

**Flexible Chelating Diphosphine Ligands and Their Interactions with Late Transition Metals****Brittany J. Barrett****Publication Date**

12-04-2017

**License**

This work is made available under a Public Domain Mark 1.0 (No Copyright) license and should only be used in accordance with that license.

**Citation for this work (American Psychological Association 7th edition)**

Barrett, B. J. (2017). *Flexible Chelating Diphosphine Ligands and Their Interactions with Late Transition Metals* (Version 1). University of Notre Dame. <https://doi.org/10.7274/9306sx63m9v>

This work was downloaded from CurateND, the University of Notre Dame's institutional repository.

For more information about this work, to report or an issue, or to preserve and share your original work, please contact the CurateND team for assistance at [curate@nd.edu](mailto:curate@nd.edu).

FLEXIBLE CHELATING DIPHOSPHINE LIGANDS AND THEIR INTERACTIONS  
WITH LATE TRANSITION METALS

A Dissertation

Submitted to the Graduate School  
of the University of Notre Dame  
in Partial Fulfillment of the Requirements  
for the Degree of

Doctor of Philosophy

by

Brittany J. Barrett

---

Vlad M. Iluc, Director

Graduate Program in Chemistry and Biochemistry

Notre Dame, Indiana

April 2017

FLEXIBLE CHELATING DIPHOSPHINE LIGANDS AND THEIR INTERACTIONS  
WITH LATE TRANSITION METALS

Abstract

By

Brittany J. Barrett

Ligand design plays an important role in the performance of transition metal catalysts. It is well known that the use of chelating ligands offer the metal center more stability, and additionally, chelating ligands can be tuned readily to influence the reactivity of the metal center. Many of these chelating ligands do not participate with the metal center throughout the course of chemical reactions, however interest has been increasing in the design of ligands that can cooperate with the metal center. Metal-ligand cooperation takes place in many forms including hemilability, charge switching, flexible coordination geometry, and ligand assisted substrate activations.

With these design features in mind, investigations centering around multidentate ligands possessing a central  $\pi$ -system were carried out. These ligands allow for a variety of coordination modes to the metal center which are adaptable, and respond to the electronic requirements of the metal center. The coordination chemistry of the trans olefin ligands *t*PCR=CRP (R = H, Me), the cis olefin ligand, *c*PCMe=CMeP, and the *o*-terphenyl ligand, PterP, will be discussed. All the ligands, except for *t*PCMe=CMeP, showed versatility in their coordination modes, and were responsive to reaction conditions.

Furthermore, the ability of the ligands *c*PCMe=CMe and PterP to stabilize difficult to observe, non-heteroatom stabilized group 10 carbenes was assessed. The reactivity of the resulting palladium and platinum carbene species was investigated. These species proved to be competent at a variety of bond activation processes, consistent with their proposed reactivity in the literature. The presented work demonstrates the cooperative tendencies of  $\pi$  based chelating ligands, and how they can be used to elucidate intermediates not commonly observed in the literature.



## TABLE OF CONTENTS

LIST OF FIGURES .....	iv
LIST OF SCHEMES .....	xiv
LIST OF ABBREVIATIONS.....	xvi
ACKNOWLEDGMENTS .....	xviii
CHAPTER 1: INTRODUCTION.....	1
1.1 Metal Ligand Cooperation.....	1
1.2 Group 10 Transition Metal Carbenes.....	8
1.3 References.....	13
CHAPTER 2: COORDINATION OF A HEMILABILE Pincer Ligand with an Olefinic Backbone to Mid-to-Late Transition Metals.....	18
2.1 Introduction.....	18
2.2 Results and Discussion .....	19
2.3 Summary .....	39
2.4 Experimental .....	42
2.5 References.....	55
CHAPTER 3: GROUP 10 METAL COMPLEXES SUPPORTED BY Pincer Ligands with a Trans Olefinic Backbone .....	59
3.1 Introduction.....	59
3.2 Results and Discussion .....	60
3.3 Reactivity Studies .....	70
3.4 DFT Calculations.....	75
3.5 Summary .....	76
3.6 Experimental.....	77
3.7 References.....	90
CHAPTER 4: METAL-LIGAND COOPERATION BETWEEN Palladium and a Diphosphine Ligand with a Cis Olefinic Backbone .....	94
4.1 Introduction.....	94
4.2 Results and Discussion .....	95
4.3 Summary .....	109
4.4 Experimental.....	110
4.5 References.....	120

CHAPTER 5: A NON-HETEROATOM STABILIZED PALLADIUM CARBENE SUPPORTED BY THE TRIDENTATE LIGAND <i>c</i> PCMe=CMeP .....	123
5.1 Introduction.....	123
5.2 Results and Discussion .....	124
5.3 Summary .....	135
5.4 Experimental.....	135
5.5 References.....	141
CHAPTER 6: AN ADAPTABLE CHELATING DIPHOSPHINE LIGAND FOR THE STABILIZATION OF PALLADIUM AND PLATINUM CARBENES .....	144
6.1 Introduction.....	144
6.2 Results and Discussion .....	145
6.3 Summary .....	164
6.4 Experimental.....	165
6.5 References.....	185
CHAPTER 7: PALLADIUM MEDIATED ARENE INSERTION INTO BULKY PALLADIUM-ARYL BONDS .....	189
7.1 Introduction.....	189
7.2 Results and Discussion .....	190
7.3 Summary .....	207
7.4 Experimental.....	208
7.5 References.....	221
APPENDIX: SELECTED NMR SPECTRA.....	225

## LIST OF FIGURES

<b>Figure 1.1:</b> Hemilabile characteristics of a neutral PNP ligand (adapted from ref. 11): (A) weak Cu–N interaction, Cu–N distance is 2.89 Å, (B) strong Cu–N interaction, Cu–N distance is 2.09 Å.....	2
<b>Figure 1.2:</b> Aromatization-dearomatization of pyridine based pincer ligands during bond activation. ....	3
<b>Figure 1.3:</b> Ligand centered reactivity of 3,5-Bis(2-phosphinophenyl)-pyridine. <sup>14</sup> .....	4
<b>Figure 1. 4:</b> Dialkylbiarylphosphine ligand design and subsequent interactions with palladium leading to C–C bond formation. <sup>34, 36</sup> .....	5
<b>Figure 1.5:</b> Dimeric palladium(0) structure formed with a preferentially cis coordinating ligand versus the monomeric palladium(0) structure formed with the flexibly coordinating wide bite angle ligand. <sup>40</sup> .....	6
<b>Figure 1.6:</b> Proposed mechanism for “long range” metal ligand cooperation exhibited by a flexible PNP acridine ligand. <sup>44</sup> .....	7
<b>Figure 1.7:</b> Coordination modes of bdps. <sup>45-46</sup> .....	8
<b>Figure 1.8:</b> Use of a sterically demanding ligand to isolate group 11 non-heteroatom stabilized carbenes. <sup>47-48</sup> .....	9
<b>Figure 1.9:</b> Previously observed group 10 non-heteroatom stabilized carbenes. ....	11
<b>Figure 2.1:</b> Coordination of 2,2'-bis(diphenylphosphino)- <i>trans</i> -stilbene (bdps) to group 6 and 9 metals.....	19
<b>Figure 2.2:</b> Thermal-ellipsoid (50% probability level) representation of <i>t</i> PCH=CHP ( <b>1</b> ). Most hydrogen atoms were omitted for clarity. Selected distances (Å) and angles (°): C(1)–C(1)# = 1.330(4), P(1)–C(11) = 1.848(2), P(1)–C(22) = 1.870(2), P(1)–C(21) = 1.852(2), C(1)#1–C(1)–C(12) = 125.6(2), C(11)–P(1)–C(22) = 101.16(9), C(11)–P(1)–C(22) = 102.81(9). ....	20
<b>Figure 2.3:</b> Thermal-ellipsoid (50% probability level) representation of ( <i>t</i> PCH=CHP)CoCl <sub>2</sub> ( <b>2</b> ). Only one of the two crystallographically independent molecules is shown. Most hydrogen atoms were omitted for clarity. Selected distances (Å) and angles (°): Co(1)–P(11) = 2.4305(17), Co(1)–P(12) =	

2.4236(18), Co(1)–Cl(11) = 2.2443(18), Co(1)–Cl(12) = 2.547(17), C(11)–C(12) = 1.317(8), P(11)–Co(1)–P(22) = 126.44(7), P(11)–Co(1)–Cl(11) = 105.66(6), P(12)–Co(1)–Cl(1) = 105.12(7), Cl(11)–Co(1)–Cl(12) = 116.59(8), P(11)–Co(1)–Cl(12) = 98.09(6), P(12)–Co(1)–Cl(12) = 105.73(7). ..... 22

**Figure 2.4:** Thermal-ellipsoid (50% probability level) representation of (*t*PCH=CHP)FeBr<sub>2</sub> (**3**). Most hydrogen atoms were omitted for clarity. Selected distances (Å) and angles (°): C(1)–C(2) = 1.320(6), Fe–P(1) = 2.5209(13), Fe–P(2) = 2.5232(14), Fe–Br(2) = 2.4038(8), Fe–Br(1) = 2.4096(8), Br(1)–Fe–Br(2) = 122.62(3), Br(1)–Fe–P(2) = 103.22(4), Br(1)–Fe–P(1) = 107.88(4), Br(2)–Fe–P(1) = 98.91(4), Br(2)–Fe–P(2) = 103.30(4), P(1)–Fe–P(2) = 122.45(5). ..... 24

**Figure 2.5:** Thermal-ellipsoid (50% probability level) representation of [(*t*PCH=CHP)CoCl][BAr<sup>F</sup><sub>4</sub>] (**4**). Only one of the two crystallographically independent cations is shown. Most hydrogen atoms were omitted for clarity. Selected distances (Å) and angles (°): Co(1)–P(11) = 2.2536(12), Co(1)–P(12) = 2.2546(12), Co(1)–Cl(1) = 2.2020(11), Co(1)–(C(11)–C(12)) = 2.068, C(11)–C(12) = 1.397(6), P(11)–Co(1)–P(12) = 172.09(5), P(11)–Co(1)–Cl(1) = 86.45(4), P(12)–Co(1)–Cl(1) = 85.84(4). ..... 26

**Figure 2.6:** Thermal-ellipsoid (50% probability level) representation of [(*t*PCH=CHP)FeBr][BAr<sup>F</sup><sub>4</sub>] (**5**). Most hydrogen atoms were omitted for clarity. Selected distances (Å) and angles (°): C(1)–C(2) = 1.332(14), Fe–P(1) = 2.4312(7), Fe–P(2) = 2.4220(7), Fe–Br = 2.3213(5), Br–Fe–P(1) = 115.41(2), Br–Fe–P(2) = 111.93(2), P(1)–Fe–P(2) = 121.38(3). ..... 27

**Figure 2.7:** Thermal-ellipsoid (50% probability level) representation of (*t*PCH=CHP)CoCl (**6**). Most hydrogen atoms were omitted for clarity. Selected distances (Å) and angles (°): Co–P(1) = 2.2138(11), Co–P(2) = 2.2145(11), Co–Cl = 2.2193(11), C(1)–C(2) = 1.442(5), P(1)–Co–P(2) = 178.76(5), Cl–Co–P(1) = 90.51(4), Cl–Co–P(2) = 89.69(4). ..... 29

**Figure 2.8:** Thermal-ellipsoid (50% probability level) representation of (*t*PCH=CHP)CoCl(CO) (**7**). Most hydrogen atoms were omitted for clarity. Selected distances (Å) and angles (°): Co–P(1) = 2.2378(14), Co–P(2) = 2.2495(14), Co–Cl = 2.348(5), C(1)–C(2) = 1.438(7), Co–C = 1.65(3), C–O = 1.18(4), P(1)–Co–P(2) = 173.11(6), Cl–Co–P(1) = 88.32(9), Cl–Co–P(2) = 92.49(10), Cl–Co–C = 101.2(7). ..... 31

**Figure 2.9:** Thermal-ellipsoid (50% probability level) representation of **8**. Only one of the two crystallographically independent molecules is shown. Most hydrogen atoms were omitted for clarity. Selected distances (Å) and angles (°): Rh(1)–P(1) = 2.2895(13), Rh(1)–Cl(1) = 2.3656(18), C(1)–C(1)# = 1.432(8), P(1)–Rh(1)–P(1)# = 179.88(7), Cl(1)–Rh(1)–P(1) = 90.07(6), Cl(1)–Rh(1)–P(1)# = 90.07(6). ..... 32

- Figure 2.10:** Thermal-ellipsoid (50% probability level) representation of **10**. Most hydrogen atoms were omitted for clarity. Selected distances (Å) and angles (°): Cu–O(1) = 2.158(2), Cu–P(1) = 2.2137(8), Cu–P(2) = 2.2179(8), C(1)–C(2) = 1.294(5), Cu–C(1) = 2.370(3), Cu–C(2) = 2.644(3), O(1)–Cu–P(1) = 103.75(6), P(1)–Cu–P(2) = 149.23(3), O(1)–Cu–P(2) = 103.57(6). ..... 34
- Figure 2.11:** Thermal-ellipsoid (50% probability level) representation of the cationic fragment of **11**. Most hydrogen atoms and the counterion were omitted for clarity. Selected distances (Å) and angles (°): Cu–P(1) = 2.2123(8), Cu–P(2) = 2.2122(8), C(1)–C(2) = 1.340(4), Cu–C(1) = 2.340(3), Cu–C(2) = 2.337(3), P(1)–Cu–P(2) = 162.34(4). ..... 36
- Figure 2.12:** Optimized geometry for [(*t*PCH=CHP)Cu]<sup>+</sup>. Most hydrogen atoms were removed for clarity. Selected distances (Å) and angles (°): Cu–P(1) = 2.316, Cu–P(2) = 2.316, C(1)–C(2) = 1.360, Cu–C(1) = 2.704, Cu–C(2) = 2.712, P(1)–Cu–P(2) = 176.67. .... 37
- Figure 2.13:** Thermal-ellipsoid (50% probability level) representation of the cationic fragment of **12**. Most hydrogen atoms and the counterion were omitted for clarity. Selected distances (Å) and angles (°): Ag–P(1) = 2.3744(6), Ag–P(2) = 2.3789(6), C(1)–C(2) = 1.326(4), P(1)–Ag–P(2) = 168.32(2). ..... 39
- Figure 3.1:** Coordination of 2,2'-bis(diphenylphosphino)-*trans*-stilbene to group 10 metals (M = Pd, Pt).<sup>3</sup> ..... 60
- Figure 3.2:** Thermal-ellipsoid (50% probability level) representation of **13**. Most hydrogen atoms were omitted for clarity. Selected distances (Å) and angles (°): Ni–P(1) = 2.1891(6), Ni–P(2) = 2.1884(6), Ni–Cl = 2.2127(6), Ni–C(1) = 1.930(2), C(1)–C(2) = 1.351(3) Å, P(1)–Ni–P(2) = 165.91(3), Cl–Ni–P(1) = 99.13(2), Cl–Ni–P(2) = 99.72(2), C(1)–Ni–P(1) = 90.13(2), C(1)–Ni–P(2) = 87.01(6), C(1)–Ni–Cl = 167.63(7). ..... 62
- Figure 3.3:** Thermal-ellipsoid (50% probability level) representation of **14**. Most hydrogen atoms were omitted for clarity. Selected distances (Å) and angles (°): Pd–P(1) = 2.2942(7), Pd–P(2) = 2.3160(7), Pd–Cl = 2.3919(7), Pd–C(1) = 2.033(3), C(1)–C(2) = 1.329(4), Cl–Pd–P(1) = 90.35(3), Cl–Pd–P(2) = 90.99(3), P(1)–Pd–P(2) = 173.59(3), C(1)–Pd–P(1) = 83.74(8), C(1)–Pd–Cl = 170.46(8). ..... 63
- Figure 3.4:** Thermal-ellipsoid (50% probability level) representation of **18**. Only one of the two crystallographically independent molecules is shown. Most hydrogen atoms and the counterion were omitted for clarity. Selected distances (Å) and angles (°): Ni(1)–Cl(1) = 2.1695(9), Ni(1)–P(11) = 2.2283(8), Ni(1)–P(12) = 2.2272(8), C(11)–C(12) = 1.398(3), Cl(1)–Ni(1)–P(11) = 85.53(3), Cl(1)–Ni(1)–P(12) = 85.56(3), Cl(1)–Ni(1)–P(11) = 105.58(7), P(12)–Ni(1)–P(11) = 171.10(3). ..... 65

**Figure 3.5:** Thermal-ellipsoid (50% probability level) representation of **19**. Only one of the two crystallographically independent molecules is shown. Most hydrogen atoms were omitted for clarity. Selected distances (Å) and angles (°): Ni(1)–P(12) = 2.1385(13), Ni(1)–P(11) = 2.1463(13), Ni(1)–C(12) = 1.968(4), Ni(1)–C(11) = 1.968(4), C(11)–C(12) = 1.406(5), P(11)–Ni(1)–P(12) = 146.35(5). ..... 66

**Figure 3.6** Thermal-ellipsoid (50% probability level) representation of **20** (left) and **21** (right). Most hydrogen atoms were omitted for clarity. Selected distances (Å) and angles (°): For **20**: Ni–Cl = 2.2498(7), Ni–P(1) = 2.2569(7), Ni–P(2) = 2.2905(7), C(1)–C(2) = 1.394(3), Cl–Ni–P(1) = 110.46(3), P(1)–Ni–P(2) = 125.10(3), Cl–Ni–P(2) = 107.24(3). For **21**: I–Ni = 2.5717(4), Ni–P(1) = 2.3039(6), Ni–P(2) = 2.2521(7), C(1)–C(2) = 1.390(3), P(1)–Ni–P(2) = 124.78(2), P(1)–Ni–I = 112.000(18), P(2)–Ni–I = 108.275(16). ..... 68

**Figure 3.7:** Thermal-ellipsoid (50% probability level) representation of **22**. Most hydrogen atoms were omitted, and some carbon atoms represented in wireframe for clarity. Selected distances (Å) and angles (°): Pd–P(1) = 2.3145(11), Pd–P(2)# = 2.3510(11), C(1)–C(2) = 1.398(5), P(1)–Pd–P(2)# = 122.74(4). ... 70

**Figure 3.8:** Thermal-ellipsoid (50% probability level) representation of **23**. Most hydrogen atoms were omitted for clarity. Selected distances (Å) and angles (°): Ni–P(1) = 2.2062(6), Ni–P(2) = 2.2095(6), Ni–C(5) = 1.982(2), Ni–C(1) = 2.1355(19), Ni–C(2) = 2.1148(19), C(1)–C(2) = 1.383(3), P(1)–Ni–P(2) = 174.07(2), P(1)–Ni–C(5) = 87.45(7), P(2)–Ni–C(5) = 87.48(7). ..... 72

**Figure 3.9:** Thermal-ellipsoid (50% probability level) representation of **25**. Most hydrogen atoms were omitted for clarity. Selected distances (Å) and angles (°): Ni–P(1) = 2.1582(7), Ni–P(2) = 2.1472(7), Ni–C(1) = 2.001(2), Ni–C(2) = 1.966(2), C(1)–C(2) = 1.429(3), P(1)–Ni–P(2) = 146.36(3). ..... 75

**Figure 3.10:**  $\sigma$  and  $\pi$  bonding interactions for  $(tPCH=CHP)^{Me}Ni$  (**19'**, left) and  $[(tPCH=CHP)^{Me}NiMe^+]$  (**23'**, right). ..... 76

**Figure 4.1:** Thermal-ellipsoid (50% probability level) representation of  $[(cPCMe=CMeP)Pd]$  (**27**). Hydrogen atoms and the solvent molecule were omitted for clarity. Selected distances (Å) and angles (°): Pd–P(1) = 2.2748(6), Pd–P(2) = 2.2892(6), Pd–C(1) = 2.198(2), Pd–C(2) = 2.186(2), C(1)–C(2) = 1.404(3), P(1)–Pd–P(2) = 140.70(2), C(1)–Pd–C(2) = 37.35(8), C(1)–Pd–P(1) = 84.08(6), C(2)–Pd–P(2) = 83.82(6). ..... 97

**Figure 4.2:** Thermal-ellipsoid (50% probability level) representation of  $[(cPCMe=CMeP)PdCl_2]$  (**28**). Hydrogen atoms were omitted for clarity. Selected distances (Å) and angles (°): Pd–P(1) = 2.3031(9), Pd–P(2) = 2.3019(10), Pd–Cl(1) = 2.3251(10), Pd–Cl(2) = 2.3194(10), C(1)–C(2) = 1.346(5), P(1)–Pd–P(2)

= 162.75(4), Cl(1)–Pd–Cl(2) = 175.05(4), Cl(1)–Pd–P(1) = 95.09(3), Cl(2)–Pd–P(2) = 84.73(4). ..... 99

**Figure 4.3:** Thermal-ellipsoid (50% probability level) representation of [(cPCMe=CMeP)PdICH<sub>3</sub>] (**29**). Most hydrogen atoms were omitted for clarity. Selected distances (Å) and angles (°): Pd–P(1) = 2.2972(11), Pd–P(2) = 2.2944(11), Pd–C(3) = 2.084(4), Pd–I = 2.6828(4), C(1)–C(2) = 1.345(6), P(1)–Pd–P(2) = 160.18(4), C(3)–Pd–I = 174.47(13), C(3)–Pd–P(1) = 84.72(12), I–Pd–P(2) = 96.36(3). ..... 102

**Figure 4.4:** Thermal-ellipsoid (50% probability level) representation of [(cPCMe=CMeP)PdI(C<sub>6</sub>H<sub>5</sub>)] (**30**). Hydrogen atoms were omitted for clarity. Selected distances (Å) and angles (°): Pd–P = 2.3229(5), Pd–P(♯) = 2.3229(5), Pd–C(21) = 2.058(3), Pd–I = 2.6992(3), C(1)–C(♯1) = 1.341(4), P–Pd–P(♯) = 157.96(3), C(21)–Pd–I = 169.85(8), C(21)–Pd–P = 84.981(18), I–Pd–P(♯) = 96.666(13). ..... 102

**Figure 4.5:** Thermal-ellipsoid (50% probability level) representation of [(cPCMe=CMeP)PdH<sub>2</sub>SiPh<sub>2</sub>] (**31**). Most hydrogen atoms were omitted for clarity. Selected distances (Å) and angles (°): Pd–P(1) = 2.3365(6), Pd–P(2) = 2.3759(6), Pd–Si = 2.3298(6), Pd–H(1) = 1.61(3), Si–H(2) = 1.41(2), Si–H(1) = 1.95(3), C(1)–C(2) = 1.339(3), P(1)–Pd–P(2) = 109.955(19), Si–Pd–H(1) = 56.0(9), Si–Pd–P(1) = 103.33(2), H(1)–Pd–P(2) = 91.0(9). ..... 105

**Figure 4.6:** Thermal-ellipsoid (50% probability level) representation of [(PCMe-CHMeP)PdCl] (**33**). Most hydrogen atoms were omitted for clarity. Selected distances (Å) and angles (°): Pd–P(1) = 2.2704(12), Pd–P(2) = 2.3140(12), Pd–Cl = 2.4174(11), Pd–C(1) = 2.108(5), C(1)–C(2) = 1.460(7), P(1)–Pd–P(2) = 177.35(5), Cl–Pd–C(1) = 174.56(15), Cl–Pd–P(1) = 91.08(4), C(1)–Pd–P(2) = 93.46(16), Pd–C(1)–C(2) = 109.6(4). ..... 107

**Figure 4.7:** Thermal-ellipsoid (50% probability level) representation of [(PC(CH<sub>3</sub>)-C(=CH<sub>2</sub>)P)PdCl] (**34**). Most hydrogen atoms were omitted for clarity. Selected distances (Å) and angles (°): Pd–P(1) = 2.2815(8), Pd–P(2) = 2.3434(8), Pd–Cl = 2.4176(8), Pd–C(1) = 2.104(3), C(1)–C(2) = 1.473(5), C(2)–C(4) = 1.366(5), C(1)–C(3) = 1.520(5), P(1)–Pd–P(2) = 176.62(3), Cl–Pd–C(1) = 173.23(10), Cl–Pd–P(1) = 91.88(3), C(1)–Pd–P(2) = 93.90(11), Pd–C(1)–C(2) = 100.6(2), C(1)–C(2)–C(4) = 122.7(3). ..... 109

**Figure 5.1:** Thermal-ellipsoid (50% probability level) representation of [(PC(CH<sub>3</sub>)-C(=CH<sub>2</sub>)P)PdBz] (**36**). Most hydrogen atoms were omitted for clarity. Selected distances (Å) and angles (°): Pd–P(1) = 2.3241(8), Pd–P(2) = 2.2792(7), Pd–C(29) = 2.170(3), Pd–C(13) = 2.161(3), C(13)–C(15) = 1.496(4), C(13)–C(14) = 1.563(4), C(15)–C(16) = 1.327(4), P(1)–Pd–P(2) = 172.60(3), C(13)–Pd–C(29) = 178.50(11), C(13)–Pd(1)–P(1) = 91.48(8), C(29)–Pd(1)–P(2) = 94.25(8), Pd–C(13)–C(15) = 103.8(17), C(16)–C(15)–C(13) = 124.8(3). ..... 126

- Figure 5.2.** Thermal-ellipsoid (50% probability level) representation of **38b**. Hydrogen atoms were omitted for clarity. Selected distances (Å) and angles (°): Pd–P(1) = 2.2385(7), Pd–P(2) = 2.3110(8), Pd–C(23) = 2.187(3), Pd–C(22) = 2.061(3), C(23)–P(1) = 1.805(3), P(1)–Pd–P(2) = 115.13(3), C(23)–Pd–C(22) = 105.52(11), C(23)–Pd–P(2) = 159.76(8), C(22)–Pd–P(1) = 153.23(8), C(23)–Pd–P(1) = 48.11(8), P(2)–Pd–C(22) = 91.62(8). ..... 128
- Figure 6.1:** VT NMR of (PterP)PtCl<sub>2</sub>, **45**. ..... 146
- Figure 6.2:** Thermal-ellipsoid (50% probability level) representation of (PterP)PtCl<sub>2</sub> (**45**). Hydrogen atoms are omitted for clarity. Selected distances (Å) and angles (°): Pt–Cl(1) = 2.3601(10), Pt–Cl(2) = 2.3490(10), Pt–P(1) = 2.2611(11), Pt–P(2) = 2.2636(11), P(1)–Pt–P(2) = 98.84(4), Cl(1)–Pt–Cl(2) = 86.22(4), P(1)–Pt–Cl(1) = 84.00(4), P(2)–Pt–Cl(2) = 90.76(4). ..... 147
- Figure 6.3:** Thermal-ellipsoid (50% probability level) representation of (PterP)PdCl<sub>2</sub> (**46**). Hydrogen atoms are omitted for clarity. Selected distances (Å) and angles (°): Pd(1)–Cl(1) = 2.3051(7), Pd(1)–Cl(2) = 2.3054(7), Pd(1)–P(1) = 2.2903(8), Pd(1)–P(2) = 2.2965(8), P(1)–Pd(1)–P(2) = 164.45(3), Cl(1)–Pd(1)–Cl(2) = 176.49(3), P(1)–Pd(1)–Cl(1) = 95.46(3), P(2)–Pd(1)–Cl(2) = 85.87(3). ..... 149
- Figure 6.4:** Thermal-ellipsoid (50% probability level) representation of (PterP)Pt (**47**). Hydrogen atoms are omitted for clarity. Selected distances (Å) and angles (°): Pt(1)–P(1) = 2.215(3), Pt(1)–P(2) = 2.229(3), P(1)–Pt(1)–P(2) = 153.95(12).. 150
- Figure 6.5:** The carbene region of the <sup>13</sup>C {<sup>1</sup>H} NMR spectrum for **48**. ..... 152
- Figure 6.6:** Thermal-ellipsoid (50% probability level) representation of (PterP)Pt=C(*p*-tol)<sub>2</sub> (**48**). Hydrogen atoms are omitted for clarity. Selected distances (Å) and angles (°): Pt–C = 1.942(3), Pt–P(1) = 2.2665(9), Pt–P(2) = 2.2891(10), P(1)–Pt–P(2) = 105.23(3), P(1)–Pt–C = 118.98(11), P(2)–Pt–C = 135.50(11), Pt–C–C(51) = 124.9(2), Pt–C–C(61) = 119.8(2), C(51)–C–C(61) = 115.0(3). ..... 153
- Figure 6.7:** Frontier molecular orbitals for **48**: bonding (bottom) and antibonding (top)  $\pi$  symmetry orbitals for the Pt=C bond in **48**. ..... 153
- Figure 6.8:** Thermal-ellipsoid (50% probability level) representation of (PterP)Pd (**49**). Hydrogen atoms are omitted for clarity. Selected distances (Å) and angles (°): Pd(1)–P(1) = 2.2612(9), Pd(1)–P(2) = 2.2472(9), P(1)–Pd(1)–P(2) = 151.23(3). ..... 156
- Figure 6.9:** Thermal-ellipsoid (50% probability level) representation of **51**. Hydrogen atoms are omitted for clarity. Selected distances (Å) and angles (°): Pd–C = 2.1794(18), Pd–P(1) = 2.2896(5), Pd–P(2) = 2.3260(5), C–P(1) = 1.8118(19), Pd–C(12) = 2.0587(19), P(1)–Pd–P(2) = 121.815(17), C(12)–Pd–C = 98.64(7), P(1)–Pd–C = 47.75(5), P(2)–Pd–C(12) = 92.84(5). ..... 158



**Figure 6.10:** Thermal-ellipsoid (50% probability level) representation of (PterP)PtHI (**52**). Hydrogen atoms are omitted for clarity. Selected distances (Å) and angles (°): Pt–I = 2.6778(6), Pt–P(1) = 2.269(2), Pt–P(2) = 2.2685(19), P(1)–Pt–P(2) = 156.21(7), P(1)–Pt–I = 102.15(6), P(2)–Pt–I = 100.28(6). ..... 159

**Figure 6.11:** Thermal-ellipsoid (50% probability level) representation of **56** (top) and **57**(bottom). Most hydrogen atoms are omitted for clarity. Selected distances (Å) and angles (°) for **56**: Pt–Si = 2.3302(16), Pt–H(1) = 1.69(6), Pt–P(1) = 2.2877(14), Pt–P(2) = 2.3335(13), Pt–H(2) = 3.28, Si–H(1) = 2.21, Si–H(2) = 1.41(5), P(1)–Pt–P(2) = 109.93(5), P(1)–Pt–Si = 100.40(6), P(2)–Pt–Si = 148.28(5), P(1)–Pt–H(1) = 163(2), P(2)–Pt–H(1) = 86(2), H(1)–Pt–Si = 64(2), Pt–Si–H(2) = 120(2); for **57**: Pd–Si = 2.3436(6), Pd–H(1) = 1.55(2), Pd–P(1) = 2.3691(5), Pd–P(2) = 2.3295(5), Pd–H(2) = 3.10, Si–H(1) = 1.87(2), Si–H(2) = 1.41(2), P(1)–Pd–Si = 146.28(2), P(2)–Pd–Si = 105.27(2), P(1)–Pd–P(2) = 108.417(19), P(1)–Pd–H(1) = 93.7(9), P(2)–Pd–H(1) = 157.7(9), H(1)–Pd–Si = 41.3(8), Pd–Si–H(2) = 108.7(10). ..... 163

**Figure 7.1:** Molecular structure of **58** (left) and **59** (right) with displacement parameters at the 50% probability level. Most hydrogen atoms are omitted for clarity. Selected distances (Å) and angles (°) for **58**: Pd(1)–P(1) = 2.2710(14), Pd(1)–P(2) = 2.3155(14), Pd(1)–Br(1) = 2.5278(7), Pd(1)–C(1) = 2.106(5), C(1)–C(2) = 1.528(7), C(2)–C(3) = 1.304(7), C(3)–C(4) = 1.486(8), C(4)–C(5) = 1.505(7), C(5)–C(6) = 1.335(7), C(6)–C(1) = 1.493(7), P(1)–Pd(1)–P(2) = 152.64(6), C(1)–Pd(1)–Br(1) = 161.39(15), C(2)–C(1)–C(6) = 109.6(4), C(5)–C(4)–C(7) = 113.2(4). For **59**: P(1)–Pd(1) = 2.2651(9), P(2)–Pd(1) = 2.2459(8), C(13)–C(14) = 1.407(4), C(14)–C(15) = 1.398(4), C(15)–C(16) = 1.382(4), C(16)–C(17) = 1.392(4), C(17)–C(18) = 1.405(5), C(18)–C(19) = 1.403(4), P(1)–Pd(1)–P(2) = 151.68(3), C(15)–C(16)–C(19) = 121.7(3), C(14)–C(13)–C(18) = 118.4(3). ..... 191

**Figure 7.2:** Molecular structure of **60a** (left) and **60b** (right) with displacement parameters at the 50% probability level. Most hydrogen atoms are omitted for clarity. Selected distances (Å) and angles (°) for **60a**: Pd(1)–P(1) = 2.3307(7), Pd(1)–Br(1) = 2.5159(5), Pd(1)–C(1) = 2.035(3), C(1)–Pd(1)–Br(1) = 164.97(12), P(1)–Pd(1)–P(1)# = 149.96(3). For **60b**: Pd(1)–P(1) = 2.3024(6), Pd(1)–Br(1) = 2.5146(4), Pd(1)–C(1) = 2.021(3), C(1)–Pd(1)–Br(1) = 168.26(9), P(1)–Pd(1)–P(1)# = 158.75(3). ..... 194

**Figure 7.3:** Molecular structure of **62** with displacement parameters at the 50% probability level. Most hydrogen atoms are omitted for clarity. Selected distances (Å) and angles (°) for **62**: Pd(1)–P(1) = 2.3261(8), Pd(1)–P(2) = 2.2595(8), Pd(1)–Br(1) = 2.5316(4), Pd(1)–C(1) = 2.102(3), C(1)–C(2) = 1.498(4), C(2)–C(3) = 1.321(4), C(3)–C(4) = 1.498(4), C(4)–C(5) = 1.505(4), C(5)–C(6) = 1.335(4), C(6)–C(1) = 1.490(4), P(1)–Pd(1)–P(2) = 149.38(3), C(1)–Pd(1)–Br(1) = 159.54(7), C(2)–C(1)–C(6) = 111.3(2), C(5)–C(4)–C(7) = 110.9(2). ..... 195

**Figure 7.4:** Molecular structure of **64a** (left) and **64b** (right) with displacement parameters at the 50% probability level. Most hydrogen atoms are omitted for

clarity. Selected distances (Å) and angles (°) for **64a**: Pd(1)-P(1) = 2.2960(15), Pd(1)-P(2) = 2.3050(8), Pd(1)-Br(1) = 2.5145(7), Pd(1)-C(1) = 2.063(6), C(1)-Pd(1)-Br(1) = 172.71(17), P(1)-Pd(1)-P(2) = 157.66(5). For **64b**: Pd(1)-P(1) = 2.3043(14), Pd(1)-P(2) = 2.2898(13), Pd(1)-Br(1) = 2.5453(7), Pd(1)-C(1) = 2.008(5), C(1)-Pd(1)-Br(1) = 165.79(16), P(1)-Pd(1)-P(2) = 159.58(5)..... 197

**Figure 7.5:** Molecular structure of **66** with displacement parameters at the 50% probability level. The counterions and hydrogen atoms are omitted for clarity. Selected distances (Å) and angles (°) for **66**: Pd(1)-P(1) = 2.3155(6), Pd(1)-P(2) = 2.3090(6), Pd(1)-Cl(1) = 2.3908(6), Pd(1)-Cl(1)# = 2.3966(6), Pd(1)-Pd(1)# = 3.639, P(1)-Pd(1)-P(2) = 97.07(2)(9), P(2)-Pd(1)-Cl(1)# = 172.10(2), P(1)-Pd(1)-Cl(1) = 170.55(2)..... 201

**Figure 7.6:** Molecular structure of **67** with displacement parameters at the 50% probability level. The triflate counterion and hydrogen atoms are omitted for clarity. Selected distances (Å) and angles (°) for **67**: Pd(1)-P(1) = 2.3553(11), Pd(1)-C(1) = 1.996(6), Pd(1)-(C(20)-C(20)#) = 2.651, P(1)-Pd(1)-P(1)# = 154.49(5), P(1)-Pd(1)-C(1) = 95.60(4)..... 203

**Figure A.1:**  $^1\text{H}$  NMR spectrum of (*t*PC(Bpin)=CP)Ni **25**. .... 225

**Figure A.2 :**  $^{13}\text{C}\{^1\text{H}\}$  NMR spectrum of (*t*PC(Bpin)=CHP)Ni (**25**). .... 226

**Figure A.3:**  $^{31}\text{P}\{^1\text{H}\}$  NMR spectrum of (*t*PC(Bpin)=CP)Ni (**25**). .... 227

**Figure A.4:**  $^1\text{H}$  NMR spectrum of (*c*PCMe=CMeP)PdBr(CH<sub>2</sub>Ph) (**35**). .... 228

**Figure A.5:**  $^{31}\text{P}\{^1\text{H}\}$  NMR spectrum of (*c*PCMe=CMeP)PdBr(CH<sub>2</sub>Ph) (**35**). .... 229

**Figure A.6:**  $^1\text{H}$  NMR spectrum of (PC(CH<sub>2</sub>)-CMeP)Pd(CH<sub>2</sub>PH) (**36**). .... 230

**Figure A.7:**  $^{31}\text{P}\{^1\text{H}\}$  NMR spectrum of (PC(CH<sub>2</sub>)-CMeP)Pd(CH<sub>2</sub>PH) (**36**). .... 231

**Figure A.8:**  $^1\text{H}$  NMR spectrum of (*c*PCMe=CMeP)Pd=C(*p*-tol)<sub>2</sub> (**37**). .... 232

**Figure A.9:**  $^{31}\text{P}\{^1\text{H}\}$  NMR spectrum of (*c*PCMe=CMeP)Pd=C(*p*-tol)<sub>2</sub> (**37**). .... 233

**Figure A.10:**  $^{13}\text{C}\{^1\text{H}\}$  NMR spectrum of (*c*PCMe=CMeP)Pd=C(*p*-tol)<sub>2</sub> (**37**). .... 234

**Figure A.11:** Carbene region of the  $^{13}\text{C}\{^1\text{H}\}$  NMR spectrum of (*c*PCMe=CMeP)Pd=C(*p*-tol)<sub>2</sub> (**37**). .... 235

**Figure A.12:**  $^1\text{H}$  NMR spectrum of **38**. Spectrum contains tetra-*p*-tolyl azine as a contaminant. .... 236

**Figure A.13:**  $^{31}\text{P}\{^1\text{H}\}$  NMR spectrum of **38**. .... 237

**Figure A.14:**  $^1\text{H}$  NMR spectrum of (*t*PCMe=CMeP)Pd (**43**). .... 238

<b>Figure A.15:</b> $^{31}\text{P}\{^1\text{H}\}$ NMR spectrum of ( <i>t</i> PCMe=CMeP)Pd ( <b>43</b> ).....	239
<b>Figure A.16:</b> $^1\text{H}$ NMR spectrum of (Pter <sup>Mes</sup> P)PdBr ( <b>58</b> ). ....	240
<b>Figure A.17:</b> $^{13}\text{C}\{^1\text{H}\}$ NMR spectrum of (Pter <sup>Mes</sup> P)PdBr ( <b>58</b> ). ....	241
<b>Figure A.19:</b> HSQC of (Pter <sup>Mes</sup> P)PdBr ( <b>58</b> ). ....	242
<b>Figure A.20:</b> $^{31}\text{P}\{^1\text{H}\}$ NMR Spectrum of (Pter <sup>Mes</sup> P)PdBr ( <b>58</b> ). ....	243
<b>Figure A.21:</b> $^1\text{H}$ NMR spectrum of mixture of isomers of (PterP)PdBr(tol) ( <b>60a-b</b> )....	244
<b>Figure A.22:</b> $^1\text{H}$ NMR spectrum of isomers of (PterP)PdBr(tol) ( <b>60a-b</b> ) after 2h at 80°C. .....	245
<b>Figure A.23:</b> $^{13}\text{C}\{^1\text{H}\}$ NMR spectrum of syn-isomer of (PterP)PdBr(tol) ( <b>60a-b</b> ). ....	246
<b>Figure A.24:</b> $^{31}\text{P}\{^1\text{H}\}$ NMR spectrum of mixture of isomers of (PterP)PdBr(tol) ( <b>60a-b</b> ).....	247
<b>Figure A.25:</b> $^1\text{H}$ NMR spectrum of syn-isomer of (PterP)PdI(tol) ( <b>61b</b> ). ....	248
<b>Figure A.26:</b> $^{13}\text{C}\{^1\text{H}\}$ NMR spectrum of syn-isomer of (PterP)PdI(tol) ( <b>61b</b> ). ....	249
<b>Figure A.27:</b> HSQC of (PterP)PdI(tol) ( <b>61b</b> ).....	250
<b>Figure A.28:</b> $^{31}\text{P}\{^1\text{H}\}$ NMR spectrum of syn-isomer of (PterP)PdI(tol) ( <b>61b</b> ). ....	251
<b>Figure A.29:</b> $^1\text{H}$ NMR spectrum of (Pter <sup>tol</sup> P)PdBr ( <b>62</b> ). ....	252
<b>Figure A.30:</b> $^{31}\text{P}\{^1\text{H}\}$ NMR spectrum of (Pter <sup>tol</sup> P)PdBr ( <b>62</b> ). ....	253
<b>Figure A.31:</b> $^1\text{H}$ NMR spectrum of (Pter <sup>tol</sup> P)PdI ( <b>63</b> ). ....	254
<b>Figure A.32:</b> $^{13}\text{C}\{^1\text{H}\}$ NMR spectrum of (Pter <sup>tol</sup> P)PdI ( <b>63</b> ).....	255
<b>Figure A.33:</b> HSQC of (Pter <sup>tol</sup> P)PdI ( <b>63</b> ).....	256
<b>Figure A.34:</b> $^{31}\text{P}\{^1\text{H}\}$ NMR spectrum of (Pter <sup>tol</sup> P)PdI ( <b>63</b> ).....	257
<b>Figure A.35:</b> $^1\text{H}$ NMR spectrum of anti-isomer of (PterP)PdBrPh ( <b>65a</b> ). ....	258
<b>Figure A.36:</b> $^{13}\text{C}\{^1\text{H}\}$ NMR spectrum of anti-isomer of (PterP)PdBrPh ( <b>65a</b> ).....	259
<b>Figure A.37:</b> HSQC of (PterP)PdBrPh ( <b>65a</b> ).....	260
<b>Figure A.38:</b> $^{31}\text{P}\{^1\text{H}\}$ NMR spectrum of anti-isomer of (PterP)PdBrPh ( <b>65a</b> ). ....	261

<b>Figure A.39:</b> $^1\text{H}$ NMR spectrum of (PterP)PdBrPh after heating to 80°C for 24 h (top). $^1\text{H}$ NMR spectrum of pure anti-isomer of (PterP)PdBrPh ( <b>65a</b> bottom). ....	262
<b>Figure A.40:</b> $^{31}\text{P}\{^1\text{H}\}$ NMR spectrum of (PterP)PdBrPh after heating to 80°C for 24 h (top). $^{31}\text{P}\{^1\text{H}\}$ NMR spectrum of pure anti-isomer of (PterP)PdBrPh ( <b>65a</b> , bottom). ....	263
<b>Figure A.41:</b> $^1\text{H}$ NMR spectrum of [(PterP)PdCl] <sub>2</sub> [2BAr <sup>F</sup> <sub>4</sub> ] ( <b>66</b> ) at room temperature.	264
<b>Figure A.42:</b> $^{13}\text{C}\{^1\text{H}\}$ NMR spectrum of [(PterP)PdCl] <sub>2</sub> [2BAr <sup>F</sup> <sub>4</sub> ] ( <b>66</b> ) at room ..... temperature. ....	265
<b>Figure A.43:</b> $^{31}\text{P}\{^1\text{H}\}$ NMR spectrum of [(PterP)PdCl] <sub>2</sub> [2BAr <sup>F</sup> <sub>4</sub> ] ( <b>66</b> ) at room temperature. ....	266
<b>Figure A.44:</b> $^{11}\text{B}\{^1\text{H}\}$ NMR spectrum of [(PterP)PdCl] <sub>2</sub> [2BAr <sup>F</sup> <sub>4</sub> ] ( <b>66</b> ) at room temperature. ....	267
<b>Figure A.45:</b> $^{19}\text{F}\{^1\text{H}\}$ NMR spectrum of [(PterP)PdCl] <sub>2</sub> [2BAr <sup>F</sup> <sub>4</sub> ] ( <b>66</b> ) at room temperature. ....	268
<b>Figure A.46:</b> $^1\text{H}$ NMR spectrum of [(PterP)Pd(tol)][OTf] ( <b>68</b> ). ....	269
<b>Figure A.47:</b> $^{13}\text{C}\{^1\text{H}\}$ NMR spectrum of [(PterP)Pd(tol)][OTf] ( <b>68</b> ). ....	270
<b>Figure A.48:</b> $^{19}\text{F}\{^1\text{H}\}$ NMR spectrum of [(PterP)Pd(tol)][OTf] ( <b>68</b> ). ....	271
<b>Figure A.49:</b> $^{31}\text{P}\{^1\text{H}\}$ NMR spectrum of [(PterP)Pd(tol)][OTf] ( <b>68</b> ). ....	272
<b>Figure A.50:</b> $^1\text{H}$ NMR spectrum of (Pter <sup>tol</sup> P)PdOTf ( <b>68</b> ). ....	273
<b>Figure A.51:</b> $^{31}\text{P}\{^1\text{H}\}$ NMR spectrum of (Pter <sup>tol</sup> P)PdOTf ( <b>68</b> ). ....	274
<b>Figure A.52:</b> $^{19}\text{F}\{^1\text{H}\}$ NMR spectrum of (Pter <sup>tol</sup> P)PdOTf ( <b>68</b> ). ....	275
<b>Figure A.53:</b> $^1\text{H}$ NMR spectrum of (Pter <sup>tol</sup> P)PdH(OTf) ( <b>69</b> ). ....	276
<b>Figure A.54:</b> Hydride region of the $^1\text{H}$ NMR spectrum of (Pter <sup>tol</sup> P)PdH(OTf) ( <b>69</b> ). ....	277
<b>Figure A.55:</b> $^{31}\text{P}\{^1\text{H}\}$ NMR spectrum of (Pter <sup>tol</sup> P)PdH(OTf) ( <b>69</b> ). ....	278
<b>Figure A.56:</b> $^{19}\text{F}\{^1\text{H}\}$ NMR spectrum of (Pter <sup>tol</sup> P)PdH(OTf) ( <b>69</b> ). ....	279

## LIST OF SCHEMES

<b>Scheme 2.1:</b> Synthesis of <i>t</i> PCH=CHP ( <b>1</b> ).....	20
<b>Scheme 2.2:</b> Synthesis of complex <b>2</b> .....	22
<b>Scheme 2.3:</b> Synthesis of compound <b>3</b> .....	23
<b>Scheme 2.4:</b> Synthesis of compounds <b>4</b> and <b>5</b> . ....	25
<b>Scheme 2.5:</b> Synthesis of complexes <b>6</b> and <b>7</b> .....	29
<b>Scheme 2.6:</b> Synthesis of compound <b>8</b> .....	32
<b>Scheme 2.7:</b> Synthesis of complexes <b>9-11</b> . ....	35
<b>Scheme 2.8:</b> Synthesis of <b>12</b> . ....	38
<b>Scheme 3.1:</b> Synthesis of complexes <b>13-15</b> . ....	61
<b>Scheme 3.2:</b> Synthesis of of <i>t</i> PCMe=CMeP ( <b>17</b> ) and complex <b>18</b> . ....	64
<b>Scheme 3.3:</b> Synthesis of complexes <b>19-20</b> . ....	68
<b>Scheme 3.4:</b> Synthesis of <b>22</b> . ....	69
<b>Scheme 3.5:</b> Reactivity of <b>19</b> towards CH <sub>3</sub> I.....	71
<b>Scheme 3.6:</b> Synthesis of complex <b>24</b> , and subsequent H-atom transfer.....	73
<b>Scheme 3.7:</b> Synthesis of ( <i>t</i> PC(Bpin)=CHP)Ni ( <b>14</b> ).....	74
<b>Scheme 4.1:</b> Synthesis of <i>c</i> PCMe=CMeP ( <b>26</b> ). ....	95
<b>Scheme 4.2:</b> Synthesis of <b>27</b> . ....	97
<b>Scheme 4.3:</b> Synthesis of <b>28</b> . ....	99
<b>Scheme 4.4:</b> Oxidative addition of CH <sub>3</sub> I and PhI to <b>27</b> . ....	101
<b>Scheme 4.5:</b> Reactivity of <b>27</b> with Ph <sub>2</sub> SiH <sub>2</sub> . ....	104
<b>Scheme 4.6:</b> Reactivity of <b>27</b> with HCl.....	106

<b>Scheme 4.7:</b> Conversion of <b>32</b> to <b>33</b> .	107
<b>Scheme 4.8:</b> Synthesis of <b>34</b> .	108
<b>Scheme 5.1:</b> Synthesis of <b>35</b> and subsequent reactivity with KOtBu.	125
<b>Scheme 5.2:</b> Synthesis of palladium carbenes <b>37a</b> and <b>37b</b> and subsequent decomposition.	127
<b>Scheme 5.3:</b> Reactivity of <b>37a</b> with CH <sub>3</sub> I.	131
<b>Scheme 5.4:</b> Reactivity of <b>37a</b> towards HCl.	132
<b>Scheme 5.5:</b> Reactivity of <b>37a</b> with Ph <sub>2</sub> SiH <sub>2</sub> .	133
<b>Scheme 5.6:</b> Isomerization of <b>27</b> to <b>43</b> , and independent synthesis of <b>43</b> .	134
<b>Scheme 6.1.</b> Synthesis of compound <b>45</b> .	146
<b>Scheme 6.2:</b> Synthesis of compound <b>46</b> .	148
<b>Scheme 6.3:</b> Synthesis of compound <b>47</b> .	150
<b>Scheme 6.4:</b> Synthesis of diarylcarbene <b>48</b> .	151
<b>Scheme 6.5:</b> Synthesis of compound <b>49</b> .	156
<b>Scheme 6.6:</b> Decomposition of <b>50</b> .	157
<b>Scheme 6.7:</b> Reactions of <b>48</b> and <b>50</b> with CH <sub>3</sub> I.	161
<b>Scheme 6.8:</b> Reactivity of carbenes <b>48</b> and <b>50</b> with Ph <sub>2</sub> SiH <sub>2</sub> .	162
<b>Scheme 7.1:</b> Synthesis of compound <b>58</b> , and subsequent dehydrohalogenation.	191
<b>Scheme 7.2:</b> Synthesis of <b>60a-b</b> and <b>61a-b</b> .	193
<b>Scheme 7.3:</b> Synthesis of <b>62</b> and <b>63</b> and subsequent dehydrohalogenation.	195
<b>Scheme 7.4:</b> Synthesis of <b>65 a-b</b> .	197
<b>Scheme 7.5:</b> Proposed mechanism for dearomative rearrangement observed in the Buchwald Group. <sup>8</sup>	199
<b>Scheme 7.6:</b> Synthesis of <b>66</b> .	200
<b>Scheme 7.7:</b> Synthesis of compound <b>67</b> .	202
<b>Scheme 7.8:</b> Synthesis of <b>68</b> , and subsequent rearrangement.	204

## LIST OF ABBREVIATIONS

Ph	phenyl
<i>p</i> -	para
<i>m</i> -	meta
<i>o</i> -	ortho
<sup><i>i</i></sup> Pr	<i>iso</i> -propyl
Ar	aryl
<sup><i>t</i></sup> Bu	<i>tert</i> -butyl
BAr <sup>F</sup> <sub>4</sub>	tetrakis[3,5-bis(trifluoromethyl)phenyl]borate
cod	1,5-cyclooctadiene
THF	tetrahydrofuran
Cy	cyclohexyl
NMR	nuclear magnetic resonance spectroscopy
Hz	hertz
ppm	parts per million
OTf	triflate
Et <sub>2</sub> O	diethylether
DCM	dichloromethane
dme	1,2-dimethoxyethane
r.t.	room temperature
Me	methyl
<sup><i>n</i></sup> Bu	<i>n</i> -butyl
dba	dibenzylideneacetone
TMS	trimethylsilyl
mes	mesityl
Et	ethyl
Tol	toluene
<i>t</i> PCH=CHP	2,2'-bis(di- <i>iso</i> -propylphosphino)- <i>trans</i> -stilbene
<i>t</i> PCMe=CMeP	2,2'-bis(di- <i>iso</i> -propylphosphino)- <i>trans</i> -diphenyl-1,2-dimethylethene
<i>c</i> PCMe=CMeP	2,2' bis(di- <i>iso</i> -propylphosphino)- <i>cis</i> -diphenyl-1,2-dimethylethene
PterP	1,2-bis(2-(di- <i>iso</i> -propylphosphino)phenyl)benzene
<i>p</i> -tol	<i>para</i> -tolyl
UV	ultraviolet
IR	infrared
dtbe	1,2-bis(di- <i>tert</i> -butylphosphino)-ethane
VT	variable temperature
Tripy	tripyrin
Tp'	hydridotris(3,5-dimethylpyrazolyl)borate)
DFT	Density Functional Theory

HSQC	heteronuclear single quantum correlation
KHMDS	Potassium bis(trimethylsilyl)amide



## ACKNOWLEDGMENTS

I want to thank my research advisor Professor Vlad Iluc for all of the support he has given me over the past couple of years. I have learned so much during my time at Notre Dame, and he was a major part of that. Vlad was a great resource for guidance and I truly appreciate his patience with me. I owe much of my success to him.

Professor Allen Oliver provided a substantial amount of guidance towards my research. He was always more the willing to offer a few suggestions when I was struggling, but additionally he was a great friend to turn to when I just needed to talk about life. I enjoyed getting to know him, and am so happy he was around to offer support.

My chemistry career would have gone nowhere if it were not for the support of Jaroslav Z, and Justin Pontius. Jaroslav was always willing to make any NMR experiment possible, and was always enthusiastic about the results. Justin was additionally a wonderful resource for teaching me the tricks of the trade.

The Iluc Research Group was a true pleasure to work with. Sean Vilanova, and Dominic Babbini were always willing to teach me a thing or two about lab techniques, but most of all they were extremely approachable and fun to be around. Julie Kessler, and Patrick Rothstein were two of the best lab mates anyone could ask for. It always made the various obstacles of graduate school much easier to face knowing that they were going through the same ones with me. We were truly in this thing together. Melissa Hoffbauer

was a wonderful person to be around in lab. Her work ethic was inspirational, and she was always willing to learn new things. Our postdocs Cezar Comanescu, and Peng Cui are responsible for much of my synthetic knowledge. I was extremely lucky to have such talented chemists to look up to. Additionally I wish Amanda Holland and Cody Work the best of luck with their future endeavors.

Finally, I would like to thank my family. I never would have gotten here if it wasn't for their unconditional support. I truly appreciate all the countless hours my parents spent listening to me carrying on about science, even though science is not exactly their area of expertise. As for my brother Kevin, as subtle as it seems, our talks about the best music to listen to brought so much joy to my life. It is amazing how much of a difference a good playlist can make while you are in the lab! Last, but not least, my mental sanity might be lost if it was not for the love and support of Luis Perla. Lou was always there for me to lean on when I needed it the most. There are no words to describe how appreciative I am.

## CHAPTER 1:

### INTRODUCTION

#### 1.1 Metal Ligand Cooperation

The use of multidentate ligands is a well-studied topic in organometallic chemistry. These ligands lead to the formation of robust metal complexes, and can be modified to alter the reactivity of the metal center.<sup>1-4</sup> By changing the backbone framework of the ligand, or the chelating atoms themselves, the flexibility and electronics of the species can be tuned. Many of these ligands remain unchanged throughout chemical reactions and are referred to as spectator ligands, however interest has been increasing towards designing ligands capable of participating with the metal center throughout the course of chemical reactions.

Pincers represent a versatile class of ligands with various examples of metal-ligand cooperation reported.<sup>5-8</sup> Additionally, the corresponding metal complexes tend to be stable and robust.<sup>9-10</sup> Many examples include a central, anionic, strong donor flanked by two neutral groups. Examples in which the central chelating moiety is neutral, have featured a pyridine or a phosphine group.<sup>11-12</sup> In addition, these neutral chelating systems have started incorporating  $\pi$ -systems as neutral donors within the ligand framework.<sup>13-18</sup> Interestingly, such ligands show different coordination modes depending on various factors such as the type of metal or its oxidation state.<sup>11-12</sup> For example, pyridine-based PNP ligands (2,6-bis(phosphinomethyl)pyridine) have shown hemilabile characteristics of the neutral

pyridine N-atom donor upon coordination to a copper metal center (Figure 1).<sup>11</sup> It was found that in the presence of bromide, the pyridine nitrogen is dissociated from the metal center; bromide extrusion with a silver salt led to pyridine coordination, stabilizing the complex (Figure 1.1).<sup>11</sup> This incorporation of a labile interaction in chelating ligand frameworks has the capability to alter the behavior of catalysts.<sup>19-20</sup> For example, Hessen and coworkers reported the catalyst,  $[(\eta^5\text{-C}_5\text{H}_4\text{CMe}_2\text{R})\text{TiCl}_3]$  ( $\text{R} = \text{CH}_3, \text{Ph}$ ).<sup>19</sup> They discovered that replacing the non-coordinating methyl substituent with a labile arene moiety transformed the ethane dimerization catalyst into a trimerization catalyst. Along with the dissociation of the labile moiety, the re-association helps stabilize metal centers, which may otherwise decompose in the absence of a substrate.<sup>11, 21-22</sup>

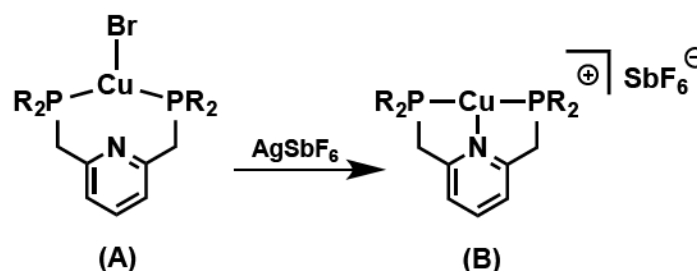


**Figure 1.1:** Hemilabile characteristics of a neutral PNP ligand (adapted from ref. 11): (A) weak Cu–N interaction, Cu–N distance is 2.89 Å, (B) strong Cu–N interaction, Cu–N distance is 2.09 Å.

Pyridine based ligand systems have also shown the ability to undergo reversible charge switching by transferring a hydrogen atom from the ligand backbone to the metal, while the central pyridine moiety can act as either a neutral or anionic moiety. This is a feature that has led to interesting reactivity towards small molecule activation as reported by the Milstein group.<sup>23</sup> They incorporated a hemilabile functionality along with charge switching behavior in their ligand framework leading to an elegant example of the acylation

of amines from alcohols with a PNN type pincer ligand (2-(di-*tert*-butylphosphinomethyl)-6-(diethylaminomethyl)pyridine). The dissociation of the amine side arm throughout the catalytic cycle allows for the activation of various substrates.<sup>24</sup> Additionally, the charge switching capabilities of the central pyridine moiety allow the ligand to cooperate with the metal center through aromatization-dearomatization processes upon accepting or donating H-atoms (Figure 1.2).<sup>25-27</sup> The dearomatized species has proven to be competent at a variety of bond activation processes in which the driving force for the reaction is the restoration of the aromatic system, an event which occurs upon H-atom acceptance from a substrate (Figure 1.2). These bond activations can occur without change in the metal's oxidation state due to the charge flipping of the pyridine nitrogen atom during the aromatization-dearomatization processes.

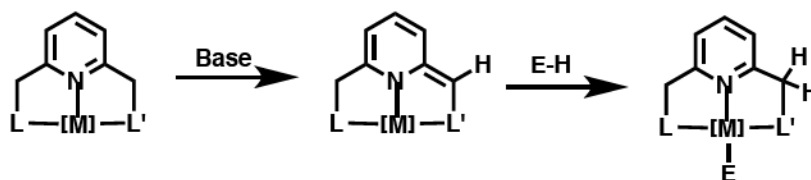


**Figure 1.2:** Aromatization-dearomatization of pyridine based pincer ligands during bond activation.

Examples such as these have inspired the design of various ligands with H-atom acceptor and donor capabilities. For example, a *p*-terphenyl diphosphine ligand reported by Agapie and coworkers demonstrated reversible H-atom migration from nickel metal to the central arene moiety in the ligand framework.<sup>28</sup> This H-atom migration displayed the ability of the ligand to accommodate multiple coordination modes including non-coordination of the central arene moiety,  $\eta^2$  coordination, and  $\eta^3$  coordination. Furthermore, this ligand was promising for H-atom storage throughout the course of

chemical reactions. The general design of ligands incorporating an aromatic moiety in the center of the framework has led to numerous interesting metal complexes.<sup>14-16, 29-33</sup> For example the terphenyl ligand system was modified by replacing the central *p*-arene moiety with a *m*-pyridine functionality, leading to ligand centered substrate activations (Figure 1.3).<sup>14</sup> Reacting these complexes with silanes and boranes resulted in hydroboration or hydrosilation of the pyridine C-N bond in the ligand framework. The resulting functionalization of the pyridine fragment led to a stronger interaction between the metal center and the pyridine  $\pi$  system due to the more electron deficient nature of the pyridine moiety. This provided an interesting example of post-synthetic modifications to a  $\pi$  based ligand system that could be utilized to tune the electronics of the metal center.

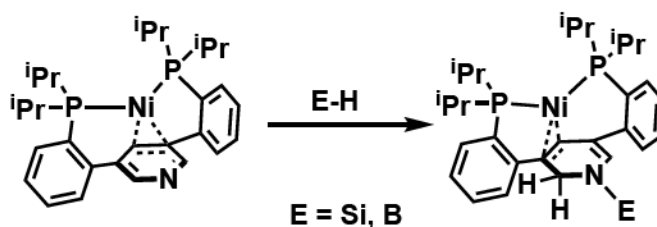


**Figure 1.3:** Ligand centered reactivity of 3,5-Bis(2-phosphinophenyl)-pyridine.<sup>14</sup>

Ligand systems containing moieties which can interact with the metal center in a  $\pi$ -based fashion have led to rich chemistry. The Buchwald group has developed a library of dialkylbiarylphosphine ligands which have proven to be useful in a variety of palladium catalyzed cross-coupling reactions (Figure 4).<sup>34-35</sup> The architecture of these ligand systems includes a “lower aryl ring” that can be modified by changing the substituents bound to the ring. These modifications can prevent unwanted side reactions between the metal center and the ligand itself, as well as allow for the sterically controlled formation of palladium(0)

complexes containing only one neutral ligand.<sup>34</sup> This lower aryl feature in the ligand framework is important for promoting reductive elimination for steric reasons, as well as stabilizing the palladium metal center through Pd-arene interactions in the absence of substrate. In addition to facilitating cross-coupling reactions, the Pd-arene interactions have also led to interesting C-C bond formation processes between the ligand itself, and an additional aromatic moiety.<sup>36</sup> This is due to the weakening of the aromatic character upon coordination of the metal center to the arene functionality (Figure 1.4).

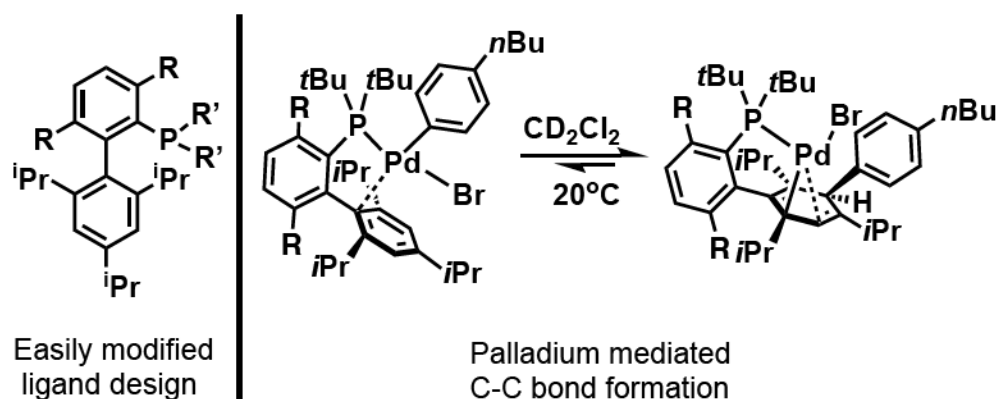


**Figure 1. 4:** Dialkylbiarylphosphine ligand design and subsequent interactions with palladium leading to C-C bond formation.<sup>34, 36</sup>

Another class of interesting ligands includes those which can flexibly coordinate to the metal center in either a cis or a trans geometry.<sup>37-42</sup> This can be important when the oxidation state of the metal center is changing throughout the course of a chemical reaction. For example, in the absence of additional neutral donor ligands, cis only coordinating ligands often lead to dimer formation upon reduction of group 10 metals from the +2 oxidation state to the 0 oxidation state.<sup>40</sup> These dimeric structures arise from the dissociation of one of the chelating atoms from the metal center, and association to an adjacent metal center. Specifically, our group recently compared the preferentially cis

coordinating  $i\text{Pr}_2\text{P}(o\text{-C}_6\text{H}_4\text{-CH}_2\text{-}o'\text{-C}_6\text{H}_4)\text{P}^i\text{Pr}_2$  to the more flexible, wide bite angle  $i\text{Pr}_2\text{P}(o\text{-C}_6\text{H}_4\text{-CH}_2\text{CH}_2\text{-}o'\text{-C}_6\text{H}_4)\text{P}^i\text{Pr}_2$ .<sup>40</sup> It was observed that in the case of the former, dimeric palladium(0) compounds resulted in the absence of an additional dative ligand, however, the wide bite angle ligand was able to accommodate the optimal trans geometry resulting in a two-coordinate palladium(0) compound (Figure 1.5).

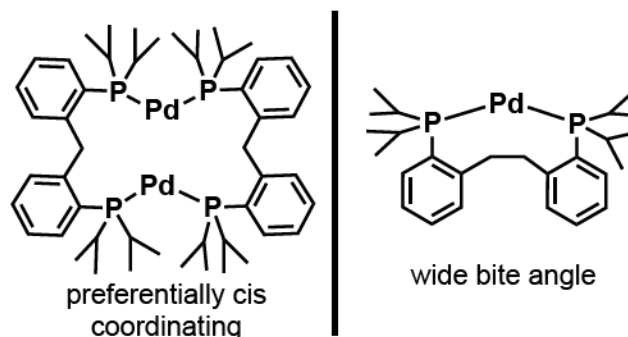


**Figure 1.5:** Dimeric palladium(0) structure formed with a preferentially cis coordinating ligand versus the monomeric palladium(0) structure formed with the flexibly coordinating wide bite angle ligand.<sup>40</sup>

Diphosphine ligands with a preference for trans coordination to group 10 metal centers tend to result in less reactive catalysts when the cycle involves a reductive elimination step. Introducing flexibility into these ligand frameworks allowing them to access a wide bite angle cis conformation can enhance the catalytic activity due to accessibility to reactive cis intermediates which promote rapid reductive elimination from the metal center.<sup>43</sup> For example, the van Leeuwen group studied the influence of the bite angle of bidentate phosphine ligands on the activity of palladium catalysts for allylic alkylation reactions. They studied diphosphine ligands with bite angles ranging from 85°-110°, and found that the ligands exhibiting the largest bite angles gave the highest catalytic activities. These



studies provide interesting opportunities to investigate the influence ligand geometry can have on the reactivity of metal complexes.

Flexibly coordinating ligands can additionally perform interesting bond activation processes. For example, the PNP acridine based ligand reported by the Milstein group showed “long range” metal ligand cooperation upon the activation of an  $H_2$  molecule.<sup>44</sup> This process was proposed to occur via a pathway in which the dissociation of the central N-atom generates a wide angle cis complex from the originally trans phosphine geometry (Figure 1.6). This allows the acridine unit to bend in towards the metal center, allowing for H-atom migration to the ligand backbone; an interesting example of metal ligand-cooperation.<sup>44</sup>

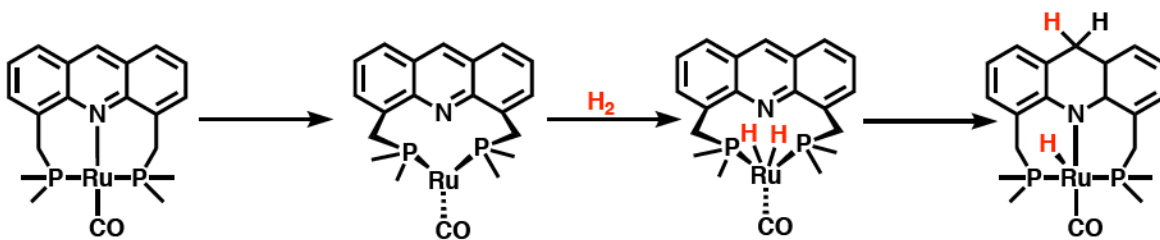


**Figure 1.6:** Proposed mechanism for “long range” metal ligand cooperation exhibited by a flexible PNP acridine ligand.<sup>44</sup>

These examples of metal-ligand cooperation drew our attention to the previously reported ligand, 2,2'-bis(diphenylphosphino)-*trans*-stilbene (bdps).<sup>45-46</sup> This ligand was originally studied in the 1970s by Bennett and coworkers. They observed a variety of coordination modes including  $\eta^2$  coordination to group 6 and 9 metals, and  $\eta^1$  coordination to group 10,  $d^8$  metals upon C-H activation of the backbone olefin moiety (Figure 1.7).<sup>45-46</sup> Although these different coordination modes were observed, the response of the ligand to changes in the electronics of the metal center was not investigated in detail. We therefore

became interested in studying the coordination of a family of similar ligand systems to late transition metals in a variety of oxidation states.

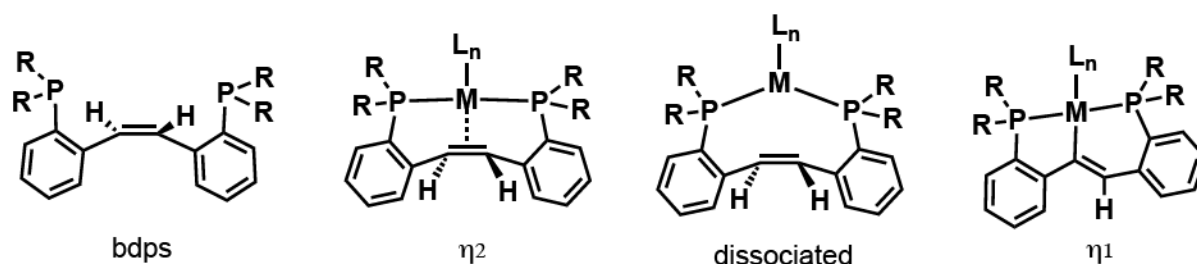


**Figure 1.7:** Coordination modes of bdps.<sup>45-46</sup>

## 1.2 Group 10 Transition Metal Carbenes

Ligand design is critical in influencing the reactivity of metal complexes. These designs can be important for generating more reactive metal centers, and additionally, can be used to stabilize reactive intermediates that are otherwise difficult to observe. For example the sterically demanding ligand, IPr<sup>\*\*</sup>, ((IPr<sup>\*\*</sup> = 1,3-bis[2,6-bis[(4-tert-butylphenyl)methyl]-4-methylphenyl]imidazol-2-ylidene) was utilized in the Straub group to stabilize previously unobservable copper and silver and gold metal diarylcarbenes (Figure 1.8).<sup>47-48</sup> The high degree of bulk exhibited by this supporting ligand played a crucial role in shielding the reactive metal carbene fragment, allowing for its isolation. This work provided an appealing example of the importance of ligand selection.

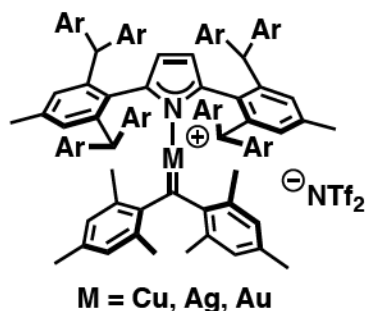


**Figure 1.8:** Use of a sterically demanding ligand to isolate group 11 non-heteroatom stabilized carbenes.<sup>47-48</sup>

Transition metal carbenes have received a great deal of attention in recent years due to their various uses in organic transformations.<sup>49-53</sup> Specifically for group 10 metal examples, many isolated carbenes feature heteroatom stabilization, while hydrocarbon analogues ( $M=CR_2$ ,  $R = H$ , alkyl, or aryl) remain rare. Isolation of such compounds is desired due to their implication in a range of catalytic reactions. For example, palladium catalyzed cross-coupling reactions between diazo compounds and an array of substrates<sup>54</sup> are proposed to involve the migratory insertion of a carbene fragment into Pd-C bonds, however, this proposal is based only on the identity of the observed organic products and not on studies of intermediate structures. Due to their transient nature, these intermediates are difficult to probe. Platinum is competent in the activation of alkynes toward nucleophilic attack. It is generally accepted that the key intermediate in this reaction involves either a platinum stabilized carbene or a metal bound carbocation.<sup>53,55-56</sup> The exact nature of this intermediate is a subject of debate, whose progress is limited again by a lack of characterized examples.

Palladium carbene species, in which the carbene is incorporated in a tridentate ligand scaffold, have been reported by us as well as in-depth reactivity studies involving

these complexes.<sup>57-66</sup> Specifically, our group was able to isolate a series of square planar palladium carbenes, using a chelating diphosphine ligand,  $[\text{PC}(\text{sp}^2)\text{P}]^{\text{R}}$  ( $\text{R} = \text{H}$ ,  $[\text{PC}(\text{sp}^2)\text{P}]^{\text{H}} = \text{bis}[2-(\text{di-}i\text{iso-propylphosphino})\text{phenyl}]\text{methylene}$ ;  $\text{R} = t\text{Bu}$ ,  $[\text{PC}(\text{sp}^2)\text{P}]^{t\text{Bu}} = \text{bis}[2-(\text{di-}i\text{iso-propylphosphino})-4\text{-}t\text{ert-butylphenyl}]\text{methylene}$ ).<sup>58-62, 67</sup> The reactivity of these species varies from nucleophilic to electrophilic as confirmed by DFT and experimental investigations.<sup>58-62, 67</sup> Although this method has been beneficial for understanding the electronic structure of these four-coordinate carbenoids, these reactions cannot be performed catalytically due to the chelating nature of the ligand framework. It is therefore desirable to synthesize palladium and platinum species in which the carbene is not anchored to the supporting ligand, so that these transformations can be advantageous in organic synthesis.

Examples of  $[\text{M}]=\text{CRR}'$  carbenes, where  $\text{M} = \text{Ni}$ ,  $\text{Pd}$ , or  $\text{Pt}$ , and  $\text{R}$  and  $\text{R}'$  are hydrogen, alkyl or aryl substituents, are uncommon. Group 10 metal cycloheptatrienyldene complexes were synthesized, however, the delocalization in the cycloheptatrienyl ring incorporates the carbene p orbital and metal to carbon  $\pi$  bonding was determined to be minimal.<sup>68-69</sup> The cycloheptatrienylium resonance form was deemed favorable, indicating that these ligands behave as mainly  $\sigma$  donors and therefore are analogous to N-heterocyclic carbenes.<sup>69</sup> In 2002, Hillhouse and coworkers isolated a nickel diphenylcarbene,  $(\text{dtbpe})\text{Ni}=\text{CPh}_2$  ( $\text{dtbpe} = 1,2\text{-bis}(\text{di-}t\text{ert-butylphosphino})\text{-ethane}$ , Figure 1.9). Its characterization by single crystal X-ray diffraction revealed a short Ni-C distance of 1.836(2) Å, consistent with double bond character.<sup>70-71</sup> Soon after, Bröring and coworkers characterized the cationic palladium diarylcarbene  $[(\text{Trpy})\text{PdC}(p\text{-tol})_2][\text{BAr}^{\text{F}}_4]$  ( $\text{Trpy} = \text{tripyrin}$ ,  $p\text{-tol} = \text{para-tolyl}$ ,  $\text{BAr}^{\text{F}}_4 = \text{tetrakis}[3,5\text{-}$

bis(trifluoromethyl)phenyl]borate, Figure 1.9).<sup>72</sup> Crystallographic analysis of this species revealed a long Pd-C distance (1.976 Å) consistent with mainly  $\sigma$  donation from the carbene to palladium. A cationic platinum example, *trans*-[Pt{P<sup>*i*</sup>Pr<sub>2</sub>(2,6-CH(Me)C<sub>6</sub>H<sub>3</sub>)}{P<sup>*i*</sup>Pr<sub>2</sub>(2,6-CH<sub>2</sub>(Me)C<sub>6</sub>H<sub>3</sub>)}][PF<sub>6</sub>], was later described by Carmona and coworkers and proved to be reactive toward nucleophiles (Figure 1.8). This species was not crystallographically characterized due to its high reactivity and poor thermal stability.<sup>56</sup>

<sup>73</sup> Additionally, Templeton and coworkers were able to observe spectroscopically a transient cationic Pt(IV) alkylidene species, [Tp'<sup>+</sup>Pt(=CHCH<sub>3</sub>)(Me)<sub>2</sub>][BAR<sup>F</sup><sub>4</sub>] (Tp' = hydridotris(3,5-dimethylpyrazolyl)borate). However, the instability of the species inhibited further characterization.<sup>74</sup> To the best of our knowledge no platinum alkylidenes or diarylcarbenes have been structurally characterized.

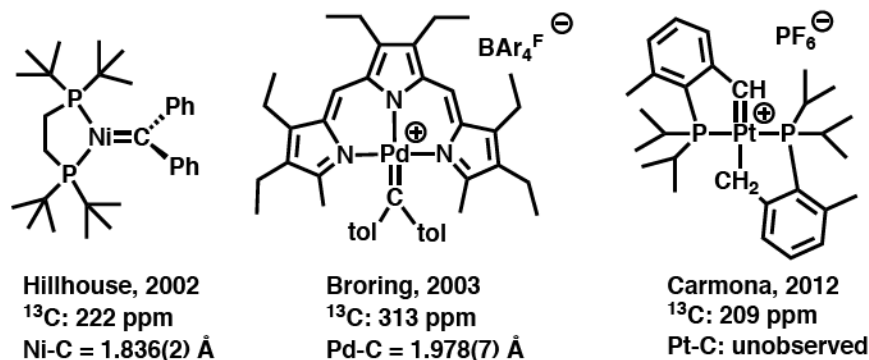


**Figure 1.9:** Previously observed group 10 non-heteroatom stabilized carbenes.

Non-heteroatom stabilized carbenes of late transition metals are difficult to isolate. For group 10 metals specifically, only a handful of examples exist. As mentioned above, the Hillhouse group was able to stabilize the three-coordinate nickel diarylcarbene (dtbpe)Ni=CPh<sub>2</sub> (dtbe = 1,2-bis(di-*tert*-butylphosphino)-ethane) from a readily available nickel(0) source (cod)<sub>2</sub>Ni (cod = cyclooctadiene).<sup>70</sup> No structurally analogous species for

the heavier group 10 metals have been reported. This lack of characterized examples may be attributed to the difficulty in finding the right starting material. For Pd(0) and Pt(0), sources commonly include four neutral phosphine ligands, not all of which are likely to dissociate from the metal center, and additionally, these phosphines tend to be difficult to remove from the reaction mixture after subsequent synthetic steps. It therefore is desirable to synthesize palladium(0) and platinum(0) precursors in the absence of monomeric phosphine donors while avoiding dimer formation. We reasoned that the use of adaptable chelating diphosphine ligands would allow for the formation of Pd(0) and Pt(0) precursors in the absence of additional neutral ligands while avoiding the need for dimer dissociation upon subsequent synthetic steps.

The work presented in the following chapters describes the synthesis and coordination chemistry of four different ligand systems. Initially, the adaptability of coordination modes for a *trans*-stilbene based ligand system will be described for group 8, 9, and 11 transition metals. Chapter 3 will discuss the coordination chemistry of the same ligand, as well as a closely related analogue, to group 10 metal centers. The H-atom acceptor capabilities of the ligand backbone will also be discussed. A structurally related ligand containing a *cis*-olefin in the ligand backbone was also investigated, and proved to be proficient at demonstrating hemilabile character with a palladium metal center. This ligand was probed further for its ability to stabilize group 10 non-heteroatom stabilized carbenes; an under-represented class of compounds in the literature. The reactivity of the resulting metal compounds will be described. The work with group 10 carbenes inspired the use of an *ortho*-terphenyl based ligand system, which will be introduced in Chapter 6. The adaptability of the ligand geometry made this ligand a good candidate for the

stabilization of group 10 carbene species. Furthermore, the reactivity of the resulting group 10 carbenes was explored. Finally, the *ortho*-terphenyl based ligand system displayed interesting reactivity in which a palladium metal center mediated the arene insertion into Pd-aryl bonds. This reactivity was probed, and will be discussed in Chapter 7.

### 1.3 References

1. Chakraborty, S.; Bhattacharya, P.; Dai, H.; Guan, H., *Acc. Chem. Res.* **2015**, *48* (7), 1995-2003.
2. Chelucci, G.; Baldino, S.; Baratta, W., *Coord. Chem. Rev.* **2015**, *300*, 29-85.
3. Zell, T.; Milstein, D., *Acc. Chem. Res.* **2015**, *48* (7), 1979-1994.
4. Deng, Q.-H.; Melen, R. L.; Gade, L. H., *Acc. Chem. Res.* **2014**, *47* (10), 3162-3173.
5. Lee, D. W.; Jensen, C. M.; Morales-Morales, D., *Organometallics* **2003**, *22* (23), 4744-4749.
6. Selander, N.; Szabo, K. J., *Chem. Rev.* **2011**, *111* (3), 2048-2076.
7. Benito-Garagorri, D.; Kirchner, K., *Acc. Chem. Res.* **2008**, *41* (2), 201-213.
8. Vankoten, G., *Pure Appl. Chem.* **1989**, *61* (10), 1681-1694.
9. Jensen, C. M., *Chem. Commun.* **1999**, (24), 2443-2449.
10. Ines, B.; SanMartin, R.; Moure, M. J.; Dominguez, E., *Adv. Synth. Catal.* **2009**, *351* (13), 2124-2132.
11. van der Vlugt, J. I.; Pidko, E. A.; Vogt, D.; Lutz, M.; Spek, A. L.; Meetsma, A., *Inorg. Chem.* **2008**, *47* (11), 4442-4444.
12. Bauer, R. C.; Gloaguen, Y.; Lutz, M.; Reek, J. N. H.; de Bruin, B.; van der Vlugt, J. I., *Dalton Trans.* **2011**, *40* (35), 8822-8829.
13. Verhoeven, D. G. A.; Moret, M.-E., *Dalton Trans.* **2016**, *45* (40), 15762-15778.
14. Horak, K. T.; VanderVelde, D. G.; Agapie, T., *Organometallics* **2015**, *34* (19), 4753-4765.

15. Horak, K. T.; Velian, A.; Day, M. W.; Agapie, T., *Chem. Commun.* **2014**, 50 (34), 4427-4429.
16. Herbert, D. E.; Lara, N. C.; Agapie, T., *Chem. Eur. J.* **2013**, 19 (48), 16453-16460.
17. Lin, S.; Day, M. W.; Agapie, T., *J. Am. Chem. Soc.* **2011**, 133 (11), 3828-3831.
18. Dixon, F. M.; Farrell, J. R.; Doan, P. E.; Williamson, A.; Weinberger, D. A.; Mirkin, C. A.; Stern, C.; Incarvito, C. D.; Liable-Sands, L. M.; Zakharov, L. N.; Rheingold, A. L., *Organometallics* **2002**, 21 (15), 3091-3093.
19. Deckers, P. J. W.; Hessen, B.; Teuben, J. H., *Angew. Chem. Int. Ed.* **2001**, 40 (13), 2516-2519.
20. Rodríguez-Lugo, R. E.; Trincado, M.; Vogt, M.; Tewes, F.; Santiso-Quinones, G.; Grützmacher, H., *Nat. Chem.* **2013**, 5 (4), 342-347.
21. Moxham, G. L.; Randell-Sly, H. E.; Brayshaw, S. K.; Woodward, R. L.; Weller, A. S.; Willis, M. C., *Angew. Chem.* **2006**, 118 (45), 7780-7784.
22. Breitenfeld, J.; Scopelliti, R.; Hu, X., *Organometallics* **2012**, 31 (6), 2128-2136.
23. Kohl, S. W.; Weiner, L.; Schwartsburd, L.; Konstantinovski, L.; Shimon, L. J. W.; Ben-David, Y.; Iron, M. A.; Milstein, D., *Science* **2009**, 324 (5923), 74-77.
24. Gunanathan, C.; Ben-David, Y.; Milstein, D., *Science* **2007**, 317 (5839), 790-792.
25. Montag, M.; Zhang, J.; Milstein, D., *J. Am. Chem. Soc.* **2012**, 134 (25), 10325-10328.
26. Feller, M.; Ben-Ari, E.; Diskin-Posner, Y.; Carmieli, R.; Weiner, L.; Milstein, D., *J. Am. Chem. Soc.* **2015**, 137 (14), 4634-4637.
27. Gnanaprakasam, B.; Milstein, D., *J. Am. Chem. Soc.* **2011**, 133 (6), 1682-1685.
28. Lin, S. B.; Day, M. W.; Agapie, T., *J. Am. Chem. Soc.* **2011**, 133 (11), 3828-3831.
29. Edouard, G. A.; Kelley, P.; Herbert, D. E.; Agapie, T., *Organometallics* **2015**, 34 (21), 5254-5277.
30. Tsui, E. Y.; Agapie, T., *Polyhedron* **2014**, 84, 103-110.
31. Lin, S.; Herbert, D. E.; Velian, A.; Day, M. W.; Agapie, T., *J. Am. Chem. Soc.* **2013**, 135 (42), 15830-15840.
32. Suseno, S.; Agapie, T., *Organometallics* **2013**, 32 (11).



33. Velian, A.; Lin, S.; Miller, A. J. M.; Day, M. W.; Agapie, T., *J. Am. Chem. Soc.* **2010**, *132* (18), 6296-6297.
34. Martin, R.; Buchwald, S. L., *Acc. Chem. Res.* **2008**, *41* (11), 1461-1473.
35. Surry, D. S.; Buchwald, S. L., *Chem. Sci.* **2010**, *2* (1), 27-50.
36. Milner, P. J.; Maimone, T. J.; Su, M.; Chen, J.; Müller, P.; Buchwald, S. L., *J. Am. Chem. Soc.* **2012**, *134* (48), 19922-19934.
37. Boron-Rettore, P.; Grove, D. M., *Helv. Chim. Acta* **1984**, *67*, 65-72.
38. Ding, K.; Miller, D. L.; Young, V. G.; Lu, C. C., *Inorg. Chem.* **2011**, *50* (6), 2545-52.
39. Koblenz, T. S.; Dekker, H. L.; de Koster, C. G.; van Leeuwen, P. W. N. M.; Reek, J. N. H., *Eur. J. Inorg. Chem.* **2011**, *2011* (31), 4837-4845.
40. Comanescu, C. C.; Iluc, V. M., *Inorg. Chem.* **2014**, *53* (16), 8517-8528.
41. Lamb, G.; Clarke, M.; Slawin, A. M. Z.; Williams, B.; Key, L., *Dalton Trans.* **2007**, (47), 5582.
42. Canac, Y.; Debono, N.; Lepetit, C.; Duhayon, C.; Chauvin, R., *Inorg. Chem.* **2011**, *50* (21), 10810-9.
43. van Leeuwen, P. W. N. M.; Kamer, P. C. J.; Reek, J. N. H.; Dierkes, P., *Chem. Rev.* **2000**, *100* (8), 2741-2770.
44. Gunanathan, C.; Gnanaprakasam, B.; Iron, M. A.; Shimon, L. J. W.; Milstein, D., *J. Am. Chem. Soc.* **2010**, *132* (42), 14763-14765.
45. Bennett, M. A.; Corlett, S.; Robertson, G. B.; Steffen, W. L., *Aust. J. Chem.* **1980**, *33* (6), 1261-1273.
46. Bennett, M. A.; Clark, P. W., *J. Organomet. Chem.* **1976**, *110* (3), 367-381.
47. Hussong, M. W.; Hoffmeister, W. T.; Rominger, F.; Straub, B. F., *Angew. Chem. Int. Ed.* **2015**, *54* (35), 10331-10335.
48. Hussong, M. W.; Rominger, F.; Krämer, P.; Straub, B. F., *Angew. Chem. Int. Ed.* **2014**, *53* (35), 9372-9375.
49. Zhang, Y.; Wang, J., *Eur. J. Org. Chem.* **2011**, *2011* (6), 1015-1026.
50. Liu, Z.; Wang, J., *J. Org. Chem.* **2013**, *78* (20), 10024-10030.
51. Xia, Y.; Xia, Y.; Zhang, Y.; Wang, J., *Org. Biomol. Chem.* **2014**, *12* (46), 9333-9336.

52. Xia, Y.; Qu, S.; Xiao, Q.; Wang, Z.-X.; Qu, P.; Chen, L.; Liu, Z.; Tian, L.; Huang, Z.; Zhang, Y.; Wang, J., *J. Am. Chem. Soc.* **2013**, *135* (36), 13502-13511.
53. Fürstner, A.; Davies, P. W., *Angew. Chem. Int. Ed.* **2007**, *46* (19), 3410-3449.
54. Xiao, Q.; Zhang, Y.; Wang, J., *Acc. Chem. Res.* **2013**, *46* (2), 236-247.
55. Fürstner, A.; Stelzer, F.; Szillat, H., *J. Am. Chem. Soc.* **2001**, *123* (48), 11863-11869.
56. Campos, J.; Peloso, R.; Carmona, E., *Angew. Chem. Int. Ed.* **2012**, *51* (33), 8255-8258.
57. Gutsulyak, D. V.; Piers, W. E.; Borau-Garcia, J.; Parvez, M., *J. Am. Chem. Soc.* **2013**, *135* (32), 11776-11779.
58. Comanescu, C. C.; Iluc, V. M., *Organometallics* **2014**, *33* (21), 6059-6064.
59. Comanescu, C. C.; Vyushkova, M.; Iluc, V., *Chem. Sci.* **2015**, *6*, 4570-4579.
60. Cui, P.; Iluc, V. M., *Chem. Sci.* **2015**, *6*, 7343-7356.
61. Cui, P.; Hoffbauer, M. R.; Vyushkova, M.; Iluc, V. M., *Chem. Sci.* **2016**, *7* (7), 4444-4452.
62. Comanescu, C. C.; Iluc, V. M., *Chem. Commun.* **2016**, *52*, 9048-9051.
63. Burford, R. J.; Piers, W. E.; Parvez, M., *Organometallics* **2012**, *31* (8), 2949-2952.
64. Burford, R. J.; Piers, W. E.; Ess, D. H.; Parvez, M., *J. Am. Chem. Soc.* **2014**, *136* (8), 3256-3263.
65. Weng, W.; Chen, C.-H.; Foxman, B. M.; Ozerov, O. V., *Organometallics* **2007**, *26* (14), 3315-3320.
66. Gessner, V. H.; Meier, F.; Uhrich, D.; Kaupp, M., *Chem. Eur. J.* **2013**, *19* (49), 16729-16739.
67. Cui, P.; Comanescu, C. C.; Iluc, V. M., *Chem. Commun.* **2015**, *51*, 6206-6209.
68. Lu, Z.; Jones, W. M.; Winchester, W. R., *Organometallics* **1993**, *12* (4), 1344-1350.
69. Herrmann, W. A.; Öfele, K.; Schneider, S. K.; Herdtweck, E.; Hoffmann, S. D., *Angew. Chem. Int. Ed.* **2006**, *45* (23), 3859-3862.
70. Mindiola, D. J.; Hillhouse, G. L., *J. Am. Chem. Soc.* **2002**, *124* (34), 9976-9977.

- 71. Iluc, V. M.; Hillhouse, G. L., *J. Am. Chem. Soc.* **2014**, *136* (17), 6479-6488.
- 72. Bröring, M.; Brandt, C. D.; Stellwag, S., *Chem. Commun.* **2003**, *18* (18), 2344-2345.
- 73. Campos, J.; Ortega-Moreno, L.; Conejero, S.; Peloso, R.; López-Serrano, J.; Maya, C.; Carmona, E., *Chem. Eur. J.* **2015**, *21* (24), 8883-8896.
- 74. Lavoie, K. D.; Frauhiger, B. E.; White, P. S.; Templeton, J. L., *J. Organomet. Chem.* **2015**, *793*, 182-191.

CHAPTER 2:  
COORDINATION OF A HEMILABILE PINCER LIGAND WITH AN OLEFINIC  
BACKBONE TO MID-TO-LATE TRANSITION METALS

## 2.1 Introduction

In this chapter, the synthesis and characterization of the neutral ligand, 2,2'-bis(*iso*-propylphosphino)-*trans*-stilbene (*t*PCH=CHP, **1**), will be discussed along with its coordination to group 8, 9, and 11 transition metals. Bennett and coworkers initially observed  $\kappa^4$ -PCCP coordination of the structurally related ligand, 2,2'-bis(diphenylphosphino)-*trans*-stilbene (bdps)<sup>1-3</sup> with group 6 and 9 metals in the 0 and +1 oxidation state, respectively (Figure 2.1). Tethered  $\pi$ -ligands have been gaining popularity in recent years due to their potential metal-ligand cooperativity.<sup>4-6</sup> Because of the possibility of observing more than one coordination mode of the ligand, an in-depth investigation of the coordination chemistry of *t*PCH=CHP (**1**) to iron, cobalt, rhodium, copper and silver in a variety of oxidation states was executed. Complementary to the results previously reported by the Bennett group, we observe more than one coordination mode with a metal center depending on its oxidation state or electronic requirements.

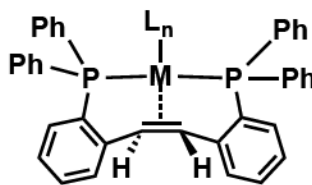
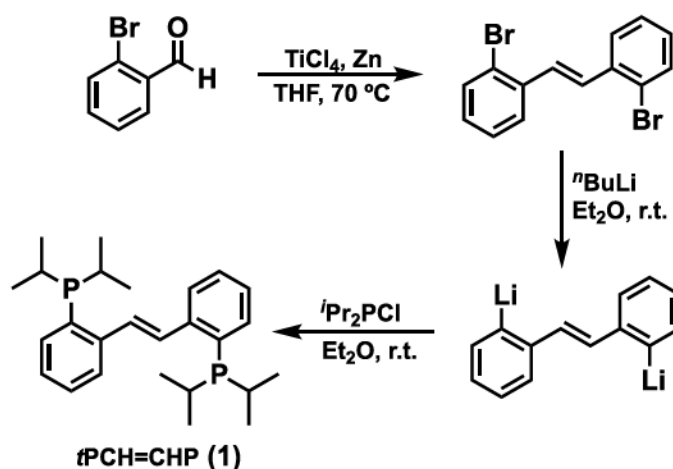


**Figure 2.1:** Coordination of 2,2'-bis(diphenylphosphino)-*trans*-stilbene (bdps) to group 6 and 9 metals.

## 2.2 Results and Discussion

The ligand precursor *o,o'*-*trans*-dibromostilbene was prepared *via* a McMurry aldehyde coupling reaction as previously described (Scheme 2.1).<sup>7</sup> A lithium halogen exchange reaction then led to *o,o'*-*trans*-dilithiostilbene, which, in turn, reacted with the desired phosphine chloride to generate 2,2'-bis(di-*iso*-propylphosphino)-*trans*-stilbene (*t*PCH=CHP, **1**). The product was isolated as a pure crystalline material in good yield by recrystallization from *n*-pentane. <sup>1</sup>H NMR spectroscopy shows equivalent environments for all methine protons and only two environments for the *iso*-propyl methyl protons. The olefin protons exhibited a downfield resonance as a singlet at 8.53 ppm. The product *t*PCH=CHP (**1**) was also characterized by <sup>31</sup>P NMR spectroscopy as a singlet at -6.52 ppm and by single crystal X-ray diffraction (Figure 2.2). The C(1)–C(1)# distance corresponding to the alkene carbon atoms is 1.330(4) Å, suggesting C=C double bond character.



**Scheme 2.1:** Synthesis of *t*PCH=CHP (1).

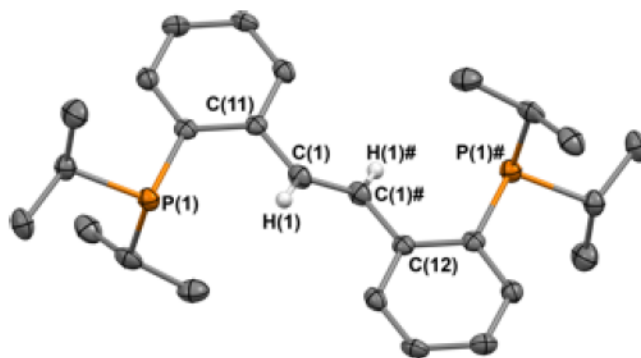
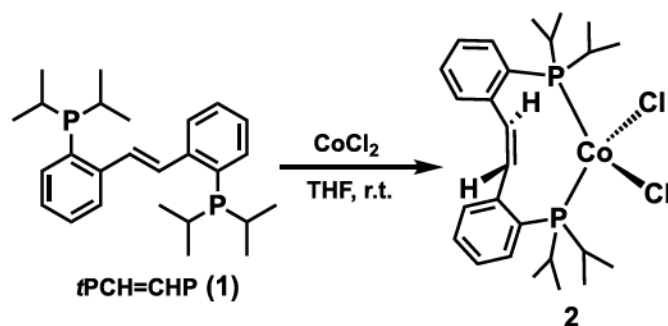


**Figure 2.2:** Thermal-ellipsoid (50% probability level) representation of *t*PCH=CHP (1).

Most hydrogen atoms were omitted for clarity. Selected distances (Å) and angles (°): C(1)–C(1)# = 1.330(4), P(1)–C(11) = 1.848(2), P(1)–C(22) = 1.870(2), P(1)–C(21) = 1.852(2), C(1)#–C(1)–C(12) = 125.6(2), C(11)–P(1)–C(22) = 101.16(9), C(11)–P(1)–C(22) = 102.81(9).

Compound 2,2'-bis(di-*iso*-propylphosphino)-*trans*-stilbene (*t*PCH=CHP, **1**) differs from the ligand previously reported by Bennett,<sup>8-9</sup> 2,2'-bis(diphenylphosphino)-*trans*-stilbene, in that the phenyl phosphine groups are replaced with *iso*-propyl groups. We hypothesized that this modification would lead to increased solubility of the resulting metal complexes and allow us to survey various oxidation states of the same metal.

Initially, metals in the +2 oxidation state were studied. The formation of  $(i\text{PCH=CHP})\text{CoCl}_2$  (**2**) was observed upon mixing **1** with  $\text{CoCl}_2$  in THF at room temperature (Scheme 2.2). The paramagnetic product was characterized by single crystal X-ray diffraction (Figure 2.3), which showed a distorted-tetrahedral geometry<sup>10-15</sup> around the metal center with angles ranging from 98.09(6) to 126.44(7)°. Compound **2** exhibits a non-coordinated olefinic backbone that retains C=C double bond character, supported by the C–C distance of 1.317(8) Å (Figure 2.3). Additionally, the distance of 3.501 Å from cobalt to the centroid of the olefin supports this interpretation. Other metrical parameters compare well with those previously reported: the Co–P distances in **2** (2.4236(18) and 2.4305(17) Å) are long compared to typical Co–P distances (2.1–2.3 Å),<sup>16-18</sup> but a similar situation was previously observed before: 2.369(5) Å in  $[(\text{Cy}_3\text{P})\text{Co}(\text{dmgH})_2\text{Cl}]$  (dmgH = dimethylglyoximate), 2.418(1) Å in  $[(\text{Ph}_3\text{P})\text{Co}(\text{dmgH})_2(\text{CH}_3)]$ ,<sup>19</sup> 2.520(2) Å in  $[\text{CoL}_2(\text{O}_3\text{SCF}_3)_2]$  ( $\text{L}=\text{P}(\text{CH}_2\text{Ph})(\text{CH}_2\text{CH}_2\text{OC}_2\text{H}_5)_2$ ),<sup>20</sup> and 2.3666(14), 2.3731(15) Å in a Co(II) tetrahedral complex supported by a P–N–P ligand,  $\text{CH}_3\text{N}(\text{CH}_2\text{CH}_2\text{PPh}_2)_2$ .<sup>16</sup> In the first three examples, the lengthening of Co–P distances was attributed to the *trans* effect of other ligands. However, such an explanation is not applicable to the P–N–P case, as well as ours, since the potentially tridentate ligand acts only in a bidentate manner, coordinating solely through the two phosphines. This elongation can be partially attributed to the steric bulk of the phosphine donors in both cases, but other factors may play an additional role. In  $\{\text{CH}_3\text{N}(\text{CH}_2\text{CH}_2\text{PPh}_2)_2\}\text{CoCl}_2$ , it was proposed that, although the cobalt complex is electron deficient (15 electron count), coordination of the nitrogen donor does not occur as a result of the steric effect of the methyl nitrogen substituent and the relatively low coordinating ability of the tertiary nitrogen. In **2**, it is also possible that sterics contribute



**Scheme 2.2:** Synthesis of complex **2**.

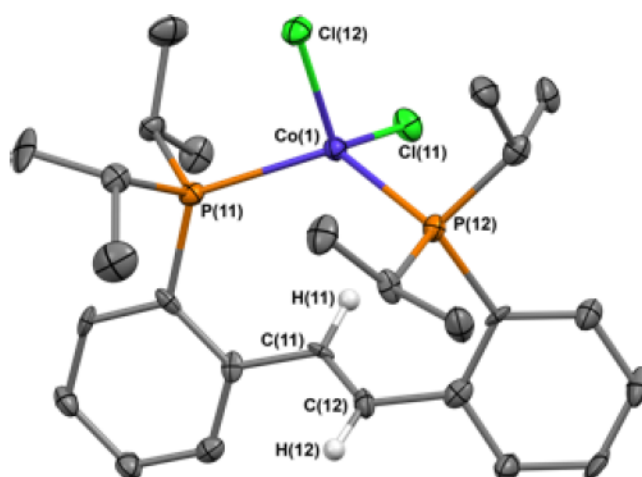
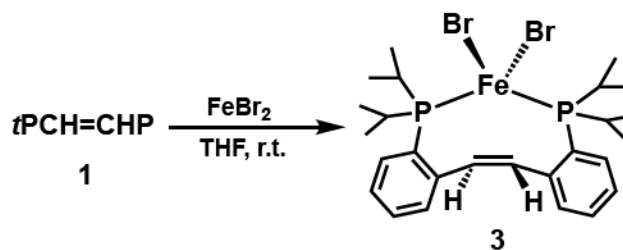


**Figure 2.3:** Thermal-ellipsoid (50% probability level) representation of (*t*PCH=CHP)CoCl<sub>2</sub> (**2**). Only one of the two crystallographically independent molecules is shown. Most hydrogen atoms were omitted for clarity. Selected distances (Å) and angles (°): Co(1)–P(11) = 2.4305(17), Co(1)–P(12) = 2.4236(18), Co(1)–Cl(11) = 2.2443(18), Co(1)–Cl(12) = 2.547(17), C(11)–C(12) = 1.317(8), P(11)–Co(1)–P(12) = 126.44(7), P(11)–Co(1)–Cl(11) = 105.66(6), P(12)–Co(1)–Cl(11) = 105.12(7), Cl(11)–Co(1)–Cl(12) = 116.59(8), P(11)–Co(1)–Cl(12) = 98.09(6), P(12)–Co(1)–Cl(12) = 105.73(7).



to the favored tetrahedral geometry over a square pyramidal or trigonal bipyramidal geometry that would result upon olefin coordination.<sup>21</sup>

In order to determine if the lack of olefin coordination is a characteristic of metals in the +2 oxidation state, the reaction of **1** with FeBr<sub>2</sub> (Scheme 2.3) in THF was carried out and resulted in the formation of an orange solution. Upon removal of volatiles and trituration with *n*-pentane, a pure tan solid, identified as (tPCH=CHP)FeBr<sub>2</sub>, **3**, was obtained. <sup>1</sup>H NMR spectroscopy showed the formation of a paramagnetic product, which was also supported by the silent <sup>31</sup>P NMR spectrum. Single crystal X-ray diffraction was used to characterize **3** (Figure 2.4), indicating a distorted tetrahedral geometry around iron<sup>22-23</sup> with angles in the 98.91(4) - 122.62(3)° range. The distortion observed (angles smaller or larger than the ideal value, 109.5°) may be attributed to the relative rigidity of the tPCH=CHP backbone. The solid state molecular structure is also consistent with a non-coordinated olefinic moiety in **3**, with a 3.596 Å distance from the metal center to the centroid of the C=C bond. The Fe–P distances of 2.5232(14) and 2.5209(13) Å are slightly elongated compared to previously reported Fe–P values,<sup>24-25</sup> likely the result of the relative rigidity of the backbone coupled with steric crowding around the metal center.



**Scheme 2.3:** Synthesis of compound **3**.

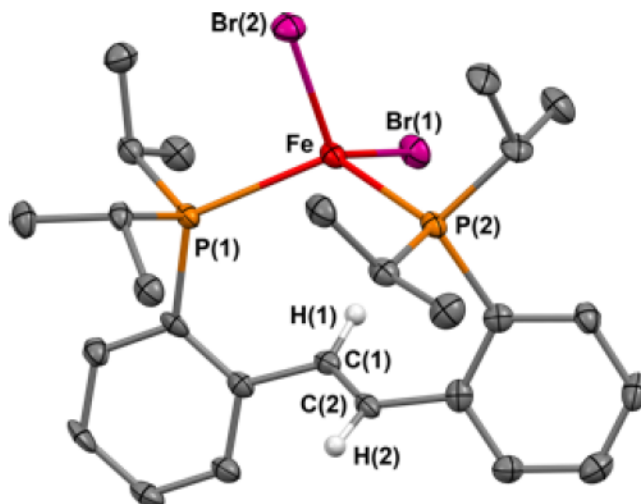
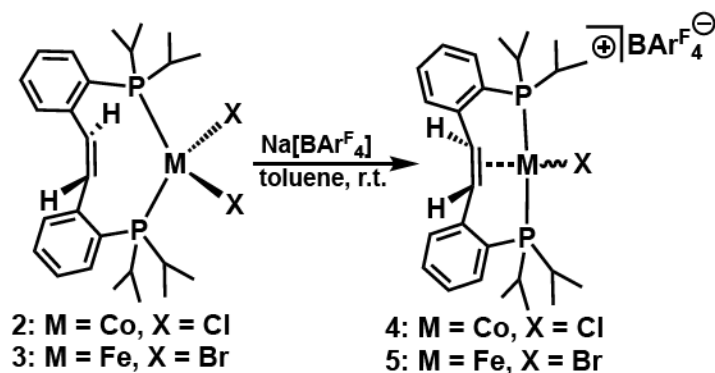


**Figure 2.4:** Thermal-ellipsoid (50% probability level) representation of  $(t\text{PCH=CHP})\text{FeBr}_2$  (**3**). Most hydrogen atoms were omitted for clarity. Selected distances (Å) and angles (°): C(1)–C(2) = 1.320(6), Fe–P(1) = 2.5209(13), Fe–P(2) = 2.5232(14), Fe–Br(2) = 2.4038(8), Fe–Br(1) = 2.4096(8), Br(1)–Fe–Br(2) = 122.62(3), Br(1)–Fe–P(2) = 103.22(4), Br(1)–Fe–P(1) = 107.88(4), Br(2)–Fe–P(1) = 98.91(4), Br(2)–Fe–P(2) = 103.30(4), P(1)–Fe–P(2) = 122.45(5).

Since we are interested in the hemilabile behavior of **1**, we reasoned that abstraction of a halide ligand from compounds **2** and **3** would render the metal centers more electron poor and induce coordination of the olefinic backbone. Consequently, compounds **2** and **3** were treated with sodium tetrakis[3,5-bis(trifluoromethyl)phenyl]borate ( $\text{NaBAr}^{\text{F}}_4$ ). After 12 hours, the formation of new paramagnetic products,  $[(t\text{PCH=CHP})\text{CoCl}][\text{BAr}^{\text{F}}_4]$  (**4**) and  $[(t\text{PCH=CHP})\text{FeBr}][\text{BAr}^{\text{F}}_4]$  (**5**), respectively, was observed as indicated by broad  $^1\text{H}$  NMR spectrum and the absence of peaks in the corresponding  $^{31}\text{P}$  NMR spectrum (Scheme 2.4).



**Scheme 2.4:** Synthesis of compounds **4** and **5**.

Analysis of complex **4** by  $^{11}\text{B}$  and  $^{19}\text{F}$  NMR spectroscopy confirmed the incorporation of the  $\text{BARF}_4^-$  counterion. Crystallization from a concentrated toluene solution layered with *n*-pentane yielded crystals suitable for X-ray diffraction. The solid state molecular structure (Figure 2.5) shows the formation of a distorted square planar complex, in which the abstraction of one chloride ligand led to the coordination of the olefin moiety. The P(11)–Co–P(12) angle of  $172.09(5)^\circ$  and the P(11)–Co–Cl(1) angle of  $86.45(4)^\circ$  support the assignment of the distorted square planar geometry. The C(11)–C(12) distance of  $1.397(6) \text{ \AA}$  is only mildly elongated for a C–C double bond, indicating that the amount of backdonation from the metal to the alkene is limited as expected for a cationic compound. The square planar geometry is also supported by the observed magnetic moment of  $1.8 \mu_{\text{B}}$ , corresponding to one unpaired electron. Examples of cobalt(II) square-planar complexes are uncommon. In general, tetrahedral examples are found when two of the ligands are weak field halides, such as in the species reported by Wang et. al., in which a PNP ligand,  $\text{CH}_3\text{N}(\text{CH}_2\text{CH}_2\text{PPh}_2)_2$ , binds to the metal center through the phosphine moieties while the amine functionality remains dissociated. In that example, two chloride

ligands are also bound to the metal center.<sup>16</sup> Similarly, Alyea et. al. also reported a tetrahedral cobalt(II) species in which the metal center is bound in a  $\kappa^2$ -P,P fashion to a PSiP ligand,  $\text{Ph}_2\text{PCH}_2\text{Si}(\text{CH}_3)_2\text{CH}_2\text{PPh}_2$ , as well as two bromide ligands.<sup>26</sup> Square planar cobalt(II) examples have been reported by the Arnold group,<sup>27</sup> who described a neutral complex containing a PNP ligand,  $\kappa^3$ -P,N,P-N( $\text{CH}_2\text{CH}_2\text{P}^i\text{Pr}_2$ )<sub>2</sub>, coordinated in a tridentate mode to a cobalt(II) center containing also a chloride ligand. Protonation of the supporting ligand led to a cationic cobalt(II) species that retained its square planar geometry.<sup>27</sup>

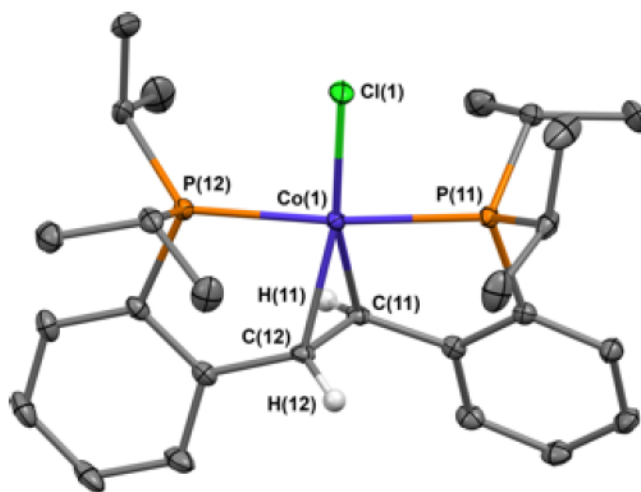


**Figure 2.5:** Thermal-ellipsoid (50% probability level) representation of  $[(t\text{PCH=CHP})\text{CoCl}][\text{BARF}_4]$  (**4**). Only one of the two crystallographically independent cations is shown. Most hydrogen atoms were omitted for clarity. Selected distances (Å) and angles (°):  $\text{Co}(1)\text{--P}(11) = 2.2536(12)$ ,  $\text{Co}(1)\text{--P}(12) = 2.2546(12)$ ,  $\text{Co}(1)\text{--Cl}(1) = 2.2020(11)$ ,  $\text{Co}(1)\text{--C}(11)\text{--C}(12) = 2.068$ ,  $\text{C}(11)\text{--C}(12) = 1.397(6)$ ,  $\text{P}(11)\text{--Co}(1)\text{--P}(12) = 172.09(5)$ ,  $\text{P}(11)\text{--Co}(1)\text{--Cl}(1) = 86.45(4)$ ,  $\text{P}(12)\text{--Co}(1)\text{--Cl}(1) = 85.84(4)$ .

Similarly to complex **4**, the iron(II) species  $[(t\text{PCH=CHP})\text{FeBr}][\text{BARF}_4]$  (**5**) contained the  $\text{BARF}_4$  counterion as indicated by  $^{11}\text{B}$  and  $^{19}\text{F}$  NMR spectroscopy. Crystals suitable for single crystal X-ray diffraction were obtained from a concentrated toluene solution layered with *n*-pentane, and illustrate the formation of a distorted trigonal

pyramidal iron(II) complex (angles ranging from 111.93(2)° to 121.38(3)°) (Figure 2.6). Distortions in the geometry are attributed to the relative rigidity of the ligand framework. Analogous to **4**, the olefin coordinates upon halide abstraction and does not experience a significant amount of  $\pi$ -backbonding from the metal center (C(1)–C(2) distance is 1.332(14) Å). Four-coordinate iron(II) complexes commonly to exhibit a tetrahedral geometry.<sup>28-30</sup> Deviations from tetrahedral geometry in compound **5** are attributed to the rigidity of the ligand backbone upon olefin coordination.

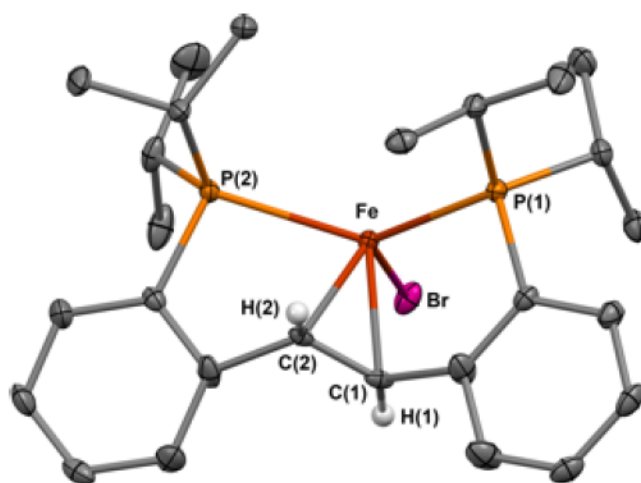
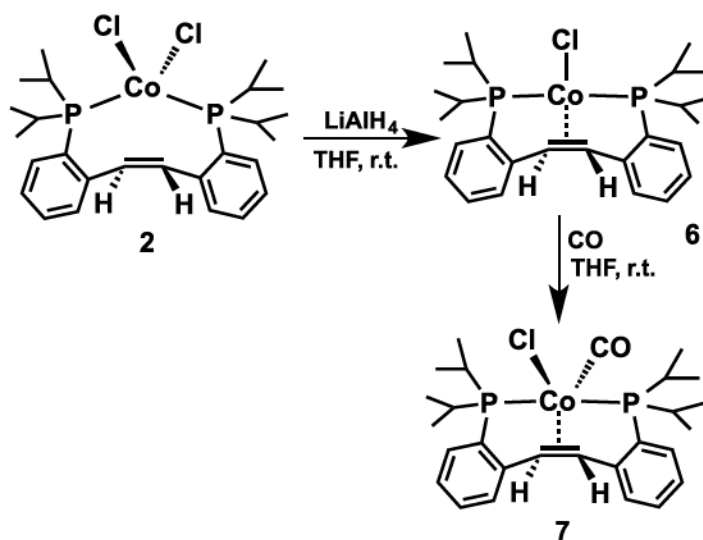


**Figure 2.6:** Thermal-ellipsoid (50% probability level) representation of [(*t*PCH=CHP)FeBr][BAr<sup>F</sup><sub>4</sub>] (**5**). Most hydrogen atoms were omitted for clarity. Selected distances (Å) and angles (°): C(1)–C(2) = 1.332(14), Fe–P(1) = 2.4312(7), Fe–P(2) = 2.4220(7), Fe–Br = 2.3213(5), Br–Fe–P(1) = 115.41(2), Br–Fe–P(2) = 111.93(2), P(1)–Fe–P(2) = 121.38(3).

A cobalt(I) complex, (*t*PCH=CHP)CoCl (**6**), was obtained upon reduction of **2** with 0.25 equivalents of LiAlH<sub>4</sub> (Scheme 2.5). The <sup>31</sup>P NMR spectrum of **6** exhibits a broad singlet at 51.08 ppm consistent with equivalent phosphorous environments. Notably, the corresponding <sup>1</sup>H NMR spectrum shows a significant upfield shift of the olefinic protons to 2.01 ppm from those values in *t*PCH=CHP (8.53 ppm). This shift is consistent with a bound olefin moiety and a considerable amount of  $\pi$ -backbonding from the metal center.

The solid-state molecular structure of **6** (Figure 2.7) agrees with this interpretation by showing an elongated C(1)–C(2) backbone distance of 1.442(5) Å and a distorted square planar geometry of the cobalt center. Notably, the C(1)–C(2) distance is longer than the Co(II) bound olefinic C–C distance observed for complex **4** (1.397(6) Å). This difference is attributed to the higher degree of  $\pi$ -backdonation for complex **6** compared to the less electron rich complex **4**. Interestingly, the Co–P distances are similar in **6** (2.2138(11) and 2.2145(11) Å) and **4** (2.2536(12) and 2.2546(12) Å), but they are shorter than in **2** (2.4305(17) and 2.4236(18) Å), presumably due to the different geometries between compound **2** and compounds **4** and **6**. The olefin was found in a near perpendicular orientation to the plane defined by P(1), Co(1), and P(2) with a dihedral angle of 78°, a feature reminiscent of Zeise’s salt.<sup>31–33</sup> A cobalt(I) structure, previously reported by Grützmacher and coworkers, Co(tropp<sup>Ph</sup>)Cl(PPh<sub>3</sub>) (tropp<sup>Ph</sup> = troylidene diphenylphosphine), contains a tetrahedral environment comprised of two phosphine ligands, an olefin, and a chloride.<sup>21</sup> The difference in geometries for Co(tropp<sup>Ph</sup>)Cl(PPh<sub>3</sub>) and **6** is likely a consequence of the rigidity of our ligand system, as well as the steric demands of the previously reported system. The broadness of the peaks observed in the <sup>1</sup>H as well as <sup>31</sup>P NMR spectra for complex **6** could be due to the presence of an equilibrium in solution between structures in



**Scheme 2.5:** Synthesis of complexes 6 and 7.

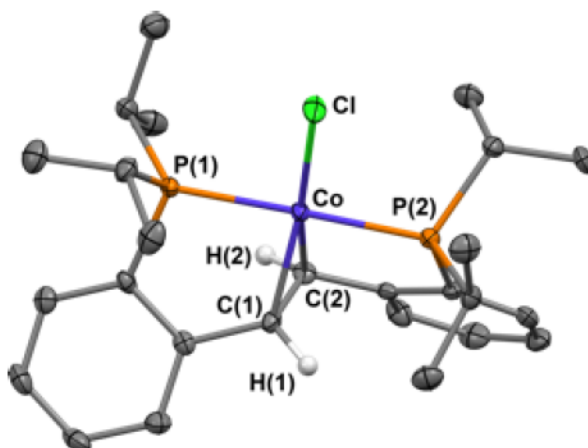


**Figure 2.7:** Thermal-ellipsoid (50% probability level) representation of  $(t\text{PCH=CHP})\text{CoCl}$  (**6**). Most hydrogen atoms were omitted for clarity. Selected distances (Å) and angles (°):  $\text{Co-P}(1) = 2.2138(11)$ ,  $\text{Co-P}(2) = 2.2145(11)$ ,  $\text{Co-Cl} = 2.2193(11)$ ,  $\text{C}(1)\text{-C}(2) = 1.442(5)$ ,  $\text{P}(1)\text{-Co-P}(2) = 178.76(5)$ ,  $\text{Cl-Co-P}(1) = 90.51(4)$ ,  $\text{Cl-Co-P}(2) = 89.69(4)$ .

which the metal center exists in a tetrahedral or a square planar environment.<sup>34</sup> The equilibrium is shifted towards the square planar species at low temperature, and a sharper <sup>31</sup>P NMR spectrum was observed at  $-70^{\circ}\text{C}$ .

To test the hemilability of the supporting ligand in **6**, the dissociation of the olefin moiety was targeted. The reaction of **6** with CO showed a rapid color change from deep purple to light orange. Examining the reaction mixture by <sup>1</sup>H NMR spectroscopy indicated the formation of a diamagnetic product, in which the olefinic protons display separate shifts at 3.64 and 4.68 ppm. The downfield shift of these protons compared to free ligand (8.52 ppm) indicates that the olefin remains bound to the metal center. <sup>31</sup>P NMR spectroscopy supports this observation, since peaks for two inequivalent phosphines, which exhibit a trans-coupling constant of 175 Hz, were observed. <sup>13</sup>C NMR spectroscopy confirms the presence of a CO ligand, with a corresponding chemical shift at 204.93 ppm. The olefinic carbon atoms are found upfield from free ligand (132.67 ppm) at 70.28 and 72.75 ppm, respectively, also consistent with the bound form of the alkene. Crystals suitable for single crystal X-ray diffraction were obtained from a concentrated solution of diethyl ether (Figure 2.8). The geometry of the complex was found to be trigonal bipyramidal as indicated by the angles ranging from 101 to 115° for the trigonal plane defined by C(1)–C(2), Cl, and CO, as well as the axial bond angle for P(1)–Co–P(2) of 173.11(6)°. The C–C distance of the olefinic moiety is 1.438(7) Å, similar to the value observed for the starting material, **6**. The formation of **7** is analogous to results reported by the Bennett group for reactions of rhodium(I) and iridium(I) complexes with CO<sup>1</sup> that led to trigonal bipyramidal complexes in which the olefin remains bound.



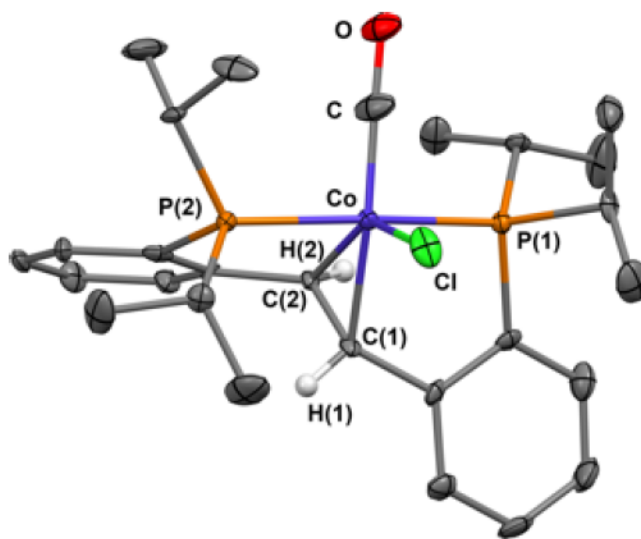
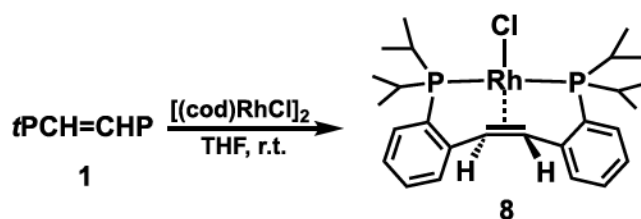


**Figure 2.8:** Thermal-ellipsoid (50% probability level) representation of (*t*PCH=CHP)CoCl(CO) (**7**). Most hydrogen atoms were omitted for clarity. Selected distances (Å) and angles (°): Co–P(1) = 2.2378(14), Co–P(2) = 2.2495(14), Co–Cl = 2.348(5), C(1)–C(2) = 1.438(7), Co–C = 1.65(3), C–O = 1.18(4), P(1)–Co–P(2) = 173.11(6), Cl–Co–P(1) = 88.32(9), Cl–Co–P(2) = 92.49(10), Cl–Co–C = 101.2(7).

A rhodium(I) complex analogous to **6**, (*t*PCH=CHP)RhCl (**8**), was obtained by reacting **1** with half an equivalent of rhodium cyclooctadiene chloride dimer ( $[(\text{cod})\text{RhCl}]_2$ ) in THF (Scheme 2.6). Similarly to **6**, the olefinic protons display an upfield shift to 3.74 ppm. The peak appears as a broad quartet, however, it is most likely an unresolved triplet of doublets due to coupling with the  $^{103}\text{Rh}$  and  $^{31}\text{P}$  nuclei. This complex is similar to the Rh(I) complex observed by Bennett with the phenyl analogue of the ligand, (bdps)RhCl (bdps = *o*-Ph<sub>2</sub>P-C<sub>6</sub>H<sub>4</sub>-CH=CH-C<sub>6</sub>H<sub>4</sub>-PPh<sub>2</sub>-*o*). In both instances, the olefin protons are shifted upfield in the  $^1\text{H}$  NMR spectrum, a consequence of the bound olefin.<sup>1</sup> X-ray crystallography (Figure 2.9) indicated a square planar complex,<sup>35-38</sup> with an elongated C(1)–C(1)# distance of 1.432(8) Å due to  $\pi$ -backbonding. The Rh–P distances of 2.2895(13) Å are similar to a previously reported square planar PNP rhodium(I) complex,

(PNP<sup>*t*</sup>Bu)RhCl (PNP<sup>*t*</sup>Bu = 2,6-bis-(di-*tert*-butylphosphino-methyl)pyridine) (2.2–2.3 Å).<sup>39–</sup>

<sup>40</sup> The olefin in the backbone approaches a perpendicular orientation to the plane defined by P(1), Rh(1), and P(1)# (dihedral angle of 73°), similarly to what was observed for compound 6.



**Scheme 2.6:** Synthesis of compound 8.

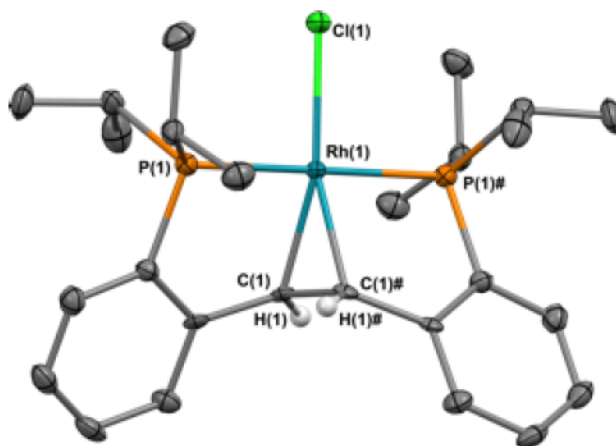


**Figure 2.9:** Thermal-ellipsoid (50% probability level) representation of **8**. Only one of the two crystallographically independent molecules is shown. Most hydrogen atoms were omitted for clarity. Selected distances (Å) and angles (°): Rh(1)–P(1) = 2.2895(13), Rh(1)–Cl(1) = 2.3656(18), C(1)–C(1)# = 1.432(8), P(1)–Rh(1)–P(1)# = 179.88(7), Cl(1)–Rh(1)–P(1) = 90.07(6), Cl(1)–Rh(1)–P(1)# = 90.07(6).

A copper(I) complex, (*t*PCH=CHP)CuI (**9**), was synthesized by stirring **1** with CuI at room temperature for one hour (Scheme 2.7). The <sup>1</sup>H NMR spectrum for this complex shows that the olefinic protons have a downfield chemical shift of 7.03 ppm indicating a

non-coordinated backbone. A high degree of symmetry was found in the alkyl region that is also consistent with this interpretation: one environment for the four methine protons, with a signal at 2.50 ppm, and two environments for the eight methyl groups, at 1.25 and 1.34 ppm. The  $^{31}\text{P}$  NMR spectrum of **9** also indicates equivalent environments for both phosphorous atoms (singlet at 7 ppm). We were unable to isolate single crystals suitable for X-ray diffraction for complex **9**. Therefore, the Cu(I) complex (*t*PCH=CHP)Cu(OTf) (**10**) was isolated from the reaction of **9** with AgOTf (Scheme 2.7).  $^1\text{H}$  NMR spectroscopy indicates that the solution structure of **10** is similar to that of **9**: a downfield shift of 7.19 ppm for the olefinic protons and one environment for the four methine positions at 2.14 ppm are observed. The corresponding  $^{31}\text{P}$  spectrum shows a singlet at 14.56 ppm, indicating that the phosphines are equivalent. Single crystals of **10** were obtained from a toluene solution layered with *n*-pentane. The solid state molecular structure (Figure 2.10) shows a distorted trigonal planar coordination environment around copper<sup>41</sup> as indicated by angles ranging from 103.57(6) - 149.23(3)° and a relatively close contact between the metal center and the olefin. The distance of 2.426 Å between copper and the olefinic backbone however, is outside the range that indicates a strong bonding interaction and can be better explained as a weak interaction or a close contact. The olefinic C–C distance of 1.294(5) Å is consistent with a double bond that is not weakened by  $\pi$ -backdonation from the metal center. J. I. van der Vlugt and coworkers described a PNP Cu(I) system, (PNP<sup>*t*Bu</sup>)CuBr and [(PNP<sup>*t*Bu</sup>)Cu][SbF<sub>6</sub>] (PNP<sup>*t*Bu</sup> = 2,6-bis[(di-*tert*-butylphosphino)methyl]pyridine), in which the geometry around the metal center is either trigonal planar or T-shaped depending on the nature of the additional ligand.<sup>42</sup> In the trigonal planar case, the metal center and the pyridine are in close contact (2.8938(17) Å),

however, are not considered to be bonding. Upon removal of bromide, the pyridine coordinates, resulting in a T-shaped complex (Figure 1.1, Chapter 1).<sup>42</sup>

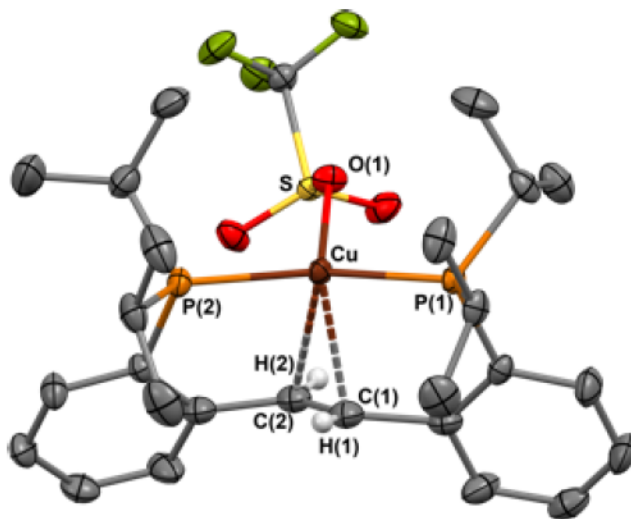
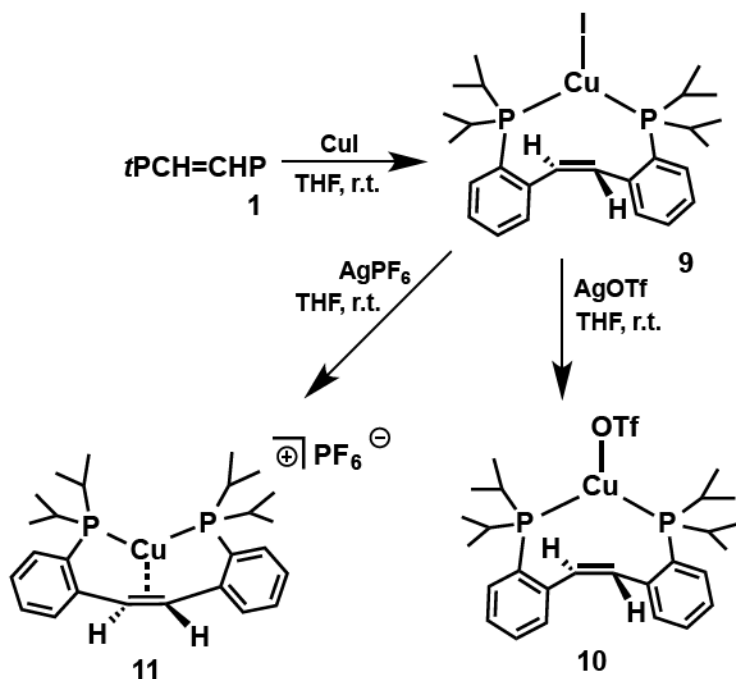


**Figure 2.10:** Thermal-ellipsoid (50% probability level) representation of **10**. Most hydrogen atoms were omitted for clarity. Selected distances (Å) and angles (°): Cu–O(1) = 2.158(2), Cu–P(1) = 2.2137(8), Cu–P(2) = 2.2179(8), C(1)–C(2) = 1.294(5), Cu–C(1) = 2.370(3), Cu–C(2) = 2.644(3), O(1)–Cu–P(1) = 103.75(6), P(1)–Cu–P(2) = 149.23(3), O(1)–Cu–P(2) = 103.57(6).

In an attempt to strengthen the coordination of the olefinic backbone to copper, removal of the iodide ligand utilizing  $\text{AgPF}_6$  was undertaken and generated  $[(t\text{PCH=CHP})\text{Cu}][\text{PF}_6]$  (**11**) (Scheme 2.7). There are several similarities between compounds **11** and **9** in their  $^1\text{H}$  NMR spectra. The olefinic protons appear as a singlet at 7.02 ppm compared to 7.03 ppm for compound **9**, and the alkyl region is nearly identical for both compounds. The cationic nature of this compound is evident in its  $^{31}\text{P}$  NMR spectrum, which shows a downfield shifted resonance at 25.41 ppm, compared to 7.00 ppm for compound **9**. The  $\text{PF}_6^-$  counterion is found upfield in the corresponding  $^{31}\text{P}$  NMR

spectrum at  $-143.28$  ppm as a septet. The absence of upfield shifted olefinic protons is indicative of a non-coordinated olefin, behavior contrasting with that of a previously observed copper(I) complex  $[(\text{PNP}^{\text{tBu}})\text{Cu}][\text{SbF}_6]$ ,<sup>42</sup> in which the central pyridine donor acted in a hemilabile fashion and dissociated in the presence of bromide.



**Scheme 2.7:** Synthesis of complexes **9-11**.

The solid state molecular structure of **11** (Figure 2.11) shows the coordination environment of the copper(I) metal center. The geometry of the metal center is distorted T-shaped, as deduced from the P–Cu–P angle of  $162.34(4)^\circ$ . This angle is smaller than the corresponding angle in  $[(\text{PNP}^{\text{tBu}})\text{Cu}][\text{SbF}_6]$ , which has a value of  $172.44(3)^\circ$ .<sup>42</sup> The olefin appears to be bound to the metal center, however the Cu–C distances of  $2.340(3)$  and  $2.337(3)$  Å are longer than those in previously observed copper olefin complexes, which show values around  $2.0$  Å.<sup>43–45</sup> Such long distances imply that the interaction between the

metal center and the olefin is weak. This observation is supported by the lack of elongation of the olefin C–C bond (1.340(4) Å).

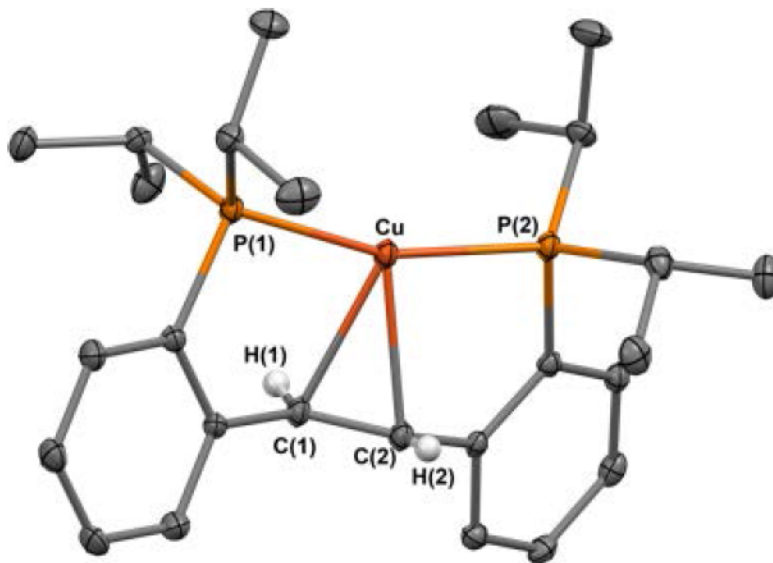


**Figure 2.11:** Thermal-ellipsoid (50% probability level) representation of the cationic fragment of **11**. Most hydrogen atoms and the counterion were omitted for clarity. Selected distances (Å) and angles (°): Cu–P(1) = 2.2123(8), Cu–P(2) = 2.2122(8), C(1)–C(2) = 1.340(4), Cu–C(1) = 2.340(3), Cu–C(2) = 2.337(3), P(1)–Cu–P(2) = 162.34(4).

To understand the bonding situation in the cationic copper(I) complexes, coordinates starting with values obtained from the X-ray structure were optimized using DFT (Figure 2.12). Interestingly, the optimized structure indicates that the olefin is not bound to copper and shows mild deviations from a linear geometry around the metal center, with a P(1)–Cu–P(2) angle of 176.67°. The distance from the olefin centroid to the metal center is 2.621 Å, compared to the value of 2.240 Å found crystallographically. These findings agree with a linear structure in which the olefin remains dissociated from the metal center. These results, coupled with the lack of evidence for olefin coordination in both  $^1\text{H}$

and  $^{13}\text{C}$  NMR spectra indicate that the weakly bound olefin observed in the solid state structure dissociates in solution to generate a two-coordinate copper(I) complex.

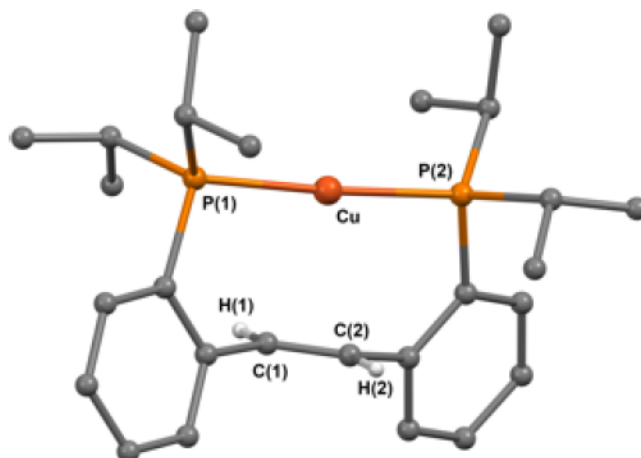


**Figure 2.12:** Optimized geometry for  $[(t\text{PCH=CHP})\text{Cu}]^+$ . Most hydrogen atoms were removed for clarity. Selected distances (Å) and angles ( $^\circ$ ): Cu–P(1) = 2.316, Cu–P(2) = 2.316, C(1)–C(2) = 1.360, Cu–C(1) = 2.704, Cu–C(2) = 2.712, P(1)–Cu–P(2) = 176.67.

The DFT results discussed above parallel our observations for the formation of the silver(I) complex  $[(t\text{PCH=CHP})\text{Ag}][\text{PF}_6]$  (**12**) that was obtained upon mixing **1** with  $\text{AgPF}_6$  (Scheme 2.8). The  $^1\text{H}$  NMR spectrum of **12** shows one environment for the four methine protons, at 2.64 ppm, and two environments for the eight *iso*-propyl methyl groups at 1.27 and 1.10 ppm, respectively, indicating a symmetrical solution structure. Additionally, the olefinic protons appear as a singlet at 7.03 ppm, slightly upfield shifted from the corresponding values in the free ligand. The phosphines are found as a doublet at 29.62 ppm in the  $^{31}\text{P}$  NMR spectrum. The broadness of the peaks is due to similar  $^{107}\text{Ag}$ - $^{31}\text{P}$  and  $^{109}\text{Ag}$ - $^{31}\text{P}$  coupling constants. The  $\text{PF}_6$  counterion is found as a septet at –143.24 ppm in the  $^{31}\text{P}$  NMR spectrum. Single crystals were obtained from a concentrated dichloromethane (DCM) solution layered with *n*-pentane. The solid state molecular

structure (Figure 2.13) indicates a nearly linear geometry around silver (P–Ag–P angle of 168.32(2)°), in which only the phosphines are coordinated to the metal center, unlike what was observed for the cationic copper(I) complex **11**. The difference between the two compounds is in agreement with the predominant preference of silver(I) to form two-coordinate complexes,<sup>46–48</sup> although, in the absence of a better donating ligand, silver(I) has been shown to coordinate to olefinic moieties.<sup>49</sup> The Ag–P distances of 2.3744(6) and 2.3789(6) Å are similar to previously reported Ag–P distances.<sup>47</sup> The observed structure is reminiscent of [(2,6-bis[(di-*tert*-butylphosphino)methyl]pyridine)Ag][BF<sub>4</sub>] containing a neutral ligand.<sup>47</sup> Compounds **12** and [(PNP)Ag][BF<sub>4</sub>], however, are different from a silver(I) complex containing a monoanionic diaryl-amido based PNP ligand, [(PNP)Ag]<sub>2</sub> (PNP = bis(*o*-di-*iso*-propylphosphine-phenyl)amine), which leads to the formation of a dimeric species.<sup>50</sup> Using a similar ligand, Bourissou observed  $\kappa^2$ -P,P-coordination of Ph<sub>2</sub>P(C<sub>6</sub>H<sub>4</sub>)Me<sub>2</sub>Si–SiMe<sub>2</sub>(C<sub>6</sub>H<sub>4</sub>)PPh<sub>2</sub> to silver(I), but a weak interaction between the Si–Si backbone and copper(I).<sup>51</sup>

**Scheme 2.8:** Synthesis of **12**.



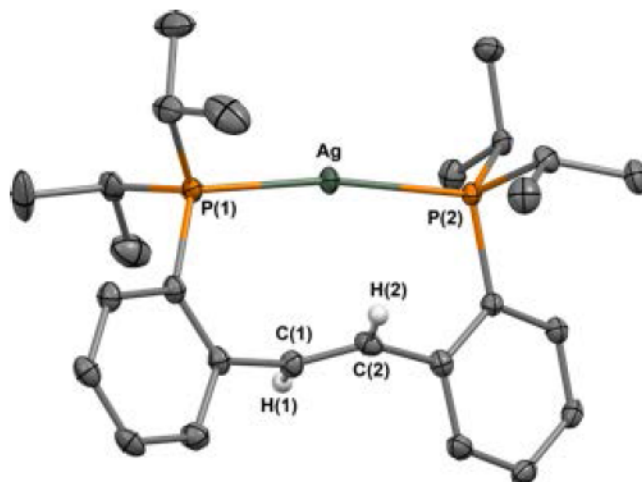


**Figure 2.13:** Thermal-ellipsoid (50% probability level) representation of the cationic fragment of **12**. Most hydrogen atoms and the counterion were omitted for clarity. Selected distances (Å) and angles (°): Ag–P(1) = 2.3744(6), Ag–P(2) = 2.3789(6), C(1)–C(2) = 1.326(4), P(1)–Ag–P(2) = 168.32(2).

### 2.3 Summary

The coordination chemistry of the neutral ligand **1**, *t*PCH=CHP, with various first-row transition metals that form stable complexes in the +1 oxidation state was studied. To determine whether the coordination mode is dependent on the oxidation state of the metal, some +2 metal complexes were also synthesized. The backbone olefinic moiety is versatile and responds to the electronic requirements of the metal. When the metal center adopts a tetrahedral geometry (in (*t*PCH=CHP)FeBr<sub>2</sub> (**3**) and (*t*PCH=CHP)CoCl<sub>2</sub>, (**2**)) or linear geometry (in [(*t*PCH=CHP)Ag][PF<sub>6</sub>] (**12**)), the coordination of the C–C double bond is not observed, however, with low valent metal centers (in (*t*PCH=CHP)CoCl (**6**), (*t*PCH=CHP)CoCl(CO) (**7**), (*t*PCH=CHP)RhCl (**8**), and [(*t*PCH=CHP)Cu][PF<sub>6</sub>] (**11**)),<sup>2</sup> coordination of the olefin occurs. Cobalt(II), iron(II), and copper(I) complexes presented an interesting case study since both non-coordination (in (*t*PCH=CHP)CoCl<sub>2</sub> (**2**), (*t*PCH=CHP)FeBr<sub>2</sub> (**3**), and (*t*PCH=CHP)Cu(OTf) (**10**) and η<sup>2</sup> coordination (in

$[(tPCH=CHP)CoCl][BAr^F_4]$  (4),  $[(tPCH=CHP)FeBr][BAr^F_4]$  (5), and  $[(tPCH=CHP)Cu][PF_6]$  (11)) of the olefinic backbone were observed. In square planar complexes,  $[(tPCH=CHP)CoCl][BAr^F_4]$  (4),  $(tPCH=CHP)CoCl$  (6) and  $(tPCH=CHP)RhCl$  (8), the olefin tends to approach a perpendicular orientation with respect to the plane of the other ligands, while a T-shape geometry (in  $[(tPCH=CHP)Cu][PF_6]$  (11)) prevents the olefin from rotating out of the plane.

The strength of the interaction between the olefin and the metal center was determined by NMR spectroscopy and X-ray crystallography (Table 2.1). The olefin peaks for free ligand are found downfield at 8.52 ppm in the  $^1H$  NMR spectrum and 132.67 ppm in the corresponding  $^{13}C$  NMR spectrum. As the olefin interacts with the metal center, the resulting shielding can significantly shift these peaks upfield, consistent with a reduction in the double bond character. This interaction is demonstrated in the cobalt(I) and rhodium(I) complexes **6-8** (Table 2.1). Similarly, the strength of the interaction can be evaluated in the solid state by examining the olefinic C–C distance determined by X-ray crystallography. Complexes with more electron rich metal centers (cobalt(I),  $(tPCH=CHP)CoCl$  and rhodium(I),  $(tPCH=CHP)RhCl$ ) contain the most elongated C–C distance in the olefinic backbone. As the metal center becomes more electron deficient, this effect begins to diminish. Intuitively, complexes lacking coordination of the olefin,  $(tPCH=CHP)CoCl_2$  and  $(tPCH=CHP)FeBr_2$ , contain short C–C distances. It can also be concluded that metal-olefin interactions in group 11 metal complexes are weak. These complexes show olefin shifts above 7 ppm in the  $^1H$  NMR spectra and 132 ppm in the corresponding  $^{13}C$  NMR spectra. Similarly, the solid state molecular structures for these complexes lack the characteristics of a bound olefin. The cationic copper(I) complex

$[(tPCH=CHP)Cu][PF_6]$  provides the best evidence for an olefin–metal interaction, displaying a small elongation of the C–C distance, similar to the distance observed in the cationic iron(II) species  $[(tPCH=CHP)FeBr][BAr^F_4]$ . The conflicting nature of the NMR spectroscopic and crystallographic data for this complex was explained by the existence of different solution and the solid state structures.

TABLE 2.1  
COMPARISON OF OLEFINIC PARAMETERS FOR DISCUSSED COMPOUNDS

Compound	Olefin $^1H$ shift (ppm)	Olefin $^{13}C$ shift (ppm)	Olefin C–C distance (Å)	M–centroid distance (Å)
$tPCH=CHP$ ( <b>1</b> )*	8.52	132.67	1.330(4)	
$(tPCH=CHP)CoCl_2$ ( <b>2</b> )	-	-	1.317(8)	3.501
$(tPCH=CHP)FeBr_2$ ( <b>3</b> )*	-	-	1.320(6)	3.596
$[(tPCH=CHP)CoCl][BAr^F_4]$ ( <b>4</b> )	-	-	1.397(6)	2.068
$[(tPCH=CHP)FeBr][BAr^F_4]$ ( <b>5</b> )*	-	-	1.332(14)	2.206
$(tPCH=CHP)CoCl$ ( <b>6</b> )*	2.01	53.89	1.442(5)	1.868
$(tPCH=CHP)CoCl(CO)$ ( <b>7</b> )	3.64, 4.68	70.28, 72.75	1.438(7)	1.901
$(tPCH=CHP)RhCl$ ( <b>8</b> )*	3.74	70.78	1.432(8)	1.964
$(tPCH=CHP)CuI$ ( <b>9</b> )	7.03	132.00	-	-
$(tPCH=CHP)CuOTf$ ( <b>10</b> )*	7.19	132.61	1.294(5)	2.426
$[(tPCH=CHP)Cu][PF_6]$ ( <b>11</b> )	7.02	135.20	1.340(4)	2.240
Optimized $[(tPCH=CHP)Cu]$	-	-		2.621
$[(tPCH=CHP)Ag][PF_6]$ ( <b>12</b> )	7.02	137.71	1.326(4)	2.860

NMR spectra were recorded in  $CDCl_3$  unless designated with (\*) in which  $C_6D_6$  was used as the NMR solvent.

The various coordination modes observed showed that  $tPCH=CHP$  is a versatile ligand and could accommodate different geometries enabling new reactivity behavior for specific metal centers. Especially encouraging is the hemilabile behavior observed for cobalt(II), iron(II), and copper(I) examples.

## 2.4 Experimental

All manipulations of air and water sensitive compounds were performed under a dry nitrogen atmosphere using an MBraun drybox. Glassware, vials, and stirring bars were dried in an oven at 120 °C overnight and evacuated for 24 h in the antechamber before being brought into the drybox. All solvents were dried by passing through a column of activated alumina, followed by storage over molecular sieves and sodium. Deuterated solvents were purchased from Cambridge Isotope Laboratories. C<sub>6</sub>D<sub>6</sub> was dried by stirring over CaH<sub>2</sub> followed by filtration. CDCl<sub>3</sub> was dried over molecular sieves. All other chemicals were commercially available and used as received. NMR spectra were obtained on Bruker 400 and Bruker 500 spectrometers at ambient temperature. Chemical shift values are reported in ppm relative to residual internal protonated solvent or to a tetramethylsilane standard while using CDCl<sub>3</sub> for <sup>1</sup>H and <sup>13</sup>C{<sup>1</sup>H} experiments. Coupling constants are reported in Hz. Magnetic moments were determined by the Evans method<sup>52-54</sup> using capillaries containing trimethoxybenzene in either CDCl<sub>3</sub> or C<sub>6</sub>D<sub>6</sub> as a reference, and trimethoxybenzene in the sample solution. IR spectrum was acquired on a FT/IR-6300 Jasco instrument. CHN analyses were performed on a CE-440 Elemental Analyzer, or by Midwest Microlab, LLC. Gaussian 03 (revision D.02)<sup>55</sup> was used for all reported calculations. The B3LYP (DFT) method was used to carry out the geometry optimizations on model compounds specified in text using the LANL2DZ basis set. The validity of the true minima was checked by the absence of negative frequencies in the energy Hessian.

### **Synthesis of 2,2'-bis(di-*iso*-propylphosphino)-*trans*-stilbene (*t*PCH=CHP, **1**).**

The precursor *o,o'*-*trans*-dibromostilbene (2.9 g, 8.63 mmol, 63.9%) was synthesized via a McMurry coupling reaction as reported in the literature.<sup>7</sup> <sup>1</sup>H NMR peaks agree with

literature values.<sup>56</sup> The precursor was then brought into the glove box and dissolved in 75 mL of diethyl ether. The solution was allowed to cool in a -35 °C freezer for 30 min, followed by the addition of *n*-butyllithium (10.8 mL, 17.3 mmol) via syringe. The mixture was allowed to warm to room temperature and then stirred for 1.5 h. The resulting solution was cooled in a -35 °C freezer for an additional 30 min before the addition of di-*iso*-propyl phosphine chloride via syringe (2.8 mL, 17.3 mmol) affording a cloudy yellow solution. After stirring overnight, the reaction was quenched with 1 mL of a degassed 10% solution of NH<sub>4</sub>Cl. The solution was then dried over Na<sub>2</sub>SO<sub>4</sub> followed by filtration through frit padded with Celite. The volatiles were removed under reduced pressure leaving behind the crude residue of *t*PCH=CHP (**1**, 2.76 g, 6.70 mmol, 78.15%), which was recrystallized from *n*-pentane. <sup>1</sup>H NMR (400 MHz, C<sub>6</sub>D<sub>6</sub>) δ: 0.88 (dd, *J*<sub>PH</sub> = 12 Hz, *J*<sub>HH</sub> = 8 Hz, 12H, CH(CH<sub>3</sub>)<sub>2</sub>), 1.02 (dd, *J*<sub>PH</sub> = 12 Hz, *J*<sub>HH</sub> = 8 Hz, 12H, CH(CH<sub>3</sub>)<sub>2</sub>), 1.95 (m, 4H, CH(CH<sub>3</sub>)<sub>2</sub>), 7.03 (td, *J*<sub>HH</sub> = 8 Hz, *J*<sub>PH</sub> = 1.6 Hz, 2H, ArH), 7.11 (td, *J*<sub>HH</sub> = 8 Hz, *J*<sub>PH</sub> = 1.2 Hz, 2H, ArH), 7.29 (dt, *J*<sub>HH</sub> = 8 Hz, *J*<sub>PH</sub> = 1.6 Hz, ArH), 7.95 (ddd, *J*<sub>HH</sub> = 6.8 Hz, *J*<sub>HH</sub> = 4 Hz, *J*<sub>PH</sub> = 0.8 Hz, 2H, ArH), 8.52 (d, *J*<sub>HH</sub> = 4 Hz, 2H, CH=CH). <sup>31</sup>P{<sup>1</sup>H} NMR (162 MHz, C<sub>6</sub>D<sub>6</sub>) δ: -6.52 (s). <sup>13</sup>C{<sup>1</sup>H} NMR (100 MHz, C<sub>6</sub>D<sub>6</sub>) δ: 19.17 (d, *J*<sub>PC</sub> = 10 Hz, CH(CH<sub>3</sub>)<sub>2</sub>), 20.33 (d, *J*<sub>PC</sub> = 19 Hz, CH(CH<sub>3</sub>)<sub>2</sub>), 23.82 (d, *J*<sub>PC</sub> = 14 Hz, CH(CH<sub>3</sub>)<sub>2</sub>), 126.24 (d, *J*<sub>PC</sub> = 4 Hz, ArC), 126.68 (s, ArC), 129.16 (s, ArC), 129.65 (dd, *J*<sub>PC</sub> = 34 Hz, *J*<sub>PC</sub> = 3 Hz, ArC), 132.67 (d, *J*<sub>PC</sub> = 3 Hz, CH=CH), 134.55 (d, *J* = 22 Hz, ArC), 145.59 (d, *J*<sub>PC</sub> = 22 Hz, ArC). MS (QTOF) *m/z*: C<sub>26</sub>H<sub>39</sub>P<sub>2</sub><sup>+</sup>, 413.25 (expected: C<sub>26</sub>H<sub>38</sub>P<sub>2</sub>, 412.24).

**Synthesis of (*t*PCH=CHP)CoCl<sub>2</sub> (**2**).** A solution of **1** (100 mg, 0.242 mmol) in 5 mL of THF was added to a suspension of CoCl<sub>2</sub> (31.6 mg, 0.242 mmol) in 2 mL of THF. The mixture was allowed to stir at room temperature for 1 h. The volatiles were removed

under reduced pressure resulting in a green residue of **2**. Trituration with 3-5 mL of *n*-pentane produced a teal powder (93.8 mg, 0.174 mmol, 71%). The teal powder was then dissolved in a minimum amount of THF and the solution was layered with *n*-pentane in order to obtain crystals suitable for X-ray diffraction. Magnetic moment:  $\mu_{\text{eff}} = 3.34 \mu_{\text{B}}$ .  $^1\text{H}$  NMR (500 MHz,  $\text{CDCl}_3$ )  $\delta$ : -0.59 ( $\nu_{1/2} = 290.35$  Hz, 12H,  $\text{CH}(\text{CH}_3)_2$ ), 3.76 ( $\nu_{1/2} = 286.53$  Hz, 12H,  $\text{CH}(\text{CH}_3)_2$ ), 6.35 ( $\nu_{1/2} = 95.51$  Hz, 4H, *ArH*), 7.44 ( $\nu_{1/2} = 133.71$  Hz, 4H, *ArH*), 12.30 ( $\nu_{1/2} = 175.74$  Hz, 4 H,  $\text{CH}(\text{CH}_3)_2$ ), 19.25 ( $\nu_{1/2} = 443.16$ , 2H,  $\text{CH}=\text{CH}$ ). Anal. Calcd for  $\text{C}_{26}\text{H}_{38}\text{Cl}_2\text{CoP}_2$ : C, 57.58; H, 7.06. Found C, 57.50; H, 7.18.

**Synthesis of  $(t\text{PCH}=\text{CHP})\text{FeBr}_2$  (**3**).** A solution of **1** (100 mg, 0.242 mmol) in 5 mL of THF was added to a suspension of iron dibromide (52.1 mg, 0.241 mmol) in 2 mL of THF and allowed to stir at room temperature for 1 h. The volatiles were removed under reduced pressure resulting in a light brown residue of **3**. Trituration with 3-5 mL of *n*-pentane yielded a pure tan powder of **3** (126.3 mg, 0.201 mmol, 83%). Crystals suitable for single crystal X-ray diffraction were obtained through recrystallization from a concentrated solution of diethyl ether. Magnetic moment:  $\mu_{\text{eff}} = 4.48 \mu_{\text{B}}$ .  $^1\text{H}$  NMR (500 MHz,  $\text{C}_6\text{D}_6$ )  $\delta$ : 0.11 ( $\nu_{1/2} = 204.99$  Hz, 6H,  $\text{CH}(\text{CH}_3)_2$ ), 2.87 ( $\nu_{1/2} = 107.62$  Hz, 6H,  $\text{CH}(\text{CH}_3)_2$ ), 5.30 ( $\nu_{1/2} = 440.72$  Hz, 12H,  $\text{CH}(\text{CH}_3)_2$ ), 6.83 ( $\nu_{1/2} = 491.97$  Hz, 8H, *ArH*), 11.66 ( $\nu_{1/2} = 645.70$  Hz, 4 H,  $\text{CH}(\text{CH}_3)_2$ ), 19.25 ( $\nu_{1/2} = 901.94$  Hz, 2H,  $\text{CH}=\text{CH}$ ). Anal. Calcd for  $\text{C}_{26}\text{H}_{38}\text{Br}_2\text{FeP}_2 \cdot \text{CHCl}_3$ : C, 43.38; H, 5.26. Found C, 42.33; H, 5.12.

**Synthesis of  $[(t\text{PCH}=\text{CHP})\text{CoCl}][\text{BAr}^{\text{F}}_4]$  (**4**).** A toluene solution of  $(t\text{PCH}=\text{CHP})\text{CoCl}_2$  (**2**, 20 mg, 0.04 mmol) was added to  $\text{Na}[\text{BAr}^{\text{F}}_4]$  (32.7 mg, 0.04 mmol). The mixture was stirred for 12 h until the solution turned from dark green to orange. The solution was filtered, followed by removal of the volatiles under reduced pressure leading

to 36.6 mg, 71.8% of **4**. Compound **4** was recrystallized from a concentrated toluene solution layered with *n*-pentane chilled to  $-35\text{ }^{\circ}\text{C}$ . Magnetic moment:  $\mu_{\text{eff}} = 1.8\text{ }\mu_{\text{B}}$ .  $^1\text{H}$  NMR (500 MHz,  $\text{CDCl}_3$ )  $\delta$ :  $-7.72$  ( $\nu_{1/2} = 503.7\text{ Hz}$ , 4H,  $\text{CH}(\text{CH}_3)_2$ ),  $-3.4$  ( $\nu_{1/2} = 194.32\text{ Hz}$ , 12H,  $\text{CH}(\text{CH}_3)_2$ ),  $-0.17$  ( $\nu_{1/2} = 503.70\text{ Hz}$ , 12H,  $\text{CH}(\text{CH}_3)_2$ ),  $3.25$  ( $\nu_{1/2} = 63.92\text{ Hz}$ , 2H,  $\text{CH}=\text{CH}$ ),  $6.16$  ( $\nu_{1/2} = 24.27\text{ Hz}$ , 2H,  $\text{ArH}$ ),  $7.40$  (4H,  $\text{BAr}_4^{\text{F}}\text{-H}$ ),  $7.57$  (8H,  $\text{BAr}_4^{\text{F}}\text{-H}$ ),  $7.85$  ( $\nu_{1/2} = 124.32\text{ Hz}$ , 2H,  $\text{ArH}$ ),  $11.34$  ( $\nu_{1/2} = 957.28\text{ Hz}$ , 2H,  $\text{ArH}$ ),  $15.17$  ( $\nu_{1/2} = 149.57$ , 2H,  $\text{ArH}$ ).  $^{19}\text{F}$  NMR (470 MHz,  $\text{CDCl}_3$ )  $\delta$ :  $-65.78$  ( $\text{BAr}_4^{\text{F}}\text{-F}$ ).  $^{11}\text{B}$  NMR (160 MHz,  $\text{CDCl}_3$ )  $\delta$ :  $-6.71$  ( $\text{BAr}_4^{\text{F}}$ ). Anal. Calcd for  $\text{C}_{58}\text{H}_{50}\text{ClCoF}_{24}\text{P}_2$ : C, 50.84; H, 3.68. Found C, 50.93; H, 3.56.

**Synthesis of  $[(t\text{PCH}=\text{CHP})\text{FeBr}][\text{BAr}_4^{\text{F}}]$  (**5**).** To a solution of  $(t\text{PCH}=\text{CHP})\text{FeBr}_2$  (**3**, 25 mg, 0.40 mmol) in 5 mL of toluene, a slurry of  $\text{NaBAr}_4^{\text{F}}$  (35.4 mg, 0.40 mmol) was added. The mixture was stirred for 12 h followed by removal of the volatiles under reduced pressure. The crude residue was triturated with *n*-pentane. Analytically pure **5** was obtained from a concentrated toluene solution layered with *n*-pentane at  $-35\text{ }^{\circ}\text{C}$  (23.6 mg, 42.1%). Magnetic moment:  $\mu_{\text{eff}} = 4.3\text{ }\mu_{\text{B}}$ .  $^1\text{H}$  NMR (400 MHz,  $\text{C}_6\text{D}_6$ )  $\delta$ :  $1.3$  ( $\nu_{1/2} = 166.45\text{ Hz}$ , 12H,  $\text{CH}(\text{CH}_3)_2$ ),  $5.43$  ( $\nu_{1/2} = 449.91\text{ Hz}$ , 12H,  $\text{CH}(\text{CH}_3)_2$ ),  $4\text{H}$ ,  $\text{CH}(\text{CH}_3)_2$ ),  $7.51$  (4H,  $\text{BAr}_4^{\text{F}}\text{-H}$ ),  $7.70$  (8H,  $\text{BAr}_4^{\text{F}}\text{-H}$ ),  $9.82$  ( $\nu_{1/2} = 192.22\text{ Hz}$ , 2H,  $\text{CH}=\text{CH}$ ),  $10.95$  ( $\nu_{1/2} = 968.66\text{ Hz}$ , 4H,  $\text{ArH}$ ),  $15.41$  ( $\nu_{1/2} = 116.84\text{ Hz}$ , 1H,  $\text{ArH}$ ),  $17.86$  ( $\nu_{1/2} = 94.23\text{ Hz}$ , 1H,  $\text{ArH}$ ),  $24.87$  ( $\nu_{1/2} = 242.23\text{ Hz}$ , 1H,  $\text{ArH}$ ),  $26.51$  ( $\nu_{1/2} = 119.49\text{ Hz}$ , 1H,  $\text{ArH}$ ).  $^{19}\text{F}$  NMR (376 MHz,  $\text{C}_6\text{D}_6$ )  $\delta$ :  $-62.89$  ( $\text{BAr}_4^{\text{F}}\text{-F}$ ).  $^{11}\text{B}$  NMR (128 MHz,  $\text{C}_6\text{D}_6$ )  $\delta$ :  $-5.82$  ( $\text{BAr}_4^{\text{F}}$ ). Anal. Calcd for  $\text{C}_{58}\text{H}_{50}\text{BBrFeP}_2\text{F}_{24}\cdot\text{CH}_2\text{Cl}_2$ : C, 47.36; H, 3.50. Found C, 47.01; H, 3.47.

**Synthesis of  $(t\text{PCH}=\text{CHP})\text{CoCl}$  (**6**).** Complex **2** (75 mg, 0.138 mmol) was dissolved in 5 mL of THF. To this solution, a suspension of 0.25 equiv. of lithium

aluminum hydride ( $\text{LiAlH}_4$ , 1.4 mg, 0.037 mmol) was added. The resulting mixture was allowed to stir for 10 min at room temperature, after which it was filtered to give a purple solution. The volatiles were removed under reduced pressure producing a purple residue, which was dissolved in a minimum amount of *n*-pentane and allowed to crystallize at  $-35^\circ\text{C}$  (15.3 mg, 0.031 mmol, 22%).  $^1\text{H}$  NMR (500 MHz,  $\text{C}_6\text{D}_6$ )  $\delta$ : 1.00 (d,  $J_{\text{PH}} = 10$  Hz, 6H,  $\text{CH}(\text{CH}_3)_2$ ), 1.25 (d,  $J_{\text{PH}} = 5$  Hz, 6H,  $\text{CH}(\text{CH}_3)_2$ ), 1.37 (d,  $J_{\text{PH}} = 5$  Hz, 6H,  $\text{CH}(\text{CH}_3)_2$ ), 1.50 (d,  $J_{\text{PH}} = 10$  Hz, 6H,  $\text{CH}(\text{CH}_3)_2$ ), 2.01 (br s, 2H,  $\text{CH}=\text{CH}$ ), 2.27 (br s, 2H,  $\text{CH}(\text{CH}_3)_2$ ), 3.29 (br s, 2H,  $\text{CH}(\text{CH}_3)_2$ ), 6.93 (t,  $J_{\text{HH}} = 5$  Hz, 2H, ArH), 6.97 (t,  $J_{\text{HH}} = 5$  Hz, 2H, ArH), 7.01 (d,  $J_{\text{HH}} = 10$  Hz, 2H, ArH), 7.14 (d,  $J_{\text{HH}} = 10$  Hz, 2H, ArH).  $^{31}\text{P}\{^1\text{H}\}$  NMR (202 MHz,  $\text{C}_6\text{D}_6$ )  $\delta$ : 58.11 (br s).  $^{13}\text{C}\{^1\text{H}\}$  NMR (100 MHz,  $\text{C}_6\text{D}_6$ )  $\delta$ : 16.34 (s,  $\text{CH}(\text{CH}_3)_2$ ), 18.37 (s,  $\text{CH}(\text{CH}_3)_2$ ), 20.15 (s,  $\text{CH}(\text{CH}_3)_2$ ), 20.32 (s,  $\text{CH}(\text{CH}_3)_2$ ), 22.88 (br s,  $\text{CH}(\text{CH}_3)_2$ ), 24.18 (br s,  $\text{CH}(\text{CH}_3)_2$ ), 53.89 (br s,  $\text{CH}=\text{CH}$ ), 124.17 (s, ArC), 125.12 (s, ArC), 125.23 (s, ArC), 129.38 (s, ArC), 130.36 (s, ArC), 160.98 (s, ArC). Anal. Calcd for  $\text{C}_{26}\text{H}_{38}\text{ClCoP}_2$ : C, 61.60; H, 7.56. Found C, 61.58; H, 7.43.

**Synthesis of  $(t\text{PCH}=\text{CHP})\text{CoCl}(\text{CO})$  (7).** A THF solution of  $(t\text{PCH}=\text{CHP})\text{CoCl}$  (6, 20 mg, 0.04 mmol) was added to a septum-capped vial along with a stir bar. The solution was then taken out of the glove box and CO was bubbled through the reaction mixture for 5 min. The starting deep purple solution rapidly turned bright orange. The reaction mixture was stirred for 1 h and the volatiles were removed under reduced pressure. The crude reaction mixture was then dissolved in diethyl ether, filtered, and allowed to sit in a  $-35^\circ\text{C}$  freezer yielding crystals of 7 (11.9 mg, 0.02 mmol, 56.4%).  $^1\text{H}$  NMR (400 MHz,  $\text{C}_6\text{D}_6$ )  $\delta$ : 0.90 (dd,  $J_{\text{PH}} = 12$  Hz,  $J_{\text{HH}} = 4$  Hz, 3 H,  $\text{CH}(\text{CH}_3)_2$ ), 1.04 (dd,  $J_{\text{PH}} = 12$  Hz,  $J_{\text{HH}} = 4$  Hz, 3H,  $\text{CH}(\text{CH}_3)_2$ ), 1.23 (m, 6H,  $\text{CH}(\text{CH}_3)_2$ ), 1.50 (m, 12H,  $\text{CH}(\text{CH}_3)_2$ ), 2.24 (m, 2H,



CH(CH<sub>3</sub>)<sub>2</sub>), 2.68 (m, 2H, CH(CH<sub>3</sub>)<sub>2</sub>), 2.92 (m, 1H, CH(CH<sub>3</sub>)<sub>2</sub>), 3.64 (m, 1H, CH=CH), 4.68 (m, 1H, CH=CH), 6.94 (m, 6H, ArH), 7.08 (t,  $J_{HH} = 5$  Hz, ArH), 7.32 (d,  $J_{HH} = 8$  Hz, ArH). <sup>31</sup>P NMR (162 MHz, C<sub>6</sub>D<sub>6</sub>) δ: 71.96 (d,  $J_{PP} = 172$  Hz), 75.05 (d,  $J_{PP} = 175$  Hz). <sup>13</sup>C NMR (100 MHz, C<sub>6</sub>D<sub>6</sub>) δ: 18.12 (d,  $J_{CP} = 4$  Hz, CH(CH<sub>3</sub>)<sub>2</sub>), 18.17 (s, CH(CH<sub>3</sub>)<sub>2</sub>), 18.60 (s, CH(CH<sub>3</sub>)<sub>2</sub>), 18.82 (d,  $J_{CP} = 5$  Hz, CH(CH<sub>3</sub>)<sub>2</sub>), 20.08 (d,  $J_{PC} = 2$  Hz, CH(CH<sub>3</sub>)<sub>2</sub>), 20.15 (s, CH(CH<sub>3</sub>)<sub>2</sub>), 20.31 (s, CH(CH<sub>3</sub>)<sub>2</sub>), 21.18 (s, CH(CH<sub>3</sub>)<sub>2</sub>), 26.28 (d,  $J_{CP} = 2$  Hz, CH(CH<sub>3</sub>)<sub>2</sub>), 26.51 (d,  $J_{CP} = 2$  Hz, CH(CH<sub>3</sub>)<sub>2</sub>), 26.70 (d,  $J_{CP} = 3$  Hz, CH(CH<sub>3</sub>)<sub>2</sub>), 26.94 (d,  $J_{CP} = 3$  Hz, CH(CH<sub>3</sub>)<sub>2</sub>), 26.99 (d,  $J_{CP} = 3$  Hz, CH(CH<sub>3</sub>)<sub>2</sub>), 26.18 (d,  $J_{CP} = 2$  Hz, CH(CH<sub>3</sub>)<sub>2</sub>), 28.04 (d,  $J_{CP} = 2$  Hz, CH(CH<sub>3</sub>)<sub>2</sub>), 28.23 (d,  $J_{CP} = 2$  Hz, CH(CH<sub>3</sub>)<sub>2</sub>), 70.28 (d,  $J_{CP} = 5$  Hz, CH=CH), 72.75 (d,  $J_{CP} = 6$  Hz, CH=CH), 125.13 (d,  $J_{CP} = 5$  Hz, ArC), 125.53 (d,  $J_{CP} = 4$  Hz, ArC), 126.15 (s, ArC), 126.26 (s, ArC), 126.91 (d,  $J_{CP} = 29$  Hz, ArC), 127.24 (d,  $J_{PC} = 30$  Hz, ArC), 127.10 (s, ArC), 130.23 (d,  $J_{CP} = 3$  Hz, ArC), 130.46 (d,  $J_{CP} = 3$  Hz, ArC), 131.64 (s, ArC), 131.96 (s, ArC), 158.78 (dd,  $J_{PC} = 26$  Hz,  $J_{PC} = 5$  Hz, ArC), 159.65 (dd,  $J_{PC} = 26$  Hz,  $J_{PC} = 5$  Hz, ArC), 204.93 (br s, CO). IR (ATR)  $\nu_{CO} = 1942$  (s) cm<sup>-1</sup>. Anal. Calcd for C<sub>27</sub>H<sub>38</sub>ClCoOP<sub>2</sub>: C, 60.62; H, 7.16. Found C, 60.39; H, 7.05.

**Synthesis of (*t*PCH=CHP)RhCl (8).** A mixture of *t*PCH=CHP (1, 25.0 mg, 0.061 mmol) and rhodium cyclooctadiene dichloride dimer ([*(cod)RhCl*]<sub>2</sub>, 14.9 mg, 0.030 mmol) in THF was allowed to stir at room temperature for 1 h. The volatiles were removed under reduced pressure and the remaining yellow residue dissolved in *n*-pentane. The solution was placed in a -35 °C freezer and crystals were obtained (23.0 mg, 0.0418 mmol, 69%). <sup>1</sup>H NMR (500 MHz, C<sub>6</sub>D<sub>6</sub>) δ: 1.00 (dd,  $J_{PH} = 13$  Hz,  $J_{HH} = 6$  Hz, 6H, CH(CH<sub>3</sub>)<sub>2</sub>), 1.12 (dd,  $J_{PH} = 16$  Hz,  $J_{HH} = 8$  Hz, 6H, CH(CH<sub>3</sub>)<sub>2</sub>), 1.22 (dd,  $J_{PH} = 16$  Hz,  $J_{HH} = 8$  Hz, 6H, CH(CH<sub>3</sub>)<sub>2</sub>), 1.55 (dd,  $J_{PH} = 16$  Hz,  $J_{HH} = 8$  Hz, 6H, CH(CH<sub>3</sub>)<sub>2</sub>), 2.22 (br m, 2H,

$\text{CH}(\text{CH}_3)_2$ ), 3.24 (m, 2H,  $\text{CH}(\text{CH}_3)_2$ ), 3.74 (br d,  $J_{\text{RhH}} = 5$  Hz, 2H,  $\text{CH}=\text{CH}$ ), 7.00 (m, 4H, ArH), 7.09 (br d,  $J_{\text{HH}} = 10$  Hz, 4H, ArH).  $^{31}\text{P}\{^1\text{H}\}$  NMR (202 MHz,  $\text{C}_6\text{D}_6$ )  $\delta$ : 57.10 (d,  $J_{\text{RhP}} = 120$  Hz).  $^{13}\text{C}\{^1\text{H}\}$  NMR (100 MHz,  $\text{C}_6\text{D}_6$ )  $\delta$ : 16.89 (s,  $\text{CH}(\text{CH}_3)_2$ ), 18.52 (t,  $J_{\text{PC}} \sim J_{\text{RhC}} = 3$  Hz,  $\text{CH}(\text{CH}_3)_2$ ), 20.49 (t,  $J_{\text{PC}} \sim J_{\text{RhC}} = 3$  Hz,  $\text{CH}(\text{CH}_3)_2$ ), 20.62 (t,  $J_{\text{PC}} \sim J_{\text{RhC}} = 4$  Hz,  $\text{CH}(\text{CH}_3)_2$ ), 24.09 (m,  $\text{CH}(\text{CH}_3)_2$ ), 70.78 (d,  $J_{\text{RhC}} = 17$  Hz,  $\text{CH}=\text{CH}$ ), 126.60 (t,  $J_{\text{PC}} = 3$  Hz, ArC), 126.25 (td,  $J_{\text{PC}} = 16$  Hz,  $J_{\text{RhC}} = 3$  Hz, ArC), 127.71 (td,  $J_{\text{RhC}} = 1$  Hz,  $J_{\text{PC}} = 7$  Hz, ArC), 130.29 (s, ArC), 131.41 (s, ArC), 158.08 (t,  $J_{\text{PC}} = 6$  Hz, ArC). Anal. Calcd for  $\text{C}_{26}\text{H}_{38}\text{ClRhP}_2 \cdot \text{C}_4\text{H}_{10}\text{O}$ : C, 57.65; H, 7.74. Found C, 57.81; H, 7.61.

**Synthesis of (*t*PCH=CHP)CuI (9).** Copper iodide (23.0 mg, 0.121 mmol) was mixed with *t*PCH=CHP (**1**, 50 mg, 0.121 mmol) in THF and stirred for 1 h at room temperature. The volatiles were removed under reduced pressure and the resulting residue was triturated with *n*-pentane (67.8 mg, 0.113 mmol, 93%).  $^1\text{H}$  NMR (500 MHz,  $\text{CDCl}_3$ )  $\delta$ : 1.25 (app q,  $J_{\text{PH}} \sim J_{\text{HH}} = 5$  Hz, 6H,  $\text{CH}(\text{CH}_3)_2$ ), 1.35 (app q,  $J_{\text{PH}} \sim J_{\text{HH}} = 5$  Hz, 6H,  $\text{CH}(\text{CH}_3)_2$ ), 2.50 (m, 4H,  $\text{CH}(\text{CH}_3)_2$ ), 7.03 (s, 2H,  $\text{CH}=\text{CH}$ ), 7.33 (m, 4H, ArH), 7.35 (m, 2H, ArH), 7.40 (app t,  $J_{\text{HH}} = 10$  Hz, 2H, ArH), 7.53 (m, 2H, ArH).  $^{31}\text{P}\{^1\text{H}\}$  NMR (202 MHz,  $\text{CDCl}_3$ )  $\delta$ : 7.00 (br s).  $^{13}\text{C}\{^1\text{H}\}$  NMR (126 MHz,  $\text{CDCl}_3$ )  $\delta$ : 19.91 (t,  $J_{\text{PC}} = 3.78$ ,  $\text{CH}(\text{CH}_3)_2$ ), 20.58 (br t,  $J_{\text{PC}} = 1.26$  Hz,  $\text{CH}(\text{CH}_3)_2$ ), 25.88 (t,  $J_{\text{PC}} = 7.56$  Hz,  $\text{CH}(\text{CH}_3)_3$ ), 127.41 (s, ArC), 129.43 (t,  $J_{\text{PC}} = 3.78$  Hz, ArC), 129.98 (s, ArC), 132.00 (t,  $J_{\text{PC}} = 6.30$  Hz,  $\text{CH}=\text{CH}$ ), 132.58 (s, ArC), 132.86 (t,  $J_{\text{PC}} = 15$  Hz, ArC), 145.71 (t,  $J_{\text{PC}} = 11.34$  Hz, ArC). Anal. Calcd for  $\text{C}_{26}\text{H}_{38}\text{CuIP}_2$ : C, 51.79; H, 6.35. Found: C 52.40; H 6.18.

**Synthesis of (*t*PCH=CHP)CuOTf (10).** To a solution of compound **9** (33.9 mg, 0.056 mmol) in THF was added silver triflate (14.4 mg, 0.056 mmol). The mixture was stirred at room temperature for 1 h. The solution was then filtered, followed by removal of

the volatiles under reduced pressure. The resulting crude oil was triturated with *n*-pentane leading to a white powder (33.4 mg, 0.053 mmol, 95%). The powder was recrystallized from a toluene solution layered with *n*-pentane at  $-35^{\circ}\text{C}$ .  $^1\text{H}$  NMR (500 MHz,  $\text{C}_6\text{D}_6$ )  $\delta$ : 1.01 (app q,  $J_{PH} = 10$  Hz,  $J_{HH} = 5$  Hz, 12 H,  $\text{CH}(\text{CH}_3)_2$ ), 1.10 (app q,  $J_{PH} = 10$  Hz,  $J_{HH} = 5$  Hz, 12H,  $\text{CH}(\text{CH}_3)_2$ ), 2.14 (m, 4H,  $\text{CH}(\text{CH}_3)_2$ ), 7.09 (m, 2H, ArH), 7.19 (m, 8 H, ArH,  $\text{CH}=\text{CH}$ ).  $^{31}\text{P}\{^1\text{H}\}$  NMR (202 MHz,  $\text{C}_6\text{D}_6$ )  $\delta$ : 14.54 (s)  $^{19}\text{F}\{^1\text{H}\}$  NMR (470 MHz,  $\text{C}_6\text{D}_6$ )  $\delta$ : 80.82 (s,  $\text{CF}_3$ ).  $^{13}\text{C}\{^1\text{H}\}$  NMR (126 MHz,  $\text{C}_6\text{D}_6$ )  $\delta$ : 19.74 (t,  $J_{PC} = 4$  Hz,  $\text{CH}(\text{CH}_3)_2$ ), 19.97 (br s,  $\text{CH}(\text{CH}_3)_2$ ), 24.64 (t,  $J_{PC} = 9$  Hz,  $\text{CH}(\text{CH}_3)_2$ ), 127.77 (s, ArC), 129.68 (t,  $J_{PC} = 4$  Hz, ArC), 130.59 (s, ArC), 132.19 (s, ArC), 132.61 (br t,  $J_{PC} = 6$  Hz,  $\text{CH}=\text{CH}$ ), 133.09 (t,  $J_{PH} = 18$  Hz, ArC), 146.24 (t,  $J_{PC} = 11$  Hz, ArC). Anal. Calcd for  $\text{C}_{26}\text{H}_{38}\text{CuF}_6\text{P}_3$ : C, 50.28; H, 6.17. Found: C 50.23; H 6.12.

**Synthesis of  $[(t\text{PCH}=\text{CHP})\text{Cu}][\text{PF}_6]$  (11).** A solution of  $(t\text{PC}=\text{CP})\text{CuI}$  (**9**, 52.5 mg, 0.12 mmol) in THF was added to a slurry of  $\text{AgPF}_6$  (30.8 mg, 0.12 mmol), and stirred at room temperature for 1 h. The volatiles were removed under reduced pressure, followed by trituration with *n*-pentane that resulted in a white powder (46.3 mg, 0.10 mmol, 84.6%).  $^1\text{H}$  NMR (400 MHz,  $\text{CDCl}_3$ )  $\delta$ : 1.11 (q,  $J_{PH} \sim J_{HH} = 8$  Hz, 12 H,  $\text{CH}(\text{CH}_3)_2$ ), 1.27 (q,  $J_{PH} \sim J_{HH} = 8$  Hz, 12 H,  $\text{CH}(\text{CH}_3)_2$ ), 2.62 (m, 4H,  $\text{CH}(\text{H}_3)_2$ ), 7.02 (s, 2H,  $\text{CH}=\text{CH}$ ), 7.60 (m, 8 H, ArH).  $^{31}\text{P}\{^1\text{H}\}$  NMR (162 MHz,  $\text{CDCl}_3$ )  $\delta$ :  $-143.28$  (septet,  $J_{PF} = 708$  Hz,  $\text{PF}_6$ ), 25.41 (s,  $\text{P}^i\text{Pr}_2$ ).  $^{19}\text{F}\{^1\text{H}\}$  NMR (376 MHz,  $\text{CDCl}_3$ )  $\delta$ :  $-76.63$  (d,  $J_{FP} = 711$  Hz,  $\text{PF}_6$ ).  $^{13}\text{C}\{^1\text{H}\}$  NMR (100 MHz,  $\text{CDCl}_3$ )  $\delta$ : 19.03 (s,  $\text{CH}(\text{CH}_3)_2$ ), 20.17 (t,  $J_{CP} = 4$  Hz,  $\text{CH}(\text{CH}_3)_2$ ), 23.55 (t,  $J_{CP} = 11$  Hz,  $\text{CH}(\text{CH}_3)_2$ ), 129.37 (s, ArC), 129.86 (s, ArC), 129.91 (s, ArC), 132.37 (s, ArC), 133.11 (s, ArC), 135.20 (br s,  $\text{CH}=\text{CH}$ ), 144.68 (t,  $J_{CP} = 11$  Hz, ArC). Anal. Calcd for  $\text{C}_{27}\text{H}_{38}\text{CuF}_3\text{O}_3\text{P}_2\text{S}$ : C, 51.88; H, 6.13. Found: C 51.79; H 6.12.

**Synthesis of [(*t*PCH=CHP)Ag][PF<sub>6</sub>] (12).** A THF solution of *t*PCH=CHP (**1**, 25 mg, 0.061 mmol) was mixed with a suspension of AgPF<sub>6</sub> (15.4 mg, 0.061 mmol) and stirred at ambient temperature for one hour. The volatiles were then removed under reduced pressure, followed by trituration of the crude residue with pentanes, resulting in a white powder of [(*t*PCH=CHP)Ag][PF<sub>6</sub>] (38.7 mg, 0.057 mmol, 96%). The product was then recrystallized from a concentrated DCM solution layered with *n*-pentane. <sup>1</sup>H NMR (400 MHz, CDCl<sub>3</sub>) δ: 1.18 (app q, *J*<sub>ph</sub> = 8 Hz, 12H, CH(CH<sub>3</sub>)<sub>2</sub>), 1.29 (m, 12H, CH(CH<sub>3</sub>)<sub>2</sub>), 2.65 (m, 4H, CH(CH<sub>3</sub>)<sub>2</sub>), 7.03 (br s, 2H, CH=CH), 7.51 (m, 2 H, ArH), 7.74 (d, *J*<sub>HH</sub> = 4 Hz, 2 H, ArH), 7.61 (m, 4 H, ArH). <sup>31</sup>P{<sup>1</sup>H} NMR (162 MHz, CDCl<sub>3</sub>) δ: -143.24 (septet, *J*<sub>PF</sub> = 714.4 Hz, PF<sub>6</sub>), 29.62 (d, unresolved <sup>107</sup>Ag-P, <sup>109</sup>Ag-P coupling, Ar-*P*Pr<sub>2</sub>). <sup>19</sup>F{<sup>1</sup>H} NMR (376 MHz, CDCl<sub>3</sub>) δ: -76.18 (d, *J*<sub>PF</sub> = 718.2 Hz, PF<sub>6</sub>). <sup>13</sup>C{<sup>1</sup>H} NMR (100 MHz, CDCl<sub>3</sub>) δ: 18.81 (s, CH(CH<sub>3</sub>)<sub>2</sub>), 20.19 (t, *J*<sub>CP</sub> = 5 Hz, CH(CH<sub>3</sub>)<sub>2</sub>), 23.87 (t, *J*<sub>PC</sub> = 10 Hz, CH(CH<sub>3</sub>)<sub>2</sub>), 126.05 (t, *J*<sub>PC</sub> = 17 Hz, ArC), 128.68 (t, *J*<sub>PC</sub> = 3 Hz, ArC), 130.87 (s, ArC), 131.80 (s, ArC), 133.28 (s, ArC), 137.71 (br s, CH=CH), 144.49 (t, *J*<sub>PC</sub> = 9 Hz, ArC). Anal. Calcd for C<sub>26</sub>H<sub>38</sub>AgF<sub>6</sub>P<sub>3</sub>: C, 46.93, H, 5.76. Found: C 46.84, H 5.77.

**X-ray single crystal diffraction** The data were collected on a Bruker APEX-II diffractometer with a monochromated Mo Kα radiation.<sup>57</sup> Data were corrected for absorption and polarized effects and analyzed for space group determination.<sup>57-58</sup> The structure was solved by direct methods (SHELXS<sup>59</sup> or OLEX2<sup>60</sup>) and refined by full-matrix least squares techniques against F<sub>o</sub><sup>2</sup> (SHELXL-97).<sup>61</sup> Unless noted, all hydrogen atoms were generated in calculated positions. Mercury was used for structure representations.<sup>62</sup>

**X-Ray Crystal Structure of *t*PCH=CHP (1).** X-Ray quality single crystals were obtained from a concentrated solution of *n*-pentane solution at -34 °C in the glovebox.

Crystal and refinement data for **1**·C<sub>7</sub>H<sub>8</sub>: Crystal data for C<sub>33</sub>H<sub>46</sub>P<sub>2</sub>; M<sub>r</sub> = 504.64; Monoclinic; space group C2/c; *a* = 13.5186(11) Å; *b* = 12.0847(9) Å; *c* = 18.2230(14) Å;  $\alpha = 90^\circ$ ;  $\beta = 93.335(2)^\circ$ ;  $\gamma = 90^\circ$ ; *V* = 2972.0(4) Å<sup>3</sup>; *Z* = 4; *T* = 120(2) K;  $\lambda = 0.71073$  Å;  $\mu = 0.165$  mm<sup>-1</sup>; *d*<sub>calc</sub> = 1.128 g·cm<sup>-3</sup>; 13722 reflections collected; 1638 unique (*R*<sub>int</sub> = 0.0504); giving *R*<sub>1</sub> = 0.0298, *wR*<sub>2</sub> = 0.0661 for 1390 data with [*I* > 2σ(*I*)] and *R*<sub>1</sub> = 0.0406, *wR*<sub>2</sub> = 0.0711 for all 1638 data. Residual electron density (e<sup>-</sup>·Å<sup>-3</sup>) max/min: 0.141/-0.195.

**X-Ray Crystal Structure of (tPCH=CHP)CoCl<sub>2</sub> (2).** X-Ray quality single crystals were obtained from a concentrated DCM solution layered with *n*-pentane at -35 °C in the glovebox. Crystal and refinement data for **2**: C<sub>26</sub>H<sub>38</sub>Cl<sub>2</sub>CoP<sub>2</sub>; M<sub>r</sub> = 542.33; Monoclinic; space group Cc; *a* = 18.254(2) Å; *b* = 18.645(2) Å; *c* = 16.109(2) Å;  $\alpha = 90^\circ$ ;  $\beta = 97.618(3)^\circ$ ;  $\gamma = 90^\circ$ ; *V* = 5434.2(12) Å<sup>3</sup>; *Z* = 8; *T* = 120(2) K;  $\lambda = 0.71073$  Å;  $\mu = 0.958$  mm<sup>-1</sup>; *d*<sub>calc</sub> = 1.326 g·cm<sup>-3</sup>; 35511 reflections collected; 11030 unique (*R*<sub>int</sub> = 0.1341); giving *R*<sub>1</sub> = 0.0583, *wR*<sub>2</sub> = 0.0652 for 6488 data with [*I* > 2σ(*I*)] and *R*<sub>1</sub> = 0.1370, *wR*<sub>2</sub> = 0.0819 for all 11030 data. Residual electron density (e<sup>-</sup>·Å<sup>-3</sup>) max/min: 0.460/-0.508.

**X-Ray Crystal Structure of (tPCH=CHP)FeBr<sub>2</sub> (3).** X-Ray quality single crystals were obtained from a concentrated solution of diethyl ether at -35 °C in the glovebox as pale yellow rods. Crystal and refinement data for **3**: C<sub>26</sub>H<sub>38</sub>Br<sub>2</sub>FeP<sub>2</sub>; M<sub>r</sub> = 628.17; Monoclinic; space group P2(1)/n; *a* = 15.9893(19) Å; *b* = 11.1028(13) Å; *c* = 16.3823(19) Å;  $\alpha = 90^\circ$ ;  $\beta = 107.936(2)^\circ$ ;  $\gamma = 90^\circ$ ; *V* = 2766.9(6) Å<sup>3</sup>; *Z* = 4; *T* = 120(2) K;  $\lambda = 0.71073$  Å;  $\mu = 3.561$  mm<sup>-1</sup>; *d*<sub>calc</sub> = 1.508 g·cm<sup>-3</sup>; 26462 reflections collected; 5729 unique (*R*<sub>int</sub> = 0.0880); giving *R*<sub>1</sub> = 0.0445, *wR*<sub>2</sub> = 0.0973 for 4035 data with [*I* > 2σ(*I*)] and *R*<sub>1</sub> = 0.0799, *wR*<sub>2</sub> = 0.1068 for all 5729 data. Residual electron density (e<sup>-</sup>·Å<sup>-3</sup>) max/min: 0.780/-0.967.

**X-Ray Crystal Structure of [(*t*PCH=CHP)CoCl][BAr<sup>F</sup><sub>4</sub>] (4).** X-Ray quality single crystals were obtained from a concentrated toluene solution layered with *n*-pentane at −35 °C in the glovebox. Crystal and refinement data for **4**: C<sub>129</sub>H<sub>108</sub>B<sub>2</sub>Cl<sub>2</sub>Co<sub>2</sub>F<sub>48</sub>P<sub>4</sub>; M<sub>r</sub> = 2904.41; Triclinic; space group P-1; *a* = 12.4634(16) Å; *b* = 23.274(3) Å; *c* = 24.594(3) Å; α = 74.884(3)°; β = 77.262(3)°; γ = 78.423(3)°; V = 6639.6(15) Å<sup>3</sup>; Z = 2; T = 120(2) K; λ = 0.71073 Å; μ = 0.453 mm<sup>−1</sup>; d<sub>calc</sub> = 1.453 g·cm<sup>−3</sup>; 154657 reflections collected; 23349 unique (R<sub>int</sub> = 0.0586); giving R<sub>1</sub> = 0.0711, wR<sub>2</sub> = 0.1898 for 17148 data with [I > 2σ(I)] and R<sub>1</sub> = 0.0983, wR<sub>2</sub> = 0.2049 for all 23349 data. Residual electron density (e<sup>−</sup>·Å<sup>−3</sup>) max/min: 1.779/−1.155.

**X-Ray Crystal Structure of [(*t*PCH=CHP)FeBr][BAr<sup>F</sup><sub>4</sub>] (5).** X-Ray quality single crystals were obtained from a concentrated toluene solution layered with *n*-pentane at −35 °C in the glovebox. Crystal and refinement data for **5**: C<sub>65</sub>H<sub>58</sub>BBrF<sub>24</sub>FeP<sub>2</sub>; M<sub>r</sub> = 1503.62; Triclinic; space group P-1; *a* = 13.1231(6) Å; *b* = 13.6718(7) Å; *c* = 18.7070(9) Å; α = 79.3172(19)°; β = 80.9439(19)°; γ = 86.7229(19)°; V = 3255.7(3) Å<sup>3</sup>; Z = 2; T = 120(2) K; λ = 0.71073 Å; μ = 1.004 mm<sup>−1</sup>; d<sub>calc</sub> = 1.534 g·cm<sup>−3</sup>; 71334 reflections collected; 11462 unique (R<sub>int</sub> = 0.0262); giving R<sub>1</sub> = 0.0407, wR<sub>2</sub> = 0.1049 for 9966 data with [I > 2σ(I)] and R<sub>1</sub> = 0.0485, wR<sub>2</sub> = 0.1090 for all 11462 data. Residual electron density (e<sup>−</sup>·Å<sup>−3</sup>) max/min: 1.490/−1.684.

**X-Ray Crystal Structure of (*t*PCH=CHP)CoCl (6).** X-Ray quality single crystals were obtained from a concentrated THF solution layered with *n*-pentane in a −35 °C freezer in the glovebox as dark purple blocks. Crystal and refinement data for **6**: C<sub>26</sub>H<sub>38</sub>ClCoP<sub>2</sub>; M<sub>r</sub> = 506.88; Monoclinic; space group P2(1)/c; *a* = 11.011(2) Å; *b* = 7.7640(14) Å; *c* = 29.925(6) Å; α = 90°; β = 90.224(4)°; γ = 90°; V = 2558.3(8) Å<sup>3</sup>; Z = 4; T = 120(2) K; λ =

0.71073 Å;  $\mu = 0.912 \text{ mm}^{-1}$ ;  $d_{\text{calc}} = 1.316 \text{ g}\cdot\text{cm}^{-3}$ ; 23379 reflections collected; 5325 unique ( $R_{\text{int}} = 0.0579$ ); giving  $R_1 = 0.0474$ ,  $wR_2 = 0.1050$  for 4386 data with  $[I > 2\sigma(I)]$  and  $R_1 = 0.0574$ ,  $wR_2 = 0.1078$  for all 5325 data. Residual electron density ( $\text{e}^{-}\cdot\text{\AA}^{-3}$ ) max/min: 0.360/−0.569.

**X-Ray Crystal Structure of (*t*PCH=CHP)CoCl(CO) (7).** X-Ray quality single crystals were obtained from a concentrated diethyl ether solution in a −35 °C freezer in the glovebox. Crystal and refinement data for **7**:  $\text{C}_{27}\text{H}_{38}\text{ClCoOP}_2$ ;  $M_r = 534.89$ ; Orthorhombic; space group  $\text{Pbca}$ ;  $a = 9.9988(6) \text{ \AA}$ ;  $b = 15.4852(10) \text{ \AA}$ ;  $c = 34.356(2) \text{ \AA}$ ;  $\alpha = 90^\circ$ ;  $\beta = 90^\circ$ ;  $\gamma = 90^\circ$ ;  $V = 5319.4(6) \text{ \AA}^3$ ;  $Z = 8$ ;  $T = 120(2) \text{ K}$ ;  $\lambda = 0.71073 \text{ \AA}$ ;  $\mu = 0.884 \text{ mm}^{-1}$ ;  $d_{\text{calc}} = 1.336 \text{ g}\cdot\text{cm}^{-3}$ ; 72798 reflections collected; 4673 unique ( $R_{\text{int}} = 0.1264$ ); giving  $R_1 = 0.0824$ ,  $wR_2 = 0.1280$  for 3927 data with  $[I > 2\sigma(I)]$  and  $R_1 = 0.1028$ ,  $wR_2 = 0.1333$  for all 4673 data. Residual electron density ( $\text{e}^{-}\cdot\text{\AA}^{-3}$ ) max/min: 0.639/−0.739.

**X-Ray Crystal Structure of (*t*PCH=CHP)RhCl (8).** X-Ray quality single crystals were obtained as yellow plates from a concentrated diethyl ether solution at −35 °C in the glovebox. Crystal and refinement data for **8**:  $\text{C}_{26}\text{H}_{38}\text{ClP}_2\text{Rh}$ ;  $M_r = 550.86$ ; Monoclinic; space group  $\text{P2/c}$ ;  $a = 11.8111(12) \text{ \AA}$ ;  $b = 15.7865(16) \text{ \AA}$ ;  $c = 14.7769(15) \text{ \AA}$ ;  $\alpha = 90^\circ$ ;  $\beta = 110.3090(17)^\circ$ ;  $\gamma = 90^\circ$ ;  $V = 2584.0(5) \text{ \AA}^3$ ;  $Z = 4$ ;  $T = 120(2) \text{ K}$ ;  $\lambda = 0.71073 \text{ \AA}$ ;  $\mu = 0.900 \text{ mm}^{-1}$ ;  $d_{\text{calc}} = 1.416 \text{ g}\cdot\text{cm}^{-3}$ ; 33562 reflections collected; 5298 unique ( $R_{\text{int}} = 0.0847$ ); giving  $R_1 = 0.0627$ ,  $wR_2 = 0.0906$  for 4019 data with  $[I > 2\sigma(I)]$  and  $R_1 = 0.0893$ ,  $wR_2 = 0.0958$  for all 5298 data. Residual electron density ( $\text{e}^{-}\cdot\text{\AA}^{-3}$ ) max/min: 1.349/−1.619.

**X-Ray Crystal Structure of (*t*PCH=CHP)Cu(OTf) (10).** X-Ray quality single crystals were obtained as clear blocks from a toluene solution layered with *n*-pentane at −35 °C in the glovebox. Crystal and refinement data for **10**: formula  $\text{C}_{27}\text{H}_{38}\text{CuF}_3\text{O}_3\text{P}_2\text{S}$ ;  $M_r$

= 625.11; Orthorhombic; space group Pbca;  $a = 10.2443(8)$  Å;  $b = 18.9199(15)$  Å;  $c = 30.626(3)$  Å;  $\alpha = 90^\circ$ ;  $\beta = 90^\circ$ ;  $\gamma = 90^\circ$ ;  $V = 5936.0(8)$  Å<sup>3</sup>;  $Z = 8$ ;  $T = 120(2)$  K;  $\lambda = 0.71073$  Å;  $\mu = 0.959$  mm<sup>-1</sup>;  $d_{\text{calc}} = 1.399$  g·cm<sup>-3</sup>; 119904 reflections collected; 5232 unique ( $R_{\text{int}} = 0.0628$ ); giving  $R_1 = 0.0379$ ,  $wR_2 = 0.0910$  for 4447 data with  $[I > 2\sigma(I)]$  and  $R_1 = 0.0476$ ,  $wR_2 = 0.0982$  for all 5232 data. Residual electron density ( $\text{e}^- \cdot \text{\AA}^{-3}$ ) max/min: 1.473/−0.541.

**X-Ray Crystal Structure of [(*t*PCH=CHP)Cu][PF<sub>6</sub>] (11).** X-Ray quality single crystals were obtained as clear blocks from a CH<sub>2</sub>Cl<sub>2</sub> solution layered with *n*-pentane at −35 °C in the glovebox. Crystal data for **11**: formula: C<sub>26</sub>H<sub>38</sub>CuF<sub>6</sub>P<sub>3</sub>;  $M_r = 621.01$ ; Monoclinic; space group P2(1)/c;  $a = 9.5653(4)$  Å;  $b = 21.5479(9)$  Å;  $c = 14.6122(6)$  Å;  $\alpha = 90^\circ$ ;  $\beta = 103.1306(16)^\circ$ ;  $\gamma = 90^\circ$ ;  $V = 2933.0(2)$  Å<sup>3</sup>;  $Z = 4$ ;  $T = 120(2)$  K;  $\lambda = 0.71073$  Å;  $\mu = 0.960$  mm<sup>-1</sup>;  $d_{\text{calc}} = 1.406$  g·cm<sup>-3</sup>; 43314 reflections collected; 5146 unique ( $R_{\text{int}} = 0.0580$ ); giving  $R_1 = 0.0411$ ,  $wR_2 = 0.0869$  for 4211 data with  $[I > 2\sigma(I)]$  and  $R_1 = 0.0559$ ,  $wR_2 = 0.0924$  for all 5146 data. Residual electron density ( $\text{e}^- \cdot \text{\AA}^{-3}$ ) max/min: 2.142/−1.079.

**X-Ray Crystal Structure of [(*t*PCH=CHP)Ag][PF<sub>6</sub>] (12).** X-Ray quality single crystals were obtained as clear blocks from a CH<sub>2</sub>Cl<sub>2</sub> solution layered with *n*-pentane at −35 °C in the glovebox. Crystal and refinement data for **12**: formula C<sub>26</sub>H<sub>38</sub>AgF<sub>6</sub>P<sub>3</sub>;  $M_r = 665.34$ ; Orthorhombic; space group P2(1)2(1)2(1);  $a = 9.8584(6)$  Å;  $b = 12.6977(7)$  Å;  $c = 23.1548(13)$  Å;  $\alpha = 90^\circ$ ;  $\beta = 90^\circ$ ;  $\gamma = 90^\circ$ ;  $V = 2898.5(3)$  Å<sup>3</sup>;  $Z = 4$ ;  $T = 120(2)$  K;  $\lambda = 0.71073$  Å;  $\mu = 0.914$  mm<sup>-1</sup>;  $d_{\text{calc}} = 1.525$  g·cm<sup>-3</sup>; 53763 reflections collected; 7281 unique ( $R_{\text{int}} = 0.0390$ ); giving  $R_1 = 0.0271$ ,  $wR_2 = 0.0590$  for 6793 data with  $[I > 2\sigma(I)]$  and  $R_1 = 0.0313$ ,  $wR_2 = 0.0611$  for all 7281 data. Residual electron density ( $\text{e}^- \cdot \text{\AA}^{-3}$ ) max/min: 0.562/−0.481.



## 2.5 References

1. Bennett, M. A.; Johnson, R. N.; Tomkins, I. B., *J. Organomet. Chem.* **1976**, *118* (2), 205-232.
2. Bennett, M. A.; Clark, P. W., *J. Organomet. Chem.* **1976**, *110* (3), 367-381.
3. Bennett, M. A.; Corlett, S.; Robertson, G. B.; Steffen, W. L., *Aust. J. Chem.* **1980**, *33* (6), 1261-1273.
4. Verhoeven, D. G. A.; Moret, M.-E., *Dalton Trans.* **2016**, *45* (40), 15762-15778.
5. Polukeev, A. V.; Wendt, O. F., *Organometallics* **2015**, *34* (17), 4262-4271.
6. Polukeev, A. V.; Marcos, R.; Ahlquist, M. S. G.; Wendt, O. F., *Chem. Sci.* **2015**, *6* (3), 2060-2067.
7. Takimiya, K.; Shibata, Y.; Ohnishi, A.; Aso, Y.; Otsubo, T.; Ogura, F., *J. Mater. Chem.* **1995**, *5* (10), 1539-1547.
8. Bennett, M. A.; Clark, P. W., *J. Organomet. Chem.* **1976**, *110* (3), 367-381.
9. Bennett, M. A.; Corlett, S.; Robertson, G. B.; Steffen, W. L., *Aust. J. Chem.* **1980**, *33* (6), 1261-1273.
10. Yang, F.; Zhou, Q.; Zhang, Y. Q.; Zeng, G.; Li, G. H.; Shi, Z.; Wang, B. W.; Feng, S. H., *Chem. Commun.* **2013**, *49* (46), 5289-5291.
11. Marlier, E. E.; Tereniak, S. J.; Ding, K. Y.; Mulliken, J. E.; Lu, C. C., *Inorg. Chem.* **2011**, *50* (19), 9290-9299.
12. Affo, W.; Ohmiya, H.; Fujioka, T.; Ikeda, Y.; Nakamura, T.; Yorimitsu, H.; Oshima, K.; Imamura, Y.; Mizuta, T.; Miyoshi, K., *J. Am. Chem. Soc.* **2006**, *128* (24), 8068-8077.
13. Sharma, R. K.; RajanBabu, T. V., *J. Am. Chem. Soc.* **2010**, *132* (10), 3295-+.
14. Mizuta, T.; Imamura, Y.; Miyoshi, K.; Yorimitsu, H.; Oshima, K., *Organometallics* **2005**, *24* (5), 990-996.
15. Hou, J. X.; Sun, W. H.; Zhang, S.; Ma, H. W.; Deng, Y.; Lu, X. M., *Organometallics* **2006**, *25* (1), 236-244.
16. Wang, M.; Yu, X. M.; Shi, Z.; Qian, M. X.; Jin, K.; Chen, J. H.; He, R., *J. Organomet. Chem.* **2002**, *645* (1-2), 127-133.
17. Dong, Q. C.; Rose, M. J.; Wong, W. Y.; Gray, H. B., *Inorg. Chem.* **2011**, *50* (20), 10213-10224.

18. Grutters, M. M. P.; van der Vlugt, J. I.; Pei, Y.; Mills, A. M.; Lutz, M.; Spek, A. L.; Müller, C.; Moberg, C.; Vogt, D., *Adv. Synth. Catal.* **2009**, *351* (13), 2199-2208.
19. Brescianipahor, N.; Calligaris, M.; Randaccio, L.; Marzilli, L. G., *Inorg. Chim. Acta.* **1979**, *32* (2), 181-187.
20. Chadwell, S. J.; Coles, S. J.; Edwards, P. G.; Hursthouse, M. B., *J. Chem. Soc. Dalton Trans.* **1995**, (21), 3551-3559.
21. Deblon, S.; Liesum, L.; Harmer, J.; Schonberg, H.; Schweiger, A.; Grutzmacher, H., *Chem. Eur. J.* **2002**, *8* (3), 601-611.
22. Snyder, B. S.; Holm, R. H., *Inorg. Chem.* **1988**, *27* (13), 2339-2347.
23. Kornev, A. N.; Belina, N. V.; Sushev, V. V.; Fukin, G. K.; Baranov, E. V.; Kurskiy, Y. A.; Poddelskii, A. I.; Abakumov, G. A.; Lonnecke, P.; Hey-Hawkins, E., *Inorg. Chem.* **2009**, *48* (12), 5574-5583.
24. Fryzuk, M. D.; Leznoff, D. B.; Ma, E. S. F.; Rettig, S. J.; Young, V. G., *Organometallics* **1998**, *17* (11), 2313-2323.
25. Hawrelak, E. J.; Bernskoetter, W. H.; Lobkovsky, E.; Yee, G. T.; Bill, E.; Chirik, P. J., *Inorg. Chem.* **2005**, *44* (9), 3103-3111.
26. Meehan, P. R.; Alyea, E. C.; Shakya, R. P.; Ferguson, G., *Polyhedron* **1998**, *17* (1), 11-16.
27. Rozenel, S. S.; Padilla, R.; Arnold, J., *Inorg. Chem.* **2013**, *52* (19), 11544-11550.
28. Hermes, A. R.; Girolami, G. S., *Organometallics* **1987**, *6* (4), 763-768.
29. Sciarone, T. J. J.; Nijhuis, C. A.; Meetsma, A.; Hessen, B., *Organometallics* **2008**, *27* (9), 2058-2065.
30. Jové, F. A.; Pariya, C.; Scoblete, M.; Yap, G. P. A.; Theopold, K. H., *Chem. Eur. J.* **2011**, *17* (4), 1310-1318.
31. Black, M.; Mais, R. H. B.; Owston, P. G., *Acta. Cryst. B.-Struct.* **1969**, *B 25*, 1753-1759.
32. Hartley, F. R., *Angew. Chem. Int. Ed.* **1972**, *11* (7), 596-606.
33. Dodoff, N. I.; Lalia-Kantouri, M.; Gdaniec, M.; Czapik, A.; Vassilev, N. G.; Markova, L. S.; Apostolova, M. D., *J. Coord. Chem.* **2012**, *65* (4), 688-704.
34. Klein, H. F.; Karsch, H. H., *Inorg. Chem.* **1975**, *14* (3), 473-477.

35. Hayashi, Y.; Szalda, D. J.; Grills, D. C.; Hanson, J. C.; Huang, K. W.; Muckerman, J. T.; Fujita, E., *Polyhedron* **2013**, *58*, 106-114.
36. Vigalok, A.; Milstein, D., *J. Am. Chem. Soc.* **1997**, *119* (33), 7873-7874.
37. Okamoto, K.; Omoto, Y.; Sano, H.; Ohe, K., *Dalton Trans.* **2012**, *41* (36), 10926-10929.
38. Vigalok, A.; Rybtchinski, B.; Shimon, L. J. W.; Ben-David, Y.; Milstein, D., *Organometallics* **1999**, *18* (5), 895-905.
39. Feller, M.; Ben-Ari, E.; Gupta, T.; Shimon, L. J. W.; Leitun, G.; Diskin-Posner, Y.; Weiner, L.; Milstein, D., *Inorg. Chem.* **2007**, *46* (25), 10479-10490.
40. Jia, G. C.; Lee, H. M.; Williams, I. D., *Organometallics* **1996**, *15* (20), 4235-4239.
41. Kumar, S.; Mani, G.; Dutta, D.; Mishra, S., *Inorg. Chem.* **2014**, *53* (2), 700-709.
42. van der Vlugt, J. I.; Pidko, E. A.; Vogt, D.; Lutz, M.; Spek, A. L.; Meetsma, A., *Inorg. Chem.* **2008**, *47* (11), 4442-4444.
43. Harmata, M.; Ghosh, S. K.; Barnes, C. L., *J. Supramol. Chem.* **2002**, *2* (1-3), 349-351.
44. Masuda, H.; Yamamoto, N.; Taga, T.; Machida, K.; Kitagawa, S.; Munakata, M., *J. Organomet. Chem.* **1987**, *322* (1), 121-129.
45. Thompson, J. S.; Harlow, R. L.; Whitney, J. F., *J. Am. Chem. Soc.* **1983**, *105* (11), 3522-3527.
46. Budagumpi, S.; Haque, R. A.; Salman, A. W.; Ghdhayeb, M. Z., *Inorg. Chim. Acta.* **2012**, *392* (0), 61-72.
47. van der Vlugt, J. I.; Siegler, M. A.; Janssen, M.; Vogt, D.; Spek, A. L., *Organometallics* **2009**, *28* (24), 7025-7032.
48. Carvajal, M. A.; Novoa, J. J.; Alvarez, S., *J. Am. Chem. Soc.* **2004**, *126* (5), 1465-1477.
49. Reisinger, A.; Trapp, N.; Knapp, C.; Himmel, D.; Breher, F.; Rügger, H.; Krossing, I., *Chem. Eur. J.* **2009**, *15* (37), 9505-9520.
50. DeMott, J. C.; Basuli, F.; Kilgore, U. J.; Foxman, B. M.; Huffman, J. C.; Ozerov, O. V.; Mindiola, D. J., *Inorg. Chem.* **2007**, *46* (16), 6271-6276.
51. Gualco, P.; Amgoune, A.; Miqueu, K.; Ladeira, S.; Bourissou, D., *J. Am. Chem. Soc.* **2011**, *133* (12), 4257-4259.

52. Bain, G. A.; Berry, J. F., *J. Chem. Ed.* **2008**, 85 (4), 532-536.
53. Sur, S. K., *J. Mag. Res.* **1989**, 82 (1), 169-173.
54. Evans, D. F., *J. Chem. Soc.* **1959**, (Jun), 2003-2005.
55. Frisch, M. J.
56. Zhang, X.; Yang, Y.; Liang, Y., *Tetrahedron Lett.* **2012**, 53 (47), 6406-6408.
57. Bruker AXS,. APEX-2. bruker-Nonius AXS, Madison, Wisconsin, USA, 2014.
58. Krause, L.; Herbst-Irmer, R.; Sheldrick, G. M.; Stalke, D., *J. Appl. Cryst.* **2015**, 48 (1), 3-10.
59. Sheldrick, G.M., *Acta Cryst.* **2015**, A71 (1), 3-8.
60. Dolomanov, O. V.; Bourhis, L. J.; Gildea, R. J.; Howard, J. A. K.; Puschmann, H., *J. Appl. Crystallogr.* **2009**, 42 (2), 339-341.
61. Sheldrick, G.M., *Acta Cryst.* **2015**, C71 (1), 3-8.
62. Macrae, C. F.; Bruno, I. J.; Chisholm, J. A.; Edgington, P. R.; McCabe, P.; Pidcock, E.; Rodriguez-Monge, L.; Taylor, R.; van de Streek, J.; Wood, P. A., *J. Appl. Cryst.* **2008**, 41 (2), 466-470.

## CHAPTER 3:

### GROUP 10 METAL COMPLEXES SUPPORTED BY PINCER LIGANDS WITH A TRANS OLEFINIC BACKBONE

#### 3.1 Introduction

In addition to investigating the hemilabile characteristics of ligand **1**, *t*PCH=CHP, it was also of interest to determine if the olefin backbone could be non-innocent and act as a hydrogen atom acceptor.<sup>1</sup> Bennett and coworkers initially reported 2,2'-bis(diphenylphosphino)-*trans*-stilbene (bdps) and observed that group 10 metals form monoanionic  $\kappa^3$ -PCP complexes in the +2 oxidation state (Figure 3.1).<sup>2-4</sup> However, the choice of an olefinic backbone allows various options such as non-coordination,  $\eta^2$ -coordination in the neutral form, and  $\eta^1$ -coordination in the vinyl form, when the backbone could function as a hydrogen atom reservoir.

To probe the ability of the olefinic backbone to switch between various coordination modes, we also replaced the olefinic protons with methyl groups and studied the coordination chemistry of 2,2'-bis(di-*iso*-propylphosphino)-*trans*-diphenyl-1,2-dimethylethene (*t*PCMe=CMeP, **17**). Furthermore, reactivity studies indicate that the vinyl backbone is non-innocent and can function as a hydrogen acceptor.

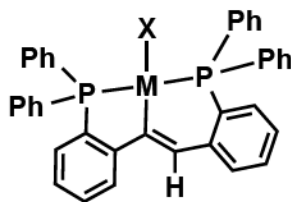
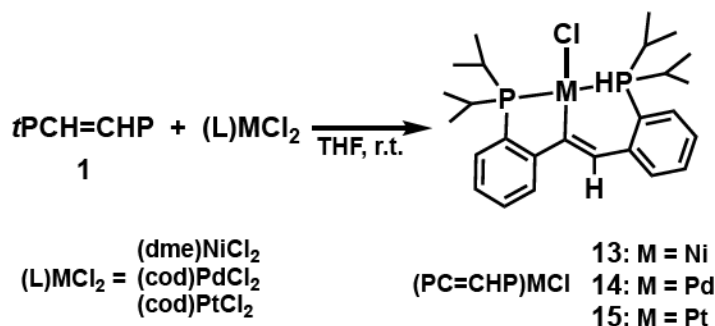


**Figure 3.1:** Coordination of 2,2'-bis(diphenylphosphino)-*trans*-stilbene to group 10 metals (M = Pd, Pt).<sup>3</sup>

### 3.2 Results and Discussion

Metal  $d^8$  complexes (PC=CHP)NiCl (**13**), (PC=CHP)PdCl (**14**), and (PC=CHP)PtCl (**15**) form readily upon the addition of **1** to the appropriate metal precursor (Scheme 3.1), similarly to what Bennett observed for the phenyl derivative.<sup>3,5</sup> Uniquely, the reaction involving the nickel precursor leads to two products: **13**, which is analogous to the previously characterized nickel complex (*o*-Ph<sub>2</sub>P-C<sub>6</sub>H<sub>4</sub>-C=CH-C<sub>6</sub>H<sub>4</sub>-PPh<sub>2</sub>-*o*)NiCl, and another product, which was not characterized because of its insolubility in common organic solvents.<sup>6</sup> Compounds **13**, **14**, and **15** result from the C-H activation of the backbone followed by rapid reductive elimination of HCl. All three  $d^8$  metals tend to favor the anionic form of the backbone consistently, a notion supported by Bennett's observations with the phenyl analogue of the ligand.<sup>3</sup> Bennett observed a similar behavior when reacting bdps (bdps = bis(diphenylphosphino)-*trans*-stilbene) with (cod)MCl<sub>2</sub> (M = Pd, Pt) and (cod)Pt(CH<sub>3</sub>)<sub>2</sub>. Ni(II) vinyl complexes are usually isolated as the insertion products of alkynes into nickel aryl bonds,<sup>7-8</sup> by oxidative addition of vinyl chloride to Ni(I)<sup>9</sup> and by cyclization reactions.<sup>10</sup> Palladium(II) salts have been known to remove vinylic hydrogens from olefins.<sup>11</sup> Other vinyl Pd(II) complexes have been isolated by oxidative addition of a C-Cl bond to a Pd(0) center<sup>12</sup> or rearrangement of Pd(II) allyl

complexes.<sup>13</sup> A similar behavior of Pt(II) was observed by Shaw for (<sup>t</sup>Bu<sub>2</sub>P(CH<sub>2</sub>)<sub>3</sub>P<sup>t</sup>Bu<sub>2</sub>)PtCl<sub>2</sub>, where after several C-H activations a similar complex, (<sup>t</sup>Bu<sub>2</sub>P(CH<sub>2</sub>)<sub>2</sub>-C=CH-P<sup>t</sup>Bu<sub>2</sub>)PtCl, was isolated, invoking an η<sup>2</sup> olefin intermediate.<sup>14</sup>



**Scheme 3.1:** Synthesis of complexes **13-15**.

The non-symmetrical coordination mode of *t*PC=CHP in **13**, **14**, and **15** is supported by the aryl region in the corresponding <sup>1</sup>H and <sup>31</sup>P NMR spectra. All species are identified by two doublets in the <sup>31</sup>P NMR spectrum and exhibit *trans* phosphorus couplings of 288, 387, and 382 Hz respectively. The platinum satellites for compound **15** are also observed in the <sup>31</sup>P NMR spectrum. In addition, compound **13** displays a broad singlet at 6.83 ppm in the <sup>1</sup>H NMR spectrum assigned to the olefinic proton. The broadness of this peak is attributed to unresolved coupling with the phosphorous atoms. The olefinic proton for compound **14** is lost in the aryl region of the spectrum, while compound **4** contains a doublet at 7.63 ppm along with Pt satellites at 7.74 and 7.51 ppm respectively (*J*<sub>PtH</sub> = 48 Hz).

The structures of compounds **13-14** were determined by single crystal X-ray diffraction and show a square planar coordination environment around the respective metal center (Figures 3.2, 3.3). In the case for **15**, the single crystal X-ray diffraction data was of low quality, however, connectivity information could be obtained and the structure is

similar to that of **13** and **14**. The C(1)–C(2) bond is in the typical range of a C–C double bond (1.351(3) Å for **13** and 1.329(4) Å for **14**). The Ni(II) complex is more distorted from a square-planar geometry (Figure 3.2), the angle P(1)–Ni–P(2) is 165.91(3)° compared to 173.59(3)° for the corresponding Pd(II) complex (Figure 3.3). In both cases, the two phenylene rings of the ligand are not coplanar, possibly to reduce the steric interaction between the vinylic and aromatic hydrogen atoms.

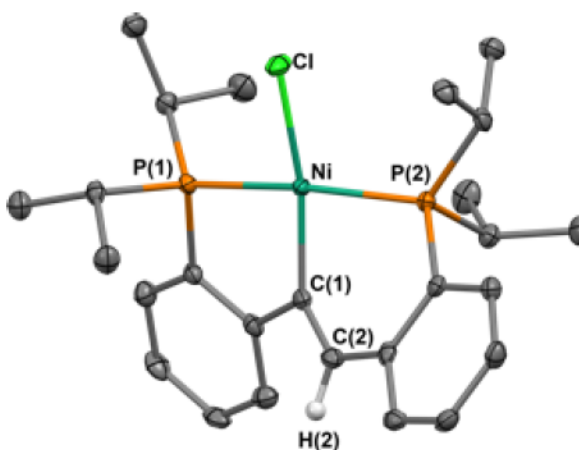


**Figure 3.2:** Thermal-ellipsoid (50% probability level) representation of **13**. Most hydrogen atoms were omitted for clarity. Selected distances (Å) and angles (°): Ni–P(1) = 2.1891(6), Ni–P(2) = 2.1884(6), Ni–Cl = 2.2127(6), Ni–C(1) = 1.930(2), C(1)–C(2) = 1.351(3) Å, P(1)–Ni–P(2) = 165.91(3), Cl–Ni–P(1) = 99.13(2), Cl–Ni–P(2) = 99.72(2), C(1)–Ni–P(1) = 90.13(2), C(1)–Ni–P(2) = 87.01(6), C(1)–Ni–Cl = 167.63(7).



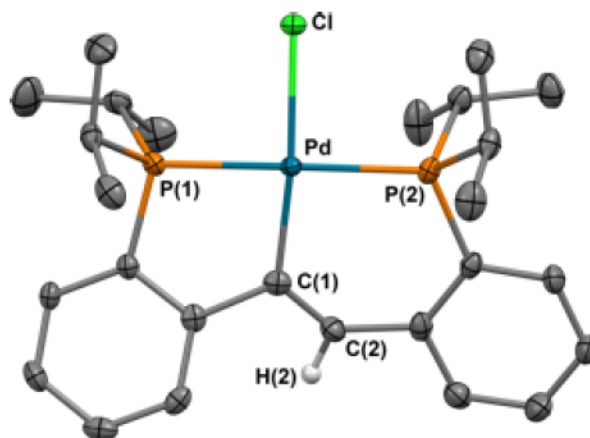
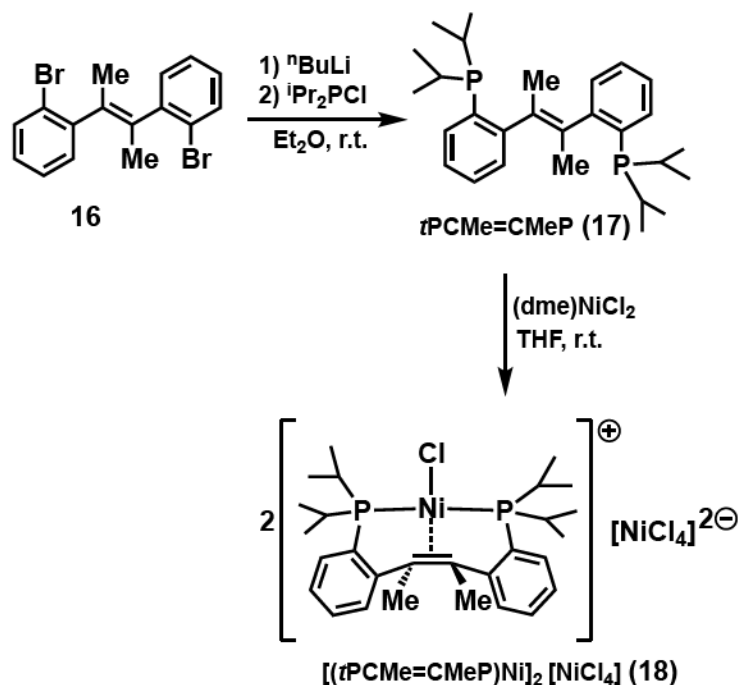


**Figure 3.3:** Thermal-ellipsoid (50% probability level) representation of **14**. Most hydrogen atoms were omitted for clarity. Selected distances (Å) and angles (°): Pd–P(1) = 2.2942(7), Pd–P(2) = 2.3160(7), Pd–Cl = 2.3919(7), Pd–C(1) = 2.033(3), C(1)–C(2) = 1.329(4), Cl–Pd–P(1) = 90.35(3), Cl–Pd–P(2) = 90.99(3), P(1)–Pd–P(2) = 173.59(3), C(1)–Pd–P(1) = 83.74(8), C(1)–Pd–Cl = 170.46(8).

Since the deprotonation of the olefinic backbone is rather unusual, we decided to study the reactions of 2,2'-bis(di-*iso*-propylphosphino)-*trans*-diphenyl-1,2-dimethylethene (*t*PCMe=CMeP, **17**), in which methyl groups replace the olefinic protons of **1**. A McMurry coupling reaction can be performed on 2'-bromoacetophenone to generate bis(2-bromophenyl)-2-butene (**16**, Scheme 3.2).<sup>15</sup> This particular reaction generates a higher yield of the *cis* (91%) than *trans* product (9%). Trituration of the crude product with *n*-hexane led to the isolation of the clean *trans* isomer due to solubility differences. From bis(2-bromophenyl)-2-butene (**16**), the same synthetic procedure used to generate *t*PCH=CHP (**1**) can be used to produce *t*PCMe=CMeP (**17**).

Reaction of two equivalents of *t*PCMe=CMeP (**17**) with three equivalents of (dme)NiCl<sub>2</sub> generates [(*t*PCMe=CMeP)NiCl]<sub>2</sub>[NiCl<sub>4</sub>], **18** (Scheme 3.2). Interestingly,  $\eta^2$  coordination is observed in **18** (Figure 3.4), a stark contrast to the  $\eta^1$  coordination mode observed with *t*PCH=CHP (**1**). The forced  $\eta^2$  coordination of the olefin in **18** causes the

formation of a cationic species, with  $\text{NiCl}_4^{2-}$  as a counteranion, which broadens the  $^1\text{H}$  NMR spectra. The methyl groups in the backbone of  $t\text{PCMe}=\text{CMeP}$  (**17**) are equivalent with a shift at 2.08 ppm, similar to the shift found in the free ligand, at 2.12 ppm. The phosphines in this complex are also equivalent and resonate as a singlet at 64.40 ppm in the corresponding  $^{31}\text{P}$  NMR spectra. The solid state molecular structure (Figure 3.4) also indicates a square planar coordination environment at the metal center and an elongated olefinic C-C distance (1.398(3) Å), consistent with the presence of  $\pi$  backbonding in **18**. The formation of **18** indicates that the absence of olefinic protons in  $t\text{PCMe}=\text{CMeP}$  renders the ligand analogous to previously reported PNP systems, in which the nitrogen donor is neutral and the corresponding nickel(II) complexes are cationic, such as  $[(\text{PONOP})\text{NiCl}][\text{Cl}]$  (PONOP = 2,6-bis(di-*tert*-butylphosphinito)-pyridine),<sup>16</sup>  $[(\text{PNHP}^{\text{Cy}})\text{NiBr}][\text{Br}]$  ( $\text{PNHP}^{\text{Cy}} = \text{HN}[\text{CH}_2\text{CH}_2\text{P}(\text{Cy})_2]_2$ ),<sup>17</sup> and  $[(\text{PNP}^{\text{tBu}})\text{Ni}(\text{NCMe})][\text{BF}_4]$  ( $\text{PNP}^{\text{tBu}} = 2,6\text{-bis}[(\text{di-}t\text{-butylphosphino)methyl]pyridine$ ).<sup>18</sup>



**Scheme 3.2:** Synthesis of  $t\text{PCMe}=\text{CMeP}$  (**17**) and complex **18**.

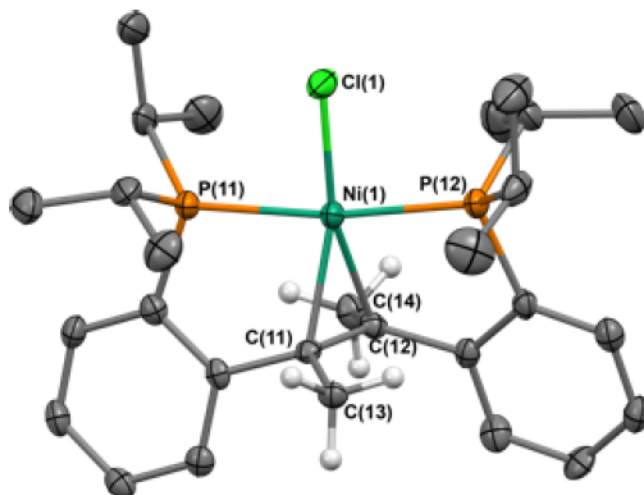


**Figure 3.4:** Thermal-ellipsoid (50% probability level) representation of **18**. Only one of the two crystallographically independent molecules is shown. Most hydrogen atoms and the counterion were omitted for clarity. Selected distances (Å) and angles (°): Ni(1)–Cl(1) = 2.1695(9), Ni(1)–P(11) = 2.2283(8), Ni(1)–P(12) = 2.2272(8), C(11)–C(12) = 1.398(3), Cl(1)–Ni(1)–P(11) = 85.53(3), Cl(1)–Ni(1)–P(12) = 85.56(3), Cl(1)–Ni(1)–P(11) = 105.58(7), P(12)–Ni(1)–P(11) = 171.10(3).

Metal  $d^{10}$  complexes were also synthesized. Compound (*t*PCH=CHP)Ni (**19**) was obtained readily from the reaction of **1** with (cod)<sub>2</sub>Ni in THF (Scheme 3.3). The product was isolated as a pure crystalline material in good yield by recrystallization from *n*-pentane. The <sup>1</sup>H NMR spectrum of **19** shows a  $C_2$  symmetric compound as indicated by the two environments for the four isopropyl methine positions at 2.14 and 1.90 ppm, respectively. The olefinic protons resonate as a singlet at 4.62 ppm. This upfield shift indicates that  $\pi$ -backbonding is present in this complex, a formulation also supported by the elongated C(11)–C(12) distance of 1.406(5) Å (Figure 3.5).<sup>19–20</sup> The trigonal planar geometry of this complex has been observed for other Ni(0) complexes. However, few examples of Ni(0) species supported solely by a chelating ligand itself exist.<sup>21</sup> Agapie and coworkers reported a diphosphine arene pincer system, which is capable of stabilizing the metal center by coordinating in an  $\eta^2$  fashion to the arene group along with the phosphine arms and generates a trigonal planar complex similar to **19**.<sup>22–23</sup> Other systems have shown the need

for an additional ligand to stabilize the metal, such as the previously reported  $\{\text{RN}(\text{CH}_2\text{P}^i\text{Pr}_2)_2\}\text{Ni}(\text{C}_2\text{H}_4)$  ( $\text{R} = \text{Me}, ^i\text{Pr}$ ), in which the amine functionality remains dissociated from the metal center. In that example, an olefin is present to donate electron density to the metal.<sup>24</sup>

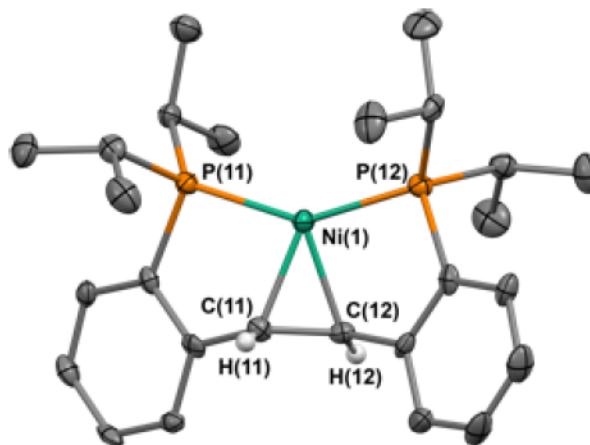
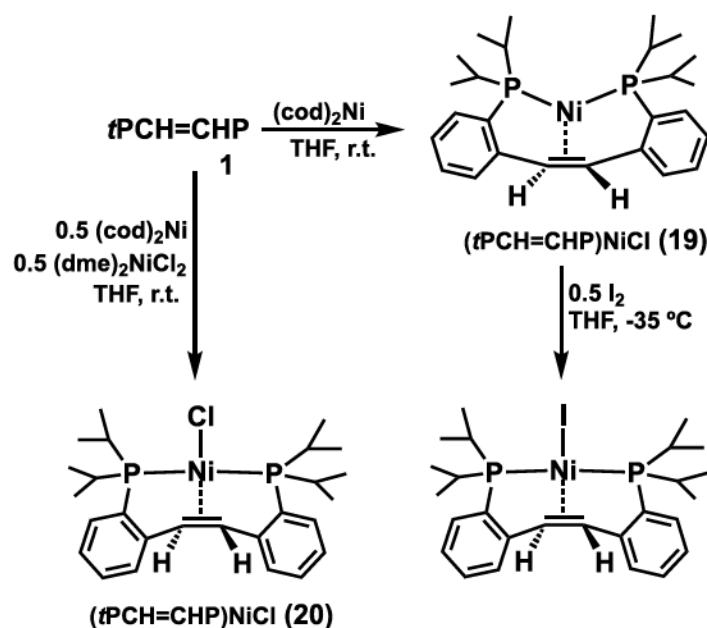


**Figure 3.5:** Thermal-ellipsoid (50% probability level) representation of **19**. Only one of the two crystallographically independent molecules is shown. Most hydrogen atoms were omitted for clarity. Selected distances (Å) and angles (°): Ni(1)–P(12) = 2.1385(13), Ni(1)–P(11) = 2.1463(13), Ni(1)–C(12) = 1.968(4), Ni(1)–C(11) = 1.968(4), C(11)–C(12) = 1.406(5), P(11)–Ni(1)–P(12) = 146.35(5).

A comproportionation reaction<sup>25-27</sup> was then attempted with in situ generated nickel(II) and nickel(0) complexes in order to generate a nickel(I) species (Scheme 3.3). Two solutions were made, one containing **1** and  $(\text{cod})_2\text{Ni}$  and the other **1** and  $(\text{dme})\text{NiCl}_2$ , which were stirred separately for 30 minutes. The mixtures were then combined and stirred for an additional hour. An NMR spectrum of the crude reaction mixture showed the presence of multiple products, of which  $(t\text{PCH}=\text{CHP})\text{NiCl}$  (**13**) was dominant. Because the fast C–H activation of the ligand (see above) we were unable to optimize the reaction conditions to avoid the side products. X-ray quality crystals were obtained from a concentrated toluene solution of the reaction mixture. The solid state molecular structure

of **20** (Figure 3.6) shows the presence of a tetrahedral Ni(I) species in which the ligand coordinates through the phosphines and the olefinic backbone.

The analogous iodide, (*t*PCH=CHP)NiI (**21**), could be obtained on a large scale by adding a chilled THF solution of a half an equivalent of I<sub>2</sub> dropwise to a chilled solution of (*t*PCH=CHP)Ni (**19**) (Scheme 3.3). The <sup>1</sup>H NMR spectrum of the resulting product showed broad peaks, consistent with the presence of a paramagnetic product, while the corresponding <sup>31</sup>P NMR spectrum was silent. Crystals suitable for X-ray diffraction were obtained from a concentrated solution of diethyl ether (Figure 3.6). The solid state molecular structure is analogous to that of (*t*PCH=CHP)NiCl (**20**) and indicates a distorted tetrahedral geometry around the metal center with angles ranging from 108.275(16) to 124.78(2)°. In general, monomeric Ni(I) species have a trigonal planar geometry,<sup>27-29</sup> such as (Pr<sub>3</sub>P)<sub>2</sub>NiX (X = Cl, Br, I),<sup>25</sup> while reported tetrahedral Ni(I) species are dimers, such as [(dtbpe)NiCl]<sub>2</sub>,<sup>30</sup> thus the presence of the olefinic backbone in **20** and **21** helps stabilize the metal center in its tetrahedral form, allowing it to maintain its monomeric nature.



**Scheme 3.3:** Synthesis of complexes **19-20**.

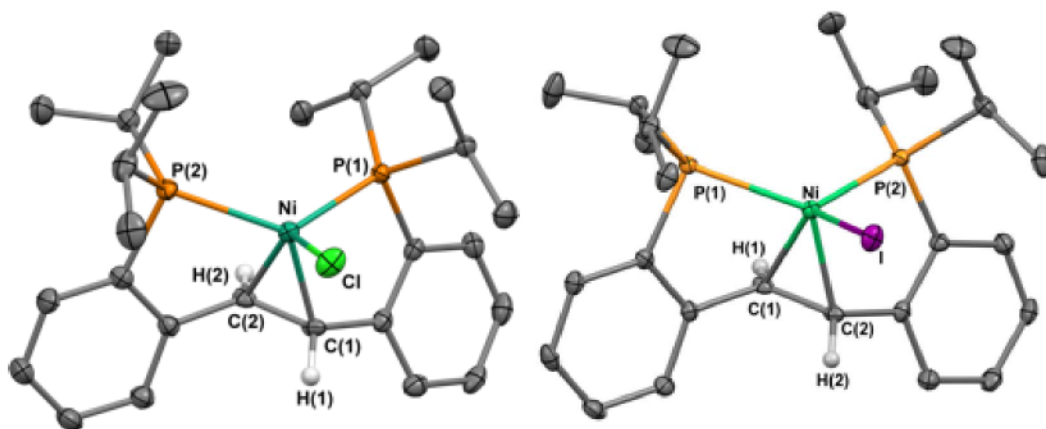
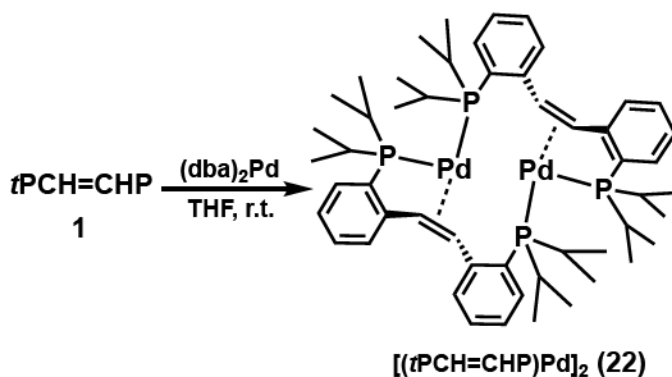


**Figure 3.6** Thermal-ellipsoid (50% probability level) representation of **20** (left) and **21** (right). Most hydrogen atoms were omitted for clarity. Selected distances (Å) and angles (°): For **20**: Ni-Cl = 2.2498(7), Ni-P(1) = 2.2569(7), Ni-P(2) = 2.2905(7), C(1)-C(2) = 1.394(3), Cl-Ni-P(1) = 110.46(3), P(1)-Ni-P(2) = 125.10(3), Cl-Ni-P(2) = 107.24(3). For **21**: I-Ni = 2.5717(4), Ni-P(1) = 2.3039(6), Ni-P(2) = 2.2521(7), C(1)-C(2) = 1.390(3), P(1)-Ni-P(2) = 124.78(2), P(1)-Ni-I = 112.000(18), P(2)-Ni-I = 108.275(16).

A palladium(0) compound was next synthesized by stirring **1** with bis(dibenzylideneacetone)palladium(0) ( $\text{Pd}(\text{dba})_2$ ) for 1 h (Scheme 3.4). Single crystal X-ray diffraction (Figure 3.7) indicated the formation of a dimer, **22**, in which each ligand binds to one palladium through one phosphine and the olefin. The remaining phosphine coordinates to an adjacent metal center. Each palladium center exhibits a distorted trigonal planar geometry with a P-Pd-P angle of  $122.74(4)^\circ$ . The  $^1\text{H}$  NMR spectrum of **22** shows the olefinic protons at 5.91 ppm, shifted upfield compared to the corresponding protons of the free ligand. All four methine positions are equivalent and appear as a broad multiplet at 2.15 ppm. Evaluation of the corresponding  $^{31}\text{P}$  NMR spectrum shows equivalent phosphorus atoms as indicated by the presence of a sharp singlet at 55.28 ppm. Both  $^1\text{H}$  and  $^{31}\text{P}$  NMR spectra indicated that **21** is found as a monomer in solution. We propose that, in solution, the dimer dissociates and forms a monomeric species similar to that observed for the nickel(0) complex **19**.



**Scheme 3.4:** Synthesis of **22**.

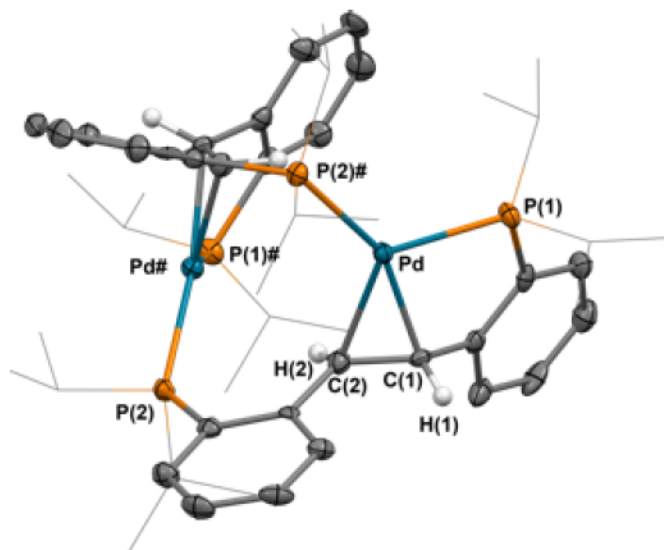


**Figure 3.7:** Thermal-ellipsoid (50% probability level) representation of **22**. Most hydrogen atoms were omitted, and some carbon atoms represented in wireframe for clarity. Selected distances (Å) and angles (°): Pd–P(1) = 2.3145(11), Pd–P(2)# = 2.3510(11), C(1)–C(2) = 1.398(5), P(1)–Pd–P(2)# = 122.74(4).

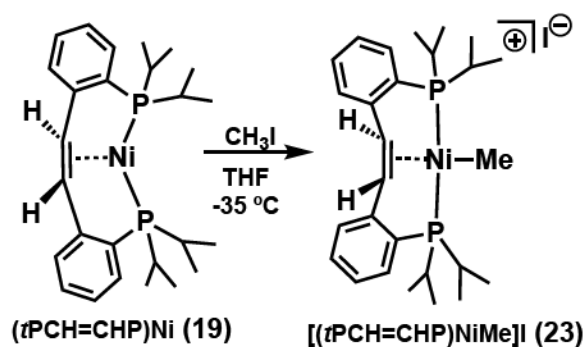
### 3.3 Reactivity Studies

Given the various coordination modes of *t*PCH=CHP (**1**) observed especially with nickel complexes, we decided to initiate a reactivity study to probe the adaptability of the ligand coordination modes throughout the course of chemical reactions. Two compounds were targeted: (*t*PCH=CHP)Ni (**19**), which shows an  $\eta^2$ -olefinic backbone, and (*t*PC=CHP)NiCl (**13**), which contains an  $\eta^1$ -vinyl backbone.

Reaction of (*t*PCH=CHP)Ni (**19**) with one equivalent CH<sub>3</sub>I (Scheme 3.5) led to the formation of the cationic methyl nickel complex, [(*t*PCH=CHP)NiMe]<sup>+</sup>I<sup>−</sup> (**23**), with no change in the coordination mode of the olefinic backbone. The formation of a cationic species upon the addition of CH<sub>3</sub>I to nickel(0) has been previously observed for an amine based PNP nickel(0) complex, (PNHP)Ni (PNHP = HN(CH<sub>2</sub>CH<sub>2</sub>NHPr<sub>2</sub>)<sub>2</sub>).<sup>31-32</sup> Compound **23** was characterized by <sup>1</sup>H and <sup>31</sup>P NMR spectroscopy in solution, and by X-



ray crystallography in the solid state.  $^1\text{H}$  NMR spectroscopy shows the olefin protons resonating as a singlet at 5.87 ppm, consistent with a bound olefin experiencing  $\pi$ -backbonding with the metal center. The new methyl ligand is found at 0.9 ppm, and is overlapping with those corresponding to the methyl *iso*-propyl groups.  $^{31}\text{P}$  NMR spectroscopy shows two equivalent environments for the phosphine atoms, which resonate as a singlet at 59.68 ppm, again, supporting the  $\eta^2$ -coordination mode of the olefinic backbone. Comparison of the solid state molecular structure (Figure 3.8) with that of  $(\text{tPCH=CHP})\text{Ni}$  (**19**) shows elongation of the Ni-C distances between the metal and the olefin from 1.968(4)-1.972(4) Å to 2.1148(19)-2.1355(19) Å. The addition of a new ligand to the coordination sphere also has the effect of shortening the C-C distance of the backbone from 1.406(5) Å to 1.383(3) Å, as expected in the presence of a more electron deficient metal center.



**Scheme 3.5:** Reactivity of **19** towards  $\text{CH}_3\text{I}$ .

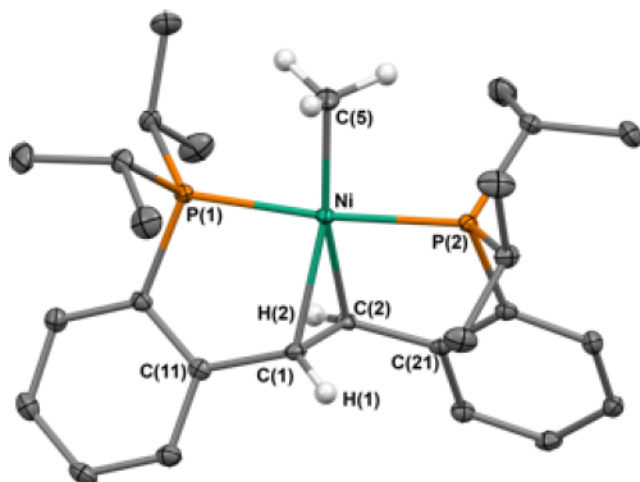
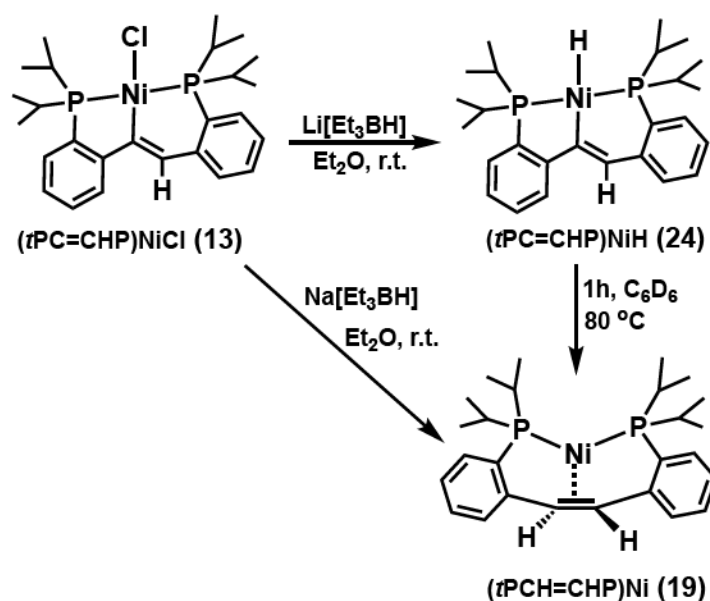


**Figure 3.8:** Thermal-ellipsoid (50% probability level) representation of **23**. Most hydrogen atoms were omitted for clarity. Selected distances (Å) and angles (°): Ni–P(1) = 2.2062(6), Ni–P(2) = 2.2095(6), Ni–C(5) = 1.982(2), Ni–C(1) = 2.1355(19), Ni–C(2) = 2.1148(19), C(1)–C(2) = 1.383(3), P(1)–Ni–P(2) = 174.07(2), P(1)–Ni–C(5) = 87.45(7), P(2)–Ni–C(5) = 87.48(7).

In order to determine whether the vinyl backbone could act as a H-atom acceptor, the nickel(II) hydride complex (*t*PC=CHP)NiH (**24**) was targeted from the corresponding chloride, (*t*PC=CHP)NiCl (**13**) (Scheme 3.6). Reaction with Li[HBET<sub>3</sub>] led to the desired nickel hydride species, as indicated by a characteristic hydride signal in the <sup>1</sup>H NMR spectrum of the crude reaction mixture at -10.65 ppm. However, after full conversion to (*t*PC=CHP)NiH (**24**) was determined by <sup>1</sup>H NMR spectroscopy, the reaction workup led to the observation of the nickel(0) complex (*t*PCH=CHP)Ni (**19**). Heating the crude reaction mixture to 80 °C for 1 h led to clean conversion to **19**. Reaction of **13** with one equivalent of Na[HBET<sub>3</sub>] led to observation of the nickel(0) complex **19** exclusively. Relevant to the hydrogen transfer described here are the reactions reported by the Agapie group with cationic diphosphine arene pincer nickel(II) complexes, which transfer the hydride from the metal to the arene backbone.<sup>22</sup> Moreover, it is important to note that the

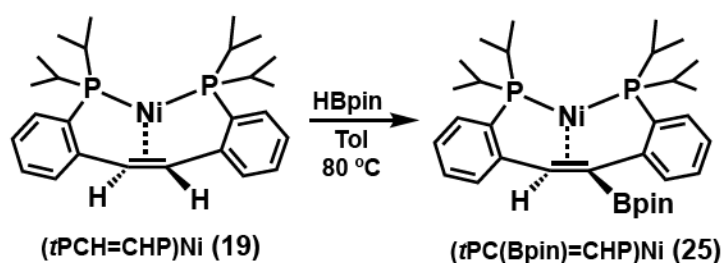
lack of hydrogen acceptor ability for supporting ligands can lead to decomposition reactions, as observed by Hu's group with  $(^{\text{Me}}\text{N}_2\text{N})\text{Ni-H}$ , where  $^{\text{Me}}\text{N}_2\text{N}$  is a pincer bis(amino)amide ligand, which underwent intramolecular decomposition and led to the formation of nickel particles and  $(^{\text{Me}}\text{N}_2\text{N})\text{H}$  by reductive elimination.<sup>33</sup> The findings described for the nickel hydride complex  $(t\text{PC=CHP})\text{NiH}$  (**24**) may have applications in nickel(0)/nickel(II) catalytic cycles that would bypass nickel(I) or nickel(III) oxidation states and mimic palladium(0)/palladium(II) catalytic cycles more efficiently than what has been reported so far.<sup>34-37</sup>



**Scheme 3.6:** Synthesis of complex **24**, and subsequent H-atom transfer.

Additional reactivity was investigated between  $(t\text{PCH=CHP})\text{Ni}$  (**19**) and pinacolborane. Upon the addition of one equivalent of pinacolborane to a toluene solution of **8**, a mixture of products was initially observed. Heating the reaction mixture to  $80^\circ\text{C}$  for 2 hours leads to full conversion to an asymmetric product **25** (Scheme 3.7). Evaluation of

the  $^{31}\text{P}$  NMR spectrum indicates that the phosphines occupy positions cis to one another, as determined by the doublets observed at 60.3, and 52.1 ppm respectively ( $J_{\text{pp}} = 52$  Hz). The  $^1\text{H}$  NMR spectrum contains an apparent doublet at 4.60 ppm, integrating to one proton. This peak is assigned to an olefin proton experiencing coupling to the two phosphines. The solid state molecular structure shows the formation of a distorted trigonal planar nickel(0) compound in which the borane has migrated to the olefin, resulting in the net loss of one  $\text{H}_2$  molecule (Figure 3.9). The borylation of unsaturated C-C bonds catalyzed by group 10 metal catalysts is known, and often employs the insertion of the olefin into the M-B (M = Ni, Pd) bond.<sup>38-43</sup> In our system, subsequent  $\beta$ -hydride elimination followed by  $\text{H}_2$  reductive elimination would generate the observed product.



**Scheme 3.7:** Synthesis of  $(t\text{PC(Bpin)=CHP})\text{Ni}$  (14).

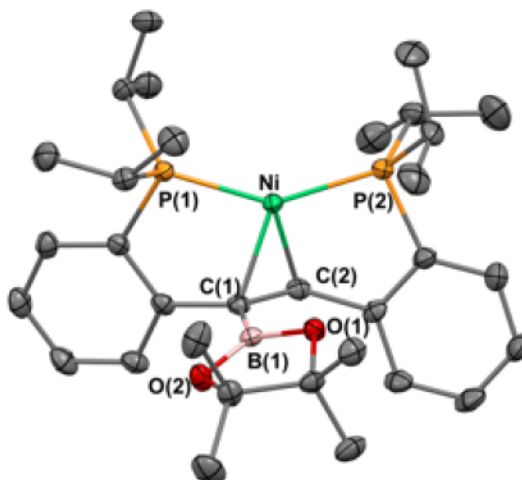


**Figure 3.9:** Thermal-ellipsoid (50% probability level) representation of **25**. Most hydrogen atoms were omitted for clarity. Selected distances (Å) and angles (°): Ni–P(1) = 2.1582(7), Ni–P(2) = 2.1472(7), Ni–C(1) = 2.001(2), Ni–C(2) = 1.966(2), C(1)–C(2) = 1.429(3), P(1)–Ni–P(2) = 146.36(3).

### 3.4 DFT Calculations

In order to compare the electronic structures of metal complexes containing a coordinated olefinic backbone, models for the two diamagnetic nickel complexes (*t*PCH=CHP)Ni (**19**) and [(*t*PCH=CHP)NiMe]I (**23**), which contain nickel in the +2 and 0 oxidation state, respectively, were investigated. Calculations were carried out with Gaussian 03 and the phosphine *iso*-propyls were replaced by methyl groups. A good agreement was found between the optimized and the experimental structures. The results of DFT calculations support the experimental findings described above: both complexes feature  $\sigma$  donation from the olefinic  $\pi$  orbital and  $\pi$  backdonation from the metal to the olefin  $\pi^*$  orbital (Figure 3.10). The amount of  $\pi$  backdonation between the two nickel complexes vary, as expected, according to the d electron count of the metal, with the nickel(0) compound featuring the largest contribution of the olefin  $\pi^*$  orbital (Figure 3.10).

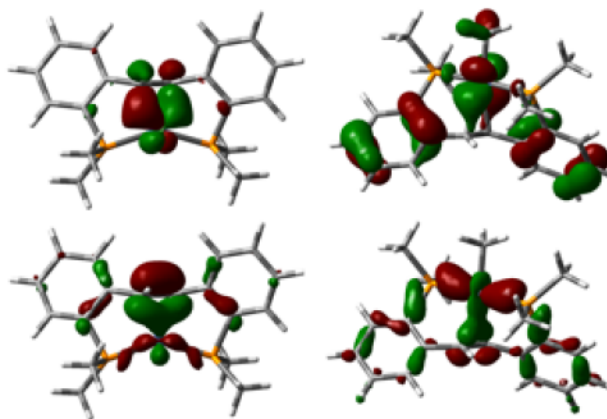


**Figure 3.10:**  $\sigma$  and  $\pi$  bonding interactions for  $(tPCH=CHP)^{Me}Ni$  (**19'**, left) and  $[(tPCH=CHP)^{Me}NiMe^+]$  (**23'**, right).

### 3.5 Summary

The neutral  $tPCH=CHP$  (**1**) pincer and its dimethyl analogue,  $tPCMe=CMeP$  (**17**), were synthesized and their coordination chemistry with group 10 metal centers was studied. The backbone olefinic moiety is versatile and responds to the electronic requirements of the metal. With metal centers in the 0 or +1 oxidation state ( $(tPCH=CHP)Ni$  (**19**),  $[(tPCH=CHP)Pd]_2$  (**22**),  $(tPCH=CHP)NiCl$  (**20**),  $(tPCH=CHP)NiI$  (**21**)),  $\eta^2$  coordination of the olefin occurred, while with metals in the +2 oxidation state dehydrohalogenation was observed leading to an  $\eta^1$  coordination of the backbone in  $(tPC=CHP)MCl$  ( $M = Ni$  (**13**),  $Pd$  (**14**),  $Pt$  (**15**)). This reactivity mode likely responds to subtle changes in the coordination environment because employing the methyl-substituted olefinic backbone analogue,  $(tPCMe=CMeP)$ , forced an  $\eta^2$  coordination of the olefin in  $[(tPCMe=CMeP)NiCl]_2[NiCl_4]$  (**18**). Reactivity studies with two nickel complexes,  $(tPCH=CHP)Ni$  (**8**), which contains an  $\eta^2$ -olefinic backbone, and  $(tPC=CHP)NiCl$  (**2**), which contains an  $\eta^1$ -vinyl backbone, indicate that while the  $\eta^2$ -coordination at nickel(0)

is unperturbed by reactions with electrophiles ( $[(tPCH=CHP)NiMe]I$  (**12**)), the vinyl backbone acts as a hydrogen acceptor at the anionic carbon when the synthesis of  $(tPC=CHP)NiH$  (**24**) is attempted, leading, ultimately, to the nickel(0) complex  $(tPCH=CHP)Ni$  (**19**). The non-innocence of the olefin backbone was extended further in the borylation of the alkene when  $(tPCH=CHP)Ni$  (**19**) was reacted with pinacolborane to generate  $(tPC(Bpin)=CHP)Ni$  (**25**). The various coordination modes observed show that this ligand class is versatile and accommodates different coordination geometries that could enable new reactivity behavior for group 10 metal centers.

### 3.6 Experimental

All manipulations of air and water sensitive compounds were performed under dry nitrogen atmosphere using a drybox. Glassware, vials, and stirring bars were dried in an oven at 120 °C overnight and evacuated for 24 h in the antechamber before being brought into the drybox. All solvents were dried by passing through a column of activated alumina, followed by storage over molecular sieves and sodium. Deuterated solvents were purchased from Cambridge Isotope Laboratories.  $C_6D_6$  was dried by stirring over  $CaH_2$  followed by filtration.  $CDCl_3$  was dried over molecular sieves. All other chemicals were commercially available and used as received. NMR spectra were obtained on Bruker 400 and Bruker 500 spectrometers at ambient temperature. Chemical shift values are reported in ppm relative to residual internal protonated solvent or to a tetramethylsilane standard while using  $CDCl_3$  for  $^1H$  and  $^{13}C\{^1H\}$  experiments. Coupling constants are reported in Hz. Magnetic moments were determined by the Evans method<sup>44-46</sup> using capillaries containing trimethoxybenzene in either  $CDCl_3$  or  $C_6D_6$  as a reference and trimethoxybenzene in the

sample solution. CHN analyses were performed on a CE-440 Elemental Analyzer or by Midwest Microlab, LLC. Gaussian 03 (revision D.02) was used for all reported calculations. The B3LYP (DFT) method was used to carry out the geometry optimizations on model compounds specified in text using the LANL2DZ basis set. The validity of the true minima was checked by the absence of negative frequencies in the energy Hessian.

**Synthesis of (*t*PC=CHP)NiCl (13).** Compound **1** (100 mg, 0.242 mmol) was dissolved in THF along with nickel(II) chloride dimethoxyethane ((dme)NiCl<sub>2</sub>, 52.6 mg, 0.242 mmol) and the resulting solution was stirred at room temperature for 1 h. The volatiles were removed under reduced pressure followed by extraction with *n*-pentane. The orange extract was set to crystallize at -34 °C (69.9 mg, 0.138 mmol, 57 %). <sup>1</sup>H NMR (400 MHz, C<sub>6</sub>D<sub>6</sub>) δ: 1.15 (dd, *J*<sub>PH</sub> = 15 Hz, *J*<sub>HH</sub> = 10 Hz, 6H, CH(CH<sub>3</sub>)<sub>2</sub>), 1.36 (dd, *J*<sub>PH</sub> = 15 Hz, *J*<sub>HH</sub> = 5 Hz, 6H, CH(CH<sub>3</sub>)<sub>2</sub>), 1.44 (app m, 12H, CH(CH<sub>3</sub>)<sub>2</sub>), 2.55 (m, 2H, CH(CH<sub>3</sub>)<sub>2</sub>), 2.63 (m, 2H, CH(CH<sub>3</sub>)<sub>2</sub>), 6.86 (br s, 1H, CH=C), 6.92 (t, *J*<sub>HH</sub> = 4 Hz, 1H, ArH), 7.01 (t, *J*<sub>HH</sub> = 8 Hz, 1H, ArH), 7.11 (m, 2H, ArH), 7.13 (t, *J*<sub>HH</sub> = 4Hz, 1H, ArH), 7.30 (t, *J*<sub>HH</sub> = 4 Hz, 1H, ArH), 7.55 (d, *J*<sub>HH</sub> = 8 Hz, 1H, ArH). <sup>31</sup>P{<sup>1</sup>H} NMR (162 MHz, C<sub>6</sub>D<sub>6</sub>) δ: 29.23 (d, *J*<sub>PP</sub> = 221.9 Hz), 61.09 (d, *J*<sub>PP</sub> = 221.9 Hz). <sup>13</sup>C{<sup>1</sup>H} NMR (100 MHz, C<sub>6</sub>D<sub>6</sub>) δ: 18.20 (d, *J*<sub>PC</sub> = 1 Hz, CH(CH<sub>3</sub>)<sub>2</sub>), 19.18 (s, CH(CH<sub>3</sub>)<sub>2</sub>), 19.22 (d, *J*<sub>PC</sub> = 2 Hz, CH(CH<sub>3</sub>)<sub>2</sub>), 19.27 (s, CH(CH<sub>3</sub>)<sub>2</sub>), 24.97 (dd, *J*<sub>PC</sub> = 2 Hz, *J*<sub>PC</sub> = 21 Hz, CH(CH<sub>3</sub>)<sub>2</sub>), 25.56 (dd, *J*<sub>PC</sub> = 2 Hz, *J*<sub>PC</sub> = 21 Hz, CH(CH<sub>3</sub>)<sub>2</sub>), 120.67 (d, *J*<sub>PC</sub> = 32 Hz, ArC), 123.51 (d, *J*<sub>PC</sub> = 16 Hz, ArC), 127.29 (d, *J*<sub>PC</sub> = 5Hz, ArC), 130.18 (d, *J*<sub>PC</sub> = 1 Hz, ArC), 130.74 (d, *J*<sub>PC</sub> = 1Hz, ArC), 130.81 (d, *J*<sub>PC</sub> = 3 Hz, ArC), 131.54 (d, *J*<sub>PC</sub> = 3 Hz, ArC), 130.02 (s, ArC), 132.40 (d, *J*<sub>PC</sub> = 8 Hz, ArC), 134.89 (d, *J*<sub>PC</sub> = 5 Hz, ArC), 147.63 (d, *J*<sub>PC</sub> = 16 Hz, ArC), 154.89 (dd, *J*<sub>PC</sub> = 5 Hz, *J*<sub>PC</sub> = 19 Hz,



C=CH), 165.10 (d,  $J_{PC} = 43$  Hz, CH=C). Anal. Calcd for  $C_{26}H_{37}ClNiP_2$ : C, 61.76; H, 7.38. Found C, 61.82; H, 7.39.

**Synthesis of (*t*PC=CHP)PdCl (14).** A mixture containing *t*PCH=CHP (**1**, 100 mg, 0.242 mmol) and dichloro(1,5-cyclooctadiene)palladium ((cod)PdCl<sub>2</sub>, 69.1 mg, 0.242 mmol) in THF was stirred at room temperature for 1 h. The volatiles were removed under reduced pressure and the remaining yellow residue was triturated with *n*-pentane. The resulting powder was dissolved in diethyl ether and allowed to crystallize at -35 °C (63.1 mg, 0.114 mmol, 47%). <sup>1</sup>H NMR (400 MHz, C<sub>6</sub>D<sub>6</sub>) δ: 1.01 (dd,  $J_{PH} = 8$  Hz,  $J_{HH} = 4$  Hz, 6H, CH(CH<sub>3</sub>)<sub>2</sub>), 1.17 (dd,  $J_{PH} = 8$  Hz,  $J_{HH} = 4$  Hz, 6H, CH(CH<sub>3</sub>)<sub>2</sub>), 1.40 (m, 12H, CH(CH<sub>3</sub>)<sub>2</sub>), 2.62 (m, 2H, CH(CH<sub>3</sub>)<sub>2</sub>), 2.80 (m, 2H, CH(CH<sub>3</sub>)<sub>2</sub>), 6.95 (t,  $J_{HH} = 8$  Hz, 1H, ArH), 6.98 (t,  $J_{HH} = 8$  Hz, 1H, ArH), 7.19 (app m, 5H, ArH), 7.32 (t,  $J_{HH} = 4$  Hz, 1H, ArH), 7.69 (d,  $J_{HH} = 8$  Hz, 1H, ArH). <sup>31</sup>P{<sup>1</sup>H} NMR (162 MHz, C<sub>6</sub>D<sub>6</sub>) δ: 35.14 (d,  $J_{PP} = 382$  Hz), 66.92 (d,  $J_{PP} = 382$  Hz). <sup>13</sup>C{<sup>1</sup>H} NMR (100 MHz, C<sub>6</sub>D<sub>6</sub>) δ: 18.35 (d,  $J_{CP} = 2$  Hz, CH(CH<sub>2</sub>)<sub>2</sub>), 18.90 (s, CH(CH<sub>3</sub>)<sub>2</sub>), 19.15 (d,  $J_{PC} = 5$  Hz, CH(CH<sub>3</sub>)<sub>2</sub>), 19.32 (d,  $J_{PC} = 4$  Hz, CH(CH<sub>3</sub>)<sub>2</sub>), 25.42 (dd,  $J_{PC} = 18$  Hz,  $J_{PC} = 2$  Hz, CH(CH<sub>3</sub>)<sub>2</sub>), 26.00 (dd,  $J_{PC} = 18$  Hz,  $J_{PC} = 2$  Hz, CH(CH<sub>3</sub>)<sub>2</sub>), 119.76 (d,  $J_{PC} = 35$  Hz, ArC), 124.58 (d,  $J_{PC} = 17$  Hz, ArC), 127.53 (d,  $J_{PC} = 5$  Hz, ArC), 130.90 (app t,  $J_{PC} = 2$  Hz, ArC), 131.21 (d,  $J_{PC} = 4$  Hz, ArC), 131.58 (d,  $J_{PC} = 2$  Hz, ArC), 131.62 (app d,  $J_{PC} = 1$  Hz, ArC), 131.78 (app d,  $J_{PC} = 1$  Hz, ArC), 131.74 (br s, ArC), 132.10 (br s, ArC), 133.55 (d,  $J_{PC} = 9$  Hz, ArC), 148.60 (d,  $J_{PC} = 10$  Hz, ArC), 153.06 (q,  $J_{PC} = 4$  Hz, CH=C), 163.62 (d,  $J_{PC} = 43$  Hz, CH=C). Anal. Calcd for  $C_{26}H_{37}ClP_2Pd$ : C, 56.43; H, 6.74. Found C, 56.78; H, 6.71.

**Synthesis of (*t*PC=CHP)PtCl (15).** A THF solution containing *t*PCH=CHP (**1**, 25mg, 0.061 mmol) and dichloro(1,5-cyclooctadiene)platinum ((cod)PtCl<sub>2</sub>, 22.8 mg, 0.061

mmol) was stirred at room temperature for 1 h. The volatiles were removed under reduced pressure and the resulting residue was triturated with *n*-pentane leading to the formation of a powder (36.4 mg, 0.057 mmol, 93%). Dissolving this powder in toluene and layering this solution with *n*-pentane at -35 °C led to the isolation of analytically pure **15**. <sup>1</sup>H NMR (400 MHz, C<sub>6</sub>D<sub>6</sub>) δ: 1.03 (dd,  $J_{PH} = 8$  Hz,  $J_{HH} = 4$  Hz, 6 Hz, CH(CH<sub>3</sub>)<sub>2</sub>), 1.14 (dd,  $J_{PH} = 8$  Hz,  $J_{HH} = 4$  Hz, 6 Hz, CH(CH<sub>3</sub>)<sub>2</sub>), 1.43 (m, 12H, CH(CH<sub>3</sub>)<sub>2</sub>), 2.81 (m, 2H, CH(CH<sub>3</sub>)<sub>2</sub>), 3.12 (m, 2H, CH(CH<sub>3</sub>)<sub>2</sub>), 7.00 (app q,  $J_{HH} = 8$  Hz, 2H, ArH), 7.15 (br m, 2H, ArH), 7.25 (m, 2H, ArH), 7.41 (t,  $J_{HH} = 8$  Hz, 1H, ArH), 7.63 (d with platinum satellites,  $J_{HH} = 4$  Hz,  $J_{HPt} = 48$  Hz, 1H, CH=C), 7.86 (dd,  $J_{HH} = 4$  Hz,  $J_{PH} = 1$  Hz, 1H, ArH). <sup>31</sup>P{<sup>1</sup>H} NMR (162 MHz, C<sub>6</sub>D<sub>6</sub>) δ: 31.46 (d with platinum satellites,  $J_{PP} = 306.2$  Hz,  $J_{PPt} = 1017.4$  Hz), 62.29 (d with platinum satellites,  $J_{PP} = 302.9$  Hz,  $J_{PPt} = 1165.6$  Hz). <sup>13</sup>C{<sup>1</sup>H} NMR (100 MHz, C<sub>6</sub>D<sub>6</sub>) δ: 18.16 (d with platinum satellites,  $J_{PtC} = 12$  Hz,  $J_{PC} = 2$  Hz, CH(CH<sub>3</sub>)<sub>2</sub>), 18.62 (d with platinum satellites,  $J_{PtC} = 10$  Hz,  $J_{PC} = 2$  Hz, CH(CH<sub>3</sub>)<sub>2</sub>), 19.00 (d,  $J_{PC} = 4$  Hz, CH(CH<sub>3</sub>)<sub>2</sub>), 19.13 (d,  $J_{PC} = 3$  Hz, CH(CH<sub>3</sub>)<sub>2</sub>), 25.14 (dd with platinum satellites,  $J_{PtC} = 13$  Hz,  $J_{PC} = 28$  Hz,  $J_{CC} = 3$  Hz, CH(CH<sub>3</sub>)<sub>2</sub>), 26.39 (dd with platinum satellites,  $J_{PtC} = 8$  Hz,  $J_{PC} = 29$  Hz,  $J_{CC} = 2$  Hz, CH(CH<sub>3</sub>)<sub>2</sub>), 117.46 (dd,  $J_{PC} = 40$  Hz,  $J_{PC} = 2$  Hz, ArC), 124.42 (d with platinum satellites,  $J_{PtC} = 17$  Hz,  $J_{PC} = 15$  Hz, ArC), 125.96 (d,  $J_{PC} = 6$  Hz, ArC), 127.45 (d,  $J_{PC} = 6$  Hz, ArC), 128.67 (d with platinum satellites,  $J_{PtC} = 12$  Hz,  $J_{PC} = 12$  Hz, CH=C), 130.59 (d with platinum satellites,  $J_{PtC} = 14$  Hz,  $J_{PC} = 2$  Hz, ArC), 131.28 (dd,  $J_{PC} = 27$  Hz,  $J_{CC} = 3$  Hz, ArC), 131.28 (d,  $J = 4$  Hz, ArC), 133.38 (d,  $J = 9$  Hz, ArC), 139.59 (d,  $J = 7$  Hz, ArC), 149.62 (d,  $J = 16$  Hz, ArC), 164.47 (d,  $J = 32$  Hz, ArC). Anal. Calcd for C<sub>26</sub>H<sub>37</sub>ClP<sub>2</sub>Pt: C, 48.64; H, 5.81. Found C, 48.37; H, 5.71.

**Synthesis of (Z)-2,3-bis(2-di-*iso*-propylphosphinephenyl)-2-butene (*t*PCMe=CMeP, **17**).** The precursor, (Z)-2,3-bis(2-bromophenyl)-2-butene (**16**), was synthesized as reported in the literature in 8.4% yield.<sup>15</sup> Compound **17** was generated via the same procedure as **1** (1.6878 g, 3.83 mmol, 72.4%). <sup>1</sup>H NMR (500 MHz, C<sub>6</sub>D<sub>6</sub>) δ: 0.95 (dd, *J*<sub>PH</sub> = 10 Hz, *J*<sub>HH</sub> = 5 Hz, 6H, CH(CH<sub>3</sub>)<sub>2</sub>, major), 1.03 (dd, *J*<sub>PH</sub> = 10 Hz, *J*<sub>HH</sub> = 5 Hz, 6H, CH(CH<sub>3</sub>)<sub>2</sub>, major), 1.17 (m, 12H, CH(CH<sub>3</sub>)<sub>2</sub>, major), 1.35 (dd, *J*<sub>PH</sub> = 10 Hz, *J*<sub>HH</sub> = 5 Hz, CH(CH<sub>3</sub>)<sub>2</sub>, minor), 1.94 (m, 4H, CH(CH<sub>3</sub>)<sub>2</sub>, major), 2.05 (s, CH<sub>3</sub>C=CCH<sub>3</sub>, minor) 2.12 (s, 6H, CH<sub>3</sub>C=CCH<sub>3</sub>, major), 7.11 (td, *J*<sub>HH</sub> = 10 Hz, *J*<sub>PH</sub> = 1 Hz, 2H, ArH, major), 7.21 (t, *J*<sub>HH</sub> = 10 Hz, 2H, ArH, major), 7.41 (dt, *J*<sub>HH</sub> = 10 Hz, *J*<sub>PH</sub> = 1 Hz, 2H, ArH, major), 7.47 (br d, *J*<sub>HH</sub> = 5 Hz, ArH, minor), 7.63 (ddd, *J*<sub>HH</sub> = 5 Hz, *J*<sub>HH</sub> = 5 Hz, *J*<sub>PH</sub> = 1 Hz, 2H, ArH, major). <sup>31</sup>P{<sup>1</sup>H} NMR (162 MHz, C<sub>6</sub>D<sub>6</sub>) δ: -3.09 (s, minor), -2.38 (s, major). <sup>13</sup>C{<sup>1</sup>H} NMR (100 MHz, C<sub>6</sub>D<sub>6</sub>) δ: 20.44 (d, *J*<sub>PC</sub> = 18 Hz, CH(CH<sub>3</sub>)<sub>2</sub>), 20.67 (d, *J*<sub>PC</sub> = 13 Hz, CH(CH<sub>3</sub>)<sub>2</sub>), 20.77 (s, CH(CH<sub>3</sub>)<sub>2</sub>), 20.94 (d, *J*<sub>PC</sub> = 15 Hz, CH(CH<sub>3</sub>)<sub>2</sub>), 24.99 (d, *J*<sub>PC</sub> = 23 Hz, -CH(CH<sub>3</sub>)<sub>2</sub>), 25.29 (d, *J*<sub>PC</sub> = 18 Hz, CH<sub>3</sub>C=CCH<sub>3</sub>), 25.96 (d, *J*<sub>PC</sub> = 24 Hz, CH(CH<sub>3</sub>)<sub>2</sub>), 126.36 (s, ArC), 129.13 (s, CH<sub>3</sub>C=CCH<sub>3</sub>), 129.46 (s, ArC), 130.03 (d, *J*<sub>PC</sub> = 11 Hz, ArC), 132.83 (d, *J*<sub>PC</sub> = 7 Hz, ArC), 135.76 (d, *J*<sub>PC</sub> = 32 Hz, ArC), 152.94 (d, *J*<sub>PC</sub> = 49 Hz, ArC). MS (QTOF) *m/z*: C<sub>28</sub>H<sub>43</sub>P<sub>2</sub><sup>+</sup>, 441.28 (expected: C<sub>28</sub>H<sub>42</sub>P<sub>2</sub>, 440.28).

**Synthesis of 2[(*t*PCMe=CMeP)NiCl]<sub>2</sub>[NiCl<sub>4</sub>] (**18**).** A solution of THF containing *t*PCMe=CMeP (**17**, 25 mg, 0.057 mmol) and (dme)NiCl<sub>2</sub> (18.5 mg, 0.085 mmol) was stirred for 1 h at ambient temperature. The volatiles were then removed under reduced pressure; trituration with *n*-pentane produced a green powder (29.8 mg, 0.023 mmol, 83%). The powder was then recrystallized from a CH<sub>2</sub>Cl<sub>2</sub> solution layered with *n*-pentane. <sup>1</sup>H NMR (400 MHz, CDCl<sub>3</sub>) δ: 1.54 (q, *J*<sub>PH</sub> = 10 Hz, 6H, CH(CH<sub>3</sub>)<sub>2</sub>), 1.61 (q, 6H, *J*<sub>PH</sub> = 10

Hz, CH(CH<sub>3</sub>)<sub>2</sub>), 1.74 (q, 12 H,  $J_{PH}$  = 10 Hz, CH(CH<sub>3</sub>)<sub>2</sub>), 2.08 (s, 6H, CH<sub>3</sub>C=CCH<sub>3</sub>), 3.00 (br s, 2H, CH(CH<sub>3</sub>)<sub>2</sub>), 3.24 (br m, 2H, CH(CH<sub>3</sub>)<sub>2</sub>), 7.94 (br s, 2H, ArH), 8.05 (br s, 2H, ArH), 9.04 (br s, 2H, ArH), 9.29 (br s, 2H, ArH). <sup>31</sup>P{<sup>1</sup>H} NMR (162 MHz, CDCl<sub>3</sub>) δ: 64.40 (s). <sup>13</sup>C{<sup>1</sup>H} NMR (100 MHz, CDCl<sub>3</sub>) δ: 18.74 (s, CH(CH<sub>3</sub>)<sub>2</sub>), 19.51 (s, CH(CH<sub>3</sub>)<sub>2</sub>), 20.43 (s, CH(CH<sub>3</sub>)<sub>2</sub>), 20.70 (s, CH(CH<sub>3</sub>)<sub>2</sub>), 26.85 (t,  $J_{PC}$  = 23 Hz, CH(CH<sub>3</sub>)<sub>2</sub>), 27.53 (t,  $J_{PC}$  = 21 Hz, CH(CH<sub>3</sub>)<sub>2</sub>), 33.15 (s, CH<sub>3</sub>C=CCH<sub>3</sub>), 123.83 (s, ArC), 128.94 (t,  $J_{PC}$  = 32 Hz, CH<sub>3</sub>C=CCH<sub>3</sub>), 131.23 (s, ArC), 132.08 (t,  $J_{PC}$  = 13 Hz, ArC), 132.65 (s, ArC), 137.42 (s, ArC), 151.93 (t,  $J_{PC}$  = 23 Hz, ArC). Anal. Calcd for C<sub>56</sub>H<sub>84</sub>Cl<sub>6</sub>Ni<sub>3</sub>P<sub>4</sub>·CH<sub>2</sub>Cl<sub>2</sub>: C, 50.53; H, 6.40. Found C, 50.52; H, 6.50.

**Synthesis of (tPCH=CHP)Ni (19).** A solution containing tPCH=CHP (**1**, 100 mg, 0.242 mmol) and nickel bis(cyclooctadiene), (cod)<sub>2</sub>Ni, was stirred at room temperature for 1 h in THF. The volatiles were removed under reduced pressure and the orange residue was dissolved in *n*-pentane and allowed to crystallize at -34 °C (79.0 mg, 0.168 mmol, 69%). <sup>1</sup>H NMR (500 MHz, C<sub>6</sub>D<sub>6</sub>) δ: 0.97 (app m, 6H, CH(CH<sub>3</sub>)<sub>2</sub>), 1.03 (dd,  $J_{PH}$  = 10 Hz,  $J_{HH}$  = 5 Hz, 6H, CH(CH<sub>3</sub>)<sub>2</sub>), 1.12 (dd,  $J_{PH}$  = 10 Hz,  $J_{HH}$  = 5 Hz, 6H, CH(CH<sub>3</sub>)<sub>2</sub>), 1.26 (dd,  $J_{PH}$  = 10 Hz,  $J_{HH}$  = 5 Hz, 6H, CH(CH<sub>3</sub>)<sub>2</sub>), 1.95 (m, 2H, CH(CH<sub>3</sub>)<sub>2</sub>), 2.19 (br m, 2H, CH(CH<sub>3</sub>)<sub>2</sub>), 4.65 (s, 2H, CH=CH), 7.07 (t,  $J_{HH}$  = 5 Hz, 2H, ArH), 7.18 (m, 4H, ArH), 7.69 (d,  $J_{HH}$  = 5 Hz, 2H, ArH). <sup>31</sup>P{<sup>1</sup>H} NMR (202 MHz, C<sub>6</sub>D<sub>6</sub>) δ: 57.85 (s). <sup>13</sup>C{<sup>1</sup>H} NMR (126 MHz, C<sub>6</sub>D<sub>6</sub>) δ: 18.36 (s, CH(CH<sub>3</sub>)<sub>2</sub>), 18.92 (t,  $J_{PC}$  = 6.3 Hz, CH(CH<sub>3</sub>)<sub>2</sub>), 20.76 (t,  $J_{PC}$  = 6.3 Hz, CH(CH<sub>3</sub>)<sub>2</sub>), 21.20 (app m, CH(CH<sub>3</sub>)<sub>2</sub>), 26.44 (t,  $J_{PC}$  = 5.04 Hz, CH(CH<sub>3</sub>)<sub>2</sub>), 74.96 (t,  $J_{PC}$  = 8.82 Hz, CH=CH), 125.49 (s, ArC), 128.35 (t,  $J_{PC}$  = 7.6 Hz, ArC), 129.51 (t,  $J_{PC}$  = 7.56, ArC), 130.93 (s, ArC), 148.82 (t,  $J_{PC}$  = 21.42 Hz, ArC), 154.63 (t,  $J_{PC}$  = 15.1 Hz, ArC). Anal. Calcd for C<sub>26</sub>H<sub>38</sub>NiP<sub>2</sub>: C, 66.27; H, 8.13. Found C, 65.81; H, 8.10.

**Synthesis of (*t*PCH=CHP)NiCl (20).** (cod)<sub>2</sub>Ni (16.7 mg, 0.061 mmol) was mixed with **1** (25 mg, 0.061 mmol) in THF and stirred for 30 minutes. Concurrently, (dme)NiCl<sub>2</sub> (13.19 mg, 0.061 mmol) was mixed with **1** (25 mg, 0.061 mmol) in THF and stirred for 30 minutes. The two solutions were mixed and stirred for an additional 2 hours. The volatiles were then removed under reduced pressure; a <sup>1</sup>H NMR spectrum of the crude reaction mixture indicated that multiple species were present, including complex **13**. Trituration with *n*-pentane followed by recrystallization from toluene solution layered with *n*-pentane led to the isolation of single crystals of (*t*PC=CP)NiCl (**20**), but because of the rapid formation of (*t*PC=CHP)NiCl (**13**) the sample was contaminated and all attempts to isolate pure **20** failed.<sup>25-26</sup>

**Synthesis of (*t*PCH=CHP)NiI (21).** A THF solution of **19** (25 mg, 0.053 mmol) was chilled to -35 °C, along with a THF solution of I<sub>2</sub> (6.7 mg, 0.026 mmol). After 30 minutes, the I<sub>2</sub> solution was added dropwise to the solution of **19** over the course of 5 minutes. The mixture was warmed to room temperature while stirring for 1 hour. The volatiles were removed under reduced pressure, followed by trituration with *n*-pentane, which resulted in a dark yellow-green powder (24.4 mg, 0.043 mmol, 80%). The powder was then recrystallized from a concentrated diethyl ether solution. Magnetic moment: μ<sub>eff</sub> = 1.63 μ<sub>B</sub>. The <sup>1</sup>H NMR spectrum is broad. <sup>1</sup>H NMR (400 MHz, C<sub>6</sub>D<sub>6</sub>) δ: 2.97 (ν<sub>1/2</sub> = 2080 Hz), 4.93 (ν<sub>1/2</sub> = 1760 Hz), 6.16 (ν<sub>1/2</sub> = 880 Hz), 7.83 (ν<sub>1/2</sub> = 360 Hz), 10.16 (ν<sub>1/2</sub> = 120 Hz), 10.63 (ν<sub>1/2</sub> = 312 Hz). Anal. Calcd for C<sub>26</sub>H<sub>38</sub>INiP<sub>2</sub>·2CHCl<sub>3</sub>: C, 40.19; H, 4.82. Found C, 40.58; H, 4.63.

**Synthesis of [(*t*PCH=CHP)Pd]<sub>2</sub> (22).** Bis(dibenzylideneacetone) palladium(0) (34.5 mg, 0.060 mmol) was mixed with *t*PCH=CHP (**1**, 25 mg, 0.061 mmol) in THF, and

stirred at room temperature for 12 h. The volatiles were removed under reduced pressure. The resulting residue was then dissolved in *n*-pentane, and passed through a silica plug using a gradient elution of *n*-pentane, diethyl ether, and THF (3.3 mg, 0.006 mmol, 10.5%).  $^1\text{H}$  NMR (400 MHz,  $\text{C}_6\text{D}_6$ )  $\delta$ : 1.02 (dd,  $J_{\text{PH}} = 8$  Hz,  $J_{\text{HH}} = 4$  Hz, 12 H,  $\text{CH}(\text{CH}_3)_2$ ), 1.21 (dd,  $J_{\text{PH}} \sim J_{\text{HH}} = 8$  Hz, 12H,  $\text{CH}(\text{CH}_3)_2$ ), 2.16 (m, 4H,  $\text{CH}(\text{CH}_3)_2$ ), 5.91 (s, 2H,  $\text{CH}=\text{CH}$ ), 7.08 (t,  $J_{\text{HH}} = 4$  Hz, 2H, ArH), 7.17 (m, 2H, ArH), 7.27 (d,  $J_{\text{HH}} = 8$  Hz, 2H, ArH), 7.60 (d,  $J_{\text{HH}} = 8$  Hz, 2H, ArH).  $^{31}\text{P}\{^1\text{H}\}$  NMR (162 MHz,  $\text{C}_6\text{D}_6$ )  $\delta$ : 55.28 (s).  $^{13}\text{C}\{^1\text{H}\}$  NMR (100 MHz,  $\text{C}_6\text{D}_6$ )  $\delta$ : 19.45 (s,  $\text{CH}(\text{CH}_3)_2$ ), 20.47 (t,  $J_{\text{PC}} = 8$  Hz,  $\text{CH}(\text{CH}_3)_2$ ), 24.72 (br s,  $\text{CH}(\text{CH}_3)_2$ ), 100.34 (t,  $J_{\text{PC}} = 7$  Hz,  $\text{CH}=\text{CH}$ ), 125.87 (t,  $J_{\text{PC}} = 2$  Hz, ArC), 129.08 (s, ArC), 129.81 (t,  $J_{\text{PC}} = 8$  Hz, ArC), 132.03 (s, ArC), 149.26 (t,  $J_{\text{PC}} = 18$  Hz, ArC), 150.89 (t,  $J_{\text{PC}} = 15$  Hz, ArC). Anal. Calcd for  $\text{C}_{52}\text{H}_{76}\text{P}_4\text{Pd}_2$ : C, 60.18; H, 7.38. Found C, 60.35; H, 7.42.

**Synthesis of [(*t*PC=CHP)NiMe]I (23).** A solution of (*t*PC=CP)Ni (**19**, 44.4 mg, 0.094 mmol) in THF was chilled in a -35 °C freezer for 30 min, along with a 1.6 M solution of iodomethane. Two equivalents of iodomethane (1.17 mL, 0.18 mmol) were added to the (*t*PC=CP)Ni (**19**) solution. The mixture was stirred for 5 minutes at ambient temperature until a yellow solid rapidly precipitated. The solvent was decanted, followed by trituration of the yellow powder with *n*-pentane (42.2 mg, 0.067 mmol, 71.3 %).  $^1\text{H}$  NMR (400 MHz,  $\text{CDCl}_3$ )  $\delta$ : 1.01 (m, 9H,  $\text{CH}_3$ ,  $\text{CH}(\text{CH}_3)_2$ ), 1.32 (m, 12H,  $\text{CH}(\text{CH}_3)_2$ ), 1.48 (app q,  $J_{\text{PH}} \sim J_{\text{HH}} = 8$  Hz, 6 H,  $\text{CH}(\text{CH}_3)_2$ ), 2.77 (br s, 2 H,  $\text{CH}(\text{CH}_3)_2$ ), 2.90 (br s, 2H,  $\text{CH}(\text{CH}_3)_2$ ), 5.66 (s, 2H,  $\text{CH}=\text{CH}$ ), 7.42 (d, 2 H,  $J_{\text{HH}} = 8$  Hz, ArH), 7.68 (m, 6 H, ArH).  $^{31}\text{P}\{^1\text{H}\}$  NMR (162 MHz,  $\text{CDCl}_3$ )  $\delta$ : 60.18 (s).  $^{13}\text{C}\{^1\text{H}\}$  NMR (100 MHz,  $\text{CDCl}_3$ )  $\delta$ : -1.52 (t,  $J_{\text{PC}} = 23$  Hz,  $\text{CH}_3$ ), 16.69 (s,  $\text{CH}(\text{CH}_3)_2$ ), 18.38 (s,  $\text{CH}(\text{CH}_3)_2$ ), 19.37 (s,  $\text{CH}(\text{CH}_3)_2$ ), 20.21 (s,  $\text{CH}(\text{CH}_3)_2$ ), 23.75 (t,  $J_{\text{PC}} = 13$  Hz,  $\text{CH}(\text{CH}_3)_2$ ), 24.95 (t,  $J_{\text{PC}} = 11$  Hz,  $\text{CH}(\text{CH}_3)_2$ ), 116.21

(s, CH=CH), 125.76 (t,  $J_{PC}$  = 20 Hz, ArC), 127.38 (t,  $J_{PC}$  = 6 Hz, ArC), 129.64 (t,  $J_{PC}$  = 2 Hz, ArC), 131.53 (s, ArC), 132.72 (s, ArC), 148.62 (t,  $J_{PC}$  = 14 Hz, ArC). Anal. Calcd for  $C_{27}H_{41}INiP_2$ : C, 52.89; H, 6.74. Found C, 53.04; H, 6.82.

**Synthesis of (*t*PC=CHP)NiH (**24**).** To a solution of (*t*PC=CHP)NiCl (**13**, 20.4 mg, 0.043 mmol) in THF, 0.04 mL of a 1M  $Li[(C_2H_5)_3BH]$  (0.04 mmol) THF solution was added. The mixture was stirred at room temperature for 1 h, after which the volatiles were removed under reduced pressure. NMR spectroscopy showed that the conversion to (*t*PCH=CHP)Ni (**19**) proceeded rapidly even at ambient temperature. Heating the NMR sample for 1 h at 80 °C showed full conversion to **19**.  $^1H$  NMR (500 MHz,  $C_6D_6$ )  $\delta$ : -10.65 (ddd,  $J_{HP}$  = 48 Hz,  $J_{HP}$  = 46 Hz,  $J_{HH}$  = 4 Hz, 1H, hydride), 0.98 (m, 12 H,  $CH(CH_3)_2$ ), 1.19 (dd,  $J_{PH}$  = 12 Hz,  $J_{HH}$  = 4 Hz, 6 H,  $CH(CH_3)_2$ ), 1.26 (dd,  $J_{PH}$  = 12 Hz,  $J_{HH}$  = 4 Hz, 6 H,  $CH(CH_3)_2$ ), 2.20 (m, 2H,  $CH(CH_3)_2$ ), 2.27 (m, 2H,  $CH(CH_3)_2$ ), 7.03 (t, 1H,  $J_{HH}$  = 8Hz, ArH), 7.09 (t,  $J_{HH}$  = 4 Hz, 1H, ArH), 7.32 (m, 4H, ArH), 7.90 (m, 1H, ArH), 8.05 (dd,  $J_{HH}$  = 8 Hz,  $J_{PH}$  = 4 Hz, 1H, ArH).  $^{31}P\{^1H\}$  NMR (162 MHz,  $C_6D_6$ )  $\delta$ : 57.53 (d,  $J_{PP}$  = 247 Hz), 84.17 (d,  $J_{PP}$  = 247 Hz). Because **24** is not stable for a reasonable amount of time at ambient temperature, an analytically pure sample suitable for elemental analysis could not be obtained.

**Synthesis of (*t*PC(Bpin)=CHP)Ni (**25**).** To a toluene solution of (*t*PCH=CHP)Ni (**19**, 20.0 mg, 0.04 mmol) was added one equivalent of HBpin (6.2  $\mu$ L, 0.04 mmol). The solution was heated to 80°C for 2 h. The volatiles were removed under reduced pressure, and the resulting crude residue was re-dissolved in *n*-pentane. The solution was stored at -35°C to induce crystallization resulting in analytically pure **25** (15.3 mg, 72%).  $^1H$  NMR (500 MHz,  $C_6D_6$ )  $\delta$ : 0.82 (s, 6 H, O- $C(CH_3)_2$ ), 0.86 (s, 6 H, O- $C(CH_3)_2$ ), 0.91 (m, 6H,

CH(CH<sub>3</sub>)<sub>2</sub>), 1.09 (dd, 3 H,  $J_{\text{HP}} = 20$  Hz,  $J_{\text{HH}} = 10$  Hz, CHCH<sub>3</sub>)<sub>2</sub>), 1.25 (m, 15 H, CH(CH<sub>3</sub>)<sub>2</sub>), 1.87 (m, 1 H, CH(CH<sub>3</sub>)<sub>2</sub>), 2.26 (m, 3H, CH(CH<sub>3</sub>)<sub>2</sub>), 4.6 (app d, 1H,  $J_{\text{HB}} = 5$  Hz, CH=C(Bpin), 6.99 (t, 1H,  $J_{\text{HH}} = 5$  Hz, ArH), 7.07 (t, 1H,  $J_{\text{HH}} = 10$  Hz, ArH), 7.17 (m, 4H, ArH), 7.64 (dd, 1H,  $J_{\text{HH}} = 8.1$  Hz,  $J_{\text{HP}} = 3$  Hz, ArH), 7.70 (dd, 1H,  $J_{\text{HH}} = 8$  Hz,  $J_{\text{HP}} = 2$  Hz, ArH). <sup>31</sup>P{<sup>1</sup>H} NMR (162 MHz, C<sub>6</sub>D<sub>6</sub>)  $\delta$ : 52.1 (d,  $J_{\text{PP}} = 62$  Hz), 60.3 (d,  $J_{\text{PP}} = 61$  Hz). ). <sup>13</sup>C{<sup>1</sup>H} NMR (100 MHz, C<sub>6</sub>D<sub>6</sub>)  $\delta$ : 17.82 (d,  $J_{\text{CP}} = 3$  Hz, CH(CH<sub>3</sub>)), 18.57 (s, CH(CH<sub>3</sub>)<sub>2</sub>), 19.27 (d,  $J_{\text{CP}} = 12$  Hz, CH(CH<sub>3</sub>)<sub>2</sub>), 20.13 (d,  $J_{\text{CP}} = 13$  Hz, CH(CH<sub>3</sub>)<sub>2</sub>), 20.70 (d,  $J_{\text{CP}} = 10$  Hz, CH(CH<sub>3</sub>)<sub>2</sub>), 20.94 (s, CH(CH<sub>3</sub>)<sub>2</sub>), 20.99 (s, CH(CH<sub>3</sub>)<sub>2</sub>), 21.08 (s, CH(CH<sub>3</sub>)<sub>2</sub>), 21.31 (d,  $J_{\text{CP}} = 10$  Hz, CH(CH<sub>3</sub>)<sub>2</sub>), 21.91 (d,  $J_{\text{CP}} = 17$  Hz, CH(CH<sub>3</sub>)<sub>2</sub>), 22.79 (d,  $J_{\text{CP}} = 12$  Hz, CH(CH<sub>3</sub>)<sub>2</sub>), 24.76 (d,  $J_{\text{CP}} = 12$  Hz, CH(CH<sub>3</sub>)<sub>2</sub>), 24.86 (s, O-C(CH<sub>3</sub>)<sub>2</sub>), 25.19 (s, O-C(CH<sub>3</sub>)<sub>2</sub>), 26.29 (d,  $J_{\text{CP}} = 13$  Hz, CH(CH<sub>3</sub>)<sub>2</sub>), 26.83 (d,  $J_{\text{CP}} = 11$  Hz, CH(CH<sub>3</sub>)<sub>2</sub>), 79.78 (dd,  $J_{\text{CP}} = 13$  Hz,  $J_{\text{CP}} = 4$  Hz, CH=C(Bpin)), 81.63 (s, CH=C(Bpin)), 124.71 (d,  $J_{\text{CP}} = 4$  Hz, ArC), 124.98 (d,  $J_{\text{CP}} = 4$  Hz, ArC), 128.49 (s, ArC), 129.28 (s, ArC), 129.57 (dd,  $J_{\text{CP}} = 12$  Hz,  $J_{\text{CP}} = 5$  Hz, ArC), 130.25 (d,  $J_{\text{CP}} = 3$  Hz, ArC), 130.37 (dd,  $J_{\text{CP}} = 9$  Hz,  $J_{\text{CP}} = 5$  Hz, ArC), 130.58 (d,  $J_{\text{CP}} = 3$  Hz, ArC), 146.20 (dd,  $J_{\text{CP}} = 31$  Hz,  $J_{\text{CP}} = 17$  Hz, ArC), 149.11 (dd,  $J_{\text{CP}} = 34$  Hz,  $J_{\text{CP}} = 8$  Hz, ArC), 155.78 (d,  $J_{\text{CP}} = 34$  Hz, ArC), 157.51 (d,  $J_{\text{CP}} = 33$  Hz, ArC).

**X-ray single crystal diffraction** The data were collected on a Bruker APEX-II diffractometer with a monochromated Mo K $\alpha$  radiation.<sup>47</sup> Data were corrected for absorption and polarized effects and analyzed for space group determination.<sup>47-48</sup> The structure was solved by direct methods (SHELXS<sup>49</sup>) and refined by full-matrix least squares techniques against  $F_o^2$  (SHELXL-97).<sup>50</sup> Unless noted, all hydrogen atoms were generated in calculated positions. Mercury was used for structure representations.<sup>50</sup>



**X-Ray Crystal Structure of (*t*PC=CHP)NiCl (13).** X-Ray quality single crystals were obtained from a concentrated CH<sub>2</sub>Cl<sub>2</sub> solution layered with *n*-pentane at -35 °C in the glovebox. The resulting crystals were bright orange blocks. Crystal and refinement data for **13**: C<sub>26</sub>H<sub>37</sub>ClNiP<sub>2</sub>; M<sub>r</sub> = 505.66; Monoclinic; space group P2(1)/n; *a* = 8.8598(10) Å; *b* = 9.8216(11) Å; *c* = 29.245(3) Å; α = 90°; β = 97.096(2)°; γ = 90°; V = 2525.3(5) Å<sup>3</sup>; Z = 4; T = 120(2) K; λ = 0.71073 Å; μ = 1.012 mm<sup>-1</sup>; d<sub>calc</sub> = 1.330 g·cm<sup>-3</sup>; 22334 reflections collected; 5171 unique (R<sub>int</sub> = 0.0488); giving R<sub>1</sub> = 0.0345, wR<sub>2</sub> = 0.0695 for 4126 data with [I>2σ(I)] and R<sub>1</sub> = 0.0521, wR<sub>2</sub> = 0.0743 for all 5171 data. Residual electron density (e<sup>-</sup>·Å<sup>-3</sup>) max/min: 0.535/-0.283.

**X-Ray Crystal Structure of (*t*PC=CHP)PdCl (14).** X-Ray quality single crystals were obtained as pale yellow blocks from a concentrated diethyl ether solution at -35 °C in the freezer in the glovebox. Crystal and refinement data for **14**: C<sub>26</sub>H<sub>37</sub>ClP<sub>2</sub>Pd; M<sub>r</sub> = 553.35; Orthorhombic; space group Pca2(1); *a* = 15.5062(11) Å; *b* = 11.0311(8) Å; *c* = 14.9547(11) Å; α = 90°; β = 90°; γ = 90°; V = 2558.0(3) Å<sup>3</sup>; Z = 4; T = 120(2) K; λ = 0.71073 Å; μ = 0.966 mm<sup>-1</sup>; d<sub>calc</sub> = 1.437 g·cm<sup>-3</sup>; 22282 reflections collected; 5276 unique (R<sub>int</sub> = 0.0346); giving R<sub>1</sub> = 0.0236, wR<sub>2</sub> = 0.0483 for 4899 data with [I>2σ(I)] and R<sub>1</sub> = 0.0280, wR<sub>2</sub> = 0.0496 for all 5276 data. Residual electron density (e<sup>-</sup>·Å<sup>-3</sup>) max/min: 0.652/-0.493.

**X-Ray Crystal Structure of [(*t*PCMe=CMeP)NiCl]<sub>2</sub>[NiCl<sub>4</sub>] (18).** X-Ray quality single crystals were obtained from a concentrated hexane layered CH<sub>2</sub>Cl<sub>2</sub> solution at -35 °C in the glovebox. The resulting crystals were dichroic plates, appearing both green and orange. Crystal and refinement data for **18**: C<sub>56</sub>H<sub>84</sub>Cl<sub>6</sub>Ni<sub>3</sub>P<sub>4</sub>; M<sub>r</sub> = 1269.94; Triclinic; space group P-1; *a* = 16.385(3) Å; *b* = 16.756(3) Å; *c* = 17.013(3) Å; α = 96.367(2)°; β =

116.335(2)°;  $\gamma = 114.271(2)^\circ$ ;  $V = 3561.9(10) \text{ \AA}^3$ ;  $Z = 2$ ;  $T = 120(2) \text{ K}$ ;  $\lambda = 0.71073 \text{ \AA}$ ;  $\mu = 1.129 \text{ mm}^{-1}$ ;  $d_{\text{calc}} = 1.184 \text{ g}\cdot\text{cm}^{-3}$ ; 36668 reflections collected; 12540 unique ( $R_{\text{int}} = 0.0482$ ); giving  $R_1 = 0.0334$ ,  $wR_2 = 0.0685$  for 8957 data with  $[I > 2\sigma(I)]$  and  $R_1 = 0.0515$ ,  $wR_2 = 0.0717$  for all 12540 data. Residual electron density ( $\text{e}^- \cdot \text{\AA}^{-3}$ ) max/min: 0.431/-0.298.

**X-Ray Crystal Structure of (tPCH=CHP)Ni (19).** X-Ray quality single crystals were obtained readily as dark orange blocks from a concentrated *n*-pentane solution at -35 °C in the glovebox. Crystal and refinement data for **19**:  $\text{C}_{26}\text{H}_{38}\text{NiP}_2$ ;  $M_r = 471.21$ ; Monoclinic; space group  $P2(1)/c$ ;  $a = 15.245(2) \text{ \AA}$ ;  $b = 10.7277(16) \text{ \AA}$ ;  $c = 31.655(5) \text{ \AA}$ ;  $\alpha = 90^\circ$ ;  $\beta = 101.825(3)^\circ$ ;  $\gamma = 90^\circ$ ;  $V = 5067.1(13) \text{ \AA}^3$ ;  $Z = 8$ ;  $T = 120(2) \text{ K}$ ;  $\lambda = 0.71073 \text{ \AA}$ ;  $\mu = 0.902 \text{ mm}^{-1}$ ;  $d_{\text{calc}} = 1.235 \text{ g}\cdot\text{cm}^{-3}$ ; 40184 reflections collected; 8912 unique ( $R_{\text{int}} = 0.1426$ ); giving  $R_1 = 0.0566$ ,  $wR_2 = 0.0807$  for 4771 data with  $[I > 2\sigma(I)]$  and  $R_1 = 0.1361$ ,  $wR_2 = 0.0931$  for all 8912 data. Residual electron density ( $\text{e}^- \cdot \text{\AA}^{-3}$ ) max/min: 0.711/-0.747.

**X-Ray Crystal Structure of (tPCH=CHP)NiCl (20).** X-Ray quality single crystals were obtained from a concentrated toluene solution at -35 °C in the glovebox. Crystal and refinement data for **20**:  $\text{C}_{26}\text{H}_{38}\text{ClNiP}_2$ ;  $M_r = 506.66$ ; Monoclinic; space group  $P2(1)/c$ ;  $a = 9.4899(9) \text{ \AA}$ ;  $b = 20.450(2) \text{ \AA}$ ;  $c = 13.0740(13) \text{ \AA}$ ;  $\alpha = 90^\circ$ ;  $\beta = 92.696(2)^\circ$ ;  $\gamma = 90^\circ$ ;  $V = 2534.4(4) \text{ \AA}^3$ ;  $Z = 4$ ;  $T = 120(2) \text{ K}$ ;  $\lambda = 0.71073 \text{ \AA}$ ;  $\mu = 1.009 \text{ mm}^{-1}$ ;  $d_{\text{calc}} = 1.328 \text{ g}\cdot\text{cm}^{-3}$ ; 35899 reflections collected; 5182 unique ( $R_{\text{int}} = 0.0651$ ); giving  $R_1 = 0.0362$ ,  $wR_2 = 0.0694$  for 4008 data with  $[I > 2\sigma(I)]$  and  $R_1 = 0.0572$ ,  $wR_2 = 0.0796$  for all 5182 data. Residual electron density ( $\text{e}^- \cdot \text{\AA}^{-3}$ ) max/min: 0.488/-0.323.

**X-Ray Crystal Structure of (tPCH=CHP)NiI (21).** X-Ray quality single crystals were obtained as green plates from a concentrated diethyl ether solution at -35 °C in the glovebox. Crystal and refinement data for **21**:  $\text{C}_{26}\text{H}_{38}\text{INiP}_2$ ;  $M_r = 598.11$ ; Monoclinic;

space group P2(1)/n;  $a = 8.0612(15)$  Å;  $b = 15.333(3)$  Å;  $c = 21.312(4)$  Å;  $\alpha = 90^\circ$ ;  $\beta = 91.438(3)^\circ$ ;  $\gamma = 90^\circ$ ;  $V = 2633.4(8)$  Å<sup>3</sup>;  $Z = 4$ ;  $T = 120(2)$  K;  $\lambda = 0.71073$  Å;  $\mu = 2.042$  mm<sup>-1</sup>;  $d_{\text{calc}} = 1.509$  g·cm<sup>-3</sup>; 59339 reflections collected; 6567 unique ( $R_{\text{int}} = 0.0531$ ); giving  $R_1 = 0.0236$ ,  $wR_2 = 0.0477$  for 5501 data with  $[I > 2\sigma(I)]$  and  $R_1 = 0.0352$ ,  $wR_2 = 0.0512$  for all 6567 data. Residual electron density (e<sup>-</sup>·Å<sup>-3</sup>) max/min: 0.604/-0.444.

**X-Ray Crystal Structure of [(*t*PCH=CHP)Pd]<sub>2</sub> (22).** X-Ray quality single crystals were obtained from a concentrated solution of *n*-pentane at -35 °C in the glovebox. Crystal and refinement data for **22**: C<sub>52</sub>H<sub>76</sub>P<sub>4</sub>Pd<sub>2</sub>;  $M_r = 1037.81$ ; Tetragonal; space group P4(1)2(1)2;  $a = 12.8344(11)$  Å;  $b = 12.8344(11)$  Å;  $c = 34.222(3)$  Å;  $\alpha = 90^\circ$ ;  $\beta = 90^\circ$ ;  $\gamma = 90^\circ$ ;  $V = 5637.1(11)$  Å<sup>3</sup>;  $Z = 4$ ;  $T = 120(2)$  K;  $\lambda = 0.71073$  Å;  $\mu = 0.781$  mm<sup>-1</sup>;  $d_{\text{calc}} = 1.223$  g·cm<sup>-3</sup>; 68395 reflections collected; 4970 unique ( $R_{\text{int}} = 0.1171$ ); giving  $R_1 = 0.0382$ ,  $wR_2 = 0.0634$  for 4420 data with  $[I > 2\sigma(I)]$  and  $R_1 = 0.0485$ ,  $wR_2 = 0.0659$  for all 4970 data. Residual electron density (e<sup>-</sup>·Å<sup>-3</sup>) max/min: 0.302/-0.312.

**X-Ray Crystal Structure of [(*t*PCH=CHP)NiMeI (23·2CH<sub>2</sub>Cl<sub>2</sub>).** X-Ray quality single crystals were obtained from a concentrated solution of dichloromethane at -35 °C in the glovebox. Crystal data for **23**: C<sub>29</sub>H<sub>45</sub>Cl<sub>4</sub>INiP<sub>2</sub>;  $M_r = 783.00$ ; Monoclinic; space group P2(1)/c;  $a = 12.3677(11)$  Å;  $b = 13.0174(11)$  Å;  $c = 21.8913(19)$  Å;  $\alpha = 90^\circ$ ;  $\beta = 102.5694(11)^\circ$ ;  $\gamma = 90^\circ$ ;  $V = 3439.9(5)$  Å<sup>3</sup>;  $Z = 4$ ;  $T = 120(2)$  K;  $\lambda = 0.71073$  Å;  $\mu = 1.883$  mm<sup>-1</sup>;  $d_{\text{calc}} = 1.512$  g·cm<sup>-3</sup>; 36026 reflections collected; 6051 unique ( $R_{\text{int}} = 0.0258$ ); giving  $R_1 = 0.0214$ ,  $wR_2 = 0.0509$  for 5412 data with  $[I > 2\sigma(I)]$  and  $R_1 = 0.0260$ ,  $wR_2 = 0.0523$  for all 6051 data. Residual electron density (e<sup>-</sup>·Å<sup>-3</sup>) max/min: 0.767/-0.464.

**X-Ray Crystal Structure of (*t*PC(Bpin)=CHP)Ni (25).** X-Ray quality single crystals were obtained from a concentrated solution of *n*-pentane at -35 °C in the glovebox.

Crystal data for **25**: C<sub>32</sub>H<sub>49</sub>BNiO<sub>2</sub>P<sub>2</sub>; M<sub>r</sub> = 597.17; Triclinic; space group P-1; *a* = 10.8552(11) Å; *b* = 11.2829(11) Å; *c* = 14.5725(15) Å; α = 87.1699(17)°; β = 79.0325(16)°; γ = 69.4133(15)°; V = 1640.0(3) Å<sup>3</sup>; Z = 2; T = 120(2) K; λ = 0.71073 Å; μ = 0.72 mm<sup>-1</sup>; d<sub>calc</sub> = 1.209 g·cm<sup>-3</sup>; 38701 reflections collected; 8232 unique (R<sub>int</sub> = 0.065); giving R<sub>1</sub> = 0.0402, wR<sub>2</sub> = 0.1019 for 6116 data with [I > 2σ(I)] and R<sub>1</sub> = 0.0656, wR<sub>2</sub> = 0.1264 for all 6116 data. Residual electron density (e<sup>-</sup>·Å<sup>-3</sup>) max/min: 0.38/-0.35.

### 3.7 References

1. Barrett, B. J.; Iluc, V. M., *Inorg. Chem.* **2014**, *53* (14), 7248-7259.
2. Bennett, M. A.; Johnson, R. N.; Tomkins, I. B., *J. Organomet. Chem.* **1976**, *118* (2), 205-232.
3. Bennett, M. A.; Clark, P. W., *J. Organomet. Chem.* **1976**, *110* (3), 367-381.
4. Bennett, M. A.; Corlett, S.; Robertson, G. B.; Steffen, W. L., *Aust. J. Chem.* **1980**, *33* (6), 1261-1273.
5. Robertso.Gb; Whimp, P. O., *Inorg. Chem.* **1974**, *13* (9), 2082-2088.
6. Bennett, M. A.; Clark, P. W., *J. Organomet. Chem.* **1976**, *110* (3), 367-381.
7. Muller, G.; Panyella, D.; Rocamora, M.; Sales, J.; Fontbardia, M.; Solans, X., *J. Chem. Soc., Dalton Trans.* **1993**, (19), 2959-2967.
8. Martinez, M.; Muller, G.; Panyella, D.; Rocamora, M., *Organometallics* **1995**, *14* (12), 5552-5560.
9. Marlier, E. E.; Tereniak, S. J.; Ding, K. Y.; Mulliken, J. E.; Lu, C. C., *Inorg. Chem.* **2011**, *50* (19), 9290-9299.
10. Yamamoto, A.; Sugimoto, M., *J. Am. Chem. Soc.* **2005**, *127* (45), 15706-15707.
11. Schuster, E. M.; Botoshansky, M.; Gandelman, M., *Angew. Chem. Int. Ed.* **2008**, *47* (24), 4555-4558.
12. Shaffer, A. R.; Schmidt, J. A. R., *Chem. Eur. J.* **2009**, *15* (11), 2662-2673.

13. Imada, Y.; Ueno, K.; Kutsuwa, K.; Murahashi, S. I., *Chem. Lett.* **2002**, (2), 140-141.
14. Briggs, J. R.; Constable, A. G.; McDonald, W. S.; Shaw, B. L., *J. Chem. Soc. Dalton Trans.* **1982**, (7), 1225-1230.
15. Yamazaki, S.; Yoshimura, T.; Yamabe, S.; Arai, T.; Tamura, H., *J. Org. Chem.* **1990**, 55 (1), 263-269.
16. Kundu, S.; Brennessel, W. W.; Jones, W. D., *Inorg. Chem.* **2011**, 50 (19), 9443-9453.
17. Vasudevan, K. V.; Scott, B. L.; Hanson, S. K., *Eur. J. Inorg. Chem.* **2012**, (30), 4898-4906.
18. van der Vlugt, J. I.; Lutz, M.; Pidko, E. A.; Vogt, D.; Spek, A. L., *Dalton Trans.* **2009**, (6), 1016-1023.
19. Ohashi, M.; Shibata, M.; Saijo, H.; Kambara, T.; Ogoshi, S., *Organometallics* **2013**, 32 (13), 3631-3639.
20. Gareau, D.; Sui-Seng, C.; Groux, L. F.; Brisse, F.; Zargarian, D., *Organometallics* **2005**, 24 (16), 4003-4013.
21. Kelley, P.; Lin, S. B.; Edouard, G.; Day, M. W.; Agapie, T., *J. Am. Chem. Soc.* **2012**, 134 (12), 5480-5483.
22. Lin, S. B.; Day, M. W.; Agapie, T., *J. Am. Chem. Soc.* **2011**, 133 (11), 3828-3831.
23. Velian, A.; Lin, S. B.; Miller, A. J. M.; Day, M. W.; Agapie, T., *J. Am. Chem. Soc.* **2010**, 132 (18), 6296-6297.
24. Kruckenberg, A.; Wadepohl, H.; Gade, L. H., *Organometallics* **2013**, 32 (18), 5153-5170.
25. Beck, R.; Shoshani, M.; Krasinkiewicz, J.; Hatnean, J. A.; Johnson, S. A., *Dalton Trans.* **2013**, 42 (5), 1461-1475.
26. Heimbach, P., *Angew. Chem. Int. Ed.* **1964**, 3 (9), 648.
27. Herbert, D. E.; Lara, N. C.; Agapie, T., *Chem. Eur. J.* **2013**, 19 (48), 16453-16460.
28. Anderson, J. S.; Iluc, V. M.; Hillhouse, G. L., *Inorg. Chem.* **2010**, 49 (21), 10203-10207.

29. Iluc, V. M.; Hillhouse, G. L., *J. Am. Chem. Soc.* **2010**, *132* (43), 15148-15150.
30. Mindiola, D. J.; Waterman, R.; Jenkins, D. M.; Hillhouse, G. L., *Inorg. Chim. Acta.* **2003**, *345*, 299-308.
31. Sgro, M. J.; Stephan, D. W., *Organometallics* **2012**, *31* (5), 1584-1587.
32. Sgro, M. J.; Stephan, D. W., *Dalton Trans.* **2012**, *41* (22), 6791-6802.
33. Breitenfeld, J.; Scopelliti, R.; Hu, X. L., *Organometallics* **2012**, *31* (6), 2128-2136.
34. Chakraborty, S.; Krause, J. A.; Guan, H., *Organometallics* **2009**, *28* (2), 582-586.
35. Chakraborty, S.; Zhang, J.; Krause, J. A.; Guan, H. R., *J. Am. Chem. Soc.* **2010**, *132* (26), 8872-8873.
36. Fan, L.; Ozerov, O. V., *Chem. Commun.* **2005**, (35), 4450-4452.
37. Liang, L. C.; Chien, P. S.; Lin, J. M.; Huang, M. H.; Huang, Y. L.; Liao, J. H., *Organometallics* **2006**, *25* (6), 1399-1411.
38. Touney, E. E.; Hoveln, R.; Buttke, C. T.; Freidberg, M. D.; Guzei, I. A.; Schomaker, J. M., *Organometallics* **2016**, *35* (20), pp 3436–3439.
39. Selander, N.; Willy, B.; Szabó, K. J., *Angew. Chem. Int. Ed.* **2010**, *49* (24), 4051-4053.
40. Ritleng, V.; Henrion, M.; Chetcuti, M. J., *ACS Catal.* **2016**, *6* (2), 890-906.
41. Reid, W. B.; Spillane, J. J.; Krause, S. B.; Watson, D. A., *J. Am. Chem. Soc.* **2016**, *138* (17), 5539-5542.
42. Onozawa, S.-y.; Tanaka, M., *Organometallics* **2001**, *20* (14), 2956-2958.
43. Kirai, N.; Iguchi, S.; Ito, T.; Takaya, J.; Iwasawa, N., *Bull. Chem. Soc. Jpn.* **2013**, *86* (7), 784-799.
44. Bain, G. A.; Berry, J. F., *J. Chem. Ed.* **2008**, *85* (4), 532-536.
45. Sur, S. K., *J. Mag. Res.* **1989**, *82* (1), 169-173.
46. Evans, D. F., *J. Chem. Soc.* **1959**, (Jun), 2003-2005.
47. Bruker AXS,. APEX-2. Bruker-Nonius AXS, Madison, Wisconsin, USA, 2014.

48. Krause, L.; Herbst-Irmer, R.; Sheldrick, G. M.; Stalke, D., *J. Appl. Cryst.* **2015**, *48* (1), 3-10.
49. Sheldrick, G., *Acta Cryst.* **2015**, *A71* (1), 3-8.
50. Macrae, C. F.; Bruno, I. J.; Chisholm, J. A.; Edgington, P. R.; McCabe, P.; Pidcock, E.; Rodriguez-Monge, L.; Taylor, R.; van de Streek, J.; Wood, P. A., *J. Appl. Cryst.* **2008**, *41* (2), 466-470.

CHAPTER 4:  
METAL-LIGAND COOPERATION BETWEEN PALLADIUM AND A DIPHOSPHINE  
LIGAND WITH A CIS OLEFINIC BACKBONE

#### 4.1 Introduction

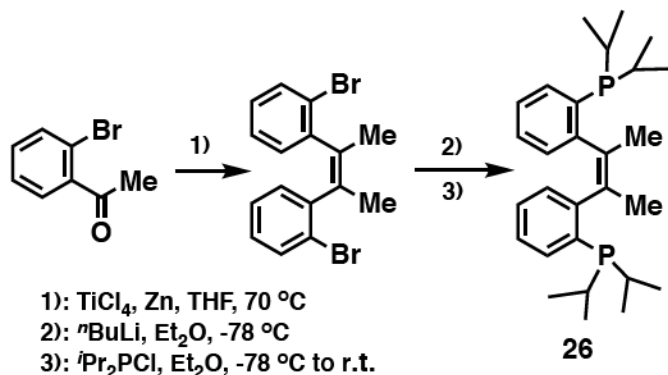
As discussed in the previous two chapters, various coordination modes of the ligand *t*PCH=CHP (**1**) with late transition metals was explored. Depending on the requirements of the metal center, we observed non-coordination, and  $\eta^2$ -coordination with group 8, 9, and 11 metals.<sup>1</sup> Group 10 metals underwent C-H activation of the olefin backbone in  $d^8$  complexes resulting in a vinyl coordination mode; behavior which was avoided through the installation of methyl groups on the olefin backbone, forcing  $\eta^2$ -coordination.<sup>2</sup> It next became interesting to study the cis analogue of *t*PCMe=CMeP (**17**) (2,2'-bis(di-*iso*-propylphosphino)-*cis*-diphenyl-1,2-dimethylethene, *c*PCMe=CMeP, **26**) to see if the strain in the backbone resulting upon coordination would influence the cooperativity of the ligand system.<sup>3</sup> Coordination of ligand **17** to group 10 transition metals results in species in which coordination of the central olefin is relatively unstrained, and therefore olefin coordination is maintained, only allowing for one additional ligand in the coordination sphere of the metal center. It was hypothesized that the higher strain resulting upon coordination of ligand **26** would enhance the hemilability of the ligand backbone. Dissociation of the olefin upon oxidative addition of a substrate is expected to occur due to a drive to minimize strain



in the ligand backbone, opening an additional coordination site at the metal center.<sup>4</sup> In this chapter the coordination modes, as well as metal-ligand cooperativity exhibited between *c*PCMe=CMeP (**26**) and palladium will be discussed.

## 4.2 Results and Discussion

The ligand precursor, (Z)-2,3-bis(2-bromophenyl)-2-butene, was synthesized via the McMurry coupling reaction of 2'-bromoacetophenone as discussed in Chapter 3.<sup>5-6</sup> The final ligand (**26**, 2,2' bis(di-*iso*-propylphosphino)-*cis*-diphenyl-1,2-dimethylethene, *c*PCMe=CMeP) is synthesized through the lithium halogen exchange of the ligand precursor, followed by treatment with di-*iso*-propyl phosphine chloride (Scheme 4.1). Compound *c*PCMe=CMeP is identified in its <sup>31</sup>P NMR spectrum by a singlet at -1.86 ppm. The high symmetry of the compound is further reflected in its <sup>1</sup>H NMR spectrum: the backbone methyl groups resonate equivalently as a singlet at 2.25 ppm.



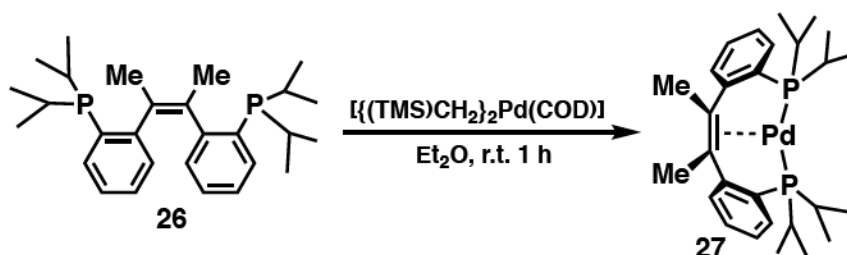
**Scheme 4.1:** Synthesis of *c*PCMe=CMeP (**26**).

Initially, the synthesis of a palladium(0) species was carried out. Reacting *c*PCMe=CMeP (**26**) with one equivalent of  $[\{(\text{TMS})\text{CH}_2\}_2\text{Pd}(\text{cod})]$  in diethyl ether at room temperature rapidly leads to the formation of a three coordinate Pd(0) species,

[(*c*PCMe=CM*e*P)Pd], **27** (Scheme 4.2). Characterization of **27** by NMR spectroscopy revealed equivalent phosphine environments as a singlet at 48.6 ppm in the <sup>31</sup>P NMR spectrum and C<sub>s</sub> symmetry in the <sup>1</sup>H NMR spectrum. The olefin methyl groups resonate as a virtual triplet due to coupling with the phosphines through the metal center at 2.21 ppm. The high symmetry in the NMR spectra is indicative of a monomeric instead of a dimeric species. This contrasts the dimeric palladium(0) species that was synthesized previously with the related ligand, *t*PCH=CHP, when the olefin and phosphine from one ligand coordinate to the metal center, along with a phosphine from an additional ligand (**22**, Chapter 3).<sup>2</sup> The different coordination mode for *c*PCMe=CM*e*P (**26**) is attributed to the increased strain of the ligand backbone as well as steric factors. The solution and solid state structures agree, as determined by X-ray crystallography (Figure 4.1); a severely distorted trigonal planar geometry is observed. The metal center is bound to the olefin, as indicated by the Pd-(C(1)-C(2) centroid) distance of 2.076 Å, as well as the elongation of the olefin C-C distance to 1.404(3) Å compared to typical olefin distances of approximately 1.34 Å.<sup>7-</sup>

<sup>8</sup> The P(1)-Pd-P(2) angle of 140.70(2)°, as well as the sum of angles around the metal center (344.59°), illustrates the degree of distortion from an ideal trigonal planar geometry. Our group has previously synthesized a monomeric trigonal planar palladium(0) species with the wide bite angle ligand *i*Pr<sub>2</sub>P(*o*-C<sub>6</sub>H<sub>4</sub>-CH<sub>2</sub>CH<sub>2</sub>-*o*'-C<sub>6</sub>H<sub>4</sub>)P<sup>*i*</sup>Pr<sub>2</sub>, L<sup>2</sup>.<sup>9</sup> The metal center is bound to an olefin of a dba ligand, as well as to the two phosphine donors on L<sup>2</sup>. The non-tethered olefin in that situation allows for a more optimal trigonal planar geometry of the metal center (P-Pd-P = 117.117(17)).<sup>9</sup> Examples of ligands containing two phosphines and a π system donor in the same ligand framework were reported.<sup>10-11</sup> Agapie and coworkers described a tris(phosphine) triphenyl benzene ligand that supports a

palladium(0) metal center. Palladium coordinates to two phosphines from the ligand and to the central phenyl ring in an  $\eta^2$  fashion. Contrasting compound **27**, a smaller P-Pd-P angle is observed ( $128.78^\circ$ ) due to the increased flexibility of their ligand side arms.<sup>10</sup> In addition, it was reported that 3,5-bis(2-phosphinophenyl)-pyridine exhibits less flexibility than the tris(phosphine) triphenyl benzene.<sup>10</sup> The coordination sphere of palladium(0) when supported by 3,5-bis(2-phosphinophenyl)-pyridine consists of the two phosphine donors and an  $\eta^1$ -N interaction to the central pyridine ring. Similarly to **27**, the P-Pd-P angle is much wider ( $155.65^\circ$ ) than  $120^\circ$  however, the overall geometry is best described as T-shaped in that situation.<sup>11</sup>



**Scheme 4.2:** Synthesis of **27**.

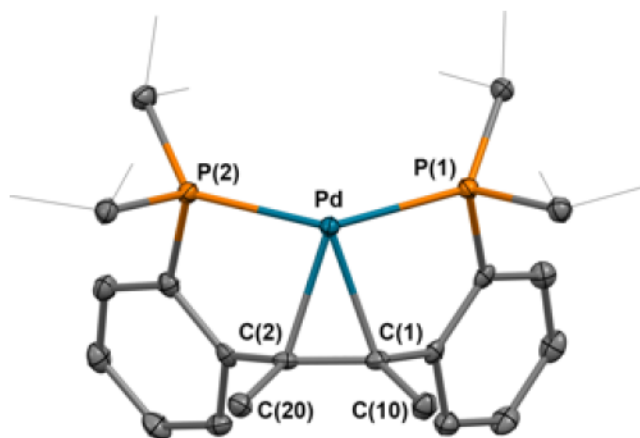
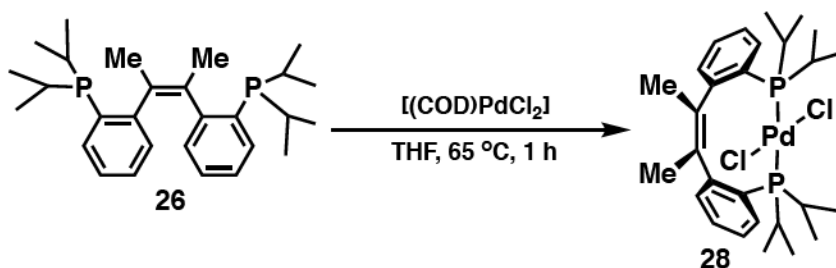


**Figure 4.1:** Thermal-ellipsoid (50% probability level) representation of  $[(cPCMe=CMcP)Pd]$  (**27**). Hydrogen atoms and the solvent molecule were omitted for clarity. Selected distances (Å) and angles ( $^\circ$ ): Pd–P(1) = 2.2748(6), Pd–P(2) = 2.2892(6), Pd–C(1) = 2.198(2), Pd–C(2) = 2.186(2) C(1)–C(2) = 1.404(3), P(1)–Pd–P(2) =  $140.70(2)$ , C(1)–Pd–C(2) =  $37.35(8)$  C(1)–Pd–P(1) =  $84.08(6)$ , C(2)–Pd–P(2) =  $83.82(6)$ .

Contrasting **27**, complexes formed with palladium(II) exhibit a dissociated olefin backbone. Reacting **26** with [(cod)PdCl<sub>2</sub>] results in a distorted square planar species, [(*c*PCMe=CMeP)PdCl<sub>2</sub>] (**28**, Scheme 4.3). The <sup>1</sup>H NMR spectrum reveals C<sub>s</sub> symmetry and supports the dissociated state of the olefin through the loss of coupling from the backbone methyl groups to the phosphines. In the <sup>31</sup>P NMR spectrum, the phosphines resonate equivalently as a singlet at 68.7 ppm. The solid state molecular structure depicts a distorted square planar compound (Figure 4.2). The P(1)-Pd-P(2) angle (162.75(4)°) is reduced from the optimal 180° due to the close proximity of the ligand backbone to the metal center (Pd-(C(1)-C(2) centroid) = 3.076 Å). The coordination mode of the ligand **26** in this palladium(II) complex is different than the one observed for the trans-analogue, *t*PCMe=CMeP (**17**), which exhibited a coordinated olefin in the resulting cationic complex.<sup>2</sup> In this case, the strained geometry of the backbone disfavors coordination of the olefin, allowing the four-coordinate species to be neutral. Similarly rigid ligands have been prepared by Vogt and coworkers.<sup>12</sup> The diphosphine 1,2-bis(2-(diphenylphosphino)phenyl)benzene is structurally similar to *c*PCMe=CMeP, however, the central olefin moiety of the latter is replaced by a central ortho substituted arene group in the former. Similarly to our observations, only a bidentate coordination of 1,2-bis(2-(diphenylphosphino)phenyl)benzene to group 10, d<sup>8</sup> metal centers was observed. However, cis coordination was observed instead of the trans coordination observed with *c*PCMe=CMeP.<sup>12</sup> Diphosphine ligands that coordinate in a cis arrangement are more numerous than trans coordinating ligands.<sup>13-14</sup> The excessive flexibility of the larger backbones required for trans coordination can often lead to the formation of dimers and oligomers. Additionally, the activation of the backbone of such large ligands can often lead

to tridentate supporting ligands, making bidentate trans coordinating ligands more elusive than their cis coordinating counterparts.<sup>13-14</sup>



**Scheme 4.3:** Synthesis of **28**.

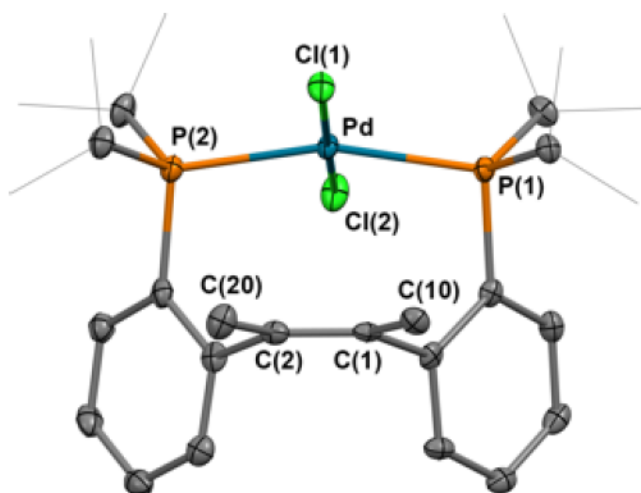
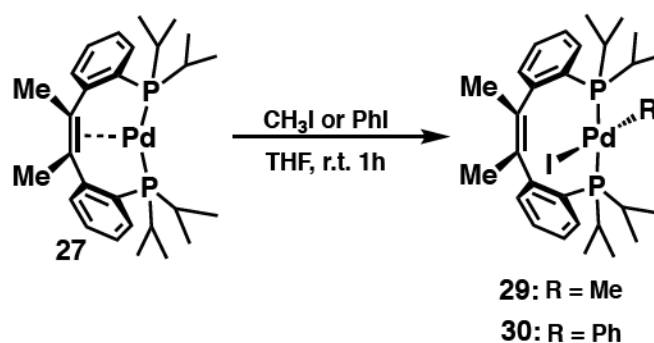


**Figure 4.2:** Thermal-ellipsoid (50% probability level) representation of  $[(cPCMe=CMcP)PdCl_2]$  (**28**). Hydrogen atoms were omitted for clarity. Selected distances (Å) and angles (°): Pd–P(1) = 2.3031(9), Pd–P(2) = 2.3019(10), Pd–Cl(1) = 2.3251(10), Pd–Cl(2) = 2.3194(10), C(1)–C(2) = 1.346(5), P(1)–Pd–P(2) = 162.75(4), Cl(1)–Pd–Cl(2) = 175.05(4), Cl(1)–Pd–P(1) = 95.09(3), Cl(2)–Pd–P(2) = 84.73(4).

Due to the different coordination modes of the ligand between **27** and **28**, we became interested in investigating oxidative addition reactions of **27** in order to determine whether hemilability of the olefinic backbone could be observed when transitioning from Pd(0) to Pd(II) complexes, as well as whether the trans phosphine coordination is preferred over cis in the final Pd(II) products. These studies were carried out with  $CH_3I$ ,  $C_6H_5I$ ,

$\text{Ph}_2\text{SiH}_2$ , and  $\text{HCl}$ . In reactions involving of  $\text{CH}_3\text{I}$  and  $\text{C}_6\text{H}_5\text{I}$ , the oxidative addition of the respective substrate results in dissociation of the olefinic backbone generating the square planar compounds  $[(c\text{PCMe}=\text{CMeP})\text{PdI}(\text{CH}_3)]$  (**29**) and  $[(c\text{PCMe}=\text{CMeP})\text{PdI}(\text{C}_6\text{H}_5)]$  (**30**, Scheme 4.4). In both species, the backbone methyl groups resonate as a singlet at 2.19 and 2.20 ppm respectively, indicating the dissociated state of the olefin. The solid state molecular structures of both compounds show trans phosphine coordination of the ligand as well as a preference for the iodide moiety to add to the metal center *syn* to the backbone olefin (Figures 4.3-4.4). It is likely that this arrangement avoids the close proximity of the backbone that would result if the alkyl (**29**) or aryl (**30**) group adds adjacent to the olefin. The presence of the backbone directs the bulkier alkyl and aryl substituent to reside in the *anti* position to minimize steric interactions. Like compound **28**, the geometry observed in **29** and **30** is distorted square planar. The P-Pd-P angles bend to  $160.18(4)^\circ$  and  $157.96(3)^\circ$  respectively from the optimal  $180^\circ$  to avoid steric interactions with the ligand backbone and the additional ligands around the metal center. This bending results in elongated Pd-(C-C centroid) distances of 3.133 and 3.173 Å, respectively compared to the distance of 2.076 Å observed upon olefin coordination in **27**. Interestingly, compound **30** has an aryl proton resonating at 4.4 ppm in the  $^1\text{H}$  NMR spectrum. This surprising upfield shift of an aryl proton is justified when examining the solid state molecular structure of the compound (Figure 4.4). The phenyl group is oriented *anti* to the olefin, and therefore resides between the two aryl groups in the ligand framework, placing one of the phenyl protons inside the shielding environment of the aromatic rings on the ligand backbone.<sup>15</sup> It should be noted that the oxidative addition of both substrates results in their trans coordination to the metal center. This is a result of isomerization and was previously observed in complexes with

ligands that have a preference for trans coordination.<sup>9,16-17</sup> A previous report from our group also shows a preference of the diphosphine  $i\text{Pr}_2\text{P}(o\text{-C}_6\text{H}_4\text{-CH}_2\text{CH}_2\text{-}o'\text{-C}_6\text{H}_4)\text{P}^i\text{Pr}_2$  ( $\text{L}^2$ ) for trans coordination to palladium metal centers. In that case, the oxidative addition of *p*-nitrobromobenzene to  $\text{L}_2\text{Pd}$  resulted in a trans Pd(II) species as the only observable product.<sup>9</sup> Additionally, the trans coordinating ligand, dbaphos, reported by Lin and Fairlamb also results in *trans*-(dbaphos)PdIPh when the oxidative addition of iodobenzene is carried out.<sup>16</sup>



**Scheme 4.4:** Oxidative addition of  $\text{CH}_3\text{I}$  and  $\text{PhI}$  to **27**.

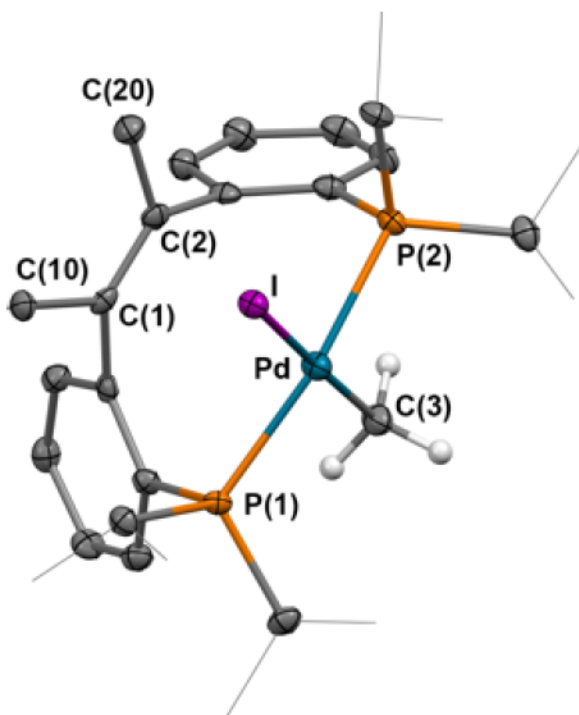


**Figure 4.3:** Thermal-ellipsoid (50% probability level) representation of  $[(cPCMe=CMeP)PdICH_3]$  (**29**). Most hydrogen atoms were omitted for clarity. Selected distances (Å) and angles (°): Pd–P(1) = 2.2972(11), Pd–P(2) = 2.2944(11), Pd–C(3) = 2.084(4), Pd–I = 2.6828(4), C(1)–C(2) = 1.345(6), P(1)–Pd–P(2) = 160.18(4), C(3)–Pd–I = 174.47(13), C(3)–Pd–P(1) = 84.72(12), I–Pd–P(2) = 96.36(3).

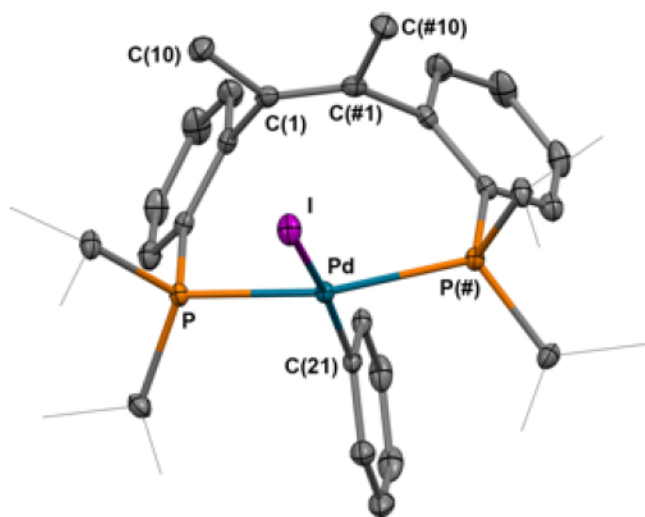
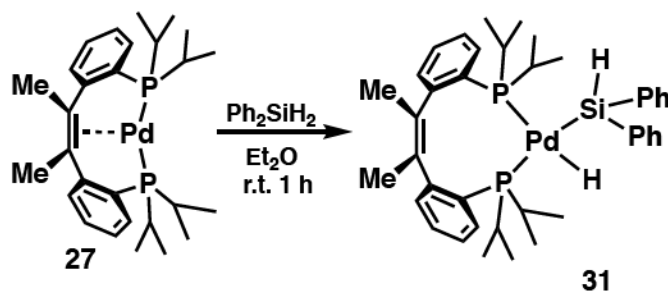


**Figure 4.4:** Thermal-ellipsoid (50% probability level) representation of  $[(cPCMe=CMeP)PdI(C_6H_5)]$  (**30**). Hydrogen atoms were omitted for clarity. Selected distances (Å) and angles (°): Pd–P = 2.3229(5), Pd–P(1) = 2.3229(5), Pd–C(21) = 2.058(3), Pd–I = 2.6992(3), C(1)–C(1) = 1.341(4), P–Pd–P(1) = 157.96(3), C(21)–Pd–I = 169.85(8), C(21)–Pd–P = 84.981(18), I–Pd–P(1) = 96.666(13).



The oxidative addition of  $\text{Ph}_2\text{SiH}_2$  proved to be an interesting case study due to the reversible nature of the Si-H bond activation process.<sup>18-20</sup> Reacting **27** with  $\text{Ph}_2\text{SiH}_2$  (Scheme 4.5) results in the rapid formation of a new compound  $[(\text{cPCMe}=\text{CMeP})\text{Pd}(\text{H}_2\text{SiPh}_2)]$  (**31**), which is readily identified in the corresponding  $^{31}\text{P}$  NMR spectrum at 37.75 ppm as a singlet. Characterization by  $^1\text{H}$  NMR spectroscopy indicates a coordinated olefin backbone as attested by the presence of a virtual triplet at 2.16 ppm. The Si-H protons resonate equivalently and are shifted upfield from free  $\text{Ph}_2\text{SiH}_2$  (5.02 ppm) to 4.55 ppm, indicating an interaction with the metal center. Furthermore, single crystal X-ray diffraction showed a distorted square planar metal center resulting from the oxidative addition of a Si-H bond from  $\text{Ph}_2\text{SiH}_2$  (Figure 4.5). The olefinic backbone is dissociated, as substantiated by the Pd-(C(1)-C(2) centroid) distance of 3.130 Å, along with the short C(1)-C(2) distance of 1.339(3) Å. In addition to the contrasting state of the olefin observed in solution and the solid state, another distinction related to the hydrogen atoms originating from the silane was noticed. The solid state structure reveals two distinct environments for these hydrogen atoms, including a palladium hydride and an unchanged Si-H bond which did not undergo a reaction with the metal center. The lack of distinct hydrogen atom signals in the  $^1\text{H}$  NMR spectrum indicates a fast equilibrium in which the Si-H bond cleavage by the metal center is reversible. Similar situations were previously reported for group 10 metals.<sup>18-20</sup> For example, Hillhouse and coworkers found that reacting the nickel(0) compound  $(\text{dtbpe})\text{Ni}$  ( $\text{dtbpe} = 1,2\text{-bis}(\text{di-}t\text{-butylphosphino})\text{ethane}$ ) with dimesitylsilane ( $\text{Mes}_2\text{SiH}_2$ ) led to a species that undergoes a dynamic process involving the reversible oxidative addition of the Si-H bond through a

Ni(0)- $\eta^2$  silane intermediate. This is observed in the  $^1\text{H}$  NMR spectrum via the SiH signal found at  $\sim 0$  ppm, an average of the resonance of the free silane and the nickel hydride resonance.<sup>18</sup> A similar observation was reported for a palladium(0) species by Fink and coworkers.<sup>20</sup> It was found that the oxidative addition of  $\text{R}_3\text{SiH}$  ( $\text{R}_3 = \text{Ph}_3, \text{Ph}_2\text{Me}, \text{PhMe}_2, \text{Et}_3$ ) to the dimeric palladium(0) species  $[(\mu\text{-dcpe})\text{Pd}]_2$  (dcpe = 1,2-bis-(dicyclohexylphosphino)ethane) produced the dynamic compound  $\text{PdH}(\text{SiHR}_3)(\text{dcpe})$ . Similarly to the report by Hillhouse and coworkers, the SiH resonance was found as an average of that for the free silane and a metal hydride species ( $-1$  to  $-2$  ppm). Comparing their results to the data obtained for complex **31**, it is concluded that a similar dynamic process is occurring, however, the presence of the olefin backbone heavily pushes the equilibrium toward the Pd(0) complex. The appearance of the SiH protons downfield at 4.55 ppm indicates that the weighted average of the species present in solution favors the unreacted ( $c\text{PCMe}=\text{CMeP}$ )Pd or a  $\sigma$ -bound Si-H species. It is also of interest to note that **31** represents the only case observed so far in which oxidative addition results in cis-coordination of the ligand **26**.



**Scheme 4.5:** Reactivity of **27** with  $\text{Ph}_2\text{SiH}_2$ .

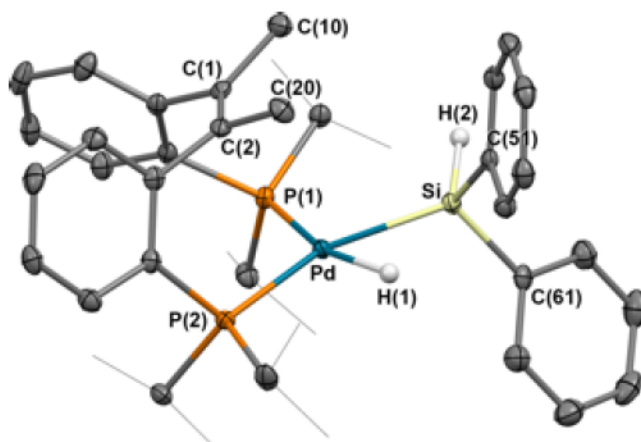
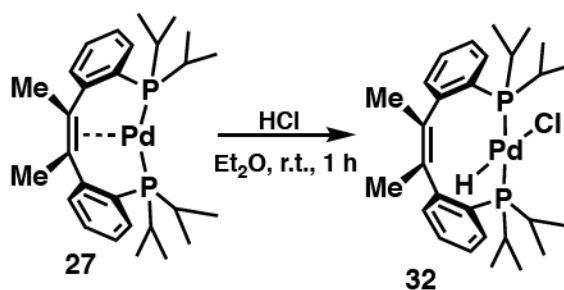


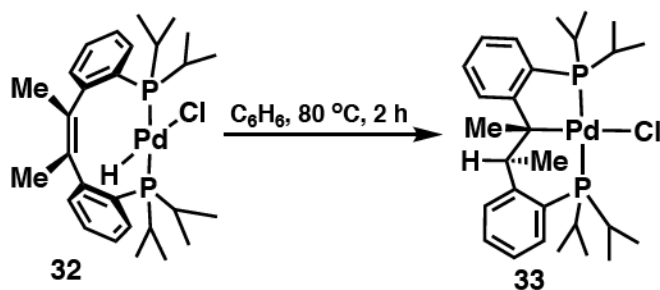
**Figure 4.5.** Thermal-ellipsoid (50% probability level) representation of  $[(cPCMe=CMcP)PdH_2SiPh_2]$  (**31**). Most hydrogen atoms were omitted for clarity. Selected distances (Å) and angles (°): Pd–P(1) = 2.3365(6), Pd–P(2) = 2.3759(6), Pd–Si = 2.3298(6), Pd–H(1) = 1.61(3), Si–H(2) = 1.41(2), Si–H(1) = 1.95(3), C(1)–C(2) = 1.339(3), P(1)–Pd–P(2) = 109.955(19), Si–Pd–H(1) = 56.0(9), Si–Pd–P(1) = 103.33(2), H(1)–Pd–P(2) = 91.0(9).

Reacting  $[(cPCMe=CMcP)Pd]$ , **27**, with one equivalent of HCl in diethyl ether at room temperature led to the clean formation of a chloro-hydride species,  $[(cPCMe=CMcP)PdHCl]$  (**32**, Scheme 4.6). The hydride is found upfield in the corresponding  $^1H$  NMR spectrum at -14.58 ppm as a singlet. Coupling between the hydride and the phosphorous nuclei was not observed even at low temperatures. The methyl groups of the ligand backbone resonate as a singlet at 2.34 ppm. The lack of coupling between the methyl groups and the phosphines is suggestive of a dissociated olefin moiety. The  $^{31}P$  NMR spectrum displays the equivalent phosphines as a singlet at 37.27 ppm. The lack of coupling observed between the hydride and the phosphines, as well as the similar chemical shift observed in the  $^{31}P$  NMR spectrum compared to the other trans compounds discussed previously (**28-30**), indicates that  $cPCMe=CMcP$  coordinates in a trans fashion.



**Scheme 4.6:** Reactivity of **27** with HCl.

Compound **32** transformed, after 12 hours, into a new asymmetric compound (**33**) as indicated by the  $^1\text{H}$  and  $^{31}\text{P}$  NMR spectra. After 4 days at room temperature, the original chloro-hydride species, **32**, was completely consumed, leading to a clean solution of compound **33**. This process can also be accomplished by heating the solution to 80 °C for 2 h (Scheme 4.7). The  $^1\text{H}$  NMR of **33** contains five separate methine resonances, as well as two separate peaks for the backbone methyl groups at 1.59 and 1.16 ppm, respectively, indicating protonation of the ligand backbone. This conclusion is further supported by the loss of the hydride signal. The inequivalent phosphine environments are found in the  $^{31}\text{P}$  NMR spectrum as trans coupling doublets at 66.09 and 18.48 ppm, respectively ( $^2J_{\text{PP}} = 356$  Hz). The solid state molecular structure, obtained from a concentrated toluene solution layered with *n*-pentane, confirms the protonation of the ligand backbone with an elongated C(1)-C(2) distance of 1.460(7) Å, along with an  $\text{sp}^3$  hybridization of C(1) and C(2) (Figure 4.6). Palladium hydrides are known to be short lived in the presence of an olefin due to the alkene insertion into the Pd-H bond.<sup>21-22</sup> Assessing the stereochemistry of the protonated backbone reveals a *syn*-addition to the olefin, allowing an intramolecular migratory insertion to be a plausible mechanism for this process.<sup>23</sup> However, an unlikely intermolecular protonation pathway followed by the isomerization of the backbone could not be ruled out.



**Scheme 4.7:** Conversion of **32** to **33**.

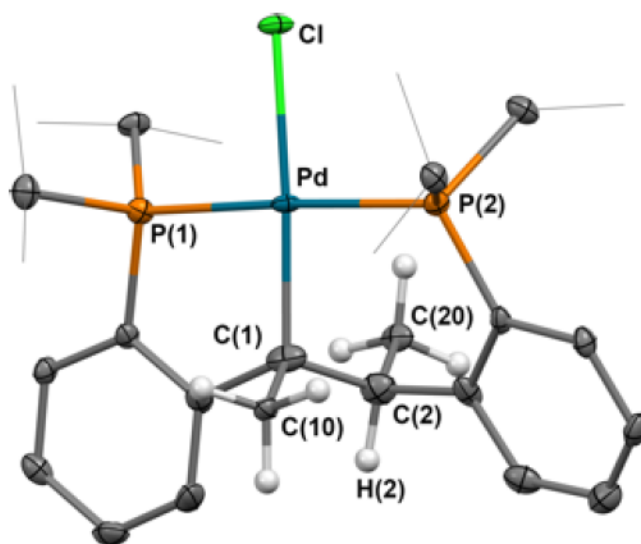
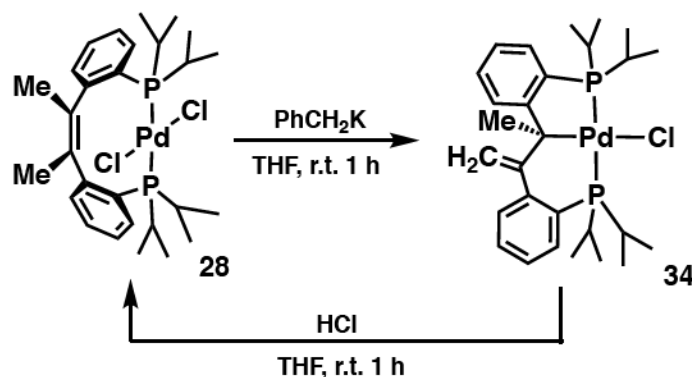


**Figure 4.6:** Thermal-ellipsoid (50% probability level) representation of [(PCMe-CHMeP)PdCl] (**33**). Most hydrogen atoms were omitted for clarity. Selected distances (Å) and angles (°): Pd–P(1) = 2.2704(12), Pd–P(2) = 2.3140(12), Pd–Cl = 2.4174(11), Pd–C(1) 2.108(5), C(1)–C(2) = 1.460(7), P(1)–Pd–P(2) = 177.35(5), Cl–Pd–C(1) = 174.56(15), Cl–Pd–P(1) = 91.08(4), C(1)–Pd–P(2) = 93.46(16), Pd–C(1)–C(2) = 109.6(4).

The formation of **33** from **32** demonstrates the hydrogen acceptor capabilities of the ligand backbone. Therefore, we decided to study if the ligand could also act as a hydrogen atom donor. Attempts at deprotonating the olefin insertion product to reform the Pd(0) species (**27**) by reacting **33** with a base failed, likely because of the presence of

multiple deprotonation sites. Consequently, the dehydrohalogenation of  $[(cPCMe=CMeP)PdCl_2]$  (**28**) was targeted instead. Reacting **28** with one equivalent of benzyl potassium led to the formation of a new asymmetric species after 1 hour (Scheme 4.8). Characterization of the product,  $[(PCMe-C(=CH_2)P)PdCl]$  (**34**), revealed the deprotonation of a methyl group on the olefin, resulting in the rearrangement of the ligand backbone. The new olefinic protons can be observed in the  $^1H$  NMR spectrum as a doublet of doublets at 4.85 and 4.63 ppm, respectively, due to the coupling with the two non-equivalent phosphines. The  $^{31}P\{^1H\}$  NMR spectrum shows the two phosphines as trans coupling doublets (356 Hz) at 68.09 and 18.49 ppm, respectively. Crystals suitable for single crystal X-ray diffraction were obtained from a concentrated *n*-pentane solution. The solid state molecular structure (Figure 4.7) confirms the rearrangement of the backbone upon the deprotonation of a methyl group. The C(2)-C(4) distance of 1.366(5) Å is indicative of a C-C double bond, while the C(1)-C(2) distance of 1.473(5) Å is characteristic of a C-C single bond. The deprotonation of the backbone was found to be reversible. Treating a THF solution of **34** with one equivalent of HCl cleanly forms **28**.



**Scheme 4.8:** Synthesis of **34**.

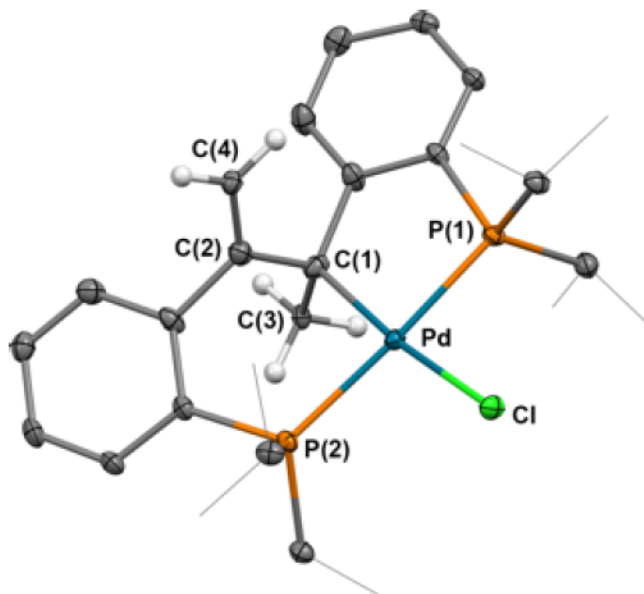


**Figure 4.7:** Thermal-ellipsoid (50% probability level) representation of  $[(\text{PC}(\text{CH}_3)\text{-C}(\text{=CH}_2)\text{P})\text{PdCl}]$  (**34**). Most hydrogen atoms were omitted for clarity. Selected distances (Å) and angles ( $^\circ$ ): Pd–P(1) = 2.2815(8), Pd–P(2) = 2.3434(8), Pd–Cl = 2.4176(8), Pd–C(1) = 2.104(3), C(1)–C(2) = 1.473(5), C(2)–C(4) = 1.366(5), C(1)–C(3) = 1.520(5), P(1)–Pd–P(2) = 176.62(3), Cl–Pd–C(1) = 173.23(10), Cl–Pd–P(1) = 91.88(3), C(1)–Pd–P(2) = 93.90(11), Pd–C(1)–C(2) = 100.6(2), C(1)–C(2)–C(4) = 122.7(3).

#### 4.3 Summary

The chelating ligand  $c\text{PCMe}=\text{CMeP}$  (**26**) was synthesized to study the coordination of the olefinic backbone in several palladium complexes. Hemilabile behavior was observed during the oxidative addition of  $\text{CH}_3\text{I}$ ,  $\text{C}_6\text{H}_5\text{I}$ ,  $\text{Ph}_2\text{SiH}_2$ , and  $\text{HCl}$  to  $(c\text{PCMe}=\text{CMeP})\text{Pd}$  (**27**). Full dissociation of the olefin occurred in all cases except for the silane substrate, when a reversible Si–H activation in conjunction with a reversible olefin dissociation were observed. The capabilities of the olefinic moiety in the ligand to act as an H-atom reservoir were probed through its protonation by a Pd–H species, as well as in the dehydrohalogenation of  $[(c\text{PCMe}=\text{CMeP})\text{PdCl}_2]$  upon the addition of a base.

#### 4.4 Experimental

All manipulations of air and water sensitive compounds were performed under a dry nitrogen atmosphere using an MBraun drybox. Glassware, vials, and stirbars were dried in an oven at 120 °C overnight and evacuated for 12 h in the antechamber before being brought into the drybox. All solvents were dried by passing through a column of activated alumina, followed by storage over molecular sieves and sodium. Deuterated solvents were purchased from Cambridge Isotope Laboratories. C<sub>6</sub>D<sub>6</sub> was dried by stirring over CaH<sub>2</sub> followed by filtration. CDCl<sub>3</sub> was dried over molecular sieves. [(TMS)CH<sub>2</sub>]<sub>2</sub>Pd(cod)]<sup>24</sup> was prepared according to literature procedures. All other chemicals were commercially available and used as received unless otherwise indicated. NMR spectra were obtained on Bruker 400 and Bruker 500 spectrometers at ambient temperature. Chemical shift values are reported in ppm relative to residual internal protio solvents or to a TMS standard while using CDCl<sub>3</sub> for <sup>1</sup>H and <sup>13</sup>C{<sup>1</sup>H} experiments. <sup>31</sup>P{<sup>1</sup>H} NMR chemical shifts are reported relative to H<sub>3</sub>PO<sub>4</sub> (85% in D<sub>2</sub>O, 0 ppm). Coupling constants are reported in Hz.

**Synthesis of (Z)-2,3-Bis(2-di-iso-propylphosphinephenyl)-2-butene (cPCMe=CMeP, 26)** The precursor (Z)-2,3-bis(2-bromophenyl)-2-butene was synthesized as previously reported in 90% yield.<sup>5-6</sup> The precursor (2.8 g, 7.3 mmol) was dissolved in 30 mL of Et<sub>2</sub>O, and chilled to -78 °C. Two equivalents of *n*-butyllithium were added to the solution via syringe (9.9 mL, 15.8 mmol). The mixture was stirred at room temperature for 1 h. The solution was once again chilled to -78 °C before adding two equivalents of di-*iso*-propyl phosphine chloride (2.3 mL, 15.8 mmol). After stirring the solution for 12 h, the mixture was quenched with 2 mL of a degassed 10% solution of NH<sub>4</sub>Cl. The solution was dried over Na<sub>2</sub>SO<sub>4</sub> followed by filtration over a pad of Celite. The



volatiles were removed under reduced pressure, leaving behind the crude residue of **26**. The compound was recrystallized from a concentrated solution of *n*-pentane in 83% yield. For **26**:  $^1\text{H}$  NMR (400 MHz,  $\text{C}_6\text{D}_6$ )  $\delta$ : 1.03 (m, 12H,  $\text{CH}(\text{CH}_3)_2$ ), 1.18 (m, 12H,  $\text{CH}(\text{CH}_3)_2$ ), 1.80 (m, 2H,  $\text{CH}(\text{CH}_3)_2$ ), 2.05 (m, 2H,  $\text{CH}(\text{CH}_3)_2$ ), 2.25 (s, 6H,  $\text{CH}_3\text{C}=\text{CCH}_3$ ), 6.87 (td,  $J_{\text{HH}} = 4$  Hz,  $J_{\text{HP}} = 3$  Hz, 2H, ArH), 6.91 (t,  $J_{\text{HH}} = 8$  Hz, 2H, ArH), 7.21 (ddd,  $J_{\text{HH}} = 8$  Hz,  $J_{\text{HP}} = 1$  Hz,  $J_{\text{HP}} = 2$  Hz, 2H, ArH), 7.49 (dd,  $J_{\text{HH}} = 7.5$  Hz,  $J_{\text{HP}} = 3.5$  Hz, 2H, ArH).  $^{31}\text{P}\{^1\text{H}\}$  NMR (162 MHz,  $\text{C}_6\text{D}_6$ )  $\delta$ : -1.86 (s).  $^{13}\text{C}\{^1\text{H}\}$  NMR (100 MHz,  $\text{C}_6\text{D}_6$ )  $\delta$ : 20.05 (d,  $J_{\text{CP}} = 13$  Hz,  $\text{CH}(\text{CH}_3)_2$ ), 20.95 (d,  $J_{\text{CP}} = 21$  Hz,  $\text{CH}(\text{CH}_3)_2$ ), 21.79 (d,  $J_{\text{CP}} = 15$  Hz,  $\text{CH}(\text{CH}_3)_2$ ), 21.79 (d,  $J_{\text{CP}} = 15$  Hz,  $\text{CH}(\text{CH}_3)_2$ ), 24.08 (d,  $J_{\text{CP}} = 10$  Hz,  $\text{CH}_3\text{C}=\text{CCH}_3$ ), 24.83 (d,  $J_{\text{CP}} = 14$  Hz,  $\text{CH}(\text{CH}_3)_2$ ), 27.63 (d,  $J_{\text{CP}} = 16$  Hz,  $\text{CH}(\text{CH}_3)_2$ ), 126.0 (s, ArC), 128.46 (s, ArC), 131.60 (dd,  $J_{\text{CP}} = 8$  Hz,  $J_{\text{CP}} = 4$  Hz, ArC), 131.97 (d,  $J_{\text{CP}} = 3$  Hz, ArC), 134.50 (d,  $J_{\text{CP}} = 6$  Hz,  $\text{CH}_3\text{C}=\text{CCH}_3$ ), 135.98 (d,  $J_{\text{CP}} = 19$  Hz, ArC), 152.98 (d,  $J_{\text{CP}} = 32$  Hz, ArC).

**Synthesis of (cPCMe=CMeP)Pd (**27**)** A mixture of cPCMe=CMeP (**26**, 50 mg, 0.11 mmol) and  $[\{(\text{TMS})\text{CH}_2\}_2\text{Pd}(\text{cod})]$  (35.3 mg, 0.11 mmol) was stirred in  $\text{Et}_2\text{O}$  at room temperature for 1 h. The volatiles were removed under reduced pressure and the crude residue dissolved in *n*-pentane. The solution was filtered over Celite and cooled to  $-35$  °C to induce crystallization. The final product, (cPCMe=CMeP)Pd (**27**), was isolated in 64% yield. The compound was stored at  $-35$  °C and kept in the dark to prevent backbone isomerization. For **27**:  $^1\text{H}$  NMR (400 MHz,  $\text{C}_6\text{D}_6$ )  $\delta$ : 0.81 (app q,  $J_{\text{HP}} = 12$  Hz,  $J_{\text{HH}} = 4$  Hz, 6H,  $\text{CH}(\text{CH}_3)_2$ ), 1.18 (app q,  $J_{\text{HP}} = 8$  Hz,  $J_{\text{HH}} = 4$  Hz, 6H,  $\text{CH}(\text{CH}_3)_2$ ), 1.30 (m, 12H,  $\text{CH}(\text{CH}_3)_2$ ), 2.21 (v t, 6H,  $(\text{CH}_3)\text{C}=\text{C}(\text{CH}_3)$ ), 2.24 (m, 4H,  $\text{CH}(\text{CH}_3)_2$ ), 6.85 (t,  $J_{\text{HH}} = 8$  Hz, 2H, ArH), 7.0 (t,  $J_{\text{HH}} = 8$  Hz, 2H, ArH), 7.06 (d,  $J_{\text{HH}} = 10$  Hz, 2H, ArH), 7.32 (d,  $J_{\text{HH}} = 10$  Hz, ArH).  $^{31}\text{P}\{^1\text{H}\}$  NMR (200 MHz,  $\text{C}_6\text{D}_6$ )  $\delta$ : 48.64 (s).  $^{13}\text{C}\{^1\text{H}\}$  NMR (126 MHz,  $\text{C}_6\text{D}_6$ )

$\delta$ : 18.89 (s, CH(CH<sub>3</sub>)<sub>2</sub>), 20.62 (t,  $J_{\text{CP}}$  = 6 Hz, CH(CH<sub>3</sub>)<sub>2</sub>), 20.67 (t,  $J_{\text{CP}}$  = 10 Hz, CH(CH<sub>3</sub>)<sub>2</sub>), 21.39 (s, CH(CH<sub>3</sub>)<sub>2</sub>), 22.32 (t,  $J_{\text{CP}}$  = 6 Hz, CH(CH<sub>3</sub>)<sub>2</sub>), 28.75 (s, CH(CH<sub>3</sub>)<sub>2</sub>), 29.01 (t,  $J_{\text{CP}}$  = 5 Hz, CH<sub>3</sub>C=CCH<sub>3</sub>), 92.97 (t,  $J_{\text{CP}}$  = 9 Hz, CH<sub>3</sub>C=CCH<sub>3</sub>), 125.33 (s, ArC), 128.97 (s, ArC), 129.48 (t,  $J_{\text{CP}}$  = 8 Hz, ArC), 132.15 (s, ArC), 146.24 (t,  $J_{\text{CP}}$  = 16 Hz, ArC), 155.65 (t,  $J_{\text{CP}}$  = 16 Hz, ArC). Anal. Calcd. for C<sub>28</sub>H<sub>42</sub>P<sub>2</sub>Pd: C, 61.48; H, 7.74. Found: C, 61.56 H, 7.83.

**Synthesis of (cPCMe=CMeP)PdCl<sub>2</sub> (28)** A THF solution of cPCMe=CMeP (**26**, 25 mg, 0.06 mmol) was added to [(cod)PdCl<sub>2</sub>] (16.2 mg, 0.06 mmol) in a Schlenk tube and heated to 65 °C. After 1 h, the volatiles were removed under reduced pressure and the resulting orange powder was triturated with *n*-pentane. The residual solid was dried under vacuum. Yield 32.9 mg, 94%. For **28**: <sup>1</sup>H NMR (500 MHz, CDCl<sub>3</sub>)  $\delta$ : 1.24 (app q, 6H,  $J_{\text{HP}}$  = 10 Hz, CH(CH<sub>3</sub>)<sub>2</sub>), 1.32 (app q, 6H,  $J_{\text{HP}}$  = 5 Hz, CH(CH<sub>3</sub>)<sub>2</sub>), 1.39 (app q, 6H,  $J_{\text{HP}}$  = 10 Hz, CH(CH<sub>3</sub>)<sub>2</sub>), 1.59 (app q, 6H,  $J_{\text{HP}}$  = 10 Hz), 1.89 (s, 6H, CH<sub>3</sub>C=CCH<sub>3</sub>), 3.08 (m, 4H, CH(CH<sub>3</sub>)<sub>2</sub>), 7.69 (m, 4H, ArH), 7.84 (d, 2H,  $J_{\text{HH}}$  = 10 Hz, ArH), 7.94 (t, 2H,  $J_{\text{HH}}$  = 5 Hz, ArH). <sup>31</sup>P{<sup>1</sup>H} NMR (200 MHz, CDCl<sub>3</sub>)  $\delta$ : 68.7 (s). <sup>13</sup>C{<sup>1</sup>H} NMR (126 MHz, CDCl<sub>3</sub>)  $\delta$ : 17.25 (s, CH(CH<sub>3</sub>)<sub>2</sub>), 18.34 (s, CH(CH<sub>3</sub>)<sub>2</sub>), 19.48 (s, CH(CH<sub>3</sub>)<sub>2</sub>), 19.80 (s, CH(CH<sub>3</sub>)<sub>2</sub>), 26.48 (t,  $J_{\text{CP}}$  = 13 Hz, CH(CH<sub>3</sub>)<sub>2</sub>), 126.88 (t,  $J_{\text{CP}}$  = 13 Hz, CH(CH<sub>3</sub>)<sub>2</sub>), 28.32 (s, CH<sub>3</sub>C=CCH<sub>3</sub>), 128.77 (t,  $J_{\text{CP}}$  = 9 Hz, ArC), 129.19 (s, CH<sub>3</sub>C=CCH<sub>3</sub>), 129.29 (t,  $J_{\text{CP}}$  = 20 Hz, ArC), 130.23 (t,  $J_{\text{CP}}$  = 3 Hz, ArC), 132.30 (s, ArC), 135.20 (s, ArC), 150.42 (t,  $J_{\text{CP}}$  = 11 Hz, ArC). Anal. Calcd. for C<sub>28</sub>H<sub>42</sub>Cl<sub>2</sub>P<sub>2</sub>Pd: C, 54.43; H, 6.85. Found: C, 54.31 H, 6.43.

**Synthesis of (cPCMe=CMeP)PdI(CH<sub>3</sub>) (29)** To a THF solution of [(cPCMe=CMeP)Pd] (**27**, 22.6 mg, 0.04 mmol) was added 2.6  $\mu$ L CH<sub>3</sub>I (0.04 mmol) and the mixture was stirred for 1 h. The volatiles were removed under reduced pressure and the resulting crude residue was triturated with *n*-pentane resulting in a pale yellow powder.

The product, **29**, was isolated in 65% (12.9 mg) yield. For **29**:  $^1\text{H}$  NMR (400 MHz,  $\text{C}_6\text{D}_6$ )  $\delta$ : -0.10 (t, 3H,  $J_{\text{HP}} = 8$  Hz,  $\text{PdCH}_3$ ), 0.91 (app q, 6 H  $J_{\text{HP}} = 8$  Hz,  $\text{CH}(\text{CH}_3)_2$ ), 1.26 (m, 6H,  $\text{CH}(\text{CH}_3)_2$ ), 1.50 (app q, 6H,  $J_{\text{HP}} = 8$  Hz,  $\text{CH}(\text{CH}_3)_2$ ), 1.75 (app q, 6H,  $J_{\text{HP}} = 8$  Hz,  $\text{CH}(\text{CH}_3)_2$ ), 2.19 (s, 6H,  $\text{CH}_3\text{C}=\text{CCH}_3$ ), 2.49 (m, 2H,  $\text{CH}(\text{CH}_3)_2$ ), 3.72 (m, 2H,  $\text{CH}(\text{CH}_3)_2$ ), 6.8 (t, 2H,  $J_{\text{HH}} = 8$  Hz,  $\text{ArH}$ ), 6.97 (t, 2H,  $J_{\text{HH}} = 8$  Hz,  $\text{ArH}$ ), 7.15 (m, 2H,  $\text{ArH}$ ), 7.28 (m, 2H,  $\text{ArH}$ ).  $^{31}\text{P}\{^1\text{H}\}$  NMR (162 MHz,  $\text{C}_6\text{D}_6$ )  $\delta$ : 36.24 (s).  $^{13}\text{C}\{^1\text{H}\}$  NMR (100 MHz,  $\text{C}_6\text{D}_6$ )  $\delta$ : 4.23 (br s,  $\text{PdCH}_3$ ), 19.75 (s,  $\text{CH}(\text{CH}_3)_2$ ), 20.53 (s,  $\text{CH}(\text{CH}_3)_2$ ), 20.60 (s,  $\text{CH}(\text{CH}_3)_2$ ), 24.49 (t,  $J_{\text{CP}} = 9$  Hz,  $\text{CH}(\text{CH}_3)_2$ ), 24.96 (t,  $J_{\text{CP}} = 9$  Hz,  $\text{CH}(\text{CH}_3)_2$ ), 26.08 (s,  $\text{CH}_3\text{C}=\text{CCH}_3$ ), 29.82 (t,  $J_{\text{CP}} = 10$  Hz,  $\text{CH}(\text{CH}_3)_2$ ), 125.06 (s,  $\text{ArC}$ ), 128.06 (obscured by  $\text{C}_6\text{D}_6$ ,  $\text{ArC}$ ), 130.91 (s,  $\text{ArC}$ ), 132.40 (t,  $J_{\text{CP}} = 5$  Hz,  $\text{ArC}$ ), 135.99 (br s,  $\text{CH}_3\text{C}=\text{CCH}_3$ ), 138.91 (t,  $J_{\text{CP}} = 16$  Hz,  $\text{ArC}$ ), 149.47 (s,  $\text{ArC}$ ). Anal. Calcd. for  $\text{C}_{29}\text{H}_{45}\text{IP}_2\text{Pd}$ : C, 50.56; H, 6.58. Found: C, 50.62 H, 6.40.

**Synthesis of (cPCMe=CMeP)PdI( $\text{C}_6\text{H}_5$ ) (**30**)** Iodobenzene (5.7  $\mu\text{L}$ , 0.05 mmol) was added to a THF solution of [(cPCMe=CMeP)Pd] (**27**, 27.8 mg, 0.05 mmol) and the resulting mixture was stirred for 1 h. The volatiles were removed under reduced pressure and the crude residue was triturated with *n*-pentane. The product was recrystallized from a concentrated  $\text{Et}_2\text{O}$  solution. Yield: 20.2 mg, 72.8%. For **30**:  $^1\text{H}$  NMR (500 MHz,  $\text{C}_6\text{D}_6$ )  $\delta$ : 0.83 (app q, 6H,  $J_{\text{HP}} = 5$  Hz,  $\text{CH}(\text{CH}_3)_2$ ), 0.97 (app q, 6H,  $J_{\text{HP}} = 5$  Hz,  $\text{CH}(\text{CH}_3)_2$ ), 1.29 (m, 2H,  $\text{CH}(\text{CH}_3)_2$ ), 1.52 (app q, 6H,  $J_{\text{HP}} = 10$  Hz,  $\text{CH}(\text{CH}_3)_2$ ), 1.70 (app q, 6H,  $J_{\text{HP}} = 10$  Hz,  $\text{CH}(\text{CH}_3)_2$ ), 2.20 (s, 6H,  $\text{CH}_3\text{C}=\text{CCH}_3$ ), 3.81 (m, 2H,  $\text{CHCH}_3$ ) 4.41 (d, 1H,  $J_{\text{HH}} = 10$  Hz,  $\text{ArH}$ ), 6.18 (t, 1H,  $J_{\text{HH}} = 5$  Hz,  $\text{ArH}$ ), 6.67 (t, 1H,  $J_{\text{HH}} = 5$  Hz,  $\text{ArH}$ ). 6.77 (m, 5H,  $\text{ArH}$ ), 7.02 (t,  $J_{\text{HH}} = 5$  Hz,  $\text{ArH}$ ), 7.14 (obscured by solvent, 2H,  $\text{ArH}$ ), 7.81 (d, 1H,  $J_{\text{HH}} = 10$  Hz,  $\text{ArH}$ ).  $^{31}\text{P}\{^1\text{H}\}$  NMR (200 MHz,  $\text{C}_6\text{D}_6$ )  $\delta$ : 32.39 (s).  $^{13}\text{C}\{^1\text{H}\}$  NMR (126 MHz,  $\text{C}_6\text{D}_6$ )  $\delta$ :

20.38 (t,  $J_{\text{CP}} = 3$  Hz,  $\text{CH}(\text{CH}_3)_2$ ), 20.56 (t,  $J_{\text{CP}} = 1$  Hz,  $\text{CH}(\text{CH}_3)_2$ ), 21.10 (s,  $\text{CH}(\text{CH}_3)_2$ ), 24.38 (t,  $J_{\text{CP}} = 6$  Hz,  $\text{CH}(\text{CH}_3)_2$ ), 24.76 (t,  $J_{\text{CP}} = 10$  Hz,  $\text{CH}(\text{CH}_3)_2$ ), 25.36 (s,  $\text{CH}_3\text{C}=\text{CCH}_3$ ), 30.51 (t,  $J_{\text{CP}} = 11$  Hz,  $\text{CH}(\text{CH}_3)_2$ ), 122.88 (s,  $\text{CH}_3\text{C}=\text{CCH}_3$ ), 124.50 (s, ArC), 125.07 (t,  $J_{\text{CP}} = 3$  Hz, ArC), 126.10 (s, ArC), 127.97 (s, ArC), 128.35 (s, ArC), 131.70 (s, ArC), 133.25 (t,  $J_{\text{CP}} = 5$  Hz, ArC), 136.41 (t,  $J_{\text{CP}} = 18$  Hz, ArC), 137.30 (s, ArC), 138.05 (t,  $J_{\text{CP}} = 4$  Hz, ArC), 139.16 (t,  $J_{\text{CP}} = 4$  Hz, ArC), 148.26 (t,  $J_{\text{CP}} = 8$  Hz, ArC). Anal. Calcd. for  $\text{C}_{34}\text{H}_{47}\text{IPd}_2$ : C, 54.38; H, 6.31. Found: C, 54.45 H, 6.35.

**Synthesis of (cPCMe=CMeP)Pd(SiH<sub>2</sub>Ph<sub>2</sub>) (31)** Diphenylsilane (0.02 mL, 0.1 mmol) was added via syringe to a diethyl ether solution of [(cPCMe=CMeP)Pd] (**27**, 33.1 mg, 0.06 mmol). The mixture was stirred at room temperature for 1 h. The volatiles were removed under reduced pressure. The crude residue was dissolved in minimum amount of *n*-pentane and stored at -35 °C. The product, [(cPCMe=CMeP)Pd(H<sub>2</sub>SiPh<sub>2</sub>)], crystallized from this concentrated solution in 48% yield (21.2 mg). For **31**: <sup>1</sup>H NMR (400 MHz, C<sub>6</sub>D<sub>6</sub>)  $\delta$ : 0.85 (app q, 6H,  $J_{\text{HP}} = 8$  Hz,  $\text{CH}(\text{CH}_3)_2$ ), 1.19 (app q, 6H,  $J_{\text{HP}} = 4$  Hz,  $\text{CH}(\text{CH}_3)_2$ ), 1.28 (app q, 12 H,  $J_{\text{HP}} = 8$  Hz,  $\text{CH}(\text{CH}_3)_2$ ), 2.15 (vt, 6H,  $\text{CH}_3\text{C}=\text{CCH}_3$ ), 2.21 (m, 2H,  $\text{CH}(\text{CH}_3)_2$ ), 2.32 (m, 2H,  $\text{CH}(\text{CH}_3)_2$ ), 4.55 (s, 2H,  $J_{\text{HSi}} = 96$  Hz, SiH<sub>2</sub>Ph<sub>2</sub>), 6.85 (td,  $J_{\text{HH}} = 8$  Hz,  $J_{\text{HP}} = 4$  Hz, ArH), 6.97 (t,  $J_{\text{HH}} = 8$  Hz, ArH), 7.10 (m, 2H, ArH), 7.15 (m, 9H, ArH), 7.2 (dd,  $J_{\text{HH}} = 8$  Hz,  $J_{\text{HP}} = 4$  Hz, ArH). <sup>31</sup>P{<sup>1</sup>H} NMR (162 MHz, C<sub>6</sub>D<sub>6</sub>)  $\delta$ : 45.75 (s). <sup>13</sup>C{<sup>1</sup>H} NMR (100 MHz, C<sub>6</sub>D<sub>6</sub>)  $\delta$ : 19.28 (s,  $\text{CH}(\text{CH}_3)_2$ ), 20.80 (t,  $J_{\text{CP}} = 6$  Hz,  $\text{CH}(\text{CH}_3)_2$ ), 21.40 (t,  $J_{\text{CP}} = 6$  Hz,  $\text{CH}(\text{CH}_3)_2$ ), 21.53 (t,  $J_{\text{CP}} = 5$  Hz,  $\text{CH}(\text{CH}_3)_2$ ), 23.33 (br s,  $\text{CH}(\text{CH}_3)_2$ ), 27.69 (s,  $\text{CH}_3\text{C}=\text{CCH}_3$ ), 28.97 (t,  $J_{\text{CP}} = 6$  Hz,  $\text{CH}(\text{CH}_3)_2$ ), 104.65 (br s,  $\text{CH}_3\text{C}=\text{CCH}_3$ ), 125.42 (s, ArC), 128.20 (s, ArC), 128.85 (s, ArC), 129.52 (s, ArC), 130.01 (t,  $J_{\text{CP}} = 7$  Hz, ArC), 131.78

(s, ArC), 135.40 (br s, ArC), 136.26 (s, ArC), 143.59 (br s, ArC), 154.44 (t,  $J_{\text{CP}} = 5$  Hz, ArC). Anal. Calcd. for  $\text{C}_{40}\text{H}_{54}\text{P}_2\text{PdSi}$ : C, 65.69; H, 7.44. Found: C, 66.21 H, 7.89.

**Synthesis of (cPCMe=CMeP)PdHCl (32)** To a diethyl ether solution of [(cPCMe=CMeP)Pd] (**27**, 20.2 mg, 0.04 mmol) was added 0.03 mL of a 1 M ethereal HCl solution. The mixture was stirred for 1 h. The volatiles were removed under reduced pressure and the resulting white powder was triturated with *n*-pentane. The solid was dried under vacuum. Yield: 17.6 mg, 82%. For **32**:  $^1\text{H}$  NMR (500 MHz,  $\text{C}_6\text{D}_6$ )  $\delta$ : -14.58 (s, 1H, PdH), 0.76 (app q, 6H,  $J_{\text{HP}} = 10$  Hz,  $\text{CH}(\text{CH}_3)_2$ ), 0.94 (app q, 6H,  $J_{\text{HP}} = 10$  Hz,  $\text{CH}(\text{CH}_3)_2$ ), 1.24 (app q, 6H,  $J_{\text{HP}} = 5$  Hz,  $\text{CH}(\text{CH}_3)_2$ ), 1.77 (app q, 6H,  $J_{\text{HP}} = 10$  Hz,  $\text{CH}(\text{CH}_3)_2$ ), 2.16 (m, 2H,  $\text{CH}(\text{CH}_3)_2$ ), 2.31 (s, 6H,  $\text{CH}_3\text{C}=\text{CCH}_3$ ), 2.81 (m, 2H,  $\text{CH}(\text{CH}_3)_2$ ), 6.77 (t, 2H,  $J_{\text{HH}} = 5$  Hz, ArH), 6.91 (m, 2H, ArH), 6.96 (t, 2H,  $J_{\text{HH}} = 5$  Hz, ArH), 7.23 (dd, 2H,  $J_{\text{HH}} = 10$  Hz,  $J_{\text{HP}} = 5$  Hz).  $^{31}\text{P}\{^1\text{H}\}$  NMR (200 MHz,  $\text{C}_6\text{D}_6$ )  $\delta$ : 37.28 (s).  $^{13}\text{C}\{^1\text{H}\}$  NMR (100 MHz,  $\text{C}_6\text{D}_6$ )  $\delta$ : 17.18 (s,  $\text{CH}(\text{CH}_3)_2$ ), 21.10 (s,  $\text{CH}(\text{CH}_3)_2$ ), 21.13 (s,  $\text{CH}(\text{CH}_3)_2$ ), 21.21 (s,  $\text{CH}(\text{CH}_3)_2$ ), 22.08 (t,  $J_{\text{CP}} = 6$  Hz,  $\text{CH}(\text{CH}_3)_2$ ), 27.17 (s,  $\text{CH}_3\text{C}=\text{CCH}_3$ ), 27.76 (t,  $J_{\text{CP}} = 9$  Hz,  $\text{CH}(\text{CH}_3)_2$ ), 124.58 (t,  $J_{\text{CP}} = 3$  Hz), 129.05 (s, ArC), 131.36 (t,  $J_{\text{CP}} = 5$  Hz, ArC), 132.64 (s, ArC), 135.15 (t,  $J_{\text{CP}} = 3$  Hz,  $\text{CH}_3\text{C}=\text{CCH}_3$ ), 137.20 (t,  $J_{\text{CP}} = 19$  Hz, ArC), 152.44 (t,  $J_{\text{CP}} = 9$  Hz, ArC).

**Synthesis of (PCMe-CHMeP)PdCl (33)** A benzene solution of [(cPCMe=CMeP)PdHCl] (**32**, 17.6 mg, 0.03 mmol) was heated to 80 °C for 2 h. The  $^1\text{H}$  and  $^{31}\text{P}\{^1\text{H}\}$  spectra of an aliquot showed clean conversion to **33**. The volatiles were removed under reduced pressure resulting in a yellow powder (17.0 mg, 96%). For **33**:  $^1\text{H}$  NMR (500 MHz,  $\text{C}_6\text{D}_6$ )  $\delta$ : 0.97 (m, 6H,  $\text{CH}(\text{CH}_3)_2$ ), 1.11 (m, 6H,  $\text{CH}(\text{CH}_3)_2$ ), 1.31 (dd, 3H,  $J_{\text{HP}} = 20$  Hz,  $J_{\text{HH}} = 5$  Hz,  $\text{CH}(\text{CH}_3)_2$ ), 1.47 (m, 9H,  $\text{CH}_3$ ,  $\text{CH}(\text{CH}_3)_2$ ), 1.54 (d, 3H,  $J_{\text{HH}} = 5$  Hz,  $\text{CH}_3$ ), 1.73 (dd, 3H,  $J_{\text{HP}} = 15$  Hz,  $J_{\text{HH}} = 5$  Hz), 2.42 (m, 2H,  $\text{CH}(\text{CH}_3)_2$ ), 2.92 (m, 1H,

CHCH<sub>3</sub>), 3.26 (m, 1H, CH(CH<sub>3</sub>)<sub>2</sub>), 3.44 (m, 1H, CH(CH<sub>3</sub>)<sub>2</sub>), 7.03 (m, 2H, ArH), 7.17 (m, 4H, ArH), 7.29 (t, 1H,  $J_{\text{HH}} = 5$  Hz, ArH), 7.56 (dd, 1H,  $J_{\text{HH}} = 10$  Hz,  $J_{\text{HP}} = 5$  Hz, ArH). <sup>31</sup>P{<sup>1</sup>H} NMR (200 MHz, C<sub>6</sub>D<sub>6</sub>) δ: 18.49 (d,  $J_{\text{PP}} = 356$  Hz), 66.09 (d,  $J_{\text{PP}} = 356$  Hz). <sup>13</sup>C{<sup>1</sup>H} NMR (100 MHz, C<sub>6</sub>D<sub>6</sub>) δ: 17.12 (dd,  $J_{\text{CP}} = 4$  Hz,  $J_{\text{CP}} = 2$  Hz, CH(CH<sub>3</sub>)<sub>2</sub>), 18.54 (s, CH(CH<sub>3</sub>)<sub>2</sub>), 19.81 (s, CH(CH<sub>3</sub>)), 19.62 (d,  $J_{\text{CP}} = 5$  Hz, CH(CH<sub>3</sub>)<sub>2</sub>), 19.85 (d,  $J_{\text{CP}} = 5$  Hz, CH(CH<sub>3</sub>)<sub>2</sub>), 20.43 (d,  $J_{\text{CP}} = 6$  Hz, CH(CH<sub>3</sub>)<sub>2</sub>), 21.20 (d,  $J_{\text{CP}} = 6$  Hz, CH(CH<sub>3</sub>)<sub>2</sub>), 22.11 (d,  $J_{\text{CP}} = 7$  Hz, CH(CH<sub>3</sub>)<sub>2</sub>), 24.16 (d,  $J_{\text{CP}} = 21$  Hz, CH(CH<sub>3</sub>)<sub>2</sub>), 25.40 (dd,  $J_{\text{CP}} = 23$  Hz,  $J_{\text{CP}} = 2$  Hz, CH(CH<sub>3</sub>)<sub>2</sub>), 26.81 (dd,  $J_{\text{CP}} = 22$  Hz,  $J_{\text{CP}} = 3$  Hz, CH(CH<sub>3</sub>)<sub>2</sub>), 27.28 (d,  $J_{\text{CP}} = 3$  Hz, CH(CH<sub>3</sub>)<sub>2</sub>), 27.48 (d,  $J_{\text{CP}} = 3$  Hz, CH(CH<sub>3</sub>)<sub>2</sub>), 36.33 (dd,  $J_{\text{CP}} = 5$  Hz,  $J_{\text{CP}} = 1$  Hz, PdC(CH<sub>3</sub>)), 55.45 (d,  $J_{\text{CP}} = 11$  Hz, CH(CH<sub>3</sub>)), 60.99 (d,  $J_{\text{CP}} = 7$  Hz, PdC(CH<sub>3</sub>)), 126.35 (d,  $J_{\text{CP}} = 20$  Hz, ArC), 126.57 (d,  $J_{\text{CP}} = 5$  Hz, ArC), 126.97 (d,  $J_{\text{CP}} = 5$  Hz, ArC), 130.93 (d,  $J_{\text{CP}} = 3$  Hz, ArC), 131.21 (d,  $J_{\text{CP}} = 2$  Hz, ArC), 131.78 (d,  $J_{\text{CP}} = 3$  Hz, ArC), 133.47 (d,  $J_{\text{CP}} = 3$  Hz, ArC), 133.53 (d,  $J_{\text{CP}} = 3$  Hz, ArC), 156.29 (s, ArC), 156.49 (s, ArC), 169.67 (s, ArC), 170.05 (s, ArC). Anal. Calcd. for C<sub>28</sub>H<sub>43</sub>ClP<sub>2</sub>Pd: C, 57.64; H, 7.43. Found: C, 57.39 H, 7.32.

**Synthesis of (PCMe-C(=CH<sub>2</sub>)P)PdCl (34)** Benzyl potassium (5.3 mg, 0.04 mmol) was added to a THF solution of [(cPCMe=CMeP)PdCl<sub>2</sub>] (**28**, 25 mg, 0.04 mmol). The mixture was allowed to stir for 1 h. The volatiles were removed under reduced pressure and the crude residue was dissolved in a minimum amount of *n*-pentane. The product crystallized at -35 °C in 77% yield (18.1 mg). For **34**: <sup>1</sup>H NMR (400 MHz, C<sub>6</sub>D<sub>6</sub>) δ: 0.84 (dd, 3H,  $J_{\text{HP}} = 12$  Hz,  $J_{\text{HH}} = 4$  Hz, CH(CH<sub>3</sub>)<sub>2</sub>), 1.16 (m, 12 H, CH(CH<sub>3</sub>)<sub>2</sub>), 1.42 (dd, 3H,  $J_{\text{HP}} = 20$  Hz,  $J_{\text{HH}} = 8$  Hz, CH(CH<sub>3</sub>)<sub>2</sub>), 1.50 (dd, 3H,  $J_{\text{HP}} = 8$  Hz,  $J_{\text{HP}} = 4$  Hz, CH<sub>3</sub>CPd), 1.55 (dd, 3H,  $J_{\text{HP}} = 20$  Hz,  $J_{\text{HH}} = 4$  Hz, CH(CH<sub>3</sub>)<sub>2</sub>), 1.73 (dd, 3H,  $J_{\text{HP}} = 20$  Hz,  $J_{\text{HH}} = 5$  Hz, CH(CH<sub>3</sub>)<sub>2</sub>),

2.43 (m, 2H,  $\text{CH}(\text{CH}_3)_2$ ), 3.05 (m, 1H,  $\text{CH}(\text{CH}_3)_2$ ), 3.39 (m, 1H,  $\text{CH}(\text{CH}_3)_2$ ), 4.63 (dd, 1H,  $J_{\text{HP}} = 3 \text{ Hz}$ ,  $J_{\text{HH}} = 2 \text{ Hz}$ ,  $\text{C}=\text{CH}_2$ ), 4.85 (br dd, 1H,  $J_{\text{HP}} = 8 \text{ Hz}$ ,  $J_{\text{HH}} = 4 \text{ Hz}$ ,  $\text{C}=\text{CH}_2$ ), 7.02 (t, 1 H,  $J_{\text{HH}} = 4 \text{ Hz}$ ,  $\text{ArH}$ ), 7.14 (m, 2H,  $\text{ArH}$ ), 7.22 (m, 3H,  $\text{ArH}$ ), 7.38 (dd, 2H,  $J_{\text{HH}} = 8 \text{ Hz}$ ,  $J_{\text{HP}} = 4 \text{ Hz}$ ,  $\text{ArH}$ ), 7.51 (d, 2H,  $J_{\text{HH}} = 4 \text{ Hz}$ ,  $\text{ArH}$ ).  $^{31}\text{P}\{^1\text{H}\}$  NMR (200 MHz,  $\text{C}_6\text{D}_6$ )  $\delta$ : 19.84,  $J_{\text{PP}} = 356 \text{ Hz}$ , 65.80 (d,  $J_{\text{PP}} = 356 \text{ Hz}$ ).  $^{13}\text{C}\{^1\text{H}\}$  NMR (126 MHz,  $\text{C}_6\text{D}_6$ )  $\delta$ : 16.27 (dd,  $J_{\text{CP}} = 6 \text{ Hz}$ ,  $J_{\text{CP}} = 4 \text{ Hz}$ ,  $\text{CH}(\text{CH}_3)_2$ ), 17.71 (t,  $J_{\text{CP}} = 4 \text{ Hz}$ ,  $\text{CH}(\text{CH}_3)_2$ ), 19.12 (d,  $J_{\text{CP}} = 5 \text{ Hz}$ ,  $\text{CH}(\text{CH}_3)_2$ ), 19.32 (d,  $J_{\text{CP}} = 5 \text{ Hz}$ ,  $\text{CH}(\text{CH}_3)_2$ ), 19.59 (dd,  $J_{\text{CP}} = 4 \text{ Hz}$ ,  $J_{\text{CP}} = 1 \text{ Hz}$ ,  $\text{CH}(\text{CH}_3)_2$ ), 19.68 (d,  $J_{\text{CP}} = 5 \text{ Hz}$ ,  $\text{CH}(\text{CH}_3)_2$ ), 19.77 (d,  $J_{\text{CP}} = 6 \text{ Hz}$ ,  $\text{CH}(\text{CH}_3)_2$ ), 20.48 (d,  $J_{\text{CP}} = 9 \text{ Hz}$ ,  $\text{CH}(\text{CH}_3)_2$ ), 24.30 (dd,  $J_{\text{CP}} = 20 \text{ Hz}$ ,  $J_{\text{CP}} = 3 \text{ Hz}$ ,  $\text{CH}(\text{CH}_3)_2$ ), 25.03 (dd,  $J_{\text{CP}} = 18 \text{ Hz}$ ,  $J_{\text{CP}} = 1 \text{ Hz}$ ,  $\text{CH}(\text{CH}_3)_2$ ), 25.12 (br s,  $\text{CH}_3\text{CPd}$ ), 25.18 (dd,  $J_{\text{CP}} = 20 \text{ Hz}$ ,  $J_{\text{CP}} = 3 \text{ Hz}$ ,  $\text{CH}(\text{CH}_3)_2$ ), 34.30 (dd,  $J_{\text{CP}} = 5 \text{ Hz}$ ,  $J_{\text{CP}} = 1 \text{ Hz}$ ,  $\text{C}=\text{CH}_2$ ), 112.73 (d,  $J_{\text{CP}} = 5 \text{ Hz}$ ,  $\text{C}=\text{CH}_2$ ), 126.80 (d,  $J_{\text{CP}} = 5 \text{ Hz}$ ,  $\text{ArC}$ ), 127.51 (d,  $J_{\text{CP}} = 4 \text{ Hz}$ ,  $\text{ArC}$ ), 128.35 (s,  $\text{ArC}$ ), 130.45 (d,  $J_{\text{CP}} = 13 \text{ Hz}$ ,  $\text{ArC}$ ), 130.40 (s,  $\text{ArC}$ ), 130.50 (s,  $\text{ArC}$ ), 131.12 (dd,  $J_{\text{CP}} = 21 \text{ Hz}$ ,  $J_{\text{CP}} = 3 \text{ Hz}$ ,  $\text{ArC}$ ), 131.53 (d,  $J_{\text{CP}} = 3 \text{ Hz}$ ,  $\text{ArC}$ ), 152.26 (d,  $J_{\text{CP}} = 18 \text{ Hz}$ ), 162.96 (dd,  $J_{\text{CP}} = 8 \text{ Hz}$ ,  $J_{\text{CP}} = 3 \text{ Hz}$ ,  $\text{ArC}$ ), 167.31 (s,  $\text{ArC}$ ), 167.59 (s,  $\text{ArC}$ ). Anal. Calcd. for  $\text{C}_{28}\text{H}_{41}\text{ClP}_2\text{Pd}$ : C, 57.84; H, 7.11. Found: C, 57.55 H, 7.48.

**X-ray single crystal diffraction** The data were collected on a Bruker APEX-II diffractometer with a monochromated Mo  $\text{K}\alpha$  or Cu  $\text{K}\alpha$  radiation.<sup>25</sup> Data were corrected for absorption and polarized effects and analyzed for space group determination.<sup>25-26</sup> The structure was solved by direct methods (SHELXS)<sup>27</sup> and refined by full-matrix least squares techniques against  $F_o^2$  (SHELXL-97).<sup>28</sup> Unless noted, all hydrogen atoms were generated in calculated positions. Mercury was used for structure representations.<sup>29</sup>

**X-Ray Crystal Structure of (cPCMe=CMeP)Pd (27).** Single crystals were obtained as yellow blocks from a concentrated *n*-pentane solution at  $-35\text{ }^{\circ}\text{C}$  in the glovebox. Crystal and refinement data for **27**:  $\frac{1}{2}\text{C}_5\text{H}_{12}$ ;  $\text{C}_{61}\text{H}_{96}\text{P}_4\text{Pd}_2$ ;  $M_r = 1166.06$ ; Monoclinic; space group  $P2(1)/n$ ;  $a = 9.5526(5)\text{ \AA}$ ;  $b = 29.7634(15)\text{ \AA}$ ;  $c = 10.6811(6)\text{ \AA}$ ;  $\alpha = 90^{\circ}$ ;  $\beta = 108.0313(17)^{\circ}$ ;  $\gamma = 90^{\circ}$ ;  $V = 2887.7(3)\text{ \AA}^3$ ;  $Z = 2$ ;  $T = 120(2)\text{ K}$ ;  $\lambda = 0.71073\text{ \AA}$ ;  $\mu = 0.770\text{ mm}^{-1}$ ;  $d_{\text{calc}} = 1.341\text{ g}\cdot\text{cm}^{-3}$ ; 46170 reflections collected; 5094 unique ( $R_{\text{int}} = 0.0471$ ); giving  $R_1 = 0.0242$ ,  $wR_2 = 0.0522$  for 4371 data with  $[I > 2\sigma(I)]$  and  $R_1 = 0.0329$ ,  $wR_2 = 0.0543$  for all 5094 data. Residual electron density ( $\text{e}^{-}\cdot\text{\AA}^{-3}$ ) max/min: 0.623/-0.513.

**X-Ray Crystal Structure of (cPCMe=CMeP)PdCl<sub>2</sub> (28).** Single crystals were obtained as orange plates from a concentrated dichloromethane solution layered with *n*-pentane at  $-35\text{ }^{\circ}\text{C}$  in the glovebox. Crystal and refinement data for **28**:  $\text{C}_{28}\text{H}_{42}\text{Cl}_2\text{P}_2\text{Pd}$ ;  $M_r = 617.86$ ; Monoclinic; space group  $P2(1)/n$ ;  $a = 12.0568(8)\text{ \AA}$ ;  $b = 14.5349(9)\text{ \AA}$ ;  $c = 16.5523(10)\text{ \AA}$ ;  $\alpha = 90^{\circ}$ ;  $\beta = 101.7870(10)^{\circ}$ ;  $\gamma = 90^{\circ}$ ;  $V = 2839.5(3)\text{ \AA}^3$ ;  $Z = 4$ ;  $T = 120(2)\text{ K}$ ;  $\lambda = 0.71073\text{ \AA}$ ;  $\mu = 0.970\text{ mm}^{-1}$ ;  $d_{\text{calc}} = 1.445\text{ g}\cdot\text{cm}^{-3}$ ; 24456 reflections collected; 4996 unique ( $R_{\text{int}} = 0.0677$ ); giving  $R_1 = 0.0492$ ,  $wR_2 = 0.0704$  for 3989 data with  $[I > 2\sigma(I)]$  and  $R_1 = 0.0709$ ,  $wR_2 = 0.0744$  for all 4996 data. Residual electron density ( $\text{e}^{-}\cdot\text{\AA}^{-3}$ ) max/min: 0.996/-1.010.

**X-Ray Crystal Structure of (cPCMe=CMeP)PdI(CH<sub>3</sub>) (29).** Single crystals were obtained as pale yellow blocks from a concentrated toluene solution layered with *n*-pentane at  $-35\text{ }^{\circ}\text{C}$  in the glovebox. Crystal and refinement data for **29**:  $\text{C}_{29}\text{H}_{45}\text{IP}_2\text{Pd}$ ;  $M_r = 688.89$ ; Monoclinic; space group  $P2(1)/n$ ;  $a = 12.0588(5)\text{ \AA}$ ;  $b = 14.8922(6)\text{ \AA}$ ;  $c = 16.9085(7)\text{ \AA}$ ;  $\alpha = 90^{\circ}$ ;  $\beta = 102.592(2)^{\circ}$ ;  $\gamma = 90^{\circ}$ ;  $V = 2963.4(2)\text{ \AA}^3$ ;  $Z = 4$ ;  $T = 120(2)\text{ K}$ ;  $\lambda = 0.71073\text{ \AA}$ ;  $\mu = 1.791\text{ mm}^{-1}$ ;  $d_{\text{calc}} = 1.544\text{ g}\cdot\text{cm}^{-3}$ ; 41798 reflections collected; 5214



unique ( $R_{\text{int}} = 0.0550$ ); giving  $R_1 = 0.0339$ ,  $wR_2 = 0.0688$  for 4442 data with  $[I > 2\sigma(I)]$  and  $R_1 = 0.0438$ ,  $wR_2 = 0.0733$  for all 5214 data. Residual electron density ( $\text{e}^- \cdot \text{\AA}^{-3}$ ) max/min: 3.708/-2.697.

**X-Ray Crystal Structure of (cPCMe=CMeP)PdI(C<sub>6</sub>H<sub>5</sub>) (30).** Single crystals were obtained as yellow blocks from a concentrated dichloromethane solution at  $-35^\circ\text{C}$  in the glovebox. Crystal and refinement data for **30**: C<sub>34</sub>H<sub>47</sub>IP<sub>2</sub>Pd;  $M_r = 750.96$ ; Orthorhombic; space group Pnma;  $a = 20.4783(14) \text{ \AA}$ ;  $b = 12.9512(9) \text{ \AA}$ ;  $c = 14.8356(10) \text{ \AA}$ ;  $\alpha = 90^\circ$ ;  $\beta = 90^\circ$ ;  $\gamma = 90^\circ$ ;  $V = 3934.7(5) \text{ \AA}^3$ ;  $Z = 4$ ;  $T = 120(2) \text{ K}$ ;  $\lambda = 0.71073 \text{ \AA}$ ;  $\mu = 1.355 \text{ mm}^{-1}$ ;  $d_{\text{calc}} = 1.268 \text{ g} \cdot \text{cm}^{-3}$ ; 68432 reflections collected; 3635 unique ( $R_{\text{int}} = 0.0395$ ); giving  $R_1 = 0.0205$ ,  $wR_2 = 0.0458$  for 3504 data with  $[I > 2\sigma(I)]$  and  $R_1 = 0.0222$ ,  $wR_2 = 0.0467$  for all 3635 data. Residual electron density ( $\text{e}^- \cdot \text{\AA}^{-3}$ ) max/min: 0.460/-0.462.

**X-Ray Crystal Structure of (cPCMe=CMeP)Pd(H<sub>2</sub>SiPh<sub>2</sub>) (31).** Single crystals were obtained as pale yellow blocks from a concentrated *n*-pentane solution at  $-35^\circ\text{C}$  in the glovebox. Crystal and refinement data for **31**: C<sub>40</sub>H<sub>54</sub>P<sub>2</sub>PdSi;  $M_r = 731.26$ ; Monoclinic; space group P2(1)/n;  $a = 12.3155(17) \text{ \AA}$ ;  $b = 18.784(3) \text{ \AA}$ ;  $c = 15.883(2) \text{ \AA}$ ;  $\alpha = 90^\circ$ ;  $\beta = 91.397(3)^\circ$ ;  $\gamma = 90^\circ$ ;  $V = 3673.1(9) \text{ \AA}^3$ ;  $Z = 4$ ;  $T = 120(2) \text{ K}$ ;  $\lambda = 0.71073 \text{ \AA}$ ;  $\mu = 0.652 \text{ mm}^{-1}$ ;  $d_{\text{calc}} = 1.322 \text{ g} \cdot \text{cm}^{-3}$ ; 56696 reflections collected; 6470 unique ( $R_{\text{int}} = 0.0454$ ); giving  $R_1 = 0.0244$ ,  $wR_2 = 0.0539$  for 5411 data with  $[I > 2\sigma(I)]$  and  $R_1 = 0.0346$ ,  $wR_2 = 0.0561$  for all 6470 data. Residual electron density ( $\text{e}^- \cdot \text{\AA}^{-3}$ ) max/min: 0.445/-0.468. H(1) and H(2) were found in the difference map and refined.

**X-Ray Crystal Structure of (PCMe-CHMeP)PdCl (33).** Single crystals were obtained as colorless plates from a toluene solution layered with *n*-pentane at  $-35^\circ\text{C}$  in the glovebox. Crystal and refinement data for **33**: C<sub>28</sub>H<sub>43</sub>ClP<sub>2</sub>Pd;  $M_r = 583.41$ ; Orthorhombic;

space group Pbca;  $a = 15.097(3)$  Å;  $b = 15.133(3)$  Å;  $c = 23.974(4)$  Å;  $\alpha = 90^\circ$ ;  $\beta = 90^\circ$ ;  $\gamma = 90^\circ$ ;  $V = 5477.2(18)$  Å<sup>3</sup>;  $Z = 8$ ;  $T = 120(2)$  K;  $\lambda = 0.71073$  Å;  $\mu = 0.907$  mm<sup>-1</sup>;  $d_{\text{calc}} = 1.415$  g·cm<sup>-3</sup>; 71292 reflections collected; 4823 unique ( $R_{\text{int}} = 0.0976$ ); giving  $R_1 = 0.0479$ ,  $wR_2 = 0.0827$  for 3694 data with  $[I > 2\sigma(I)]$  and  $R_1 = 0.0724$ ,  $wR_2 = 0.0886$  for all 4823 data. Residual electron density (e<sup>-</sup>·Å<sup>-3</sup>) max/min: 1.185/-0.759.

**X-Ray Crystal Structure of (PCMe-CHMeP)PdCl (34).** Single crystals were obtained as brown cubes from a concentrated *n*-pentane solution at  $-35^\circ\text{C}$  in the glovebox. Crystal and refinement data for **34**: C<sub>28</sub>H<sub>41</sub>ClP<sub>2</sub>Pd;  $M_r = 581.40$ ; Orthorhombic; space group Pbca;  $a = 15.1228(4)$  Å;  $b = 15.1248(3)$  Å;  $c = 24.0229(6)$  Å;  $\alpha = 90^\circ$ ;  $\beta = 90^\circ$ ;  $\gamma = 90^\circ$ ;  $V = 5494.7(2)$  Å<sup>3</sup>;  $Z = 8$ ;  $T = 120(2)$  K;  $\lambda = 1.54178$  Å;  $\mu = 7.534$  mm<sup>-1</sup>;  $d_{\text{calc}} = 1.406$  g·cm<sup>-3</sup>; 93951 reflections collected; 5418 unique ( $R_{\text{int}} = 0.0560$ ); giving  $R_1 = 0.0374$ ,  $wR_2 = 0.0895$  for 5042 data with  $[I > 2\sigma(I)]$  and  $R_1 = 0.0404$ ,  $wR_2 = 0.0916$  for all 5418 data. Residual electron density (e<sup>-</sup>·Å<sup>-3</sup>) max/min: 1.619/-1.694.

#### 4.5 References

1. Barrett, B. J.; Iluc, V. M., *Inorg. Chem.* **2014**, *53* (14), 7248-7259.
2. Barrett, B. J.; Iluc, V. M., *Organometallics* **2014**, *33* (10), 2565-2574.
3. Barrett, B. J.; Iluc, V. M., *Inorg. Chim. Acta* **2016**.
4. Sgro, M. J.; Stephan, D. W., *Angew. Chem. Int. Ed.* **2012**, *51* (45), 11343-11345.
5. Yamazaki, S.; Yoshimura, T.; Yamabe, S.; Arai, T.; Tamura, H., *J. Org. Chem.* **1990**, *55* (1), 263-269.
6. Barrett, B. J.; Iluc, V. M., *Inorg. Chem.* **2014**, *53* (14), 7248-7259.

7. Canovese, L.; Visentin, F.; Chessa, G.; Uguagliati, P.; Dolmella, A., *J. Organomet. Chem.* **2000**, *601* (1), 1-15.
8. van Asselt, R.; Elsevier, C. J.; Smeets, W. J. J.; Spek, A. L., *Inorg. Chem.* **1994**, *33* (7), 1521-1531.
9. Comanescu, C. C.; Iluc, V. M., *Inorg. Chem.* **2014**, *53* (16), 8517-8528.
10. Suseno, S.; Agapie, T., *Organometallics* **2013**, *32* (11), 3161-3164.
11. Horak, K. T.; VanderVelde, D. G.; Agapie, T., *Organometallics* **2015**, *34* (19), 4753-4765.
12. van der Vlugt, J. I.; van Duren, R.; Batema, G. D.; den Heeten, R.; Meetsma, A.; Fraanje, J.; Goubitz, K.; Kamer, P. C. J.; van Leeuwen, P. W. N. M.; Vogt, D., *Organometallics* **2005**, *24* (22), 5377-5382.
13. Bessel, C. A.; Aggarwal, P.; Marschilok, A. C.; Takeuchi, K. J., *Chem. Rev.* **2001**, *101* (4), 1031-1066.
14. Freixa, Z.; van Leeuwen, P. W. N. M., *Coord. Chem. Rev.* **2008**, *252* (15-17), 1755-1786.
15. Boekelheide, V.; Hylton, T. A., *J. Am. Chem. Soc.* **1970**, *92* (12), 3669-3675.
16. Jarvis, A. G.; Sehnal, P. E.; Bajwa, S. E.; Whitwood, A. C.; Zhang, X.; Cheung, M. S.; Lin, Z.; Fairlamb, I. J. S., *Chem. Eur. J.* **2013**, *19* (19), 6034-6043.
17. Yin, J.; Buchwald, S. L., *J. Am. Chem. Soc.* **2002**, *124* (21), 6043-6048.
18. Iluc, V. M.; Hillhouse, G. L., *Tetrahedron* **2006**, *62* (32), 7577-7582.
19. Nakata, N.; Fukazawa, S.; Kato, N.; Ishii, A., *Organometallics* **2011**, *30* (17), 4490-4493.
20. Boyle, R. C.; Mague, J. T.; Fink, M. J., *J. Am. Chem. Soc.* **2003**, *125* (11), 3228-3229.
21. Takaya, J.; Iwasawa, N., *J. Am. Chem. Soc.* **2008**, *130* (46), 15254-15255.
22. Takaya, J.; Kirai, N.; Iwasawa, N., *J. Am. Chem. Soc.* **2011**, *133* (33), 12980-12983.
23. Doherty, N. M.; Bercaw, J. E., *J. Am. Chem. Soc.* **1985**, *107* (9), 2670-2682.
24. Lee, H. G.; Milner, P. J.; Buchwald, S. L., *Org. Lett.* **2013**, *15* (21), 5602-5605.

25. Bruker AXS,. APEX-2. bruker-Nonius AXS, Madison, Wisconsin, USA, 2014.
26. Krause, L.; Herbst-Irmer, R.; Sheldrick, G. M.; Stalke, D., *J. Appl. Cryst.* **2015**, *48* (1), 3-10.
27. Sheldrick, G., *Acta Cryst.* **2015**, *A71* (1), 3-8.
28. Sheldrick, G., *Acta Cryst.* **2015**, *C71* (1), 3-8.
29. Macrae, C. F.; Bruno, I. J.; Chisholm, J. A.; Edgington, P. R.; McCabe, P.; Pidcock, E.; Rodriguez-Monge, L.; Taylor, R.; van de Streek, J.; Wood, P. A., *J. Appl. Cryst.* **2008**, *41* (2), 466-470.

CHAPTER 5:  
A NON-HETEROATOM STABILIZED PALLADIUM CARBENE SUPPORTED BY THE  
TRIDENTATE LIGAND *c*PCMe=CMeP

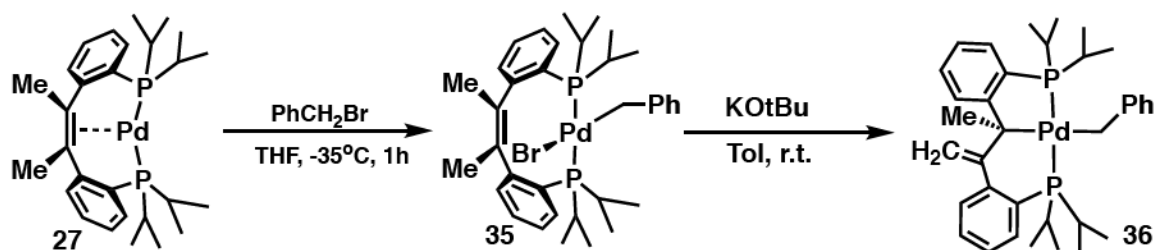
## 5.1 Introduction

In this chapter, the synthesis, characterization, and reactivity of a palladium carbene species will be discussed. The ligand *c*PCMe=CMeP (**26**) was explored for its ability to support non-heteroatom stabilized group 10 carbenes, the isolation of which remains rare. Examples in which monodentate ligands are utilized lack the observation of the reactive carbene itself, however reactivity is consistent with the presence of a transient carbene species throughout the course of chemical reactions.<sup>1-6</sup> Recently, the strategy of incorporating the carbene fragment into a chelating ligand framework has led to the successful isolation of group 10 carbenes.<sup>7-10</sup> This strategy has been beneficial for conducting in-depth reactivity investigations for the corresponding complexes.<sup>7, 9, 11-14</sup> We became interested in determining if ligand **26** could be used for the successful isolation of a species containing a carbene which is not incorporated within the chelating ligand framework, but instead is formed from an additional ligand. Furthermore, we were interested in determining if **26** would exhibit  $\kappa^2$  coordination via the phosphines resulting in a trigonal planar complex, or if the olefin would coordinate, resulting in a square planar complex.

## 5.2 Results and Discussion

The palladium(0) compound (*c*PCMe=CMeP)Pd (**27**, Chapter 4) is an attractive starting material for the synthesis of a palladium carbene. The monomeric form of this species prevents the need for dimer dissociation, and the ability of the chelate ligand itself to stabilize the metal center alleviates the need to remove additional neutral ligands. Various routes for the synthesis of transition metal carbene species have been reported. Among these routes, deprotonation of a metal bound  $sp^3$  carbon is common.<sup>7, 9, 15</sup> Initially, attempts to synthesize a palladium carbene involved oxidative addition of benzylbromide to (*c*PCMe=CMeP)Pd (**27**), followed by deprotonation of the resulting benzylic position on (*c*PCMe=CMeP)PdBr(CH<sub>2</sub>Ph), **35** (Scheme 5.1). This route was appealing as it mimics the synthetic route used in our group previously to generate the palladium carbene species, (PC( $sp^2$ )P)PdP(CH<sub>3</sub>)<sub>3</sub>.<sup>9</sup> Addition of benzylbromide to a cold solution of **27** in THF cleanly leads to the formation of product **35** (Scheme 5.1). The proposed structure is a square planar compound in which oxidative addition leads to the dissociation of the backbone olefin, as observed for oxidative addition reactions in Chapter 4. If the olefin maintains  $\eta^2$  coordination, the resulting species is expected to be cationic with a bromide counter ion, however this is not supported by the NMR spectra. The methyl groups on the olefin are observed in the <sup>1</sup>H NMR spectrum as a singlet at 2.30 ppm. The lack of coupling of the methyl groups to the phosphines suggests a dissociated olefin. The new benzylic protons are observed in <sup>1</sup>H NMR as a triplet at 3.81 ppm ( $J_{HP}$  = 5 Hz). Reacting compound **35** with one equivalent of potassium *tert*-butoxide in toluene at room temperature rapidly led to the formation of a new species, **36** (Scheme 5.1). The <sup>1</sup>H NMR spectrum is reminiscent of (PCMe-C(=CH<sub>2</sub>)P)PdCl (**34**, Chapter 4), indicating deprotonation of the ligand backbone

instead of the benzylic position. The olefin protons are observed as apparent triplets at 4.12 and 4.55 ppm respectively. The  $^{31}\text{P}$  NMR spectrum shows the two phosphines as *trans* coupling doublets ( $J_{\text{P-P}} = 352$  Hz) at 58.34 and 21.41 ppm respectively, supporting the rearrangement of the backbone upon the deprotonation of a methyl group. Crystals suitable for single crystal X-ray diffraction were obtained from a concentrated *n*-pentane solution, and confirm the deprotonation of the ligand backbone. The C(15)-C(16) bond distance of 1.327(4) Å is indicative of a C-C double bond, while the C(13)-C(15) bond distance of 1.496(4) Å is characteristic of a C-C single bond (Figure 5.1).



**Scheme 5.1:** Synthesis of 35 and subsequent reactivity with KOtBu.

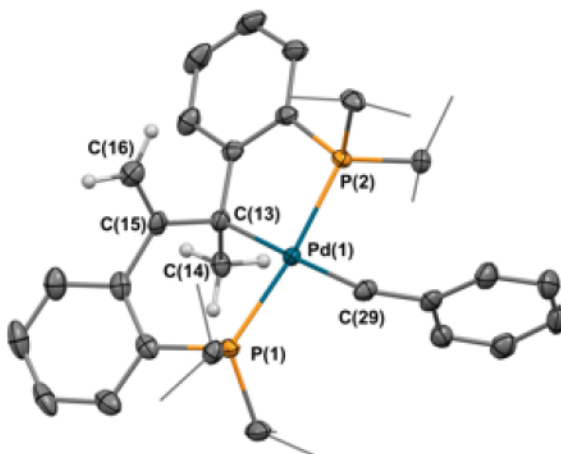
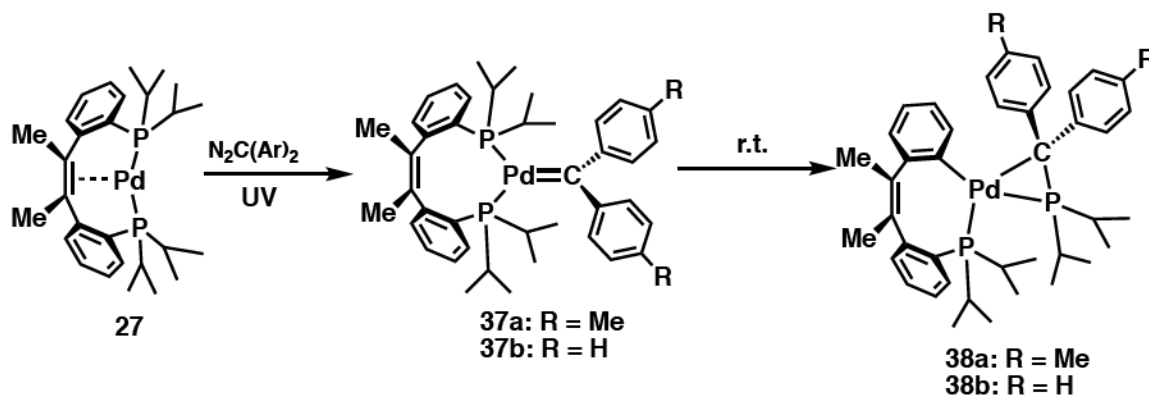


**Figure 5.1:** Thermal-ellipsoid (50% probability level) representation of  $[(PC(CH_3)C(=CH_2)P)PdBz]$  (**36**). Most hydrogen atoms were omitted for clarity. Selected distances (Å) and angles (°): Pd–P(1) = 2.3241(8), Pd–P(2) = 2.2792(7), Pd–C(29) = 2.170(3), Pd–C(13) = 2.161(3), C(13)–C(15) = 1.496(4), C(13)–C(14) = 1.563(4), C(15)–C(16) = 1.327(4), P(1)–Pd–P(2) = 172.60(3), C(13)–Pd–C(29) = 178.50(11), C(13)–Pd(1)–P(1) = 91.48(8), C(29)–Pd(1)–P(2) = 94.25(8), Pd–C(13)–C(15) = 103.8(17), C(16)–C(15)–C(13) = 124.8(3).

Another route commonly used to synthesize transition metal carbene complexes involves the decomposition of diazo reagents.<sup>1-2, 6, 16-22</sup> Initially, this method was carried out with one equivalent of  $(cPCMe=CMeP)Pd$  (**27**) and one equivalent of either di-*p*-tolyl diazomethane  $[(p\text{-tol})_2CN_2]$  or diphenyl diazomethane  $[(Ph)_2CN_2]$  in THF at room temperature, but no reaction was observed. The application of heat to the reaction mixture only led to decomposition of the diazo compound to the corresponding azine species  $((Ar)_2C=N-N=C(Ar)_2)$ .<sup>19, 23-25</sup> Azine formation has been reported to occur through the coupling of diazo compounds with a carbene fragment.<sup>15, 26-27</sup> It is therefore reasonable to propose that a carbene species is an intermediate in this reaction. The reaction mixture was next exposed to UV radiation for 1 hour in  $C_6D_6$  and a new singlet at 48.08 ppm for **37a**, and 49.32 ppm for **37b** in the  $^{31}P$  NMR spectrum was observed. Additional exposure to UV to get full conversion to the new compound resulted in the formation of two new



doublets in the  $^{31}\text{P}$  NMR spectrum at 37.38 and 13.05 ppm respectively ( $^2J_{\text{P-P}} = 14$  Hz) for **38a**, and 38.21 and 13.78 ppm respectively for **38b**, along with unreacted Pd(0) starting material (48.70 ppm) **27**. All the compounds present in solution were soluble in *n*-pentane, however the species represented by the cis coupling doublets (**38a**, **38b**) crystallizes out of solution, and a solid state molecular structure was obtained. Analysis of the solid state structure of **38b** revealed a distorted square planar compound in which one of the the P-C<sub>Ar</sub> bonds of the ligand framework has been cleaved (Figure 5.2). This resulted in  $\kappa^2$  P-C<sub>Ar</sub> coordination of the remaining fragment of ligand **26**. The cleaved phosphine maintained its coordination to the metal, however a new P-C bond had formed between the phosphine and the diarylcarbene, presumably because of the decomposition of the palladium carbene species (**37a**, **37b**) (Scheme 5.2).



**Scheme 5.2:** Synthesis of palladium carbenes **37a** and **37b** and subsequent decomposition.

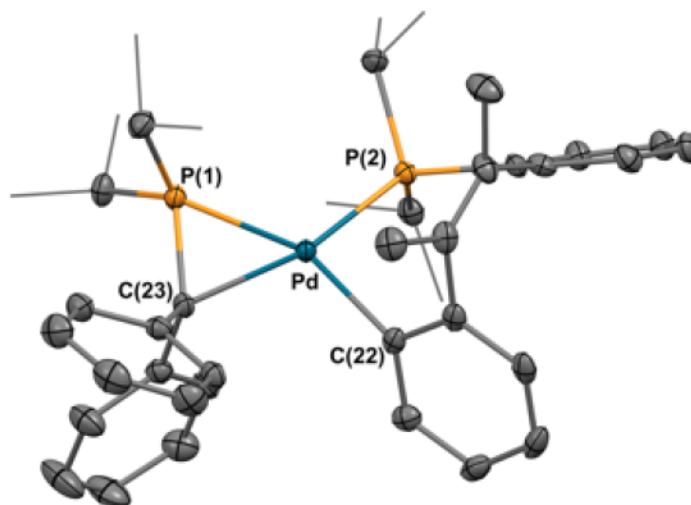


**Figure 5.2.** Thermal-ellipsoid (50% probability level) representation of **38b**. Hydrogen atoms were omitted for clarity. Selected distances (Å) and angles (°): Pd–P(1) = 2.2385(7), Pd–P(2) = 2.3110(8), Pd–C(23) = 2.187(3), Pd–C(22) = 2.061(3), C(23)–P(1) = 1.805(3), P(1)–Pd–P(2) = 115.13(3), C(23)–Pd–C(22) = 105.52(11), C(23)–Pd–P(2) = 159.76(8), C(22)–Pd–P(1) = 153.23(8), C(23)–Pd–P(1) = 48.11(8), P(2)–Pd–C(22) = 91.62(8).

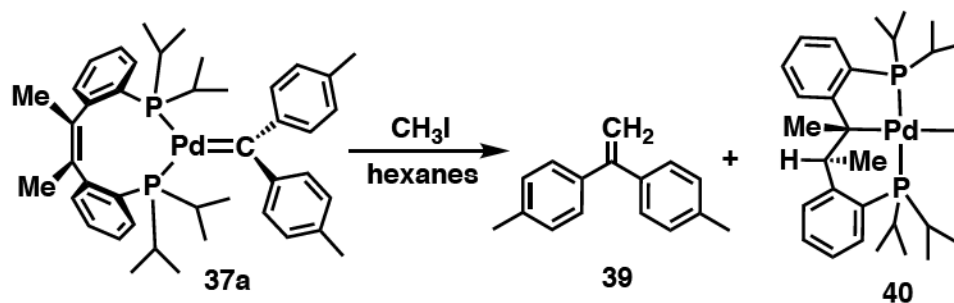
Characterization of the species corresponding to the singlet at 48.08 ppm in the  $^{31}\text{P}$  NMR spectrum was next attempted. It was hypothesized that reacting the (*c*PCMe=CMeP)Pd starting material (**27**) with excess *p*-tol<sub>2</sub>CN<sub>2</sub> would allow for full consumption of **27** before the observation of **38a**. After reacting **27** with 2.5 equivalents of the diazo compound, only one species (**37a**) was observed in the  $^{31}\text{P}$  NMR spectrum at 48.08 ppm after 1 hour of UV exposure. The  $^{13}\text{C}$  NMR spectrum of the solution displayed a diagnostic peak at 300.2 ppm as a triplet ( $J_{\text{C-P}} = 63$  Hz). This downfield shift in the  $^{13}\text{C}$  NMR spectrum is indicative of a metal-carbene species present in solution.<sup>19-20, 22, 28</sup> The appearance of a triplet results from coupling to the two equivalent phosphorus atoms. Comparing the NMR data of compound **37a** to our group's internal carbene ((PC(sp<sup>2</sup>))<sup>*t*Bu</sup> PdP(CH<sub>3</sub>)<sub>3</sub>) reveals several distinct differences. The far downfield shift of **37a** is not comparable with of the carbene carbon shift previously observed (134.17 ppm).<sup>11</sup> This,

along with the lack of coupling to the phosphines in the previously observed structure, leads to the conclusion that compound **37a** is not analogous. Hillhouse and coworkers previously synthesized a tridentate nickel carbene ((dtbpe)Ni=CPh<sub>2</sub>), dtbpe = 1,2-bis(di-tert-butylphosphino)ethane), also through the utilization of diazo compounds.<sup>20</sup> Their species contains a carbene resonance at 221.8 ppm as a triplet in the <sup>13</sup>C NMR spectrum ( $J_{C-P}$  = 51 Hz). This downfield shift, along with the comparable magnitude of the coupling to their equivalent phosphines is suggestive of a similar structure in **37a**.

Although evidence supports the formation of the target compound, the clean synthesis of this species has proven to be difficult. Within hours after the synthesis of **37a** or **37b**, the formation of the side product **38a** or **38b**, as well as Pd(0) starting material, **27**, is observed. The formation of the Pd(0) starting material occurs upon coupling of two carbene fragments, generating tetraarylethylene. In addition to the quick decomposition of the palladium carbene species, the use of excess diazo reagent leads to the formation of impurities that are difficult to separate from the reaction mixture. In the presence of UV light, the diazo compound undergoes coupling upon loss of N<sub>2</sub> to form the corresponding azine species.<sup>19, 23-24</sup> Possible issues with the procedure could result from using aromatic solvents due to their absorption of UV light. It was therefore hypothesized that using hexanes might improve the results. The use of hexanes allowed the synthesis to be run at room temperature with one equivalent of diazo reagent, and results in reproducible formation of the palladium carbene after 90 minutes of UV exposure averaging an 80% yield by <sup>31</sup>P NMR spectroscopy. With a better method to synthesize the desired compound, we attempted characterization via single crystal X-ray diffraction. However, the high

solubility along with the instability of the species has impeded the formation of suitable crystals for X-ray diffraction.

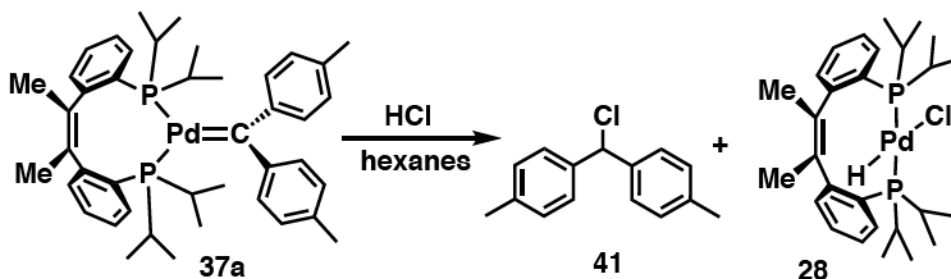
With a synthetic method capable of synthesizing the carbene species with minimal impurities present in solution, preliminary reactivity studies were undertaken. Addition of excess  $\text{CH}_3\text{I}$  to a hexane solution of **37a** at room temperature led to the formation of a new organic species (Scheme 5.3). Isolation of this compound by column chromatography revealed the formation of di(*p*-tolyl)ethylene, **39**, by  $^1\text{H}$  and  $^{13}\text{C}$  NMR spectroscopy. Evaluation of the crude mixture by  $^{31}\text{P}$  NMR spectroscopy revealed the formation of two new phosphorus containing species observed as a singlet at 35.55 ppm and two *trans* coupling doublets at 67.99 and 17.58 ppm respectively ( $J_{\text{P-P}} = 346$  Hz), along with the decomposition product **38a**. It was speculated that one of the new species could result from (*c*PCMe=CMeP)Pd, **27**, reacting with the excess  $\text{CH}_3\text{I}$  in solution. The presence of **27** in solution is a consequence of synthesizing the carbene in situ. Comparing the NMR of the previously observed (*c*PCMe=CMeP)PdI( $\text{CH}_3$ ) (**29**, Chapter 4) with the reaction mixture confirmed this hypothesis. As for the asymmetric compound (**40**), the spectroscopic signatures observed in the  $^1\text{H}$  and  $^{31}\text{P}$  NMR spectra were reminiscent of the previously observed compound, (PCMe-CHMeP)PdCl (**33**, Chapter 4) resulting from olefin insertion into a Pd-H bond. Based on the observed organic product, this result is unsurprising. Throughout the course of the chemical reaction, the I- $\text{CH}_3$  bond is cleaved across the Pd=C bond. Subsequent  $\beta$ -hydride elimination would result in the observed organic product, as well as a PdI(H) species. This species could undergo the analogous olefin insertion process that was observed previously in the related compound (*c*PCMe=CMeP)PdHCl (**32**, Chapter 4).



**Scheme 5.3:** Reactivity of **37a** with  $\text{CH}_3\text{I}$ .

The reactivity of the palladium carbene (**37a**) was further assessed with  $\text{HCl}$ . The addition of excess  $\text{HCl}$  to a solution of **37a** in hexanes rapidly results in the formation of a yellow precipitate (Scheme 5.4). The crude mixture revealed the presence of  $(c\text{PCMe}=\text{CMeP})\text{PdHCl}$  (**32**, Chapter 4), along with an unidentified organic product. Triturating the yellow precipitate with *n*-pentane, followed by cooling the resulting filtrate allows for the removal of **32** from the reaction mixture. The  $^1\text{H}$  NMR spectrum of the supernate shows the organic product as the major species in solution, and was identified as 4,4'-(chloromethylene)bis(methylbenzene) (**41**). The tolyl groups are equivalent, and resonate as two doublets in the aryl region (7.14 and 7.26 ppm) and as a singlet in the alkyl region at 2.32 ppm. The methine proton is found as a singlet at 5.79 ppm. Pathways for the insertion of carbenes into X-H bonds have been proposed in the literature.<sup>29</sup> For nonpolar X-H bonds ( $\text{X} = \text{C}, \text{Si}$ ), this process is believed to occur through a concerted mechanism, however for polar X-H bonds ( $\text{X} = \text{N}, \text{O}$ ) an ylide intermediate is postulated, followed by 1,2-proton migration. Given the polarity of the H-Cl bond, the ylide pathway is plausible. Alternatively, nucleophilic attack of the carbene on the proton would be expected to generate a palladium alkyl chloride species. Reductive elimination of alkyl

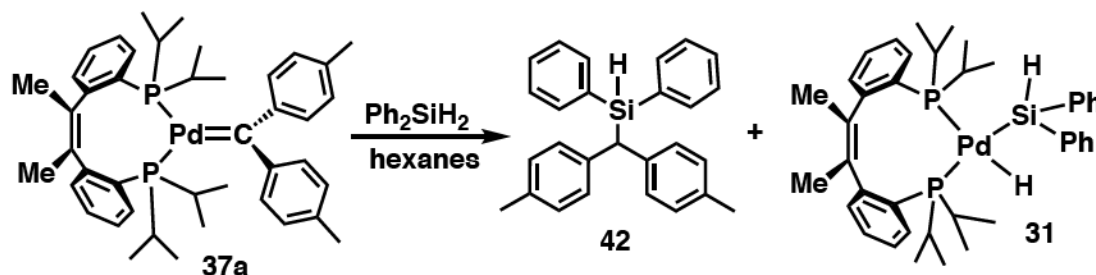
halides from palladium however, is not facile and would be unlikely to generate the observed organic product.



**Scheme 5.4:** Reactivity of **37a** towards HCl.

Late transition metal carbenes are competent in various catalytic E-H (E = Si, N, O, S) bond insertion reactions.<sup>30-34</sup> Specifically, carbene insertion into silicon-hydrogen bonds has proven to be a powerful method for the formation of new Si-C bonds. Common examples often include the use of rhodium, iridium, or copper; recently,<sup>16, 30-32, 35</sup> palladium has shown similar reactivity in silicon-silicon carbene insertion reactions.<sup>16</sup> Carbenoid insertion into E-H bonds is proposed to occur via two major pathways, depending on the polarity of the E-H bond. For substrates with mild polarity, such as silanes, this process may occur through a concerted insertion into the E-H bond.<sup>32-33</sup> More polar bonds, such as O-H, S-H and N-H, proceed by a stepwise process, in which the heteroatom is attacked by the carbene, forming an ylide intermediate, followed by hydrogen atom transfer.<sup>35</sup> The ability of **37a** to activate Si-H bonds was assessed through the reaction of **37a** with one equivalent of diphenylsilane ( $\text{Ph}_2\text{SiH}_2$ ) in hexanes (Scheme 5.5). After 30 minutes of stirring, the solution had turned from deep red, to light orange. The crude reaction mixture showed the full consumption of  $\text{Ph}_2\text{SiH}_2$  resulting in an organic product, as well as a new

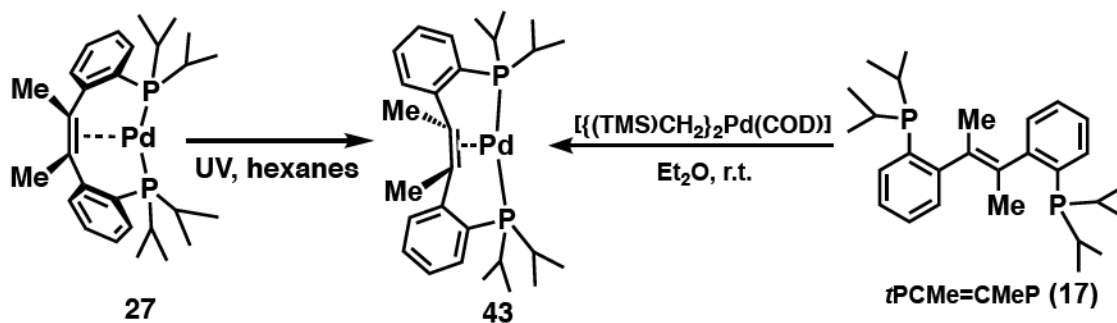
phosphine containing species by  $^1\text{H}$  and  $^{31}\text{P}$  NMR spectroscopy. Isolation of the organic species was possible by column chromatography, and was determined to be (di-*p*-tolylmethyl)diphenyl silane (**42**) occurring via carbene insertion into the Si-H bond as depicted in Scheme 5.5. The new methine proton is found in the  $^1\text{H}$  NMR spectrum as a doublet at 4.09 ppm ( $J_{\text{H-H}} = 4$  Hz), while the silicon bound proton is easily identified as a doublet at 5.18 ppm with silicon satellites ( $J_{\text{H-Si}} = 100$  Hz). The identity of the phosphine species was hypothesized to be the result of (*c*PCMe=CMeP)Pd (**27**) reacting with excess silane in solution (Scheme 5.5). The formation of compound **27** results from the carbene species reacting with  $\text{Ph}_2\text{SiH}_2$ . Comparing the reaction mixture NMR data to the NMR data obtained for (*c*PCMe=CMeP)PdH<sub>2</sub>SiPh<sub>2</sub> (**31**, Chapter 4) confirms this hypothesis.



**Scheme 5.5:** Reactivity of **37a** with  $\text{Ph}_2\text{SiH}_2$ .

It was next considered whether the palladium carbene (**37a**) could perform these transformations catalytically. The catalytic insertion of the carbene into the Si-H bond of  $\text{Ph}_2\text{SiH}_2$  was targeted. The reaction of (*p*-tol)<sub>2</sub>CN<sub>2</sub> with one equivalent of  $\text{Ph}_2\text{SiH}_2$  under UV radiation with 5 mol% loading of (*c*PCMe=CMeP)Pd (**27**) was monitored by NMR spectroscopy. After one hour of UV exposure, 70% of the  $\text{Ph}_2\text{SiH}_2$  reagent was unreacted, however additional UV exposure did not lead to further consumption. The  $^{31}\text{P}$  NMR spectrum revealed that the only detectable phosphine containing species present in the

reaction mixture was the isomerized form of the palladium(0) starting material, (*t*PCMe=CMeP)Pd, **43**. In order to confirm this, a solution of (*c*PCMe=CMeP)Pd (**27**) was exposed to UV radiation (Scheme 5.6). After one hour compound **27** was fully converted to compound **43**.



**Scheme 5.6:** Isomerization of **27** to **43**, and independent synthesis of **43**.

Independent synthesis of compound **43** is readily achieved by reacting *t*PCMe=CMeP (**17**) with one equivalent of ((TMS)CH<sub>2</sub>)<sub>2</sub>Pd(cod) in diethyl ether at room temperature for one hour (Scheme 5.6). This species is identified in the <sup>31</sup>P NMR spectrum as a singlet at 51.93 ppm. To determine if the formation of compound **43** during catalytic reactions with compound **27** was a deconstructive process, the synthesis of the carbene from this species was attempted. Reacting **43** with one equivalent of (*p*-tol)<sub>2</sub>CN<sub>2</sub> with traditional heating led to an unisolable mixture of products. The reaction was then attempted with exposure to UV radiation, however similar unisolable mixtures were obtained.

The reactivity of **37a** was additionally assessed with olefins, amines, boranes, and ketones, however in all cases only decomposition of the carbene and unreacted substrate was observed.



### 5.3 Summary

The synthesis and reactivity of a palladium carbene supported by the chelating ligand *c*PCMe=CMeP is described. Multiple methods were attempted to synthesize the target species, however the use of diazo reagents was ultimately the best pathway to synthesize the desired compound. Characterization by multinuclear NMR was carried out, however a solid state molecular structure has not been obtained. Preliminary reactivity investigations demonstrated the reactivity of the species towards electrophiles, and the capability of the carbene to insert into Si-H and Cl-H bonds. Catalytic investigations towards the carbene insertion into Si-H bonds revealed the tendency of the backbone of the ligand framework to isomerize from a cis conformation to a trans, ultimately killing the catalyst. A new ligand design was therefore implemented, and will be discussed in Chapter 6.

### 5.4 Experimental

All manipulations of air and water sensitive compounds were performed under dry nitrogen atmosphere using an MBraun drybox. Glassware, vials, and stir bars were dried in an oven at 120 °C overnight and evacuated for 12 hours in the antechamber before being brought into the drybox. All solvents were dried by passing through a column of activated alumina, followed by storage over molecular sieves and sodium. Deuterated solvents were purchased from Cambridge Isotope Laboratories. C<sub>6</sub>D<sub>6</sub> and C<sub>6</sub>D<sub>5</sub>CD<sub>3</sub> were dried by stirring over CaH<sub>2</sub> followed by filtration. CDCl<sub>3</sub>, and C<sub>6</sub>D<sub>12</sub> were dried over molecular sieves. (*p*-tol)<sub>2</sub>CN<sub>2</sub>,<sup>36</sup> and [(TMS)CH<sub>2</sub>]<sub>2</sub>Pd(cod)]<sup>37</sup> were prepared according to literature procedures. All other chemicals were commercially available and used as received. NMR spectra were

obtained on Bruker 400 and Bruker 500 spectrometers at ambient temperature unless stated otherwise. Chemical shift values are reported in ppm relative to residual internal protio solvents or to a TMS standard for  $^1\text{H}$  and  $^{13}\text{C}\{^1\text{H}\}$  experiments.  $^{31}\text{P}\{^1\text{H}\}$  NMR chemical shifts are relative to an external standard of  $\text{PPh}_3$  in  $\text{C}_6\text{D}_6$ .  $^{29}\text{Si}\{^1\text{H}\}$  NMR chemical shifts are relative to an external standard of TMS in  $\text{CDCl}_3$ . Coupling constants are reported in Hz.

Experimental procedure for the synthesis and characterization of compounds **26-27**, **29**, **31-32** can be found in Chapter 4.

**Synthesis of (cPCMe=CMeP)PdBr(CH<sub>2</sub>Ph) (35).** To an  $\text{Et}_2\text{O}$  solution of (cPCMe=CMeP)Pd (**27**, 25.0 mg, 0.04 mmol) was added one equivalent of benzylbromide (7.6  $\mu\text{L}$ , 0.04 mmol). The mixture was stirred at room temperature for 1 hour. The volatiles were removed, and the resulting residue was triturated with *n*-pentane leaving **35** as a yellow powder (29.5 mg, 0.04 mmol, 93%).  $^1\text{H}$  NMR (400 MHz,  $\text{CDCl}_3$ )  $\delta$ : 0.89 (app q, 6 H,  $J = 4$  Hz,  $\text{CH}(\text{CH}_3)_2$ ), 1.10 (app q, 6 H,  $J = 4$  Hz,  $\text{CH}(\text{CH}_3)_2$ ), 1.31 (app q, 6 H,  $J = 4$  Hz,  $\text{CH}(\text{CH}_3)_2$ ), 1.50 (app q, 6 H,  $J = 4$  Hz,  $\text{CH}(\text{CH}_3)_2$ ), 2.30 (s, 6 H,  $\text{C}(\text{CH}_3)=\text{C}(\text{CH}_3)$ ), 2.59 (m, 2 H,  $\text{CH}(\text{CH}_3)_2$ ), 2.83 (m, 2 H,  $\text{CH}(\text{CH}_3)_2$ ), 4.50 (s, 2 H,  $\text{PdCH}_2(\text{Ph})$ ), 1.94 (t, 2 H,  $J_{\text{HH}} = 6$  Hz,  $\text{ArH}$ ), 7.33 (m, 2 H,  $\text{ArH}$ ), 7.36 (m, 3 H,  $\text{ArH}$ ), 7.40 (m, 3 H,  $\text{ArH}$ ), 7.45 (m, 2 H,  $\text{ArH}$ ), 7.48 (m, 1 H,  $\text{ArH}$ ).  $^{31}\text{P}\{^1\text{H}\}$  NMR (162 MHz,  $\text{CDCl}_3$ )  $\delta$ : 31.86 (s).

**Synthesis of (PC(=CH<sub>2</sub>)-CMeP)Pd(CH<sub>2</sub>Ph) (36).** A THF solution of potassium *tert*-butoxide (3.1 mg, 0.03 mmol) was added dropwise to a THF solution of (cPCMe=CMeP)PdBr(CH<sub>2</sub>Ph) **35** (20.0 mg, 0.03 mmol). The mixture was allowed to stir for 1 hour. The solution was filtered over a pad of celite, and the volatiles were removed under reduced pressure. The crude residue was triturated with *n*-pentane leaving behind the

powder of **36** (15.7 mg, 0.02 mmol, 89.0 %).  $^1\text{H}$  NMR (500 MHz,  $\text{C}_6\text{D}_6$ )  $\delta$ : 0.77 (dd, 3 H,  $J_{\text{HP}} = 10$  Hz,  $J_{\text{HH}} = 5$  Hz,  $\text{CH}(\text{CH}_3)_2$ ), 0.97 (m, 4 H,  $\text{CH}(\text{CH}_3)_2$ ), 1.01 (m, 3 H,  $\text{CH}(\text{CH}_3)_2$ ), 1.07 (m, 7 H,  $\text{CH}(\text{CH}_3)_2$ ), 1.16 (m, 6 H,  $\text{CH}(\text{CH}_3)_2$ ), 1.32 (dd, 3 H,  $J_{\text{HP}} = 15$  Hz,  $J_{\text{HH}} = 10$  Hz,  $\text{CH}(\text{CH}_3)_2$ ), 1.58 (d, 3 H,  $J = 5$  Hz,  $\text{C}(\text{CH}_2)\text{-C}(\text{CH}_3)$ ), 2.14 (m, 1 H,  $\text{CH}(\text{CH}_3)_2$ ), 2.45 (m, 3 H,  $\text{CH}(\text{CH}_3)_2$ ), 4.12 (t, 1 H,  $J_{\text{HH}} = 3$  Hz,  $\text{C}(\text{CH}_2)\text{-C}(\text{CH}_3)$ ), 4.55 (t, 1 H,  $J_{\text{HH}} = 3$  Hz,  $\text{C}(\text{CH}_2)\text{-C}(\text{CH}_3)$ ), 6.93 (t, 1 H,  $J_{\text{HH}} = 5$  Hz,  $\text{ArH}$ ), 6.98 (m, 1 H,  $\text{ArH}$ ), 7.04 (t, 1 H,  $J_{\text{HH}} = 5$  Hz,  $\text{ArH}$ ), 7.18 (m, 4 H,  $\text{ArH}$ ), 7.25 (m, 1 H,  $\text{ArH}$ ), 7.29 (t,  $J_{\text{HH}} = 10$  Hz,  $\text{ArH}$ ), 7.45 (d, 2 H,  $J_{\text{HH}} = 10$  Hz,  $\text{ArH}$ ), 7.53 (dd, 1 H,  $J_{\text{HH}} = 5$  Hz,  $J_{\text{HH}} = 5$  Hz,  $\text{ArH}$ ), 7.76 (d, 1 H,  $J_{\text{HH}} = 10$  Hz,  $\text{ArH}$ ).  $^{31}\text{P}\{^1\text{H}\}$  NMR (202 MHz,  $\text{C}_6\text{D}_6$ )  $\delta$ : 21.41 (d,  $J_{\text{PP}} = 343$  Hz), 58.43 (d,  $J_{\text{PP}} = 343$  Hz).

**Synthesis of [(cPCMe=CMeP)Pd=C(*p*-tol) $_2$ ] (37).** Compound [(cPCMe=CMeP)Pd] (**27**) was dissolved in hexanes and added to a quartz J-Young NMR tube along with (*p*-tol) $_2\text{CN}_2$  and a  $\text{C}_6\text{D}_6$  capillary. The solution was exposed to UV radiation and monitored by  $^{31}\text{P}\{^1\text{H}\}$  NMR spectroscopy. After 1 h of UV exposure, a mixture of products was observed, including 85% [(cPCMe=CMeP)Pd=C(*p*-tol) $_2$ ] (**37**), 15% decomposition of the carbene to **38**. Further exposure of the solution to UV radiation results in further conversion to the insertion product **38**. Storing the mixture obtained after 1 h UV exposure in the dark at room temperature results in full conversion to **38** after 12 h.  $^1\text{H}$  NMR (500 MHz,  $\text{C}_6\text{D}_6$ )  $\delta$ : 0.99 (app q, 6 H,  $J = 5$  Hz,  $\text{CH}(\text{CH}_3)_2$ ), 1.07 (m, 12 H,  $\text{CH}(\text{CH}_3)_2$ ), 1.37 (app q, 6 H,  $J = 5$  Hz,  $\text{CH}(\text{CH}_3)_2$ ), 2.05 (br s, 3 H,  $\text{C}_6\text{H}_4(\text{CH}_3)$ ), 2.18 (br s, 3 H,  $\text{C}_6\text{H}_4(\text{CH}_3)$ ), 2.22 (s, 6 H,  $\text{C}(\text{CH}_3)=\text{C}(\text{CH}_3)$ ), 2.37 (m, 4 H,  $\text{CH}(\text{CH}_3)_2$ ), 6.8 (m, 4 H,  $\text{ArH}$ ), 6.88 (t, 3 H,  $J_{\text{HH}} = 10$  Hz,  $\text{ArH}$ ), 7.09 (d, 2 H,  $J_{\text{HH}} = 10$  Hz,  $\text{ArH}$ ), 7.21 (d, 2 H,  $J_{\text{HH}} = 5$  Hz,  $\text{ArH}$ ), 7.55 (d, 2 H,  $J_{\text{HH}} = 10$  Hz,  $\text{ArH}$ ), 7.76 (t, 1 H,  $J_{\text{HH}} = 5$  Hz,  $\text{ArH}$ ), 7.92 (m, 2 H,

ArH).  $^{13}\text{C}\{^1\text{H}\}$  NMR (126 MHz,  $\text{C}_6\text{D}_6$ )  $\delta$ : 19.01 (s,  $\text{CH}(\text{CH}_3)_2$ ), 20.14 (s,  $\text{CH}(\text{CH}_3)_2$ ), 21.30 (s,  $\text{CH}(\text{CH}_3)_2$ ), 21.68 (s,  $\text{C}_6\text{H}_4(\text{CH}_3)$ ), 21.78 (s,  $\text{C}_6\text{H}_4(\text{CH}_3)$ ), 22.57 (t,  $J_{\text{CP}} = 6$  Hz,  $\text{CH}(\text{CH}_3)_2$ ), 23.64 (s,  $\text{C}(\text{CH}_3)=\text{C}(\text{CH}_3)$ ), 27.41 (t,  $J_{\text{CP}} = 4$  Hz,  $\text{CH}(\text{CH}_3)_2$ ), 33.44 (t,  $J_{\text{CP}} = 6$  Hz,  $\text{CH}(\text{CH}_3)_2$ ), 124.62 (t,  $J_{\text{CP}} = 13$  Hz, ArC), 125.60 (s, ArC), 127.74 (s, ArC), 128.36 (s, ArC), one C atom obscured by solvent, 128.76 (s, ArC), 128.91 (s, ArC), 129.11 (s, ArC), 129.29 (t,  $J_{\text{CP}} = 4$  Hz, ArC), 129.34 (s, ArC), 130.19 (s, ArC), 130.34 (s, ArC), 130.47 (s, ArC), 131.56 (t,  $J_{\text{CP}} = 4$  Hz, ArC), 131.94 (s, ArC), 133.98 (s, ArC), 150.97 (t,  $J_{\text{CP}} = 9$  Hz, ArC), 155.74 (t,  $J_{\text{CP}} = 14$  Hz, ArC), 156.73 (t,  $J_{\text{CP}} = 14$  Hz, ArC), 300.29 (t,  $J_{\text{CP}} = 62$  Hz,  $\text{Pd}=\text{C}$ ).  $^{31}\text{P}\{^1\text{H}\}$  NMR (202 MHz,  $\text{C}_6\text{D}_6$ )  $\delta$ : 48.07 (s).

**Synthesis of 38b.** A  $\text{C}_6\text{D}_6$  solution of **37b** was allowed to sit at room temperature overnight. The volatiles were removed under reduced pressure resulting in a crude oily residue. The residue was re-dissolved in *n*-pentane and chilled to  $-35^\circ\text{C}$  to induce crystallization. The product,  $[(2''\text{-di-}i\text{-propylphosphino-}\{(Z)\text{-3-phenylbut-2-en-2-yl}\})\text{Pd}(\eta^2\text{-P,C-Pr}_2\text{P}=\text{C}(p\text{-tol})_2)]$ , crystallizes out as a mixture with tetra-*para*-tolyl azine, and was not isolated in its pure form.  $^1\text{H}$  NMR (500 MHz,  $\text{C}_6\text{D}_6$ )  $\delta$ : 0.81 (m, 1 H,  $\text{CH}(\text{CH}_3)_2$ ), 0.88 (t, 3 H,  $J_{\text{HP}} = 8$  Hz,  $\text{C}(\text{CH}_3)=\text{C}(\text{CH}_3)$ ), 0.92 (dd, 3 H,  $J_{\text{HP}} = 8$  Hz,  $J_{\text{HH}} = 4$  Hz,  $\text{CH}(\text{CH}_3)_2$ ), 0.97 (dd, 3 H,  $J_{\text{HP}} = 12$  Hz,  $J_{\text{HH}} = 4$  Hz,  $\text{CH}(\text{CH}_3)_2$ ), 1.09 (m, 6 H,  $\text{CH}(\text{CH}_3)_2$ ), 1.23 (m, 6 H,  $\text{CH}(\text{CH}_3)_2$ ), 1.54 (dd,  $J_{\text{HP}} = 12$  Hz,  $J_{\text{HH}} = 4$  Hz,  $\text{CH}(\text{CH}_3)_2$ ), 1.98 (s, 3 H,  $\text{C}_6\text{H}_4(\text{CH}_3)$ ), 1.99 (s, 3 H,  $\text{C}_6\text{H}_4(\text{CH}_3)$ ), 2.10 (s, 3 H,  $\text{C}(\text{CH}_3)=\text{C}(\text{CH}_3)$ ), 2.29 (m, 2 H,  $\text{CH}(\text{CH}_3)_2$ ), 2.67 (m, 1 H,  $\text{CH}(\text{CH}_3)_2$ ), 6.72 (t, 1 H,  $J_{\text{HH}} = 4$  Hz, ArH), 6.82 (t, 2 H,  $J_{\text{HH}} = 8$  Hz, ArH), 6.93 (d, 2 H,  $J_{\text{HH}} = 8$  Hz, ArH), 7.05 (m, 3 H, ArH), 7.12 (m, 2 H, ArH), 7.37 (d, 2 H,  $J_{\text{HH}} = 4$  Hz, ArH), 7.61 (d, 2 H,  $J_{\text{HH}} = 4$  Hz, ArH), some aromatic resonances are

obscured by azine side product.  $^{31}\text{P}\{^1\text{H}\}$  NMR (162 MHz,  $\text{C}_6\text{D}_6$ )  $\delta$ : 13.05 (d,  $J_{\text{PP}} = 13$  Hz), 37.4 (d,  $J_{\text{PP}} = 14$  Hz).

**General procedure for reactivity experiments between**

**(*c*PCMe=CMeP)Pd=C(*p*-tol) $_2$  and  $\text{CH}_3\text{I}$ ,  $\text{HCl}$  or  $\text{Ph}_2\text{SiH}_2$ .** (*c*PCMe=CMeP)Pd (30 mg, 0.054 mmol) was dissolved in *n*-hexane along with (*p*-tol) $_2\text{CN}_2$  (14.6 mg, 0.066 mmol). The solution was transferred to a J Young NMR tube along with a  $\text{C}_6\text{D}_6$  capillary. The mixture was exposed to UV radiation for 1.5 h. The reaction was monitored by  $^{31}\text{P}$  NMR to ensure adequate conversion to (*c*PCMe=CMeP)Pd=(*p*-tol) $_2$ . Once at least 80% conversion to carbene was achieved, 1 molar equivalent of reagent was added to the solution. The mixture was monitored by  $^{31}\text{P}$  NMR spectroscopy to ensure full consumption of the carbene before reaction workup. Typical reaction times were 3 h. Reaction workup included concentrating the mixture and allowing the palladium species to crystallize from solution in a  $-35$  °C freezer. The organic product was purified by column chromatography.

**1,1-di(*p*-tolyl)ethylene (39):**  $^1\text{H}$  NMR (400 MHz,  $\text{C}_6\text{D}_6$ )  $\delta$ : 2.12 (s, 6H,  $\text{C}_6\text{H}_5\text{CH}_3$ ), 5.41 (s, 2H,  $\text{CH}_2\text{C}(\text{p-tol})_2$ ), 6.97 (d, 4H, ArH,  $J_{\text{HH}} = 8$  Hz), 7.32 (d, 4H, ArH,  $J_{\text{HH}} = 8$  Hz).  $^{13}\text{C}\{^1\text{H}\}$  NMR (100 MHz,  $\text{C}_6\text{D}_6$ )  $\delta$ : 21.1 (s,  $\text{C}_6\text{H}_5\text{CH}_3$ ), 113.0 (s,  $\text{CH}_2\text{C}(\text{p-tol})_2$ ), 128.7 (s, ArC), 129.2 (s, ArC), 137.5 (s, ArC), 139.5 (s, ArC).

**4,4'-(chloromethylene)bis(methylbenzene) (41).**  $^1\text{H}$  NMR (500 MHz,  $\text{CDCl}_3$ )  $\delta$ : 2.32 (s, 6 H,  $\text{C}_6\text{H}_4(\text{CH}_3)$ ), 5.79 (s,  $\text{CH}(\text{p-tol})_2$ ), 7.14 (d,  $J_{\text{HH}} = 8$  Hz, ArH), 7.26 (d,  $J_{\text{HH}} = 8$  Hz, ArH).

**(di-*p*-tolylmethyl)diphenylsilane (42):**  $^1\text{H}$  NMR (400 MHz,  $\text{CDCl}_3$ )  $\delta$ : 2.26 (s, 6H,  $\text{C}_6\text{H}_4\text{CH}_3$ ), 4.09 (d, 1H,  $\text{CH}(\text{p-tol})_2$ ,  $J_{\text{HH}} = 1$  Hz), 5.18 (d, 1H,  $\text{SiHPh}_2$ ,  $J_{\text{HH}} = 1$  Hz,  $J_{\text{HSi}} = 160$

Hz), 6.98 (d, 4H, ArH,  $J_{\text{HH}} = 8$  Hz), 7.05 (d, 4H, ArH,  $J_{\text{HH}} = 8$  Hz), 7.26 (m, 4 H, ArH), 7.31 (m, 6H, ArH).  $^{13}\text{C}\{^1\text{H}\}$  NMR (100 MHz,  $\text{CDCl}_3$ )  $\delta$ : 29.9 (s,  $\text{C}_6\text{H}_4\text{CH}_3$ ), 127.9 (s, ArC), 129.2 (s, ArC), 129.2 (s, ArC), 129.7 (s, ArC), 133.5 (s, ArC), 135.0 (s, ArC), 135.9 (s, ArC), 129.0 (s, ArC).

**Synthesis of (*t*PCMe=CMeP)Pd (43).** [ $\{(\text{TMS})\text{CH}_2\}_2\text{Pd}(\text{cod})$ ] (21.2 mg, 0.07 mmol) was added to an  $\text{Et}_2\text{O}$  solution of (*t*PCMe=CMeP) (**17**, 30.0 mg, 0.07 mmol) and allowed to stir at room temperature for 2 h. The volatiles were removed under reduced pressure. The crude residue was dissolved in *n*-pentane and chilled to  $-35^\circ\text{C}$  to induce crystallization (32.0 mg, 0.06 mmol, 86%).  $^1\text{H}$  NMR (400 MHz,  $\text{C}_6\text{D}_6$ )  $\delta$ : 1.03 (m, 12 H,  $\text{CH}(\text{CH}_3)_2$ ), 1.20 (app q, 6 H,  $J = 8$  Hz,  $\text{CH}(\text{CH}_3)_2$ ), 1.41 (app q, 6 H,  $J = 8$  Hz,  $\text{CH}(\text{CH}_3)_2$ ), 1.56 (s, 6 H,  $\text{C}(\text{CH}_3)=\text{C}(\text{CH}_3)$ ), 2.02 (m, 2H,  $\text{CH}(\text{CH}_3)_2$ ), 2.20 (m, 2 H,  $\text{CH}(\text{CH}_3)_2$ ), 7.16 (m, 2 H, ArH), 7.27 (t, 2 H,  $J_{\text{HH}} = 8$  Hz, ArH), 7.39 (d, 2 H,  $J_{\text{HH}} = 4$  Hz, ArH), 7.45 (d, 2 H,  $J_{\text{HH}} = 8$  Hz, ArH).  $^{31}\text{P}\{^1\text{H}\}$  NMR (162 MHz,  $\text{C}_6\text{D}_6$ )  $\delta$ : 51.97 (s).

**X-ray single crystal diffraction** The data were collected on a Bruker APEX-II diffractometer with a monochromated Mo  $\text{K}\alpha$  radiation.<sup>38</sup> Data were corrected for absorption and polarized effects and analyzed for space group determination.<sup>38-39</sup> The structure was solved by direct methods (SHELXS<sup>40</sup> or OLEX2<sup>41</sup>) and refined by full-matrix least squares techniques against  $F_o^2$  (SHELXL-97).<sup>42</sup> Unless noted, all hydrogen atoms were generated in calculated positions. Mercury was used for structure representations.<sup>43</sup>

**X-Ray Crystal Structure of [(PC(CH<sub>3</sub>)-C(=CH<sub>2</sub>)P)PdBz] (36).** X-Ray quality single crystals were obtained as colorless plates from a concentrated solution of *n*-pentane at  $-35^\circ\text{C}$  in the glovebox. Crystal and refinement data for **36**:  $\text{C}_{35}\text{H}_{48}\text{P}_2\text{Pd}$ ;  $M_r = 637.13$ ; Monoclinic; space group C2/c;  $a = 27.721(4)$  Å;  $b = 10.2881(13)$  Å;  $c = 22.342(3)$  Å;  $\alpha =$

90°;  $\beta = 97.519(4)^\circ$ ;  $\gamma = 90^\circ$ ;  $V = 6317.2(14) \text{ \AA}^3$ ;  $Z = 8$ ;  $T = 120(2) \text{ K}$ ;  $\lambda = 0.71073 \text{ \AA}$ ;  $\mu = 0.711 \text{ mm}^{-1}$ ;  $d_{\text{calc}} = 1.340 \text{ g}\cdot\text{cm}^{-3}$ ; 55026 reflections collected; 6963 unique ( $R_{\text{int}} = 0.0582$ ); giving  $R_1 = 0.0394$ ,  $wR_2 = 0.1154$  for 6963 data with  $[I > 2\sigma(I)]$  and  $R_1 = 0.0564$ ,  $wR_2 = 0.1277$  for all 55026 data. Residual electron density ( $\text{e}^- \cdot \text{\AA}^{-3}$ ) max/min: 1.25/-1.07.

**X-Ray Crystal Structure of 38b.** X-Ray quality single crystals were obtained as yellow blocks from a concentrated solution of *n*-pentane at -35 °C in the glovebox. Crystal data for **38b**:  $\text{C}_{35}\text{H}_{45}\text{P}_2\text{Pd}$ ;  $M_r = 523.59$ ; Orthorhombic; space group  $P2(1)2(1)2(1)$ ;  $a = 12.5503(8) \text{ \AA}$ ;  $b = 15.3033(10) \text{ \AA}$ ;  $c = 21.7717(14) \text{ \AA}$ ;  $\alpha = 90^\circ$ ;  $\beta = 90^\circ$ ;  $\gamma = 90^\circ$ ;  $V = 4181.5(5) \text{ \AA}^3$ ;  $Z = 6$ ;  $T = 120(2) \text{ K}$ ;  $\lambda = 0.71073 \text{ \AA}$ ;  $\mu = 0.550 \text{ mm}^{-1}$ ;  $d_{\text{calc}} = 1.248 \text{ g}\cdot\text{cm}^{-3}$ ; 73954 reflections collected; 10535 unique ( $R_{\text{int}} = 0.0664$ ); giving  $R_1 = 0.0330$ ,  $wR_2 = 0.0736$  for 10535 data with  $[I > 2\sigma(I)]$  and  $R_1 = 0.0428$ ,  $wR_2 = 0.0736$  for all 73954 data. Residual electron density ( $\text{e}^- \cdot \text{\AA}^{-3}$ ) max/min: 0.71/-0.65.

## 5.5 References

1. Xiao, Q.; Zhang, Y.; Wang, J., *Acc. Chem. Res.* **2012**, *46* (2), 236-247.
2. Zhang, Y.; Wang, J., *Eur. J. Org. Chem.* **2011**, *2011* (6), 1015-1026.
3. Xie, X. L.; Zhu, S. F.; Guo, J. X.; Cai, Y.; Zhou, Q. L., *Angew. Chem. Int. Ed.* **2014**, *53* (11), 2978-2981.
4. Kudirka, R.; Devine, S.; Adams, C. S.; Van Vranken, D. L., *Angew. Chem.* **2009**, *121* (20), 3731-3734.
5. Ye, F.; Qu, S.; Zhou, L.; Peng, C.; Wang, C.; Cheng, J.; Hossain, M.; Liu, Y.; Zhang, Y.; Wang, Z.-X.; Wang, J., *J. Am. Chem. Soc.* **2015**, *137* (13), 4435-4444.
6. Zhao, X.; Jing, J.; Lu, K.; Zhang, Y.; Wang, J., *Chem. Commun.* **2010**, *46* (10), 1724-1726.
7. Gutsulyak, D. V.; Piers, W. E.; Borau-Garcia, J.; Parvez, M., *J. Am. Chem. Soc.* **2013**, *135* (32), 11776-11779.

8. Weng, W.; Chen, C.-H.; Foxman, B. M.; Ozerov, O. V., *Organometallics* **2007**, *26* (14), 3315-3320.
9. Comanescu, C. C.; Iluc, V. M., *Organometallics* **2014**, *33* (21), 6059-6064.
10. Gessner, V. H.; Meier, F.; Uhrich, D.; Kaupp, M., *Chem. Eur. J.* **2013**, *19* (49), 16729-16739.
11. Cui, P.; Comanescu, C. C.; Iluc, V. M., *Chem. Commun.* **2015**, *51* (28), 6206-6209.
12. Comanescu, C. C.; Vyushkova, M.; Iluc, V. M., *Chem. Sci.* **2015**, *6* (8), 4570-4579.
13. Cui, P.; Iluc, V. M., *Chem. Sci.* **2015**, *6* (12), 7343-7354.
14. Cui, P.; Hoffbauer, M. R.; Vyushkova, M.; Iluc, V. M., *Chem. Sci.* **2016**, *7* (7), 4444-4452.
15. Whited, M. T.; Grubbs, R. H., *Acc. Chem. Res.* **2009**, *42* (10), 1607-1616.
16. Liu, Z.; Tan, H.; Fu, T.; Xia, Y.; Qiu, D.; Zhang, Y.; Wang, J., *J. Am. Chem. Soc.* **2015**, *137* (40), 12800-12803.
17. Koduri, N. D.; Wang, Z.; Cannell, G.; Cooley, K.; Lemma, T.; Miao, K.; Nguyen, M.; Frohock, B.; Castaneda, M.; Scott, H.; Albinescu, D.; Hussaini, S. R., *J. Org. Chem.* **2014**, *79* (16), 7405-7414.
18. Xia, Y.; Xia, Y.; Zhang, Y.; Wang, J., *Organic & Biomolecular Chemistry* **2014**, *12* (46), 9333-9336.
19. Hussong, M. W.; Rominger, F.; Krämer, P.; Straub, B. F., *Angew. Chem. Int. Ed.* **2014**, *53* (35), 9372-9375.
20. Mindiola, D. J.; Hillhouse, G. L., *J. Am. Chem. Soc.* **2002**, *124* (34), 9976-9977.
21. Waterman, R.; Hillhouse, G. L., *J. Am. Chem. Soc.* **2003**, *125* (44), 13350-13351.
22. Iluc, V. M.; Hillhouse, G. L., *J. Am. Chem. Soc.* **2014**, *136* (17), 6479-6488.
23. Giri, B. P.; Prasad, G.; Mehrotra, K. N., *Can. J. Chem.* **1979**, *57* (10), 1157-1161.
24. Qiu, L.; Huang, D.; Xu, G.; Dai, Z.; Sun, J., *Org. Lett.* **2015**, *17* (7), 1810-1813.
25. Bellow, J. A.; Stoian, S. A.; van Tol, J.; Ozarowski, A.; Lord, R. L.; Groysman, S., *J. Am. Chem. Soc.* **2016**, *138* (17), 5531-5534.



26. Kornecki, K. P.; Briones, J. F.; Boyarskikh, V.; Fullilove, F.; Autschbach, J.; Schrote, K. E.; Lancaster, K. M.; Davies, H. M. L.; Berry, J. F., *Science* **2013**, *342* (6156), 351-354.
27. Straub, B. F.; Hofmann, P., *Angew. Chem. Int. Ed.* **2001**, *40* (7), 1288-1290.
28. Zhu, S.-F.; Zhou, Q.-L., *Acc. Chem. Res.* **2012**, *45* (8), 1365-1377.
29. Dakin, L. A.; Schaus, S. E.; Jacobsen, E. N.; Panek, J. S., *Tetrahedron Lett.* **1998**, *39* (49), 8947-8950.
30. Yasutomi, Y.; Suematsu, H.; Katsuki, T., *J. Am. Chem. Soc.* **2010**, *132* (13), 4510-4511.
31. Zhu, S.-F.; Zhou, Q.-L., *Acc. Chem. Res.* **2012**, *45* (8), 1365-1377.
32. Gillingham, D.; Fei, N., *Chem. Soc. Rev.* **2013**, *42* (12), 4918-4931.
33. Pereira, A.; Champouret, Y.; Martín, C.; Álvarez, E.; Etienne, M.; Belderráin, T. R.; Pérez, P. J., *Chem. Eur. J.* **2015**, *21* (27), 9769-9775.
34. Buck, R. T.; Coe, D. M.; Drysdale, M. J.; Ferris, L.; Haigh, D.; Moody, C. J.; Pearson, N. D.; Sanghera, J. B., *Tetrahedron: Asymmetry* **2003**, *14* (7), 791-816.
35. Duckett, S. B.; Galvez-Lopez, M.-D.; Perutz, R. N.; Schott, D., *Dalton Trans.* **2004**, (17), 2746-2749.
36. Lee, H. G.; Milner, P. J.; Buchwald, S. L., *Org. Lett.* **2013**, *15* (21), 5602-5605.
37. Bruker AXS, APEX-2. Bruker-Nonius AXS, Madison, Wisconsin, USA, **2014**.
38. Krause, L.; Herbst-Irmer, R.; Sheldrick, G. M.; Stalke, D., *J. Appl. Cryst.* **2015**, *48* (1), 3-10.
39. Sheldrick, G., *Acta Cryst.* **2015**, *A71* (1), 3-8.
40. Dolomanov, O. V.; Bourhis, L. J.; Gildea, R. J.; Howard, J. A. K.; Puschmann, H., *J. Appl. Crystallogr.* **2009**, *42* (2), 339-341.
41. Sheldrick, G., *Acta Cryst.* **2015**, *C71* (1), 3-8.
42. Macrae, C. F.; Bruno, I. J.; Chisholm, J. A.; Edgington, P. R.; McCabe, P.; Pidcock, E.; Rodriguez-Monge, L.; Taylor, R.; van de Streek, J.; Wood, P. A., *J. Appl. Cryst.* **2008**, *41* (2), 466-470.

CHAPTER 6:  
AN ADAPTABLE CHELATING DIPHOSPHINE LIGAND FOR THE STABILIZATION OF  
PALLADIUM AND PLATINUM CARBENES

## 6.1 Introduction

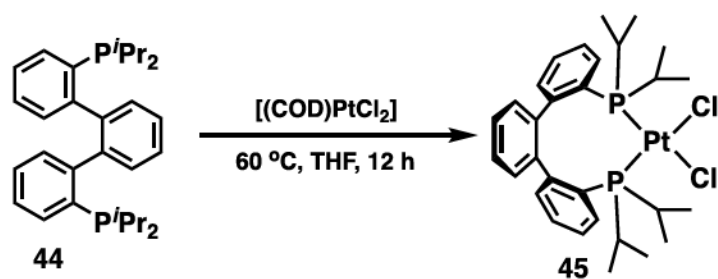
The results presented in the previous chapter indicate that the isolation of group 10 non-heteroatom stabilized carbenes can be accomplished through the utilization of chelating ligands, complementing the observations of the Hillhouse group in their formation of the three coordinate carbene, (dtbe)Ni=CPh<sub>2</sub>.<sup>1-3</sup> The ligand *c*PCMe=CMeP (**26**) was capable of supporting the target complex, however the tendency of the ligand to isomerize to its trans configuration provided a deactivation pathway for the catalyst when catalytic transformations were attempted. Therefore, it was of interest to synthesize a ligand structurally similar to **26** that would resist isomerization. The Vogt group previously reported the ligand, 1,2-bis(2-diphenylphosphino)benzene, and explored its coordination chemistry to platinum(II) metal centers.<sup>4</sup> The ligand framework itself is highly reminiscent of **26**; containing an arene moiety in the place of the *cis*-olefin fragment. The synthesis of the analogous ligand, 1,2-bis(2-di-*iso*-propylphosphino)benzene, PterP, (**44**) was carried out. The coordination chemistry of the ligand to palladium and platinum metal centers was investigated, and the respective carbene complexes synthesized. The reactivity of the

palladium and platinum carbene species was compared to **37a** and will be discussed in this chapter.

## 6.2 Results and Discussion

The ligand precursor, 1,2-di(bromophenyl)benzene was synthesized from a Suzuki cross-coupling reaction as reported in the literature. From this compound, the same synthetic procedure utilized to generate ligands **1**, **17**, and **26** can be used to generate the ligand, PterP, **44**, 1,2-bis(2-(di-*iso*-propylphosphino)phenyl)benzene. The ligand was characterized by multinuclear NMR spectroscopy, and shows the phosphines inequivalent environments, resonating at -3.7 ppm as a singlet in the  $^{31}\text{P}$  NMR spectrum.

The reaction of PterP (**44**) with an equivalent of  $[(\text{cod})\text{PtCl}_2]$  at 60 °C in THF for 12 h led to the isolation of  $[(\text{PterP})\text{PtCl}_2]$  (**45**, Scheme 6.1). Characterization of **45** by NMR spectroscopy at room temperature revealed broad resonances in both the  $^1\text{H}$  and  $^{31}\text{P}$  NMR spectra, indicating a dynamic process. Variable temperature NMR spectroscopic studies (Figure 6.2) showed a  $C_s$  symmetric compound at 60 °C, as indicated by the equivalent environments in the  $^{31}\text{P}$  NMR spectrum. However, upon cooling to -60 °C, the phosphine environments become non-equivalent and correspond to a *cis* coordination environment around the metal center ( $^2J_{\text{pp}} = 16$  Hz). The solid state molecular structure of **45** (Figure 6.2) confirms the *cis* arrangement of the phosphines around the platinum center,<sup>4</sup> leaving the chlorides to occupy positions *trans* to each of the phosphine donors.



**Scheme 6.1:** Synthesis of compound **45**.

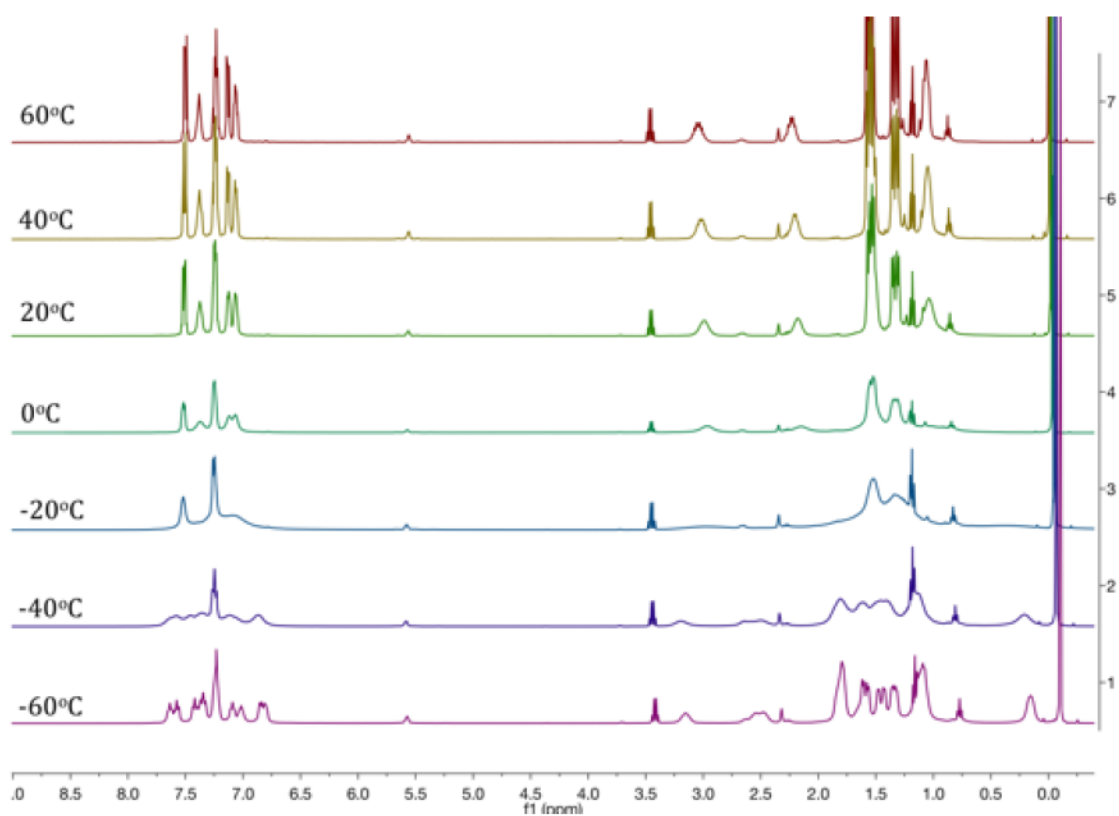


**Figure 6.1:** VT NMR of  $(\text{PterP})\text{PtCl}_2$ , **45**.

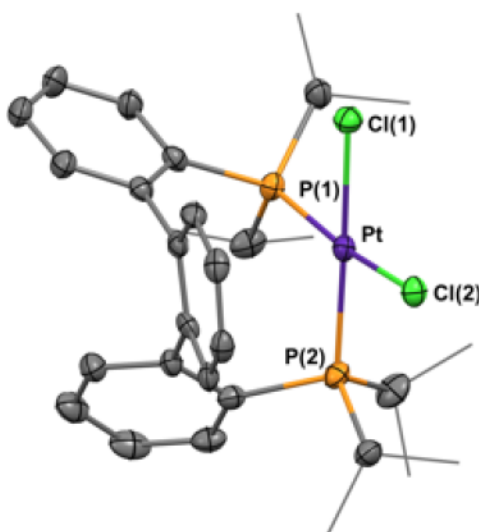
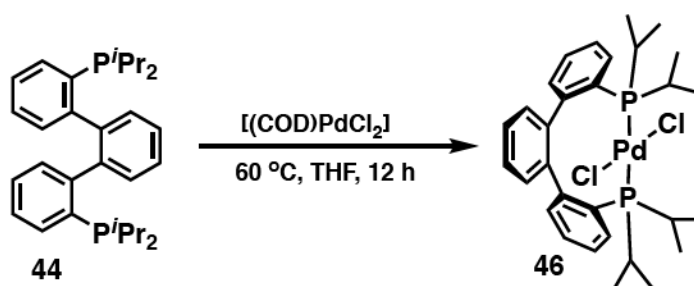


**Figure 6.2:** Thermal-ellipsoid (50% probability level) representation of (PterP)PtCl<sub>2</sub> (**45**). Hydrogen atoms are omitted for clarity. Selected distances (Å) and angles (°): Pt–Cl(1) = 2.3601(10), Pt–Cl(2) = 2.3490(10), Pt–P(1) = 2.2611(11), Pt–P(2) = 2.2636(11), P(1)–Pt–P(2) = 98.84(4), Cl(1)–Pt–Cl(2) = 86.22(4), P(1)–Pt–Cl(1) = 84.00(4), P(2)–Pt–Cl(2) = 90.76(4).

The palladium(II) analogue can be readily synthesized by reacting **44** with [(cod)PdCl<sub>2</sub>] to form [(PterP)PdCl<sub>2</sub>] (**46**, Scheme 6.2). In contrast to **45**, the diphosphine ligand exhibits a trans coordination mode to the metal center (Figure 6.3). The different ligand geometries in **45** and **46** make PterP an attractive candidate for the stabilization of monomeric, two-coordinate Pd(0) and Pt(0) species, which are desirable precursors for carbene formation. For example, our group recently compared the preferentially cis coordinating <sup>i</sup>Pr<sub>2</sub>P(*o*-C<sub>6</sub>H<sub>4</sub>-CH<sub>2</sub>-*o*'-C<sub>6</sub>H<sub>4</sub>)P<sup>i</sup>Pr<sub>2</sub> to the more flexible, wide bite angle <sup>i</sup>Pr<sub>2</sub>P(*o*-C<sub>6</sub>H<sub>4</sub>-CH<sub>2</sub>CH<sub>2</sub>-*o*'-C<sub>6</sub>H<sub>4</sub>)P<sup>i</sup>Pr<sub>2</sub>.<sup>5</sup> We observed that, in the case of the former, dimeric palladium(0) compounds resulted in the absence of an additional dative ligand, however, the wide bite angle ligand was able to accommodate the optimal trans geometry resulting

in a two-coordinate palladium(0) compound. This choice of a flexible diphosphine ligand<sup>6</sup> allowed the preparation of two coordinate palladium(0) and platinum(0) precursors which play a key role in the formation of the desired carbene species. The formation of monomeric Pd(0) and Pt(0) compounds is a strategic synthetic target since it alleviates the need for dimer<sup>7</sup> dissociation in subsequent reactions that might impede carbene formation. Additionally, the accessibility to cis coordination is necessary for the formation of a 3-coordinate carbene species.



**Scheme 6.2:** Synthesis of compound 46.

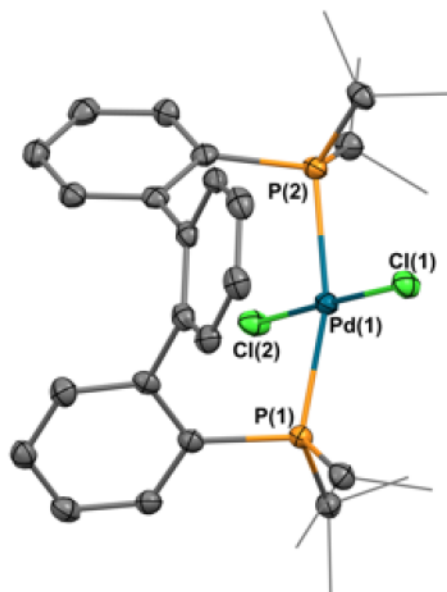
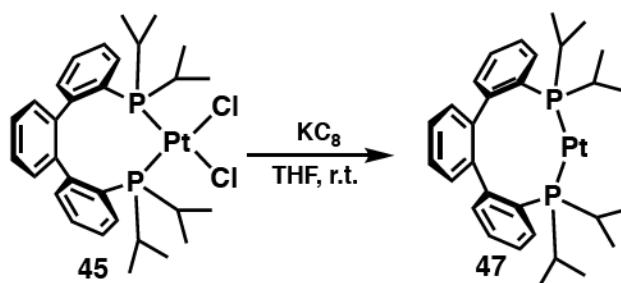


**Figure 6.3:** Thermal-ellipsoid (50% probability level) representation of (PterP)PdCl<sub>2</sub> (**46**). Hydrogen atoms are omitted for clarity. Selected distances (Å) and angles (°): Pd(1)–Cl(1) = 2.3051(7), Pd(1)–Cl(2) = 2.3054(7), Pd(1)–P(1) = 2.2903(8), Pd(1)–P(2) = 2.2965(8), P(1)–Pd(1)–P(2) = 164.45(3), Cl(1)–Pd(1)–Cl(2) = 176.49(3), P(1)–Pd(1)–Cl(1) = 95.46(3), P(2)–Pd(1)–Cl(2) = 85.87(3).

Compound **45** can be reduced to [(PterP)Pt] (**47**) by reacting it with 2 equivalents of KC<sub>8</sub> at room temperature in THF (Scheme 6.3). The resulting species was characterized by NMR spectroscopy as well as single crystal X-ray diffraction. The solid state molecular structure shows a bent geometry around the metal center as indicated by the P–Pt–P angle of 153.95° (Figure 6.3). Although di-coordinate platinum(0) species are known,<sup>8–10</sup> four or three coordinate complexes are common when bidentate ligands are employed.<sup>11–15</sup> Additionally, it is interesting to note that the structurally related para and meta substituted terphenyl systems reported by Agapie and co-workers (2,2''-bis(di-*iso*-propylphosphino)terphenyl) commonly exhibit an interaction between the metal center and the central aryl moiety.<sup>16–18</sup> Contrasting these examples, the ortho substituted analogue described here renders the ligand too rigid to allow such an interaction. Additionally, the

transformation from cis to trans diphosphine coordination of PterP from platinum(II) to platinum(0) demonstrates that the ligand is coordinately flexible.



**Scheme 6.3:** Synthesis of compound **47**.

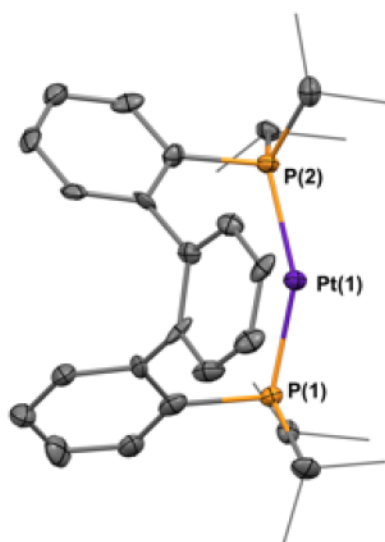
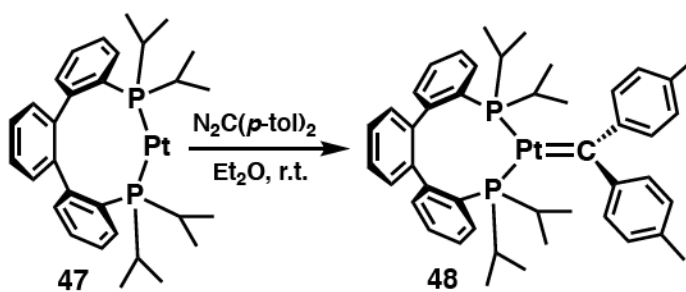


**Figure 6.4:** Thermal-ellipsoid (50% probability level) representation of (PterP)Pt (**47**). Hydrogen atoms are omitted for clarity. Selected distances (Å) and angles (°): Pt(1)–P(1) = 2.215(3), Pt(1)–P(2) = 2.229(3), P(1)–Pt(1)–P(2) = 153.95(12).

Reacting an Et<sub>2</sub>O solution of **47** with an equivalent of (*p*-tol)<sub>2</sub>CN<sub>2</sub> leads to the formation of a major product, [(PterP)Pt=C(*p*-tol)<sub>2</sub>] (**48**), after 2 h at room temperature (Scheme 6.4). The tolyl methyl groups resonate separately in the <sup>1</sup>H NMR spectrum at 2.19



and 2.22 ppm. This finding, along with the aryl region integrating to 20 total protons, indicates that the *p*-tolyl groups were incorporated into the complex. Furthermore, the  $^{13}\text{C}$  NMR spectrum exhibits a diagnostic downfield shift at 262.8 ppm (Figure 6.5) as a triplet, along with platinum satellites at 269.9 and 255.8 ppm ( $^2J_{\text{CP}} = 66$  Hz,  $^1J_{\text{CPt}} = 1775$  Hz). This downfield chemical shift is reminiscent of other electrophilic group 10 metal carbenes. Specifically, the cationic platinum carbene, *trans*-[Pt{P<sup>*i*</sup>Pr<sub>2</sub>(2,6-CH(Me)C<sub>6</sub>H<sub>3</sub>){P<sup>*i*</sup>Pr<sub>2</sub>(2,6-CH<sub>2</sub>(Me)C<sub>6</sub>H<sub>3</sub>)}}]<sup>+</sup> resonates downfield at 209 ppm; interestingly, the value of the C-Pt coupling constant reported for this complex (740 Hz) is lower than that for **48**.<sup>19</sup> Additionally, our group recently observed a correlation between the electronic properties of the carbene fragment and its observed chemical shift in the  $^{13}\text{C}$  NMR spectrum. For instance, the nucleophilic carbene [{PC(sp<sup>2</sup>)P}<sup>*t*</sup>BuPd(PMe<sub>3</sub>)] resonates relatively upfield at 136 ppm; bond polarity inversion of the carbene fragment results in electrophilic character for [{PC(sp<sup>2</sup>)P<sup>*t*</sup>Bu}Pd(PMe<sub>3</sub>)]<sup>+</sup>, which has a downfield shift, at 284 ppm.<sup>20-21</sup> Notably, the structurally analogous trigonal planar nickel carbene [(dtbpe)Ni=CPh<sub>2</sub>] exhibits similar spectroscopic characteristics to **48**, resonating as a triplet at 222 ppm ( $J_{\text{PP}} = 51$  Hz).<sup>22</sup>



**Scheme 6.4:** Synthesis of diarylcarbene **48**.

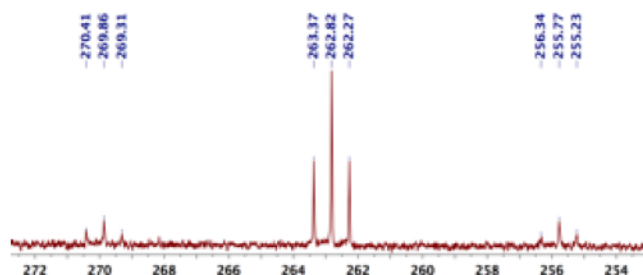


**Figure 6.5:** The carbene region of the  $^{13}\text{C}\{^1\text{H}\}$  NMR spectrum for **48**.

The solid state molecular structure of **48** (Figure 6.6) confirms the synthesis of a trigonal planar platinum carbene species (sum of angles is  $359.68^\circ$  for C and  $359.71^\circ$  for Pt). The Pt-C distance of  $1.942(3)$  Å is shorter than typical Pt-C NHC distances ( $\sim 2.0$  Å)<sup>23-25</sup> and slightly shorter than for previously reported heteroatom stabilized platinum carbenes ( $1.95\text{--}2.0$  Å).<sup>26-28</sup> Similarly to the previously reported nickel diphenylcarbene (dtbpe)Ni=CPh<sub>2</sub>, the plane of the carbene ligand is almost perpendicular to the plane defined by P(1)-Pt-P(2).<sup>22, 29</sup> This orientation allows  $\pi$  overlap between the platinum d orbital and a carbene p orbital. Geometry optimizations using Gaussian03 (B3LYP functional, LANL2DZ basis set) performed on **48** matched the observed solid state structure. The frontier molecular orbitals calculated for a model of **48**, **48'**, in which the *iso*-propyl phosphine groups were replaced by methyl groups, revealed the  $\pi$  bonding and antibonding orbitals as HOMO-1 and LUMO, respectively, found in the P(1)-Pt-P(2) plane (Figure 6.7). Both these orbitals have a small  $\sigma$  P-Pt antibonding character.

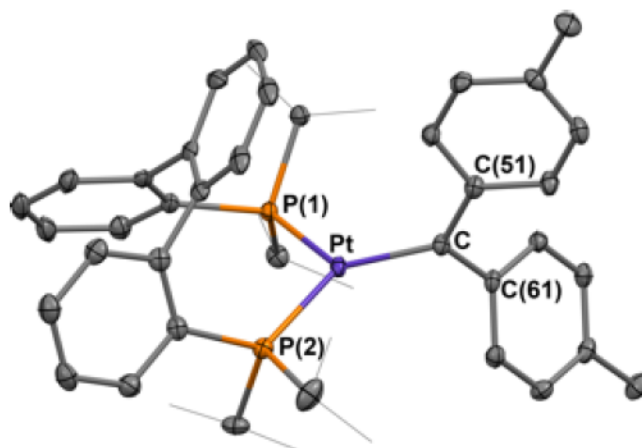


**Figure 6.6:** Thermal-ellipsoid (50% probability level) representation of  $(\text{PterP})\text{Pt}=\text{C}(p\text{-tol})_2$  (**48**). Hydrogen atoms are omitted for clarity. Selected distances ( $\text{\AA}$ ) and angles ( $^\circ$ ):  $\text{Pt}-\text{C} = 1.942(3)$ ,  $\text{Pt}-\text{P}(1) = 2.2665(9)$ ,  $\text{Pt}-\text{P}(2) = 2.2891(10)$ ,  $\text{P}(1)-\text{Pt}-\text{P}(2) = 105.23(3)$ ,  $\text{P}(1)-\text{Pt}-\text{C} = 118.98(11)$ ,  $\text{P}(2)-\text{Pt}-\text{C} = 135.50(11)$ ,  $\text{Pt}-\text{C}-\text{C}(51) = 124.9(2)$ ,  $\text{Pt}-\text{C}-\text{C}(61) = 119.8(2)$ ,  $\text{C}(51)-\text{C}-\text{C}(61) = 115.0(3)$ .

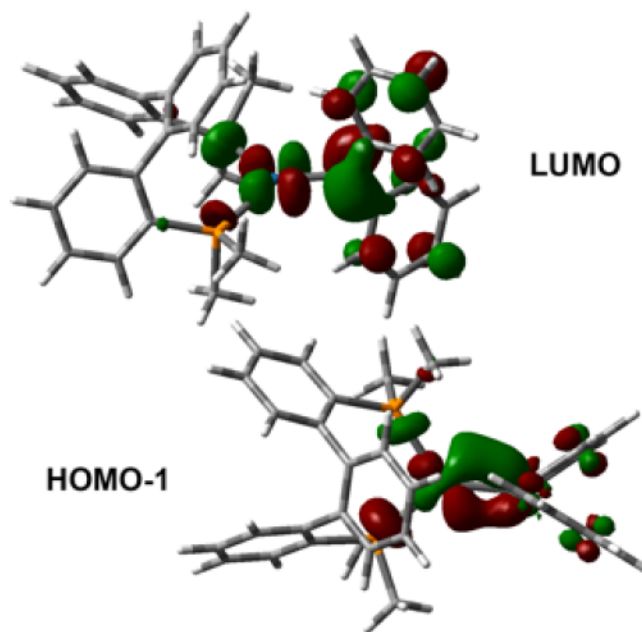


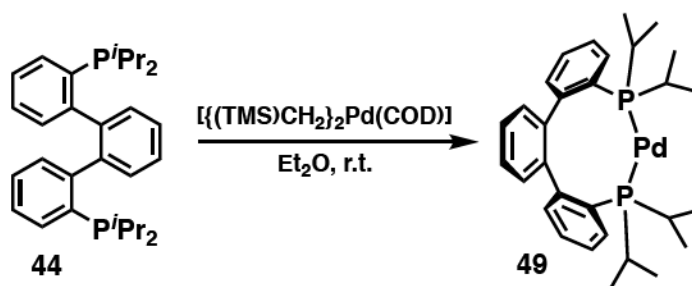
**Figure 6.7:** Frontier molecular orbitals for **48**: bonding (bottom) and antibonding (top)  $\pi$  symmetry orbitals for the  $\text{Pt}=\text{C}$  bond in **48**.

It is of interest to compare the bonding observed in **48** to other examples of group 10 metal carbenes reported in the literature. Like the nickel carbene reported by Hillhouse and coworkers, the bond between the metal center and the carbene fragment has a high  $\pi$  character due to the trigonal planar geometry of the metal center.<sup>22, 29</sup> This is supported by the short M-C distances of 1.942(3) Å in **48** and 1.836(2) Å in (dtbpe)Ni=CPh<sub>2</sub>. Additionally, the presence of two separate resonances for the *p*-tolyl methyl protons in the <sup>1</sup>H NMR spectrum of **48** indicates hindered rotation around the Pt-C bond, supporting double bond character. In contrast, our group synthesized a variety of 4-coordinate palladium carbenes. These complexes range from exhibiting nucleophilic character centered on the carbene carbon to cationic character upon 2-electron oxidation.<sup>20, 30-31</sup> The square planar geometry of the metal center (and the higher coordination number) resulted in a filled  $\pi$  antibonding orbital (HOMO) for the neutral nucleophilic carbene; the bonding is best described as a Pd-C ylide-type single bond with zwitterionic character. This is further supported by the long Pd-C distance of 2.076(3) Å. The sequential oxidation of this carbene resulted in the contraction of the Pd-C distance to 1.968(3) Å, consistent with an increase in bond order. This distance was, however, comparable to the distances observed in palladium N-heterocyclic carbenes, and best described as a cationic carbon center stabilized by  $\pi$ -backdonation from the metal center. The weak  $\pi$  donor capabilities of the 4-coordinate cationic palladium center results in additional electron stabilization from the bound aryl groups. This lack of  $\pi$  donor capabilities for group 10 metal carbenes with higher coordination numbers is further observed for the 4-coordinate palladium example reported by Bröring and coworkers, ((Trpy)PdC(*p*-tol)<sub>2</sub>)[BAR<sup>F</sup><sub>4</sub>]), which exhibits a relatively long Pd-C distance of 1.98 Å.<sup>32</sup> This effect is amplified for the platinum carbenes

of octahedral geometry observed by Templeton and coworkers ( $[\text{Tp}^*\text{Pt}(=\text{CHCH}_3)(\text{Me})_2][\text{BAr}^{\text{F}}_4]$ ).<sup>28</sup> The carbene carbon exhibits a pronounced downfield chemical shift in the  $^{13}\text{C}$  NMR spectrum at 431 ppm. This was attributed to the cationic carbene experiencing only a weak  $\pi$  donation from the 6-coordinate metal center.

We determined that the bidentate ligand scaffold was vital for the isolation of the desired platinum carbene by employing monodentate phosphine ligands. The synthesis of the di-coordinate platinum(0) compound  $[(\text{PCy}_3)_2\text{Pt}]$  was therefore carried out.<sup>10</sup> This species reacted with one equivalent of  $(p\text{-tol})_2\text{CN}_2$  until the diazo reagent was fully consumed. Instead of observing the formation of a platinum carbene, however, we observed the full conversion of the diazo species to the corresponding azine  $((p\text{-tol})_2\text{C}=\text{N}-\text{N}=\text{C}(p\text{-tol})_2)$  by  $^1\text{H}$  NMR spectroscopy (Scheme 6). Compound  $[(\text{PCy}_3)_2\text{Pt}]$  was found unchanged at the end of the reaction. Azine formation has been reported to occur through the coupling of diazo compounds with a carbene fragment.<sup>33-35</sup> It is therefore reasonable to propose that a platinum carbene species is an intermediate in this reaction, however, it is spectroscopically undetectable. This indicates that our coordinately flexible bidentate ligand aids in stabilizing the platinum carbene moiety, making its isolation feasible.

We next became interested in isolating the analogous palladium carbene. The palladium(0) precursor can be readily synthesized by reacting PterP with  $[\{(\text{TMS})_2\text{CH}_2\}_2\text{Pd}(\text{cod})]$ <sup>36</sup> in diethyl ether at room temperature (Scheme 1). The resulting compound,  $[(\text{PterP})\text{Pd}]$  (**49**), was characterized by NMR spectroscopy and single crystal X-ray diffraction (Figure 6.8). Comparable to **47**, the species is di-coordinate and the ligand imposes a bent geometry on the metal center ( $\text{P}(1)\text{-Pd-P}(2) = 151.23(3)^\circ$ ).



**Scheme 6.5:** Synthesis of compound **49**.

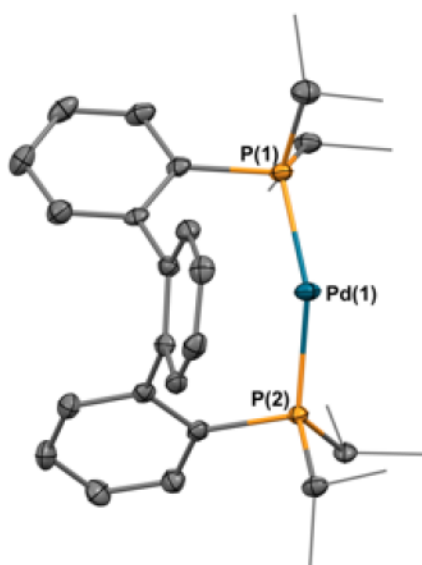
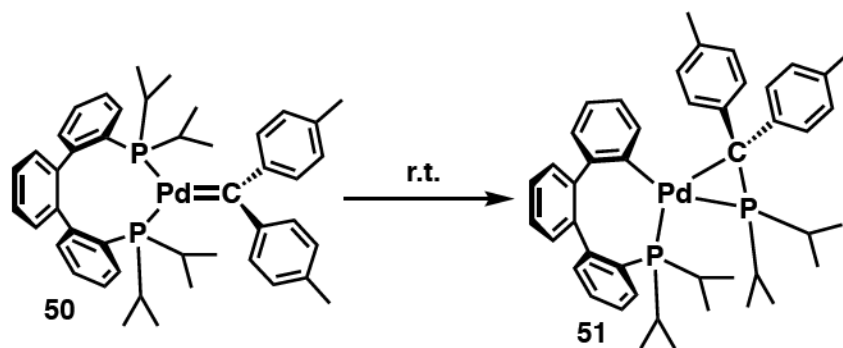


**Figure 6.8:** Thermal-ellipsoid (50% probability level) representation of (PterP)Pd (**49**). Hydrogen atoms are omitted for clarity. Selected distances (Å) and angles (°): Pd(1)–P(1) = 2.2612(9), Pd(1)–P(2) = 2.2472(9), P(1)–Pd(1)–P(2) = 151.23(3).

When **49** reacts with (*p*-tol)<sub>2</sub>CN<sub>2</sub> at room temperature, multiple species are observed in solution. Heating the reaction mixture leads to the formation of an azine species, a transformation also observed for [(Cy<sub>3</sub>P)<sub>2</sub>Pt] (see above). Exposing the reaction mixture to UV radiation for 1 h leads to a major species in solution, assignable in the <sup>31</sup>P NMR spectrum as a singlet at 48.2 ppm. This species, **50**, is the desired palladium carbene, as

indicated by the presence of a triplet at 296.6 ppm in the  $^{13}\text{C}$  NMR spectrum ( $^2J_{\text{CP}} = 63$  Hz). Attempts to obtain single crystals suitable for X-ray diffraction were hampered by its high solubility and instability, however, DFT calculations indicated that **50** is structurally and electronically similar to **48**. The comparable chemical shifts in the  $^{31}\text{P}$  and  $^{13}\text{C}$  NMR spectra, as well as the comparable C-P coupling constants for **48** and **50**, indicate that these two species are analogous. It is of interest to note that to the best of our knowledge, no other palladium non-heteroatom stabilized carbene exhibiting a trigonal planar geometry has been isolated.

We found that when **50** is left at room temperature overnight, full conversion to a new asymmetric product, **51** (Scheme 6.6), is observed by NMR spectroscopy. This behavior is analogous to the palladium carbenes discussed in Chapter 5, (cPCMe=CMcP)Pd=C(Ar)<sub>2</sub>, **37a**, and **37b**. The solid state molecular structure (Figure 6.9) of **51** confirms this claim. On the other hand, the platinum carbene (**48**) is remarkably stable, no decomposition is observed even if heated in solution for 10 days at 120°C.



**Scheme 6.6:** Decomposition of **50**.

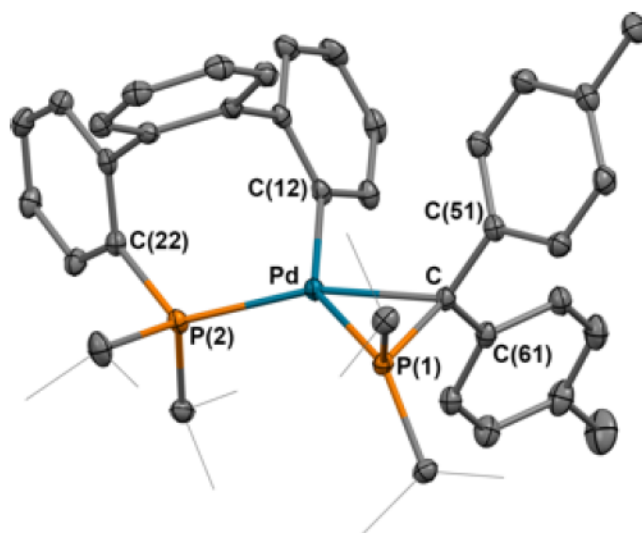


**Figure 6.9:** Thermal-ellipsoid (50% probability level) representation of **51**. Hydrogen atoms are omitted for clarity. Selected distances (Å) and angles (°): Pd–C = 2.1794(18), Pd–P(1) = 2.2896(5), Pd–P(2) = 2.3260(5), C–P(1) = 1.8118(19), Pd–C(12) = 2.0587(19), P(1)–Pd–P(2) = 121.815(17), C(12)–Pd–C = 98.64(7), P(1)–Pd–C = 47.75(5), P(2)–Pd–C(12) = 92.84(5).

In addition to the isolation of the platinum (**48**) and palladium (**50**) diarylcarbenes, their reactivity was assessed. Reacting **48** with an equivalent of iodomethane leads to the clean formation of 1,1-di(*p*-tolyl)ethylene (**39**, Chapter 5, Scheme 6.7), along with (PterP)PtHI (**52**), which could be separated due to their differences in solubility. This is analogous to the results observed for the reaction of (*c*PCMe=CMeP)Pd=C(*p*-tol)<sub>2</sub> with iodomethane (Chapter 5). Compound **52** was characterized by single crystal X-ray diffraction (Figure 6.10) and multinuclear NMR spectroscopy. The hydride was not identified in the electron density map of the crystal structure however, it is easily identified in the <sup>1</sup>H NMR spectrum by a triplet at -13.1 ppm, with platinum satellites (<sup>1</sup>*J*<sub>HPt</sub> = 1200 Hz). Regeneration of the diarylcarbene **48** from **52** could be achieved through the addition of KN(TMS)<sub>2</sub> followed by the addition of the diazo reagent (Scheme 6.7).



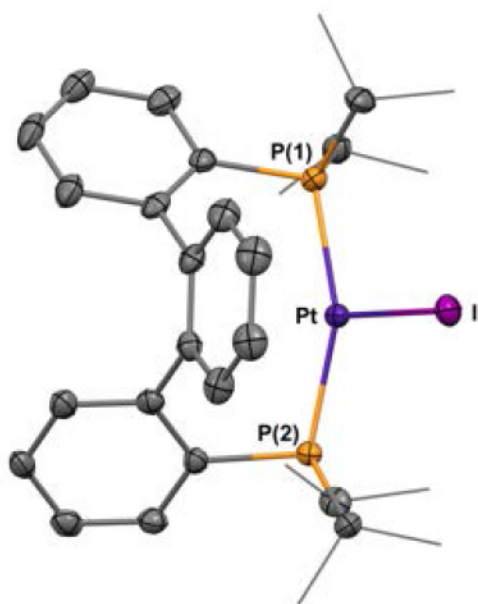


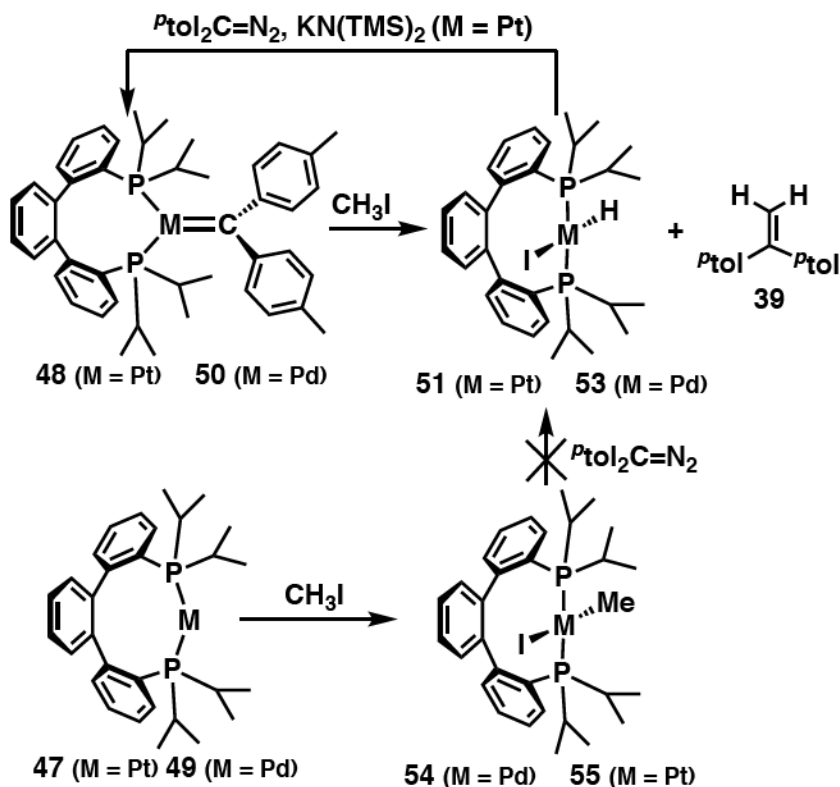
**Figure 6.10:** Thermal-ellipsoid (50% probability level) representation of (PterP)PtHI (**52**). Hydrogen atoms are omitted for clarity. Selected distances (Å) and angles (°): Pt–I = 2.6778(6), Pt–P(1) = 2.269(2), Pt–P(2) = 2.2685(19), P(1)–Pt–P(2) = 156.21(7), P(1)–Pt–I = 102.15(6), P(2)–Pt–I = 100.28(6).

The analogous reaction with **50** and iodomethane led only to a trace amount of the expected organic product. The crude reaction mixture revealed that **50** reacts similarly to the platinum analogue **48**, however many additional products are also formed. In addition to (PterP)PdHI (**53**), the decomposition product **51** was observed in the reaction mixture, as well as the oxidative addition product (PterP)PdI(CH<sub>3</sub>) (**54**). The presence of **54** was confirmed by its independent synthesis, and is attributed to palladium coupling of the diazo substrate, generating the corresponding olefin along with palladium(0). The small amount of organic product formed indicates that **50** undergoes decomposition before it can react fully with the substrate. Further inspection of the crude reaction mixture reveals multiple carbene related species, including the corresponding azine and 1,1,2,2-tetra-*p*-tolylethene, likely a consequence of the in-situ generation of **50**. We hypothesize that the latter is a

result of palladium coupling of the diazo starting material to generate the corresponding olefin, a reaction that has precedent in transition metal chemistry. For example, ruthenium, copper, and gold compounds have proven to be competent at this transformation catalytically.<sup>37-42</sup> Such a process would represent an additional pathway for the formation of the oxidative addition product (**54**), which would result from the presence of palladium(0) (**49**) in solution, formed by the dissociation of the carbene from **50**, explaining the relatively large amount of **54** formed. These results indicate, that the instability of the palladium carbene inhibits its reactivity with a given substrate and therefore, leads to complicated reaction mixtures. It should be noted that the platinum analogue does not lead to the same coupling between two (*p*-tol)<sub>2</sub>C: fragments even upon extended heating at 120°C, highlighting the increased stability of **48** compared to **50**.

Group 10 metal carbenes have been invoked as intermediates in the catalytic coupling of tosylhydrazones with benzyl, vinyl, and alkyl halides.<sup>43-45</sup> This reaction is proposed to occur via the oxidative addition of the R-X (R = benzyl, vinyl, or alkyl group, X = any halogen) substrate to palladium(0), followed by the formation of the carbene from the tosylhydrazone reagent. Insertion of the carbene into the Pd-R bond, followed by  $\beta$ -hydride elimination, releases the organic product. Palladium(0) is regenerated through the addition of a base. In order to probe this proposed mechanism, we attempted to generate the same organic product through the reaction of (PterP)PdI(CH<sub>3</sub>) (**54**) and (PterP)PtI(CH<sub>3</sub>) (**55**) with (*p*-tol)<sub>2</sub>CN<sub>2</sub> (Scheme 6.7), however, no reaction occurred. This result could be due to the presence of the chelating phosphine ligand, which would lead to an unlikely five-coordinate carbene intermediate upon oxidative addition of the substrate. In our case, more likely, the R-X bond is cleaved in a cooperative manner by the metal center and the

carbene moiety, similar to what was observed for the four coordinate group 10 metal carbenes reported previously by our group.<sup>30</sup>

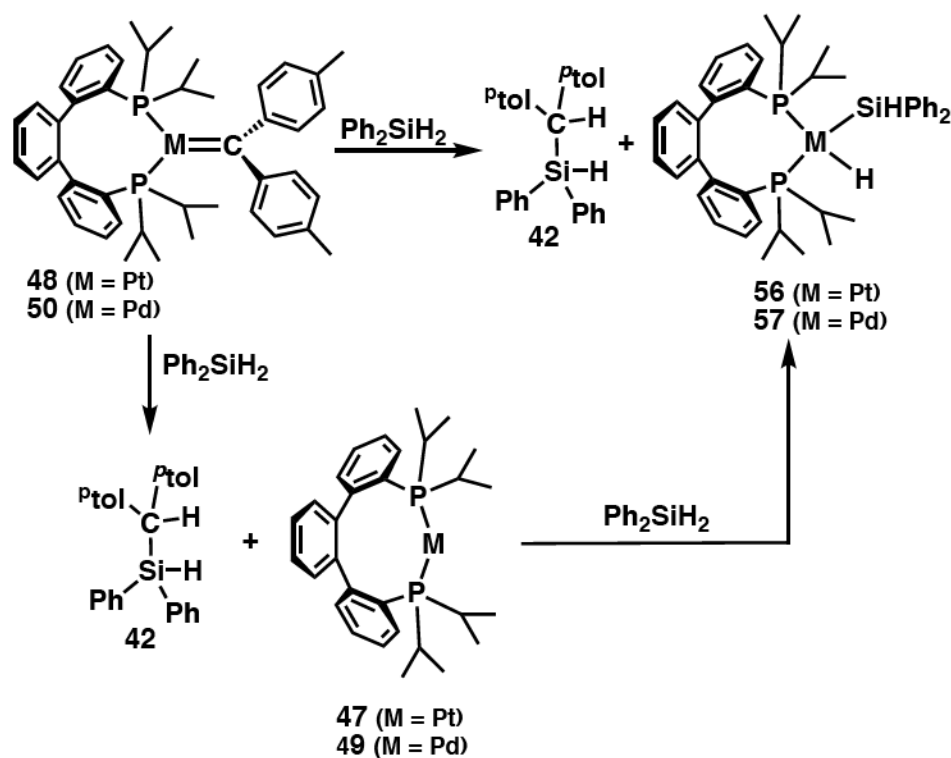


**Scheme 6.7:** Reactions of **48** and **50** with  $CH_3I$ .

The reactivity of the palladium and platinum diarylcarbenes was further assessed with silanes, and akin to the reaction with iodomethane, the results are analogous to the reactivity observed with  $(cPCMe=CMcP)Pd=C(p\text{-}tol)_2$  (**37**, Chapter 5). Reacting **48** with two equivalents of  $Ph_2SiH_2$  led to the formation of (di-*p*-tolylmethyl)diphenylsilane, resulting from carbene insertion into a Si-H bond of the substrate (Scheme 6.8) in agreement with the proposed literature mechanism in which a concerted insertion of the carbene fragment into the Si-H bond forms the observed organic product.<sup>46-47</sup> Additionally, the clean formation of  $(PterP)PtH(SiHPh_2)$  (**56**) is observed; this is proposed to occur from

the reaction of (PterP)Pt (**47**) with unreacted Ph<sub>2</sub>SiH<sub>2</sub> (Scheme 6.8). The formation of **56** was confirmed via its independent synthesis from **47** and Ph<sub>2</sub>SiH<sub>2</sub> (Figure 6.11).

The reaction of the palladium diarylcarbene (**50**) with Ph<sub>2</sub>SiH<sub>2</sub> shows only trace amounts of the expected organic product (Scheme 6.8). Analysis of the reaction mixture reveals two palladium products: 62% of the metal silane adduct (PterP)Pd(Ph<sub>2</sub>SiH<sub>2</sub>), **57**, and 38% of the carbene decomposition product (**51**). The large amount of silane adduct formed indicates that once again, the instability of the palladium carbene impedes its reactivity with a desired substrate, and instead undergoes coupling to form the corresponding olefin or azine species along with palladium(0) **49** (see above).



**Scheme 6.8:** Reactivity of carbenes **48** and **50** with Ph<sub>2</sub>SiH<sub>2</sub>.

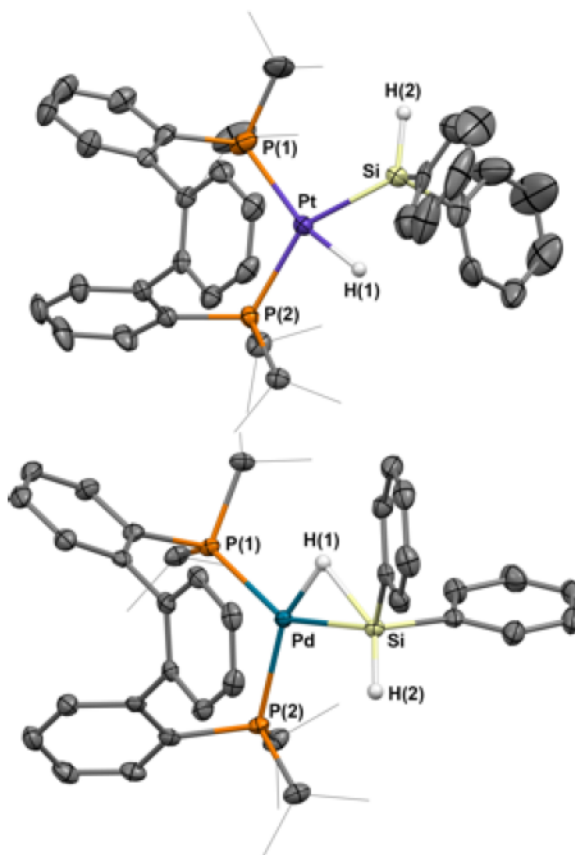


**Figure 6.11:** Thermal-ellipsoid (50% probability level) representation of **56** (top) and **57** (bottom). Most hydrogen atoms are omitted for clarity. Selected distances (Å) and angles (°) for **56**: Pt–Si = 2.3302(16), Pt–H(1) = 1.69(6), Pt–P(1) = 2.2877(14), Pt–P(2) = 2.3335(13), Pt–H(2) = 3.28, Si–H(1) = 2.21, Si–H(2) = 1.41(5), P(1)–Pt–P(2) = 109.93(5), P(1)–Pt–Si = 100.40(6), P(2)–Pt–Si = 148.28(5), P(1)–Pt–H(1) = 163(2), P(2)–Pt–H(1) = 86(2), H(1)–Pt–Si = 64(2), Pt–Si–H(2) = 120(2); for **57**: Pd–Si = 2.3436(6), Pd–H(1) = 1.55(2), Pd–P(1) = 2.3691(5), Pd–P(2) = 2.3295(5), Pd–H(2) = 3.10, Si–H(1) = 1.87(2), Si–H(2) = 1.41(2), P(1)–Pd–Si = 146.28(2), P(2)–Pd–Si = 105.27(2), P(1)–Pd–P(2) = 108.417(19), P(1)–Pd–H(1) = 93.7(9), P(2)–Pd–H(1) = 157.7(9), H(1)–Pd–Si = 41.3(8), Pd–Si–H(2) = 108.7(10).

As for **56**, the formation of **57** was confirmed through its independent synthesis. Evaluation of **56** and **57** via NMR spectroscopy indicates that both complexes are undergoing dynamic processes, but to a different extent. The palladium silane adduct shows equivalent environments for the two silane protons at 1.74 ppm. This value is shifted upfield from free silane (5.5 ppm), indicating an interaction with the metal center.

Palladium silane adducts have been previously reported and commonly exhibit dynamic behavior.<sup>48-49</sup> It has been proposed that the two silane protons can exchange through an  $\eta^2$ -silane intermediate, explaining the equivalent environments observed in the  $^1\text{H}$  NMR spectrum. In contrast to **57**, the platinum analogue, **56**, shows two distinct environments for the silane protons (-3.73 and 5.10 ppm). Additionally, its  $^{31}\text{P}$  NMR spectrum shows two non-equivalent phosphine environments as unresolved doublets at 40.36 and 35.78 ppm. This asymmetry indicates a larger extent of silane oxidative addition compared to that in the palladium analogue, however, the  $^1\text{H}$  NMR and  $^{31}\text{P}$  NMR signatures are reminiscent of previously reported platinum silane adducts that exhibit fluxional behavior.<sup>50</sup> Examining the  $^{29}\text{Si}$  NMR spectra for each of the compounds provides additional support for the larger extent of oxidative addition of the silane to the platinum analogue compared to the palladium analogue. The signal in the platinum compound is an apparent doublet at 6.6 ppm with platinum satellites ( $J_{\text{SiP}} = 149$  Hz,  $J_{\text{SiPt}} = 1221$  Hz). In contrast, the palladium species exhibits a singlet in the  $^{29}\text{Si}$  NMR spectrum at -9.23 ppm. In the solid-state molecular structures (Figure 6.11) of both species, the Si-M-P (M = Pt, Pd) angle is larger than the optimal  $90^\circ$  for a square planar geometry, however, this value is larger for the palladium ( $105.27(2)^\circ$ ) than the platinum analogue ( $100.40(6)^\circ$ ).

### 6.3 Summary

The synthesis and characterization of trigonal planar palladium and platinum diarylcarbenes has been described. The palladium carbene was spectroscopically characterized in solution, however, the instability of the species impeded its solid-state characterization. The observed palladium carbene is analogous to the isolated platinum

carbene, as indicated by their similar spectroscopic signatures and further support was provided by DFT calculations. The PterP ligand allowed the synthesis of trans, two-coordinate palladium(0) and platinum(0) compounds and was capable of adopting a wide angle, cis arrangement upon carbene formation, highlighting its flexibility. Additionally, the ability of PterP to stabilize di-coordinate Pd(0) and Pt(0) monomeric compounds alleviates the need to break apart dimeric species, which commonly form with ligands exhibiting a preference for cis coordination. The reactivity of the isolated palladium and platinum diarylcarbenes was investigated with CH<sub>3</sub>I and Ph<sub>2</sub>SiH<sub>2</sub>. It was found that both species were competent at performing the respective transformations stoichiometrically, although the instability of the palladium compound led to more decomposition than in the case of platinum. The reactivity observed was analogous to that observed with (cPCMe=CMeP)Pd=C(*p*-tol)<sub>2</sub> (**37a**) in Chapter 5.

## 6.4 Experimental

All manipulations of air and water sensitive compounds were performed under dry nitrogen atmosphere using an MBraun drybox. Glassware, vials, and stir bars were dried in an oven at 120 °C overnight and evacuated for 12 hours in the antechamber before being brought into the drybox. All solvents were dried by passing through a column of activated alumina, followed by storage over molecular sieves and sodium. Deuterated solvents were purchased from Cambridge Isotope Laboratories. C<sub>6</sub>D<sub>6</sub> and C<sub>6</sub>D<sub>5</sub>CD<sub>3</sub> were dried by stirring over CaH<sub>2</sub> followed by filtration. CDCl<sub>3</sub>, and C<sub>6</sub>D<sub>12</sub> were dried over molecular sieves. KC<sub>8</sub>,<sup>51</sup> (*p*-tol)<sub>2</sub>CN<sub>2</sub>,<sup>52</sup> and [{(TMS)CH<sub>2</sub>}<sub>2</sub>Pd(cod)]<sup>36</sup> were prepared according to literature procedures. All other chemicals were commercially available and used as received. NMR

spectra were obtained on Bruker 400 and Bruker 500 spectrometers at ambient temperature unless stated otherwise. Chemical shift values are reported in ppm relative to residual internal protio solvents or to a TMS standard for  $^1\text{H}$  and  $^{13}\text{C}\{^1\text{H}\}$  experiments.  $^{195}\text{Pt}\{^1\text{H}\}$  NMR chemical shifts are relative to an external standard of  $\text{Na}_2\text{PtCl}_4$  in  $\text{D}_2\text{O}$ , and  $^{31}\text{P}\{^1\text{H}\}$  NMR chemical shifts are relative to an external standard of  $\text{PPh}_3$  in  $\text{C}_6\text{D}_6$ .  $^{29}\text{Si}\{^1\text{H}\}$  NMR chemical shifts are relative to an external standard of TMS in  $\text{CDCl}_3$ . Coupling constants are reported in Hz. CHN analyses were performed on a CE-440 Elemental Analyzer or by Midwest Microlab. Gaussian 03 (revision D.02) was used for all reported calculations. The B3LYP (DFT) method was used to carry out the geometry optimizations on model compounds specified in text using the LANL2DZ basis set. The validity of the true minima was checked by the absence of negative frequencies in the energy Hessian.

**Synthesis of 1,2-bis(2-bromophenyl)benzene.** The ligand precursor was synthesized according to a modified procedure.<sup>53</sup> *o*-diiodobenzene (1.1 g, 3.3 mmol), 2-bromophenylboronic acid (6.7 g, 33.3 mmol),  $\text{PPh}_3$  (843.6 mg, 3.2 mmol),  $\text{Pd}(\text{PPh}_3)_4$  (350.3 mg, 0.03 mmol) and 100 mL of THF were added to a Schlenk flask under an inert atmosphere. A 2 M KOH solution was purged with  $\text{N}_2$ , and 30 mL was transferred into the mixture. The mixture was stirred under an atmosphere of  $\text{N}_2$  at 60 °C for 24 hours. The organic layer was separated from the aqueous layer and filtered through silica. All the volatiles were removed under reduced pressure. The residue was re-dissolved in hexanes, and washed with  $\text{H}_2\text{O}_2$ . The organic layer was separated from the aqueous layer, dried over  $\text{Na}_2\text{SO}_4$ , and filtered over silica. If needed, the product was further purified by column chromatography (silica, *n*-hexane). The product, 1,2-bis(2-bromophenyl)benzene, was isolated as a colorless oil (1.1 g, 86%).



**Synthesis of PterP (44).** A solution of 1,2-bis(2-bromophenyl)benzene (500.0 mg, 1.3 mmol) in 15 mL of Et<sub>2</sub>O was chilled to –78 °C for 30 minutes, followed by the addition of *n*-butyllithium (1.62 mL, 2.6 mmol) by syringe. The mixture was warmed to room temperature and stirred for 1 hour. The solution was chilled to –78 °C for 30 minutes before the addition of chlorodi-*iso*-propylphosphine (0.42 mL, 2.6 mmol) via syringe. The solution was stirred at room temperature for 12 hours. The reaction mixture was quenched with 1 mL degassed 10% solution of NH<sub>4</sub>Cl in H<sub>2</sub>O. The solution was dried over anhydrous Na<sub>2</sub>SO<sub>4</sub> and filtered through a pad of Celite. The volatiles were removed under reduced pressure. PterP (44) was isolated by recrystallization from a concentrated *n*-pentane solution at –35 °C. Yield: 477mg, 80%. **For 44:** <sup>1</sup>H NMR (500 MHz, C<sub>6</sub>D<sub>6</sub>) δ: 0.67 (dd, 6H, CH(CH<sub>3</sub>)<sub>2</sub>, *J*<sub>HH</sub> = 7 Hz, *J*<sub>HP</sub> = 13 Hz), 0.90 (dd, 6H, CH(CH<sub>3</sub>)<sub>2</sub>, *J*<sub>HH</sub> = 7 Hz, *J*<sub>HP</sub> = 11 Hz), 0.97 (dd, 6H, CH(CH<sub>3</sub>)<sub>2</sub>, *J*<sub>HH</sub> = 5 Hz, *J*<sub>HP</sub> = 12 Hz), 1.11 (dd, 6H, CH(CH<sub>3</sub>)<sub>2</sub>, *J*<sub>HH</sub> = 7 Hz, *J*<sub>HP</sub> = 15 Hz), 1.71 (m, 2H, CH(CH<sub>3</sub>)<sub>2</sub>), 1.96 (m, 2H, CH(CH<sub>3</sub>)<sub>2</sub>), 7.00 (td, 2H, ArH, *J*<sub>HH</sub> = 7.5 Hz, *J*<sub>HP</sub> = 1.5 Hz), 7.08 (t, 2H, ArH, *J*<sub>HH</sub> = 7 Hz), 7.21 (m, 6H, ArH), 7.77 (ddd, 2H, ArH, *J*<sub>HH</sub> = 7.5 Hz, *J*<sub>HH</sub> = 3.5 Hz, *J*<sub>HP</sub> = 1 Hz). <sup>13</sup>C{<sup>1</sup>H} NMR (126 MHz, C<sub>6</sub>D<sub>6</sub>) δ: 20.1 (d, CH(CH<sub>3</sub>)<sub>2</sub>, *J*<sub>CP</sub> = 4 Hz), 20.2 (d, CH(CH<sub>3</sub>)<sub>2</sub>, *J*<sub>CP</sub> = 2 Hz), 20.6 (d, CH(CH<sub>3</sub>)<sub>2</sub>, *J*<sub>CP</sub> = 12 Hz), 20.8 (d, CH(CH<sub>3</sub>)<sub>2</sub>, *J*<sub>CP</sub> = 22 Hz), 23.2 (d, CH(CH<sub>3</sub>)<sub>2</sub>, *J*<sub>CP</sub> = 15 Hz), 27.8 (d, CH(CH<sub>3</sub>)<sub>2</sub>, *J*<sub>CP</sub> = 17 Hz), 126.40 (s, ArC), 126.6 (s, ArC), 127.9 (s, ArC), 131.9 (d, ArC, *J*<sub>CP</sub> = 3 Hz), 132.5 (d, ArC, *J*<sub>CP</sub> = 2 Hz), 133.4 (t, ArC, *J*<sub>CP</sub> = 7 Hz), 141.5 (d, ArC, *J*<sub>CP</sub> = 5 Hz), 150.3 (d, ArC, *J*<sub>CP</sub> = 31 Hz). <sup>31</sup>P{<sup>1</sup>H} NMR (200 MHz, C<sub>6</sub>D<sub>6</sub>) δ: –3.7 (s).

**Synthesis of [(PterP)PtCl<sub>2</sub>] (45).** In a scintillation vial, a solution of PterP (44, 75.0 mg, 0.16 mmol) in 5 mL of THF was added to a solution of [(cod)PtCl<sub>2</sub>] (60.6 mg, 0.16 mmol, 5 mL of THF). The mixture was heated for 12 hours at 60 °C in a Schlenk tube.

The volatiles were removed under reduced pressure and the residue was triturated with *n*-pentane (3×5 mL). The solvent was decanted, and the resulting white powder was washed with *n*-pentane and dried under reduced pressure. Yield: 90 mg, 76%. **For 45:**  $^1\text{H}$  NMR (400 MHz,  $\text{CDCl}_3$ , 20 °C)  $\delta$ : 1.06 (br s, 6H,  $\text{CH}(\text{CH}_3)_2$ ), 1.35 (dd, 6H,  $\text{CH}(\text{CH}_3)_2$ ,  $J_{\text{HP}} = 16$  Hz,  $J_{\text{HH}} = 8$  Hz), 1.56 (m, 12H,  $\text{CH}(\text{CH}_3)_2$ ), 2.20 (br m, 2H,  $\text{CH}(\text{CH}_3)_2$ ), 3.02 (br m, 2H,  $\text{CH}(\text{CH}_3)_2$ ), 7.09 (br m, 2H, ArH), 7.15 (app t, 2H, ArH,  $J_{\text{HH}} = 4$ Hz), 7.27 (app t, 4H, ArH,  $J_{\text{HH}} = 4$ Hz), 7.40 (br m, 2H, ArH), 7.53 (dd, 2H, ArH,  $J_{\text{HP}} = 5.6$ Hz,  $J_{\text{HH}} = 3.6$ Hz).  $^1\text{H}$  NMR (400 MHz,  $\text{CDCl}_3$ , 60 °C)  $\delta$ : 1.06 (br dd, 6H,  $\text{CH}(\text{CH}_3)_2$ ,  $J_{\text{HH}} = 4$  Hz,  $J_{\text{HP}} = 8$  Hz), 1.34 (dd, 6H,  $\text{CH}(\text{CH}_3)_2$ ,  $J_{\text{HP}} = 16$  Hz,  $J_{\text{HH}} = 8$  Hz), 1.56 (m, 12H,  $\text{CH}(\text{CH}_3)_2$ ), 2.24 (m, 2H,  $\text{CH}(\text{CH}_3)_2$ ), 3.05 (m, 2H,  $\text{CH}(\text{CH}_3)_2$ ), 7.07 (br m, 2H, ArH), 7.14 (dd, 2H, ArH,  $J_{\text{HH}} = J_{\text{HP}} = 4$ Hz), 7.24 (app t, 4H, ArH,  $J_{\text{HH}} = 4$  Hz), 7.39 (br m, 2H, ArH), 7.51 (dd, 2H, ArH,  $J_{\text{HP}} = 8$  Hz,  $J_{\text{HH}} = 4$  Hz).  $^{13}\text{C}\{^1\text{H}\}$  NMR (100 MHz,  $\text{CDCl}_3$ , 20 °C)  $\delta$ : 21.1 (d,  $\text{CH}(\text{CH}_3)_2$ ,  $J_{\text{CP}} = 5.8$  Hz), 22.2 (s,  $\text{CH}(\text{CH}_3)_2$ ), 22.7 (s,  $\text{CH}(\text{CH}_3)_2$ ), 23.0 (s,  $\text{CH}(\text{CH}_3)_2$ ), 23.0 (br s,  $\text{CH}(\text{CH}_3)_2$ ), 26.8 (d,  $\text{CH}(\text{CH}_3)_2$ ,  $J_{\text{CP}} = 30$  Hz), 28.0 (br t,  $\text{CH}(\text{CH}_3)_2$ ,  $J_{\text{CP}} = 15.5$  Hz), 125.6 (d, ArC,  $J_{\text{CP}} = 6.4$  Hz), 127.8 (s, ArC), 129.9 (s, ArC), 130.5 (br s, ArC), 132.9 (br s, ArC), 133.7 (d, ArC,  $J_{\text{CP}} = 8.4$  Hz), 140.4 (br s, ArC), 147.3 (s, ArC), 147.4 (s, ArC).  $^{31}\text{P}\{^1\text{H}\}$  NMR (162 MHz,  $\text{CDCl}_3$ , 20 °C)  $\delta$ : 13.6 (br s,  $J_{\text{PPt}} = 3759$  Hz).  $^{31}\text{P}\{^1\text{H}\}$  NMR (162 MHz,  $\text{CDCl}_3$ , -60 °C)  $\delta$ : 8.8 (d,  $J_{\text{PP}} = 13$  Hz,  $J_{\text{PPt}} = 3679$  Hz), 15.9 (d,  $J_{\text{PP}} = 13$  Hz,  $J_{\text{PPt}} = 3826$  Hz).  $^{195}\text{Pt}\{^1\text{H}\}$  NMR (86 MHz,  $\text{CDCl}_3$ , 20 °C)  $\delta$ : -4075.8 (t,  $J_{\text{PtP}} = 3752$  Hz). Anal. Calcd. for  $\text{C}_{30}\text{H}_{40}\text{Cl}_2\text{P}_2\text{Pt}$ : C, 49.46; H, 5.53. Found: C, 49.52; H, 5.44.

**Synthesis of [(PterP)PdCl<sub>2</sub>] (46).** A solution of PterP (**44**, 25.0 mg, 0.05 mmol) in 5 mL of THF was added to a solution of [(cod)PdCl<sub>2</sub>] (15.5 mg, 0.05 mmol) in 5 mL of THF and heated to 65 °C for 2 hours in a Schlenk tube. The volatiles were removed under

reduced pressure. The resulting residue was triturated with *n*-pentane (5×5 mL) and dried under reduced pressure. [(PterP)PdCl<sub>2</sub>] (**46**) was isolated as a pale yellow powder. Yield: 29 mg, 83 %. **For 46:** <sup>1</sup>H NMR (500 MHz, CDCl<sub>3</sub>) δ: 1.22 (app q, 6H CH(CH<sub>3</sub>)<sub>2</sub>, *J*<sub>HH</sub> = *J*<sub>HP</sub> = 10 Hz), 1.45 (app q, 6H, CH(CH<sub>3</sub>)<sub>2</sub>, *J*<sub>HH</sub> = *J*<sub>HP</sub> = 5 Hz), 1.66 (m, 12 H, CH(CH<sub>3</sub>)<sub>2</sub>), 3.05 (m, 2H, CH(CH<sub>3</sub>)<sub>2</sub>), 3.17 (m, 2H, CH(CH<sub>3</sub>)<sub>2</sub>), 7.09 (dd, 2H, ArH, *J*<sub>HH</sub> = 5 Hz, *J*<sub>HP</sub> = 10 Hz), 7.20 (t, 2H, ArH, *J*<sub>HH</sub> = 5 Hz), 7.25 (t, 2H, ArH, *J*<sub>HH</sub> = 5 Hz), 7.36 (dd, 2H, ArH, *J*<sub>HH</sub> = 5 Hz, *J*<sub>HP</sub> = 10 Hz), 7.40 (dd, 2H, ArH, *J*<sub>HH</sub> = 5 Hz, *J*<sub>HP</sub> = 2 Hz), 7.55 (m, 2H, ArH). <sup>13</sup>C{<sup>1</sup>H} NMR (126 MHz, CDCl<sub>3</sub>) δ: 19.4 (s, CH(CH<sub>3</sub>)<sub>2</sub>), 19.6 (s, CH(CH<sub>3</sub>)<sub>2</sub>), 20.4 (s, CH(CH<sub>3</sub>)<sub>2</sub>), 24.5 (t, CH(CH<sub>3</sub>)<sub>2</sub>, *J*<sub>CP</sub> = 8 Hz), 25.0 (t, CH(CH<sub>3</sub>)<sub>2</sub>, *J*<sub>CP</sub> = 11 Hz), 24.4 (t, CH(CH<sub>3</sub>)<sub>2</sub>, *J*<sub>CP</sub> = 10 Hz), 126.2 (t, ArC, *J*<sub>CP</sub> = 3 Hz), 127.4 (s, ArC), 128.0 (s, ArC), 130.8 (s, ArC), 132.6 (s, ArC), 133.6 (t, ArC, *J*<sub>CP</sub> = 5 Hz), 137.0 (t, ArC, *J*<sub>CP</sub> = 19 Hz), 141.7 (t, ArC, *J*<sub>CP</sub> = 1 Hz), 145.9 (t, ArC, *J*<sub>CP</sub> = 8 Hz). <sup>31</sup>P{<sup>1</sup>H} NMR (200 MHz, CDCl<sub>3</sub>) δ: 33.1 (s). Anal. Calcd. for C<sub>30</sub>H<sub>40</sub>Cl<sub>2</sub>P<sub>2</sub>Pd: C, 56.31; H, 6.30. Found: C, 55.95; H, 6.25.

**Synthesis of [(PterP)Pt] (**47**).** A suspension of KC<sub>8</sub> (17.4 mg, 0.13 mmol) in 5 mL of THF was added dropwise to a solution of [(PterP)PtCl<sub>2</sub>] (**45**, 46.1 mg, 0.06 mmol) in 5 mL of THF. The mixture was stirred at room temperature for 10 min. The volatiles were removed under reduced pressure, followed by extraction with *n*-pentane. The crude product was isolated as an orange powder (40.1 mg, 96%). Analytically pure **47** was isolated by recrystallization from a concentrated solution of *n*-pentane at −35 °C (10 mg, 36%). **For 47:** <sup>1</sup>H NMR (500 MHz, C<sub>6</sub>D<sub>6</sub>) δ: 1.11 (app q, 6H, CH(CH<sub>3</sub>)<sub>2</sub>, *J*<sub>HH</sub> = 5 Hz), 1.20 (m, 12H, CH(CH<sub>3</sub>)<sub>2</sub>), 1.29 (app q, 6H, CH(CH<sub>3</sub>)<sub>2</sub>, *J*<sub>HP</sub> = 10 Hz), 2.29 (m, 4H, CH(CH<sub>3</sub>)<sub>2</sub>), 6.91 (t, 2H, ArH, *J*<sub>HH</sub> = 10 Hz), 7.00 (t, 2H, ArH, *J*<sub>HH</sub> = 7.5 Hz), 7.04 (m, 2 H, ArH), 7.16 (m, 4H, ArH), 7.43 (d, 2H, ArH, *J*<sub>HH</sub> = 6.5 Hz). <sup>13</sup>C{<sup>1</sup>H} NMR (100 MHz, C<sub>6</sub>D<sub>6</sub>) δ: 18.1 (s, CH(CH<sub>3</sub>)<sub>2</sub>),

21.3 (s, CH(CH<sub>3</sub>)<sub>2</sub>), 21.3 (t, CH(CH<sub>3</sub>)<sub>2</sub>,  $J_{\text{CP}} = 5.3$  Hz), 22.4 (t, CH(CH<sub>3</sub>)<sub>2</sub>,  $J_{\text{CP}} = 3.5$  Hz), 23.9 (t, CH(CH<sub>3</sub>)<sub>2</sub>,  $J_{\text{CP}} = 11.4$  Hz), 29.4 (t, CH(CH<sub>3</sub>)<sub>2</sub>,  $J_{\text{CP}} = 8.6$  Hz), 125.0 (s, ArC), 125.7 (s, ArC), 127.2 (s, ArC), 131.4 (s, ArC), 132.1 (s, ArC), 132.5 (s, ArC), 141.6 (s, ArC), 149.6 (d,  $J_{\text{CP}} = 8$  Hz, ArC). <sup>31</sup>P{<sup>1</sup>H} NMR (162 MHz, C<sub>6</sub>D<sub>6</sub>)  $\delta$ : 63.3 (s,  $J_{\text{PPt}} = 4597$  Hz). <sup>195</sup>Pt{<sup>1</sup>H} NMR (86 MHz, C<sub>6</sub>D<sub>6</sub>)  $\delta$ : -5759.1 (t,  $J_{\text{PPt}} = 4515$  Hz). Anal. Calcd. for C<sub>30</sub>H<sub>40</sub>P<sub>2</sub>Pt: C, 54.79; H, 6.13. Found: C, 54.65; H, 5.88.

**Synthesis of [(PterP)Pt=C(*p*-tol)<sub>2</sub>] (48).** A solution of [(PterP)Pt] (**47**, 43.9 mg, 0.07 mmol) in 5 mL of Et<sub>2</sub>O was mixed with a solution of (*p*-tol)<sub>2</sub>CN<sub>2</sub> (14.8 mg, 0.07 mmol) in 5 mL of Et<sub>2</sub>O. The reaction mixture was stirred at room temperature for 2 hours. The volatiles were removed under reduced pressure and the residue was re-dissolved in *n*-pentane. The solution was filtered through a pad of Celite, and concentrated in vacuo. The product crystallized at -35 °C from this concentrated solution. Yield: 18 mg, 40%. **For 48:** <sup>1</sup>H NMR (500 MHz, C<sub>6</sub>D<sub>6</sub>)  $\delta$ : 0.99 (m, 12H, CH(CH<sub>3</sub>)<sub>2</sub>), 1.09 (app q, 6H, CH(CH<sub>3</sub>)<sub>2</sub>,  $J = 7.2$  Hz), 1.40 (app q, 6H, CH(CH<sub>3</sub>)<sub>2</sub>,  $J = 8$  Hz), 2.24 (s, 3H, C<sub>6</sub>H<sub>4</sub>CH<sub>3</sub>), 2.27 (br t, 3H, C<sub>6</sub>H<sub>4</sub>CH<sub>3</sub>,  $J_{\text{HP}} = 4$  Hz), 2.45 (m, 2H, CH(CH<sub>3</sub>)<sub>2</sub>), 2.54 (m, 2H, CH(CH<sub>3</sub>)<sub>2</sub>), 6.85 (m, 2H, ArH), 6.89 (m, 2H, ArH), 7.08 (br m, 2H, ArH), 7.20 (m, 5H, ArH), 7.39 (m, 2H, ArH), 7.45 (m, 2H, ArH), 7.49 (m, 2H, ArH). <sup>13</sup>C{<sup>1</sup>H} NMR (126 MHz, C<sub>6</sub>D<sub>6</sub>)  $\delta$ : 18.2 (s, CH(CH<sub>3</sub>)<sub>2</sub>,  $J_{\text{CPt}} = 141$  Hz), 20.3 (s, CH(CH<sub>3</sub>)<sub>2</sub>,  $J_{\text{CPt}} = 26$  Hz), 20.8 (s, CH(CH<sub>3</sub>)<sub>2</sub>,  $J_{\text{CPt}} = 20$  Hz), 21.5 (s, C<sub>6</sub>H<sub>4</sub>CH<sub>3</sub>), 21.59 (t, CH(CH<sub>3</sub>)<sub>2</sub>,  $J_{\text{CP}} = 1$  Hz), 27.2 (t, CH(CH<sub>3</sub>)<sub>2</sub>,  $J_{\text{CP}} = 10$  Hz), 31.8 (s, C<sub>6</sub>H<sub>4</sub>CH<sub>3</sub>), 35.6 (t, CH(CH<sub>3</sub>)<sub>2</sub>,  $J_{\text{CP}} = 14$  Hz,  $J_{\text{CPt}} = 95$  Hz), 126.4 (s, ArC), 126.5 (t, ArC,  $J_{\text{CP}} = 10$  Hz), 127.4 (s, ArC), 127.4 (s, ArC), 129.0 (s, ArC), 129.8 (s, ArC), 130.1 (s, ArC), 132.4 (br s, ArC), 133.3 (t, ArC,  $J_{\text{CP}} = 4$  Hz), 133.6 (t, ArC,  $J_{\text{CP}} = 5$  Hz), 142.5 (s, ArC), 146.9 (t, ArC,  $J_{\text{CP}} = 8$  Hz), 154.5 (t, ArC,  $J_{\text{CP}} = 11$  Hz), 155.4 (t, ArC,  $J_{\text{CP}} = 25$  Hz),

262.8 (t, Pt=C(*p*-tol)<sub>2</sub>,  $J_{\text{CP}} = 65.5$  Hz,  $J_{\text{CPt}} = 1775$  Hz).  $^{31}\text{P}\{^1\text{H}\}$  NMR (200 MHz, C<sub>6</sub>D<sub>6</sub>)  $\delta$ : 51.8 (s,  $J_{\text{PPt}} = 2234$  Hz).  $^{195}\text{Pt}\{^1\text{H}\}$  NMR (86 MHz, C<sub>6</sub>D<sub>6</sub>)  $\delta$ : -3702.0 (t,  $J_{\text{PPt}} = 2234$  Hz). Anal. Calcd. for C<sub>45</sub>H<sub>54</sub>P<sub>2</sub>Pt: C, 63.44; H, 6.39. Found: C, 63.50; H, 6.31.

**Synthesis of [(PterP)Pd] (49). Method A:** In a 20 mL scintillation vial, a solution of PterP (**1**, 50.0 mg, 0.11 mmol) in 5 mL of Et<sub>2</sub>O was added to [(cod)Pd(CH<sub>2</sub>TMS)<sub>2</sub>] (33.6 mg, 0.11 mmol). The mixture was stirred at room temperature for 1 hour. The orange solution was filtered through a pad of Celite, concentrated under reduced pressure, and layered with *n*-pentane. The product, **49** crystallized from this solution at -35 °C. Yield: 28 mg, 46%. **Method B:** Potassium graphite (KC<sub>8</sub>, 12.0 mg, 0.09 mmol) was suspended in THF (5 mL) and added to a solution of **3** (27.7 mg, 0.04 mmol) in 5 mL of THF dropwise. The solution was allowed to stir at room temperature for 30 min. The volatiles were removed under reduced pressure. The residue was extracted with 10 mL of *n*-pentane. The *n*-pentane solution was filtered through a plug of Celite and concentrated under reduced pressure. Pure **49** crystallized from this concentrated solution at -35 °C. Yield: 11 mg, 45%. **For 49:**  $^1\text{H}$  NMR (400 MHz, C<sub>6</sub>D<sub>6</sub>)  $\delta$ : 1.02 (app q, 6H CH(CH<sub>3</sub>)<sub>2</sub>,  $J = 14$  Hz), 1.11 (m, 12H, CH(CH<sub>3</sub>)<sub>2</sub>), 1.24 (app q, 6H, CH(CH<sub>3</sub>)<sub>2</sub>,  $J = 17$  Hz), 2.16 (m, 4H, CH(CH<sub>3</sub>)<sub>2</sub>), 6.92 (td, 2H, ArH,  $J_{\text{HH}} = 7$  Hz,  $J_{\text{HP}} = 2$  Hz), 6.98 (t, 2H, ArH,  $J_{\text{HH}} = 7$  Hz), 7.03 (m, 2H, ArH), 7.07 (m, 2H, ArH), 7.17 (d, 2H, ArH,  $J_{\text{HH}} = 7$  Hz), 7.39, (d, 2H, ArH,  $J_{\text{HH}} = 8$  Hz).  $^{13}\text{C}\{^1\text{H}\}$  NMR (100 MHz, C<sub>6</sub>D<sub>6</sub>)  $\delta$ : 18.2 (s, CH(CH<sub>3</sub>)<sub>2</sub>), 21.3 (s, CH(CH<sub>3</sub>)<sub>2</sub>), 22.5 (t, CH(CH<sub>3</sub>)<sub>2</sub>,  $J_{\text{CP}} = 7$  Hz), 28.0 (t, CH(CH<sub>3</sub>)<sub>2</sub>,  $J_{\text{CP}} = 7$  Hz), 124.1 (s, ArC), 125.9 (s, ArC), 127.1 (s, ArC), 131.6 (s, ArC), 132.2 (s, ArC), 132.3 (t, ArC,  $J_{\text{CP}} = 4$  Hz), 136.6 (s, ArC), 140.4 (t, ArC,  $J_{\text{CP}} = 11$  Hz), 149.8 (t, ArC,  $J_{\text{CP}} = 11$  Hz).  $^{31}\text{P}\{^1\text{H}\}$  NMR (162 MHz, C<sub>6</sub>D<sub>6</sub>)  $\delta$ : 34.1 (s). Anal. Calcd. for C<sub>35</sub>H<sub>52</sub>P<sub>2</sub>Pd·C<sub>5</sub>H<sub>12</sub>: C, 65.57; H, 8.18. Found: C, 65.91; H, 8.52.

**Synthesis of [(PterP)Pd=C(*p*-tol)<sub>2</sub>] (50).** Compound [(PterP)Pd] (49) was dissolved in hexanes and added to a quartz J-Young NMR tube along with (*p*-tol)<sub>2</sub>CN<sub>2</sub> and a C<sub>6</sub>D<sub>6</sub> capillary. The solution was exposed to UV radiation and monitored by <sup>31</sup>P{<sup>1</sup>H} NMR spectroscopy. After 1 h of UV exposure, a mixture of products was observed, including 73% [(PterP)Pd=C(*p*-tol)<sub>2</sub>] (7), 17% [(PterP)Pd] (49), 7% decomposition of the carbene to [(2''-disopropylphosphino-{1,1':2',1''-terphenyl}-2-yl)Pd(η<sup>2</sup>-P,C-<sup>*i*</sup>Pr<sub>2</sub>P=C(*p*-tol)<sub>2</sub>)] (51), and 4% of an unidentified product. Further exposure of the solution to UV radiation results in further conversion to the insertion product 51. Storing the mixture obtained after 1 h UV exposure in the dark at room temperature results in full conversion to 51 after 12 h (*vide infra*). **For 50:** <sup>1</sup>H NMR (500 MHz, C<sub>6</sub>D<sub>12</sub>) δ: 0.80 (app q, 6H, CH(CH<sub>3</sub>)<sub>2</sub>, *J* = 5 Hz), 0.88 (app q, 6H, CH(CH<sub>3</sub>)<sub>2</sub>, *J* = 5 Hz), 1.01 (app q, 6H, CH(CH<sub>3</sub>)<sub>2</sub>, *J* = 10 Hz), 1.44 (app q, 6H, CH(CH<sub>3</sub>)<sub>2</sub>, *J* = 5 Hz), 2.20 (s, 3H, C<sub>6</sub>H<sub>4</sub>CH<sub>3</sub>), 2.33 (s, 3H, C<sub>6</sub>H<sub>4</sub>CH<sub>3</sub>), 2.50 (m, 2H, CH(CH<sub>3</sub>)<sub>2</sub>), 6.82 (m, 6H, ArH), 6.94 (m, 2H, ArH), 7.09 (m, 6H, ArH), 7.18 (dd, 2H, ArH, *J*<sub>HH</sub> = 5 Hz, *J*<sub>HP</sub> = 10 Hz), 7.25 (d, 2H, ArH, *J*<sub>HH</sub> = 10 Hz), 7.41 (dd, 2H, ArH, *J*<sub>HH</sub> = 5 Hz, *J*<sub>HP</sub> = 10 Hz). <sup>13</sup>C{<sup>1</sup>H} NMR (126 MHz, C<sub>6</sub>D<sub>5</sub>CD<sub>3</sub>, -15 °C) δ: 17.8 (s, CH(CH<sub>3</sub>)<sub>2</sub>), 22.0-19.0 (obscured by solvent peak, CH(CH<sub>3</sub>)<sub>2</sub>), 22.7 (app t, CH(CH<sub>3</sub>)<sub>2</sub>, *J*<sub>CP</sub> = 11 Hz), 33.0 (t, CH(CH<sub>3</sub>)<sub>2</sub>, *J*<sub>CP</sub> = 11 Hz), 122.3 (s, ArC), 126.1 (s, ArC), 126.3 (t, ArC, *J*<sub>CP</sub> = 13 Hz), 127.1 (s, ArC), 131.9 (s, ArC), 133.1 (t, ArC, *J*<sub>CP</sub> = 9 Hz), 134.5 (s, ArC), 135.9 (s, ArC), 141.9 (s, ArC), 146.8 (dd, ArC, *J*<sub>CP</sub> = 4 Hz, *J*<sub>CP</sub> = 9 Hz), 155.2 (t, ArC, *J*<sub>CP</sub> = 15 Hz), 156.2 (t, ArC, *J*<sub>CP</sub> = 14 Hz, ArC), 160.2 (s, ArC), 296.4 (t, Pd=C(*p*-tol)<sub>2</sub>, *J*<sub>CP</sub> = 63 Hz). <sup>31</sup>P{<sup>1</sup>H} NMR (200 MHz, C<sub>6</sub>D<sub>12</sub>) δ: 52.4 (s).

**Synthesis of 51.** A benzene solution of [(PterP)Pd] (6, 54.9 mg, 0.10 mmol, 0.7 mL) and (*p*-tol)<sub>2</sub>CN<sub>2</sub> (21.4 mg, 0.10 mmol) was added to a quartz J-Young NMR tube and

exposed to UV radiation for 5 h. The volatiles were removed under reduced pressure. The crude residue was dissolved in 2 mL of *n*-pentane. [(2''-di-*iso*-propylphosphino-{1,1':2',1''-terphenyl}-2-yl)Pd( $\eta^2$ -P,C-*i*Pr<sub>2</sub>P=C(*p*-tol)<sub>2</sub>)] (**51**) crystalized at -35 °C as pale orange crystals. Yield: 40 mg, 73%. **For 51:** <sup>1</sup>H NMR (500 MHz, C<sub>6</sub>D<sub>6</sub>)  $\delta$ : 0.27 (dd, 3H, CH(CH<sub>3</sub>)<sub>2</sub>,  $J_{\text{HH}} = 7$  Hz,  $J_{\text{HP}} = 18$  Hz), 0.92 (m, 6H, CH(CH<sub>3</sub>)<sub>2</sub>), 1.0 (dd, 3H, CH(CH<sub>3</sub>)<sub>2</sub>,  $J_{\text{HH}} = 7$  Hz,  $J_{\text{HP}} = 15$  Hz), 1.09 (dd, 3H, CH(CH<sub>3</sub>)<sub>2</sub>,  $J_{\text{HH}} = 7$  Hz,  $J_{\text{HP}} = 11$  Hz), 1.17 (dd, 3H, CH(CH<sub>3</sub>)<sub>2</sub>,  $J_{\text{HH}} = 7$  Hz,  $J_{\text{HP}} = 17$  Hz), 1.34 (dd, 3H, CH(CH<sub>3</sub>)<sub>2</sub>,  $J_{\text{HH}} = 7$  Hz,  $J_{\text{HP}} = 15$  Hz), 1.52 (dd, 3H CH(CH<sub>3</sub>)<sub>2</sub>,  $J_{\text{HH}} = 7$  Hz,  $J_{\text{HP}} = 16$  Hz), 1.99 (m, 1H, CH(CH<sub>3</sub>)<sub>2</sub>), 2.11 (s, 3H, C<sub>6</sub>H<sub>4</sub>CH<sub>3</sub>), 2.16 (s, 3H, C<sub>6</sub>H<sub>4</sub>CH<sub>3</sub>), 2.29 (m, 1H, CH(CH<sub>3</sub>)<sub>2</sub>), 2.37 (m, 1H, CH(CH<sub>3</sub>)<sub>2</sub>), 2.47 (m, 1H, CH(CH<sub>3</sub>)<sub>2</sub>), 6.80 (tt, 1H, ArH,  $J_{\text{HH}} = 7$  Hz,  $J_{\text{HP}} = 2$  Hz), 6.99 (m, 14 H, ArH), 7.32 (d, 2H, ArH,  $J_{\text{HH}} = 8$  Hz), 7.36 (t, 1H, ArH,  $J_{\text{HH}} = 7$  Hz), 7.40 (dd, 1H, ArH,  $J_{\text{HH}} = 7$  Hz,  $J_{\text{HP}} = 2$  Hz), 7.53 (d, 2H, ArH,  $J_{\text{HH}} = 8$  Hz). <sup>13</sup>C{<sup>1</sup>H} NMR (126 Hz, C<sub>6</sub>D<sub>6</sub>)  $\delta$ : 18.4 (br s, CH(CH<sub>3</sub>)<sub>2</sub>), 19.8 (d, CH(CH<sub>3</sub>)<sub>2</sub>,  $J_{\text{CP}} = 7$  Hz), 20.2 (d, CH(CH<sub>3</sub>)<sub>2</sub>,  $J_{\text{CP}} = 7$  Hz), 20.4 (d, CH(CH<sub>3</sub>)<sub>2</sub>,  $J_{\text{CP}} = 3$  Hz), 20.5 (d, CH(CH<sub>3</sub>)<sub>2</sub>,  $J_{\text{CP}} = 3$  Hz), 20.7 (d, CH(CH<sub>3</sub>)<sub>2</sub>,  $J_{\text{CP}} = 4$  Hz), 21.0(s, C<sub>6</sub>H<sub>4</sub>CH<sub>3</sub>), 21.0(d, CH(CH<sub>3</sub>)<sub>2</sub>,  $J_{\text{CP}} = 14$  Hz), 21.2 (s, C<sub>6</sub>H<sub>4</sub>CH<sub>3</sub>), 22.3 (d, CH(CH<sub>3</sub>)<sub>2</sub>,  $J_{\text{CP}} = 6$  Hz), 22.5 (d, CH(CH<sub>3</sub>)<sub>2</sub>,  $J_{\text{CP}} = 4$  Hz), 23.1 (d, CH(CH<sub>3</sub>)<sub>2</sub>,  $J_{\text{CP}} = 23.7$  (d, CH(CH<sub>3</sub>)<sub>2</sub>,  $J_{\text{CP}} = 18$  Hz), 32.3 (dd, CH(CH<sub>3</sub>)<sub>2</sub>,  $J_{\text{CP}} = 13$  Hz,  $J_{\text{CP}} = 10$  Hz), 122.5 (s, ArC), 124.6 (dd, ArC,  $J_{\text{CP}} = 6$  Hz,  $J_{\text{CP}} = 3$  Hz), 125.3 (s, ArC), 126.3 (d, ArC,  $J_{\text{CP}} = 6$  Hz), 127.2 (dd, ArC,  $J_{\text{CP}} = 6$  Hz,  $J_{\text{CP}} = 3$  Hz), 127.5 (s, ArC), 128.4 (s, ArC), 129.0 (s, ArC), 129.2 (s, ArC), 128.8 (app t, ArC,  $J_{\text{CP}} = 4$  Hz), 130.9 (d, ArC,  $J_{\text{CP}} = 7$  Hz), 131.5 (s, ArC), 131.9 (s, ArC), 133.1 (d, ArC,  $J_{\text{CP}} = 9$  Hz), 134.5 (s, ArC), 134.8 (s, ArC), 136.9 (s, ArC), 140.7 (d, ArC,  $J_{\text{CP}} = 3$  Hz), 141.6 (d, ArC,  $J_{\text{CP}} = 4$  Hz), 147.1 (dd, C(*p*-tol)<sub>2</sub>,  $J_{\text{CP}} = 8$  Hz,  $J_{\text{CP}} = 4$  Hz), 148.2 (d, ArC,  $J_{\text{CP}} = 3$  Hz), 149.2 (d, ArC,  $J_{\text{CP}} = 4$  Hz), 149.6 (s, ArC), 149.8 (s, ArC), 167.8 (d,

ArC,  $J_{\text{CP}} = 21$  Hz), 168.6 (d, ArC,  $J_{\text{CP}} = 21$  Hz).  $^{31}\text{P}\{^1\text{H}\}$  NMR (200 MHz,  $\text{C}_6\text{D}_6$ )  $\delta$ : 13.6 (d,  $J_{\text{PP}} = 14$  Hz), 38.2 (d,  $J_{\text{PP}} = 14$  Hz). Anal. Calcd. for  $\text{C}_{45}\text{H}_{54}\text{P}_2\text{Pd}$ : C, 70.81; H, 7.13. Found: C, 70.67; H, 6.99.

**Synthesis of  $[(\text{Cy}_3\text{P})_2\text{Pt}]$ .** To a suspension of  $[(\text{cod})\text{PtCl}_2]$  (30.0 mg, 0.08 mmol) in 5 mL of THF was added a solution of  $\text{Cy}_3\text{P}$  (45.0 mg, 0.16 mmol) in 5 mL of THF. The mixture was stirred at room temperature for 12 hours. The volatiles were removed under reduced pressure and the residue was triturated with *n*-pentane (5×5 mL). The residue was dried under reduced pressure.  $[(\text{Cy}_3\text{P})_2\text{PtCl}_2]$  was isolated as a white powder. Yield: 53.2 mg, 80.2%. The  $^1\text{H}$  and  $^{31}\text{P}\{^1\text{H}\}$  NMR spectra are consistent with the reported literature values.<sup>54</sup> The product,  $[(\text{PCy}_3)_2\text{PtCl}_2]$ , was used in the next step without further purification. In a 20 mL scintillation vial,  $[(\text{PCy}_3)\text{PtCl}_2]$  (53.2 mg, 0.06 mmol) was dissolved in 5 mL of THF. A suspension of  $\text{KC}_8$  (17.4 mg, 0.13 mmol) in 5 mL of THF was added to this solution. The mixture was stirred at room temperature for 3 hours. The volatiles were removed under reduced pressure. The product was extracted in *n*-pentane and filtered through a pad of Celite. The volatiles were removed under reduced pressure and the product,  $[(\text{PCy}_3)_2\text{Pt}]$  was isolated as a yellow powder. Yield: 27.0 mg, 55%. The  $^1\text{H}$  and  $^{31}\text{P}\{^1\text{H}\}$  NMR spectra are consistent with the reported literature values.<sup>9</sup>

**Reaction of  $[(\text{Cy}_3\text{P})_2\text{Pt}]$  with  $(p\text{-tol})_2\text{CN}_2$ .**  $[(\text{Cy}_3\text{P})_2\text{Pt}]$  (27.0 mg, 0.04 mmol) was dissolved in  $\text{C}_6\text{D}_6$  and added to  $(p\text{-tol})_2\text{CN}_2$  (7.8 mg, 0.04 mmol). The mixture was monitored by  $^1\text{H}$  and  $^{31}\text{P}\{^1\text{H}\}$  NMR spectroscopy until full conversion of  $(p\text{-tol})_2\text{CN}_2$  to  $(p\text{-tol})_2\text{C}=\text{N}-\text{N}=\text{C}(p\text{-tol})_2$  was achieved (12 h). No conversion of  $[(\text{PCy}_3)_2\text{Pt}]$  was observed. The  $^1\text{H}$  NMR spectrum for  $(p\text{-tol})_2\text{C}=\text{N}-\text{N}=\text{C}(p\text{-tol})_2$  is consistent with the reported literature values.<sup>55</sup>



**Reaction between [(PterP)Pt=C(*p*-tol)<sub>2</sub>] (48) and H<sub>2</sub>SiPh<sub>2</sub>.** A C<sub>6</sub>D<sub>6</sub> solution of [(PterP)Pt=C(*p*-tol)<sub>2</sub>] (**5**, 28.1 mg, 0.04 mmol) was added to a J-Young NMR tube along with two equivalents of Ph<sub>2</sub>SiH<sub>2</sub> (0.02 mL, 0.08 mmol). The solution was heated to 120°C for 3 days and monitored by <sup>31</sup>P{<sup>1</sup>H} NMR spectroscopy to ensure full consumption of **5**. The volatiles were removed and the crude residue was dissolved in *n*-pentane. The solution was chilled to –35°C to induce precipitation of [(PterP)Pt(H)SiHPh<sub>2</sub>] (**56**), leaving the organic product, (di-*p*-tolylmethyl)diphenylsilane (69% crude NMR yield), in the mother liquor. The final organic product was purified by column chromatography (silica, hexanes). **For (di-*p*-tolylmethyl)diphenylsilane:** <sup>1</sup>H NMR (400 MHz, CDCl<sub>3</sub>) δ: 2.26 (s, 6H, C<sub>6</sub>H<sub>4</sub>CH<sub>3</sub>), 4.09 (d, 1H, CH(*p*-tol)<sub>2</sub>, *J*<sub>HH</sub> = 1 Hz), 5.18 (d, 1H, SiHPh<sub>2</sub>, *J*<sub>HH</sub> = 1 Hz, *J*<sub>HSi</sub> = 160 Hz), 6.98 (d, 4H, ArH, *J*<sub>HH</sub> = 8 Hz), 7.05 (d, 4H, ArH, *J*<sub>HH</sub> = 8 Hz), 7.26 (m, 4 H, ArH), 7.31 (m, 6H, ArH). <sup>13</sup>C{<sup>1</sup>H} NMR (100 MHz, CDCl<sub>3</sub>) δ: 29.9 (s, C<sub>6</sub>H<sub>4</sub>CH<sub>3</sub>), 127.9 (s, ArC), 129.2 (s, ArC), 129.2 (s, ArC), 129.7 (s, ArC), 133.5 (s, ArC), 135.0 (s, ArC), 135.9 (s, ArC), 129.0 (s, ArC).

**Synthesis of [(PterP)Pt(H)SiHPh<sub>2</sub>] (56).** An equivalent of Ph<sub>2</sub>SiH<sub>2</sub> (7.6 μL, 0.04 mmol) was added via syringe to a solution of [(PterP)Pt] (**47**, 26.8 mg, 0.04 mmol) in Et<sub>2</sub>O. The mixture was stirred at room temperature for one hour. The volatiles were removed under reduced pressure. The crude residue was washed with cold *n*-pentane leaving **56** as a clean tan powder (31 mg, 90%). **For 56:** <sup>1</sup>H NMR (400 MHz, C<sub>6</sub>D<sub>6</sub>) δ: –3.73 (dd, 1H, PtH, *J*<sub>HP</sub> = 144 Hz, *J*<sub>HP</sub> = 20 Hz, *J*<sub>HPt</sub> = 868 Hz), 0.88 (m, 4H, CH(CH<sub>3</sub>)<sub>2</sub>), 1.04 (m, 14H, CH(CH<sub>3</sub>)<sub>2</sub>), 1.24 (m, 6H, CH(CH<sub>3</sub>)<sub>2</sub>), 2.44 (m, 3H, CH(CH<sub>3</sub>)<sub>2</sub>), 3.21 (m, 1H, CH(CH<sub>3</sub>)<sub>2</sub>), 5.10 (m, 1H, SiH), 6.85 (m, 6H, ArH), 6.92 (t, 1H, ArH, *J*<sub>HH</sub> = 8 Hz), 7.0 (t, 1H, ArH, *J*<sub>HH</sub> = 8 Hz), 7.07 (m, 3H, ArH), 7.18 (m, 2H, ArH), 7.30 (t, 3H, ArH, *J*<sub>HH</sub> = 8 Hz), 7.39 (t, 2H,

ArH,  $J_{\text{HH}} = 8$  Hz), 7.98 (d, 2H, ArH,  $J_{\text{HH}} = 8$  Hz), 8.07 (d, 2H, ArH,  $J_{\text{HH}} = 8$  Hz).  $^{13}\text{C}\{^1\text{H}\}$  NMR (100 MHz,  $\text{C}_6\text{D}_6$ )  $\delta$ : 17.8 (br s,  $\text{CH}(\text{CH}_3)_2$ ), 18.4 (br s,  $\text{CH}(\text{CH}_3)_2$ ), 20.0 (s,  $\text{CH}(\text{CH}_3)_2$ ), 20.1 (s,  $\text{CH}(\text{CH}_3)_2$ ), 20.4 (s,  $\text{CH}(\text{CH}_3)_2$ ), 20.2 (s,  $\text{CH}(\text{CH}_3)_2$ ), 22.4 (br m,  $\text{CH}(\text{CH}_3)_2$ ), 22.3 (d,  $\text{CH}(\text{CH}_3)_2$ ,  $J_{\text{CP}} = 11$  Hz), 26.7 (br d,  $\text{CH}(\text{CH}_3)_2$ ,  $J_{\text{CP}} = 23$  Hz), 27.9 (d,  $\text{CH}(\text{CH}_3)_2$ ,  $J_{\text{CP}} = 14$  Hz), 28.1 (d,  $\text{CH}(\text{CH}_3)_2$ ,  $J_{\text{CP}} = 13$  Hz), 33.9 (br d,  $\text{CH}(\text{CH}_3)_2$ ,  $J_{\text{CP}} = 23$  Hz), 126.1 (s, ArC), 126.7 (s, ArC), 127.1 (s, ArC), 127.2 (s, ArC), 27.3 (s, ArC), 127.6 (s, ArC), 126.7 (s, ArC), 128.1 (ArC, obscured by solvent peaks), 129.5 (s, ArC), 130.1 (s, ArC), 130.8 (br s, ArC), 132.9 (d, ArC,  $J_{\text{CP}} = 7$  Hz), 133.5 (d, ArC,  $J_{\text{CP}} = 7$  Hz), 136.6 (s, ArC,  $J_{\text{CPt}} = 30$  Hz), 137.8 (s, ArC,  $J_{\text{CPt}} = 34$  Hz), 140.8 (s, ArC), 141.5 (s, ArC), 146.2 (s, ArC), 146.4 (s, ArC), 147.3 (s, ArC), 148.2 (s, ArC).  $^{31}\text{P}\{^1\text{H}\}$  NMR (162 MHz,  $\text{C}_6\text{D}_6$ )  $\delta$ : 34.7 (unresolved d,  $J_{\text{PPt}} = 2718$  Hz), 40.4 (unresolved d,  $J_{\text{PPt}} = 1837$  Hz).  $^{195}\text{Pt}\{^1\text{H}\}$  NMR ( $\text{C}_6\text{D}_6$ , 86 MHz)  $\delta$ : -3644.2 (dd,  $J_{\text{PtP}} = 2750$  Hz,  $J_{\text{PtP}} = 1848$  Hz).  $^{29}\text{Si}\{^1\text{H}\}$  NMR ( $\text{C}_6\text{D}_6$ , 80 MHz)  $\delta$ : 6.6 (app d,  $J_{\text{SiP}} = 149$  Hz,  $J_{\text{SiPt}} = 1221$  Hz) Anal. Calcd. for  $\text{C}_{42}\text{H}_{52}\text{P}_2\text{PtSi}$ : C, 59.91; H, 6.23. Found: C, 60.01; H, 6.20.

**Reaction between [(PterP)Pd=C(*p*-tol)<sub>2</sub>] (50) and H<sub>2</sub>SiPh<sub>2</sub>.** To an *n*-hexane solution of [(PterP)Pd] (**6**, 20.0 mg, 0.04 mmol) was added an equivalent of (*p*-tol)<sub>2</sub>CN<sub>2</sub> (7.8 mg, 0.04 mmol). The solution was transferred to a quartz J-Young NMR tube along with a  $\text{C}_6\text{D}_6$  capillary. The mixture was exposed to UV radiation and monitored by  $^{31}\text{P}\{^1\text{H}\}$  NMR spectroscopy to ensure adequate conversion to [(PterP)Pd=C(*p*-tol)<sub>2</sub>] (**50**). Next, a molar equivalent of Ph<sub>2</sub>SiH<sub>2</sub> was added (6.5  $\mu\text{L}$ , 0.04 mmol). The reaction was monitored by  $^{31}\text{P}\{^1\text{H}\}$  NMR spectroscopy to ensure full consumption of **7**. The evaluation of the crude  $^1\text{H}$  NMR spectrum revealed 14% conversion to (di-*p*-tolylmethyl)diphenylsilane. The

$^{31}\text{P}\{^1\text{H}\}$  NMR spectrum showed 62% conversion to  $[(\text{PterP})\text{Pd}(\text{H})\text{SiHPh}_2]$  (**57**) and 38% conversion to the decomposition product **51**.

**Synthesis of  $[(\text{PterP})\text{Pd}(\text{H})\text{SiHPh}_2]$  (**57**).** To an  $\text{Et}_2\text{O}$  solution of  $[(\text{PterP})\text{Pd}]$  (**49**, 50.0 mg, 0.09 mmol) was added one equivalent of  $\text{Ph}_2\text{SiH}_2$  (0.02 mL, 0.09 mmol). The mixture was stirred at room temperature for 1 h. The volatiles were removed and the crude residue was re-dissolved in *n*-pentane. The solution was chilled to  $-35^\circ\text{C}$  resulting in the recrystallized product (**57**, 48 mg, 72%). **For 57:**  $^1\text{H}$  NMR (400 MHz,  $\text{C}_6\text{D}_6$ )  $\delta$ : 0.94 (app q, 6H,  $\text{CH}(\text{CH}_3)_2$ ,  $J_{\text{HP}} = 6$  Hz), 1.13 (app q, 6H,  $\text{CH}(\text{CH}_3)_2$ ,  $J_{\text{HP}} = 8$  Hz), 1.20 (m, 12H,  $\text{CH}(\text{CH}_3)_2$ ), 1.74 (s, 2H,  $\text{SiH}_2$ ), 2.24 (m, 2H,  $\text{CH}(\text{CH}_3)_2$ ), 2.56 (m, 2H,  $\text{CH}(\text{CH}_3)_2$ ), 6.88 (m, 8 H,  $\text{ArH}$ ), 7.06 (dd, 2H,  $\text{ArH}$ ,  $J_{\text{HH}} = 8$  Hz,  $J_{\text{HP}} = 4$  Hz), 7.22 (m, 4H,  $\text{ArH}$ ), 7.30 (t, 4H,  $\text{ArH}$ ,  $J_{\text{HH}} = 8$  Hz), 7.98 (d, 4H,  $\text{ArH}$ ,  $J_{\text{HH}} = 8$  Hz).  $^{13}\text{C}\{^1\text{H}\}$  NMR (100 MHz,  $\text{C}_6\text{D}_6$ )  $\delta$ : 18.9 (s,  $\text{CH}(\text{CH}_3)_2$ ), 20.4 (s,  $\text{CH}(\text{CH}_3)_2$ ), 20.7 (t,  $\text{CH}(\text{CH}_3)_2$ ,  $J_{\text{CP}} = 3$  Hz), 22.6 (t,  $\text{CH}(\text{CH}_3)_2$ ,  $J_{\text{CP}} = 7$  Hz), 26.3 (t,  $\text{CH}(\text{CH}_3)_2$ ,  $J_{\text{CP}} = 5$  Hz), 29.6 (t,  $\text{CH}(\text{CH}_3)_2$ ,  $J_{\text{CP}} = 10$  Hz), 126.4 (s,  $\text{ArC}$ ), 126.9 (s,  $\text{ArC}$ ), 127.5 (s,  $\text{ArC}$ ), 128.0 (s,  $\text{ArC}$ ), 130.5 (s,  $\text{ArC}$ ), 130.9 (s,  $\text{ArC}$ ), 131.9 (d,  $\text{ArC}$ ,  $J_{\text{CP}} = 3$  Hz), 133.0 (t,  $\text{ArC}$ ,  $J_{\text{CP}} = 4$  Hz), 136.5 (s,  $\text{ArC}$ ), 140.1 (s,  $\text{ArC}$ ), 43.2 (s,  $\text{ArC}$ ), 47.7 (t,  $\text{ArC}$ ,  $J_{\text{CP}} = 11$  Hz).  $^{31}\text{P}\{^1\text{H}\}$  NMR (162 MHz,  $\text{C}_6\text{D}_6$ )  $\delta$ : 30.4 (s).  $^{29}\text{Si}\{^1\text{H}\}$  NMR ( $\text{C}_6\text{D}_6$ , 80 MHz)  $\delta$ : -9.2 (s). Anal. Calcd. for  $\text{C}_{42}\text{H}_{52}\text{P}_2\text{PdSi}$ : C, 66.96; H, 6.96. Found: C, 67.12; H, 7.14.

**Reaction between  $[(\text{PterP})\text{Pt}=\text{C}(p\text{-tol})_2]$  (**48**) and  $\text{CH}_3\text{I}$ .** An equivalent of  $\text{CH}_3\text{I}$  (2.5  $\mu\text{L}$ , 0.04 mmol) was added to a  $\text{C}_6\text{D}_6$  solution of  $[(\text{PterP})\text{Pt}=\text{C}(p\text{-tol})_2]$  (**48**, 25.0 mg, 0.04 mmol). The mixture was heated to  $120^\circ\text{C}$  for 12 h in a Schlenk flask. The volatiles were removed under reduced pressure. The residue was extracted with *n*-pentane. The organic product, 1,1-di(*p*-tolyl)ethylene (**39**, 5.5 mg, 71%), was isolated from this *n*-

pentane solution. The residual powder contained [(PterP)Pt(H)I] (**52**, 22 mg, 86%). **For 52:**  $^1\text{H}$  NMR (400 MHz,  $\text{C}_6\text{D}_6$ )  $\delta$ : -13.10 (t, 1H, PtH,  $J_{\text{HP}} = 3$  Hz,  $J_{\text{HPt}} = 1200$  Hz), 0.86 (app q, 6H,  $\text{CH}(\text{CH}_3)_2$ ,  $J_{\text{HP}} = 8$  Hz), 1.04 (app q, 6H,  $\text{CH}(\text{CH}_3)_2$ ,  $J_{\text{HP}} = 4$  Hz), 1.26 (app q, 6H,  $\text{CH}(\text{CH}_3)_2$ ,  $J_{\text{HP}} = 8$  Hz), 1.47 (app q, 6H,  $\text{CH}(\text{CH}_3)_2$ ,  $J_{\text{HP}} = 8$  Hz), 2.20 (m, 2H,  $\text{CH}(\text{CH}_3)_2$ ), 2.93 (m, 2H,  $\text{CH}(\text{CH}_3)_2$ ), 6.83 (m, 4H, ArH), 6.92 (t, 2H, ArH,  $J_{\text{HP}} = 8$  Hz), 7.0 (m, 2H, ArH), 7.29 (dd, 2H, ArH,  $J_{\text{HH}} = 8$  Hz,  $J_{\text{HP}} = 4$  Hz), 7.34 (m, 2H, ArH).  $^{13}\text{C}\{^1\text{H}\}$  NMR (100 MHz,  $\text{C}_6\text{D}_6$ )  $\delta$ : 20.2 (s,  $\text{CH}(\text{CH}_3)_2$ ,  $J_{\text{CPt}} = 19$  Hz), 21.0 (s,  $\text{CH}(\text{CH}_3)_2$ ), 21.6 (s,  $\text{CH}(\text{CH}_3)_2$ ), 21.8 (t,  $\text{CH}(\text{CH}_3)_2$ ), 23.2 (t,  $\text{CH}(\text{CH}_3)_2$ ,  $J_{\text{CP}} = 15$  Hz), 29.2 (t,  $\text{CH}(\text{CH}_3)_2$ ,  $J_{\text{CP}} = 12$  Hz), 124.7 (t, ArC,  $J_{\text{CP}} = 4$  Hz), 127.2 (s, ArC), 128.0 (s, ArC), 132.6 (s, ArC,  $J_{\text{CPt}} = 17$  Hz), 132.6 (s, ArC), 132.9 (t, ArC,  $J_{\text{CP}} = 4$  Hz), 138.8 (t, ArC,  $J_{\text{CP}} = 23$  Hz), 140.6 (t, ArC,  $J_{\text{CP}} = 3$  Hz), 149.6 (t, ArC,  $J_{\text{CP}} = 8$  Hz).  $^{31}\text{P}\{^1\text{H}\}$  NMR (162 MHz,  $\text{C}_6\text{D}_6$ )  $\delta$ : 35.2 (s,  $J_{\text{PPt}} = 2874$  Hz). **For**

**Conversion of [(PterP)Pt(H)I] (**52**) to [(PterP)Pt=C(*p*-tol) $_2$ ] (**48**).** An equivalent of  $\text{KN}(\text{SiMe}_3)_2$  (4.7 mg, 0.02 mmol) was added to an  $\text{Et}_2\text{O}$  solution of [(PterP)Pt(H)I] (**52**, 18.4 mg, 0.02 mmol) in a scintillation vial. The mixture was allowed to stir at room temperature for 2 h. The volatiles were removed under reduced pressure, and the residue was extracted with *n*-pentane. The solution was filtered over a pad of Celite. The  $^1\text{H}$  and  $^{31}\text{P}\{^1\text{H}\}$  NMR spectra indicated full conversion to [(PterP)Pt] (**47**). The addition of an equivalent of (*p*-tol) $_2\text{CN}_2$  led to quantitative conversion to [(PterP)Pt=C(*p*-tol) $_2$ ] (**48**).

**Reaction between [(PterP)Pd=C(*p*-tol) $_2$ ] (**50**) and  $\text{CH}_3\text{I}$ .** [(PterP)Pd] (**49**, 20.0 mg, 0.04 mmol) was dissolved in *n*-hexane along with (*p*-tol) $_2\text{CN}_2$  (7.8 mg, 0.04 mmol). The solution was transferred to a quartz J-Young NMR tube along with a  $\text{C}_6\text{D}_6$  capillary. The mixture was exposed to UV radiation for 1 h. The reaction was monitored by  $^{31}\text{P}\{^1\text{H}\}$  NMR spectroscopy to ensure adequate conversion to [(PterP)Pd=C(*p*-tol) $_2$ ] (**7**). Once the

conversion to carbene **50** was achieved, an equivalent of CH<sub>3</sub>I (2.2  $\mu$ L, 0.04 mmol) was added to the solution. The mixture was monitored by <sup>31</sup>P{<sup>1</sup>H} NMR spectroscopy to ensure full consumption of the carbene. Typical reaction times were 3 h. By <sup>1</sup>H NMR spectroscopy, 13% conversion to 1,1-di(*p*-tolyl)ethylene) was detected. The two isomers of the byproduct [(PterP)Pd(H)I] (**53**) were observed, as indicated by two upfield resonances at –10.45 (t, PdH, *J*<sub>HP</sub> = 12 Hz) and –11.11 (t, PdH, *J*<sub>HP</sub> = 12 Hz), supporting the formation of the iodohydride complex. Evaluation of the crude <sup>31</sup>P{<sup>1</sup>H} NMR spectrum reveals a mixture of **53** (36.01 (s), and 34.90 ppm (s)), **54**, and the decomposition product **51**.

**Synthesis of [(PterP)Pd(CH<sub>3</sub>)I] (**54**).** An equivalent of CH<sub>3</sub>I (3  $\mu$ L, 0.04 mmol) was added to an Et<sub>2</sub>O solution of [(PterP)Pd] (**49**, 24.3 mg, 0.04 mmol). The mixture was stirred for 1 h at room temperature. The volatiles were removed under reduced pressure and the resulting residue was triturated with *n*-pentane. The residue was dried under reduced pressure and the product **54** was isolated as a tan powder (29 mg, 96%). **For 54:** <sup>1</sup>H NMR (400 MHz, C<sub>6</sub>D<sub>6</sub>, major isomer)  $\delta$ : –0.11 (t, 3H, PdCH<sub>3</sub>, *J*<sub>HP</sub> = 8 Hz), 1.07 (app q, 6H, CH(CH<sub>3</sub>)<sub>2</sub>, *J*<sub>HP</sub> = 8 Hz), 1.29 (app q, 6H, CH(CH<sub>3</sub>)<sub>2</sub>, *J*<sub>HP</sub> = 8 Hz), 1.46 (app q, 6H, CH(CH<sub>3</sub>)<sub>2</sub>, *J*<sub>HP</sub> = 4 Hz), 1.72 (app q, 6H, CH(CH<sub>3</sub>)<sub>2</sub>, *J*<sub>HP</sub> = 8 Hz), 2.53 (m, 2H, CH(CH<sub>3</sub>)<sub>2</sub>), 3.52 (m, 2H, CH(CH<sub>3</sub>)<sub>2</sub>), 6.88 (t, 2H, ArH, *J*<sub>HH</sub> = 8 Hz), 6.95 (t, 2H, ArH, *J*<sub>HH</sub> = 8 Hz), 7.13 (app t, 2H, ArH, *J*<sub>HP</sub> = 4 Hz), 7.3 (m, 6H, ArH). <sup>1</sup>H NMR (400 MHz, C<sub>6</sub>D<sub>6</sub>, minor isomer)  $\delta$ : 0.26 (t, 3H, PdCH<sub>3</sub>, *J*<sub>HP</sub> = 4 Hz), CH(CH<sub>3</sub>)<sub>2</sub> signals are obscured by major isomer, 2.84 (m, 2H, CH(CH<sub>3</sub>)<sub>2</sub>), 4.08 (m, 2H, CH(CH<sub>3</sub>)<sub>2</sub>), 7.07 (m, 2H, ArH), 7.56 (m, 2H, ArH), 6 aryl protons are obscured by the major isomer. <sup>13</sup>C{<sup>1</sup>H} NMR (100 MHz, C<sub>6</sub>D<sub>6</sub>, major isomer)  $\delta$ : 4.7 (t, (PdCH<sub>3</sub>, *J*<sub>CP</sub> = 2 Hz), 20.3 (s, CH(CH<sub>3</sub>)<sub>2</sub>), 20.5 (s, CH(CH<sub>3</sub>)<sub>2</sub>), 21.3 (s, CH(CH<sub>3</sub>)<sub>2</sub>),

24.4 (t, CH(CH<sub>3</sub>)<sub>2</sub>,  $J_{\text{CP}} = 9$  Hz), 24.7 (t, CH(CH<sub>3</sub>)<sub>2</sub>,  $J_{\text{CP}} = 8$  Hz), 32.1 (t, CH(CH<sub>3</sub>)<sub>2</sub>,  $J_{\text{CP}} = 9$  Hz), 125.7 (t, ArC,  $J_{\text{CP}} = 2$  Hz), 127.3 (s, ArC), 128.1 (s, ArC), 130.3 (s, ArC), 130.8 (s, ArC), 134.2 (t, ArC,  $J_{\text{CP}} = 4$  Hz), 139.3 (t, ArC,  $J_{\text{CP}} = 26$  Hz), 141.3 (t, ArC,  $J_{\text{CP}} = 3$  Hz), 146.4 (t, ArC,  $J_{\text{CP}} = 8$  Hz). <sup>13</sup>C{<sup>1</sup>H} NMR (100 MHz, C<sub>6</sub>D<sub>6</sub>, minor isomer)  $\delta$ : -5.0 (br s, PdCH<sub>3</sub>), 19.2 (s, CH(CH<sub>3</sub>)<sub>2</sub>), 19.8 (s, CH(CH<sub>3</sub>)<sub>2</sub>), 19.9 (t, CH(CH<sub>3</sub>)<sub>2</sub>,  $J_{\text{CP}} = 2$  Hz), 24.0 (t, CH(CH<sub>3</sub>)<sub>2</sub>,  $J_{\text{CP}} = 8$  Hz), 25.1 (t, CH(CH<sub>3</sub>)<sub>2</sub>,  $J_{\text{CP}} = 8$  Hz), 28.3 (t, CH(CH<sub>3</sub>)<sub>2</sub>,  $J_{\text{CP}} = 12$  Hz), 122.7 (s, ArC), 124.6 (s, ArC), 126.6 (s, ArC), 130.6 (s, ArC), 132.6 (s, ArC), 133.7 (t, ArC,  $J_{\text{CP}} = 4$  Hz), 138.4 (t, ArC,  $J_{\text{CP}} = 17$  Hz), 143.1 (s, ArC), 145.1 (t, ArC,  $J_{\text{CP}} = 8$  Hz). <sup>31</sup>P{<sup>1</sup>H} NMR (162 MHz, C<sub>6</sub>D<sub>6</sub>)  $\delta$ : 36.9 (s, major isomer), 31.7 (s, minor isomer). Anal. Calcd. for C<sub>31</sub>H<sub>43</sub>IP<sub>2</sub>Pd: C, 52.37; H, 6.10. Found: C, 51.99; H, 5.83.

**Synthesis of [(PterP)Pt(CH<sub>3</sub>)I] (**55**).** To an Et<sub>2</sub>O solution of [(PterP)Pt] (**47**, 20.9 mg, 0.03 mmol) was added one equivalent of CH<sub>3</sub>I (2  $\mu$ L, 0.03 mmol). The mixture was allowed to stir for 1 h at room temperature resulting in the formation of a precipitate. The suspension was decanted, and the resulting powder was triturated with *n*-pentane and dried under reduced pressure. [(PterP)Pt(CH<sub>3</sub>)I] (**55**, 20 mg, 94%) was isolated as a tan powder.

**For **55**:** <sup>1</sup>H NMR (400 MHz, C<sub>6</sub>D<sub>6</sub>)  $\delta$ : -0.11 (t, 3H, PtCH<sub>3</sub>,  $J_{\text{HP}} = 8$  Hz,  $J_{\text{HPt}} = 72$  Hz), 1.07 (app q, 6H, CH(CH<sub>3</sub>)<sub>2</sub>,  $J_{\text{HP}} = 4$  Hz), 1.28 (m, 6H, CH(CH<sub>3</sub>)<sub>2</sub>), 1.47 (m, 6H, CH(CH<sub>3</sub>)<sub>2</sub>), 1.68 (app q, 6H, CH(CH<sub>3</sub>)<sub>2</sub>,  $J_{\text{HP}} = 8$  Hz), 2.63 (m, 2H, CH(CH<sub>3</sub>)<sub>2</sub>), 3.62 (m, 2H, CH(CH<sub>3</sub>)<sub>2</sub>), 6.86 (t, 2H, ArH,  $J_{\text{HH}} = 4$  Hz), 6.94 (t, 2H, ArH,  $J_{\text{HH}} = 4$  Hz), 7.09 (dd, 2H, ArH,  $J_{\text{HH}} = 6$  Hz,  $J_{\text{HP}} = 4$  Hz), 7.3 (m, 6H, ArH). <sup>13</sup>C{<sup>1</sup>H} NMR (100 MHz, C<sub>6</sub>D<sub>6</sub>)  $\delta$ : -7.9 (t, PtCH<sub>3</sub>,  $J_{\text{CP}} = 6$  Hz), 20.2 (s, CH(CH<sub>3</sub>)<sub>2</sub>,  $J_{\text{CPt}} = 21$  Hz), 20.9 (s, CH(CH<sub>3</sub>)<sub>2</sub>), 21.1 (s, CH(CH<sub>3</sub>)<sub>2</sub>), 24.1 (t, CH(CH<sub>3</sub>)<sub>2</sub>,  $J_{\text{CP}} = 12$  Hz), 24.2 (t, CH(CH<sub>3</sub>)<sub>2</sub>,  $J_{\text{CP}} = 7$  Hz), 31.0 (t, CH(CH<sub>3</sub>)<sub>2</sub>,  $J_{\text{CP}} = 14$  Hz), 125.5 (t, ArC,  $J_{\text{CP}} = 3$  Hz), 127.3 (s, ArC), 127.68 (s, ArC), 130.6 (s, ArC,  $J_{\text{CPt}} = 29$  Hz), 131.3 (s,

ArC), 134.0 (t, ArC,  $J_{\text{CP}} = 4$  Hz), 138.9 (t, ArC,  $J_{\text{CP}} = 22$  Hz), 142.1 (s, ArC), 146.4 (t, ArC,  $J_{\text{CP}} = 8$  Hz).  $^{31}\text{P}\{^1\text{H}\}$  NMR (162 MHz,  $\text{C}_6\text{D}_6$ )  $\delta$ : 30.8 (s).  $^{195}\text{Pt}\{^1\text{H}\}$  NMR ( $\text{C}_6\text{D}_6$ , 86 MHz)  $\delta$ : -3123.5 (t,  $J_{\text{PP}} = 2901$  Hz). Anal. Calcd. for  $\text{C}_{31}\text{H}_{43}\text{IP}_2\text{Pt}$ : C, 46.56; H, 5.42. Found: C, 46.50; H, 5.66.

**Reaction of [(PterP)Pt(CH<sub>3</sub>)I] (**55**) or [(PterP)Pd(CH<sub>3</sub>)I] (**54**) with (*p*-tol)<sub>2</sub>CN<sub>2</sub>.**

To a THF solution of either [(PterP)Pt(CH<sub>3</sub>)I] (**55**, 20.8 mg, 0.03 mmol) or [(PterP)Pd(CH<sub>3</sub>)I] (**54**, 18.0 mg, 0.03 mmol) was added one equivalent of (*p*-tol)<sub>2</sub>CN<sub>2</sub> (7.0 mg, 0.03 mmol). The mixture was allowed to stir at room temperature for 4 h. Evaluation of the crude reaction mixture by  $^1\text{H}$  and  $^{31}\text{P}$  NMR spectroscopy showed no reaction. Exposing the reaction mixtures to UV radiation lead to decomposition of the diazo reagent to the corresponding azine compound, leaving the palladium and platinum starting materials unchanged.

**X-ray single crystal diffraction** The data were collected on a Bruker APEX-II diffractometer with a monochromated Mo  $\text{K}\alpha$  radiation.<sup>56</sup> Data were corrected for absorption and polarized effects and analyzed for space group determination.<sup>56-57</sup> The structure was solved by direct methods (SHELXS)<sup>58</sup> and refined by full-matrix least squares techniques against  $F_o^2$  (SHELXL-2014).<sup>59</sup> Unless noted, all hydrogen atoms were generated in calculated positions. Mercury was used for structure representations.<sup>60</sup>

**X-Ray crystal structure of [(PterP)PtCl<sub>2</sub>] $\cdot$ C<sub>6</sub>H<sub>6</sub> (**45** $\cdot$ C<sub>6</sub>H<sub>6</sub>).** Single crystals were obtained as clear plates from a concentrated  $\text{C}_6\text{D}_6$  solution at room temperature in the glovebox. Crystal and refinement data for **45** $\cdot$ C<sub>6</sub>H<sub>6</sub>:  $\text{C}_{36}\text{H}_{46}\text{Cl}_2\text{P}_2\text{Pt}$ ;  $M_r = 806.66$ ; Monoclinic; space group  $P2(1)/n$ ;  $a = 9.9849(7)$  Å;  $b = 21.4059(14)$  Å;  $c = 15.5615(10)$  Å;  $\alpha = 90^\circ$ ;  $\beta = 91.320(2)^\circ$ ;  $\gamma = 90^\circ$ ;  $V = 3325.2(4)$  Å<sup>3</sup>;  $Z = 4$ ;  $T = 120(2)$  K;  $\lambda = 0.71073$  Å;

$\mu = 4.501 \text{ mm}^{-1}$ ;  $d_{\text{calc}} = 1.611 \text{ g}\cdot\text{cm}^{-3}$ ; 47949 reflections collected; 5852 unique ( $R_{\text{int}} = 0.0714$ ); giving  $R_1 = 0.0281$ ,  $wR_2 = 0.0560$  for 4621 data with  $[I > 2\sigma(I)]$  and  $R_1 = 0.0466$ ,  $wR_2 = 0.0602$  for all 5852 data. Residual electron density ( $\text{e}^{-}\cdot\text{\AA}^{-3}$ ) max/min: 1.837/−1.808.

**X-Ray crystal structure of [(PterP)PdCl<sub>2</sub>] (46).** Single crystals were obtained as yellow needles from a concentrated THF solution layered with *n*-pentane at −35 °C in the glovebox. Crystal and refinement data for **3**: C<sub>30</sub>H<sub>40</sub>Cl<sub>2</sub>P<sub>2</sub>Pd;  $M_r = 639.86$ ; Triclinic; space group *P*-1;  $a = 11.1678(7) \text{ \AA}$ ;  $b = 15.7553(9) \text{ \AA}$ ;  $c = 16.9878(10) \text{ \AA}$ ;  $\alpha = 88.891(2)^{\circ}$ ;  $\beta = 73.797(2)^{\circ}$ ;  $\gamma = 80.222(2)^{\circ}$ ;  $V = 2827.4(3) \text{ \AA}^3$ ;  $Z = 4$ ;  $T = 120(2) \text{ K}$ ;  $\lambda = 0.71073 \text{ \AA}$ ;  $\mu = 0.977 \text{ mm}^{-1}$ ;  $d_{\text{calc}} = 1.503 \text{ g}\cdot\text{cm}^{-3}$ ; 60818 reflections collected; 9962 unique ( $R_{\text{int}} = 0.0408$ ); giving  $R_1 = 0.0313$ ,  $wR_2 = 0.0756$  for 8177 data with  $[I > 2\sigma(I)]$  and  $R_1 = 0.0426$ ,  $wR_2 = 0.0803$  for all 9962 data. Residual electron density ( $\text{e}^{-}\cdot\text{\AA}^{-3}$ ) max/min: 0.962/−0.550.

**X-Ray crystal structure of [(PterP)Pt] (47).** Single crystals were obtained as yellow blocks from a concentrated *n*-pentane solution at −35 °C in the glovebox. Crystal and refinement data for **4**: C<sub>30</sub>H<sub>40</sub>P<sub>2</sub>Pt;  $M_r = 657.65$ ; Triclinic; space group *P*-1;  $a = 10.4152(16) \text{ \AA}$ ;  $b = 17.115(3) \text{ \AA}$ ;  $c = 17.993(3) \text{ \AA}$ ;  $\alpha = 69.156(4)^{\circ}$ ;  $\beta = 89.994(4)^{\circ}$ ;  $\gamma = 80.636(4)^{\circ}$ ;  $V = 2951.6(8) \text{ \AA}^3$ ;  $Z = 4$ ;  $T = 120(2) \text{ K}$ ;  $\lambda = 0.71073 \text{ \AA}$ ;  $\mu = 4.877 \text{ mm}^{-1}$ ;  $d_{\text{calc}} = 1.480 \text{ g}\cdot\text{cm}^{-3}$ ; 54024 reflections collected; 10422 unique ( $R_{\text{int}} = 0.0921$ ); giving  $R_1 = 0.0945$ ,  $wR_2 = 0.2311$  for 7847 data with  $[I > 2\sigma(I)]$  and  $R_1 = 0.1138$ ,  $wR_2 = 0.2477$  for all 10422 data. Residual electron density ( $\text{e}^{-}\cdot\text{\AA}^{-3}$ ) max/min: 3.415/−2.528.

**X-Ray crystal structure of [(PterP)Pt=C(*p*-tol)<sub>2</sub>] (48).** Single crystals were obtained as dark red blocks from a concentrated solution of *n*-pentane at −35 °C in the glovebox. Crystal and refinement data for **5**: C<sub>45</sub>H<sub>54</sub>P<sub>2</sub>Pt;  $M_r = 851.91$ ; Monoclinic; space group *P*2<sub>1</sub>/*c*;  $a = 14.9955(10) \text{ \AA}$ ;  $b = 14.4043(9) \text{ \AA}$ ;  $c = 18.4309(12) \text{ \AA}$ ;  $\alpha = 90^{\circ}$ ;  $\beta =$



103.3790(10)°;  $\gamma = 90^\circ$ ;  $V = 3873.0(4) \text{ \AA}^3$ ;  $Z = 4$ ;  $T = 120(2) \text{ K}$ ;  $\lambda = 0.71073 \text{ \AA}$ ;  $\mu = 3.736 \text{ mm}^{-1}$ ;  $d_{\text{calc}} = 1.461 \text{ g}\cdot\text{cm}^{-3}$ ; 89959 reflections collected; 9615 unique ( $R_{\text{int}} = 0.0819$ ); giving  $R_1 = 0.0315$ ,  $wR_2 = 0.0573$  for 7469 data with  $[I > 2\sigma(I)]$  and  $R_1 = 0.0544$ ,  $wR_2 = 0.0634$  for all 9615 data. Residual electron density ( $\text{e}^- \cdot \text{\AA}^{-3}$ ) max/min: 1.875/−1.473.

**X-Ray crystal structure of [(PterP)Pd]·½C<sub>5</sub>H<sub>12</sub> (49·½C<sub>5</sub>H<sub>12</sub>).** Single crystals were obtained as yellow needles from a concentrated *n*-pentane solution at −35 °C in the glovebox. Crystal and refinement data for **49·½C<sub>5</sub>H<sub>12</sub>**: C<sub>65</sub>H<sub>92</sub>P<sub>4</sub>Pd<sub>2</sub>;  $M_r = 1210.07$ ; Monoclinic; space group  $P2_1/c$ ;  $a = 18.1059(11) \text{ \AA}$ ;  $b = 10.3894(6) \text{ \AA}$ ;  $c = 31.9405(19) \text{ \AA}$ ;  $\alpha = 90^\circ$ ;  $\beta = 100.5762(12)^\circ$ ;  $\gamma = 90^\circ$ ;  $V = 5906.2(6) \text{ \AA}^3$ ;  $Z = 4$ ;  $T = 120(2) \text{ K}$ ;  $\lambda = 0.71073 \text{ \AA}$ ;  $\mu = 0.756 \text{ mm}^{-1}$ ;  $d_{\text{calc}} = 1.361 \text{ g}\cdot\text{cm}^{-3}$ ; 89377 reflections collected; 10395 unique ( $R_{\text{int}} = 0.0579$ ); giving  $R_1 = 0.0385$ ,  $wR_2 = 0.0912$  for 7971 data with  $[I > 2\sigma(I)]$  and  $R_1 = 0.0574$ ,  $wR_2 = 0.0977$  for all 10395 data. Residual electron density ( $\text{e}^- \cdot \text{\AA}^{-3}$ ) max/min: 2.437/−2.412.

**X-Ray crystal structure of 51.** Single crystals were obtained as orange blocks from a concentrated *n*-pentane solution at −35 °C in the glovebox. Crystal and refinement data for **51**: C<sub>45</sub>H<sub>54</sub>P<sub>2</sub>Pd;  $M_r = 763.22$ ; Monoclinic; space group  $P2_1/c$ ;  $a = 12.1666(3) \text{ \AA}$ ;  $b = 12.6383(3) \text{ \AA}$ ;  $c = 25.2046(6) \text{ \AA}$ ;  $\alpha = 90^\circ$ ;  $\beta = 91.1130(10)^\circ$ ;  $\gamma = 90^\circ$ ;  $V = 3874.86(16) \text{ \AA}^3$ ;  $Z = 4$ ;  $T = 120(2) \text{ K}$ ;  $\lambda = 1.54178 \text{ \AA}$ ;  $\mu = 4.856 \text{ mm}^{-1}$ ;  $d_{\text{calc}} = 1.308 \text{ g}\cdot\text{cm}^{-3}$ ; 74785 reflections collected; 7560 unique ( $R_{\text{int}} = 0.0424$ ); giving  $R_1 = 0.0250$ ,  $wR_2 = 0.0674$  for 7051 data with  $[I > 2\sigma(I)]$  and  $R_1 = 0.0272$ ,  $wR_2 = 0.0689$  for all 7560 data. Residual electron density ( $\text{e}^- \cdot \text{\AA}^{-3}$ ) max/min: 0.965/−0.485.

**X-Ray crystal structure of [(PterP)Pt(H)SiHPh<sub>2</sub>] (56).** Single crystals were obtained as pale yellow blocks from a concentrated *n*-pentane solution at −35°C in the glovebox. Crystal and refinement data for **9**: C<sub>32</sub>H<sub>52</sub>P<sub>2</sub>PtSi;  $M_r = 841.95$ ; Orthorhombic;

space group *Pbca*;  $a = 17.0851(7)$  Å;  $b = 18.5952(8)$  Å;  $c = 23.7353(11)$  Å;  $\alpha = 90^\circ$ ;  $\beta = 90^\circ$ ;  $\gamma = 90^\circ$ ;  $V = 7540.7(6)$  Å<sup>3</sup>;  $Z = 8$ ;  $T = 120(2)$  K;  $\lambda = 0.71073$  Å;  $\mu = 3.867$  mm<sup>-1</sup>;  $d_{\text{calc}} = 1.483$  g·cm<sup>-3</sup>; 116275 reflections collected; 6635 unique ( $R_{\text{int}} = 0.1308$ ); giving  $R_1 = 0.0348$ ,  $wR_2 = 0.0606$  for 4506 data with  $[I > 2\sigma(I)]$  and  $R_1 = 0.0729$ ,  $wR_2 = 0.0672$  for all 6635 data. Residual electron density (e<sup>-</sup>·Å<sup>-3</sup>) max/min: 0.938/−0.948.

**X-Ray crystal structure of [(PterP)Pd(H)SiHPh<sub>2</sub>] (**57**·C<sub>5</sub>H<sub>12</sub>).** Single crystals were obtained as pale yellow blocks from a concentrated *n*-pentane solution at −35°C in the glovebox. Crystal and refinement data for **57**·C<sub>5</sub>H<sub>12</sub>: C<sub>47</sub>H<sub>62.15</sub>P<sub>2</sub>PdSi; Mr = 823.54; Triclinic; space group *P*-1;  $a = 9.7476(3)$  Å;  $b = 13.3740(5)$  Å;  $c = 17.3877(6)$  Å;  $\alpha = 72.9060(10)^\circ$ ;  $\beta = 83.9190(10)^\circ$ ;  $\gamma = 81.8410(10)^\circ$ ;  $V = 2139.73(13)$  Å<sup>3</sup>;  $Z = 2$ ;  $T = 120(2)$  K;  $\lambda = 0.71073$  Å;  $\mu = 0.567$  mm<sup>-1</sup>;  $d_{\text{calc}} = 1.278$  g·cm<sup>-3</sup>; 57530 reflections collected; 7535 unique ( $R_{\text{int}} = 0.0396$ ); giving  $R_1 = 0.0256$ ,  $wR_2 = 0.0632$  for 6926 data with  $[I > 2\sigma(I)]$  and  $R_1 = 0.0286$ ,  $wR_2 = 0.0643$  for all 7535 data. Residual electron density (e<sup>-</sup>·Å<sup>-3</sup>) max/min: 0.700/−0.343.

**X-Ray crystal structure of [(PterP)Pt(H)I] (**52**).** Single crystals were obtained as colorless blocks from a concentrated diethyl ether solution at −35°C in the glovebox. Crystal and refinement data for **11**: C<sub>30</sub>H<sub>40</sub>IP<sub>2</sub>Pt; Mr = 784.55; Tetragonal; space group *I*-4;  $a = 23.0436(16)$  Å;  $b = 23.0436(16)$  Å;  $c = 13.4662(12)$  Å;  $\alpha = 90^\circ$ ;  $\beta = 90^\circ$ ;  $\gamma = 90^\circ$ ;  $V = 7150.7(12)$  Å<sup>3</sup>;  $Z = 8$ ;  $T = 120(2)$  K;  $\lambda = 0.71073$  Å;  $\mu = 4.891$  mm<sup>-1</sup>;  $d_{\text{calc}} = 1.458$  g·cm<sup>-3</sup>; 54859 reflections collected; 6276 unique ( $R_{\text{int}} = 0.0457$ ); giving  $R_1 = 0.0178$ ,  $wR_2 = 0.0359$  for 5877 data with  $[I > 2\sigma(I)]$  and  $R_1 = 0.0217$ ,  $wR_2 = 0.0379$  for all 6276 data. Residual electron density (e<sup>-</sup>·Å<sup>-3</sup>) max/min: 0.711/−0.379.

**X-Ray crystal structure of [(PterP)Pt(CH<sub>3</sub>)I] (**55**).** Single crystals were obtained as colorless blocks from a concentrated solution of toluene layered with *n*-pentane at –35°C in the glovebox. Crystal and refinement data for **55**: C<sub>30</sub>H<sub>40</sub>IP<sub>2</sub>Pt; M<sub>r</sub> = 799.58; Monoclinic; space group *P2<sub>1</sub>/n*; *a* = 10.2030(9) Å; *b* = 14.0134(13) Å; *c* = 20.8771(19) Å; α = 90°; β = 93.5760(10)°; γ = 90°; V = 2979.2(5) Å<sup>3</sup>; Z = 3; T = 120(2) K; λ = 0.71073 Å; μ = 5.8721 mm<sup>-1</sup>; d<sub>calc</sub> = 1.783 g·cm<sup>-3</sup>; 45156 reflections collected; 5254 unique (R<sub>int</sub> = 0.0395); giving R<sub>1</sub> = 0.0157, wR<sub>2</sub> = 0.0343 for 4809 data with [I > 2σ(I)] and R<sub>1</sub> = 0.0196, wR<sub>2</sub> = 0.0351 for all 5254 data. Residual electron density (e<sup>-</sup>·Å<sup>-3</sup>) max/min: 0.481/–0.366.

## 6.5 References

1. Mindiola, D. J.; Hillhouse, G. L., *J. Am. Chem. Soc.* **2002**, *124* (34), 9976-9977.
2. Iluc, V. M.; Hillhouse, G. L., *J. Am. Chem. Soc.* **2014**, *136* (17), 6479-6488.
3. Waterman, R.; Hillhouse, G. L., *J. Am. Chem. Soc.* **2003**, *125* (44), 13350-13351.
4. van der Vlugt, J. I.; van Duren, R.; Batema, G. D.; den Heeten, R.; Meetsma, A.; Fraanje, J.; Goubitz, K.; Kamer, P. C. J.; van Leeuwen, P. W. N. M.; Vogt, D., *Organometallics* **2005**, *24* (22), 5377-5382.
5. Comanescu, C. C.; Iluc, V. M., *Inorg. Chem.* **2014**, *53* (16), 8517-8528.
6. Barrett, B. J.; Iluc, V. M., *Inorg. Chim. Acta* **2016**, *460*, 35-42.
7. Barrett, B. J.; Iluc, V. M., *Organometallics* **2014**, *33* (10), 2565-2574.
8. Bauer, J.; Braunschweig, H.; Dewhurst, R. D.; Radacki, K., *Chem. Eur. J.* **2013**, *19* (27), 8797-8805.
9. Bauer, J.; Braunschweig, H.; Damme, A.; Radacki, K., *Angew. Chem. Int. Ed.* **2012**, *51* (40), 10030-10033.
10. Mann, B. E.; Musco, A., *J. Chem. Soc., Dalton Trans.* **1980**, (5), 776-785.

11. Yoshida, T.; Yamagata, T.; Tulip, T. H.; Ibers, J. A.; Otsuka, S., *J. Am. Chem. Soc.* **1978**, *100* (7), 2063-2073.
12. Saito, S.; Tando, K.; Kabuto, C.; Yamamoto, Y., *Organometallics* **2000**, *19* (18), 3740-3743.
13. Hoyte, S. A.; Spencer, J. L., *Organometallics* **2011**, *30* (20), 5415-5423.
14. Zhang, K.; Hu, J.; Chan, K. C.; Wong, K. Y.; Yip, J. H. K., *Eur. J. Inorg. Chem.* **2007**, *2007* (3), 384-393.
15. Carr, N.; Mole, L.; Orpen, A. G.; Spencer, J. L., *J. Chem. Soc., Dalton Trans.* **1992**, *18* (18), 2653-2662.
16. Lin, S. B.; Day, M. W.; Agapie, T., *J. Am. Chem. Soc.* **2011**, *133* (11), 3828-3831.
17. Horak, K. T.; Velian, A.; Day, M. W.; Agapie, T., *Chem. Commun.* **2014**, *50* (34), 4427-4429.
18. Herbert, D. E.; Lara, N. C.; Agapie, T., *Chem. Eur. J.* **2013**, *19* (48), 16453-16460.
19. Campos, J.; Peloso, R.; Carmona, E., *Angew. Chem. Int. Ed.* **2012**, *51* (33), 8255-8258.
20. Cui, P.; Iluc, V. M., *Chem. Sci.* **2015**, *6*, 7343-7356.
21. Cui, P.; Comanescu, C. C.; Iluc, V. M., *Chem. Commun.* **2015**, *51*, 6206-6209.
22. Mindiola, D. J.; Hillhouse, G. L., *J. Am. Chem. Soc.* **2002**, *124* (34), 9976-9977.
23. Roy, S.; Mondal, K. C.; Meyer, J.; Niepötter, B.; Köhler, C.; Herbst-Irmer, R.; Stalke, D.; Dittrich, B.; Andrada, D. M.; Frenking, G.; Roesky, H. W., *Chem. Eur. J.* **2015**, *21* (26), 9312-9318.
24. Blase, V.; Flores-Figueroa, A.; Schulte to Brinke, C.; Hahn, F. E., *Organometallics* **2014**, *33* (17), 4471-4478.
25. Bauer, J.; Braunschweig, H.; Brenner, P.; Kraft, K.; Radacki, K.; Schwab, K., *Chem. Eur. J.* **2010**, *16* (39), 11985-11992.
26. Gosavi, T.; Wagner, C.; Merzweiler, K.; Schmidt, H.; Steinborn, D., *Organometallics* **2005**, *24* (4), 533-538.
27. Rendina, L. M.; Vittal, J. J.; Puddephatt, R. J., *Organometallics* **1995**, *14* (2), 1030-1038.

28. Lavoie, K. D.; Frauhiger, B. E.; White, P. S.; Templeton, J. L., *J. Organomet. Chem.* **2015**, *793*, 182-191.
29. Iluc, V. M.; Hillhouse, G. L., *J. Am. Chem. Soc.* **2014**, *136* (17), 6479-6488.
30. Comanescu, C. C.; Iluc, V. M., *Organometallics* **2014**, *33* (21), 6059-6064.
31. Comanescu, C. C.; Vyushkova, M.; Iluc, V., *Chem. Sci.* **2015**, *6*, 4570-4579.
32. Bröring, M.; Brandt, C. D.; Stellwag, S., *Chem. Commun.* **2003**, *18* (18), 2344-2345.
33. Bellow, J. A.; Stoian, S. A.; van Tol, J.; Ozarowski, A.; Lord, R. L.; Groysman, S., *J. Am. Chem. Soc.* **2016**, *138* (17), 5531-5534.
34. Kornecki, K. P.; Briones, J. F.; Boyarskikh, V.; Fullilove, F.; Autschbach, J.; Schrote, K. E.; Lancaster, K. M.; Davies, H. M. L.; Berry, J. F., *Science* **2013**, *342* (6156), 351-354.
35. Qiu, L.; Huang, D.; Xu, G.; Dai, Z.; Sun, J., *Org. Lett.* **2015**, *17* (7), 1810-1813.
36. Lee, H. G.; Milner, P. J.; Buchwald, S. L., *Org. Lett.* **2013**, *15* (21), 5602-5605.
37. Basato, M.; Tubaro, C.; Biffis, A.; Bonato, M.; Buscemi, G.; Lighezzolo, F.; Lunardi, P.; Vianini, C.; Benetollo, F.; Del Zotto, A., *Chem. Eur. J.* **2009**, *15* (6), 1516-1526.
38. Koduri, N. D.; Wang, Z.; Cannell, G.; Cooley, K.; Lemma, T. M.; Miao, K.; Nguyen, M.; Frohock, B.; Castaneda, M.; Scott, H.; Albinescu, D.; Hussaini, S. R., *J. Org. Chem.* **2014**, *79* (16), 7405-7414.
39. Zhu, C.; Xu, G.; Ding, D.; Qiu, L.; Sun, J., *Org. Lett.* **2015**, *17* (17), 4244-4247.
40. Xu, G.; Zhu, C.; Gu, W.; Li, J.; Sun, J., *Angew. Chem. Int. Ed.* **2015**, *54* (3), 883-887.
41. Zhou, Y.; Trewyn, B. G.; Angelici, R. J.; Woo, L. K., *J. Am. Chem. Soc.* **2009**, *131* (33), 11734-11743.
42. Pereira, A.; Champouret, Y.; Martín, C.; Álvarez, E.; Etienne, M.; Belderráin, T. R.; Pérez, P. J., *Chem. Eur. J.* **2015**, *21* (27), 9769-9775.
43. Liu, Z.; Wang, J., *J. Org. Chem.* **2013**, *78* (20), 10024-10030.
44. Zhang, Y.; Wang, J., *Eur. J. Org. Chem.* **2011**, *2011* (6), 1015-1026.
45. Xiao, Q.; Zhang, Y.; Wang, J., *Acc. Chem. Res.* **2013**, *46* (2), 236-247.

46. Zhu, S.-F.; Zhou, Q.-L., *Acc. Chem. Res.* **2012**, *45* (8), 1365-1377.
47. Gillingham, D.; Fei, N., *Chem. Soc. Rev.* **2013**, *42* (12), 4918-4931.
48. Boyle, R. C.; Mague, J. T.; Fink, M. J., *J. Am. Chem. Soc.* **2003**, *125* (11), 3228-3229.
49. Nakata, N.; Fukazawa, S.; Kato, N.; Ishii, A., *Organometallics* **2011**, *30* (17), 4490-4493.
50. Chan, D.; Duckett, S. B.; Heath, S. L.; Khazal, I. G.; Perutz, R. N.; Sabo-Etienne, S.; Timmins, P. L., *Organometallics* **2004**, *23* (24), 5744-5756.
51. Weitz, I. S.; Rabinovitz, M., *J. Chem. Soc., Perkin Trans. 1* **1993**, (1), 117-120.
52. Duckett, S. B.; Galvez-Lopez, M.-D.; Perutz, R. N.; Schott, D., *Dalton Trans.* **2004**, (17), 2746-2749.
53. King, B. T.; Kroulík, J.; Robertson, C. R.; Rempala, P.; Hilton, C. L.; Korinek, J. D.; Gortari, L. M., *J. Org. Chem.* **2007**, *72* (7), 2279-2288.
54. Al-Najjar, I. M., *Inorg. Chim. Acta.* **1987**, *128* (1), 93-104.
55. Giri, B. P.; Prasad, G.; Mehrotra, K. N., *Can. J. Chem.* **1979**, *57* (10), 1157-1161.
56. Bruker AXS, APEX-2. Bruker-Nonius AXS, Madison, Wisconsin, USA, 2014.
57. Krause, L.; Herbst-Irmer, R.; Sheldrick, G. M.; Stalke, D., *J. Appl. Cryst.* **2015**, *48* (1), 3-10.
58. Sheldrick, G., *Acta Cryst.* **2015**, *A71* (1), 3-8.
59. Sheldrick, G., *Acta Cryst.* **2015**, *C71* (1), 3-8.
60. Macrae, C. F.; Bruno, I. J.; Chisholm, J. A.; Edgington, P. R.; McCabe, P.; Pidcock, E.; Rodriguez-Monge, L.; Taylor, R.; van de Streek, J.; Wood, P. A., *J. Appl. Cryst.* **2008**, *41* (2), 466-470.

CHAPTER 7:  
PALLADIUM MEDIATED ARENE INSERTION INTO BULKY PALLADIUM-ARYL  
BONDS

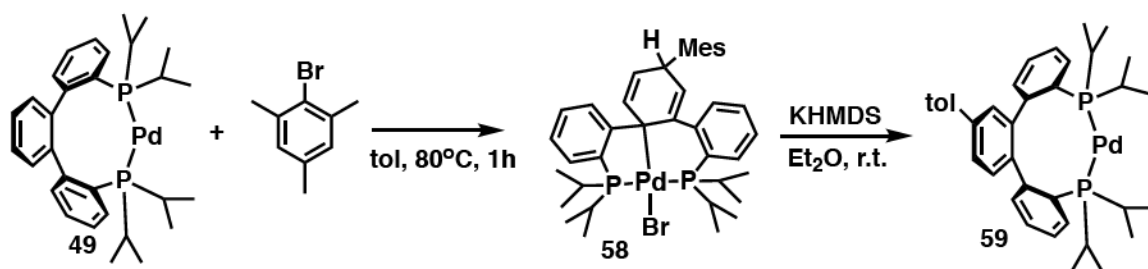
### 7.1 Introduction

In this chapter, the migration of palladium bound aromatic groups to the central arene of the PterP ligand framework will be discussed. The arylation of arenes catalyzed by palladium metal centers is known, and is believed to be the result of  $\pi$ -interactions between the metal center and the aromatic group to be functionalized.<sup>1-3</sup> These interactions disrupt the aromaticity of the system, and make the aryl group susceptible to nucleophilic attack.<sup>4</sup> The supporting ligand, PterP (**44**), results in strained species in which the central aromatic moiety shields a face of the metal center. This arene moiety is held at a close proximity to the metal center, however, the strain in the ligand framework makes  $\pi$ -interactions between the metal and the ligand backbone difficult to observe. For complexes experiencing steric crowding around the metal center, these  $\pi$ -interactions help facilitate the migration of palladium bound bulky substituents to the ligand backbone. The conditions necessary for facilitating this reactivity were explored, and the resulting complexes characterized. Attempts to observe coordination of the arene backbone to the metal center will also be discussed.

## 7.2 Results and Discussion

The initial investigation of the oxidative addition of BrMes to (PterP)Pd (**49**) led to unexpected results. It was found that at room temperature, a complicated mixture of products was obtained. Heating the reaction mixture to 80°C for 1 hour lead to the formation of one clean product (**58**, Scheme 7.1). Analysis of the compound by  $^{31}\text{P}$  and  $^1\text{H}$  NMR spectroscopy revealed the formation of an asymmetric compound. Interestingly, closer inspection of the  $^1\text{H}$  NMR spectrum revealed that 3 originally aromatic protons were shifted upfield to 4.62, 5.61, and 5.65 ppm respectively. An HSQC experiment indicated that these peaks correlate to carbon atoms which are similarly shifted upfield (40.58, 123.33, and 128.47 ppm). While two of the carbon atoms are still relatively downfield, the resonance at 40.58 ppm was quite striking, and indicates a loss in the aromaticity of the ligand backbone. This hypothesis was confirmed upon inspection of the solid state molecular structure, which revealed the migration of the mesityl functionality to the central arene of the ligand backbone (Figure 7.1). This results in a 4-coordinate palladium(II) metal center in which two originally aromatic carbon atoms of the ligand backbone have become  $\text{sp}^3$  hybridized ( $\text{C}(2)\text{-C}(1)\text{-C}(6) = 109.6(4)$ ,  $\text{C}(5)\text{-C}(4)\text{-C}(7) = 113.2(4)$ , Figure 7.1). The restoration of the aromaticity of the ligand backbone was accomplished through treatment of the species with a base, resulting in a palladium(0) metal center exhibiting a functionalized backbone (**59**). This assignment was confirmed upon analysis of the solid state molecular structure (Figure 7.1). The formerly  $\text{sp}^3$  hybridized carbon atoms of the backbone have returned to  $\text{sp}^2$  hybridization as indicated by the angles for  $\text{C}(14)\text{-C}(13)\text{-C}(18) = 118.4(3)$ , and  $\text{C}(15)\text{-C}(16)\text{-C}(19) = 121.7(3)$ .





**Scheme 7.1:** Synthesis of compound **58**, and subsequent dehydrohalogenation.

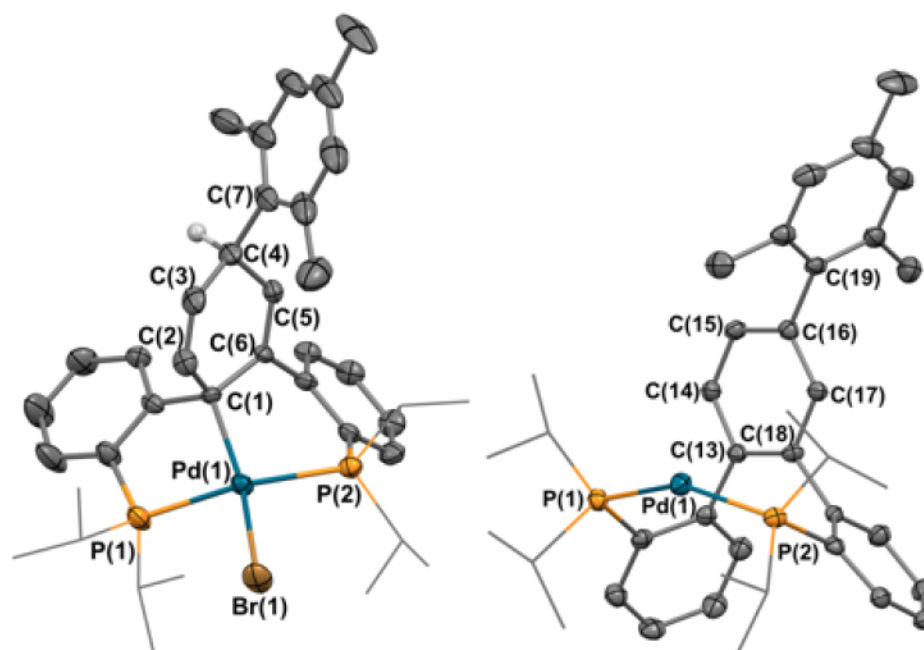
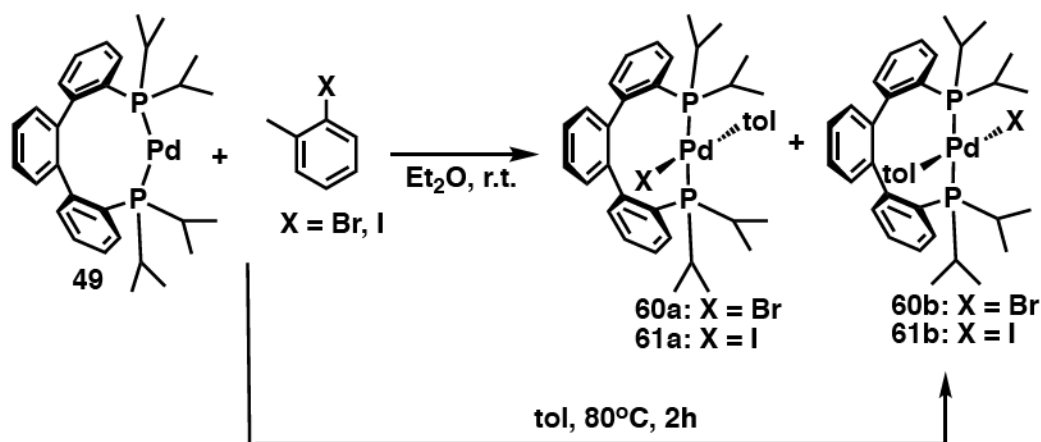


**Figure 7.1:** Molecular structure of **58** (left) and **59** (right) with displacement parameters at the 50% probability level. Most hydrogen atoms are omitted for clarity. Selected distances (Å) and angles (°) for **58**: Pd(1)-P(1) = 2.2710(14), Pd(1)-P(2) = 2.3155(14), Pd(1)-Br(1) = 2.5278(7), Pd(1)-C(1) = 2.106(5), C(1)-C(2) = 1.528(7), C(2)-C(3) = 1.304(7), C(3)-C(4) = 1.486(8), C(4)-C(5) = 1.505(7), C(5)-C(6) = 1.335(7), C(6)-C(1) = 1.493(7), P(1)-Pd(1)-P(2) = 152.64(6), C(1)-Pd(1)-Br(1) = 161.39(15), C(2)-C(1)-C(6) = 109.6(4), C(5)-C(4)-C(7) = 113.2(4). For **59**: P(1)-Pd(1) = 2.2651(9), P(2)-Pd(1) = 2.2459(8), C(13)-C(14) = 1.407(4), C(14)-C(15) = 1.398(4), C(15)-C(16) = 1.382(4), C(16)-C(17) = 1.392(4), C(17)-C(18) = 1.405(5), C(18)-C(19) = 1.403(4), P(1)-Pd(1)-P(2) = 151.68(3), C(15)-C(16)-C(19) = 121.7(3), C(14)-C(13)-C(18) = 118.4(3).

Next, there was interest in determining what factors were important for the migration event to occur. The steric bulk of the mesityl moiety was hypothesized to increase the favorability of the migration event, due to the resulting drive to minimize steric interactions between the mesityl group and the ligand backbone. To test this, the less bulky substrates 2-bromotoluene, and 2-iodotoluene were investigated (Scheme 7.2). Unlike the results obtained in the case for the mesityl group, both 2-bromotoluene and 2-iodotoluene underwent oxidative addition to the metal center. Interestingly, at room temperature two isomers were observed in the  $^1\text{H}$  NMR spectrum for the reactions with both reagents (**60a-b**, and **61a-b**). When the solutions are heated to 80°C for 2 h, full conversion to one isomer (**60b**, **61b**) was observed. Inspection of the  $^1\text{H}$  NMR spectrum containing the mixture of isomers reveals that each compound has one upfield aromatic proton, however for one isomer, this upfield shift is more prominent than in the case for the other. An upfield shift of an aromatic proton was observed previously for (*c*PCMe=CMeP)PdIPh (**30**, Chapter 4), due to a proton of the palladium bound phenyl group residing in the shielding environment of the phenyl groups in the ligand backbone. Therefore, it was hypothesized that the isomer experiencing a greater amount of shielding results from the toluene substituent residing anti to the central arene of the ligand backbone. It therefore experiences shielding from the two phenyl groups on the periphery of the ligand framework. The isomer containing a smaller degree of shielding results from the toluene group occupying the position syn to the central arene group; experiencing shielding from only one aromatic moiety.



**Scheme 7.2:** Synthesis of **60a-b** and **61a-b**.

For compounds **60a** and **60b**, solid state molecular structures were obtained (Figure 7.2). The structure for the syn-isomer was obtained only after heating of the reaction mixture to achieve full conversion to one isomer. Obtaining NMR spectra of the crystals used to collect the solid state molecular structure indicates that no isomerization back to the anti-isomer occurs at the low temperature conditions utilized to induce crystalization. Both compounds exhibit trans coordination of the ligand to the metal center, leaving the bromide and toluene ligands to occupy positions trans to one another. Both structures display distortions in the square planar geometry of the metal center due to the bending of the phosphine arms to minimize steric interactions between the ligand backbone and the additional ligands on palladium ( $\text{P}(1)\text{-Pd}(1)\text{-P}(2)$  range =  $149.96\text{-}158.75^\circ$ ).

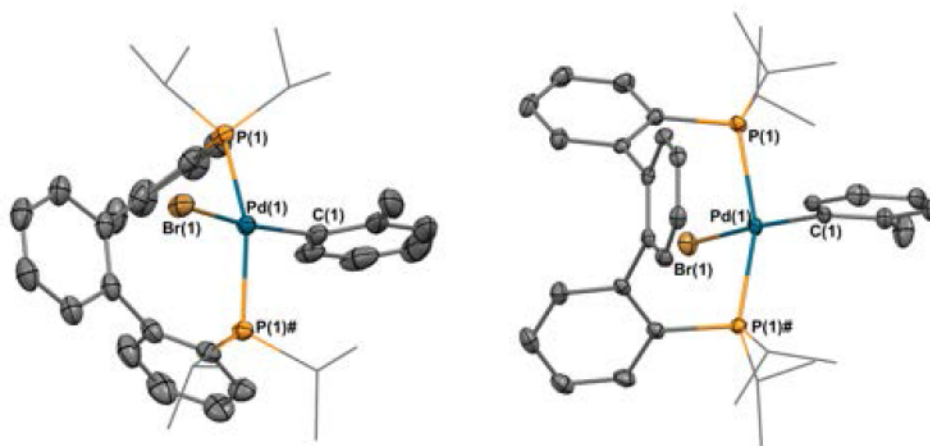
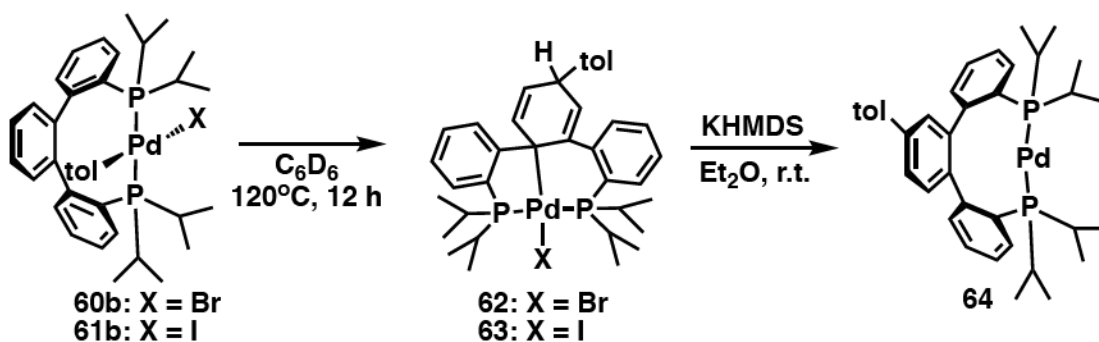


**Figure 7.2:** Molecular structure of **60a** (left) and **60b** (right) with displacement parameters at the 50% probability level. Most hydrogen atoms are omitted for clarity. Selected distances (Å) and angles (°) for **60a**: Pd(1)-P(1) = 2.3307(7), Pd(1)-Br(1) = 2.5159(5), Pd(1)-C(1) = 2.035(3), C(1)-Pd(1)-Br(1) = 164.97(12), P(1)-Pd(1)-P(1)# = 149.96(3). For **60b**: Pd(1)-P(1) = 2.3024(6), Pd(1)-Br(1) = 2.5146(4), Pd(1)-C(1) = 2.021(3), C(1)-Pd(1)-Br(1) = 168.26(9), P(1)-Pd(1)-P(1)# = 158.75(3).

Prolonged heating of compounds **60b** and **61b** at 80°C lead to no migration event of the toluene substituent to the ligand backbone. Increasing the heat to 120°C however, lead to full conversion to an asymmetric compound after 12 hours in both cases (**62**: X = Br, **63**: X = I, Scheme 7.3). The products obtained were reminiscent of **58** in the  $^1\text{H}$  NMR spectrum; once again displaying 3 protons in the 4–6 ppm range indicating dearomatization of the ligand backbone. In the case for the iodo-analogue (**63**), the solid state molecular structure confirmed the migratory insertion of the ligand backbone (Figure 7.3). Once again, two of the originally aromatic backbone carbon atoms have become  $\text{sp}^3$  hybridized upon migration of the tolyl substituent to the ligand backbone. As for the mesityl analogue, restoration of the aromaticity of the ligand backbone was accomplished upon treatment with a base (Scheme 7.3).



**Scheme 7.3:** Synthesis of **62** and **63** and subsequent dehydrohalogenation.

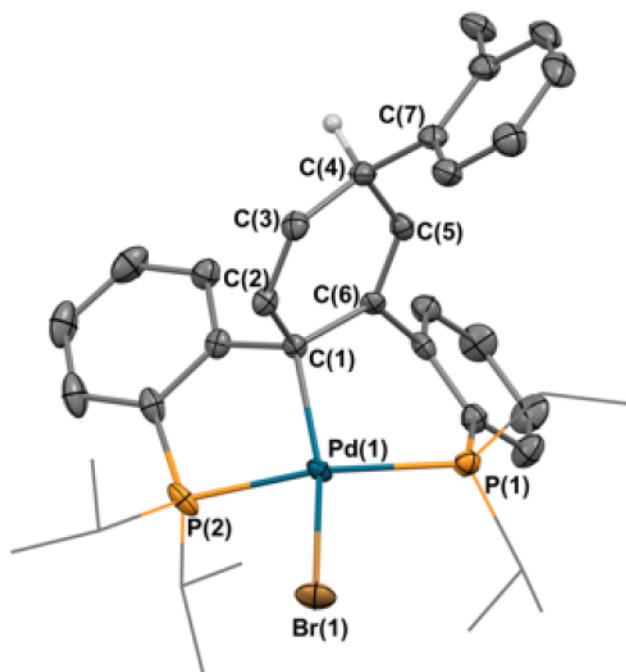
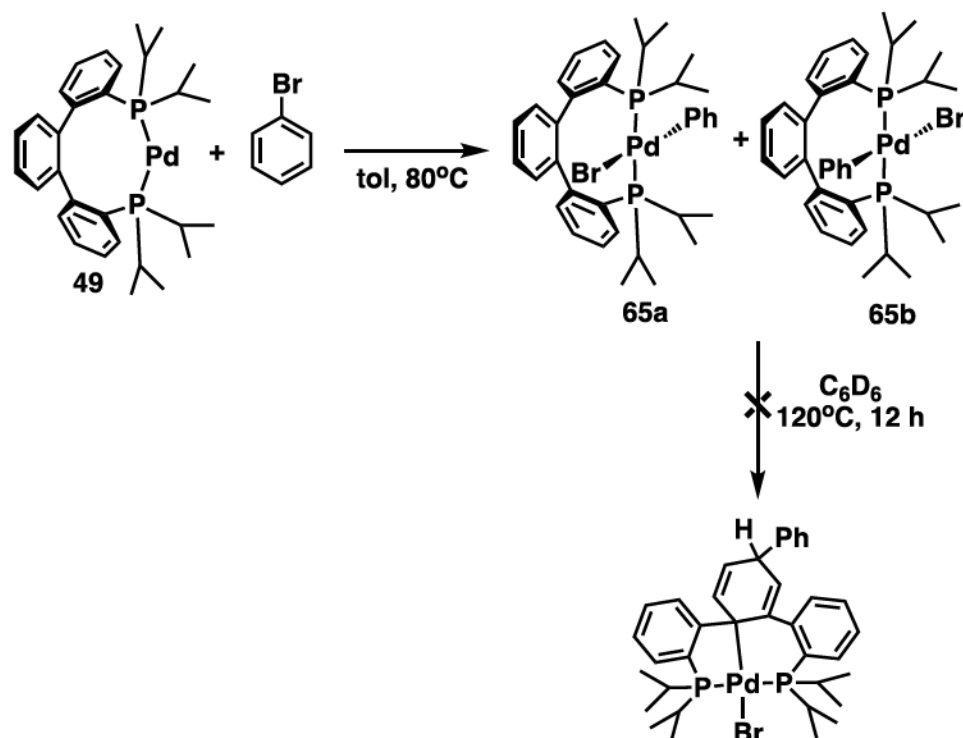


**Figure 7.3:** Molecular structure of **62** with displacement parameters at the 50% probability level. Most hydrogen atoms are omitted for clarity. Selected distances (Å) and angles (°) for **62**: Pd(1)-P(1) = 2.3261(8), Pd(1)-P(2) = 2.2595(8), Pd(1)-Br(1) = 2.5316(4), Pd(1)-C(1) = 2.102(3), C(1)-C(2) = 1.498(4), C(2)-C(3) = 1.321(4), C(3)-C(4) = 1.498(4), C(4)-C(5) = 1.505(4), C(5)-C(6) = 1.335(4), C(6)-C(1) = 1.490(4), P(1)-Pd(1)-P(2) = 149.38(3), C(1)-Pd(1)-Br(1) = 159.54(7), C(2)-C(1)-C(6) = 111.3(2), C(5)-C(4)-C(7) = 110.9(2).

Given that the less bulky toluene compounds underwent migration to the ligand backbone only after being heated to 120°C, it was next of interest to determine if even less bulky phenyl substituents would migrate at all. Oxidative addition of bromobenzene to (PterP)Pd (**49**) was next carried out (Scheme 7.4). Unlike the toluene examples, the room temperature reaction only produced one isomer in solution (**65a**). Heating of the solution to 80°C afforded the isomerization of the complex, however full conversion to the second isomer (**65b**) was not achieved even after 10 days of heating. The solid state molecular structures of both isomers were obtained, and are reminiscent of the toluene analogues (Figure 7.4). The structure of the anti-isomer was obtained from a reaction which was not subjected to heating, indicating that it is the more kinetically favorable isomer. Both isomers contain trans coordination of the diphosphine ligand, **44**, and show distortions from an optimal square planar geometry due to the bending of the phosphine arms away from the ligand backbone.

Attempts to induce the migration of the phenyl ligand to the arene backbone were next carried out, however, after heating the solution to 120°C overnight, a complicated mixture of products was observed (Scheme 7.4). The reaction was also attempted using microwave radiation at varying temperatures however, similar mixtures of products were observed.



**Scheme 7.4:** Synthesis of 65 a-b.

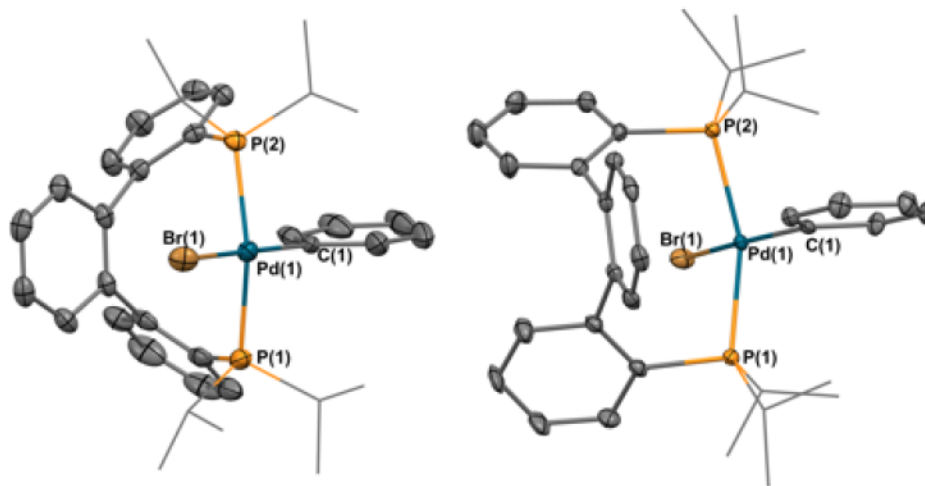
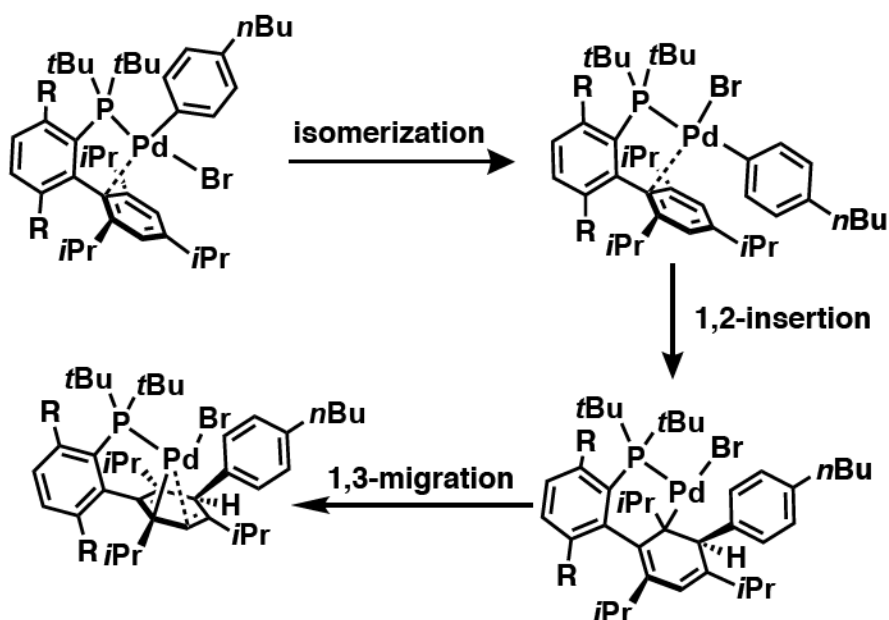


**Figure 7.4:** Molecular structure of **64a** (left) and **64b** (right) with displacement parameters at the 50% probability level. Most hydrogen atoms are omitted for clarity. Selected distances (Å) and angles (°) for **64a**: Pd(1)-P(1) = 2.2960(15), Pd(1)-P(2) = 2.3050(8), Pd(1)-Br(1) = 2.5145(7), Pd(1)-C(1) = 2.063(6), C(1)-Pd(1)-Br(1) = 172.71(17), P(1)-Pd(1)-P(2) = 157.66(5). For **64b**: Pd(1)-P(1) = 2.3043(14), Pd(1)-P(2) = 2.2898(13), Pd(1)-Br(1) = 2.5453(7), Pd(1)-C(1) = 2.008(5), C(1)-Pd(1)-Br(1) = 165.79(16), P(1)-Pd(1)-P(2) = 159.58(5).

It is known in the literature that the interaction of metal centers with the  $\pi$ -system of aromatic rings can make these rings susceptible to nucleophilic attack. Generally, this is more commonly reported for early transition metals<sup>4-7</sup>, while examples of group 10 species exhibiting similar reactivity are less common.<sup>8-11</sup> The palladium catalyzed arylation of arenes has been proposed to occur via a concerted aryl migratory insertion mechanism, initiated by palladium-arene interactions.<sup>1, 3</sup> However, this is speculative, and is used to explain proton abstraction processes which are not observed in our system. Phosphine ligands that are designed around a biaryl scaffold are often used as the supporting ligands for palladium catalyzed coupling reactions.<sup>12-15</sup> One of the features of biaryl ligand systems that makes them attractive is the ability of  $\eta^1$  or  $\eta^2$  interactions between the palladium metal center and the biaryl ligand system to stabilize the catalyst in the absence of substrate.<sup>16-20</sup> Only in few reported examples does this interaction lead to a functionalized arene of the supporting ligand when group 10 metals are employed. The Agapie group observed that their tris(phosphine) ligand with a benzene linker undergoes functionalization when nickel and palladium metal centers are used.<sup>9</sup> In their compounds with only two of the three phosphine donors coordinated to the metal center, they observe that the interaction of either nickel or palladium with the central benzene moiety of the ligand backbone leads to the nucleophilic attack of the benzene linker by the dissociated phosphine. This generates a complex containing a phosphonium moiety.<sup>9</sup> Similarly, the Buchwald group noticed similar reactivity for some of their bulkier biphenylphosphine ligand systems (Scheme 7.5).<sup>8, 21-22</sup> The ligand design places the “lower” phenyl group within the coordination sphere of a palladium metal center. This leads to the reversible rearrangement of their palladium(II) aryl halide compound into a dearomatized species in



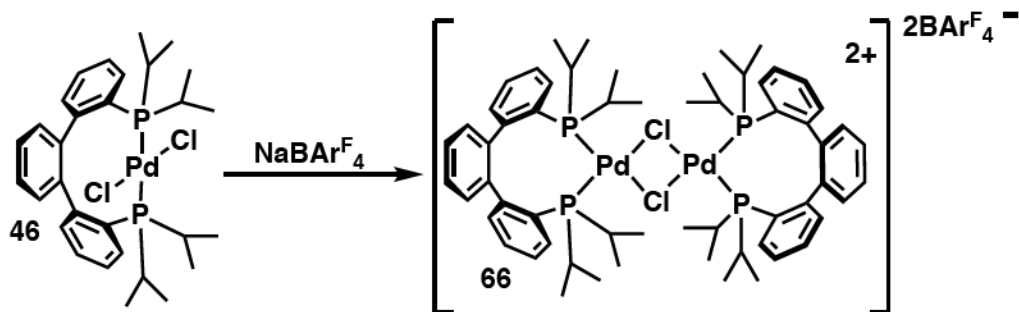
which the aryl group migrates to the “lower” phenyl ring of the ligand framework to reduce the steric crowding of the metal center. This behavior was studied in detail by Buchwald and coworkers, and it was concluded that the likely mechanism involves an initial interaction of the palladium metal center with the “lower” phenyl group. A 1,2 insertion next gives a dearomatized species in which C-C bond formation between the ligand and the palladium bound aryl moiety occurs in conjunction with Pd-C bond formation of the same “lower” phenyl ring. Finally, a 1,3 shift of the palladium metal center gives their observed final product (Scheme 7.5). It should be noted that this process was not observed for less bulky biaryl ligand scaffolds.



**Scheme 7.5:** Proposed mechanism for dearomative rearrangement observed in the Buchwald Group.<sup>8</sup>

A common feature in these processes is either an  $\eta^1$  or  $\eta^2$  interaction with the aromatic moiety, which ultimately leads to the observed reactivity.<sup>2, 23</sup> These types of interactions between group 10 metal centers and aromatic groups are well established.<sup>9, 17, 24-32</sup> We therefore became interested in observing such an interaction in our system. It was

hypothesized that abstraction of a halide ligand from (PterP)PdCl<sub>2</sub>, **46**, would force the arene moiety to stabilize the electron deficient metal center. Therefore, (PterP)PdCl<sub>2</sub> (**46**) was treated with NaBAr<sup>F</sup><sub>4</sub> (Scheme 7.6), which led to the formation of one product (**66**). By <sup>1</sup>H, <sup>11</sup>B, and <sup>19</sup>F NMR spectroscopy, the presence of the BAr<sup>F</sup><sub>4</sub> counterion was confirmed, supporting the removal of a chloride ligand from the metal center. The <sup>1</sup>H, and <sup>31</sup>P NMR spectra display C<sub>2</sub> symmetry, however, both are considerably broad. The solid state molecular structure revealed the formation of a chloride bridging dimer (Figure 7.5). No interaction between the metal center and the ligand arene was observed, as determined from the long distance of 3.448 Å from the metal center to the arene centroid. The broadness of the NMR spectra is attributed to the cis geometry of the ligand backbone. A similar observation was made for the complex (PterP)PtCl<sub>2</sub> (**45**) which demonstrates cis coordination of the same ligand to the metal center as well (Chapter 6).



**Scheme 7.6:** Synthesis of **66**.

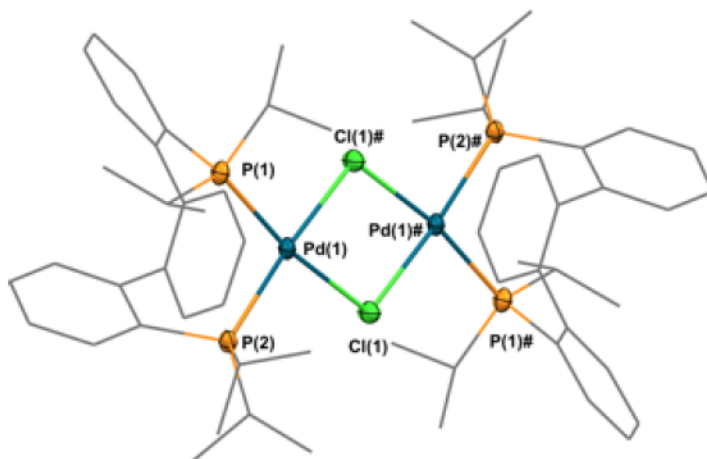
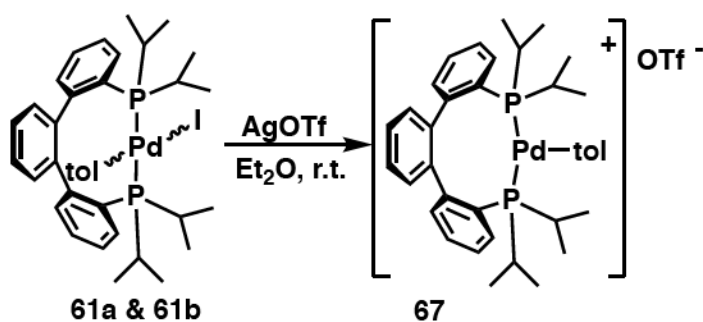


**Figure 7.5:** Molecular structure of **66** with displacement parameters at the 50% probability level. The counterions and hydrogen atoms are omitted for clarity. Selected distances (Å) and angles (°) for **66**: Pd(1)-P(1) = 2.3155(6), Pd(1)-P(2) = 2.3090(6), Pd(1)-Cl(1) = 2.3908(6), Pd(1)-Cl(1)# = 2.3966(6), Pd(1)-Pd(1)# = 3.639, P(1)-Pd(1)-P(2) = 97.07(2)(9), P(2)-Pd(1)-Cl(1)# = 172.10(2), P(1)-Pd(1)-Cl(1) = 170.55(2).

The next goal was to prevent the formation of a dimeric species to determine if an interaction between the metal center and the arene could be forced. Reacting (PterP)PdI(tol) (**61**) with AgOTf leads to the rapid formation of a new compound (**67**, Scheme 7.7). The  $^1\text{H}$  NMR spectrum indicates that the triflate anion is not coordinated to the metal center due to the lack of shielded aromatic protons from the tolyl ligand. Coordination of triflate to the metal center is expected to result in the tolyl ligand residing in one of the two shielding environments of the ligand backbone, as was observed for the oxidative addition complexes **60a-b**, **61a-b**, and **64a-b**. Additionally, coordination of the metal center to the arene backbone is expected to shift the aromatic protons upfield. The lack of shifted resonances indicates that such an interaction is not present. Evaluation of the  $^{13}\text{C}$  NMR spectrum also does not show any shifted aromatic resonances, supporting the dissociated state of the arene. Crystals suitable for single crystal X-ray diffraction were

obtained from a concentrated DCM solution layered with *n*-pentane (Figure 7.6). The structure shows a distorted T-shape palladium(II) cation with a triflate anion (P(1)-Pd(1)-P(1)# = 154.49(5)). The palladium metal center is 2.651 Å from the centroid of the closest C-C bond of the ligand arene (C(20)-C(20)#). This distance is comparable to an interaction reported for the palladium(0) compound (dcpBiph)<sub>2</sub>Pd (dcpBiph = 2-(dicyclohexylphosphino)-biphenyl) by the Fink group.<sup>17</sup> It was observed that the palladium(0) interacted in an  $\eta^1$  fashion with a biphenyl carbon atom, indicated by the close distance of 2.676(5) Å.<sup>17</sup> It is important to note however, that this distance is longer than those generally reported for palladium complexes interacting with the  $\pi$ -system of an aryl group. Palladium arene  $\eta^2$  interactions have been reported at distances of 2.066 Å, and  $\eta^1$  interactions have been reported at distances of 2.1970 Å.<sup>9, 14</sup> Based on these comparisons, the palladium in [(PterP}Pd(tol)][OTf] (**67**) is not believed to be coordinated to the arene backbone. This cationic species proved to be unstable. Heating in DCM at 40°C led to the formation of palladium black.



**Scheme 7.7:** Synthesis of compound **67**.

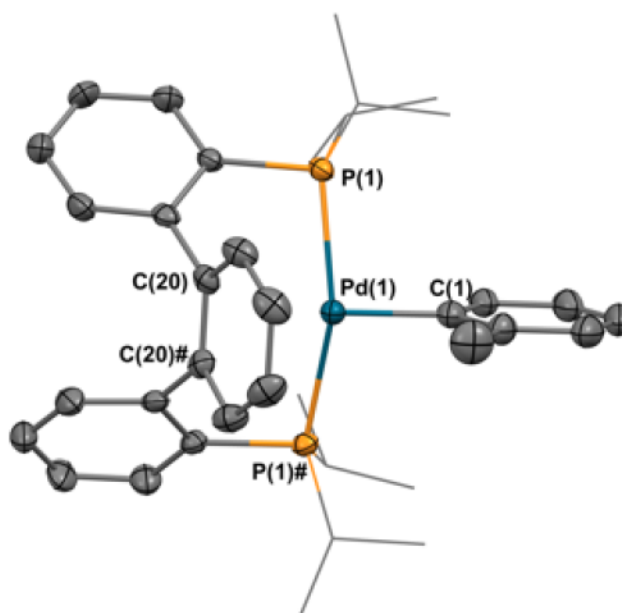
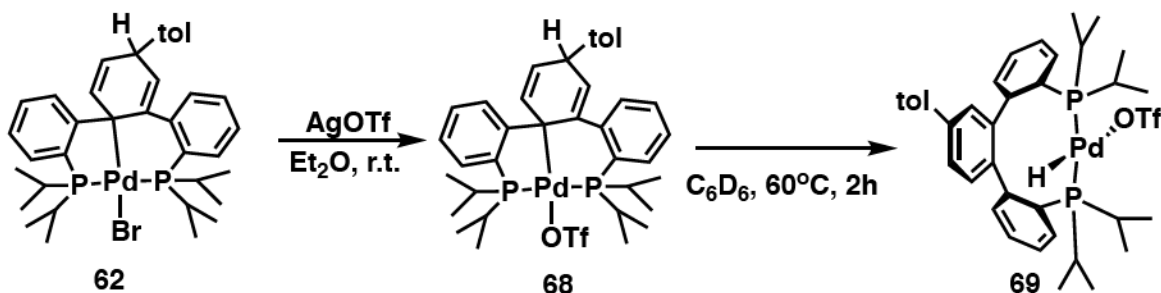


**Figure 7.6:** Molecular structure of **67** with displacement parameters at the 50% probability level. The triflate counterion and hydrogen atoms are omitted for clarity. Selected distances (Å) and angles (°) for **67**: Pd(1)-P(1) = 2.3553(11), Pd(1)-C(1) = 1.996(6), Pd(1)-(C(20)-C(20)#) = 2.651, P(1)-Pd(1)-P(1)# = 154.49(5), P(1)-Pd(1)-C(1) = 95.60(4).

The example mentioned above of aryl migration to a biphenyl phosphine ligand from the Buchwald group was a reversible process, however reversibility has not been observed for our system.<sup>8</sup> It was hypothesized that replacing a halide ligand in a complex that has already undergone aryl migration with a weakly coordinating triflate ligand might induce the migration of the aromatic group back to the metal center. Therefore (Pter<sup>tol</sup>P)PdBr (**62**) was reacted with AgOTf, leading to the formation of a new species (**68**) with spectroscopic signatures reminiscent of the starting material indicating similar connectivity (Scheme 7.8). The presence of the triflate ligand was confirmed by <sup>19</sup>F NMR spectroscopy. At room temperature, there is no indication that the species is undergoing rearrangement to restore aromaticity in the ligand backbone through migration of the tolyl

moiety to the metal center. The compound was next heated to 60°C for 2 h, which led to the formation of a new compound (**69**, Scheme 7.8). By  $^{31}\text{P}$  NMR spectroscopy, the phosphines resonate equivalently as a singlet at 33.2 ppm. The  $^1\text{H}$  NMR spectrum however, shows a high degree of asymmetry. The *iso*-propyl methyl groups consist of seven different resonances, and additionally all four of the *iso*-propyl methine positions resonate independently. The tolyl moiety is accounted for; the tolyl methyl group is identified as a singlet at 2.45 ppm. The aryl region integration to 16 protons also supports the presence of the tolyl functionality. There are no protons resonating between 3-6 ppm, indicating that the aromaticity of the backbone has been restored. Examining the hydride region of the spectrum reveals a triplet at -19.01 ppm. Crystals suitable for single crystal X-ray diffraction have not been obtained, however the NMR data suggests the occurrence of hydride elimination from the dearomatized backbone. This would restore the aromaticity of the ligand backbone, and generate a palladium(II) compound with a functionalized ligand (Scheme 7.8). The asymmetry observed in the  $^1\text{H}$  NMR spectrum for the ligand backbone is consistent with the tolyl moiety breaking the symmetry of the molecule, however, it would also be reasonable to assume that while the phosphines are inequivalent, they are quite similar and appear to resonate as a singlet.



**Scheme 7.8:** Synthesis of **68**, and subsequent rearrangement.

The mechanism for the migratory insertion of the arene into Pd-aryl bonds remains unclear. In a general sense, either a 1,4-migratory insertion or a 1,2-migratory insertion into the ligand backbone followed by 1,3-allylic shift of the palladium metal center would lead to the observed connectivity in the final product; this could occur in several ways. A possible mechanism could involve dissociation of the halide ligand, encouraging the palladium to interact with the arene. Subsequent 1,4-migratory insertion or 1,2-insertion and 1,3-migration, as discussed above, followed by recombination with the halide ligand would lead to the observed product. The lack of arene-palladium interactions in the cationic compounds **66** and **67**, as well as the instability of the T-shaped species (**67**) however, does not offer support for this stepwise mechanism. Another possibility involves the dissociation of a phosphine arm, offering more flexibility to the complex; allowing the metal center to interact with the arene moiety more easily. If one of the phosphine arms dissociates from the metal center, the mechanism would proceed analogously to that described by Buchwald and coworkers (Figure 7.5). If dissociation of the phosphine occurs however, it is expected that an additional product would be observed. The dissociation of a phosphine arm would induce flexibility into the ligand backbone, allowing for the C-H activation of the non-substituted ortho carbon on the central aryl group. The formation of palladacycles from biarylphosphine ligands has been reported.<sup>33-34</sup> It was observed that biphenyl ligands lacking substitution in the lower aryl ring are susceptible to palladacycle formation. Additionally, biphenyl ligand systems substituted in only one ortho position of the lower aryl ring form palladacycles even more readily than their unsubstituted analogues.<sup>33</sup> This is not observed for the Buchwald system that undergoes migratory insertion because both ortho positions are substituted with *iso*-propyl groups.<sup>8</sup> No evidence of this C-H activation

has been observed for our diphosphine ligand system, indicating that dissociation of a phosphine arm is not a likely step in the reaction mechanism. It is therefore proposed that the reaction mechanism does not require the dissociation of either the halide or the phosphine, and instead proceeds through a concerted 1,4-insertion or a 1,2-insertion followed by 1,3-allylic migration of the metal center facilitated by weak palladium-aryl interactions. Finally, a 1,4-migratory insertion for this process seems more likely than a 1,2-insertion followed by a 1,3-allylic shift due to the rigidity of the ligand framework, however such a mechanism cannot be ruled out.

The hydride elimination from the dearomatized ring generating **69** is again, an interesting process. Evaluation of the solid state molecular structures of the products resulting upon aryl group migration (**58**, **62-63**) always contain the aryl moiety syn to the metal center. Additionally, evaluation of the NMR spectra for these species shows signals for only one product, indicating that the migration always occurs in a syn conformation; supporting the mechanism described above. This result would prevent hydride elimination from the aryl substituted carbon atom, due to its anti-location with respect to the metal center. It is therefore proposed that a 1,3-hydride migration around the central ring occurs. Similar situations have been previously proposed in the Agapie group.<sup>29</sup> They observe H-atom migration from a nickel metal center to the central arene of their structurally related, *p*-terphenyl diphosphine ligand system. Upon deuterium labeling studies of the ligand backbone, they observed the migration of a non-labeled H-atom from nickel to the arene backbone, and additionally observed H/D scrambling throughout all positions of the central arene. This was attributed to 1,2-H atom shifts occurring over the  $\pi$ -system of the arenium



moiety.<sup>29</sup> If 1,3-hydride migration occurs in our backbone, it would allow for  $\beta$ -hydride elimination and result in the observed product.

### 7.3 Summary

Investigating the oxidative addition of aryl halides to (PterP)Pd (**49**) led to the palladium assisted arylation of the central arene in the ligand framework. The bulky mesityl substituent led to the exclusive formation of the dearomatized, migrated species (Pter<sup>mes</sup>P)PdBr (**58**), while the less bulky substrates, 2-bromotoluene and 2-iodotoluene led to isolation of the square planar oxidative addition products (**60a-b**, **61a-b**). Migration of the toluene substituent required harsher conditions than for the mesityl analogue, indicating that the drive for the migratory insertion is the reduction of steric interactions around the metal center. Reducing the bulk of the aromatic substituent even further to a phenyl group resulted in no observation of the migration event.

It is generally accepted in the literature that these types of migration events are often facilitated by palladium-arene interactions. Attempts to isolate a compound in which such interactions could be observed were unsuccessful. Abstraction of a chloride ligand from (PterP)PdCl<sub>2</sub> (**46**) led to the formation of a dimeric compound, [(PterP)PdCl]<sub>2</sub>•2[BAr<sup>F</sup><sub>4</sub>], **66**. Attempts to avoid dimer dissociation with the goal of forcing arene coordination produced T-shape cationic complex [(PterP)Pd(tol)][OTf], **67**. While the arene was at a comparable distance to a previously reported example, the interaction is farther than most reported examples and is therefore better described as a close contact.

Finally, attempts to observe the reversibility of the migration event were carried out by replacing a halide ligand with a the weaker triflate ligand. Instead of observing the

reversal of the aryl group migration, hydride abstraction was observed, leading to rearomatization of the ligand backbone generating the palladium hydride complex (PterP)Pd(H)OTf, **69**.

## 7.4 Experimental

All manipulations of air and water sensitive compounds were performed under a dry nitrogen atmosphere using an MBraun drybox. Glassware, vials, and stirring bars were dried in an oven at 120 °C overnight and evacuated for 24 h in the antechamber before being brought into the drybox. All solvents were dried by passing through a column of activated alumina, followed by storage over molecular sieves and sodium. Deuterated solvents were purchased from Cambridge Isotope Laboratories. C<sub>6</sub>D<sub>6</sub> was dried by stirring over CaH<sub>2</sub> followed by filtration. CDCl<sub>3</sub> was dried over molecular sieves. All other chemicals were commercially available and used as received. NMR spectra were obtained on Bruker 400 and Bruker 500 spectrometers at ambient temperature. Chemical shift values are reported in ppm relative to residual internal protonated solvent or to a tetramethylsilane standard while using CDCl<sub>3</sub> for <sup>1</sup>H and <sup>13</sup>C{<sup>1</sup>H} experiments. Coupling constants are reported in Hz. Magnetic moments were determined by the Evans method<sup>52-54</sup> using capillaries containing trimethoxybenzene in either CDCl<sub>3</sub> or C<sub>6</sub>D<sub>6</sub> as a reference, and trimethoxybenzene in the sample solution.

**Synthesis of (Pter<sup>mes</sup>)P)PdBr (58).** A toluene solution of (PterP)Pd (48.8 mg, 0.09 mmol) and bromomesitylene (13 μL, 0.09 mmol) was heated to 80 °C for 1h. The volatiles were removed under reduced pressure. The crude residue was triturated with *n*-pentane resulting in the formation of an orange solid (50 mg, 0.07 mmol, 78%). For **58**: <sup>1</sup>H NMR (400 MHz, C<sub>6</sub>D<sub>6</sub>) δ: 0.63 (dd, 3H, *J*<sub>HP</sub> = 12 Hz, *J*<sub>HH</sub> = 8 Hz, CH(CH<sub>3</sub>)<sub>2</sub>), 0.75 (dd, 3H, *J*<sub>HP</sub> =

8 Hz,  $J_{\text{HH}} = 8$  Hz,  $\text{CH}(\text{CH}_3)_2$ ), 1.11 (m, 6H,  $\text{CH}(\text{CH}_3)_2$ ), 1.59 (m, 6H,  $\text{CH}(\text{CH}_3)_2$ ), 1.67, (dd, 3H,  $J_{\text{HP}} = 12$  Hz,  $J_{\text{HH}} = 8$  Hz,  $\text{CH}(\text{CH}_3)_2$ ), 1.91 (dd, 3H,  $J_{\text{HP}} = 12$  Hz,  $J_{\text{HH}} = 4$  Hz,  $\text{CH}(\text{CH}_3)_2$ ), 2.17 (s, 3H, mes- $\text{CH}_3$ ), 2.24 (br s, 3H, mes- $\text{CH}_3$ ), 2.44 (br s, 4 H, mes- $\text{CH}_3$ , overlapping  $\text{CH}(\text{CH}_3)_2$ ), 2.63 (m, 1H,  $\text{CH}(\text{CH}_3)_2$ ), 2.81 (m, 1H,  $\text{CH}(\text{CH}_3)_2$ ), 2.90 (m, 1H,  $\text{CH}(\text{CH}_3)_2$ ), 4.62 (m, 1H,  $\text{CH}(\text{mes})$ ), 5.61 (br s, 1H,  $\text{CH}=\text{CH}-\text{CH}(\text{mes})$ ), 5.65 (app dq,  $J_{\text{HH}} = 8$  Hz,  $J_{\text{HH}} = 4$  Hz, 1H,  $\text{CH}=\text{CH}-\text{CH}(\text{mes})$ ), 6.72 (m, 1H,  $\text{C}(\text{Ph})=\text{CH}-\text{CH}(\text{mes})$ ), 6.79 (s, 2H, ArH), 6.93 (m, 1H, ArH), 6.96 (m, 2H, ArH), 7.11 (t, 1H,  $J_{\text{HH}} = 4$  Hz, ArH), 7.14 (m, 1H, ArH), 7.25 (m, 2H, ArH), 7.76 (d, 1H,  $J_{\text{HH}} = 8$  Hz, ArH).  $^{13}\text{C}$   $\{^1\text{H}\}$  NMR (100 MHz,  $\text{C}_6\text{D}_6$ )  $\delta$ : 16.82 (dd,  $J_{\text{CP}} = 6$  Hz,  $J_{\text{CP}} = 2$  Hz,  $\text{CHCH}_3$ ), 18.06 (s,  $\text{CHCH}_3$ ), 19.04 (d,  $J_{\text{CP}} = 1$  Hz,  $\text{C}_6\text{H}_2(\text{CH}_3)_3$ ), 19.19 (d,  $J_{\text{CP}} = 5$  Hz,  $\text{CHCH}_3$ ), 19.58 (d,  $J_{\text{CP}} = 2$  Hz,  $\text{CHCH}_3$ ), 19.97 (d,  $J_{\text{CP}} = 4$  Hz,  $\text{CHCH}_3$ ), 20.23 (s,  $\text{C}_6\text{H}_2(\text{CH}_3)_3$ ), 20.88 (s,  $\text{C}_6\text{H}_2(\text{CH}_3)_3$ ), 22.96 (d,  $J_{\text{CP}} = 2$  Hz,  $\text{CHCH}_3$ ), 23.11 (d,  $J_{\text{CP}} = 3$  Hz,  $\text{CHCH}_3$ ), 24.63 (d,  $J_{\text{CP}} = 5$  Hz,  $\text{CHCH}_3$ ), 24.73 (d,  $J_{\text{CP}} = 5$  Hz,  $\text{CHCH}_3$ ), 26.97 (dd,  $J_{\text{CP}} = 11$  Hz,  $J_{\text{CP}} = 5$  Hz,  $\text{CHCH}_3$ ), 27.83 (d,  $J_{\text{CP}} = 19$  Hz,  $\text{CHCH}_3$ ), 40.7 (s,  $\text{CH}(\text{mes})$ ), 123.93 (d,  $J_{\text{CP}} = 5$  Hz, ArC), 125.95 (s, ArC), 125.99 (s, ArC), 126.10 (s, ArC), 126.91 (d,  $J_{\text{CP}} = 4$  Hz, ArC), 128.35 (s, ArC), 128.82 (s, ArC), 128.98 (s, ArC), 129.30 (s, ArC), 129.47 (br s, ArC), 130.36 (s, ArC), 130.62 (s, ArC), 130.94 (br s, ArC), 131.64 (d,  $J_{\text{CP}} = 2$  Hz, ArC), 133.33 (d,  $J_{\text{CP}} = 6$  Hz, ArC), 132.81 (s, ArC), 133.86 (s, ArC), 135.45 (s, ArC), 135.88 (s, ArC), 136.79 (s, ArC), 145.18 (d,  $J_{\text{CP}} = 8$  Hz, ArC), 151.49 (d,  $J_{\text{CP}} = 15.6$  Hz, ArC), 160.19 (d,  $J_{\text{CP}} = 26$  Hz, ArC).  $^{31}\text{P}\{^1\text{H}\}$  NMR (162 MHz,  $\text{C}_6\text{D}_6$ )  $\delta$ : 27.42 (d,  $J_{\text{PP}} = 288$  Hz), 49.05 (d,  $J_{\text{PP}} = 288$  Hz).

**Synthesis of (Pter<sup>mes</sup>P)Pd (**59**).** Potassium bis(trimethylsilyl) amide (KHMDs, 8.8 mg, 0.04 mmol) was added to an  $\text{Et}_2\text{O}$  solution of (Pter<sup>mes</sup>P)PdBr (**58**, 33.7 mg, 0.04 mmol). The mixture was allowed to stir for 1 h followed by removal of the volatiles under reduced

pressure. The crude residue was dissolved in *n*-pentane and filtered over a pad of celite. The solution was cooled to -35°C to induce crystallization of **59** (23.3 mg, 0.03 mmol, 77%). For **59**:  $^1\text{H}$  NMR (400 MHz,  $\text{C}_6\text{D}_6$ )  $\delta$ : 0.92 (m, 6 H,  $\text{CH}(\text{CH}_3)$ ), 1.06 (m, 12 H,  $\text{CH}(\text{CH}_3)_2$ ), 1.21 (m, 6 H,  $\text{CH}(\text{CH}_2)_3$ ), 1.99 (m, 1 H,  $\text{CH}(\text{CH}_3)_2$ ), 2.09 (m, 2 H,  $\text{CH}(\text{CH}_3)_2$ ), obscured by mesityl-Me), 2.12 (s, 3 H, mes- $\text{CH}_3$ ), 2.15 (s, 3 H, mes- $\text{CH}_3$ ), 2.12 (m, 1 H,  $\text{CH}(\text{CH}_3)_2$ , obscured by mesityl-Me), 2.56 (s, 3 H, mes- $\text{CH}_3$ ), 6.81 (s, 1 H, ArH), 6.90 (m, 5 H, ArH), 7.01 (m, 5 H, ArH), 7.13 (m, 2 H, ArH, overlapping solvent), 7.49 (d, 2 H,  $J_{\text{HH}} = 4$  Hz, ArH).  $^{31}\text{P}\{^1\text{H}\}$  NMR (162 MHz,  $\text{C}_6\text{D}_6$ )  $\delta$ : 32.88 (d,  $J_{\text{PP}} = 175$ ), 34.44 (d,  $J_{\text{PP}} = 177$  Hz).  $^{13}\text{C}\{^1\text{H}\}$  NMR (100 MHz,  $\text{C}_6\text{D}_6$ )  $\delta$ : 17.42 (s, mes- $\text{CH}_3$ ), 18.06 (s, mes- $\text{CH}_3$ ), 21.01 (s,  $\text{CH}(\text{CH}_3)_2$ ), 21.07 (d,  $J_{\text{CP}} = 4$  Hz,  $\text{CH}(\text{CH}_3)_2$ ), 21.19 (s, mes- $\text{CH}_3$ ), 21.37 (d,  $J_{\text{CP}} = 3$  Hz,  $\text{CH}(\text{CH}_3)_2$ ), 21.51 (br s,  $\text{CH}(\text{CH}_3)_2$ ), 21.57 (t,  $J_{\text{CP}} = 2$  Hz,  $\text{CH}(\text{CH}_3)$ ), 22.04 (d,  $J_{\text{CP}} = 10$  Hz,  $\text{CH}(\text{CH}_3)_2$ ), 22.36 (s,  $\text{CH}(\text{CH}_3)_2$ ), 22.53 (t,  $J_{\text{CP}} = 3$  Hz,  $\text{CH}(\text{CH}_3)_2$ ), 22.67 (d,  $J_{\text{CP}} = 10$  Hz,  $\text{CH}(\text{CH}_3)_2$ ), 22.98 (sd,  $J_{\text{CP}} = 12$  Hz,  $J_{\text{CP}} = 3$  Hz,  $\text{CH}(\text{CH}_3)_2$ ), 27.16 (t,  $J_{\text{CP}} = 6$  Hz,  $\text{CH}(\text{CH}_3)_2$ ), 28.60 (t,  $J_{\text{CP}} = 6$  Hz,  $\text{CH}(\text{CH}_3)_2$ ), 125.02 (s, ArC), 125.82 (d,  $J_{\text{CP}} = 2$  Hz, ArC), 126.04 (d,  $J_{\text{CP}} = 2$  Hz, ArC), 127.14 (s, ArC), 127.23 (s, ArC), two peaks obscured by solvent, 128.45 (s, ArC), 128.56 (s, ArC), 131.06 (s, ArC), 132.08 (s, ArC), 132.14 (s, ArC), 132.25 (s, ArC), 132.36 (s, ArC), 132.51 (s, ArC), 132.59 (s, ArC), 135.52 (s, ArC), 136.43 (s, ArC), 136.66 (s, ArC), 137.51 (s, ArC), 139.98 (s, ArC), 140.24 (dd,  $J_{\text{CP}} = 16$  Hz,  $J_{\text{CP}} = 4$  Hz, ArC), 140.81 (dd,  $J_{\text{CP}} = 17$  Hz,  $J_{\text{CP}} = 4$  Hz, ArC), 149.37 (dd,  $J_{\text{CP}} = 20$  Hz,  $J_{\text{CP}} = 4$  Hz, ArC), 150.13 (dd,  $J_{\text{CP}} = 21$  Hz,  $J_{\text{CP}} = 5$  Hz, ArC).

**Synthesis of (PterP)PdBr(tol) (60a-b).** To an ether solution of (PterP)Pd (86.3 mg, 0.15 mmol) was added 2-bromotoluene (19  $\mu\text{L}$ , 0.16 mmol). The mixture was allowed to stir for 1 h. The volatiles were removed under reduced pressure. The crude powder was

trituated with *n*-pentane resulting in the compound as a yellow powder (75.2 mg, 0.10 mmol, 68%). Characterization by NMR spectroscopy revealed a mixture of syn and anti isomers. Heating the C<sub>6</sub>D<sub>6</sub> solution of the mixture resulted in almost full conversion to the syn isomer. For **60a**: <sup>1</sup>H NMR (400 MHz, C<sub>6</sub>D<sub>6</sub>, anti-isomer) δ: 1.12 (app q, 8 H, *J* = 6 Hz, CH(CH<sub>3</sub>)<sub>2</sub> overlaps CH(CH<sub>3</sub>)<sub>2</sub>), 1.30 (app d, 15 H, *J* = 6 Hz, CH(CH<sub>3</sub>)<sub>2</sub>), 1.46 (obscured by major isomer, 3 H, CH(CH<sub>3</sub>)<sub>2</sub>), 2.76 (s, 3H, C<sub>6</sub>H<sub>4</sub>(CH<sub>3</sub>)), 3.52 (br m, 2H, CH(CH<sub>3</sub>)<sub>2</sub>), 4.37 (d, 1H, *J*<sub>HH</sub> = 8 Hz, ArH), 5.84 (t, 1H, *J*<sub>HH</sub> = 8 Hz, ArH), 6.50 (br m, 2H, ArH), 6.56 (t, 1H, *J*<sub>HH</sub> = 6 Hz, ArH), 6.64 (d, 1H, *J*<sub>HH</sub> = 9 Hz, ArH), 6.84 (br s, 2H, ArH), 7.02 (t, 2H, *J*<sub>HH</sub> = 7 Hz, ArH), 7.20 (obscured by major isomer, 4 H, ArH), 7.31 (obscured by major isomer, 2 H, ArH). For **60b**: <sup>1</sup>H NMR (400 MHz, C<sub>6</sub>D<sub>6</sub>, syn-isomer) δ: 0.28 (app q, 6 H, *J* = 8 Hz, CH(CH<sub>3</sub>)<sub>2</sub>), 1.05 (app q, 6 H, *J* = 8 Hz, CH(CH<sub>3</sub>)<sub>2</sub>), 1.52 (app q, 6 H, *J* = 8 Hz, CH(CH<sub>3</sub>)<sub>2</sub>), 1.66 (app q, 6 H, *J* = 8 Hz, CH(CH<sub>3</sub>)<sub>2</sub>), 2.43 (m, 2H, CH(CH<sub>3</sub>)<sub>2</sub>), 2.75 (s, 3H, C<sub>6</sub>H<sub>4</sub>(CH<sub>3</sub>)), 3.48 (m, 2H, CH(CH<sub>3</sub>)<sub>2</sub>), 4.56 (d, 1H, *J*<sub>HH</sub> = 6 Hz, ArH), 6.53 (br m, 1H, ArH), 6.69 (m, 2H, ArH), 7.17 (m, 6 H, ArH), 7.28 (dd, 2 H, *J*<sub>HH</sub> = 4 Hz, *J*<sub>HH</sub> = 6 Hz, ArH), 7.52 (dd, 2 H, *J*<sub>HH</sub> = 4 Hz, *J*<sub>HH</sub> = 6 Hz, ArH), 7.56 (m, 2 H, ArH). <sup>13</sup>C {<sup>1</sup>H} NMR (100 MHz, CDCl<sub>3</sub>, syn-isomer) δ: 16.52 (s, C<sub>6</sub>H<sub>4</sub>(CH<sub>3</sub>)), 20.11 (t, *J*<sub>CP</sub> = 2 Hz, CH(CH<sub>3</sub>)<sub>2</sub>), 20.33 (s, CH(CH<sub>3</sub>)<sub>2</sub>), 25.15 (t, *J*<sub>CP</sub> = 10 Hz, CH(CH<sub>3</sub>)<sub>2</sub>), 25.41 (t, *J*<sub>CP</sub> = 8 Hz, CH(CH<sub>3</sub>)<sub>2</sub>), 26.34 (t, *J*<sub>CP</sub> = 8 Hz, CH(CH<sub>3</sub>)<sub>2</sub>), 26.57 (s, CH(CH<sub>3</sub>)<sub>2</sub>), 122.45 (s, ArC), 124.82 (s, ArC), 126.28 (t, *J*<sub>CP</sub> = 2 Hz, ArC), 126.80 (s, ArC), 127.13 (s, ArC), 127.17 (s, ArC), 130.59 (s, ArC), 131.18 (s, ArC), 132.50 (s, ArC), 134.63 (t, *J*<sub>CP</sub> = 10 Hz, ArC), 135.75 (t, *J*<sub>CP</sub> = 4 Hz), 136.53 (t, *J*<sub>CP</sub> = 34 Hz, ArC), 143.82 (s, ArC), 144.32 (t, *J*<sub>CP</sub> = 14 Hz, ArC), 150.94 (s, ArC). For **60a**: <sup>31</sup>P{<sup>1</sup>H} NMR (162 MHz, C<sub>6</sub>D<sub>6</sub>, anti-isomer) δ: 32.54 (s). For **60b**: <sup>31</sup>P{<sup>1</sup>H} NMR (162 MHz, C<sub>6</sub>D<sub>6</sub>, syn-isomer) δ: 28.75 (s).

**Synthesis of (PterP)PdI(tol) (61a-b).** To an ether solution of (PterP)Pd (71.5.7 mg, 0.13 mmol) was added 2-iodotoluene (18  $\mu$ L, 0.14 mmol). The mixture was allowed to stir for 1h. The volatiles were removed under reduced pressure. The crude powder was triturated with *n*-pentane resulting in the compound as a yellow powder (79.0 mg, 0.11 mmol, 87%). Characterization by NMR spectroscopy revealed a mixture of syn and anti isomers. Heating the C<sub>6</sub>D<sub>6</sub> solution of the mixture resulted in full conversion to the syn-isomer. For **61b**: <sup>1</sup>H NMR (400 MHz, CDCl<sub>3</sub>, syn-isomer)  $\delta$ : 0.25 (app q, 6 H,  $J$  = 8 Hz, CH(CH<sub>3</sub>)<sub>2</sub>), 1.07 (app q, 6 H,  $J$  = 6 Hz, CH(CH<sub>3</sub>)<sub>2</sub>), 1.54 (app q, 6 H,  $J$  = 6 Hz, CH(CH<sub>3</sub>)<sub>2</sub>), 1.62 (app q, 6 H,  $J$  = 8 Hz, CH(CH<sub>3</sub>)<sub>2</sub>), 2.48 (m, 2 H, CH(CH<sub>3</sub>)<sub>2</sub>), 2.70 (s, 3 H, C<sub>6</sub>H<sub>4</sub>(CH<sub>3</sub>)), 3.68 (m, 2 H, CH(C<sub>3</sub>)<sub>2</sub>), 4.57 (d, 1 H,  $J_{\text{HH}}$  = ArH), 6.55 (t, 1 H,  $J_{\text{HH}}$  = 8 Hz, ArH), 6.65 (d, 1 H,  $J_{\text{HH}}$  = 8 H, ArH), 6.71 (t, 1 H,  $J_{\text{HH}}$  = 8 Hz, ArH), 7.18 (m, 6H, ArH), 7.26 (dd, 2 H,  $J_{\text{HH}}$  = 6 Hz,  $J_{\text{HH}}$  = 3 Hz, ArH), 7.50 (dd, 2 H,  $J_{\text{HH}}$  = 6 Hz,  $J_{\text{HH}}$  = 3 Hz, ArH), 7.56 (m, 2 H, ArH). For **61b**: <sup>13</sup>C {<sup>1</sup>H} NMR (100 MHz, CDCl<sub>3</sub>, syn-isomer)  $\delta$ : 16.57 (s, CH(CH<sub>3</sub>)<sub>2</sub>), 20.50 (s, CH(CH<sub>3</sub>)<sub>2</sub>), 20.58 (t,  $J_{\text{CP}}$  = 2 Hz, (CH(CH<sub>3</sub>)<sub>2</sub>), 24.99 (t,  $J_{\text{CP}}$  = 8 Hz, CH(CH<sub>3</sub>)<sub>2</sub>), 25.80 (s, C<sub>6</sub>H<sub>4</sub>(CH<sub>3</sub>)), 26.36 (t,  $J_{\text{CP}}$  = 9 Hz, CH(CH<sub>3</sub>)<sub>2</sub>), 26.86 (t,  $J_{\text{CP}}$  = 10 Hz, CH(CH<sub>3</sub>)<sub>2</sub>), 125.25 (s, ArC), 126.40 (s, ArC), 127.02 (s, ArC), 127.12 (s, ArC), 127.30 (s, ArC), 130.37 (s, ArC), 132.68 (s, ArC), 134.83 (t,  $J_{\text{CP}}$  = 4 Hz, ArC), 135.92 (t,  $J_{\text{CP}}$  = 4 Hz, ArC), 137.34 (t,  $J_{\text{CP}}$  = 18 Hz, ArC), 142.06 (s, ArC), 143.73 (s, ArC), 144.20 (t,  $J_{\text{CP}}$  = 8 Hz, ArC), 151.35 (s, ArC). For **61b**: <sup>31</sup>P{<sup>1</sup>H} NMR (162 MHz, CDCl<sub>3</sub> syn-isomer)  $\delta$ : 26.63 (s).

**Synthesis of (Pter<sup>tol</sup>P)PdBr (62).** Compound (PterP)PdBr(tol) (53.0 mg, 0.07 mmol) was dissolved in toluene and transferred to a schlenk flask. The solution was heated to 120 °C for 12 h. The solvent was removed under reduced pressure leaving behind the crude residue of (Pter(tol)P)PdBr. The residue was triturated with *n*-pentane resulting in

the formation of a yellow powder (49.9 mg, 0.07 mmol, 94%). For **62**:  $^1\text{H}$  NMR (400 MHz,  $\text{C}_6\text{D}_6$ )  $\delta$ : 0.57 (m, 6 H,  $\text{CH}(\text{CH}_3)_2$ ), 1.11 (m, 6 H,  $\text{CH}(\text{CH}_3)_2$ ), 1.58 (m, 9 H,  $\text{CH}(\text{CH}_3)_2$ ), 1.85 (dd, 3 H,  $J_{\text{HP}} = 16$  Hz,  $J_{\text{HH}} = 8$  Hz,  $\text{CH}(\text{CH}_3)$ ), 2.12 (s, 3 H,  $\text{C}_6\text{H}_4(\text{CH}_3)$ ), 2.40 (m, 1 H,  $\text{CH}(\text{CH}_3)_2$ ), 2.70 (m, 2 H,  $\text{CH}(\text{CH}_3)_2$ ), 2.94 (m, 1 H,  $\text{CH}(\text{CH}_3)_2$ ), 4.36 (br d, 1H,  $J_{\text{HH}} = 4$  Hz,  $\text{CH}(\text{tol})$ ), 5.45 (s, 1 H,  $\text{C}=\text{CH}-\text{CH}(\text{tol})$ ), 5.54 (d, 1 H,  $J_{\text{HH}} = 12$  Hz,  $\text{C}(\text{Ph})=\text{CH}-\text{CH}(\text{tol})$ ), 6.61 (m, 1 H,  $\text{ArH}$ ), 6.93 (m, 3 H,  $\text{ArH}$ ), 7.02 (m, 1 H,  $\text{ArH}$ ), 7.05 (t, 1 H,  $J_{\text{HH}} = 8$  Hz,  $\text{ArH}$ ), 7.11 (m, 3 H,  $\text{ArH}$ ), 7.20 (m, 1 H,  $\text{ArH}$ ), 7.30 (t, 1 H,  $J_{\text{HH}} = 8$  Hz,  $\text{ArH}$ ), 7.37 (d, 1 H,  $J_{\text{HH}} = 8$  Hz,  $\text{ArH}$ ), 7.80 (d, 1 H,  $J_{\text{HH}} = 8$  Hz,  $\text{ArH}$ ).  $^{31}\text{P}\{^1\text{H}\}$  NMR (162 MHz,  $\text{C}_6\text{D}_6$ )  $\delta$ : 28.64 (d,  $J_{\text{PP}} = 363$  Hz), 52.22 (d,  $J_{\text{PP}} = 366$  Hz).

**Synthesis of (Pter<sup>tol</sup>P)PdI (63).** Compound (PterP)PdI(tol) (40.0 mg, 0.06 mmol) was dissolved in toluene and transferred to a schlenk flask. The solution was heated to 120 °C for 12 h. The solvent was removed under reduced pressure leaving behind the crude residue of (Pter(tol)P)PdI. The residue was triturated with *n*-pentane resulting in the formation of a yellow powder (38 mg, 0.05 mmol, 95%). For **63**:  $^1\text{H}$  NMR (400 MHz,  $\text{C}_6\text{D}_6$ )  $\delta$ : 0.44 (m, 6 H,  $\text{CH}(\text{CH}_3)_2$ ), 1.10 (m, 6 H,  $\text{CH}(\text{CH}_3)_2$ ), 1.37 (dd, 3 H,  $J_{\text{HP}} = 12$  Hz,  $J_{\text{HH}} = 8$  Hz,  $\text{CH}(\text{CH}_3)_2$ ), 1.50 (dd, 3 H,  $J_{\text{HP}} = 16$  Hz,  $J_{\text{HH}} = 8$  Hz,  $\text{CH}(\text{CH}_3)_2$ ), 1.64 (dd, 3 H,  $J_{\text{HP}} = 16$  Hz,  $J_{\text{HH}} = 8$  Hz,  $\text{CH}(\text{CH}_3)_2$ ), 1.75 (dd, 3 H,  $J_{\text{HP}} = 12$  Hz,  $J_{\text{HH}} = 8$  Hz,  $\text{CH}(\text{CH}_3)_2$ ), 2.08 (s, 3 H,  $\text{C}_6\text{H}_4(\text{CH}_3)$ ), 2.15 (m, 1 H,  $\text{CH}(\text{CH}_3)_2$ ), 2.71 (m, 1 H,  $\text{CH}(\text{CH}_3)_2$ ), 2.92 (m, 1 H,  $\text{CH}(\text{CH}_3)_2$ ), 3.05 (br m, 1 H,  $\text{CH}(\text{CH}_3)_2$ ), 4.23 (br d, 1 H,  $J_{\text{HH}} = 8$  Hz,  $\text{CH}(\text{tol})$ ), 5.42 (br s, 1 H,  $\text{C}=\text{CH}-\text{CH}(\text{tol})$ ), 5.53 (br d, 1 H,  $J_{\text{HH}} = 12$  Hz,  $J_{\text{HH}} = 4$  Hz,  $\text{C}(\text{Ph})=\text{CH}-\text{CH}(\text{tol})$ ), 6.42 (m, 1 H,  $\text{ArH}$ ), 6.87 (m, 3 H,  $\text{ArH}$ ), 7.01 (m, 2 H,  $\text{ArH}$ ), 7.13 (m, 5 H,  $\text{ArH}$ ), 7.27 (m, 2 H,  $\text{ArH}$ ), 7.77 (d, 1 H,  $J_{\text{HH}} = 8$  Hz,  $\text{ArH}$ ).  $^{13}\text{C}$   $\{^1\text{H}\}$  NMR (100 MHz,  $\text{C}_6\text{D}_6$ )  $\delta$ : 18.11 (s,  $\text{CH}(\text{CH}_3)_2$ ), 18.45 (s,  $\text{CH}(\text{CH}_3)_2$ ), 19.33 (s,  $\text{C}_6\text{H}_4(\text{CH}_3)$ ), 19.36 (s,  $\text{CH}(\text{CH}_3)_2$ ), 20.05 (br d,

$J_{\text{CP}} = 8 \text{ Hz}$ ,  $\text{CH}(\text{CH}_3)_2$ ), 20.34 (s,  $\text{CH}(\text{CH}_3)_2$ ), 20.53 (d,  $J_{\text{CP}} = 3 \text{ Hz}$ ,  $\text{CH}(\text{CH}_3)_2$ ), 20.63 (d,  $J_{\text{CP}} = 5 \text{ Hz}$ ,  $\text{CH}(\text{CH}_3)_2$ ), 23.77 (dd,  $J_{\text{CP}} = 13 \text{ Hz}$ ,  $J_{\text{CP}} = 6 \text{ Hz}$ ,  $\text{CH}(\text{CH}_3)_2$ ), 24.56 (d,  $J_{\text{CP}} = 20 \text{ Hz}$ ,  $\text{CH}(\text{CH}_3)_2$ ), 26.07 (dd,  $J_{\text{CP}} = 15 \text{ Hz}$ ,  $J_{\text{CP}} = 6 \text{ Hz}$ ,  $\text{CH}(\text{CH}_3)_2$ ), 28.05 (d,  $J_{\text{CP}} = 25 \text{ Hz}$ ,  $\text{CH}(\text{CH}_3)_2$ ), 41.23 (s,  $\text{CH}(\text{tol})$ ), 119.83 (d,  $J_{\text{CP}} = 6 \text{ Hz}$ ,  $\text{C}(\text{Ph})=\text{CH}-\text{CH}(\text{tol})$ ), 126.21 (d,  $J_{\text{CP}} = 4 \text{ Hz}$ ,  $\text{C}=\text{CH}-\text{CH}(\text{tol})$ ), 126.44 (s,  $\text{C}_6\text{H}_3(\text{tol})$ ), 124.44 (s, ArC), 126.75 (s, ArC), 127.91 (s, ArC), 128.91 (s, ArC), 128.97 (s, ArC), 129.61 (s, ArC), 130.60 (d,  $J_{\text{CP}} = 7 \text{ Hz}$ , ArC), 131.69 (d,  $J_{\text{CP}} = 2 \text{ Hz}$ ,  $\text{C}_6\text{H}_3(\text{tol})$ ), 132.71 (s, ArC), 135.13 (s, ArC), 136.51 (s, ArC), 141.84 (s, ArC), 143.09 (d,  $J_{\text{CP}} = 11 \text{ Hz}$ , ArC), 152.11 (d,  $J_{\text{CP}} = 19 \text{ Hz}$ , ArC), 160.42 (d,  $J_{\text{CP}} = 22 \text{ Hz}$ , ArC).  $^{31}\text{P}\{^1\text{H}\}$  NMR (162 MHz,  $\text{C}_6\text{D}_6$ )  $\delta$ : 30.34 (d,  $J_{\text{PP}} = 356 \text{ Hz}$ ), 54.42 (d,  $J_{\text{PP}} = 356 \text{ Hz}$ ).

**Synthesis of (Pter<sup>tol</sup>P)Pd (64).** Potassium bis(trimethylsilyl) amide (KHMDs, 12.4 mg, 0.06 mmol) was added to an  $\text{Et}_2\text{O}$  solution of (Pter<sup>tol</sup>P)PdBr (**62**, 46.0 mg, 0.06 mmol). The mixture was allowed to stir for 1 hour followed by removal of the volatiles under reduced pressure. The crude residue was dissolved in *n*-pentane and filtered over a pad of celite. The solution was cooled to  $-35^\circ\text{C}$  to induce crystallization of **64** (25.6 mg, 0.04 mmol, 72%).  $^1\text{H}$  NMR (400 MHz,  $\text{C}_6\text{D}_6$ )  $\delta$ : 0.94-1.23 (m, 24 H,  $\text{CH}(\text{CH}_3)_2$ ), 2.12 (m, 4 H,  $\text{CH}(\text{CH}_3)_2$ ), 2.45 (s,  $\text{C}_6\text{H}_4(\text{CH}_3)$ ), 6.93 (t, 2 H,  $J_{\text{HH}} = 4 \text{ Hz}$ , ArH), 7.02 (m, 3 H, ArH), 7.11 (br s, 2 H, ArH), 7.12 (br s, 1 H, ArH), 7.17 (m, 3 H, ArH, overlapping with solvent), 7.38 (m, 1 H, ArH), 7.49 (d, 2 H,  $J_{\text{HH}} = 8 \text{ Hz}$ , ArH).  $^{31}\text{P}\{^1\text{H}\}$  NMR (162 MHz,  $\text{C}_6\text{D}_6$ )  $\delta$ : 33.56 (d,  $J_{\text{PP}} = 217 \text{ Hz}$ ), 35.1 (d,  $J_{\text{PP}} = 217 \text{ Hz}$ ).

**Synthesis of (PterP)PdBrPh (65).** To an  $\text{Et}_2\text{O}$  solution of (PterP)Pd (**49**, 25.0 mg, 0.04 mmol) was added bromobenzene (4.6  $\mu\text{L}$ , 0.04 mmol). The mixture was allowed to stir for 1 hour resulting in the precipitation of (PterP)PdBrPh. The solution was decanted,



and the yellow powder washed with *n*-pentane leaving the clean powder of **65** (26.4 mg, 0.04 mmol, 90%).  $^1\text{H}$  NMR (400 MHz,  $\text{C}_6\text{D}_6$ )  $\delta$ : 0.99 (app q, 6 H,  $J = 8$  Hz,  $\text{CH}(\text{CH}_3)_2$ ), 1.06 (app q, 6 H,  $J = 8$  Hz,  $\text{CH}(\text{CH}_3)_2$ ), 1.38 (m, 2 H,  $\text{CH}(\text{CH}_3)_2$ ), 1.50 (app q, 6 H,  $J = 8$  Hz,  $\text{CH}(\text{CH}_3)_2$ ), 1.64 (app q, 6 H,  $J = 8$  Hz,  $\text{CH}(\text{CH}_3)_2$ ), 3.77 (m, 2 H,  $\text{CH}(\text{CH}_3)_2$ ), 4.51 (d, 1 H,  $J_{\text{HH}} = 8$  Hz, *ArH*), 6.21 (t, 1 H,  $J_{\text{HH}} = 8$  Hz, *ArH*), 6.68 (d, 1 H,  $J_{\text{HH}} = 8$  Hz, *ArH*), 6.81 (m, 5 H, *ArH*), 7.02 (m, 2 H, *ArH*), 7.32 (m, 6 H, *ArH*), 7.80 (d, 1 H,  $J_{\text{HH}} = 8$  Hz, *ArH*).  $^{13}\text{C}$   $\{^1\text{H}\}$  NMR (100 MHz,  $\text{C}_6\text{D}_6$ )  $\delta$ : 20.16 (t,  $J_{\text{CP}} = 2$  Hz,  $\text{CH}(\text{CH}_3)_2$ ), 20.78 (t,  $J_{\text{CP}} = 2$  Hz,  $\text{CH}(\text{CH}_3)_2$ ), 21.08 (s,  $\text{CH}(\text{CH}_3)_2$ ), 24.09 (t,  $J_{\text{CP}} = 7$  Hz,  $\text{CH}(\text{CH}_3)_2$ ), 24.46 (t,  $J_{\text{CP}} = 9$  Hz,  $\text{CH}(\text{CH}_3)_2$ ), 29.31 (t,  $J_{\text{CP}} = 10$  Hz,  $\text{CH}(\text{CH}_3)_2$ ), 122.57 (s, *ArC*), 124.60 (s, *ArC*), 125.86 (t,  $J_{\text{CP}} = 3$  Hz, *ArC*), 126.13 (s, *ArC*), 127.12 (s, *ArC*), 131.42 (s, *ArC*), 131.86 (s, *ArC*), 135.16 (t,  $J_{\text{CP}} = 4$  Hz, *ArC*), 136.43 (t,  $J_{\text{CP}} = 15$  Hz, *ArC*), 137.48 (t,  $J_{\text{CP}} = 3$  Hz, *ArC*), 138.62 (t,  $J_{\text{CP}} = 4$  Hz, *ArC*), 141.94 (s, *ArC*), 145.63 (t,  $J_{\text{CP}} = 8$  Hz, *ArC*), 152.83 (s, *ArC*).  $^{31}\text{P}\{^1\text{H}\}$  NMR (162 MHz,  $\text{C}_6\text{D}_6$ )  $\delta$ : 33.68 (s).

**Synthesis of [(PterP)PdCl]<sub>2</sub>[2BAr<sup>F</sup><sub>4</sub>] (**66**).** To a toluene solution of (PterP)PdCl<sub>2</sub> (**46**, 21.8 mg, 0.04 mmol) was added NaBAr<sup>F</sup><sub>4</sub> (33.7 mg, 0.04 mmol). The mixture was stirred for 1 h resulting in the formation of a red precipitate. The volatiles were removed under reduced pressure, followed by trituration of the crude residue with *n*-pentane. The product was redissolved in DCM, and layered with *n*-pentane and stored at -35°C to induce crystallization (35.8 mg, 0.02 mmol, 64%). For **66**:  $^1\text{H}$  NMR (400 MHz,  $\text{CD}_2\text{Cl}_2$ )  $\delta$ : 1.16 (br m, 12 H,  $\text{CH}(\text{CH}_3)_2$ ), 1.35 (br m, 5 H,  $\text{CH}(\text{CH}_3)_2$ ), 1.72 (br s, 6 H,  $\text{CH}(\text{CH}_3)_2$ ), 2.27 (br s, 2 H,  $\text{CH}(\text{CH}_3)_2$ ), 2.53 (m, 2 H,  $\text{CH}(\text{CH}_3)_2$ ), 7.11 (br s, 2 H, *ArH*), 7.33 (br m, 5 H, *ArH*), 7.41 (br m, 2 H, *ArH*), 7.55 (s, 4 H, *ArH*), 7.67 (m, 2 H, *ArH*), 7.71 (s, 8 H, *ArH*).  $^{13}\text{C}$   $\{^1\text{H}\}$  NMR (100 MHz,  $\text{CD}_2\text{Cl}_2$ )  $\delta$ : 21.16 (s,  $\text{CH}(\text{CH}_3)_2$ ), 21.80 (s,  $\text{CH}(\text{CH}_3)_2$ ), 22.39 (s,

CH(CH<sub>3</sub>)<sub>2</sub>), 23.18 (br s, CH(CH<sub>3</sub>)<sub>2</sub>), 28.26 (br s, CH(CH<sub>3</sub>)<sub>2</sub>), 30.03 (br s, CH(CH<sub>3</sub>)<sub>2</sub>), 117.89 (app t,  $J_{\text{CP}} = 5$  Hz, ArC), 120.93 (s, ArC), 123.64 (s, ArC), 126.35 (s, ArC), 127.79 (app d,  $J = 5$  Hz, ArC), 129.06 (br s, ArC), 129.43 (br s, ArC), 129.69 (s, ArC), 131.94 (br s, ArC), 132.79 (s, ArC), 133.03 (s, ArC), 134.41 (d,  $J = 8$  Hz, ArC), 135.20 (s, ArC), 140.28 (s, ArC), 146.05 (d,  $J = 13$  Hz, ArC), 162.15 (q,  $J_{\text{CB}} = 50$  Hz, ArC). <sup>31</sup>P{<sup>1</sup>H} NMR (162 MHz, CD<sub>2</sub>Cl<sub>2</sub>) δ: 47.77 (br s). <sup>11</sup>B{<sup>1</sup>H} NMR (128 MHz, CD<sub>2</sub>Cl<sub>2</sub>) δ: -6.62 (s). <sup>19</sup>F{<sup>1</sup>H} NMR (376 MHz, CD<sub>2</sub>Cl<sub>2</sub>) δ: -65.86 (s).

**Synthesis of [(PterP)Pd(tol)][OTf] (67).** To an ether solution of (PterP)PdI(tol) (25 mg, 0.04 mmol) was added 1 equivalent of AgOTf (9.2 mg, 0.04 mmol). The mixture was allowed to stir for 1 h followed by removal of the volatiles under reduced pressure. The crude residue was washed with ether. The final product was extracted with DCM and filtered. The solution was layered with *n*-pentane and stored at -35°C to induce recrystallization (22.5 mg, 0.03 mmol, 87%). For **67**: <sup>1</sup>H NMR (400 MHz, CD<sub>2</sub>Cl<sub>2</sub>) δ: 0.76 (app q, 6 H,  $J = 8$  Hz, CH(CH<sub>3</sub>)<sub>2</sub>), 1.05 (app q, 6 H,  $J = 8$  Hz, CH(CH<sub>3</sub>)<sub>2</sub>), 1.19 (app q, 6 H,  $J = 8$  Hz, CH(CH<sub>3</sub>)<sub>2</sub>), 1.47 (app q, 6 H,  $J = 8$  Hz, CH(CH<sub>3</sub>)<sub>2</sub>), 2.08 (s, 3H, C<sub>6</sub>H<sub>4</sub>(CH<sub>3</sub>)), 2.49 (m, 4 H, CH(CH<sub>3</sub>)<sub>2</sub>), 6.83 (m, 1 H, ArH), 6.92 (m, 3 H, ArH), 7.46 (m, 8 H, ArH), 7.71 (m, 4 H, ArH). <sup>13</sup>C {<sup>1</sup>H} NMR (100 MHz, CD<sub>2</sub>Cl<sub>2</sub>) δ: 17.65 (s, CH(CH<sub>3</sub>)<sub>2</sub>), 18.26 (s, C<sub>6</sub>H<sub>4</sub>(CH<sub>3</sub>), 19.74 (s, CH(CH<sub>3</sub>)<sub>2</sub>), 19.80 (s, CH(CH<sub>3</sub>)<sub>2</sub>), 21.74 (t,  $J_{\text{CP}} = 11$  Hz, CH(CH<sub>3</sub>)<sub>2</sub>), 26.57 (s, CH(CH<sub>3</sub>)<sub>2</sub>), 28.89 (t,  $J_{\text{CP}} = 10$  Hz, CH(CH<sub>3</sub>)<sub>2</sub>), 125.77 (s, ArC), 127.39 (s, ArC), 128.98 (t,  $J_{\text{CP}} = 3$  Hz, ArC), 129.09 (s, ArC), 129.58 (s, ArC), 131.11 (s, ArC), 132.69 (br s, ArC), 132.89 (t,  $J_{\text{CP}} = 5$  Hz, ArC), 133.44 (t,  $J_{\text{CP}} = 12$  Hz, ArC), 133.72 (br s, ArC), 133.86 (s, ArC), 137.34 (s, ArC), 137.62 (s, ArC), 145.47 (t,  $J_{\text{CP}} = 10$  Hz, ArC). <sup>19</sup>F {<sup>1</sup>H} NMR (376 MHz, CD<sub>2</sub>Cl<sub>2</sub>) δ: -81.93 (s). <sup>31</sup>P{<sup>1</sup>H} NMR (162 MHz, CD<sub>2</sub>Cl<sub>2</sub>) δ: 24.42 (s).

**Synthesis of (Pter<sup>tol</sup>P)PdOTf (68).** A THF solution of AgOTf (12.1 mg, 0.05 mmol) was added to a THF solution of **62** (30.6 mg, 0.05 mmol). The mixture was stirred at room temperature for 1 h. The solution was filtered over a pad of celite and the volatiles were removed under reduced pressure, the crude residue was dissolved in Et<sub>2</sub>O and chilled to -35°C to induce precipitation of the orange solid (26.4 mg, 0.04 mmol, 79%). For **68**: <sup>1</sup>H NMR (400 MHz, C<sub>6</sub>D<sub>6</sub>) δ: 0.44 (m, 6 H, CH(CH<sub>3</sub>)<sub>2</sub>), 1.02 (dd, 3 H, *J*<sub>HP</sub> = 12 Hz, *J*<sub>HH</sub> = 4 Hz, CH(CH<sub>3</sub>)<sub>2</sub>), 1.19 (dd, 3 H, *J*<sub>HP</sub> = 16 Hz, *J*<sub>HH</sub> = 8 Hz, CH(CH<sub>3</sub>)<sub>2</sub>), 1.30 (dd, 3 H *J*<sub>HP</sub> = 16 Hz, *J*<sub>HH</sub> = 8 Hz, CH(CH<sub>3</sub>)<sub>2</sub>), 1.49 (dd, 3 H, *J*<sub>HP</sub> = 20 Hz, *J*<sub>HH</sub> = 8 Hz, CH(CH<sub>3</sub>)<sub>2</sub>), 1.60 (m, 6 H, CH(CH<sub>3</sub>)<sub>2</sub>), 1.94 (m, 1 H, CH(CH<sub>3</sub>)<sub>2</sub>), 2.00 (s, 2 H, C<sub>6</sub>H<sub>4</sub>(CH<sub>3</sub>)), 2.50 (m, 1 H, CH(CH<sub>3</sub>)<sub>2</sub>), 2.65 (m, 1 H, CH(CH<sub>3</sub>)<sub>2</sub>), 3.01 (m, 1 H, CH(CH<sub>3</sub>)<sub>2</sub>), 4.02 (dm, 1 H, *J*<sub>HH</sub> = 8 Hz, CH(tol)), 5.43 (br q, 1 H, *J*<sub>HH</sub> = 2 Hz, C=CH-CH(tol)), 5.47 (dm, *J*<sub>HH</sub> = 8 Hz, C=CH-CH(tol)), 6.77 (td, *J*<sub>HH</sub> = 7 Hz, *J*<sub>HH</sub> = 4 Hz, ArH), 6.85 (m, 3 H, ArH), 6.94 (d, *J*<sub>HH</sub> = 8 Hz, ArH), 7.0 (m, 4 H, ArH), 7.08 (t, *J*<sub>HH</sub> = 6 Hz, ArH), 7.13 (m, 1 H, ArH), 7.26 (d, *J*<sub>HH</sub> = 8 Hz, ArH). <sup>19</sup>F{<sup>1</sup>H} NMR (376 MHz, CD<sub>2</sub>Cl<sub>2</sub>) δ: -79.88 (s). <sup>31</sup>P{<sup>1</sup>H} NMR (162 MHz, C<sub>6</sub>D<sub>6</sub>) δ: 29.50 (d, *J*<sub>PP</sub> = 315 Hz), 54.55 (d, *J*<sub>PP</sub> = 315 Hz).

**Synthesis of (Pter<sup>tol</sup>P)PdH(OTf) (69).** A C<sub>6</sub>D<sub>6</sub> solution of **68** (22.5 mg, 0.03 mmol) was heated to 60°C and monitored by NMR spectroscopy to track the progress of the reaction. After 2 h, full conversion to **69** was achieved. Prolonged heating led to the formation of palladium black. The volatiles from the crude mixture were removed under reduced pressure, and the remaining residue was triturated with *n*-pentane leaving the product as a yellow powder (15.2 mg, 0.02 mmol, 67%). For **69**: <sup>1</sup>H NMR (400 MHz, C<sub>6</sub>D<sub>6</sub>) δ: -19.01 (t, 1 H, *J*<sub>HP</sub> = 4 Hz, PdH), 0.65 (app q, 6 H, *J* = 8 Hz, CH(CH<sub>3</sub>)<sub>2</sub>), 0.96 (app q, 3 H, *J* = 8 Hz, CH(CH<sub>3</sub>)<sub>2</sub>), 1.07 (app q, 3 H, *J* = 6 Hz, CH(CH<sub>3</sub>)<sub>2</sub>), 1.12 (app q, 3 H, *J* = 6 Hz,

CH(CH<sub>3</sub>)<sub>2</sub>), 1.27 (app q, 3 H,  $J = 8$  Hz, CH(CH<sub>3</sub>)<sub>2</sub>), 1.38 (m, 6 H, CH(CH<sub>3</sub>)<sub>2</sub>), 2.0 (m, 2H, CH(CH<sub>3</sub>)<sub>2</sub>), 2.48 (s, 3 H, C<sub>6</sub>H<sub>4</sub>(CH<sub>3</sub>)), 2.55 (m, 1 H, CH(CH<sub>3</sub>)<sub>2</sub>), 2.75 (m, 1 H, CH(CH<sub>3</sub>)<sub>2</sub>), 6.83 (q, 2 H,  $J_{\text{HH}} = 8$  Hz, ArH), 6.96 (m, 5 H, ArH), 7.13 (m, 4 H, ArH), 7.23 (d, 1 H,  $J_{\text{HH}} = 8$  Hz, ArH), 7.34 (d, 1 H,  $J_{\text{HH}} = 4$  Hz, ArH), 7.41 (m, 2 H, ArH). <sup>19</sup>F{<sup>1</sup>H} NMR (376 MHz, CD<sub>2</sub>Cl<sub>2</sub>)  $\delta$ : -80.12 (s). <sup>31</sup>P{<sup>1</sup>H} NMR (162 MHz, C<sub>6</sub>D<sub>6</sub>)  $\delta$ : 33.22 (s).

**X-ray single crystal diffraction** The data were collected on a Bruker APEX-II diffractometer with a monochromated Mo K $\alpha$  radiation.<sup>35</sup> Data were corrected for absorption and polarized effects and analyzed for space group determination.<sup>35-36</sup> The structure was solved by direct methods (SHELXS<sup>37</sup> of OLEX2<sup>38</sup>) and refined by full-matrix least squares techniques against  $F_o^2$  (SHELXL-97).<sup>39</sup> Unless noted, all hydrogen atoms were generated in calculated positions. Mercury was used for structure representations.<sup>40</sup>

**X-Ray Crystal Structure of (Pter<sup>mes</sup>P)PdBr (58).** Single crystals were obtained as yellow needles from a concentrated Et<sub>2</sub>O solution at -35 °C in the glovebox. Crystal and refinement data for **58**: C<sub>39</sub>H<sub>51</sub>BrP<sub>2</sub>Pd;  $M_r = 768.04$ ; Monoclinic; space group P2(1)/n;  $a = 17.8978(10)$  Å;  $b = 10.0274(5)$  Å;  $c = 23.6513(13)$  Å;  $\alpha = 90^\circ$ ;  $\beta = 109.575(2)^\circ$ ;  $\gamma = 90^\circ$ ;  $V = 3999.3(9)$  Å<sup>3</sup>;  $Z = 4$ ;  $T = 120(2)$  K;  $\lambda = 1.54178$  Å;  $\mu = 1.566$  mm<sup>-1</sup>;  $d_{\text{calc}} = 1.276$  g·cm<sup>-3</sup>; 57954 reflections collected; 8355 unique ( $R_{\text{int}} = 0.1119$ ); giving  $R_1 = 0.0416$ ,  $wR_2 = 0.0773$  for 8355 data with [ $I > 2\sigma(I)$ ] and  $R_1 = 0.0930$ ,  $wR_2 = 0.0959$  for all 57954 data. Residual electron density (e<sup>-</sup>·Å<sup>-3</sup>) max/min: 0.91/-0.81.

**X-Ray Crystal Structure of (Pter<sup>mes</sup>P)Pd (59•C<sub>7</sub>H<sub>8</sub>).** Single crystals were obtained as yellow rods from a concentrated *n*-pentane solution at -35 °C in the glovebox. Crystal and refinement data for **59•C<sub>7</sub>H<sub>8</sub>**: C<sub>46</sub>H<sub>58</sub>P<sub>2</sub>Pd;  $M_r = 779.26$ ; Triclinic; space group P-1;  $a = 10.5192(14)$  Å;  $b = 11.0543(15)$  Å;  $c = 17.780(2)$  Å;  $\alpha = 89.569(2)^\circ$ ;  $\beta =$

82.203(2)°;  $\gamma = 79.929(2)^\circ$ ;  $V = 2016.6(5) \text{ \AA}^3$ ;  $Z = 2$ ;  $T = 120(2) \text{ K}$ ;  $\lambda = 1.54178 \text{ \AA}$ ;  $\mu = 0.570 \text{ mm}^{-1}$ ;  $d_{\text{calc}} = 1.283 \text{ g}\cdot\text{cm}^{-3}$ ; 63406 reflections collected; 10030 unique ( $R_{\text{int}} = 0.0349$ ); giving  $R_1 = 0.0347$ ,  $wR_2 = 0.0830$  for 10030 data with  $[I > 2\sigma(I)]$  and  $R_1 = 0.0437$ ,  $wR_2 = 0.0906$  for all 63406 data. Residual electron density ( $\text{e}^- \cdot \text{\AA}^{-3}$ ) max/min: 1.52/-0.72.

**X-Ray Crystal Structure of *anti*-(PterP)PdBr(tol) (60a).** Single crystals were obtained as colorless rods from a toluene solution layered with *n*-pentane solution at  $-35^\circ\text{C}$  in the glovebox. Crystal and refinement data for **60a**:  $\text{C}_{37}\text{H}_{47}\text{BrP}_2\text{Pd}$ ;  $M_r = 740.05$ ; Orthorhombic; space group Pnma;  $a = 26.524(2) \text{ \AA}$ ;  $b = 12.8797(12) \text{ \AA}$ ;  $c = 9.7495(9) \text{ \AA}$ ;  $\alpha = 90^\circ$ ;  $\beta = 90^\circ$ ;  $\gamma = 90^\circ$ ;  $V = 3330.6(5) \text{ \AA}^3$ ;  $Z = 4$ ;  $T = 120(2) \text{ K}$ ;  $\lambda = 1.54178 \text{ \AA}$ ;  $\mu = 6.980 \text{ mm}^{-1}$ ;  $d_{\text{calc}} = 1.476 \text{ g}\cdot\text{cm}^{-3}$ ; 64132 reflections collected; 3439 unique ( $R_{\text{int}} = 0.0548$ ); giving  $R_1 = 0.0277$ ,  $wR_2 = 0.0734$  for 3439 data with  $[I > 2\sigma(I)]$  and  $R_1 = 0.0290$ ,  $wR_2 = 0.0747$  for all 64132 data. Residual electron density ( $\text{e}^- \cdot \text{\AA}^{-3}$ ) max/min: 1.31/-0.72.

**X-Ray Crystal Structure of *syn*-(PterP)PdBr(tol) (60b).** Single crystals were obtained as colorless rods from a toluene solution layered with *n*-pentane at  $-35^\circ\text{C}$  in the glovebox. Crystal and refinement data for **60b**:  $\text{C}_{40}\text{H}_{40}\text{P}_2\text{BrPd}$ ;  $M_r = 581.40$ ; Orthorhombic; space group Pnma;  $a = 15.72038(8) \text{ \AA}$ ;  $b = 12.9153(6) \text{ \AA}$ ;  $c = 16.7946(9) \text{ \AA}$ ;  $\alpha = 90^\circ$ ;  $\beta = 90^\circ$ ;  $\gamma = 90^\circ$ ;  $V = 3409.8(3) \text{ \AA}^3$ ;  $Z = 4$ ;  $T = 120(2) \text{ K}$ ;  $\lambda = 1.54178 \text{ \AA}$ ;  $\mu = 7.534 \text{ mm}^{-1}$ ;  $d_{\text{calc}} = 1.498 \text{ g}\cdot\text{cm}^{-3}$ ; 53036 reflections collected; 4495 unique ( $R_{\text{int}} = 0.0473$ ); giving  $R_1 = 0.0255$ ,  $wR_2 = 0.0595$  for 4495 data with  $[I > 2\sigma(I)]$  and  $R_1 = 0.0357$ ,  $wR_2 = 0.0631$  for all 5418 data. Residual electron density ( $\text{e}^- \cdot \text{\AA}^{-3}$ ) max/min: 0.88/-0.37.

**X-Ray Crystal Structure of (Pter<sup>tol</sup>P)PdBr (62).** Single crystals were obtained as brown cubes from a concentrated *n*-pentane solution at  $-35^\circ\text{C}$  in the glovebox. Crystal and refinement data for **62**:  $\text{C}_{37}\text{H}_{46}\text{BrP}_2\text{Pd}$ ;  $M_r = 739.53$ ; Triclinic; space group P-1;  $a =$

14.5938(7) Å;  $b = 15.2733(7)$  Å;  $c = 16.4461(7)$  Å;  $\alpha = 75.964(2)^\circ$ ;  $\beta = 70.549(2)^\circ$ ;  $\gamma = 83.500(2)^\circ$ ;  $V = 3351.2(3)$  Å<sup>3</sup>;  $Z = 4$ ;  $T = 120(2)$  K;  $\lambda = 1.54178$  Å;  $\mu = 1.866$  mm<sup>-1</sup>;  $d_{\text{calc}} = 1.466$  g·cm<sup>-3</sup>; 10018 reflections collected; 16825 unique ( $R_{\text{int}} = 0.0660$ ); giving  $R_1 = 0.0361$ ,  $wR_2 = 0.0703$  for 16825 data with [ $I > 2\sigma(I)$ ] and  $R_1 = 0.0692$ ,  $wR_2 = 0.0800$  for all 10018 data. Residual electron density (e<sup>-</sup>·Å<sup>-3</sup>) max/min: 0.83/-0.98.

**X-Ray Crystal Structure of *anti*-(PterP)PdBrPh (65a).** Single crystals were obtained as yellow blocks from a toluene solution layered with *n*-pentane solution at -35 °C in the glovebox. Crystal and refinement data for **65a**: C<sub>36</sub>H<sub>45</sub>BrP<sub>2</sub>Pd;  $M_r = 581.40$ ; Triclinic; space group P-1;  $a = 10.3069(6)$  Å;  $b = 10.7725(6)$  Å;  $c = 18.8886(11)$  Å;  $\alpha = 93.878(3)^\circ$ ;  $\beta = 101.895(3)^\circ$ ;  $\gamma = 112.197(2)^\circ$ ;  $V = 1875.44(19)$  Å<sup>3</sup>;  $Z = 2$ ;  $T = 120(2)$  K;  $\lambda = 1.54178$  Å;  $\mu = 1.666$  mm<sup>-1</sup>;  $d_{\text{calc}} = 1.286$  g·cm<sup>-3</sup>; 37903 reflections collected; 7704 unique ( $R_{\text{int}} = 0.0466$ ); giving  $R_1 = 0.0322$ ,  $wR_2 = 0.0776$  for 7704 data with [ $I > 2\sigma(I)$ ] and  $R_1 = 0.0469$ ,  $wR_2 = 0.0776$  for all 37903 data. Residual electron density (e<sup>-</sup>·Å<sup>-3</sup>) max/min: 1.107/-0.48.

**X-Ray Crystal Structure of *syn*-(PterP)PdBrPh (65b).** Single crystals were obtained as yellow plates from a concentrated toluene solution layered with *n*-pentane at -35 °C in the glovebox. Crystal and refinement data for **65b**: C<sub>36</sub>H<sub>45</sub>BrP<sub>2</sub>Pd;  $M_r = 726.02$ ; Monoclinic; space group P2(1)/c;  $a = 13.1300(9)$  Å;  $b = 11.9276(9)$  Å;  $c = 24.4957(17)$  Å;  $\alpha = 90^\circ$ ;  $\beta = 92.660(1)^\circ$ ;  $\gamma = 90^\circ$ ;  $V = 3832.1(5)$  Å<sup>3</sup>;  $Z = 4$ ;  $T = 120(2)$  K;  $\lambda = 1.54178$  Å;  $\mu = 1.631$  mm<sup>-1</sup>;  $d_{\text{calc}} = 1.258$  g·cm<sup>-3</sup>; 75525 reflections collected; 9541 unique ( $R_{\text{int}} = 0.0770$ ); giving  $R_1 = 0.0339$ ,  $wR_2 = 0.0633$  for 9541 data with [ $I > 2\sigma(I)$ ] and  $R_1 = 0.0549$ ,  $wR_2 = 0.0688$  for all 75525 data. Residual electron density (e<sup>-</sup>·Å<sup>-3</sup>) max/min: 0.92/-1.11.

**X-Ray Crystal Structure of [(PterP)PdCl]•2[BAr<sup>F</sup><sub>4</sub>] (66).** Single crystals were obtained as orange cubes from a DCM solution layered with *n*-pentane solution at –35 °C in the glovebox. Crystal and refinement data for **66**: C<sub>62</sub>H<sub>52</sub>BClF<sub>24</sub>P<sub>2</sub>Pd; M<sub>r</sub> = 1467.70; Triclinic; space group P-1; *a* = 12.8457(7) Å; *b* = 15.6948(9) Å; *c* = 18.3956(10) Å; α = 112.309(1)°; β = 99.386(1)°; γ = 104.394(1)°; V = 3183.3(3) Å<sup>3</sup>; Z = 2; T = 120(2) K; λ = 1.54178 Å; μ = 0.493 mm<sup>-1</sup>; d<sub>calc</sub> = 1.531 g·cm<sup>-3</sup>; 97151 reflections collected; 15813 unique (R<sub>int</sub> = 0.0271); giving R<sub>1</sub> = 0.0365, wR<sub>2</sub> = 0.0944 for 15813 data with [I > 2σ(I)] and R<sub>1</sub> = 0.0423, wR<sub>2</sub> = 0.1000 for all 15813 data. Residual electron density (e<sup>-</sup>·Å<sup>-3</sup>) max/min: 1.15/-0.84.

**X-Ray Crystal Structure of [(PterP)Pd(tol)][OTf] (67).** Single crystals were obtained as orange blocks from a DCM solution layered with THF at –35 °C in the glovebox. Crystal and refinement data for **67**: C<sub>38</sub>H<sub>44</sub>F<sub>3</sub>O<sub>3</sub>P<sub>2</sub>PdS; M<sub>r</sub> = 809.75; Orthorhombic; space group Pnma; *a* = 17.522(6) Å; *b* = 13.912(5) Å; *c* = 14.795(5) Å; α = 90°; β = 90°; γ = 90°; V = 3606(2) Å<sup>3</sup>; Z = 4; T = 120(2) K; λ = 1.54178 Å; μ = 0.714 mm<sup>-1</sup>; d<sub>calc</sub> = 1.491 g·cm<sup>-3</sup>; 82274 reflections collected; 4647 unique (R<sub>int</sub> = 0.0934); giving R<sub>1</sub> = 0.0419, wR<sub>2</sub> = 0.0886 for 4647 data with [I > 2σ(I)] and R<sub>1</sub> = 0.0724, wR<sub>2</sub> = 0.1022 for all 82274 data. Residual electron density (e<sup>-</sup>·Å<sup>-3</sup>) max/min: 0.97/-0.93.

## 7.5 References

1. Alberico, D.; Scott, M. E.; Lautens, M., *Chem. Rev.* **2007**, *107* (1), 174-238.
2. Campeau, L.-C.; Fagnou, K., *Chem. Commun.* **2006**, (12), 1253-1264.
3. García-Cuadrado, D.; de Mendoza, P.; Braga, A. A. C.; Maseras, F.; Echavarren, A. M., *J. Am. Chem. Soc.* **2007**, *129* (21), 6880-6886.

4. Keane, J. M.; Harman, D. W., *Organometallics* **2005**, *24* (8), 1786-1798.
5. Pape, A. R.; Kaliappan, K. P.; Kündig, P. E., *Chem. Rev.* **2000**, *100* (8), 2917-2940.
6. Keane, J. M.; Chordia, M. D.; Mocella, C. J.; Sabat, M.; Trindle, C. O.; Harman, W. D., *J. Am. Chem. Soc.* **2004**, *126* (21), 6806-6815.
7. Harman, W. D., *Coord. Chem. Rev.* **2004**, *248* (9-10), 853-866.
8. Milner, P. J.; Maimone, T. J.; Su, M.; Chen, J.; Müller, P.; Buchwald, S. L., *J. Am. Chem. Soc.* **2012**, *134* (48), 19922-19934.
9. Suseno, S.; Agapie, T., *Organometallics* **2013**, *32* (11), 3161-3164.
10. Nielsen, D. K.; Doyle, A. G., *Angew. Chem. Int. Ed.* **2011**, *50* (27), 6056-6059.
11. Feller, M.; Ben-Ari, E.; Iron, M. A.; Diskin-Posner, Y.; Leitun, G.; Shimon, L. J. W.; Konstantinovski, L.; Milstein, D., *Inorg. Chem.* **2010**, *49* (4), 1615-1625.
12. Bedford, R. B.; Cazin, C.; Holder, D., *Coord. Chem. Rev.* **2004**, *248* (21-24), 2283-2321.
13. Kočovský, P., *J. Organomet. Chem.* **2003**, *687* (2), 256-268.
14. Barder, T. E., *J. Am. Chem. Soc.* **2006**, *128* (3), 898-904.
15. Barder, T. E.; Biscoe, M. R.; Buchwald, S. L., *Organometallics* **2007**, *26* (9), 2183-2192.
16. Goutierre, A.-S.; Trinh, H.; Larini, P.; Jazzar, R.; Baudoin, O., *Organometallics* **2017**, *36* (1), 129-135.
17. Reid, S. M.; Boyle, R. C.; Mague, J. T.; Fink, M. J., *J. Am. Chem. Soc.* **2003**, *125* (26), 7816-7817.
18. Kumar, A. P. G.; Dotta, P.; Hermatschweiler, R.; Pregosin, P. S.; Albinati, A.; Rizzato, S., *Organometallics* **2005**, *24* (6), 1306-1314.
19. DeAngelis, A. J.; Gildner, P. G.; Chow, R.; Colacot, T. J., *J. Org. Chem.* **2015**, *80* (13), 6794-6813.
20. Chahen, L.; Therrien, B.; Süß-Fink, G., *J. Organomet. Chem.* **2006**, *691* (20), 4257-4264.
21. Sather, A. C.; Buchwald, S. L., *Acc. Chem. Res.* **2016**, *49* (10), 2146-2157.



22. Lee, H.; Milner, P. J.; Buchwald, S. L., *J. Am. Chem. Soc.* **2014**, *136* (10), 3792-3795.
23. Martín-Matute, B.; Mateo, C.; Cárdenas, D. J.; Echavarren, A. M., *Chem. Eur. J.* **2001**, *7* (11), 2341-2348.
24. Horak, K. T.; VanderVelde, D. G.; Agapie, T., *Organometallics* **2015**, *34* (19), 4753-4765.
25. Edouard, G. A.; Kelley, P.; Herbert, D. E.; Agapie, T., *Organometallics* **2015**, *34* (21), 5254-5277.
26. Tsui, E. Y.; Agapie, T., *Polyhedron* **2014**, *84*, 103-110.
27. Horak, K. T.; Velian, A.; Day, M. W.; Agapie, T., *Chem. Commun.* **2014**, *50* (34), 4427-4429.
28. Lin, S.; Herbert, D. E.; Velian, A.; Day, M. W.; Agapie, T., *J. Am. Chem. Soc.* **2013**, *135* (42), 15830-15840.
29. Lin, S.; Day, M. W.; Agapie, T., *J. Am. Chem. Soc.* **2011**, *133* (11), 3828-3831.
30. Velian, A.; Lin, S.; Miller, A. J. M.; Day, M. W.; Agapie, T., *J. Am. Chem. Soc.* **2010**, *132* (18), 6296-6297.
31. Malacea, R.; Chahdoura, F.; Devillard, M.; Saffon, N.; Gómez, M.; Bourissou, D., *Adv. Synth. Catal.* **2013**, *355* (11-12), 2274-2284.
32. Harman, H. W.; Peters, J. C., *J. Am. Chem. Soc.* **2012**, *134* (11), 5080-5082.
33. Strieter, E. R.; Buchwald, S. L., *Angew. Chem.* **2006**, *118* (6), 939-942.
34. Racowski, J. M.; Ball, N. D.; Sanford, M. S., *J. Am. Chem. Soc.* **2011**, *133* (45), 18022-18025.
35. Bruker AXS, APEX-2. Bruker-Nonius AXS, Madison, Wisconsin, USA, 2014.
36. Krause, L.; Herbst-Irmer, R.; Sheldrick, G. M.; Stalke, D., *J. Appl. Cryst.* **2015**, *48* (1), 3-10.
37. Sheldrick, G., *Acta Cryst.* **2015**, *A71* (1), 3-8.
38. Dolomanov, O. V.; Bourhis, L. J.; Gildea, R. J.; Howard, J. A. K.; Puschmann, H., *J. Appl. Crystallogr.* **2009**, *42* (2), 339-341.

39. Sheldrick, G., *Acta Cryst.* **2015**, *C71* (1), 3-8.
40. Macrae, C. F.; Bruno, I. J.; Chisholm, J. A.; Edgington, P. R.; McCabe, P.; Pidcock, E.; Rodriguez-Monge, L.; Taylor, R.; van de Streek, J.; Wood, P. A., *J. Appl. Cryst.* **2008**, *41* (2), 466-470.

APPENDIX:  
SELECTED NMR SPECTRA

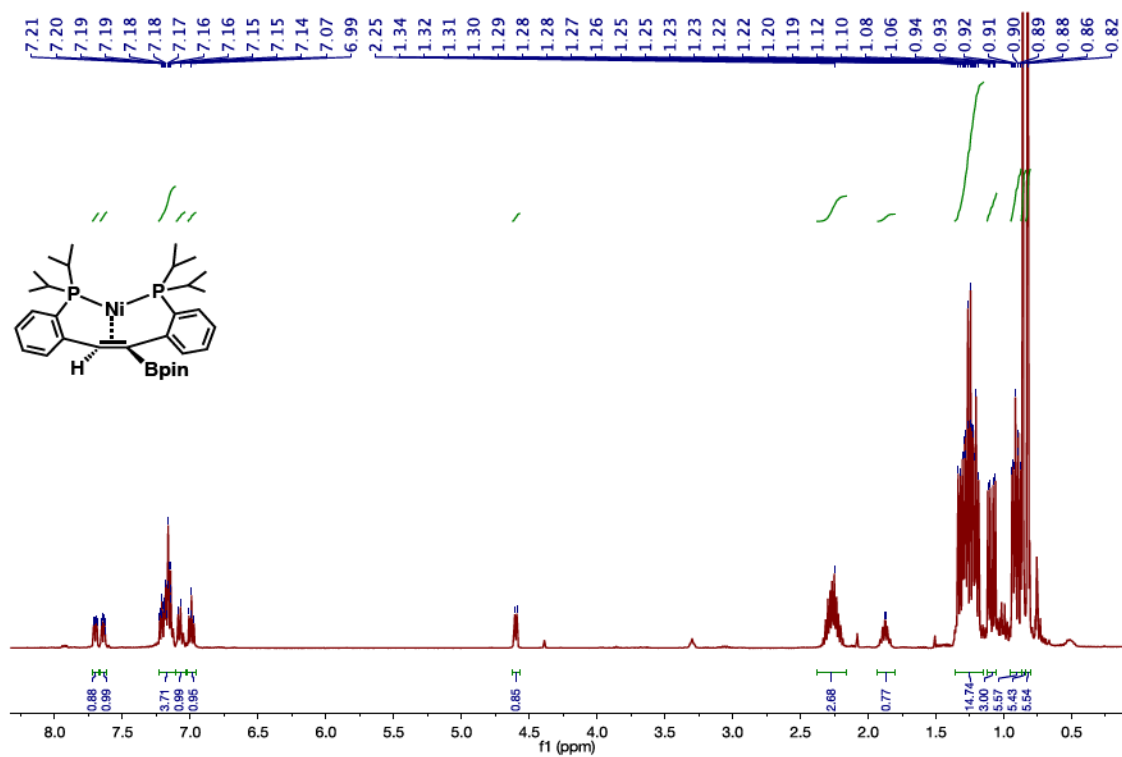


**Figure A.1:**  $^1\text{H}$  NMR spectrum of  $(t\text{PC}(\text{Bpin})=\text{CP})\text{Ni}$  **25**.

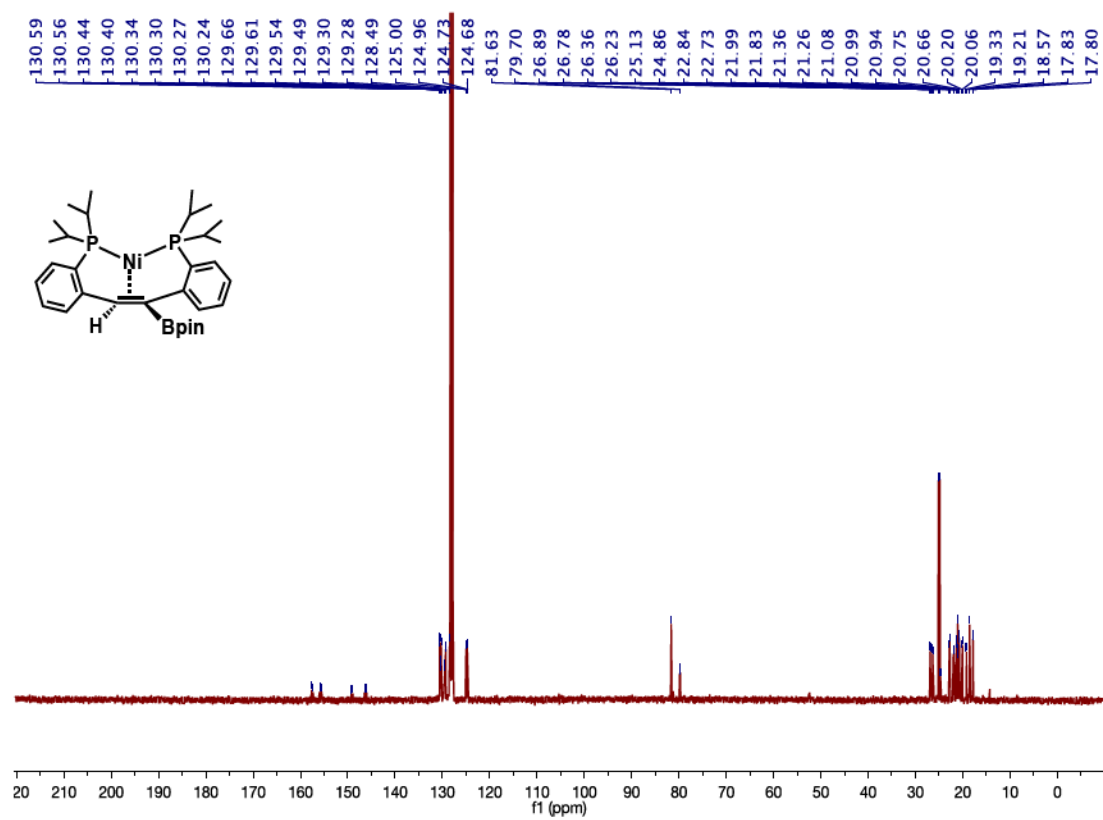


**Figure A.2** :  $^{13}C\{^1H\}$  NMR spectrum of  $(tPC(Bpin)=CHP)Ni$  (**25**).

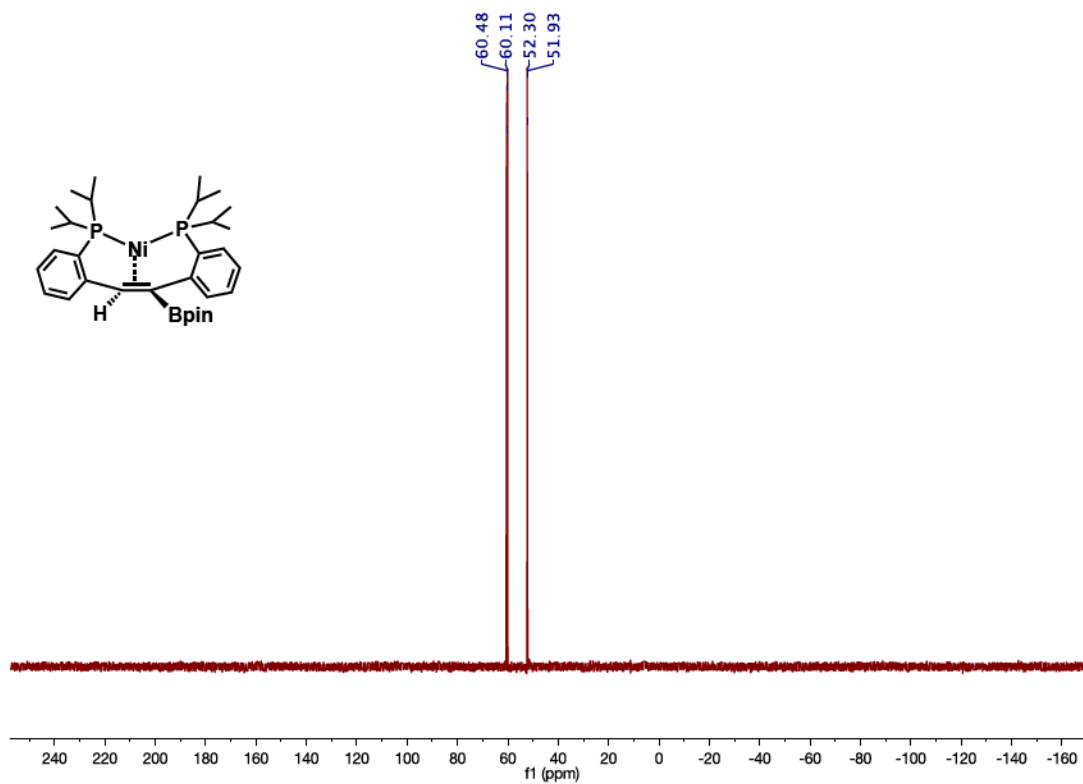


**Figure A.3:**  $^{31}P\{^1H\}$  NMR spectrum of  $(tPC(Bpin)=CP)Ni$  (**25**).

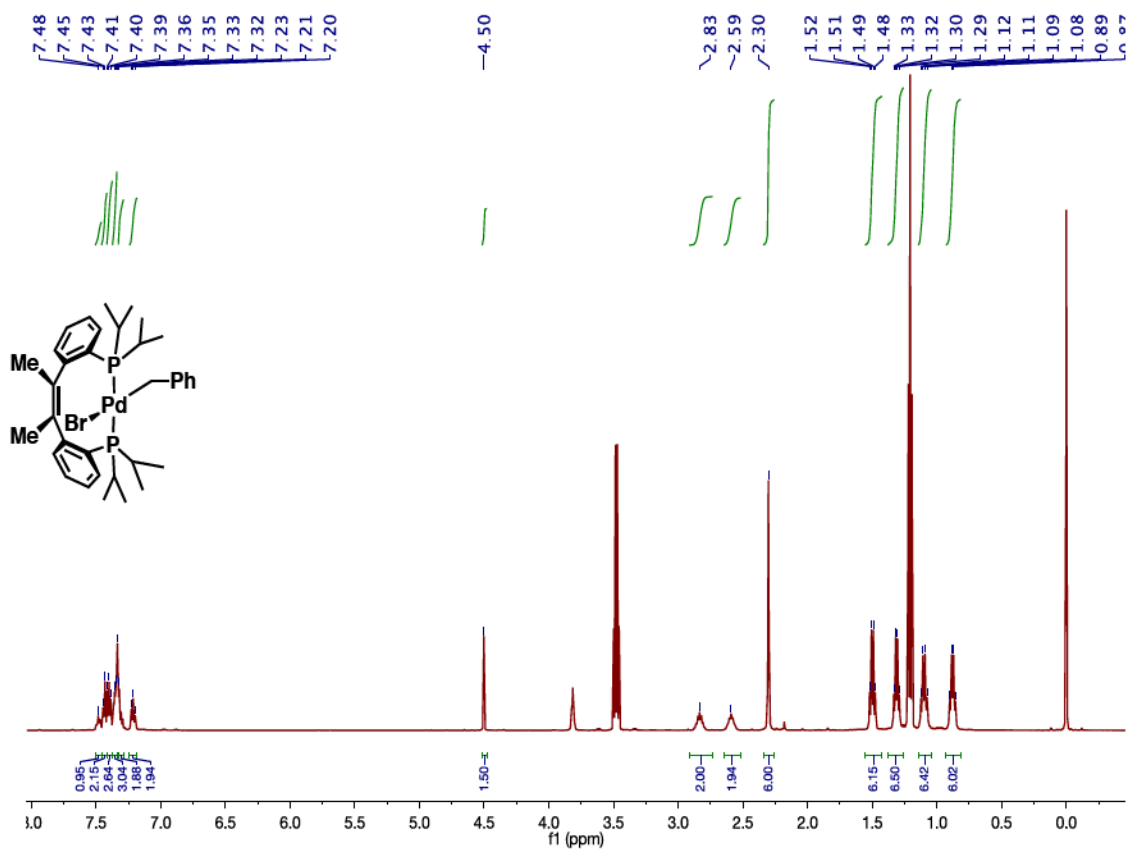


**Figure A.4:**  $^1H$  NMR spectrum of  $(cPCMe=CMeP)PdBr(CH_2Ph)$  (35).

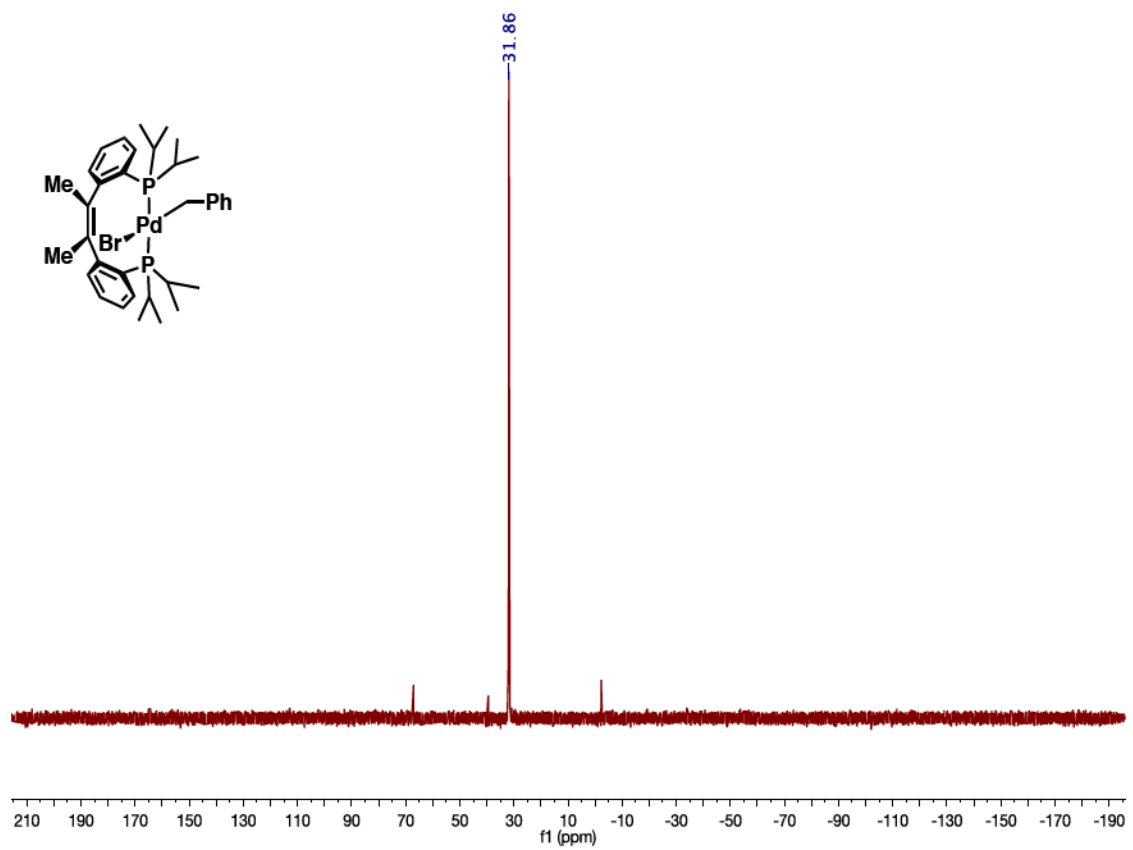


**Figure A.5:**  $^{31}P\{^1H\}$  NMR spectrum of  $(cPCMe=CMcP)PdBr(CH_2Ph)$  (**35**).

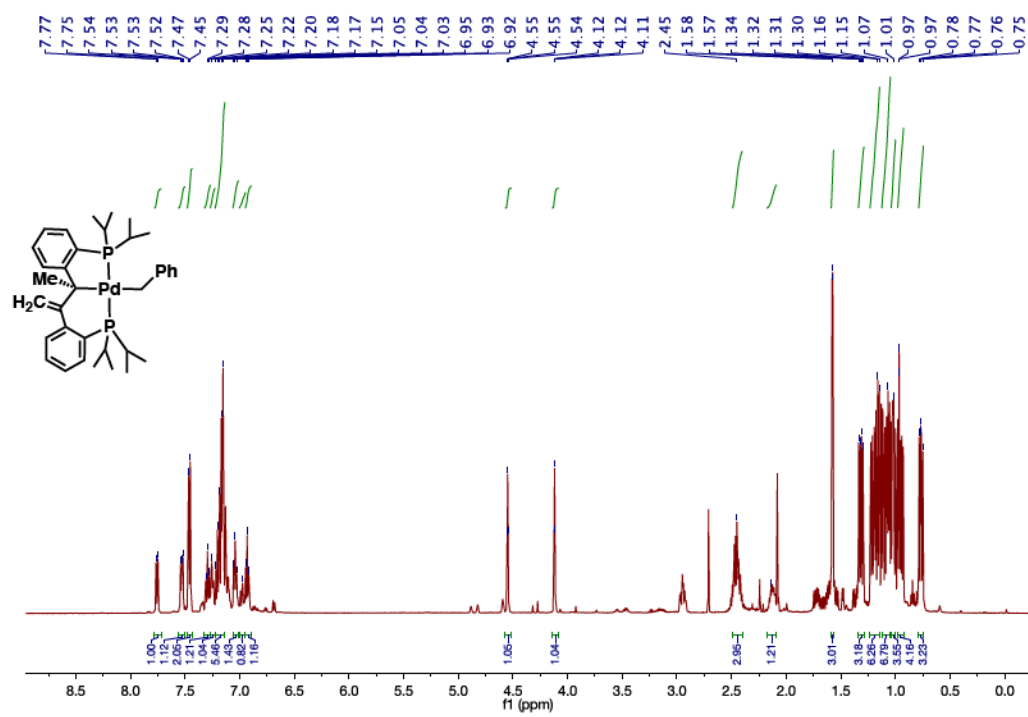


**Figure A.6:**  $^1\text{H}$  NMR spectrum of  $(\text{PC}(\text{CH}_2)\text{-CMeP})\text{Pd}(\text{CH}_2\text{PH})$  (36).



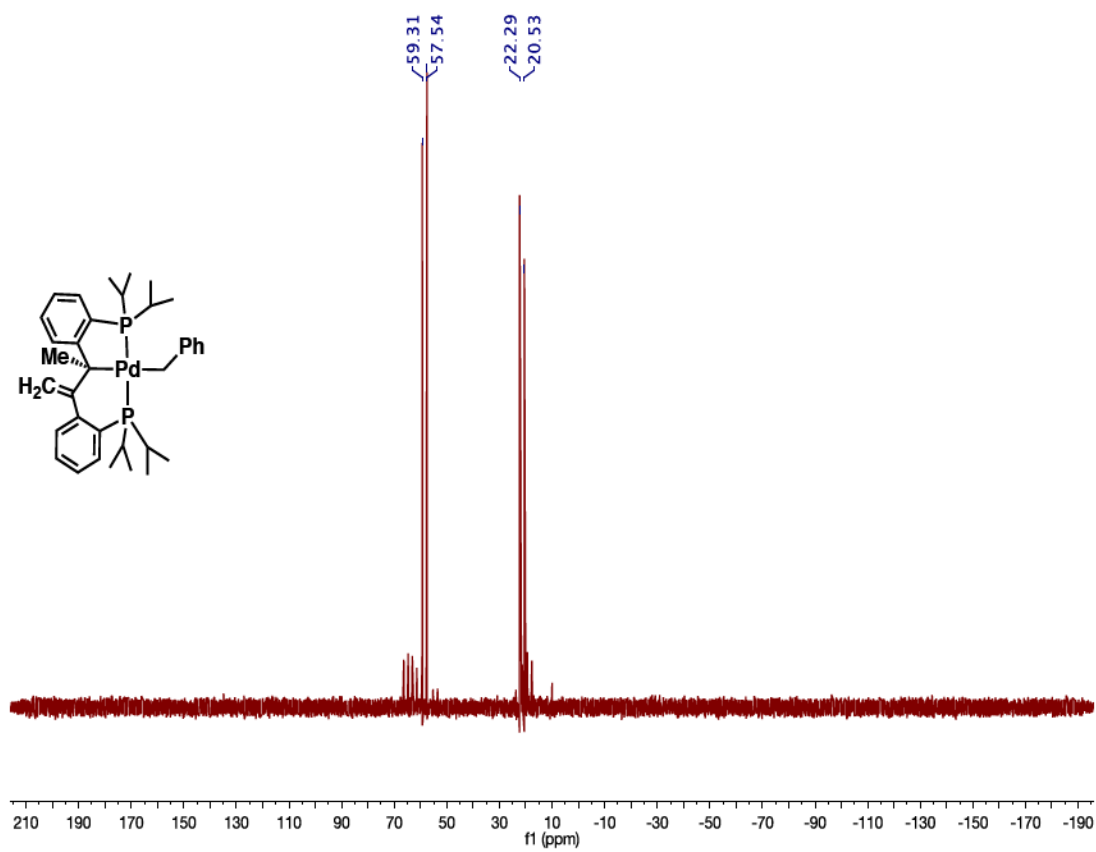


**Figure A.7:** <sup>31</sup>P{<sup>1</sup>H} NMR spectrum of (PC(CH<sub>2</sub>)-CMeP)Pd(CH<sub>2</sub>PH) (**36**).

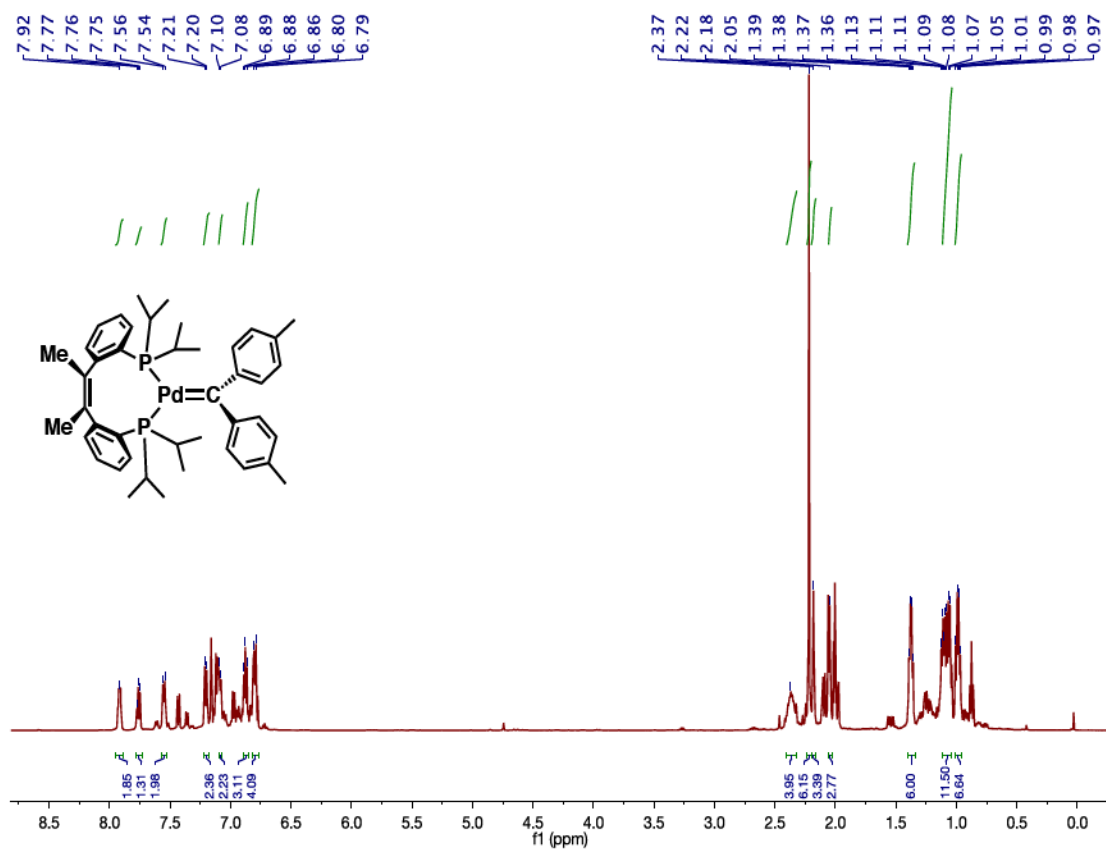


**Figure A.8:**  $^1\text{H}$  NMR spectrum of  $(c\text{PCMMe}=\text{CMMeP})\text{Pd}=\text{C}(p\text{-tol})_2$  (37).

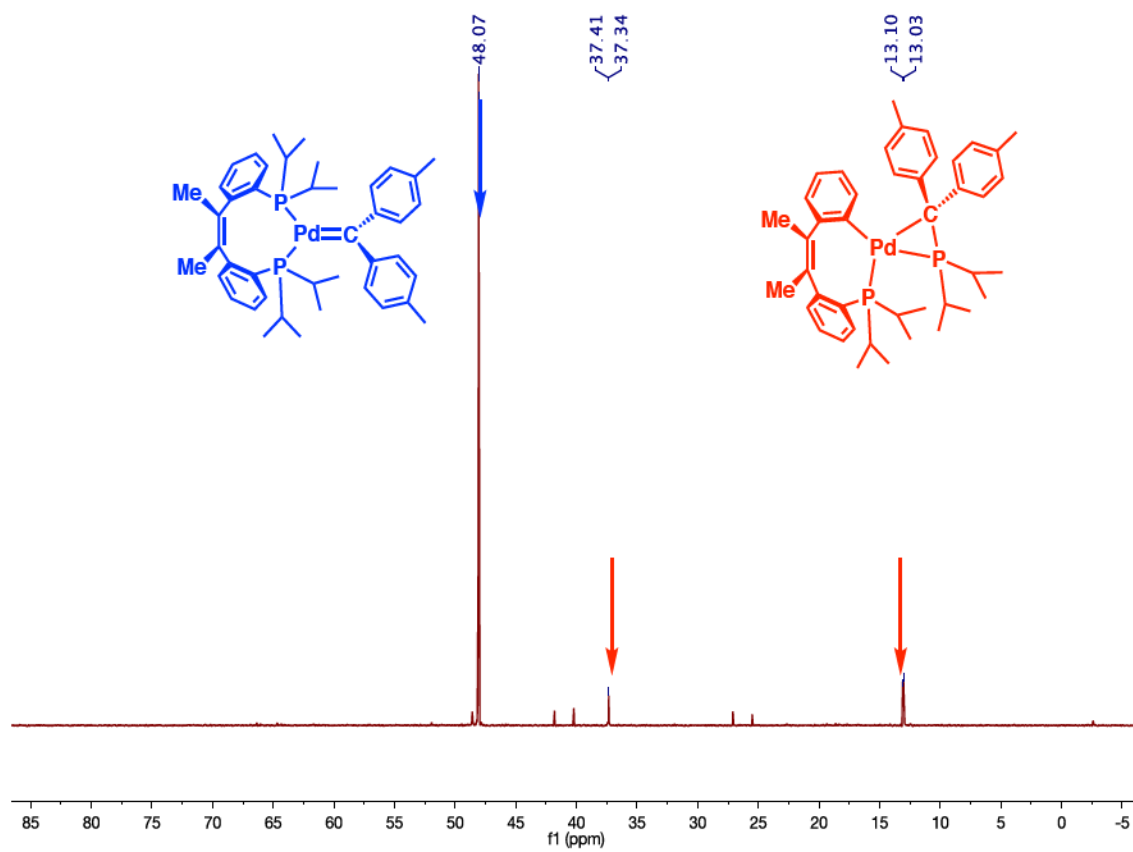


**Figure A.9:**  $^{31}\text{P}\{^1\text{H}\}$  NMR spectrum of  $(\text{cPCMMe}=\text{CMMeP})\text{Pd}=\text{C}(\text{p-tol})_2$  (37).

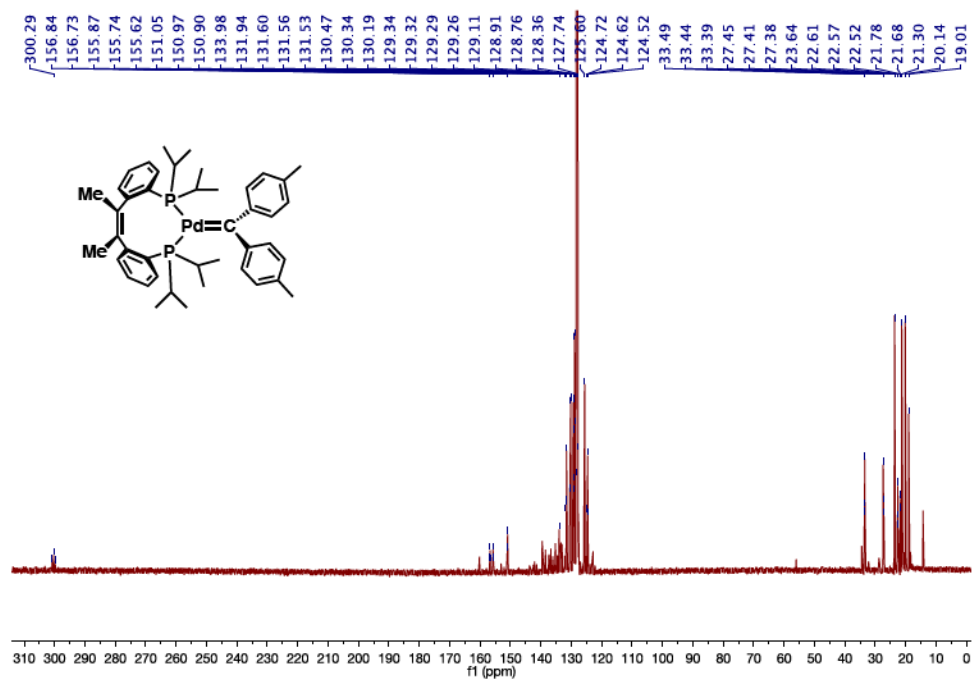


**Figure A.10:**  $^{13}C\{^1H\}$  NMR spectrum of  $(cPCMe=CMeP)Pd=C(p\text{-tol})_2$  (37).

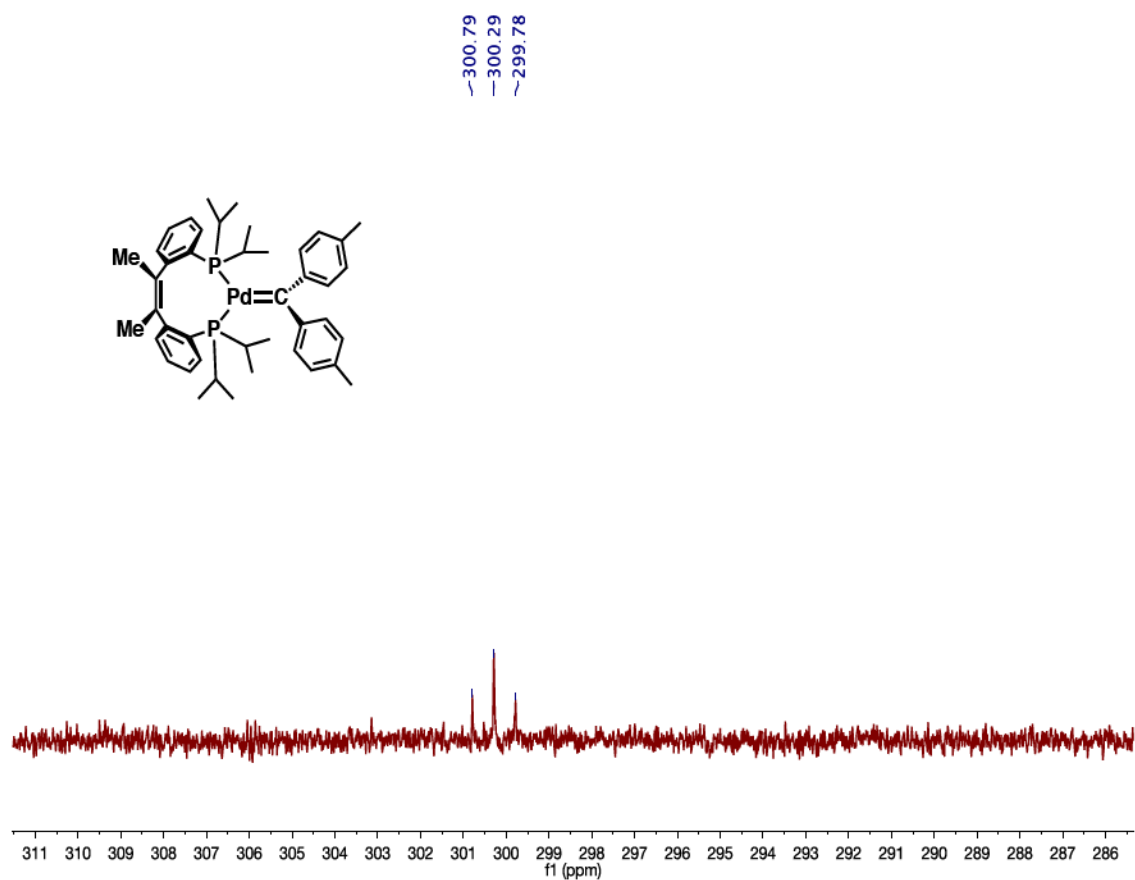


**Figure A.11:** Carbene region of the  $^{13}\text{C}\{^1\text{H}\}$  NMR spectrum of  $(c\text{PCMe}=\text{CMeP})\text{Pd}=\text{C}(p\text{-tol})_2$  (**37**).

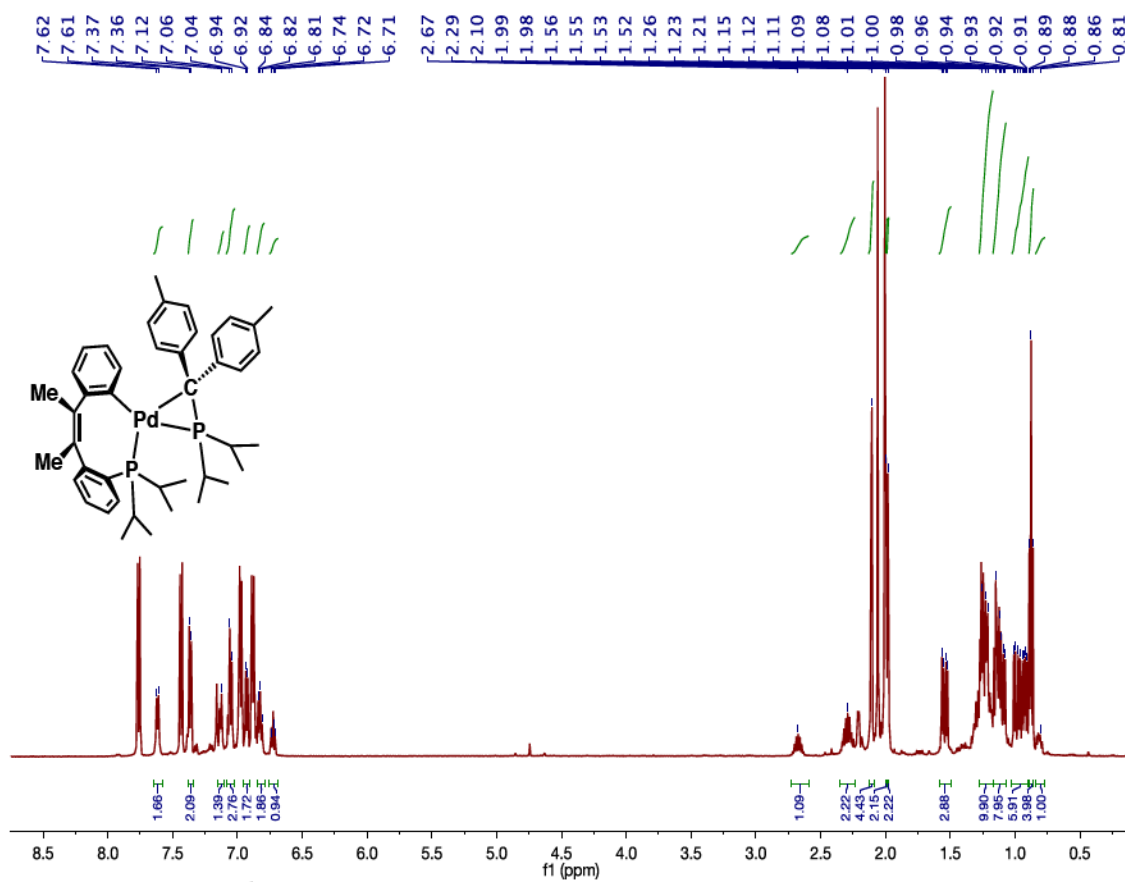


**Figure A.12:**  $^1\text{H}$  NMR spectrum of **38**. Spectrum contains tetra-*p*-tolyl azine as a contaminant.

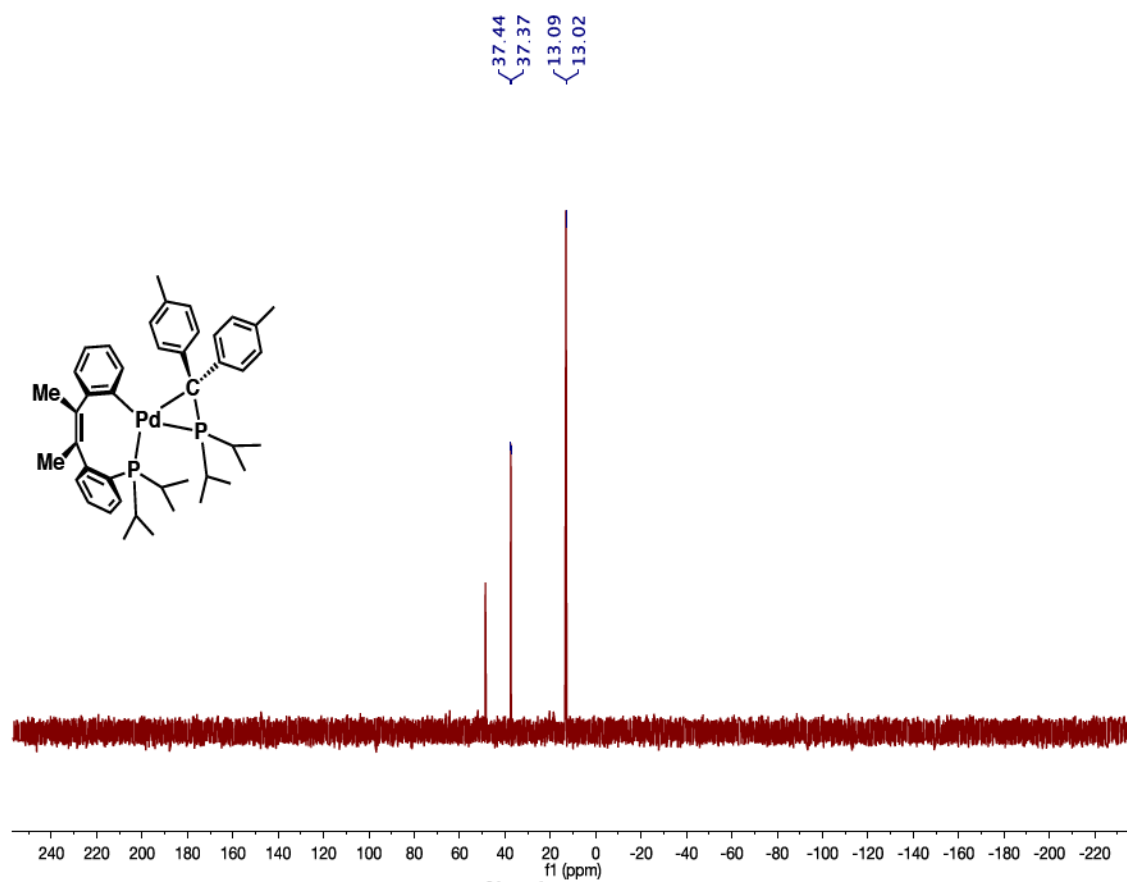


**Figure A.13:**  $^{31}\text{P}\{^1\text{H}\}$  NMR spectrum of **38**.

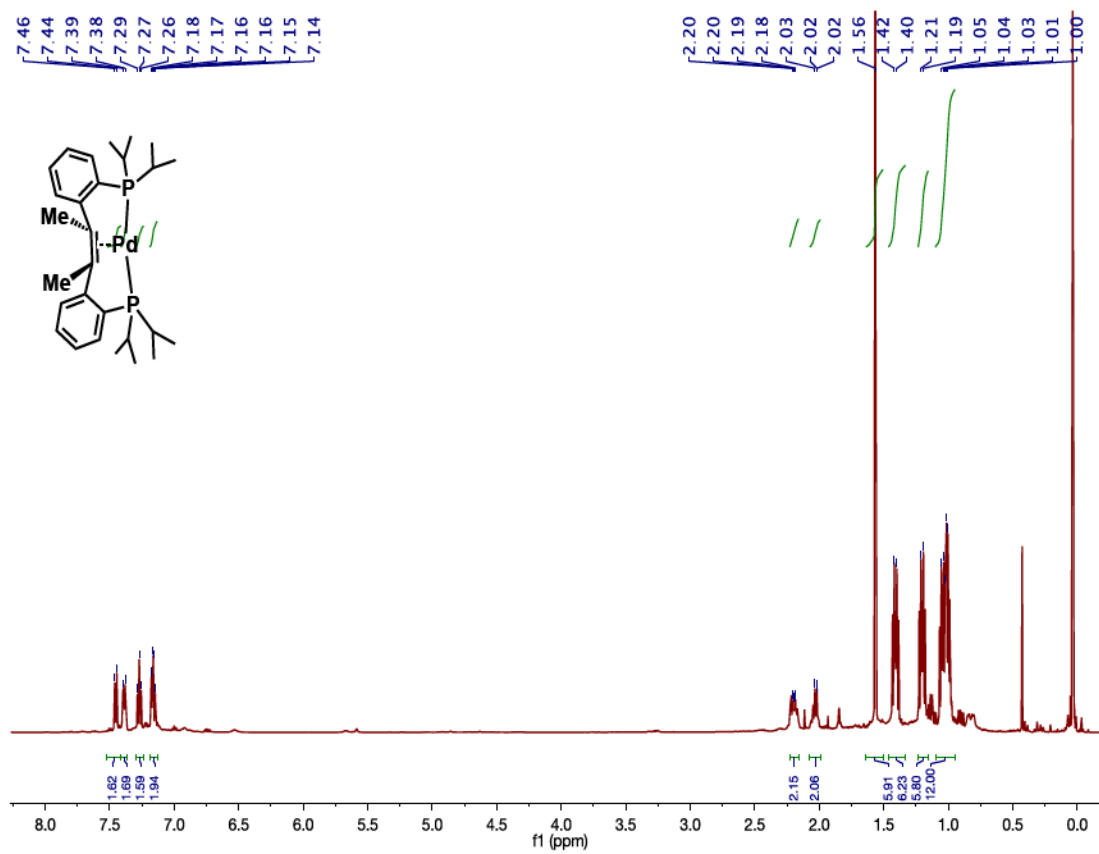


**Figure A.14:**  $^1H$  NMR spectrum of  $(tPCMe=CMeP)Pd$  (43).



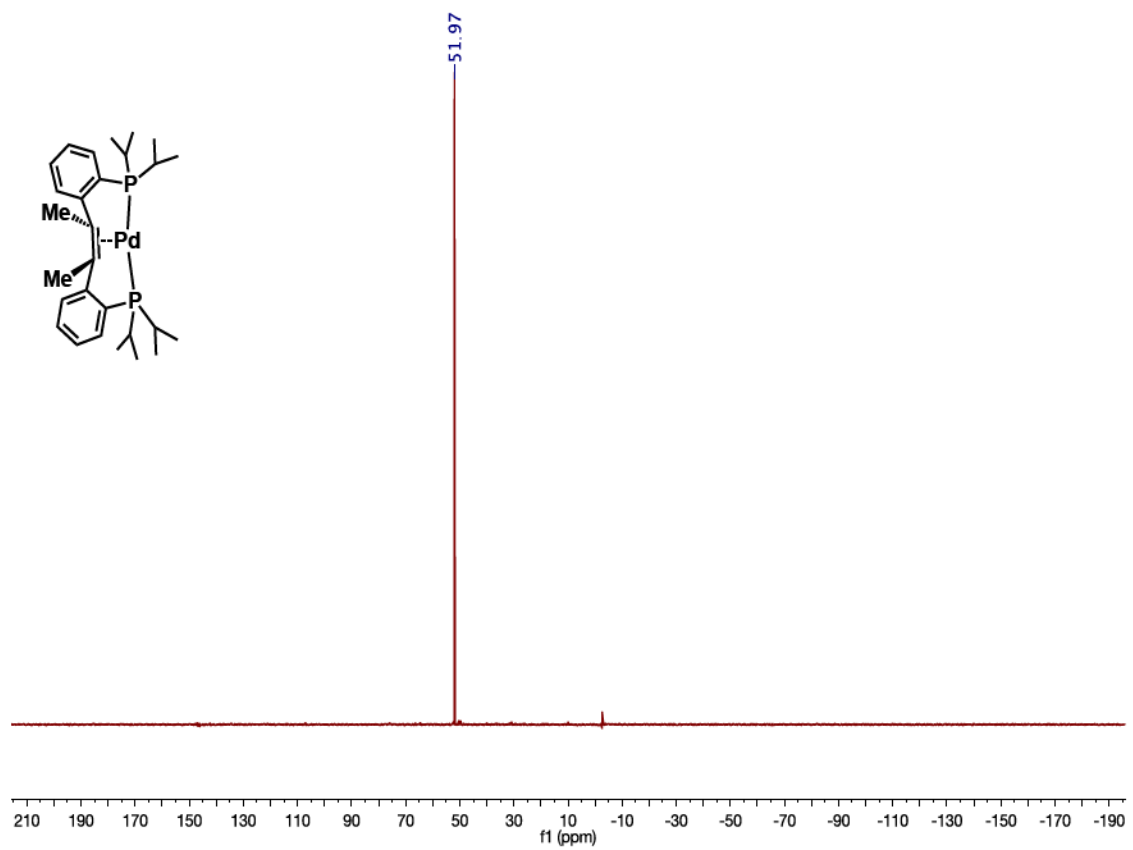


**Figure A.15:**  $^{31}P\{^1H\}$  NMR spectrum of  $(tPCMe=CMeP)Pd$  (**43**).

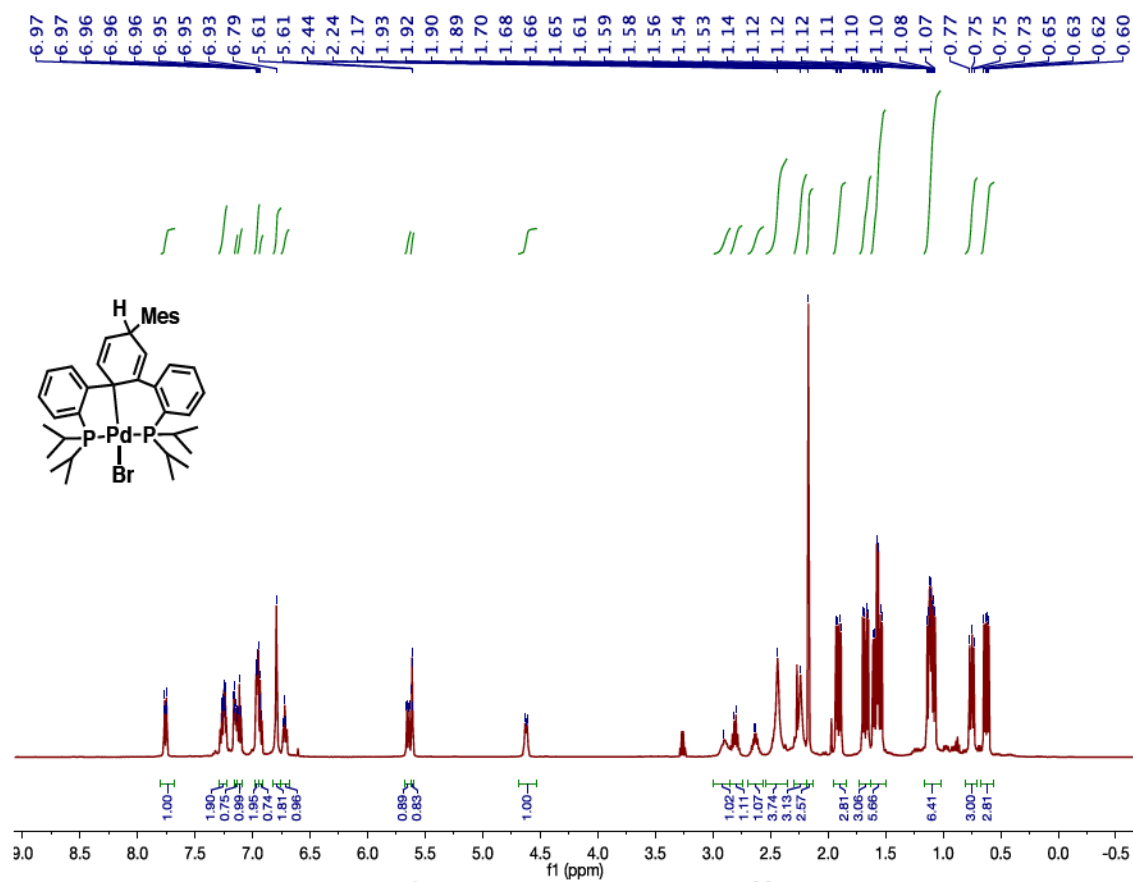
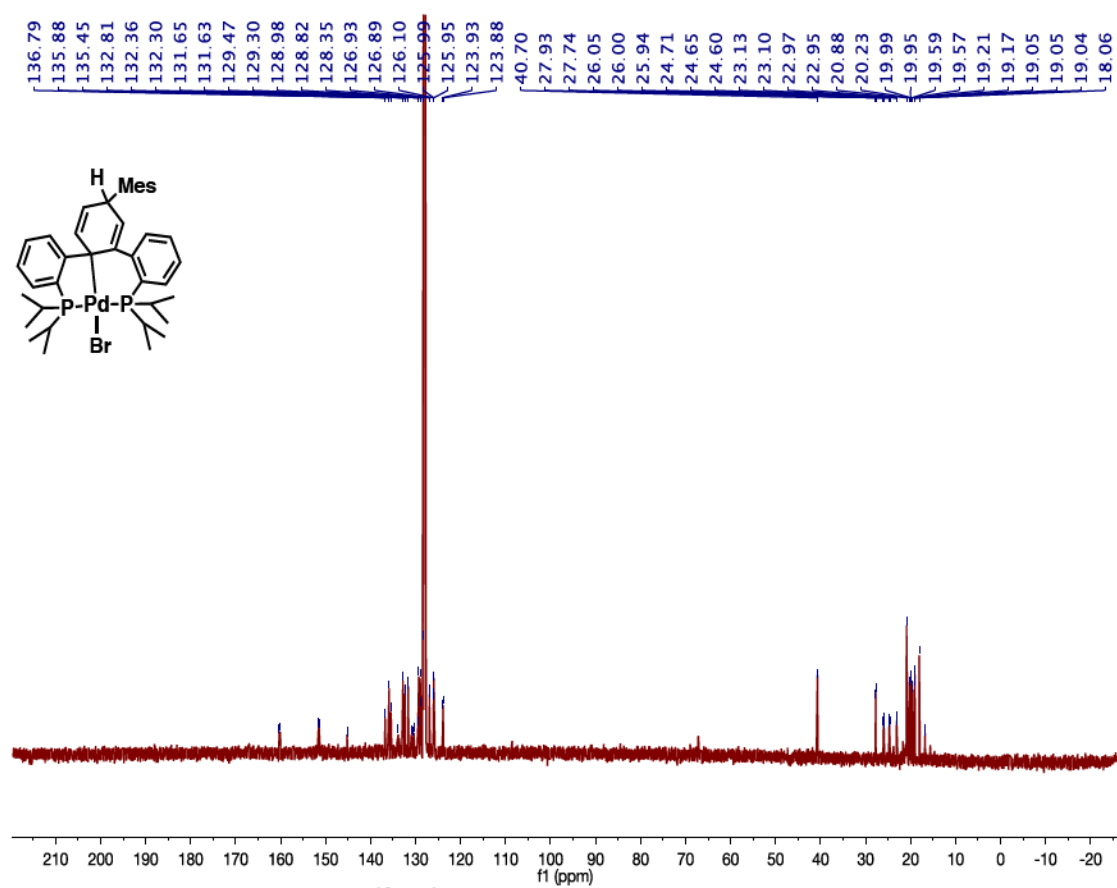
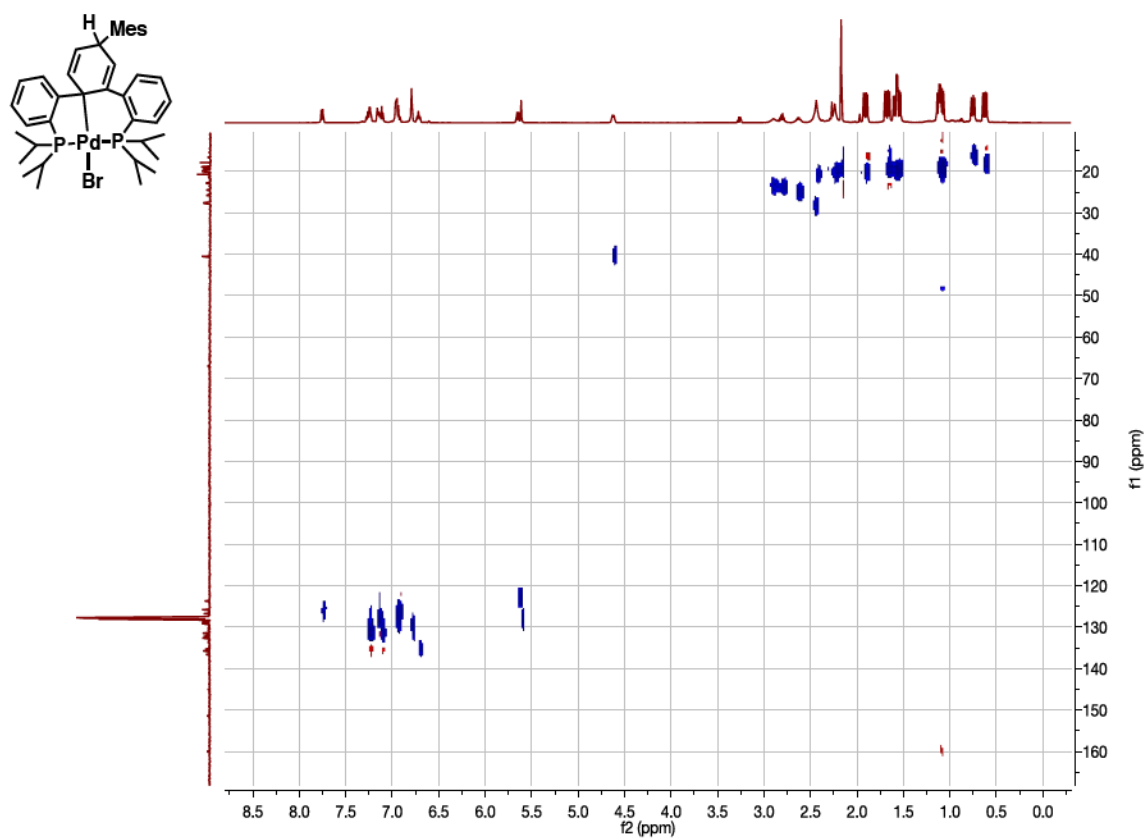


Figure A.16: <sup>1</sup>H NMR spectrum of (Pter<sup>Mes</sup>P)<sub>2</sub>PdBr (**58**).



**Figure A.17:**  $^{13}\text{C}\{^1\text{H}\}$  NMR spectrum of (Pter<sup>mes</sup>P)PdBr (**58**).



**Figure A.19:** HSQC of (Pter<sup>mes</sup>P)PdBr (**58**).

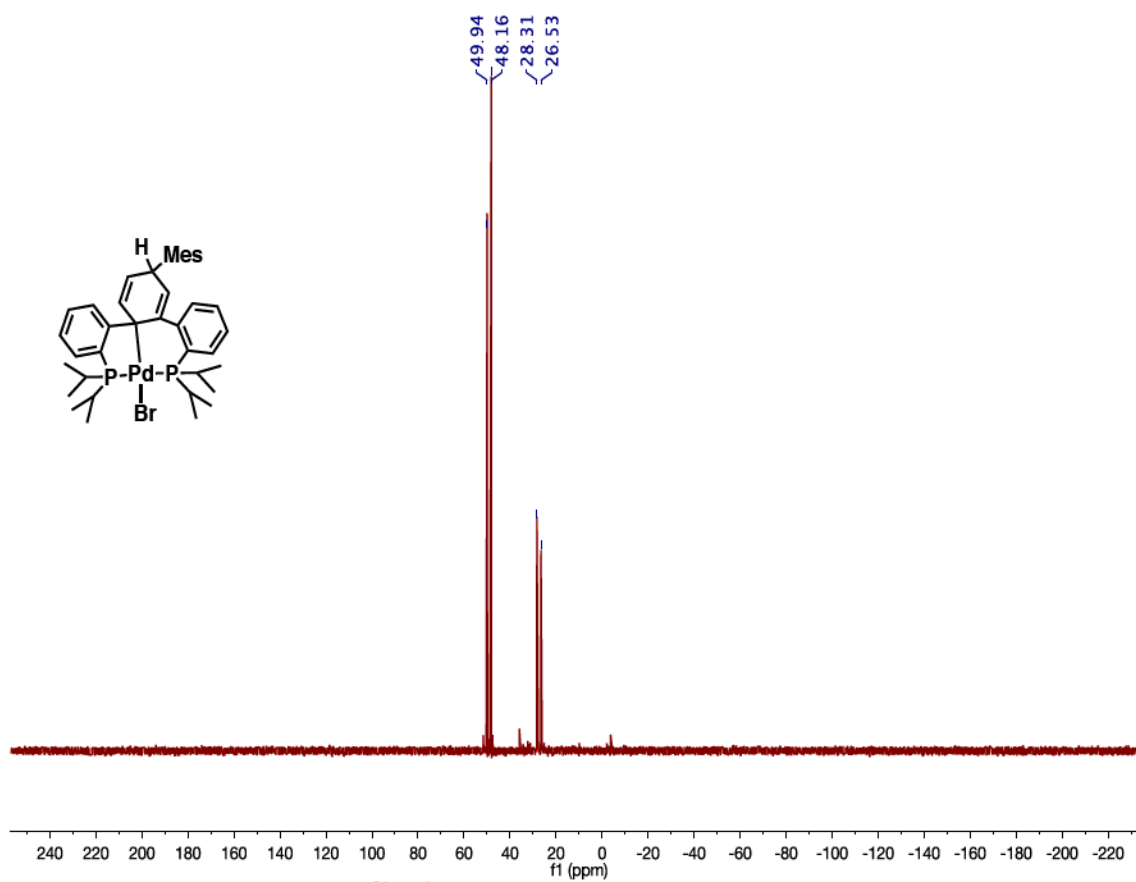


**Figure A.20:**  $^{31}\text{P}\{^1\text{H}\}$  NMR Spectrum of (Pter<sup>mes</sup>PdBr) (**58**).

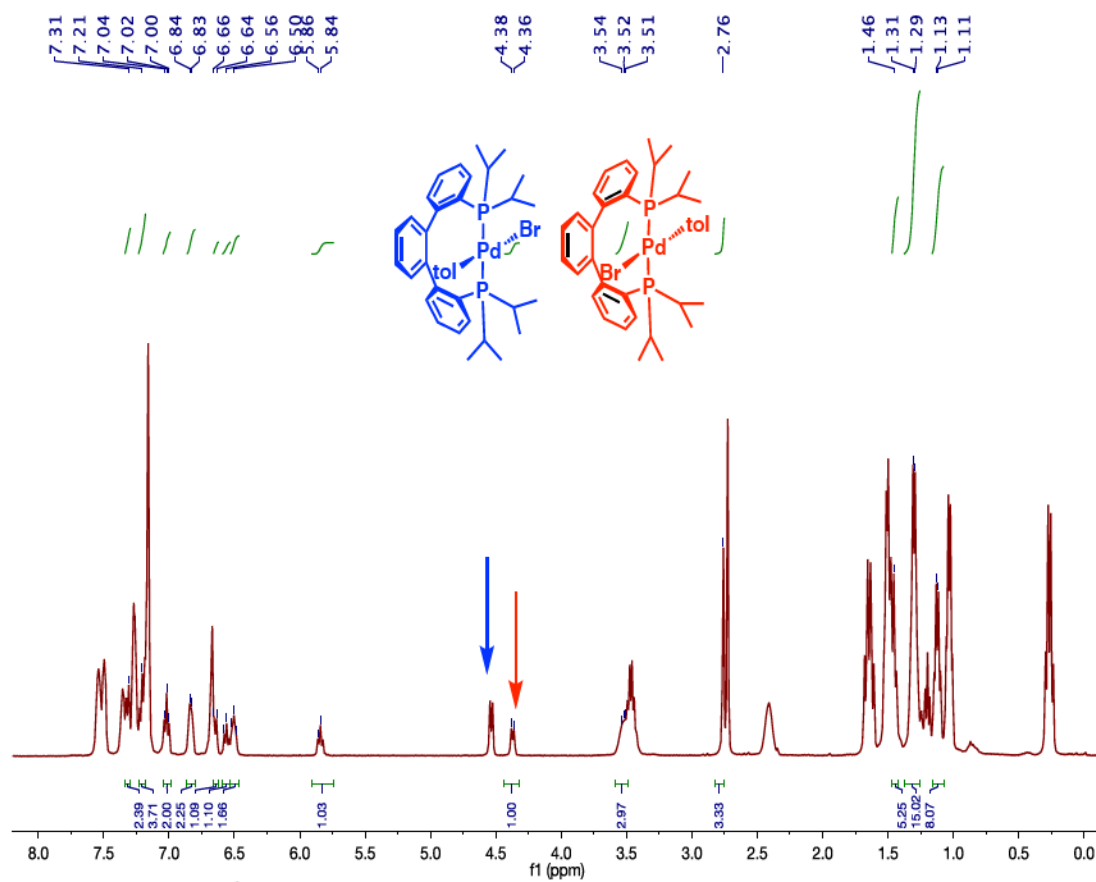


**Figure A.21:**  $^1\text{H}$  NMR spectrum of mixture of isomers of  $(\text{PterP})\text{PdBr}(\text{tol})$  (60a-b).

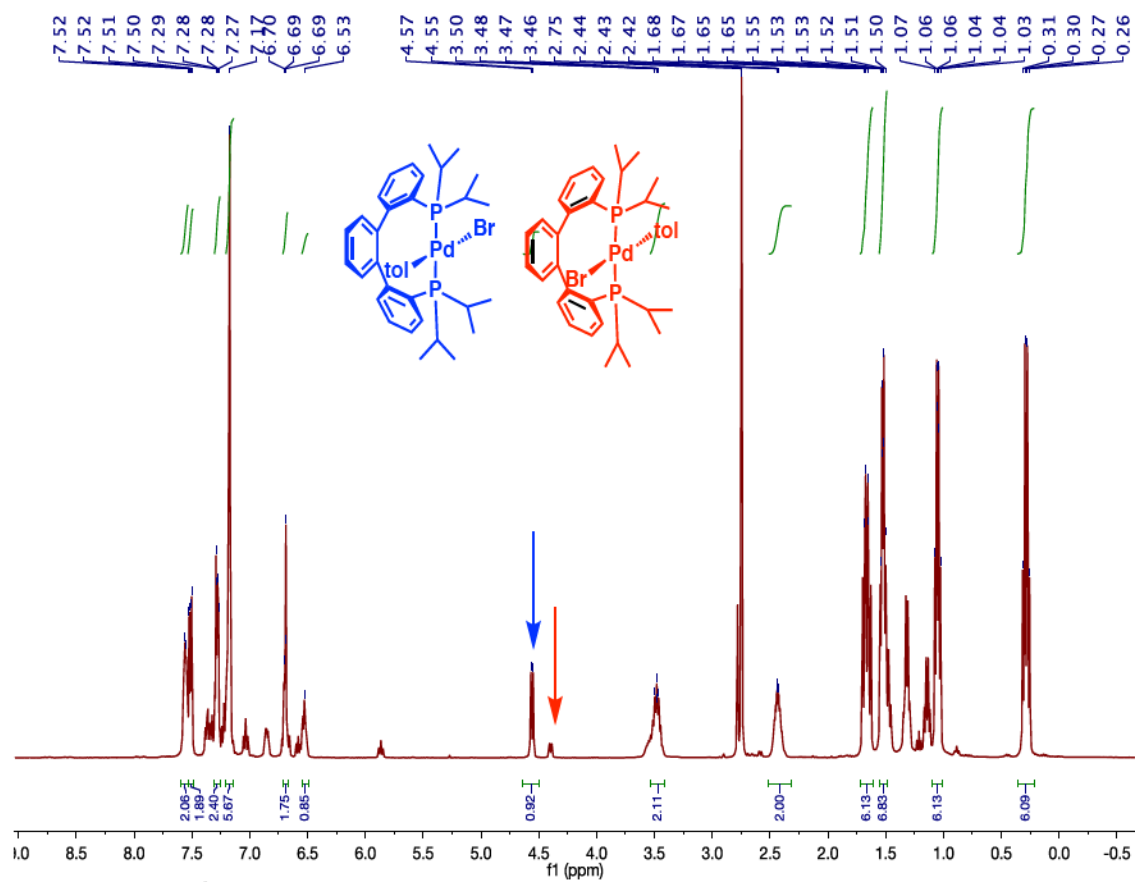


**Figure A.22:**  $^1\text{H}$  NMR spectrum of isomers of  $(\text{PterP})\text{PdBr}(\text{tol})$  (**60a-b**) after 2h at  $80^\circ\text{C}$ .

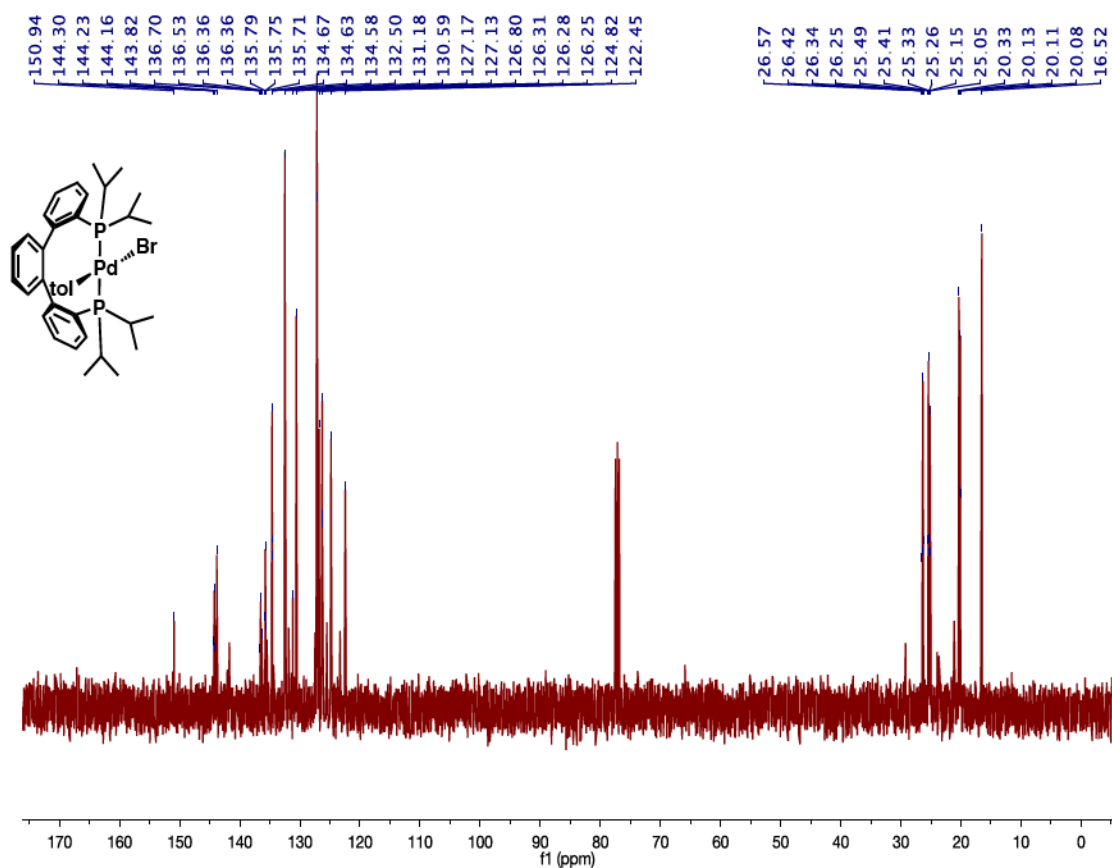


**Figure A.23:**  $^{13}\text{C}\{^1\text{H}\}$  NMR spectrum of syn-isomer of (PterP)PdBr(tol) (**60a-b**).



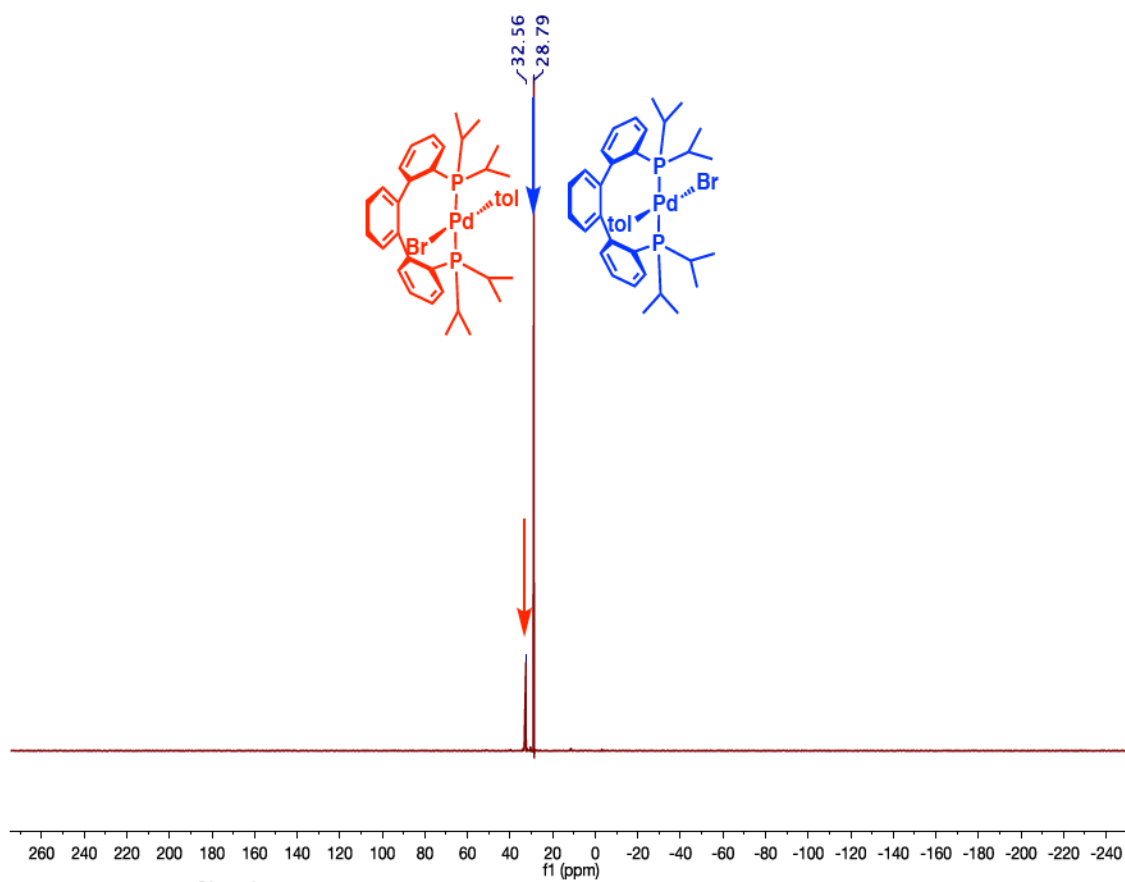


**Figure A.24:**  $^{31}\text{P}\{^1\text{H}\}$  NMR spectrum of mixture of isomers of (PterP)PdBr(tol) (**60a-b**).

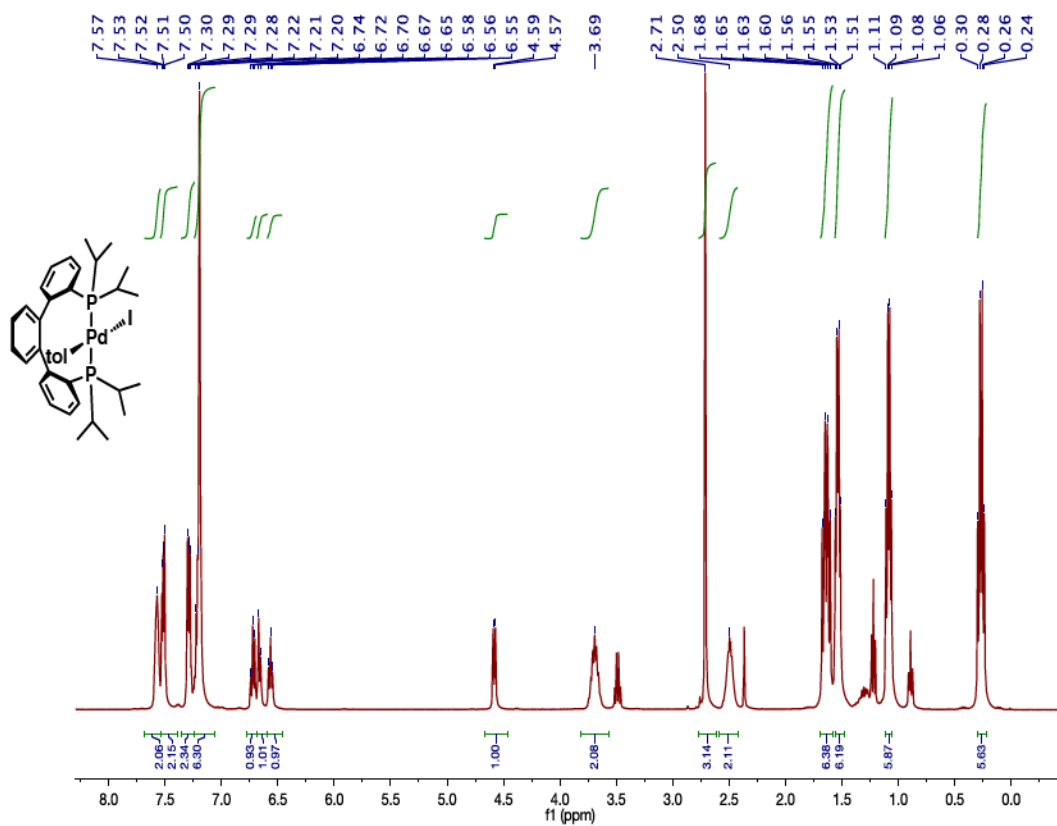


**Figure A.25:**  $^1\text{H}$  NMR spectrum of syn-isomer of  $(\text{PterP})\text{PdI}(\text{tol})$  (**61b**).

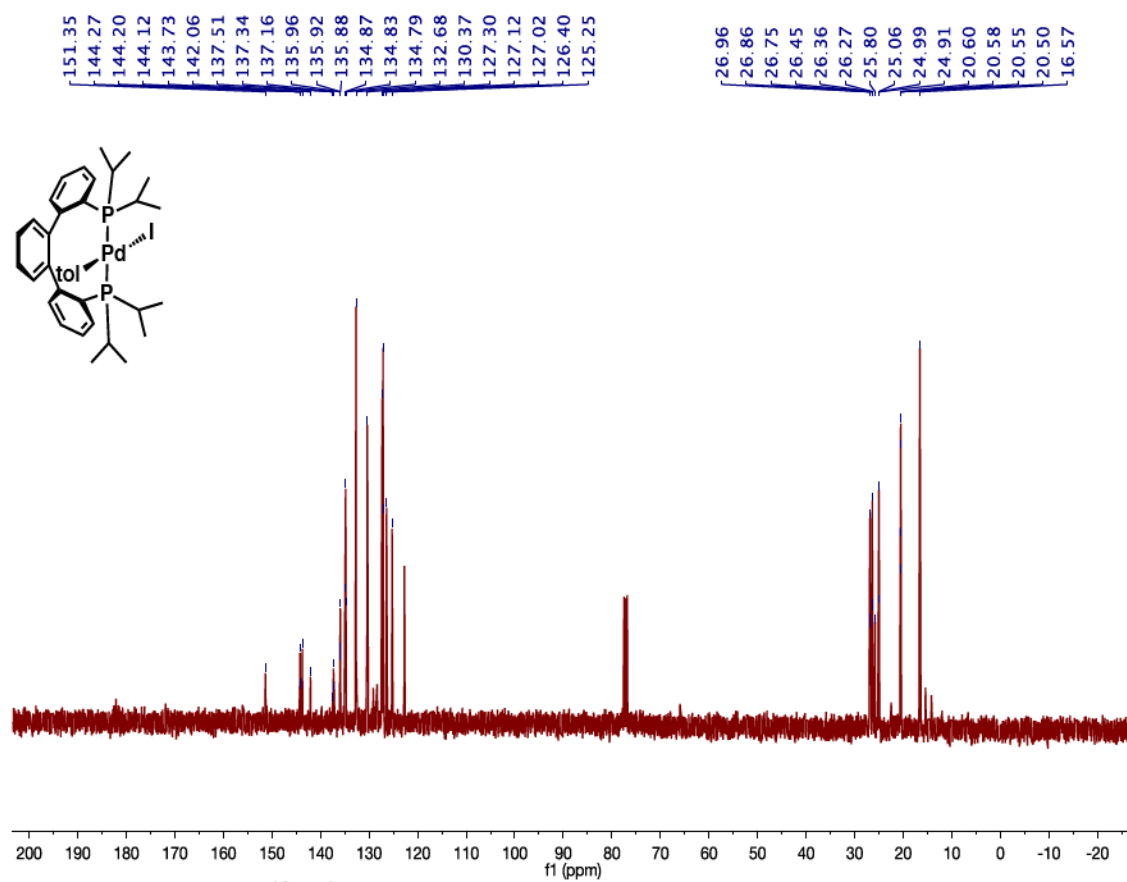


**Figure A.26:**  $^{13}\text{C}\{^1\text{H}\}$  NMR spectrum of syn-isomer of (PterP)PdI(tol) (**61b**).

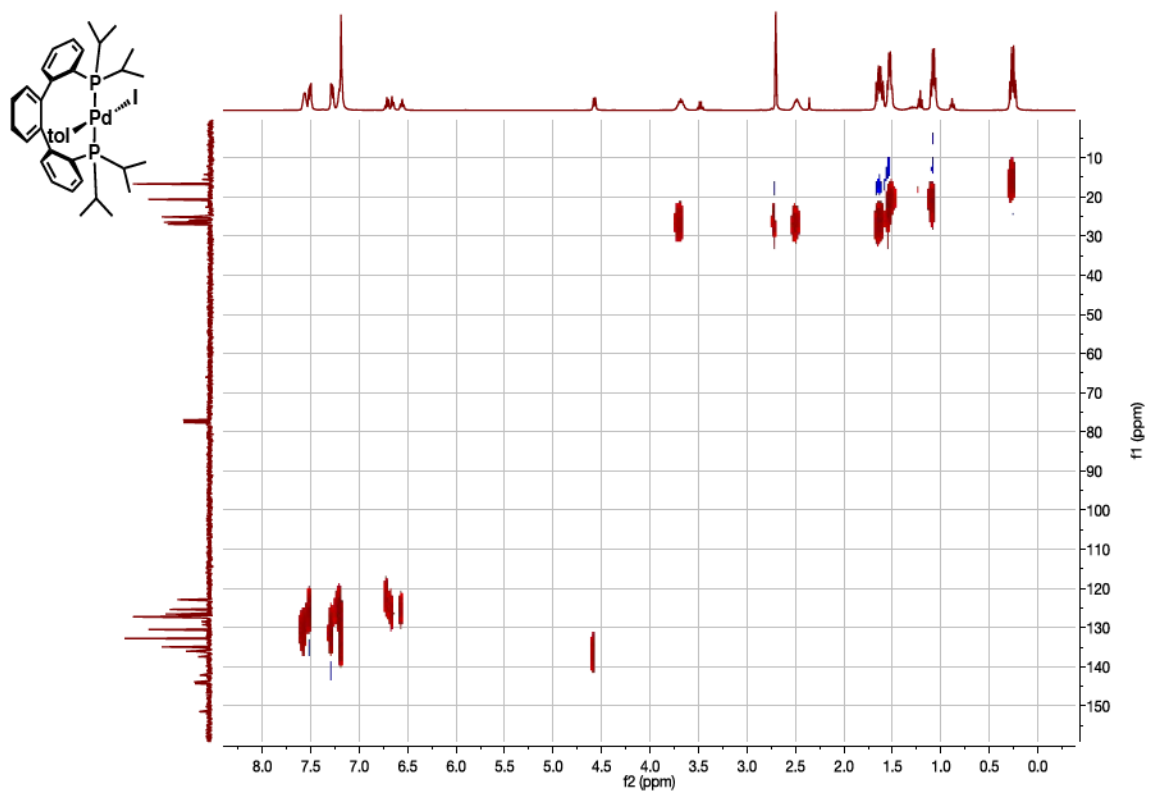


**Figure A.27:** HSQC of (PterP)PdI(tol) (**61b**).

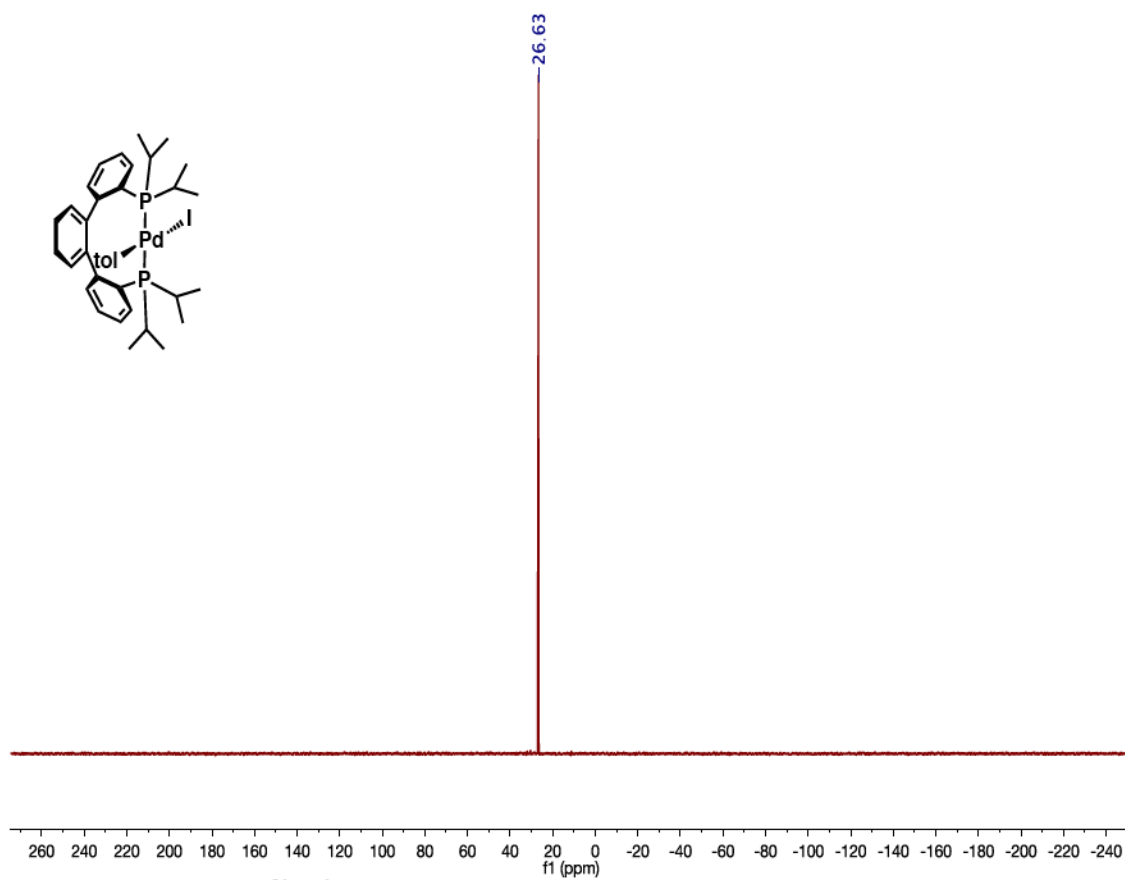


**Figure A.28:**  $^{31}\text{P}\{^1\text{H}\}$  NMR spectrum of syn-isomer of (PterP)PdI(tol) (**61b**).

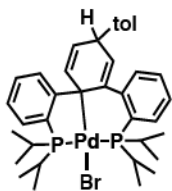


**Figure A.29:**  $^1\text{H}$  NMR spectrum of  $(\text{Pter}^{\text{tolP}})\text{PdBr}$  (**62**).

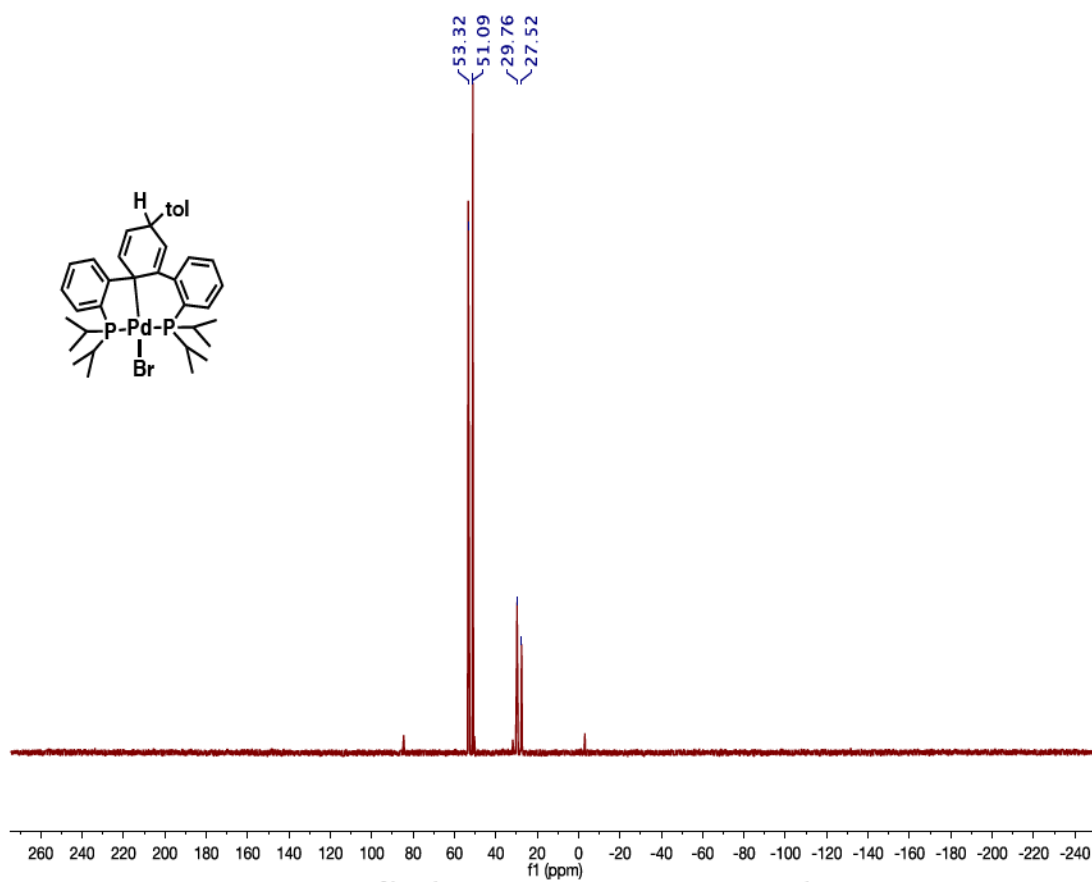


**Figure A.30:**  $^{31}\text{P}\{^1\text{H}\}$  NMR spectrum of (Pter<sup>tol</sup>P)PdBr (**62**).

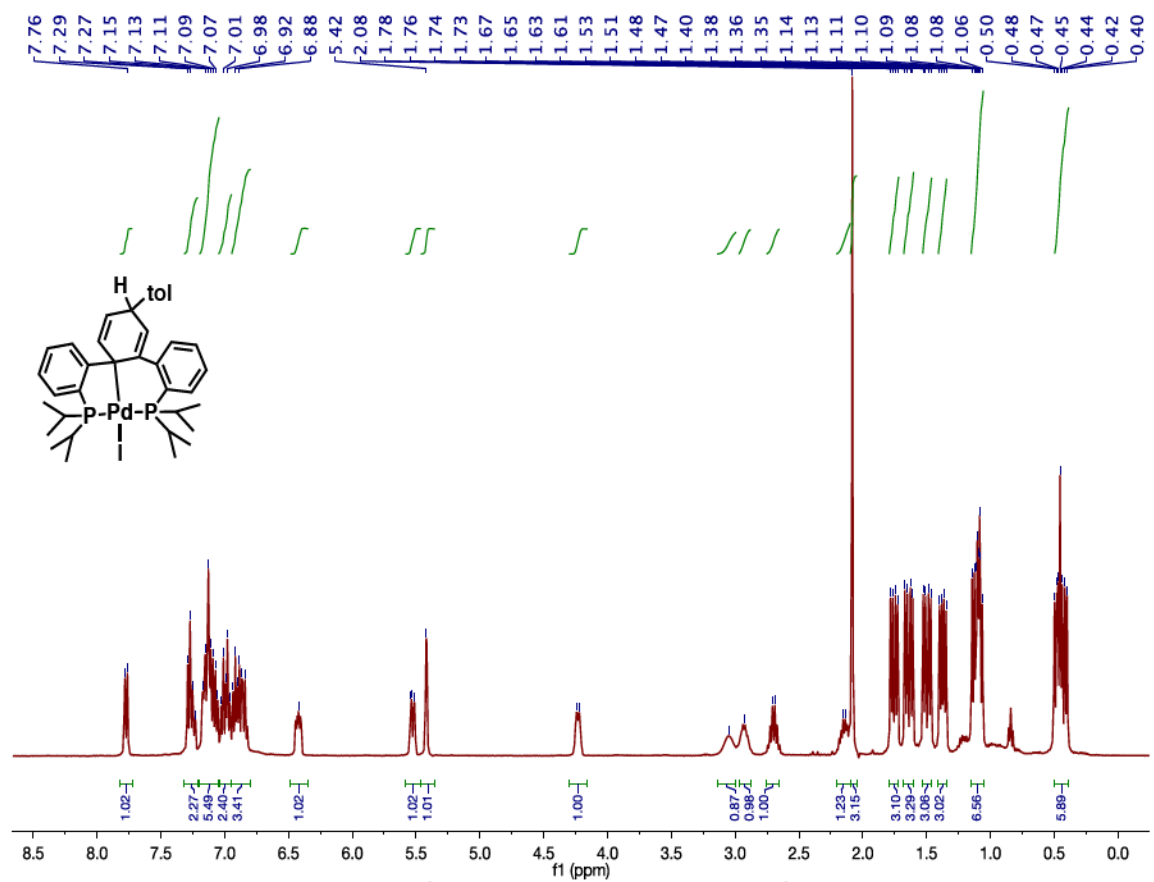
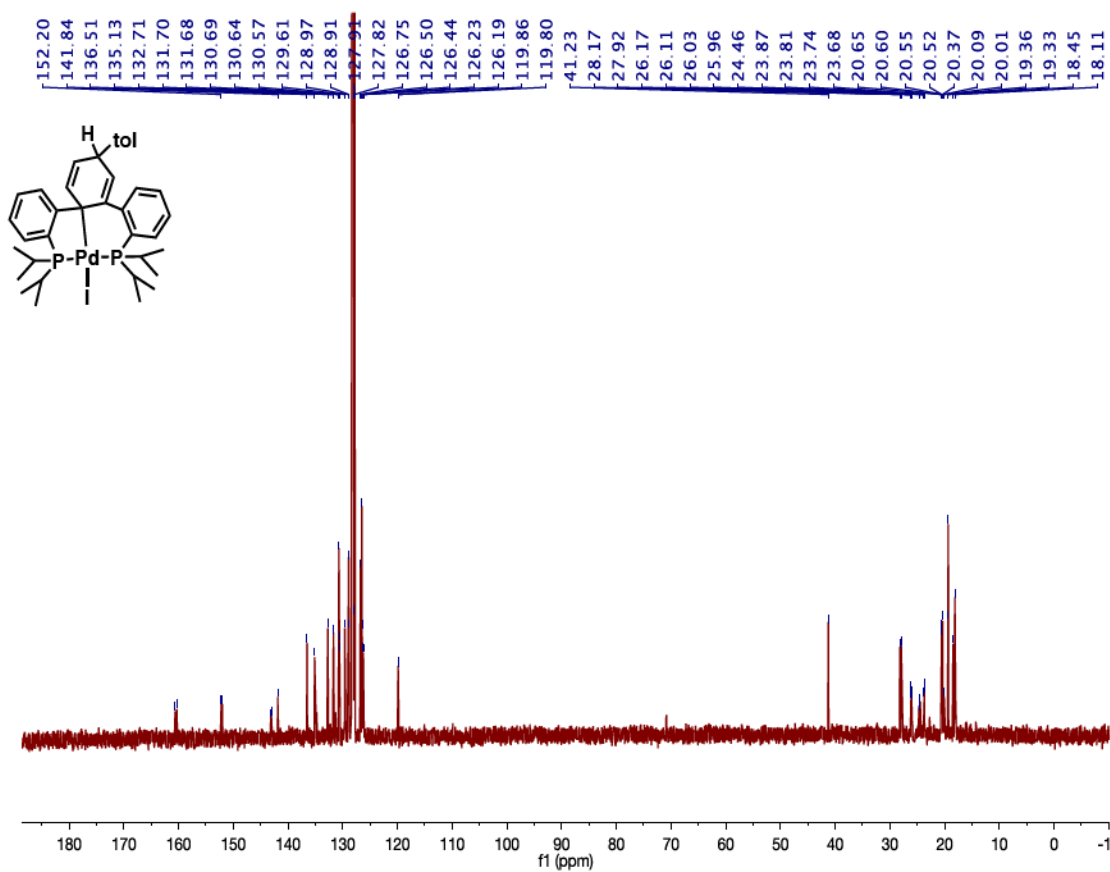
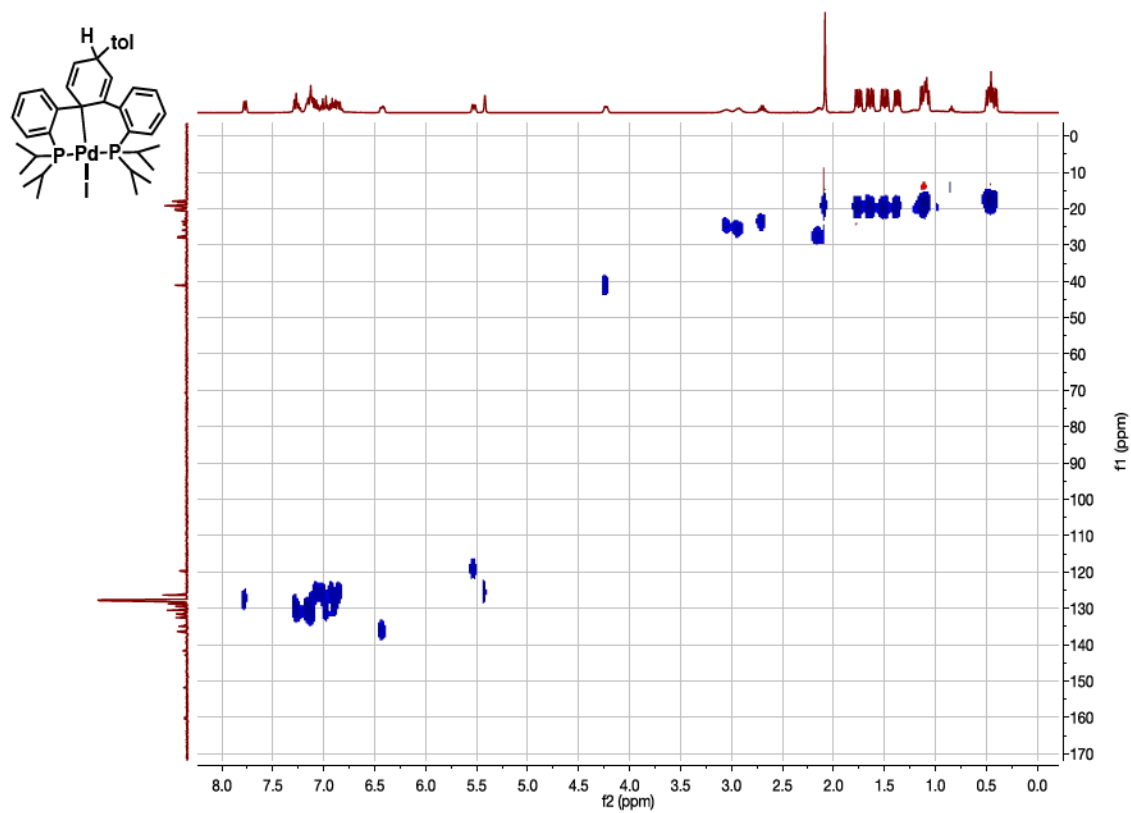


Figure A.31:  $^1\text{H}$  NMR spectrum of  $(\text{Pter}^{\text{tol}}\text{P})\text{PdI}$  (63).

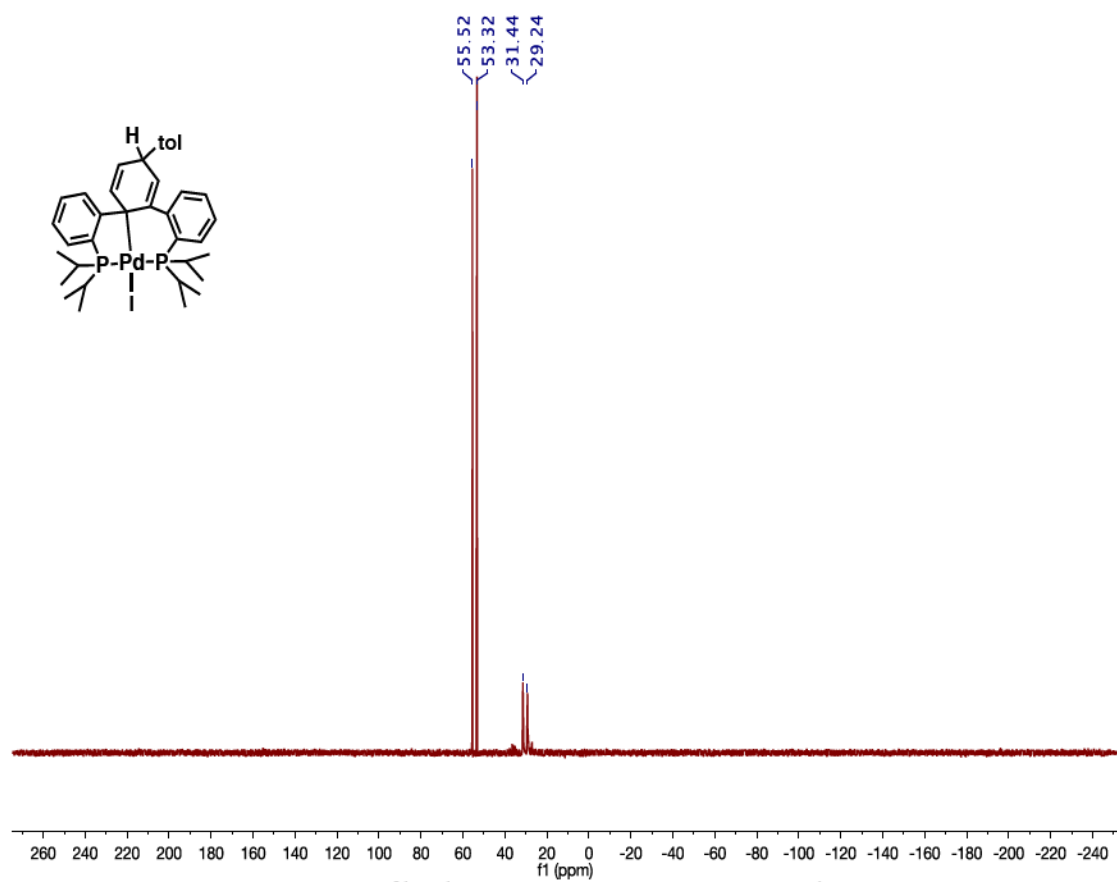




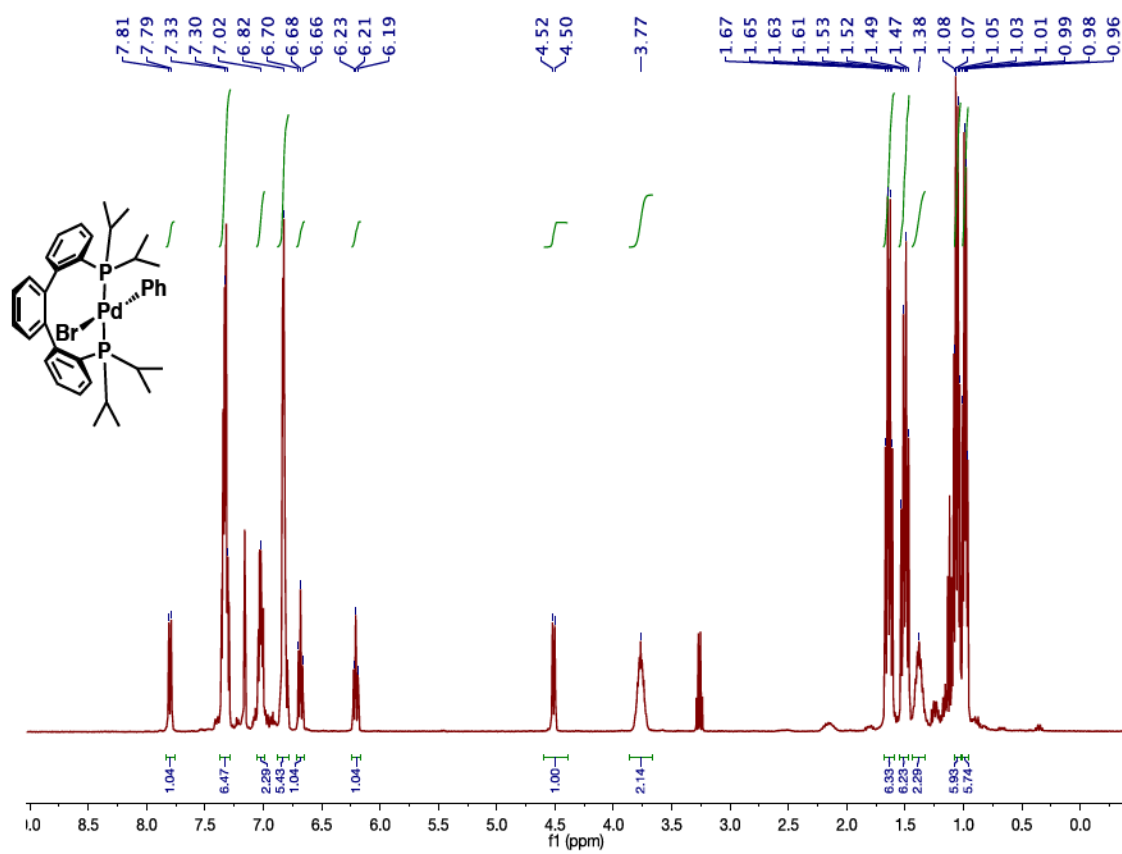
**Figure A.32:**  $^{13}\text{C}\{^1\text{H}\}$  NMR spectrum of (Pter<sup>tol</sup>P)PdI (63).



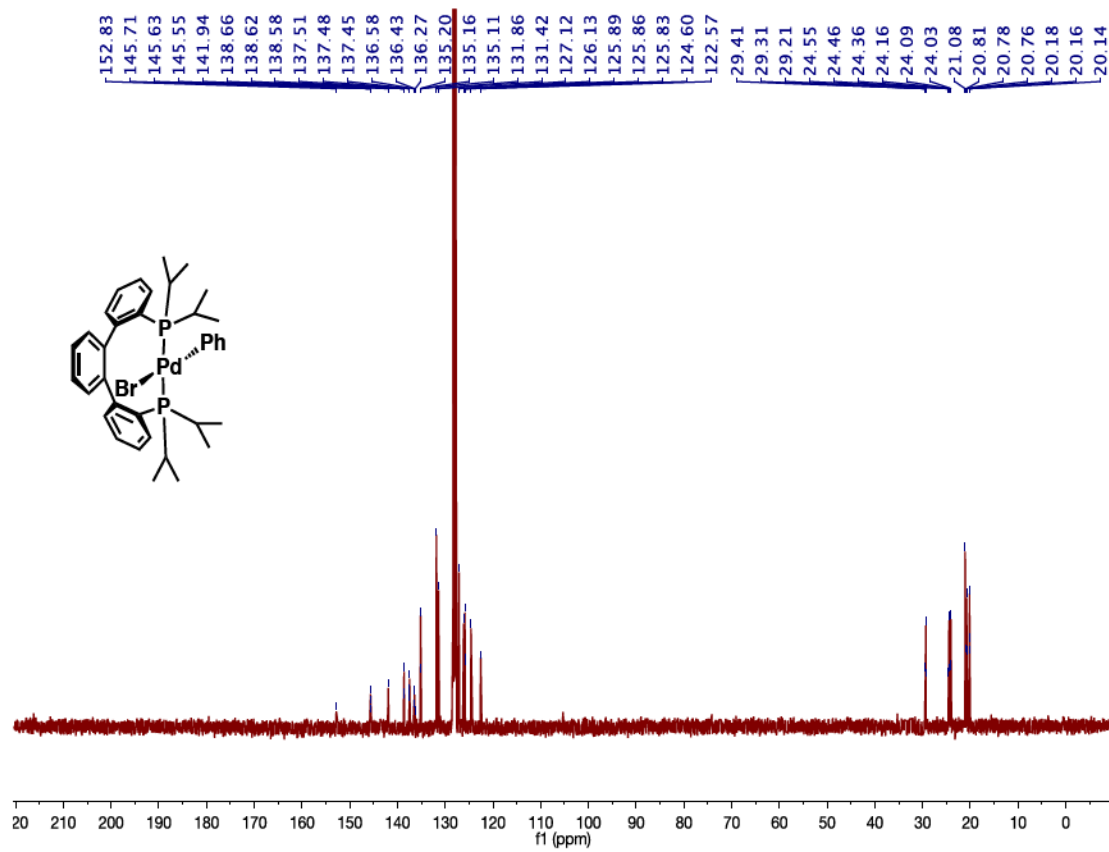
**Figure A.33:** HSQC of (Pter<sup>tol</sup>P)PdI (**63**).



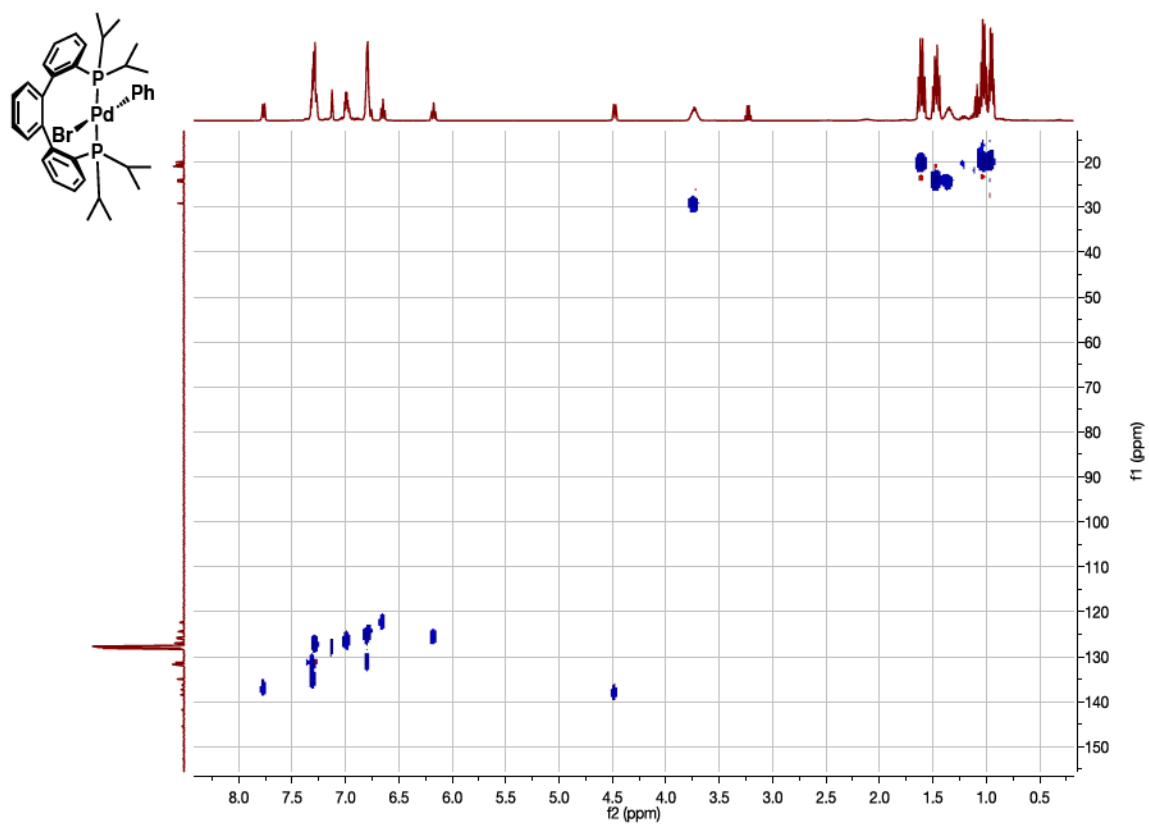
**Figure A.34:**  $^{31}\text{P}\{^1\text{H}\}$  NMR spectrum of  $(\text{Pter}^{\text{tol}}\text{P})\text{PdI}$  (63).



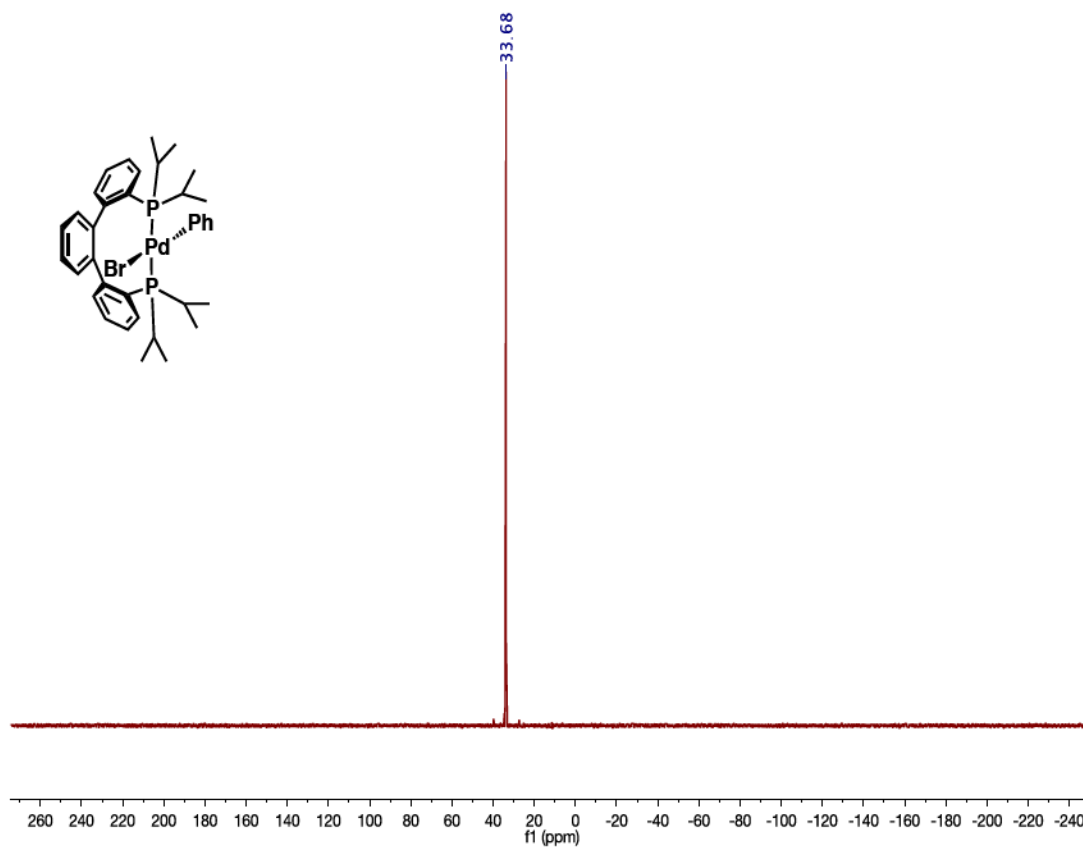
**Figure A.35:**  $^1\text{H}$  NMR spectrum of anti-isomer of  $(\text{PterP})\text{PdBrPh}$  (65a).



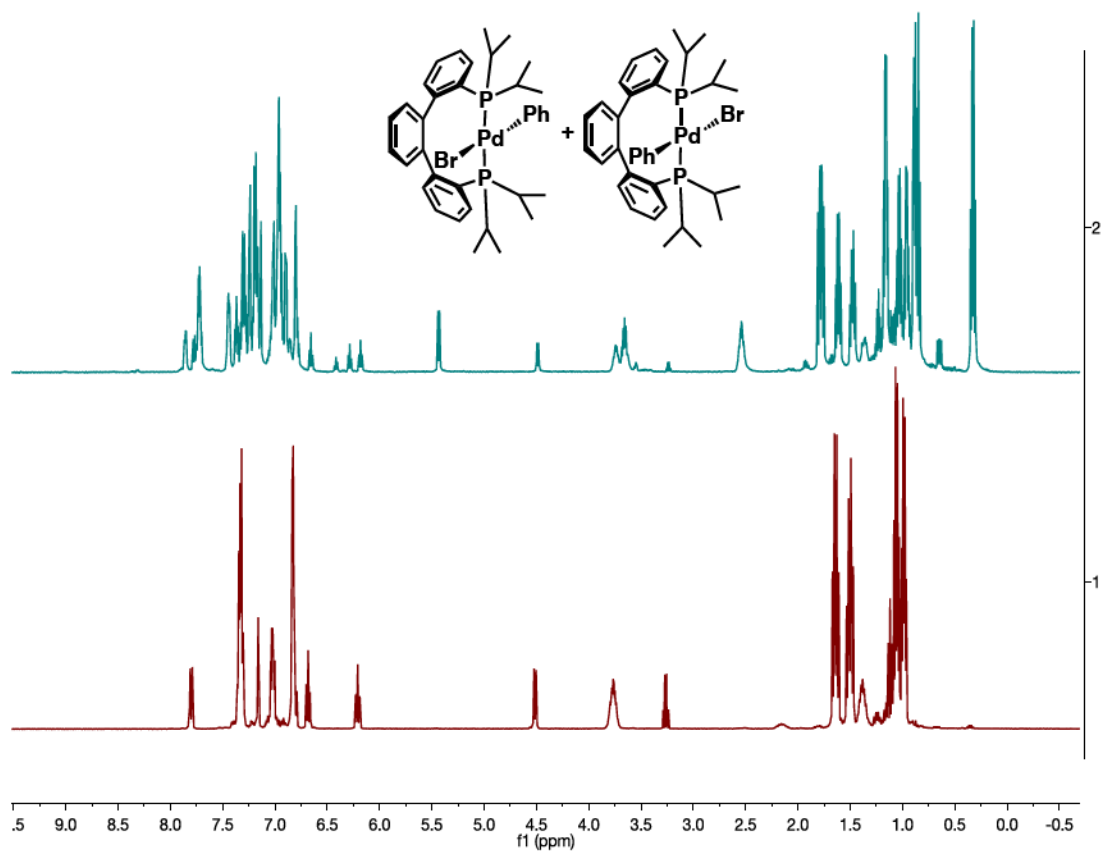
**Figure A.36:**  $^{13}\text{C}\{^1\text{H}\}$  NMR spectrum of anti-isomer of (PterP)PdBrPh (65a).



**Figure A.37:** HSQC of (PterP)PdBrPh (**65a**).

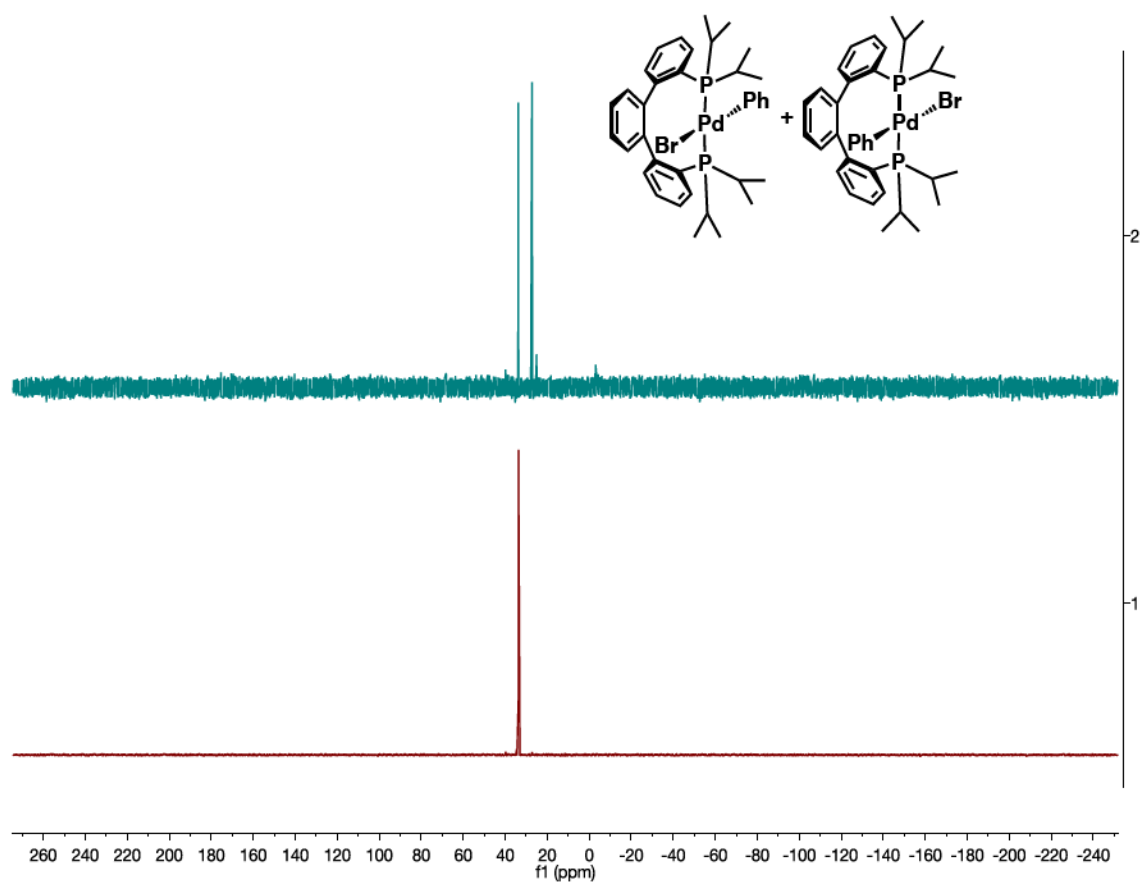


**Figure A.38:**  $^{31}\text{P}\{^1\text{H}\}$  NMR spectrum of anti-isomer of (PterP)PdBrPh (**65a**).

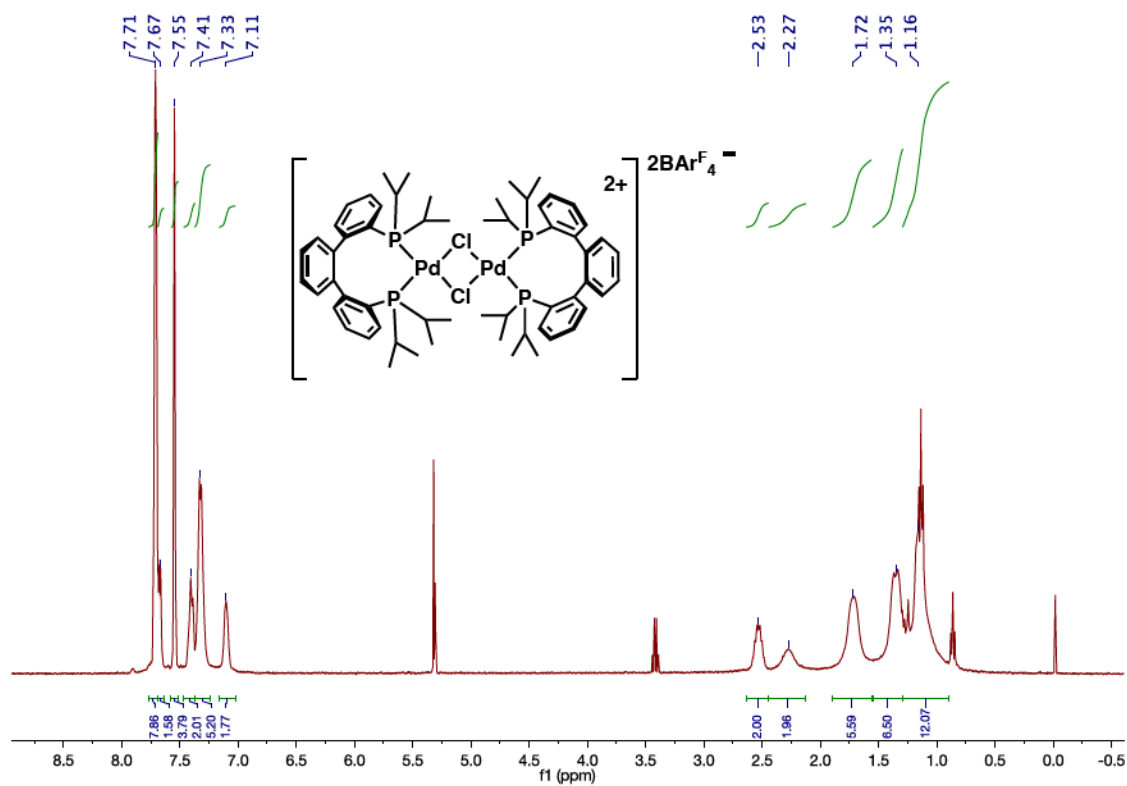


**Figure A.39:**  $^1\text{H}$  NMR spectrum of  $(\text{PterP})\text{PdBrPh}$  after heating to  $80^\circ\text{C}$  for 24 h (top).  $^1\text{H}$  NMR spectrum of pure anti-isomer of  $(\text{PterP})\text{PdBrPh}$  (**65a** bottom).

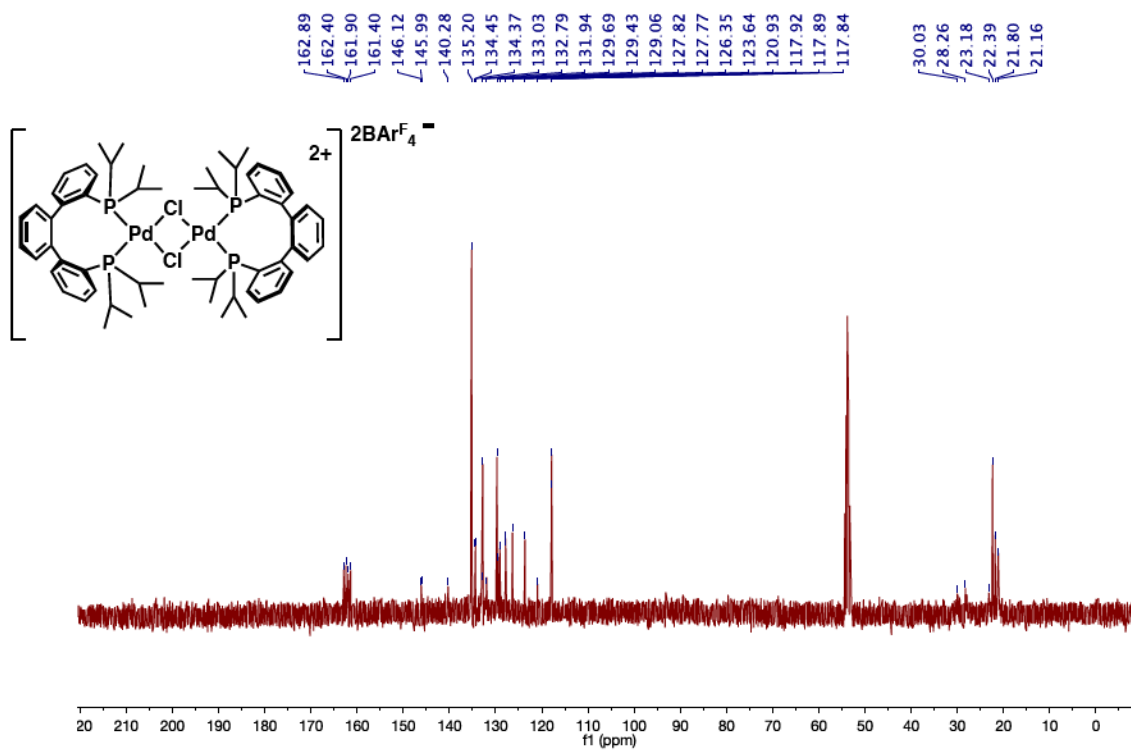




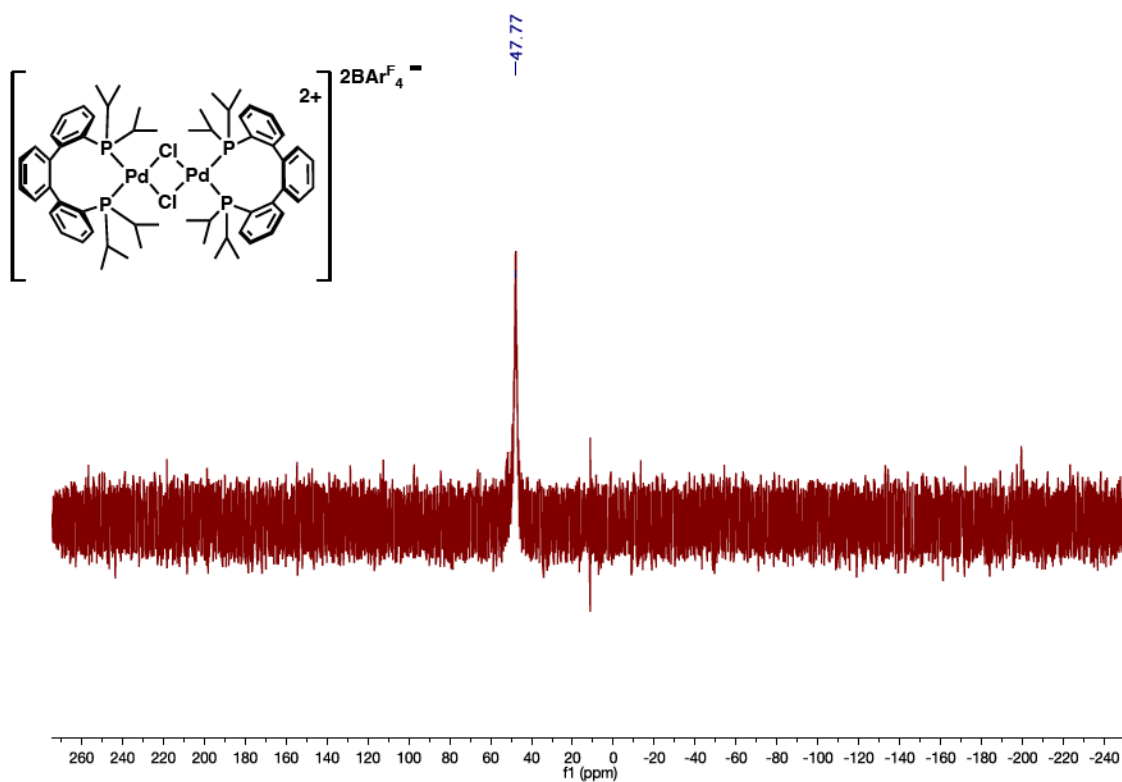
**Figure A.40:**  $^{31}\text{P}\{^1\text{H}\}$  NMR spectrum of (PterP)PdBrPh after heating to 80°C for 24 h (top).  $^{31}\text{P}\{^1\text{H}\}$  NMR spectrum of pure anti-isomer of (PterP)PdBrPh (**65a**, bottom).



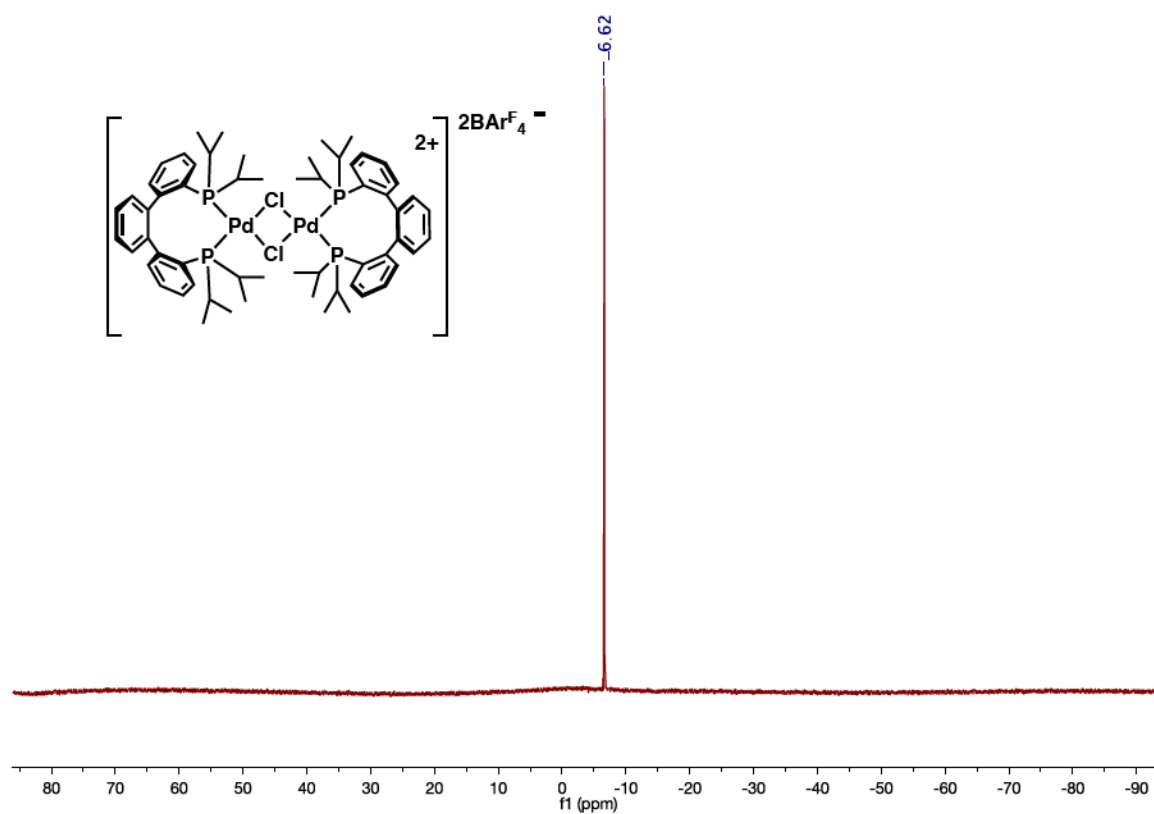
**Figure A.41:**  $^1\text{H}$  NMR spectrum of  $[(\text{PterP})\text{PdCl}]_2[2\text{BAr}^{\text{F}}_4]$  (66) at room temperature.



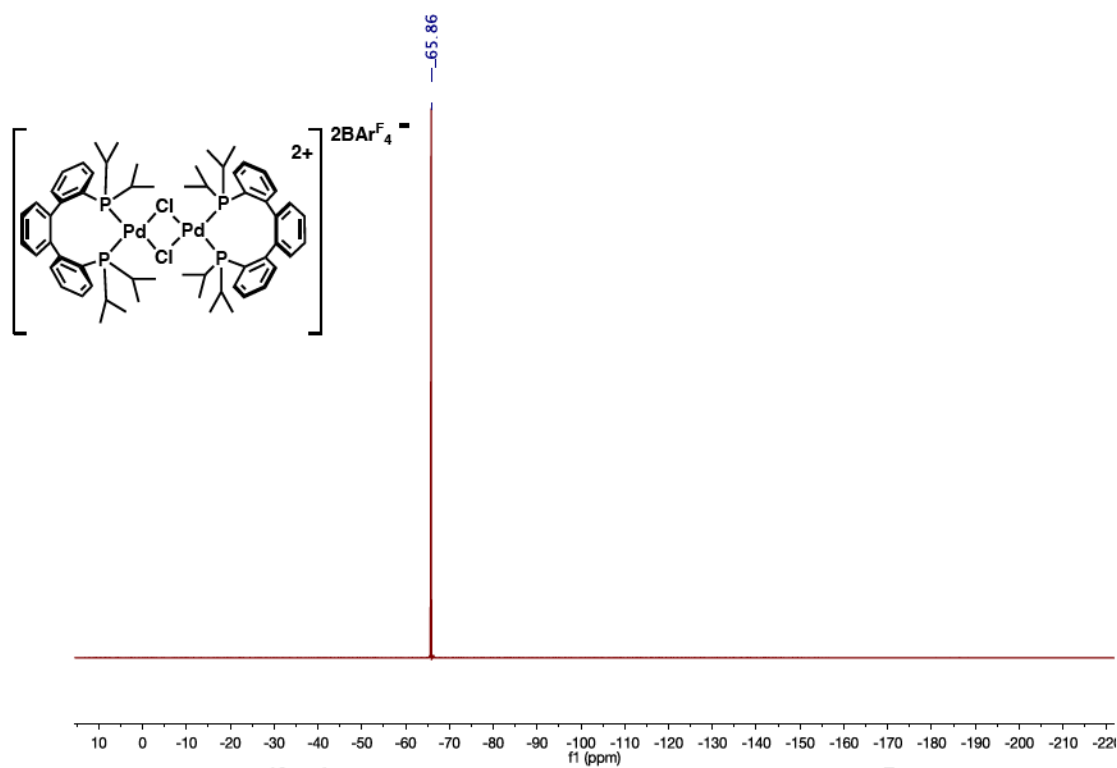
**Figure A.42.**  $^{13}\text{C}\{^1\text{H}\}$  NMR spectrum of  $[(\text{PterP})\text{PdCl}]_2[2\text{BArF}_4]$  (**66**) at room temperature.



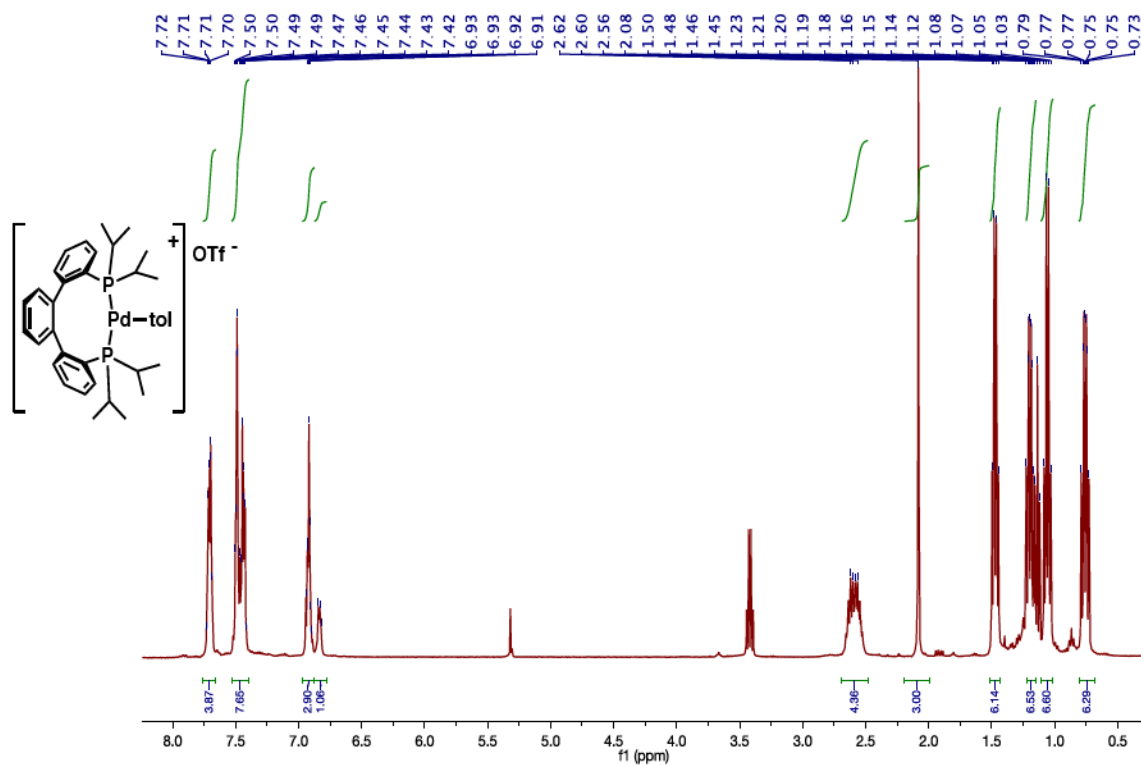
**Figure A.43:**  $^{31}\text{P}\{^1\text{H}\}$  NMR spectrum of  $[(\text{PterP})\text{PdCl}]_2[2\text{BAr}^{\text{F}}_4]$  (**66**) at room temperature.



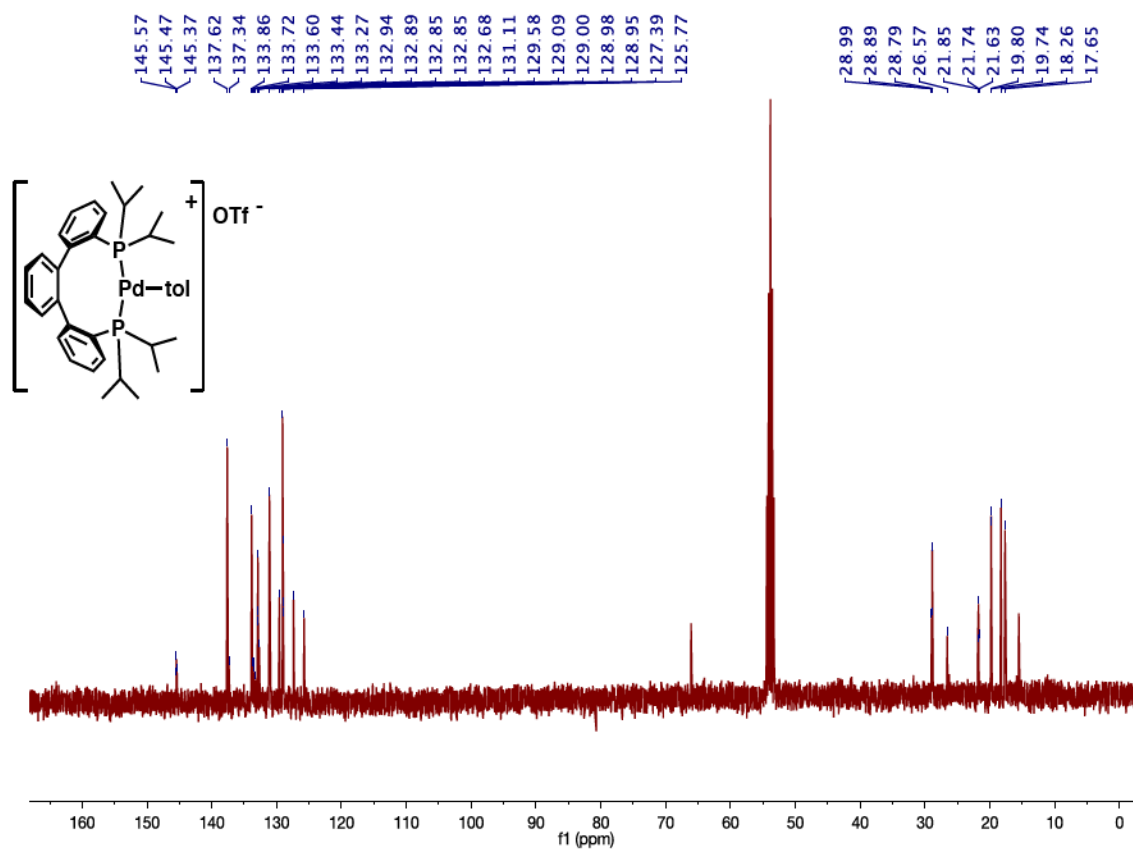
**Figure A.44:**  $^{11}\text{B}\{^1\text{H}\}$  NMR spectrum of  $[(\text{PterP})\text{PdCl}]_2[2\text{BAr}^{\text{F}}_4]$  (66) at room temperature.



**Figure A.45:**  $^{19}\text{F}\{^1\text{H}\}$  NMR spectrum of  $[(\text{PterP})\text{PdCl}]_2[2\text{BAr}^{\text{F}}_4]$  (**66**) at room temperature.

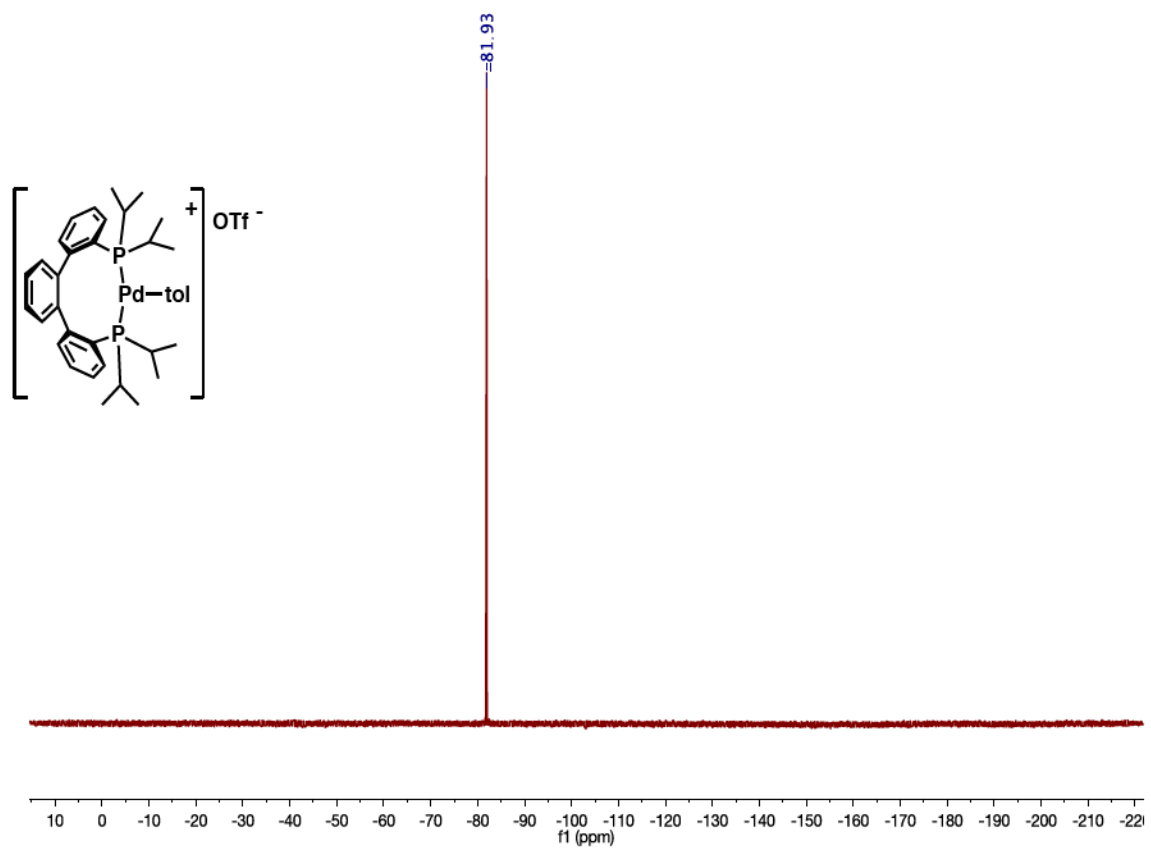


**Figure A.46:** <sup>1</sup>H NMR spectrum of  $[(PterP)Pd(tol)][OTf]$  (68).

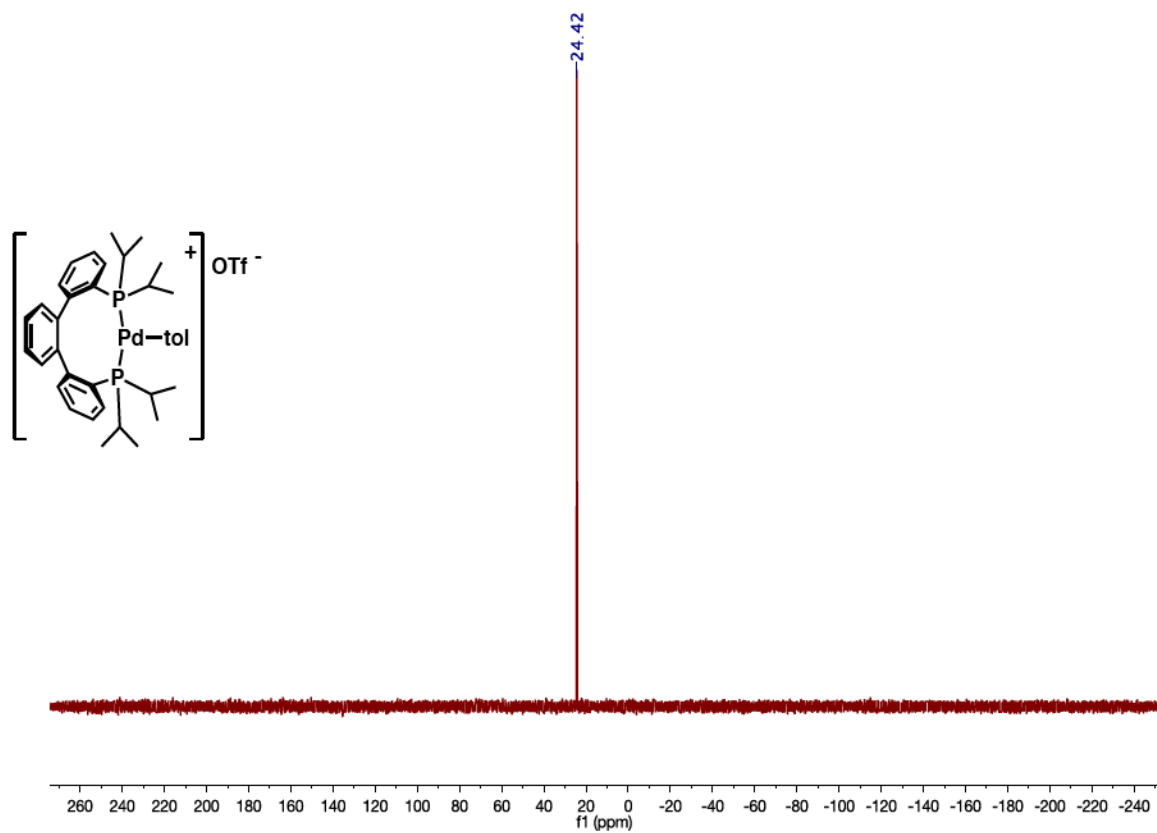


**Figure A.47:**  $^{13}C\{^1H\}$  NMR spectrum of  $[(PterP)Pd(tol)][OTf]$  (**68**).

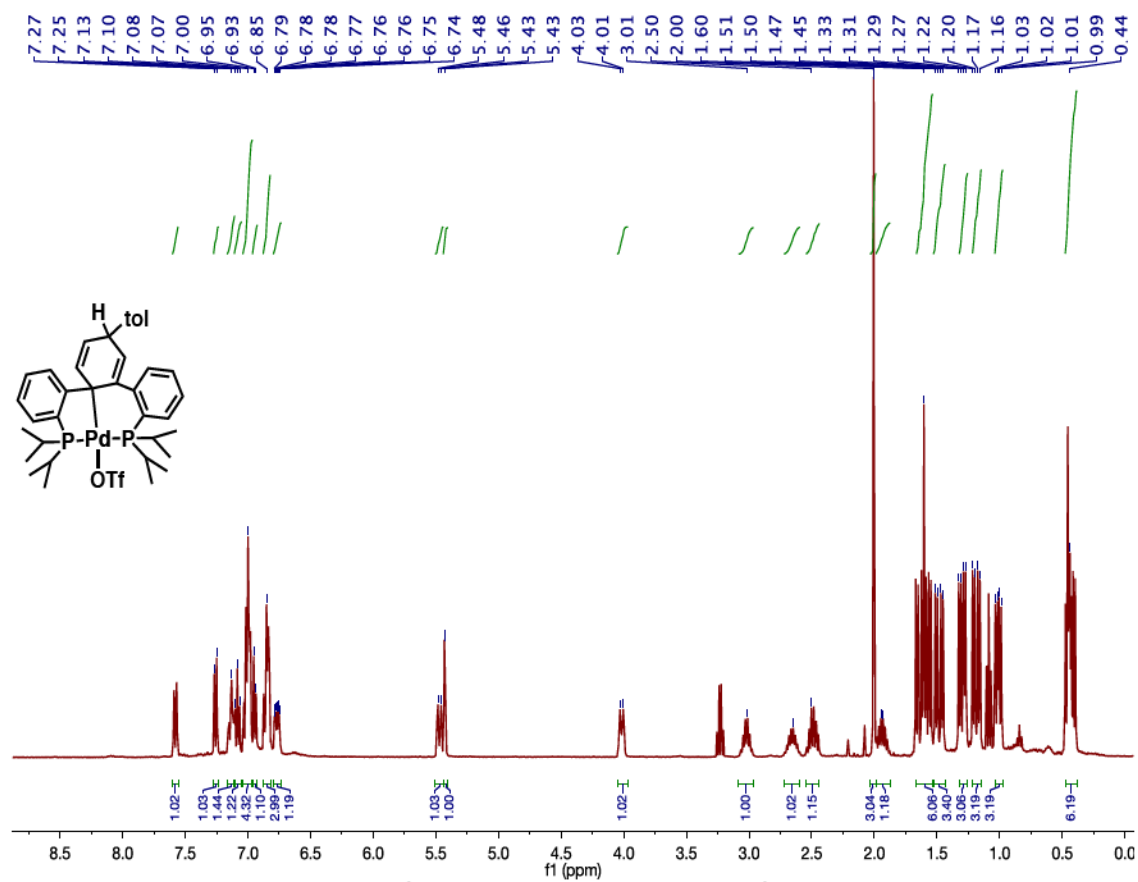




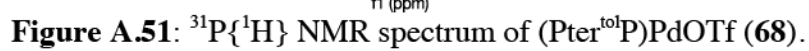
**Figure A.48:**  $^{19}\text{F}\{^1\text{H}\}$  NMR spectrum of  $[(\text{PterP})\text{Pd}(\text{tol})][\text{OTf}]$  (68).



**Figure A.49:**  $^{31}P\{^1H\}$  NMR spectrum of  $[(PterP)Pd(tol)][OTf]$  (**68**).



**Figure A.50:**  $^1\text{H}$  NMR spectrum of  $(\text{Pter}^{\text{tol}}\text{P})\text{PdOTf}$  (68).



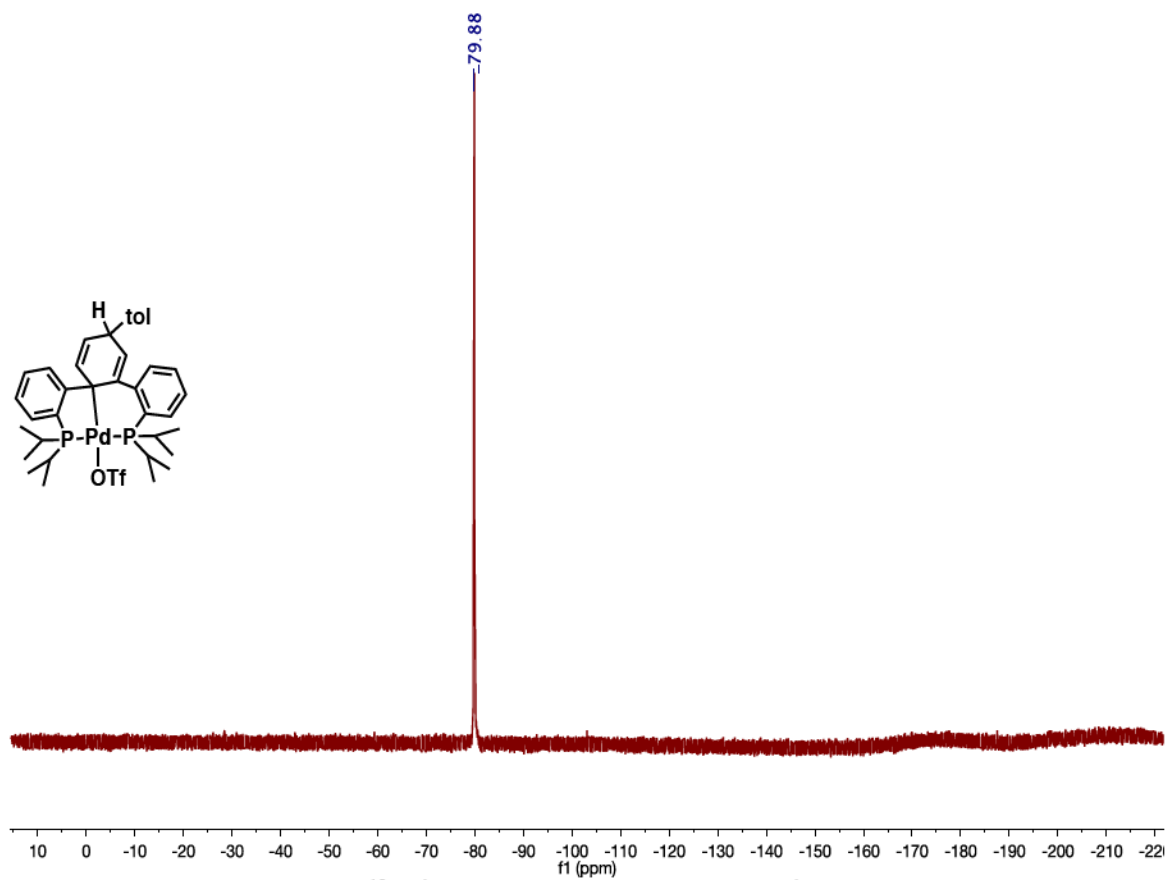


**Figure A.52:**  $^{19}\text{F}\{^1\text{H}\}$  NMR spectrum of (Pter<sup>tol</sup>P)PdOTf (**68**).

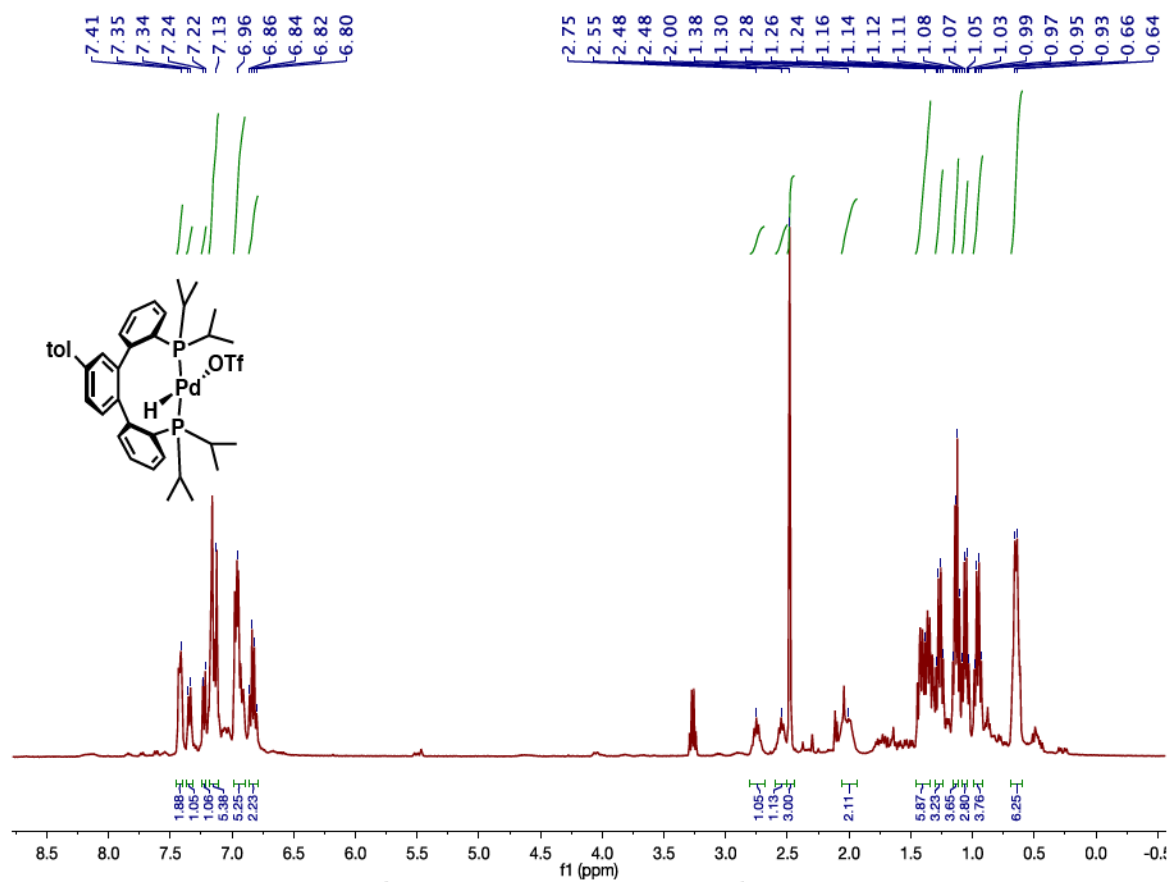


**Figure A.53:**  $^1\text{H}$  NMR spectrum of  $(\text{Pter}^{\text{tol}}\text{P})\text{PdH}(\text{OTf})$  (69).

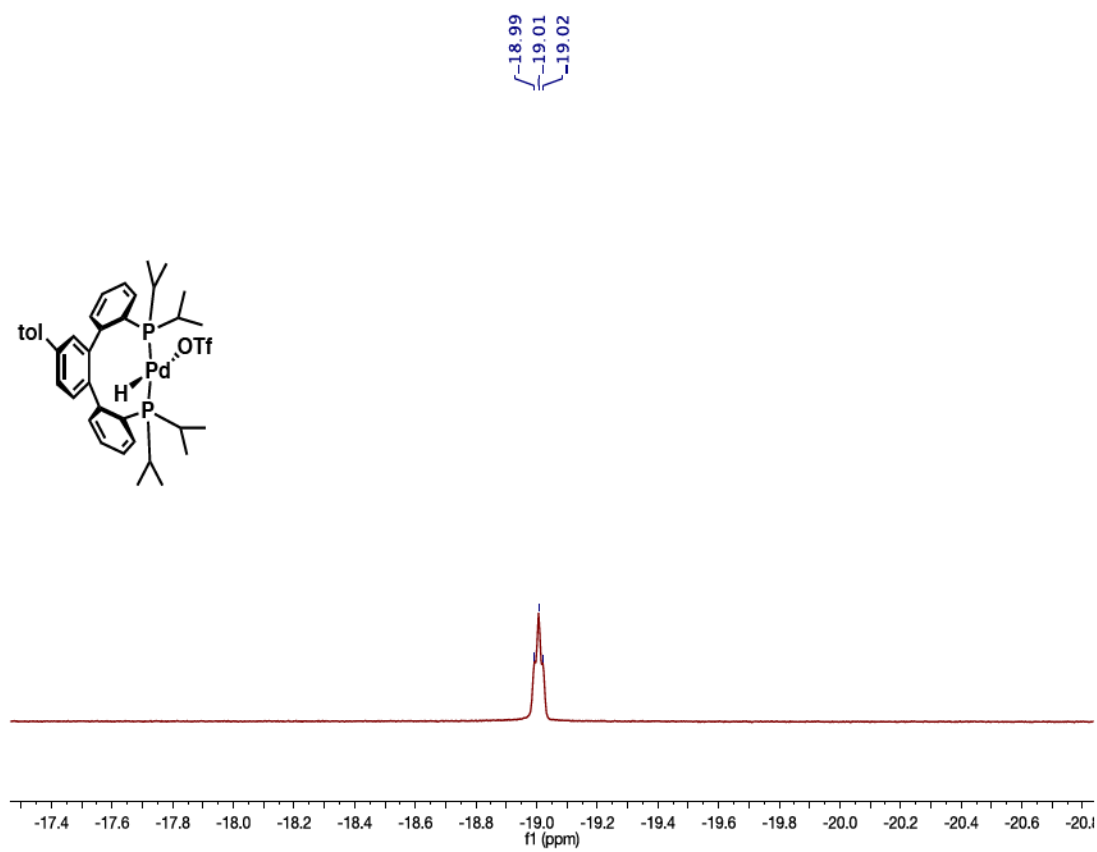


**Figure A.54:** Hydride region of the  $^1\text{H}$  NMR spectrum of (Pter<sup>tol</sup>)PdH(OTf) (**69**).

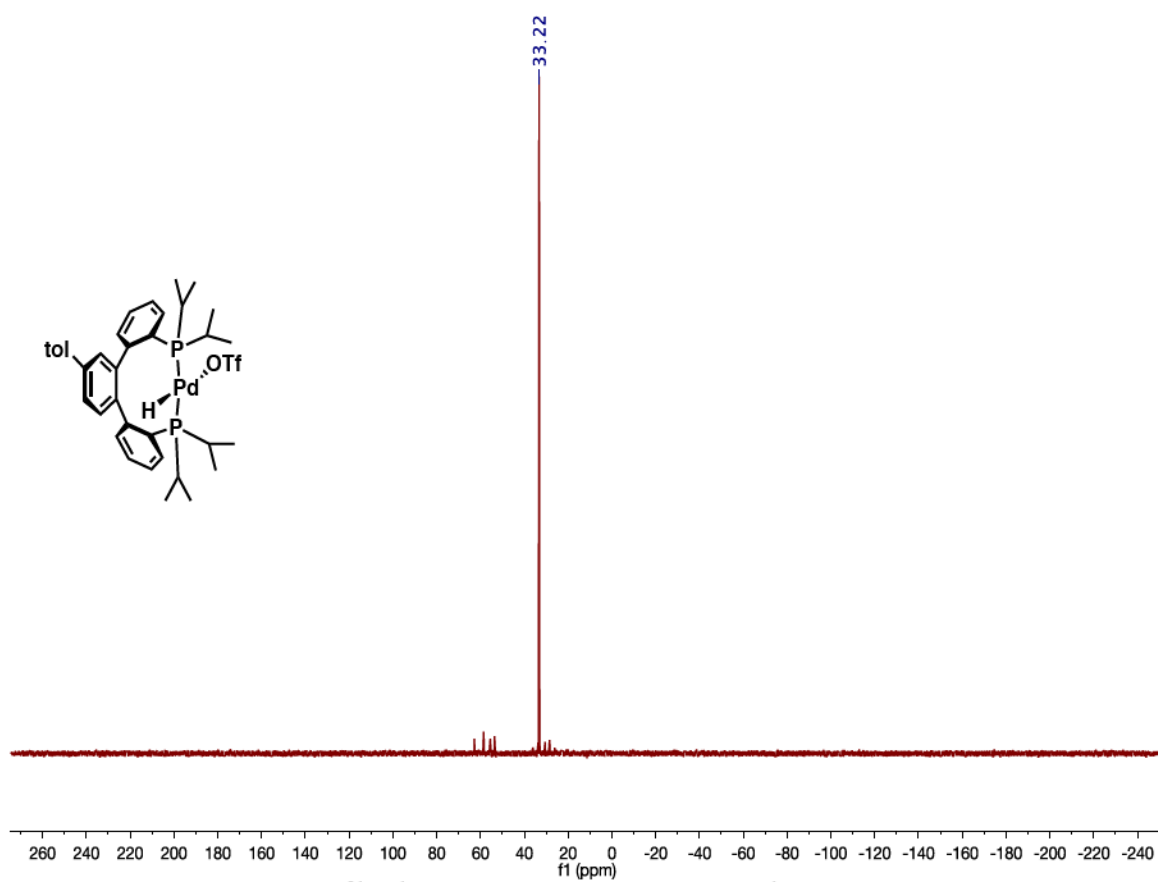


**Figure A.55:**  $^{31}\text{P}\{^1\text{H}\}$  NMR spectrum of (Pter<sup>tol</sup>)PdH(OTf) (**69**).



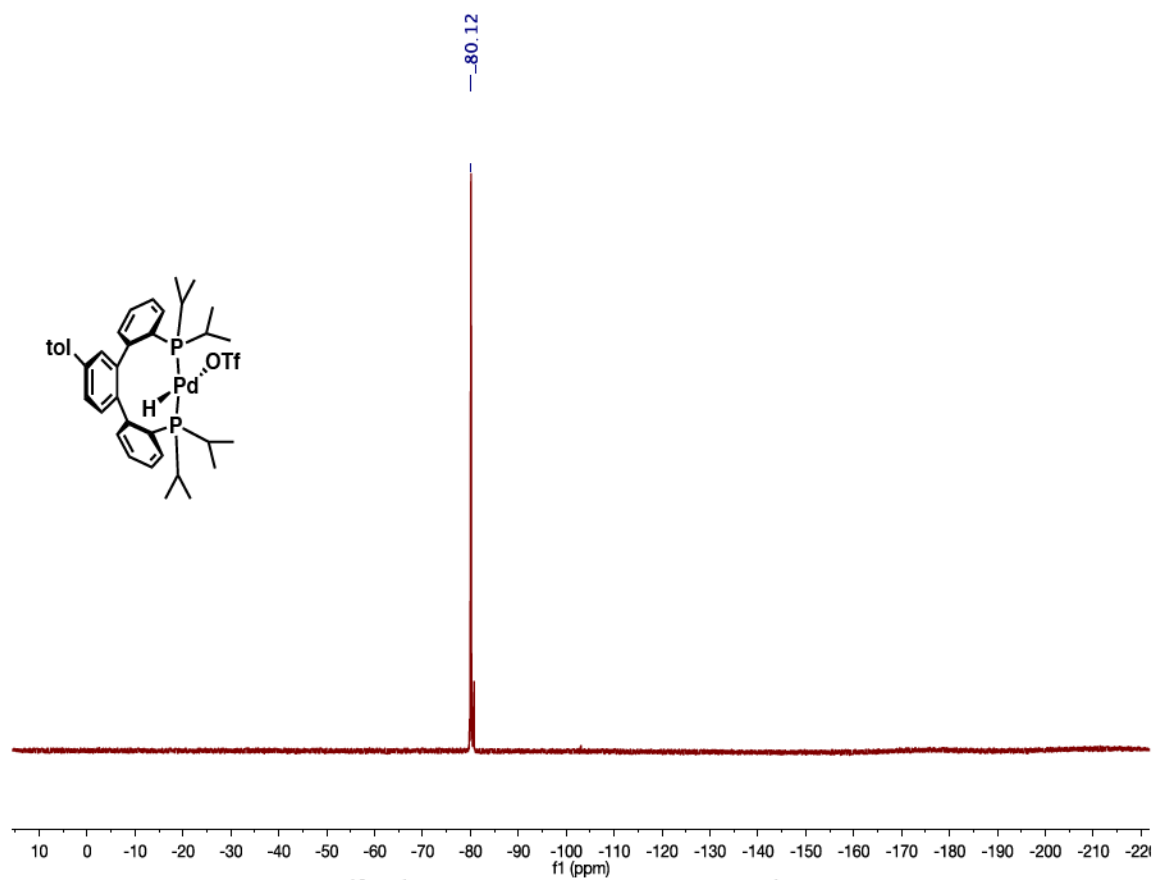


**Figure A.56:**  $^{19}\text{F}\{^1\text{H}\}$  NMR spectrum of  $(\text{Pter}^{\text{tol}}\text{P})\text{PdH}(\text{OTf})$  (69).